DISSERTATION

THE DESIGN AND SYNTHESIS OF SUPER REDUCING ORGANIC PHOTOCATALYSTS THROUGH MECHANISTIC UNDERSTANDING WITH APPLICATION TOWARDS UNACTIVATED ARENE ACTIVATION

Submitted by

Alexander Richard Green

Department of Chemistry

In partial fulfillment of the requirements

For the Degree of Doctor of Philosophy

Colorado State University

Fort Collins, Colorado

Summer 2024

Doctoral Committee:

Advisor: Garret Miyake

Robert Paton
Travis Bailey
Brad Reisfeld

ABSTRACT

THE DESIGN AND SYNTHESIS OF SUPER REDUCING ORGANIC PHOTOCATALYSTS THROUGH MECHANISTIC UNDERSTANDING WITH APPLICATION TOWARDS UNACTIVATED ARENE ACTIVATION

The work described in this dissertation focuses on the understanding of an organic photocatalyst system through a degradation and mechanistic study, leading to development of a new class of organic photocatalyst and improved application. The design of new organic photocatalysts is crucial for eliminating the need to use rare and expensive ruthenium and iridium that have dominated the field of photoredox catalysis for the past decade. Additionally, most of the catalysts describe here-in operate through a unique two electron, one proton activation mechanism to generate a closed shell species which enables direct quenching towards unactivated arenes such as benzene, without the use of a stoichiometric amount of reductant such as solvated electrons coming from pyrophoric metals. The progress described within this dissertation provides a deeper understanding of tunable organic reductants and their function.

DEDICATION

To my amazing co-workers in the Miyake group, and notable mentors who helped get to this point: Dr. Bonnie Buss, Dr. Max Kudisch, Dr. Cam Chrisman, and Dr. Amreen Bains. To Dr. Garret Miyake for giving me the opportunity needed to grow throughout this PhD and my admirable team of collaborators at Colorado Boulder who has made significant contributions to this work: Dr. Niels Damrauer, Dr. Nicholas F. Pompetti, and Arindam Sau.

To my friends who joined me through this journey and made the world full of color, notably Garrett Hoteling, Luke Salzer, Dakota Lorenz, Brennan McBride, Macayla Barnes, and Fran Luong. To my loved ones and family who supported me through these five years and encouraged this achievement, especially Elana J. Cope.

TABLE OF CONTENTS

ABSTRACT……..……..ii

DEDICATION…….……...…….iii

CHAPTER 1 - INTRODUCTION……...…….……..…1

DISSERTATION STRUCTURE…….……2

MOTIVATIONS…….…….2

REFERENCES……5

CHAPTER 2 - C–F BOND ACTIVATION BY AN ORGANIC PHOTOREDOX CATALYST.
OVERVIEW……...6

INTRODUCTION…….……7

RESULTS AND DISCUSSION…….9

CONCLUSION…….19

REFERENCES…….20

CHAPTER 3 - MECHANISTIC INVESTIGATION OF A PHOTOCATALYST MODEL REVEALS FUNCTION BY PERYLENE-LIKE CLOSED SHELL SUPER-PHOTOREDUCTANT CAPABLE OF REDUCING UNACTIVATED ARENES.

OVERVIEW…….……24

INTRODUCTION…….……25

RESULTS AND DISCUSSION……..…….……27

CONCLUSION……..……48

REFERENCES……..51

CHAPTER 4 – SPECTROSCOPICALLY GUIDED DISCOVERY OF PHOTOANNULATION IN BAY-SUBSTITUTED BENZO[GHI]PERYLENE UNLOCKS UNPRECEDENTED PHOTO-BIRCH REDUCTIONS

OVERVIEW……..54

INTRODUCTION…….……....55

RESULTS AND DISCUSSION…….58

CONCLUSION……..76

REFERENCES……..77

APPENDIX A: SUPPLEMENTARY INFORMATION FOR CHAPTER 2……..…..79

APPENDIX B: SUPPLEMENTARY INFORMATION FOR CHAPTER 3……...….402

APPENDIX C: SUPPLEMENTARY INFORMATION FOR CHAPTER 4……517

CHAPTER 1 – INTRODUCTION

DISSERTATION STRUCTURE

This dissertation consists of four chapters. Chapter 3 is adapted from previously published work and Chapters 2 and 4 are a draft of unpublished work. Below is a list of the chapters including a summary of the content:

Chapter 2: Current unpublished work from the manuscript draft titled "*C–F bond activation by an organic photoredox catalyst"* by Xin Liu, Alexander R. Green, Mihai V. Popescu Arindam Sau, Nicholas F. Pompetti, Yingzi Li, Yucheng Zhao, Robert S. Paton, Niels H. Damrauer, and Garret M. Miyake. This chapter focuses on the use of organic photocatalysts in the benzo[ghi]perylene (BPI) family to reduce fluorinated compounds to generate aryl radicals, susceptible through radical-radical coupling. The mechanism of this system was probed, and a dual function of open shell and closed shell state of the catalyst was suggested to be operative.

Chapter 3: Adapted from: Arindam Sau[1], Nicholas F. Pompetti[1], Alexander R. Green[1], Mihai V. Popescu, Robert S. Paton, Garret M. Miyake, and Niels H. Damrauer. *Mechanistic Investigation of a Photocatalyst Model Reveals Function by Perylene-Like Closed Shell Super-Photoreductant Capable of Reducing Unactivated Arenes. ACS Catal. 2024, 14, 4, 2252–2263*. This chapter focuses on the degradation pathway of a previously established light driven system in photoredox using BPIs, which led to the design and understanding of a new class of photocatalysts; benzo perylene diester (BPDE). Key takeaways from this work revolve around a unique 2 electron 1 proton activation of the BPDE pre-catalyst to generate a perylene like active species, which we monitor reactivity with unactivated arenes. This mode of operation suggests future improved catalysis, shown in Chapter 4.

Chapter 4: Current unpublished work from a manuscript draft labeled *"Spectroscopically guided discovery of photoannulation in bay-substituted benzo[ghi]perylene unlocks unprecedented photo-Birch reductions"* by Amreen K. Bains, Arindam Sau, Alexander R. Green, Brandon Portela, Graham Haung, Anna M. Wolff, Ludovic F. Patin, Robert S. Paton, Neils H. Damrauer, and Garret M. Miyake. In this work, the BPDE catalyst system was expanded with structural modifications. The result of these modifications showed a post synthetic annulation to form a benzo coronene diester, (BCDE), which follows a similar path of activation to the BPDE when applied to the reduction of arenes. This new system was applied to a broad reaction scope and overcame limitations of the first reductive system using BPIs.

MOTIVATIONS

Over the past decade, photo redox catalysis has become a critical tool for small and macromolecule synthesis. Photo redox catalysis represents many ideals of green chemistry, including performing reactions under mild conditions fueled by solar energy without stoichiometric reagents.[1] Rare heavy earth metals are typically used as photo redox catalysts such as iridium and ruthenium, which come with a high environmental cost.[2] Due to these limitations, organic photocatalysts (OPCs) are a sustainable alternative, which not only can replace the previous catalysts but also offer unique properties that we may exploit for synthetic challenges.

Our group specializes in the design, synthesis, and mechanistic understanding of OPCs and the application towards small molecule methodology and controlled polymer synthesis.[3] Topics covered in this work will revolve around reductive photocatalysts, where a substrate gains and electron from the photocatalyst through single electron transfer (Figure 1.1A). Previous work established that a unique organic dye known as benzo[ghi] perylene can be used as a photocatalyst towards activating inert substrates such as benzene, which typically uses pyrophoric metals such

as lithium or sodium in stoichiometric quantities.[4] Reducing unactivated arenes has proven difficult due to the lack of thermodynamic driving force from organic catalysts, yet many reduced arenes and olefins are found in value products.[5] The strategy that enables us to accomplish challenging reactivity that only metals could do in the past comes from the absorption of multiple photons of energy in the same system to thermodynamically drive a reaction forward, inspired by nature's Z-scheme, or in photo redox catalysis – consecutive photoinduced electron transfer (Figure 1.1B).[6]

The goal of this work is to display a story arc that started with a novel system that contained many limitations from mechanistic understanding, to limited applicability. Through degradation studies, design of a model catalyst and fundamental understanding of the catalytically active species (intermediate responsible for electron transfer to the substrate), to rationale catalyst design and synthesis of new photocatalyst families, we demonstrate a full picture of an exponentially improved system, pushing the boundaries of highly reductive organic photocatalysis.

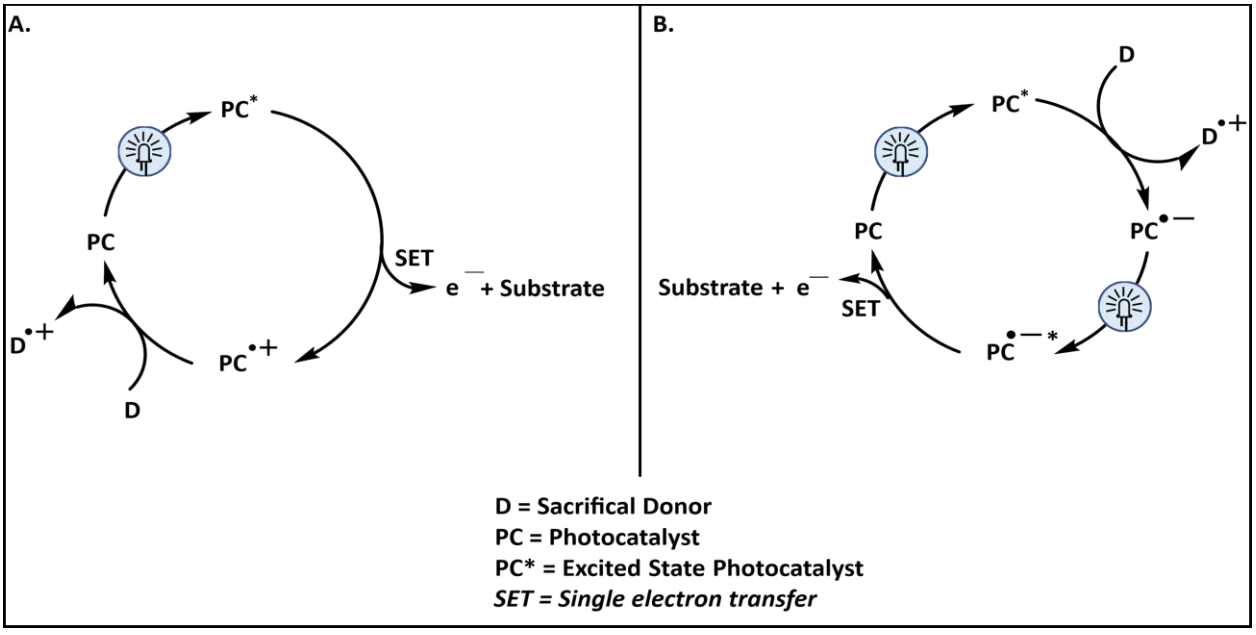

Figure 1.1. Oxidative quenching in photocatalyzed reducing mechanisms. A) Traditional photocatalyzed mechanism where the electron undergoes single electron transfer from the excited

state photocatalyst. B) Abbreviated mechanism for consecutive photoinduced electron transfer, utilizing multiple photons in one catalytic cycle which enables stronger reduction potentials from the excited state photocatalyst.

REFERENCES

(1) Romero, N. A.; Nicewicz, D. A., *Chem. Rev.* **2016,** 116 (17), 10075-10166.
(2) Michel P. The toxic damage from mining rare elements. *Nature and Environment.* **2021**, https://www.dw.com/en/toxic-and-radioactive-the-damage-from-mining-rare-elements/a-57148185.
(3) McCarthy, B.G., Pearson, R.M., Lim, C.H., Sartor, M. S., Damrauer, N.H., Miyake, G.M., J. *Am. Chem. Soc*. **2018***,* 140, 5088−5101
(4) Cole, J. P.; Chen, D. F.; Kudisch, M.; Pearson, R. M.; Lim, C. H.; Miyake, G. M., *J. Am. Chem. Soc.* **2020,** 142 (31), 13573-13581.
(5) Joshi, D.K., Sutton, J.W., Carver, S., Blanchard, J.P., *Org. Pro. Res. Dev.* **2005**, 9, 997-1002.
(6) Chatterjee, A.; Konig, B., *Angew. Chem. Int. Ed. Engl.* **2019,** *58* (40), 14289-14294.

[1]CHAPTER 2 – C–F BOND ACTIVATION BY AN ORGANIC PHOTOREDOX CATALYST.

OVERVIEW

Photoredox catalyzed activation of organohalides has offered a broadly applicable strategy in chemical synthesis because the halide serves as a versatile functional group for elimination, substitution, and cross-coupling reactions.[1-3] However, activation of carbon-halogen bonds has thus far rarely extended to organofluorines which are the most commercially abundant organohalide. Current approaches based on photoredox chemistry for activation of carbon-fluorine (C–F) bonds are limited by the substrates and transition-metal catalysts needed.[4-19] Therefore, developing a general method for the direct activation of organofluorines would have major implications for organic synthesis. Here we report an organic photoredox catalyst system that can efficiently reduce C–F bonds to generate carbon-centered radicals that can be intercepted for hydrodefluorination and cross-coupling reactions. This system enables the general use of organofluorines as synthons under mild reaction conditions. Furthermore, we extend this methodology toward the defluorination of polyfluoroalkyl substances (PFAS) and fluorinated polymers, a critical challenge in the breakdown of persistent and environmentally damaging forever chemicals.

INTRODUCTION

[1] *Author contributions. A.R.G., M.V.P, and A.S. contributed equally. A.R.G, X.L. and G.M.M. conceived the idea. X.L., A.R.G., and Y.Z. executed the reaction methodology development. N.F.P., A.S., N.H.D., X.L. and A.R.G. conceived of and contributed to mechanistic studies. Y.L., M.V.P. and R.S.P. performed DFT calculations. X.L., N.F.P., A.S., R.S.P., N.H.D., and G.M.M co-wrote the manuscript. All authors read and edited the manuscript.*

Organofluorines have tremendous impacts in medicinal[20], agrochemical[21], and materials sciences[22] as fluorine incorporation results in structures imparting specific beneficial attributes or used to tune properties derived from secondary interactions with the molecular environment. Numerous top-selling pharmaceuticals and agrochemicals contain fluorine because of the favorable interactions derived from hydrogen bonding at protein active sites[23]. Substitution of hydrogen in the structure of the commodity plastic polyethylene with fluorine leads to high-performance polytetrafluoroethylene (Teflon®) with superior thermal, mechanical, and stability properties[24], inspiring continued development of fluorine-containing polymers for use in high-end applications.[25] Due to opportunities imparted by fluorine incorporation, significant efforts have been made to develop synthetic methods for the synthesis of fluorine-containing compounds.[26] From an alternative perspective, the prevalence of fluorinated organic molecules makes the carbon-fluorine (C–F) bond an attractive functional group for further chemical modification.[27] However, properties such as strong C–F bond strength, hydrophobicity, and high thermal stability that impart unique properties into fluorinated compounds also equate to chemical inertness (Fig. 1a). Consequently, not only are C–F bonds challenging to activate but their stability results in environmental persistence. Serious concerns regarding environmental contamination of fluorinated molecules exist because they are pervasive in the environment and long-term exposure can result in adverse health effects.[28]

Although C–F bond activation has received significant attention, these approaches largely rely on transition metal or main group Lewis-acid catalysts[29,30] and have been beset by scope limitations and issues of substrate generality. Recently, the advent of low-energy, visible-light photoredox catalysis has offered a broadly applicable carbon-halogen (halogen = Cl, Br, or I) bond activation strategy, which has led to an increase in the use of radical chemistry to tackle synthetic

problems (Fig. 1b).[31,32] However, no general strategy has yet emerged for direct C–F bond activation of alkyl and aryl fluorides, per- and polyfluoroalkyl substances (PFAS), or fluorinated polymers. To date, most work in photoredox catalyzed C–F bond activation has centered on nucleophilic aromatic substitution by an oxidative reaction mechanism[4,5], limited to specific substrates (polyfluorinated arenes[6], trifluoromethyls[7-13], or fluoroamides[14,15]), required stoichiometric reagents[16,17], used high energy UV light[33], relied on an anionic bimetallic complex[18], or was limited to only a few catalyst turnovers.[19]

The fundamental challenge in photoredox-catalyzed C–F bond activation is that the reducing power of known photoredox catalysts is insufficient to engage this inert bond. To accommodate a diverse range of chemical complexities and C–F bond strengths, this activation step would require a significant thermodynamic driving force by developing a photoredox catalyst system with a strong electron transfer capability. Our interests in photoredox catalysis originated with the development of strongly reducing organic photoredox catalysts (PCs) for application in organocatalyzed atom transfer radical polymerization.[34] Subsequently, we were motivated to develop a catalyst system for challenging C–F bond activations. En route to this goal, we took note of reports that perylene diimide or an acridinium salt can merge the energetics of two photons into a single high-energy chemical transformation, where a photoexcited reduced form of the catalyst is competent in the reduction of aryl chlorides.[35,36] Additionally, a closed-shell electron-rich photocatalyst results from two sequential one-electron reductions of naphthalene monoimide, which can also be used for activation of the C–Cl bond in aryl chlorides for hydrodechlorination and cross-coupling reactions.[37,38] These reports led us to question whether developing a two-photon catalytic system with a more negative reduction potential could be potent enough for C–F

activation, and whether catalyst design should consider the role of open- versus closed-shell species to engage relevant photochemical events.

RESULTS AND DISCUSSION

Our approach for the development of a new catalytic system for C–F bond activation was inspired by our previous observation of a purely organic photo-Birch catalytic system.[39] By using benzo[ghi]perylene monoimide (**BPI**) in conjunction with tetramethylammonium hydroxide (Me_4NOH), arenes can be reduced to cyclohexadienes. However, multiple catalyst loadings and long reaction time limited its application. Subsequent mechanistic investigations showed that the imide ring in **BPI** was undergoing rapid degradation under highly basic conditions.[40] To alleviate the problem of catalyst degradation and extensive reaction times, we were motivated to use tetra-n-butylammonium fluoride (nBu$_4$NF) as a less basic sacrificial electron donor (Fig. 2.1c). Here, we report the successful realization of this idea and demonstrate that a combination of **BPI** and nBu$_4$NF under blue light gives rise to a reducing environment potent enough to activate C–F bond in a wide range of organofluorines (including aryl fluorides, alkyl fluorides, PFAS, and fluorinated polymers). Following an electron transfer (ET) event, the C–F bond is cleaved generating carbon-centered radicals that can be used for either hydrodefluorination (by including *tert*-amyl alcohol) or cross-coupling reactions (by including a coupling partner, instead of an alcohol) (Fig. 2.1e). During optimization, most other fluoride sources were found to be not soluble in the reaction condition while other electron donors and proton sources resulted in inferior yields (Fig. 2.1d). It has been shown that the tert-amyl alcohol (tAmylOH) adducts with Me_4NF exhibits greater fluoride (F^-) nucleophilicity and lower alcohol nucleophilicity than adducts with other alcohols.[41]

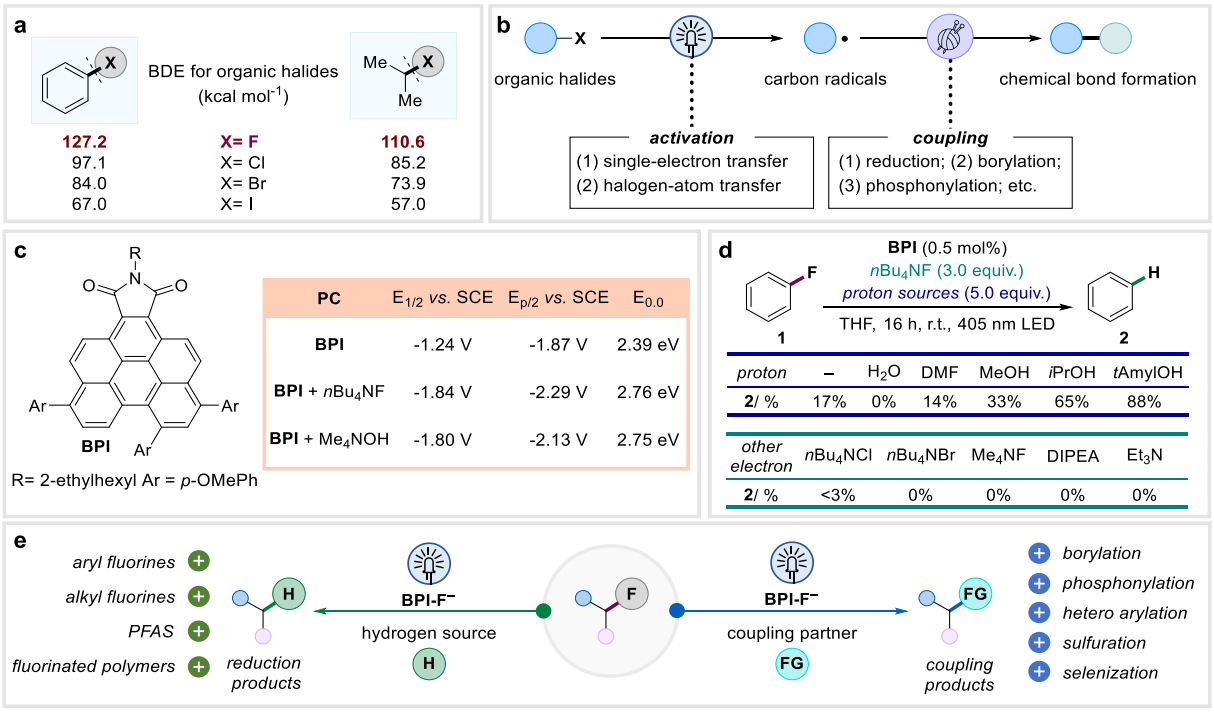

Fig. 2.1. Direct activation of organofluorines and fluorinated polymers. a, Bond dissociation energies (BDE) of organohalides. b, Mechanistic approaches for activation of carbon-halogen bonds via visible light. c, Deliberate tuning of redox potentials of the BPI with fluoride or hydroxide. d, The optimized hydrodefluorination of fluorobenzene. DMF, dimethylformamide. DIPEA, N,N-diisopropylethylamine. e, Development of a general strategy for C–F bond activation driven by visible light.

The hypothesized mechanistic outline for the hydrodefluorination of fluorobenzene **1** is depicted in Fig. 2a. First, a ring-opening intermediate **BPI-RO** with an amide and a carboxylate functional group is formed through a hydrolyzing reaction under dark conditions. Then, visible light generates the excited-state **BPI-RO***, which is reductively quenched by F^- to yield the open-shell intermediate **BPI-RO**$^{\bullet-}$ and a fluoride radical ($F^{\bullet}$). Thereafter, a second photoexcitation event yields the strongly reducing excited-state radical anion species **BPI-RO**$^{\bullet-*}$, which can abstract a hydrogen atom from *t*AmylOH or nBu$_4$NF to yielding a closed-shell species **BPI-RO-H**$^-$. Upon excitation, **BPI-RO-H**$^{-*}$ reduces the substrate via proton-coupled electron transfer (PCET) or photoinduced electron transfer followed by proton transfer (PET/PT), to generate either Ph-F$^{\bullet-}$ or

Ph-H while generating **BPI-RO**$^{\bullet-}$. The Ph-F$^{\bullet-}$ species yields a carbon-centered radical that can abstract a hydrogen atom from the *n*Bu$_4$NF to yield benzene **2** as the reduction product.

To investigate these mechanistic hypotheses, we performed a series of experiments. Initially, to make the assignments of peaks simpler and to structurally elucidate the mode of reactivity between the **BPI** and *n*Bu$_4$NF, we undertook intermediate studies using the symmetric variant **BPI-N**. We successfully isolated the intermediate formed from **BPI-N** and *n*Bu$_4$NF. The ^{1}H-, ^{13}C-, 2D-NMR, and UV-vis indicate that the intermediate is an asymmetric ring-opening compound (**BPI-N-RO**) with amide and carboxylate groups. Density functional theory (DFT) studies suggest that free hydroxide (OH^-) from F^- reaction with water can lead to the formation of ring-opening intermediate with an overall -14.0 kcal/mol exergonic process. Moreover, the absence of any signal in ^{19}F-NMR of the isolated product indicated that neither a covalent fluoride adducts nor a fluoro-Meisenheimer complex is formed. The NMR experiments showed that the **BPI** also demonstrates identical reactivity with *n*Bu$_4$NF which suggests the forming of **BPI-RO**. Notably, **BPI-RO** is stable in solution and a hypsochromic shift relative to **BPI** (λ_{max} = 565 nm [**BPI**], 483 nm [**BPI-RO**], (Fig. S2.14-S2.16) is observed in the absorption spectrum, indicative not anion-π formation which typically observed a bathochromic shift. Other common F^- sources were unsuccessful in forming this adduct (Fig. S2.49–S2.51), while the purity of *n*Bu$_4$NF was found to be essential to stability and catalytic performance of the catalyst. Because high water content will result in the F^- rapid form the thermodynamically stable HF^{2-}, which possesses lower HOMO levels and poor electron donating ability. Computed standard oxidation potentials in THF suggest that the *t*AmylOH bound F– is a more favorable electron-donor compared to either *t*Amyl alkoxide or amine. Quenching experiments of **BPI-RO** with fluorobenzene reveal that reactivity requires the two-photon process, as **BPI-RO** is unreactive (Fig. S2.37). Upon irradiation with the same

excitation wavelength as the reaction conditions with excess nBu$_4$NF in the absence of alcohol, a radical anion species is observed by electron paramagnetic resonance (EPR) spectroscopy (Fig. S2.36) and UV-vis (Fig. S2.31). We posit that this is evidence of **BPI-RO** being transformed into radical anion **BPI-RO**$^{\bullet-}$ through a photoinduced reduction by F$^-$. In our original work, this EPR spectrum was assigned to **BPI**$^{\bullet-}$, but we now believe that this is not correct and that it corresponds to the presence of **BPI-RO**$^{\bullet-}$ under non-alcohol reaction conditions.

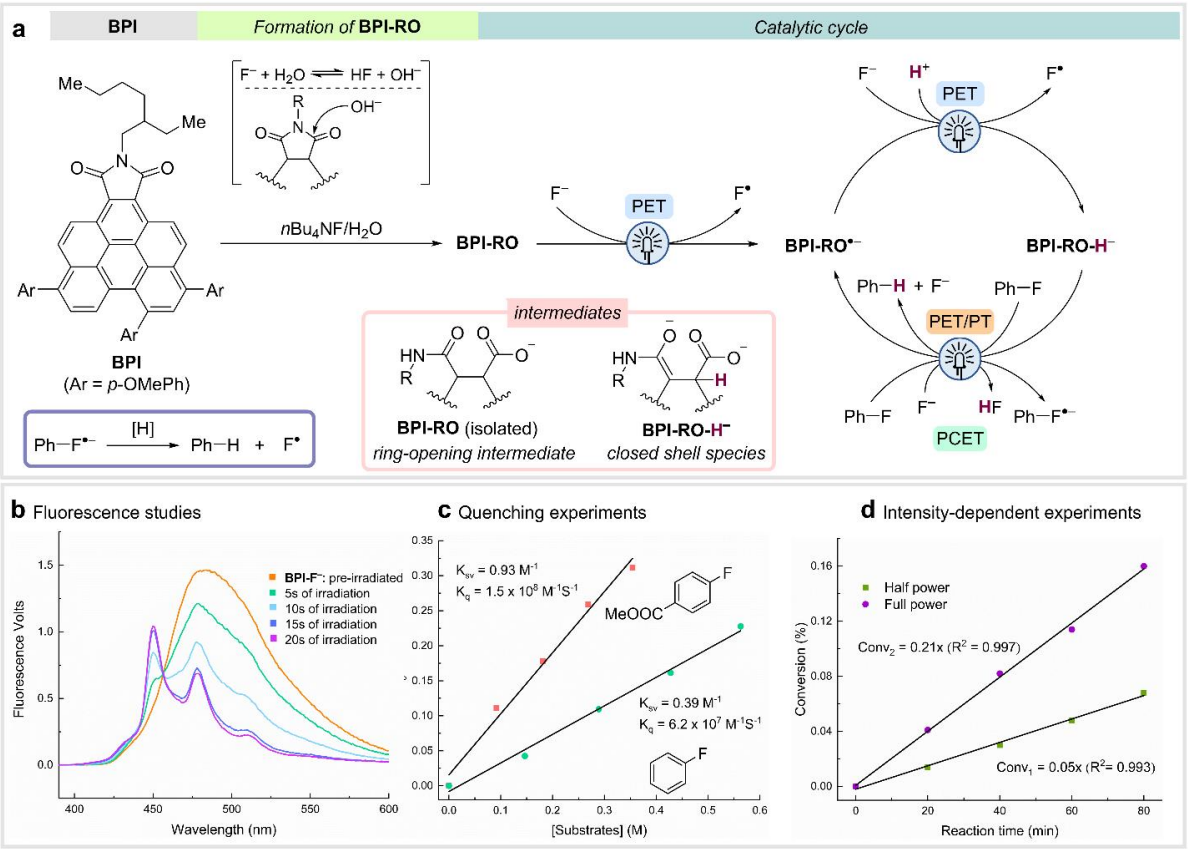

Fig. 2.2. Mechanism and analysis for photoredox catalyzed C–F bond activation. a, Proposed mechanism for the photoredox-catalyzed dehalogenation of fluorobenzene. nBu, butyl; LED, light-emitting diodes; PET, photoinduced electron transfer; HAT, hydrogen atom transfer. b, Fluorescence studies. c, Quenching experiments. d, Light intensity-dependent experiments.

It is important to highlight that, in the presence of a proton source (*t*AmylOH), **BPI-RO**$^{\bullet-}$ is rapidly transformed into a closed-shell species following a second interaction with visible light (an

emission band was observed at λ_{max} = 450 nm, Fig. 2.2b) and no radical anion is detected. The new species is air-stable and photoluminescent with a lifetime on the order of 10 ns, which we posit is the closed-shell singlet species **BPI-RO-H**$^{-}$, and not in a doublet state (which is likely protonated by the alcohol) (Fig. S2.39–S2.42). Computed thermochemistry and reduction potential indicate that the closed-shell species **BPI-RO-H**$^{-}$ is a stable intermediate with a new C–H bond adjacent to the carbonyl group via protonation; the redox potential of excited state **BPI-RO-H**$^{-*}$ up to -3.64 V vs. SCE. Indeed, ^{13}C-, and ^{1}H-NMR experiments support the formation of the new intermediate (Fig. S2.43–S2.45), while photoluminescence quenching of this species is observed with aryl fluorides such as methyl 4-fluorobenzoate and fluorobenzene, demonstrating the super reducing power (Fig. 2.2c). In support of the closed-shell mechanism involves an overall two-photon excitation process, a near quadratic dependency of the conversion of fluorobenzene to the irradiation density is observed (Fig. 2.2d).[46] Lastly, deuterium-labeling experiments support that both the *n*Bu$_4$NF and alcohol can serve as the proton source in this system (Table. S2.19-S2.22), which suggests both PCET and PET/ET process are possible.[37]

To evaluate the competency of this catalytic system in C–F bond activation, we first explored the scope of the hydrodefluorination of organofluorines (Fig. 2.3a). A variety of both electron-poor and electron-rich aryl fluorides possessing different functional groups (e.g., free alcohol, carboxylic acid, amine, and nitrile) were tolerated by the catalytic system and afforded the corresponding products (**3** to **10**) in good to excellent yields while no Birch-type arene reduction products were observed under these reaction conditions. Furthermore, this methodology could be extended to alkyl fluorides and was efficient in the defluorination of primary, secondary, and tertiary alkyl fluorides in good to high yields (**11** to **16**). This reactivity was also efficient with Cl or Br-based organohalides (see supplementary materials for details). As a demonstration of the

notable reactivity of this system, we successfully reduced polyfluorinated compounds under our conditions and the substrates were efficiently converted to hydrodefluorination products (**17** to **24**). Moreover, several natural products and drug derivatives were also amenable to hydrodefluorination to the corresponding products (**25** to **28**) in useful to good yield.

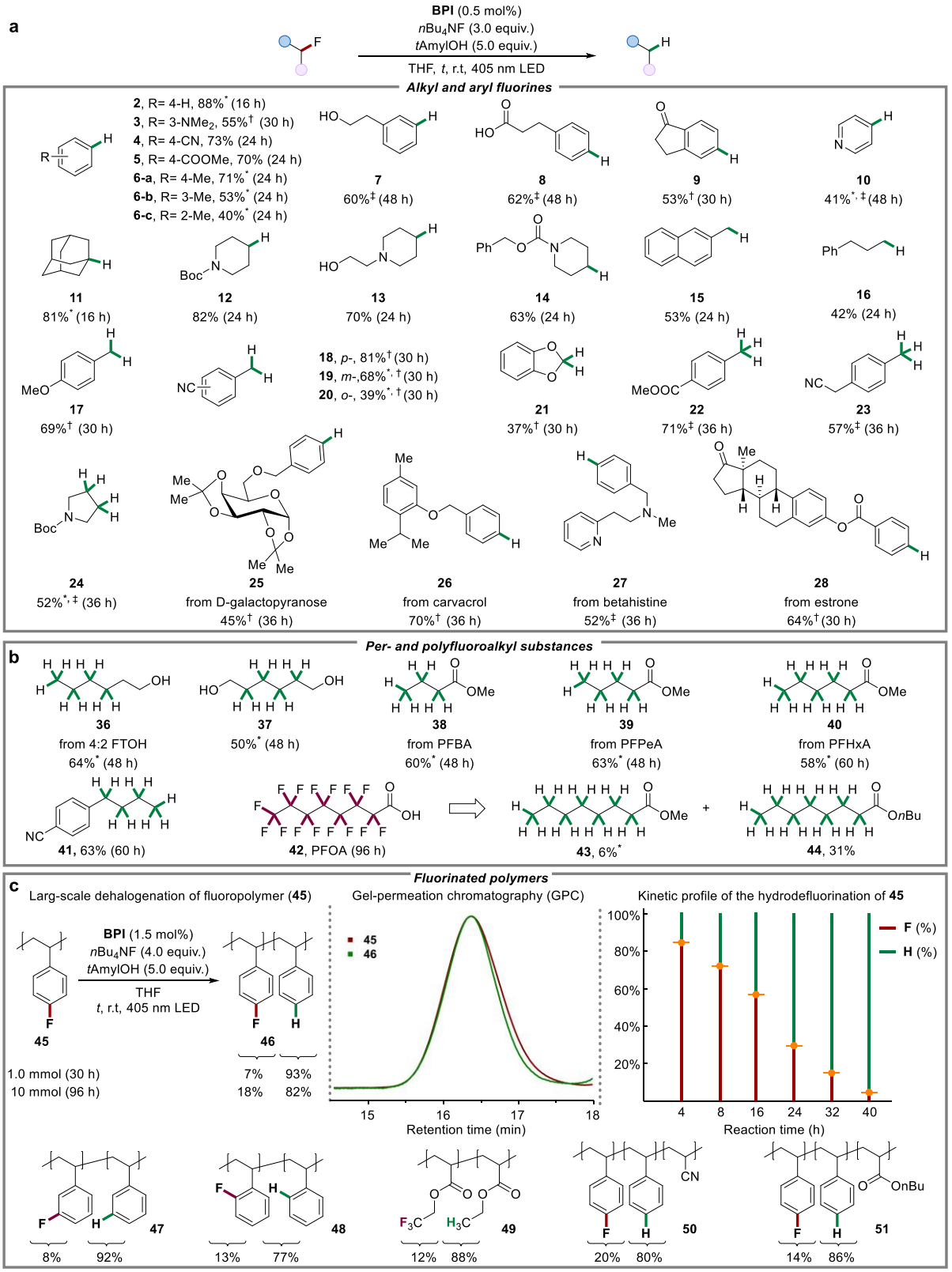
a
BPI (0.5 mol%)
nBu4NF (3.0 equiv.)
tAmylOH (5.0 equiv.)
THF, t, r.t, 405 nm LED
Alkyl and aryl fluorines
2, R= 4-H, 88%* (16 h)
3, R= 3-NMe2, 55%† (30 h)
4, R= 4-CN, 73% (24 h)
5, R= 4-COOMe, 70% (24 h)
6-a, R= 4-Me, 71%* (24 h)
6-b, R= 3-Me, 53%* (24 h)
6-c, R= 2-Me, 40%* (24 h)
7 60%‡ (48 h)
8 62%‡ (48 h)
9 53%† (30 h)
10 41%*, ‡ (48 h)
11 81%* (16 h)
12 82% (24 h)
13 70% (24 h)
14 63% (24 h)
15 53% (24 h)
16 42% (24 h)
17 69%† (30 h)
18, p-, 81%† (30 h)
19, m-,68%*, † (30 h)
20, o-, 39%*, † (30 h)
21 37%† (30 h)
22 71%‡ (36 h)
23 57%‡ (36 h)
24 52%*, ‡ (36 h)
25 from D-galactopyranose 45%† (36 h)
26 from carvacrol 70%† (36 h)
27 from betahistine 52%‡ (36 h)
28 from estrone 64%† (30 h)
b
Per- and polyfluoroalkyl substances
36 from 4:2 FTOH 64%* (48 h)
37 50%* (48 h)
38 from PFBA 60%* (48 h)
39 from PFPeA 63%* (48 h)
40 from PFHxA 58%* (60 h)
41, 63% (60 h)
42, PFOA (96 h)
43, 6%*
44, 31%
c
Fluorinated polymers
Larg-scale dehalogenation of fluoropolymer (45)
BPI (1.5 mol%)
nBu4NF (4.0 equiv.)
tAmylOH (5.0 equiv.)
THF
t, r.t, 405 nm LED
45
46
1.0 mmol (30 h)
10 mmol (96 h)
7% 93%
18% 82%
Gel-permeation chromatography (GPC)
45
46
Retention time (min)
Kinetic profile of the hydrodefluorination of 45
F (%)
H (%)
Reaction time (h)
47 8% 92%
48 13% 77%
49 12% 88%
50 20% 80%
51 14% 86%

*Fig. 2.3. Substrate scope for the hydrodefluorination reaction. a, Scope for the hydrodefluorination of aryl and alkyl fluorides. Isolated yields are given. *The yields were calculated by GC measurements. †BPI (1.0 mol%) was used. ‡BPI (2.0 mol%) was used. Boc, tert-butoxycarbonyl; Ph, Phenyl. b, Scope for the per- and polyfluoroalkyl substances. See supplementary materials for detailed reaction conditions. The yields were calculated by GC measurements. c, Scope for the fluorinated polymers. See supplementary materials for detailed reaction conditions. The conversions were determined by ^{19}F-NMR.*

The broad success in the scope of C–F bond activation with our catalyst system led us to question if hydrodefluorination of PFAS could be achieved, which would offer a mild strategy to address the challenge of PFAS degradation.[47–49] Using methanol as the hydrogen donor, several PFAS, including perfluorooctanoic acid (PFOA), could be converted to the defluorinated products (**36** to **40,** and **44**) in high yield (Fig. 2.3b), representing a mild reaction methodology for breaking down these persistent chemicals. Interestingly, the carboxylic acid PFOA is defluorinated to the *n*-butyl ester (**44**) through additional reaction with *n*Bu_4NF. Given that our strategy can be implemented with small molecules, we envisioned that this C–F bond activation strategy could be applied to fluorinated polymers, which display prolonged stability under ambient conditions, limited potential in end-of-life recycling, and increasing concern over environmental contamination.[50] Poly(4-fluorostyrene) **45** undergoes complete hydrodefluorination to **46** in a 10 mmol scale reaction while the gel permeation chromatography (GPC) trace was virtually identical before and after the reaction, demonstrating the lack of chain scission accompanying polymer hydrodefluorination (Fig. 2.3c). Notably, monitoring the reaction profile revealed that this strategy can also controllably tune the polymer fluorine content by reaction time. To further extend the scope of macromolecular transformations, a variety of fluorinated polymer derivatives including poly(fluorostyrene), fluorinated polyacrylate, and poly(fluorostyrene)-derived copolymers (**47** to **51**) could also be transformed to the targeted hydrodefluorination products.

We next investigated the possibility of extending this methodology to cross-coupling processes by intercepting the carbon-centered radical generated from aryl fluoride reduction (Fig. 2.4). When similar conditions as hydrodefluorination were attempted for borylation, a low yield of desired product was obtained with a substantial amount of the reduction product identified. In this case, the high concentration of hydrogen donor favors hydrodefluorination, thus rendering the coupling reaction uncompetitive. We reasoned that favoring the open-shell manifold by omitting the hydrogen source could improve conditions for cross-coupling. Through this modulation, a diverse range of electron-poor and -rich aryl fluorides were borylated to the corresponding products (**52** to **61**) through the desired radical coupling reaction with bis(pinacolato)diboron. The diborylation product **62** could also be obtained starting from 1,4-difluorobenzene. Notably, aryl boronates other than pinacol boronate could be generated using the corresponding diboron esters (**63** and **64**). Considering that borylation reagents are heavily used in drug and bioactive molecule syntheses, borylated derivatives of (-)-menthol (**65**), geraniol (**66**) and cholesterol (**67**) were generated in good yields up to 60%. Furthermore, this cross-coupling reactivity could be applied to achieve phosphonylation (**70** to **73**), (hetero) arylation (**74** to **80**), sulfuration, and selenization (**81** to **86**).

To further demonstrate the utility of this chemical reactivity, we targeted a double functionalization of 1,4-difluorobenzene (Fig. S2.8). The mono-borylation product **88** can be obtained using optimized conditions (see supporting information for details) and served as a common intermediate for further transformations such as Chan-Lam amination, S_NAr amination, and cyanation, which were isolated with moderate yields (**89** to **91**). Compared with sequential processes, a one-pot bifunctionalization is more challenging. We demonstrated this goal by sequentially adding the coupling partners for sulfuration and borylation (see supplementary materials for details), and the corresponding product **92** could be isolated in useful yield.

Moreover, the use of this bifunctional product in sulfamidation and Suzuki-Miyaura cross-coupling was effective, as demonstrated by the high yields of **93** and **94**.

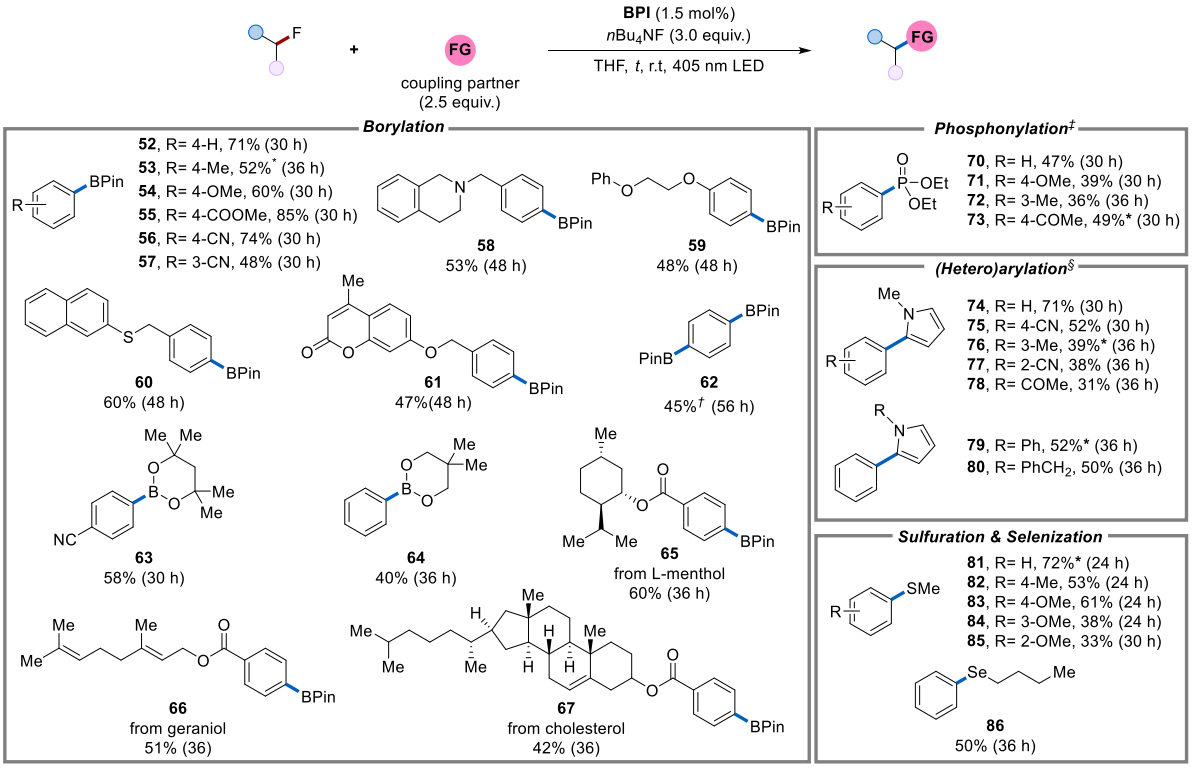

*Fig. 2.4. Intermolecular couplings from challenging aryl fluoride precursors. *The yields were calculated by GC measurements. †6.0 equiv. of coupling partner was used. ‡BPI (2.0 mol%), coupling partner (5.0 equiv.) and acetonitrile (1.0 mL, co-solvent) were used. §BPI (2.0 mol%), coupling partner (20.0 equiv.) and DMSO (1.0 mL, co-solvent) were used. BPin, pinacolborane.*

CONCLUSION

We anticipate that this mild catalyst system for challenging C–F bond activation will facilitate the use of organofluorines in chemical synthesis and provide a new means for breaking down persistent fluorinated compounds. The apparent opportunity to manipulate photoredox catalysts to operate in either an open- or closed-shell electronic configuration for controlling chemoselectivity is intriguing in photoredox catalysis and it may offer strategies to further expand the reaction capabilities. Efforts to more completely explore mechanistic details controlling these different strategies are ongoing in our laboratories.

REFERENCES

1. Cheung, K. P. S., Sarkar, S. & Gevorgyan, V. Visible light-induced transition metal catalysis. *Chem. Rev.* **122**, 1543–1625 (2022).
2. Pitre, S. P. & Overman, L. E. Strategic use of visible-light photoredox catalysis in natural product synthesis. *Chem. Rev.* **122**, 1717–1751 (2022).
3. Narayanam, J. M. R. & Stephenson, C. R. J. Visible light photoredox catalysis: applications in organic synthesis. *Chem. Soc. Rev.* **40**, 102–113 (2011).
4. Pistritto, V. A., Schutzbach-Horton, M. E. & Nicewicz, D. A. Nucleophilic aromatic substitution of unactivated fluoroarenes enabled by organic photoredox catalysis. *J. Am. Chem. Soc.* **142**, 17187–17194 (2020).
5. Huang, H. & Lambert, T. H. Electrophotocatalytic S_NAr reactions of unactivated aryl fluorides at ambient temperature and without base. *Angew. Chem. Int. Ed.* **59**, 658–662 (2020).
6. Senaweera, S. & Weaver, J. D. Photocatalytic C–F reduction and functionalization. *Aldrichmica Acta* **49**, 45–54 (2016).
7. Chen, K., Berg, N., Gschwind, R. & König, B. Selective single C(sp^3)–F bond cleavage in trifluoromethylarenes: merging visible-light catalysis with Lewis acid activation. *J. Am. Chem. Soc*. **139**, 18444–18447 (2017).
8. Wang, H., & Jui, N. T. Catalytic defluoroalkylation of trifluoromethylaromatics with unactivated alkenes. *J. Am. Chem. Soc.* **140**, 163–166 (2018).
9. Vogt, D. B., Seath, C. P., Wang, H. & Jui, N. T. Selective C–F functionalization of unactivated trifluoromethylarenes. *J. Am. Chem. Soc.* **141**, 13203–13211 (2019).
10. Liu, C., Li, K. & Shang, R. Arenethiolate as a dual function catalyst for photocatalytic defluoroalkylation and hydrodefluorination of trifluoromethyls. *ACS Catal.* **12**, 4103–4109 (2022).
11. Campbell, M. W., Polites, V. C., Patel, S., Lipson, J. E., Majhi, J. & Molander, G. A. Photochemical C–F activation enables defluorinative alkylation of trifluoroacetates and -acetamides. *J. Am. Chem. Soc.* **143**, 19648–19654 (2021).
12. Shreiber, S. T., Granados, A., Matsuo, Bianca., Majhi, J., Campbell, M. W., Patel, S. & Molander, G. A. Visible-light-induced C–F bond activation for the difluoroalkylation of indoles. *Org. Lett.* **24**, 8542–8546 (2022).
13. Liu, C., Shen, N. & Shang, R. Photocatalytic defluoroalkylation and hydrodefluorination of trifluoromethyls using *o*-phosphinophenolate. *Nat. Commun.* **13**, 354 (2022).
14. Sandoval, B. A., Clayman, P. D., Oblinsky, D. G., Oh, S., Nakano, Y., Bird, M., Scholes, G. D. & Hyster, T. K. Photoenzymatic reductions enabled by direct excitation of flavin-dependent "Ene"-reductases. *J. Am. Chem. Soc.* **143**, 1735–1739 (2021).
15. Ye, J. -H., Bellotti, P., Heusel, C. & Glorius, F. Photoredox-catalyzed defluorinative functionalizations of polyfluorinated aliphatic amides and esters. *Angew. Chem. Int. Ed.* **61**, e202115456 (2022).
16. Glaser, F., Larsen, C. B., Kerzig, C. & Wenger, O. S. Aryl dechlorination and defluorination with an organic super-photoreductant. *Photochem. Photobiol. Sci.* **19**, 1035–1041 (2020).
17. Ding, T.-H., Qu, J.-P. & Kang, Y.-B. Visible-light-induced, base-promoted transition-metal-free dehalogenation of aryl fluorides, chlorides, bromides, and iodides. *Org. Lett.* **22**, 3084–3088 (2020).
18. Moore, J. T., Dorantes, M. J., Pengmei, Z., Schwartz, T. M., Schaffner, J., Apps, S. L., Gaggioli, C. A., Das, U., Gagliardi, L., Blank, D. A., & Lu, C. C. Light-driven hydrodefluorination of

electron-rich aryl fluorides by an anionic rhodium-gallium photoredox catalyst. *Angew. Chem. Int. Ed.* **61**, e202205575 (2022).
19. Wang, S., Wang, H., & König, B. Photo-induced thiolate catalytic activation of inert Caryl-hetero bonds for radical borylation. *Chem.* **7**, 1653–1665 (2021).
20. Wang, J., Sánchez-Roselló, M., Luis Aceña, J., del Pozo, C., Sorochinsky, A. E., Fustero, S., Soloshonok, V. A. & Liu, H. Fluorine in pharmaceutical industry: fluorine-containing drugs introduced to the market in the last decade (2001–2011). *Chem. Rev.* **114**, 2432–2506 (2014).
21. Jeschke, P. The unique role of fluorine in the design of active ingredients for modern crop protection. *ChemBioChem* **5**, 570–589 (2004).
22. Pagliaro, M. & Ciriminna, R. New fluorinated functional materials. *J. Mater. Chem.* **15**, 4981–4991 (2005).
23. Müller, K., Faeh, C. & Diederich, F. Fluorine in pharmaceuticals: looking beyond intuition. *Science* **317**, 1881–1886 (2007).
24. Puts, G. J., Crouse, P. & Ameduri, B. M. Polytetrafluoroethylene: synthesis and characterization of the original extreme polymer. *Chem. Rev.* **119**, 1763–1805 (2019).
25. Améduri, B. The promising future of fluoropolymers. *Macromol. Chem. Phys.* **221**, 1900573 (2020).
26. Furuya, T., Kamlet, A. S. & Ritter, T. Catalysis for fluorination and trifluoromethylation. *Nature* **473**, 470–477 (2011).
27. Amii, H. & Uneyama, K. C− F bond activation in organic synthesis. *Chem. Rev.* **109**, 2119–2183 (2009).
28. Joudan, S. & Lundgren, R. J. Taking the "F" out of forever chemicals. *Science* **377**, 816–817 (2022).
29. Stahl, T., Klare, H. F. T. & Oestreich, M. Main-group Lewis acids for C–F bond activation. *ACS Catal.* **3**, 1578–1587 (2013).
30. Aizenberg, M. & Milstein, D. Catalytic activation of carbon-fluorine bonds by a soluble transition metal complex. *Science* **265**, 359–361 (1994).
31. Prier, C. K., Rankic, D. A. & MacMillan, D. W. C. Visible light photoredox catalysis with transition metal complexes: applications in organic synthesis. *Chem. Rev.* **113**, 5322–5363 (2013).
32. Yoon, T. P., Ischay, M. A., Du, J. Visible light photocatalysis as a greener approach to photochemical synthesis. *Nature Chem.* **2**, 527-532 (2010).
33. Toriumi, N., Yamashita, K. & Iwasawa, N. Metal-free photoredox-catalyzed hydrodefluorination of fluoroarenes utilizing amide solvent as reductant. *Chem. Eur. J.* **27**, 12635–12641 (2021).
34. Theriot, J. C., Lim, C.-H., Yang, H., Ryan, M. D., Musgrave, C. B. & Miyake, G. M. Organocatalyzed atom transfer radical polymerization driven by visible light. *Science* **352**, 1082–1086 (2016).
35. Ghosh, I., Ghosh, T., Bardagi, J. I. & König, B. Reduction of aryl halides by consecutive visible light-induced electron transfer processes. *Science* **346**, 725–728 (2014).
36. MacKenzie, I. A., Wang, L., Onuska, N. P. R., Williams, O. F., Begam, K., Moran, A. M., Dunietz, B. D. & Nicewicz, D. A. Discovery and characterization of an acridine radical photoreductant. *Nature* **580**, 76–90 (2020).
37. Rieth, A. L., Gonzalez, M. I., Kudisch, B., Nava, M. & Nocera, D. G. How radical are "radical" photocatalysts? A closed-shell Meisenheimer complex is identified as a super-reducing photoreagent. *J. Am. Chem. Soc*. **143**, 14352–14359 (2021).

38. Cowper, N. G. W., Chernowsky, C. P., Williams, O. P. & Wickens, Z. K. Potent reductants via electron-primed photoredox catalysis: unlocking aryl chlorides for radical coupling. *J. Am. Chem. Soc.* **142**, 2093–2099 (2020).
39. Cole, J. P., Chen, D.-F., Kudisch, M., Pearson, R. M., Lim, C.-H. & Miyake, G. M. Organocatalyzed Birch reduction driven by visible light. *J. Am. Chem. Soc.* **142**, 13573–13581 (2020).
40. Sau, A., Pompetti, N. F., Green, A. R., Popescu, M. V., Paton, R. S., Miyake, G. M. & Damrauer, N. H. Mechanistic investigation of a photocatalyst model reveals function by perylene-like closed shell super-photoreductant capable of reducing unactivated arenes. *ACS Catal.* **14**, 2252–2263 (2024).
41. Morales-Colón, M. T., See, Y. Y., Lee, S. J., Scott, P. J. H., Bland, D. C. & Sanford, M. S. Org. Lett. 23, 4493–4498 (2021).
42. Speckmeier, E., Fischer, T. G., Zeitler, K. A toolbox approach to construct broadly applicable metal-free catalysts for photoredox chemistry: deliberate tuning of redox potentials and importance of halogens in donor–acceptor cyanoarenes. *J. Am. Chem. Soc*. **140**, 15353–15365 (2018).
43. Cole, J. P., Chen, D.-F., Kudisch, M., Pearson, R. M., Lim, C.-H. & Miyake, G. M. Organocatalyzed Birch reduction driven by visible light. *J. Am. Chem. Soc.* **142**, 13573–13581 (2020).
44. Morales-Colón, M. T., See, Y. Y., Lee, S. J., Scott, P. J. H., Bland, D. C. & Sanford, M. S. Org. Lett. 23, 4493–4498 (2021).
45. Saha. S. Anion-induced electron transfer. *Acc. Chem. Res.* **51**, 2225–2236 (2018).
46. Guha, S., Goodson, F. S., Corson, L. J. & Saha. S. Boundaries of anion/naphthalenediimide interactions: from anion−π interactions to anion-induced charge-transfer and electron-transfer phenomena. *J. Am. Chem. Soc.* **134**, 13679–13691 (2012).
47. Dawson, R. E., Hennig, A., Weimann, D. P., Emery, D., Ravikumar, V., Montenegro, J., Takeuchi, T., Gabutti, S., Mayor, M., Mareda, J., Schalley, C. A. & Matile, S. Experimental evidence for the functional relevance of anion–π interactions. *Nat. Chem.* **2**, 533–538 (2010).
48. Aragay, G., Frontera, A., Lloveras, V., Vidal-Gancedo, J. & Ballester, P. Different nature of the interactions between anions and $HAT(CN)_6$: from reversible anion−π complexes to irreversible electron-transfer processes ($HAT(CN)_6$ = 1,4,5,8,9,12-hexaazatriphenylene). *J. Am. Chem. Soc.* **135**, 2620–2627 (2013).
49. Sun, H. & DiMagno, S. G. Anhydrous tetrabutylammonium fluoride. *J. Am. Chem. Soc.* **127**, 2050–2051 (2005).
50. Glaser, F., Kerzig, Christoph. & Wenger, O. S. Multi-photon excitation in photoredox catalysis: concepts, applications, methods. *Angew. Chem. Int. Ed.* **59**, 10266–10284 (2020)
51. Trojanowicz, M., Bojanowska-Czajka, A., Bartosiewicz, I. & Kulisa, K. Advanced oxidation/reduction processes treatment for aqueous perfluorooctanoate (PFOA) and perfluorooctanesulfonate (PFOS) - a review of recent advances. *Chem. Eng. J.* **336**, 170–199 (2018).
52. Longendyke, G. K., Katel, S. & Wang, Y. PFAS fate and destruction mechanisms during thermal treatment: a comprehensive review. *Environ. Sci.: Process Impacts.* **24**, 196–208 (2022).
53. Douvris, C. & Ozerov, O. V. Hydrodefluorination of perfluoroalkyl groups using silylium-carborane catalysts. *Science* **321**, 1188–1190 (2008).

54. Lohmann, R., Cousins, I. T., DeWitt, J. C., Glüge, J., Goldenman, G., Herzke, D., Lindstrom, A. B., Miller, M. F., Ng, C. A., Patton, S., Scheringer, M., Trier, X. & Wang, Z. Are fluoropolymers really of low concern for human and environmental health and separate from other PFAS? *Environ. Sci. Technol.* **54**, 12820–12828 (2020).

[2]CHAPTER 3 – MECHANISTIC INVESTIGATION OF A PHOTOCATALYST MODEL REVEALS FUNCTION BY PERYLENE-LIKE CLOSED SHELL SUPER-PHOTOREDUCTANT CAPABLE OF REDUCING UNACTIVATED ARENES.

OVERVIEW

Benzo[ghi]perylene monoimides (BPIs) have recently been employed as organic photocatalysts for challenging reductions, enabling Birch and defluorination reactions. In probing their function, we identify a thermal degradation product involving imide ring opening and this in turn motivates development and synthesis of a high-symmetry model system – a benzo[ghi]perylene diester (**BPDE**) – whose structural simplicity is useful for mechanistic exploration relevant to the broader photocatalyst class. Using electrochemical and spectroscopic tools, we probe both the singly and doubly reduced states of **BPDE** and report the generation of **[BP-H]**$^{-}$, a 2-electron, 1-proton activated closed-shell super-reductant. This catalytically active species, after visible photon absorption, operates from its singlet excited state where the motions of the added proton are coupled to an electron transfer event which enables direct reduction of inert substrates like benzene and fluorobenzene. Birch chemistry on benzene has been previously realized only by solvated electrons or electrochemistry. The function of this model system uncovered in these mechanistic explorations suggests modes of operation for this photocatalyst class which will enable future optimizations.

---

[2] *Author contributions. A.R.G., N.F.P and A.S. contributed equally. A.R.G, N.F.P., A.S., N.H.D and G.M.M. conceived the idea. A.R.G. executed the catalyst design, synthesis, and reaction development. A.R.G performed experiments relating to degradation of the catalyst. N.F.P and A.S. contributed to all the electrochemistry and spectroscopic investigations. M.V.P. and R.S.P. performed DFT calculations. A.R.G, N.F.P., A.S., N.H.D., and G.M.M co-wrote the manuscript. All authors read and edited the manuscript.*

INTRODUCTION

Using visible light to activate small molecules through redox processes is a growing strategy for synthetic chemists.[1-6] For processes driven by absorption of a single photon in a photocatalyst (PC), an absolute potential of > 3V is in principle achievable considering that 400 nm photons in the blue edge of the visible spectrum carry 3.1 eV of energy. However, additional electrochemical and photochemical considerations significantly limit what potentials can be deployed. For example, from the perspective of PCs that drive reductive transformations, one must also consider the PC oxidation potential as well as loss of energy prior to a successful electron transfer to a target substrate, due to non-radiative intra-PC phenomena. In practice, reductive transformations requiring more than ~ -2 V cannot be carried out without harvesting the combined energies of more than one photon. Following the work of Ghosh *et al.*, where aryl halides including aryl chlorides could be activated using perylene diimide (PDI) and 440 nm blue light,[7] several organic and metal-based photocatalytic systems have been developed that rely on consecutive photoinduced electron transfer events (ConPET).[8] In such systems, an initial photo-induced redox event modifies the PC which then absorbs a second photon to produce a highly redox-potent excited state. This general scheme has been invoked in describing the function of highly reducing organic photocatalytic dyes,[9, 10] with implantation in synthetic transformations such as dehalogenations,[7, 11, 12] detosylations,[13] and Birch reductions.[14, 15]

Several of the organic photosensitizers developed to utilize ConPET (xanthones,[16] dicyanoanthracenes,[17] napthalene and perylene imides[18]) are proposed to operate out of an open shell PC intermediate which allows for a single electron transfer (SET) from the excited doublet to the substrate. However, PCs that operate from an open shell state are air sensitive and often demonstrate short excited-state lifetimes[10, 18, 19] that can limit diffusional bimolecular electron

transfer yields, thereby impacting their synthetic utility.[10] On the other hand, the open-shell radical anionic states of the PCs can in principle be further reduced to generate closed shell species (for example, of polyaromatic imide photocatalysts[20, 21]) that are more stable with much longer excited state lifetimes. These may also be able to act as potent photo reductants. For example, as illustrated by Rieth *et al.*, the doublet excited state of naphthalene monoimide radical anion ($NMI^{\cdot -}$) only lives for 24 ps whereas the closed shell Meisenheimer-like $[NMI(H)]^-$ complex that is electrochemically produced and represents the further addition of an electron and a proton, shows ~ three orders of magnitude longer fluorescence lifetime of 20 ns while at the same time having a comparable excited state reduction potential (≈–3.1 V vs Fc^+/Fc).[20] Importantly, $[NMI(H)]^-$ was shown to act as a reductant with methyl-4-chlorobenzoate under 440 nm irradiation. The reactivity of this system is suggestive that a closed shell reductant is operative.

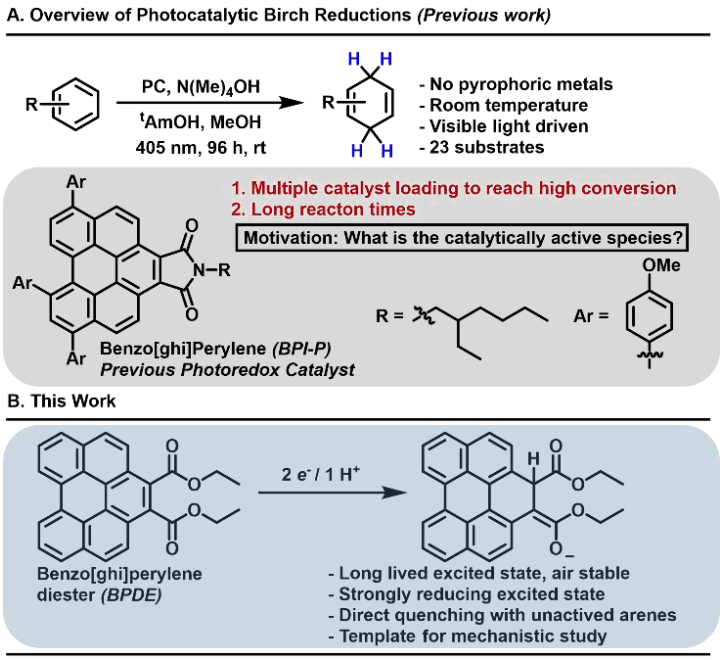

Figure 3.1. A) Previous scheme for visible light driven Birch reduction using BPI photocatalysts and their identified limitations. B) Activation pathway using newly developed BPDE.

Discovered by Cole et al. in 2020, the Benzo[ghi]perylene imide (BPI) photocatalyst family exhibits potency for Birch reduction of unactivated arenes,[14] which traditionally requires the use of pyrophoric metals (Na, Li) and liquid ammonia.[22, 23] However, long reactions times and the need for multiple catalyst loadings limit practical application of the photo-Birch system in synthesis (Figure 3.1A). Rational catalyst design with improved reactivity would require a priori knowledge of major photodegradation pathways, along with mechanistic understanding of the photoactive redox state of the PC, as demonstrated in PDI and cyano-arene based organic PCs.[24, 25] In this current work we show that the major degradation of BPI catalysts involves the hydrolysis of the imide ring, motivating synthesis of a new PC (Benzo[ghi]perylene diester or **BPDE**) that bypasses imide hydrolysis and provides a structurally simpler platform through its symmetry for spectroscopic interrogation. Through the use of cyclic voltammetry, spectroelectrochemistry, absorption spectroscopy, and fluorimetry, we probe both the singly and doubly reduced states of **BPDE** and identify the relevant highly reducing photoactive redox state. Although the yield of photo-Birch via **BPDE** is low, its use as a model for this mechanistic exploration uncovers a critical mode of operation for this class of photocatalysts which will enable future optimizations.

RESULTS AND DISCUSSION

Challenges emerge improving original PC design, even after introducing enhanced solubility: As noted above, major limitations for practical application of BPI derivatives in photo-Birch stem from long reaction times and requirements for multiple catalyst loadings.[14] We initially hypothesized that long reaction times were due to poor solubility of BPI-P (structure in Figure 3.2A) in methanol resulting in a predominately heterogenous system. Since benzyl alcohol substituents are known to solubilize metalloporphyrin complexes in water or alcoholic solvent,[26] a derivative was synthesized using 4-benzyl alcohol as the core extension substituent (BPI-M,

Figure 3.2A), and this PC proved to be methanol soluble. Notably, the thermodynamic and photophysical properties are not significantly perturbed (Table S3.5, Fig. S3.14). Using the same reaction conditions as those previously reported, the conversion of benzene to cyclohexadiene was monitored to benchmark performance. However, even with a completely homogeneous system, this PC did not show better performance. In 48 hours, BPI-M drives 30% conversion of benzene to cyclohexadiene, 5% lower than what was observed using BPI-P (Table S3.2).

Observations of underlying hydroxide-induced structural changes to BPI. Although the overall photo-Birch reaction time and yield were not improved, the enhanced solubility of BPI-M enabled in-situ spectroscopic monitoring under relevant reaction conditions. First, we probed the interaction of BPI-M with tetramethylammonium hydroxide (TMAOH) under the hypothesis that hydroxide could lead to degradation of the catalyst. Upon addition of TMAOH to a solution of BPI-M in methanol, the charge transfer (CT) transition[27] centered at 500 nm in the UV-Vis spectrum is lost with a concomitant appearance of a new band centered at 408 nm (Figure 3.2C). The observed change demonstrates a thermal reaction with OH– resulting in a new species, denoted [BPI-M-OH]−. This solution was then irradiated with 405 nm light, wherein the broad 408 nm absorption band is rapidly lost, and a spectrum emerges that is characterized by two well-resolved features centered at 374 and 392 nm (Figure 3.2C). Notably, this change persists, and we do not observe the reformation of [BPI-M-OH]− nor BPI-M after monitoring the solution for 24 hours, suggesting that the catalyst has undergone a light-driven structural change.

Parallel to the UV-Vis absorption measurements, the associated structural changes of BPI-M with TMAOH were tracked in-situ using ^{13}C NMR and high-resolution mass spectrometry (HRMS). The ^{13}C NMR spectrum collected for BPI-M shows a single resonance at 170 ppm assigned to the imide carbonyl carbon and indicating that core-substitutional asymmetry in this

molecule is sufficiently remote from this site to obviate detection of two different ^{13}C resonances. Analysis of the product associated with $[BPI\text{-}M\text{-}OH]^-$, on the other hand, reveals the emergence of a new signal at 178 ppm. The significance of this resonance within a region associated with carbonyl ^{13}C sites, argues against an intact imide ring after nucleophilic addition of OH^- since this would result in the formation of a sp3 hybridized carbon center (Figure 3.2B). Instead, this signal suggests a chemical inequivalence for a pair of carbonyl sites. We posit this chemical inequivalence is due to imide ring-opening in the presence of OH^-, resulting in carboxylate and amide functionalities. Imide hydrolysis in the presence of OH^- has been previously reported.28 Additionally, it is noted that a breaking of the imide ring would explain loss of the lowest energy CT band. An aliquot of the crude mixture (BPI-M + TMAOH) was ana-lyzed using HRMS and a signal is observed that matches the predicted mass of the protonated ring opened species: BPI-Ring Opened (BPI-RO) (Figure 3.2B). We attempted to isolate BPI-RO to explore whether it is active on its own in photo-Birch. However, this compound proved sensitive to ring-closure during isolation of this transient species. In reaction conditions we found that through an acid workup (with slowly added 0.1M HCl), the crude mixture containing BPI-RO is driven to a benzo[ghi]perylene anhydride (BPA, Figure 3.2B). The BPA com-pound exhibits some properties akin to BPI-M including a CT-like transition and a single carbonyl signature (164 ppm in $CDCl_3$) in the ^{13}C NMR spectrum. As a photocatalyst, however, BPA is less effective than the parent (20% conversion of benzene to cyclohexadiene monitored via 1H NMR in 24 hours as compared to 30% using BPI-M).

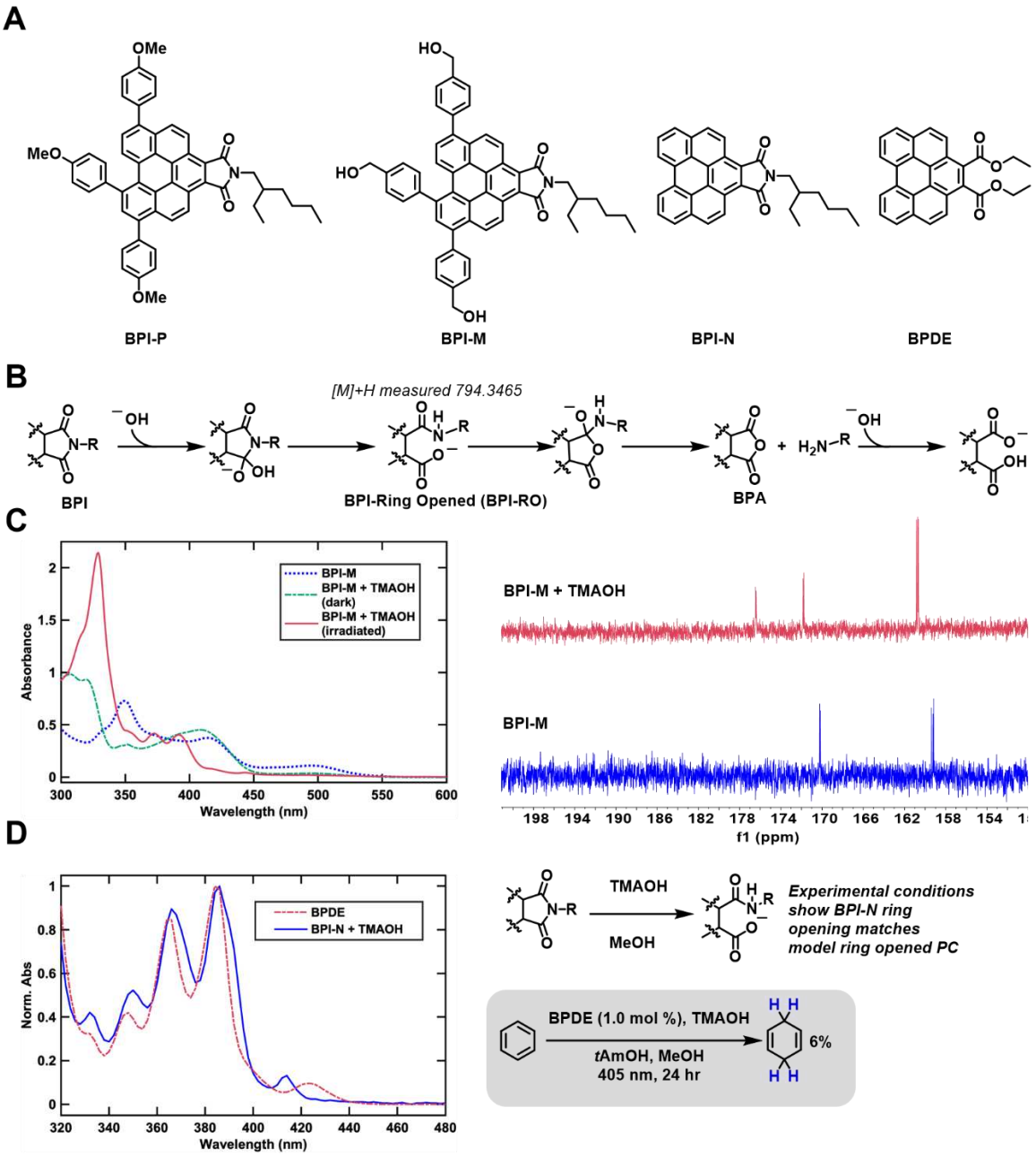

Figure 3.2. A) Photocatalysts used in mechanistic study. B) Proposed mechanism for thermal degradation of BPI-M via hydroxide. C) Absorbance and ^{13}C NMR spectra monitoring the changes associated with BPI-M interacting with TMAOH in methanol. D) Absorbance spectra highlighting the similarities between the newly synthesized (BPDE) and BPI-N in the presence of TMAOH. BPDE can act as model ring opened catalyst comparable to the thermally ring-opened BPI-N structure.

Motivation for a ring-opened model system: Due to the poorer reactivity of BPA in photo-Birch reduction of benzene, we hypothesized that the BPI-RO is relevant to reactivity. However, because BPI-RO is challenging to isolate, a model photo-catalyst was sought that is representative of the ring-opened species but stable against anhydride formation. Recognizing that a benzo[ghi]perylene diester would represent one of the simplest proxies for BPI-RO, we synthesized BPDE (Figure 3.2A) using a one-pot Diels-Alder cycloaddition between perylene and diethyl acetylenedicarboxylate. Notably, the UV-Vis absorption spectrum is similar to that seen for the non-core extended BPI-N (Figure 3.2A) after exposure to hydroxide (Figure 3.2D). Spectral features of BPDE are highlighted by the relatively weak α-band (Clar's notation[29]) at ~ 425 nm which acts as the lowest electronic excited state (S1) whereas the more prominent p-band (S2) is vibronically resolved with the 0-0 transition centered at 385 nm. The new BPDE functions as a photocatalyst in the reduction of benzene to cyclohexadiene (6% conversion). This efficacy is comparable to that of BPI N, which exhibits 3% conversion as reported previously.[14] BPDE also exhibits reactivity in hydrodehalogenation of fluorobenzene and chlorobenzene in which benzene formation was monitored via NMR, albeit in low NMR yields (19% on fluorobenzene, 25% on chlorobenzene) (Fig. S3.1). We note that in terms of performance, BPDE is inferior to the higher performing BPI-P. However, the observed photoinduced substrate re-duction reactivity suggests that BPDE can indeed be used as a model ring-opened compound for further mechanistic understanding and can act as a template for future modification. Understanding how the aryl substitutions onto the benzo[ghi]perylene core affects PC performance is currently being studied.

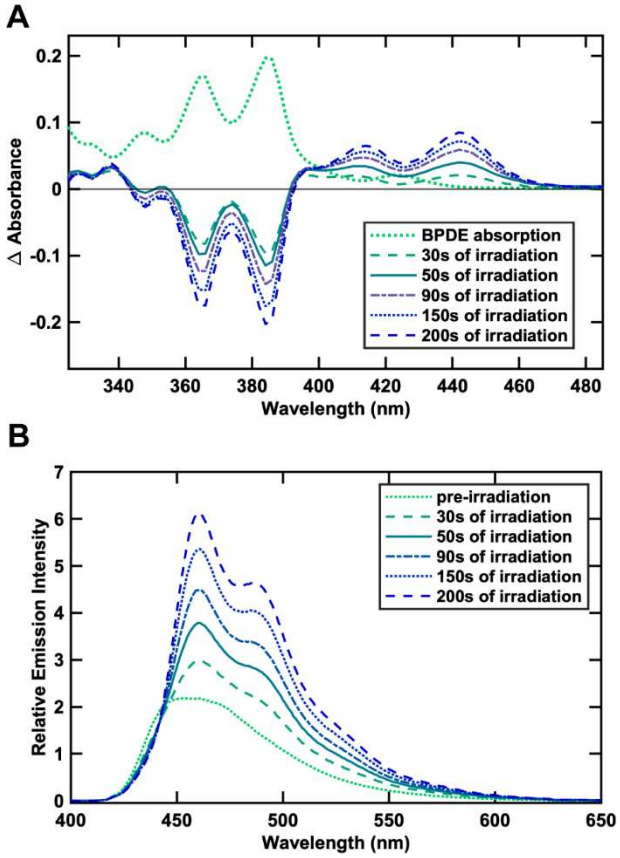

Figure 3.3. Changes in the absorption (A) and emission (B) spectrum of 35 μM BPDE under irradiation in presence of 180 mM TMAOH in a 2:1 THF:MeOH solvent system. The emission spectra were collected by exciting the sample at 420 nm.

Photochemical investigation of BPDE reveals a new species whose fluorescence is quenched by benzene: The generality of function as a photocatalyst in both Birch and hydrodehalogenation, combined with the simplicity and symmetry of the compound, motivated us to explore how this model PC functions during photocatalysis. We began by monitoring BPDE reactivity with excess TMAOH (~5000 equiv.) in the dark via UV-Visible spectroscopy in a THF/MeOH (2:1) solvent system. THF was used as a co-solvent because BPDE is insoluble in pure MeOH. As shown in Fig. S3.19, the absorption spectrum of BPDE remains the same upon introduction of OH- other than the expected dilution effect due to the added MeOH. Next, we sought to explore if photoexcited BPDE would react with TMAOH. This reaction was performed

by irradiating BPDE in presence of 180 mM TMAOH (~ 5000 equiv.) inside a photoreactor fitted with two 385nm LEDs. As shown in Figure 3.3A, the vibronic absorption peaks of parent benzo[ghi]perylene core diminish over minutes, concomitant with the appearance of two new peaks at 425 and 445 nm that resemble a new red-shifted vibronic progression. Observation of an isosbestic point at 390 nm suggests a 1-to-1 conversion from BPDE to another species. During this absorption spectrum sequence, photoluminescence spectra were also collected after each period of irradiation. As can be seen in Figure 3B, a bright vibronically resolved spectrum emerges that is distinct from the broad and featureless fluorescence spectrum of BPDE. A quantum yield determination after 200s of irradiation indicates Φ_{em}=0.94 for the new species (Fig. S3.22). It also has a fluorescence lifetime of ~7 ns that is shorter compared to that of BPDE (τ_{em}=16.2 ns). At the same time, the newly formed species was found to be tolerant to air exposure even after 24-hours which, along with a very high emission quantum yield and multi-nanoseconds lifetime, suggests that it is not an open shelled radical anion. In a preliminary consideration of the role played by this new species within catalysis, photoluminescence spectra were measured in the presence of substrate. Selective photoexcitation for the new species at 450 nm was required because these samples still maintain unreacted BPDE. Interestingly, the fluorescence intensity of the new species is found to be diminished after addition of benzene (Fig. S3.23). For example, in the presence of 0.30 M benzene, the 0, 0 peak height drops by 11%. This is, to our knowledge, evidence for the first example of excited state reactivity of an organic photoreductant observed in the presence of an arene as inert as benzene. More detailed explorations of quenching properties are explored later in this work after identification of the emitting chromophore and establishment of protocols to more cleanly produce it for more systematic explorations.

Electrochemical and spectroelectrochemical interrogation of BPDE; connecting redox events to photochemical product: Cole et al previously demonstrated that OH^- was critical for BPI-P driven photo-Birch reactivity. To understand the role of hydroxide in our system as an electron donor, we were motivated by the work reported by Saha et al. who showed that electron rich anions are capable of reducing π-acids in their ground state or upon photoexcitation.[30,31] In order to investigate the reduced states of BPDE, we turned to electrochemistry, replacing the chemical reductant with an electrode. Cyclic voltammetry studies of BPDE are shown in Figure 3.4A. In experiments that sweep with a negative potential limit of –2.5 V vs Fc^+/Fc, a first redox event occurs in THF that is reversible with a half-wave potential of –2.22 V vs Fc^+/Fc. This potential corresponds to BPDE + $e^- \rightleftharpoons BPDE^{\bullet-}$. When scanning into more negative potentials, a second redox event is observed with a half-wave potential of –2.61 V vs Fc^+/Fc that corresponds to dianion formation $BPDE^{\bullet-} + e^- \rightleftharpoons BPDE^{2-}$. However, this redox event displays an apparent diminished return current (anodic peak) of the first reduction (see Figure 4A), and likely second reduction, and is accompanied by the appearance of a new anodic-current feature seen at approximately –1.00 V vs Fc^+/Fc. These observations together suggest that a chemical product formed at negative potentials capable of dianion formation (more negative than –2.62 V vs Fc^+/Fc) then requires a substantively positive potential (more positive than ~ –1 V vs Fc^+/Fc) to return BPDE. The reversibility of this wave exhibits scan-rate dependence: after increasing the scan rate from 0.1 V/s to 0.4 V/s the new feature exhibits partial reversibility (cathodic current) and an approximate $E_{1/2}$ = –1.1 V vs Fc^+/Fc (Fig. S3.10).

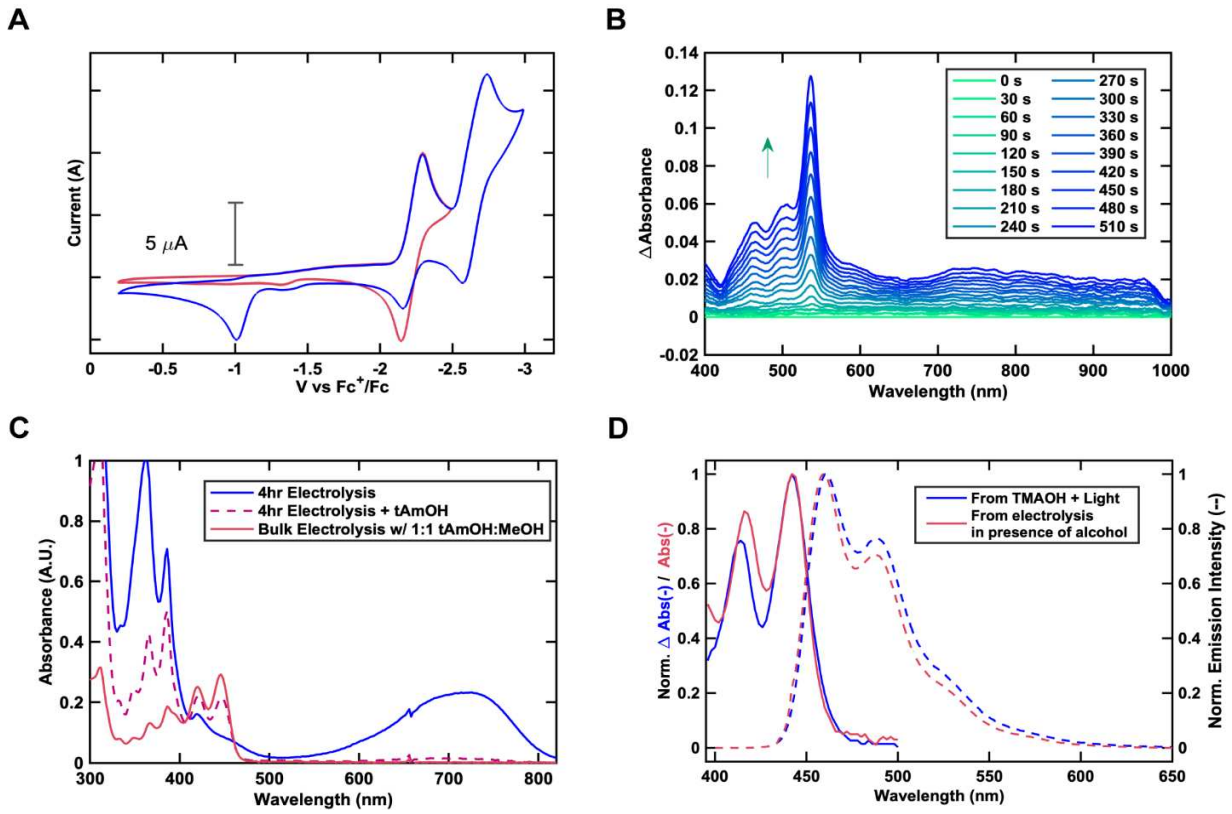

Figure 3.4. (A) Cyclic voltammogram of 1.0 mM BPDE in 0.1 M $TBAPF_6$ THF solution, scanning at 100 mV s^{-1} from 0 to –2.5 V (pink trace) and 0 to –3.0 V (blue trace) vs Fc^+/Fc using a Pt disk working electrode, Pt wire counter electrode, and leak-free Ag/$AgNO_3$ reference electrode. (B) Spectroelectrochemical study of BPDE in 0.1 M $TBAPF_6$ THF solution with the Pt mesh working electrode held just past the $1e^-$ reducing potential at –2.4 V vs Fc^+/Fc. (C) Absorbance spectrum of BPDE after 4 hours of bulk electrolysis at -2.85 V vs Fc^+/Fc in THF (blue), bulk electrolyzed solution following addition of tAmOH (dashed pink), and the solution after continued bulk electrolysis at –2.85V vs Fc^+/Fc in a 2:0.5:0.5 THF:MeOH:tAmOH solvent system (red). (D) Comparing the absorption and emission spectra of the electrochemically formed $[BP\text{-}H]^-$ species to that formed by the reaction of BPDE, irradiation 405 nm for 200 s, and TMAOH.

Spectral characterization of the one-electron reduction product **BPDE**$^{\bullet-}$ via spectroelectrochemistry is presented in Figure 3.4B. In THF, a progression of peaks is observed at 463 nm, 504 nm, and 537 nm, as well as a broad and featureless absorption extending well past the 1000 nm detection limit of the spectrometer. The intense peak at 537 nm is consistent with the reported absorption spectrum of benzo[ghi]perylene radical anion.[32] Notably these features do not match with the emergent vibronic progression observed for **BPDE** under irradiation in presence

of TMAOH (Figure 3.3A). We attempted to generate **BPDE**$^{\bullet-}$ within THF via bulk electrolysis in order to analyze its excited state lifetime by transient absorption. However, after removal of the electrode, the radical anion was unstable even under a strictly inert atmosphere and without any substrate present, as observed through UV-Vis changes on a minute time scale, and this made transient absorption characterization difficult. As a surrogate, bulk electrolysis was performed to generate the radical anion of the parent catalyst, i.e., **BPI-P**$^{\bullet-}$, which was more stable (generated in DMAc at –2 V vs Fc^+/Fc). TA experiments indicate that **BPI-P**$^{\bullet-}$ has a lifetime of ~10ps. (Fig. S3.17). Such a short-lived excited state is expected to preclude the radical anion from engaging in excited state reactivity via diffusion limited bimolecular collisions. From these observations, and the UV-Vis absorption dissimilarity with irradiated **BPDE** in the presence of TMAOH (Figure 3.3A), it is unlikely that the radical anion is operative in the reduction of substrates as a major pathway in the photo-Birch mechanism. Similar challenges to directly using an organic radical anion to drive photoinduced electron transfer reactions with solution phase substrates have recently been noted by others as well in their consideration of both monoimide[20] and diimide[21] species. Hence, we move our investigation onto the doubly reduced **BPDE**$^{2-}$ and its relationship to the new oxidative feature found in cyclic voltammetry.

Spectral characterization after the second reductive wave using spectroelectrochemistry encounters some complexity due to kinetic considerations involving the interconversion of species during the measurement, for example **BPDE**$^{\bullet-}$ to **BPDE**$^{2-}$. As such, we engaged in longer bulk electrolysis experiments to drive more product formation in an H-Cell. A sequence of three related experiments is shown in Figure 3.4C. *First*, a concentrated solution of **BPDE** in THF (with 0.1 M $TBAPF_6$) was electrolyzed at –2.85 V vs Fc^+/Fc for four hours. The UV-Vis absorption spectrum of an aliquot taken from the H-cell is shown in the blue trace and indicates the emergence of new

absorption features including a broad band at ~ 710 nm and an intense peak at 360 nm which are assigned to **BPDE**$^{2-}$. We suspect that the sharp shoulder at 386 nm is due to **BPDE** suggesting that bulk electrolysis is not complete. However, there is no evidence for **BPDE**$^{\cdot-}$ given the absence of a peak at 537 nm. *Second*, we then considered spectral changes upon addition of an alcohol to the aliquot taken from the H-cell, guided by the fact that the reaction conditions rely on inclusion of tert-amyl alcohol (tAmOH) or MeOH environments. As can be seen in the dashed purple trace of Figure 4C, addition of 200 μL tAmOH (see Fig. S3.11 for a similar experiment using MeOH) leads to loss of the prominent ~ 710 nm and 360 nm features. A vibronic progression peaked at 386 nm becomes evident as the 360 nm band is lost and this corresponds to the starting **BPDE** that had not been electrolyzed (vide supra). Importantly, we also observe the emergence of a pair of peaks at 420 and 446 nm suggestive of a second vibronic progression. These are effectively coincident with the peaks observed when **BPDE** is irradiated in the presence of TMAOH in a THF/MeOH mixture (Figure 3.3A). *Third*, returning to the H-cell, 1.00 mL of 1:1 tAmOH:MeOH was added and electrolysis was continued for one hour at –2.85 V vs Fc^{+}/Fc. As shown in the red trace of Figure 3.4C, the system appears to drive closer to completion of the product characterized by the vibronic progression peaked at 446 nm. A small amount of **BPDE** remains evident, as inferred, for example, by the structured peak shape of the 0-2 vibronic transition. The absorption spectrum from this experiment is shown in Figure 3.4D superposed with the difference absorption data from Figure 3.3A after **BPDE** was irradiated for 200 s in the presence of TMAOH in a THF/MeOH mixture. The spectral similarity highlights that the same product is emerging in both electrochemical and photolysis experiments, supporting the idea that hydroxide can act as a sacrificial electron donor to **BPDE**. Figure 3.4D also shows close correspondence between emission spectra collected following excitation at 450 nm for both samples.

*Two electron, one proton activation of **BPDE** forms a catalytically active species **[BP-H]⁻**:* Taken as a whole, the electrochemical observations suggest that in THF, in the absence of a proton source, the primary electrolysis (–2.85 V vs Fc^+/Fc) product is **$BPDE^{2-}$**. When protons are available (e.g. tAmOH or MeOH), either upon addition of protic solvent to a mixture of **$BPDE^{2-}$** and **BPDE** (second experiment above), or during active electrolysis that is producing **$BPDE^{2-}$** from **BPDE** in the presence of a protic solvent (third experiment above), a stable product is formed whose absorption spectral features match the photochemical product generated when **BPDE** is irradiated in the presence of TMAOH in a THF/MeOH mixture (Figure 3.3A). Without TMAOH, BPDE upon irradiation shows no changes, as monitored by UV-Vis, suggesting that TMAOH is needed to generate ***[BP-H]⁻*** (Figure S3.19B). To understand the CV data of Figure 3.4A in this context, we posit that at large negative potentials – beyond the $E_{1/2}$ = -2.61 V vs Fc^+/Fc needed to generate **$BPDE^{2-}$** – the same product is formed with an amount limited by the availability of protons and the scan rate competing with the rate of product formation. Although the CV experiment was run in THF, some proton availability is possible through the presence of tetrabutylammonium, a source of protons through Hofmann elimination.[33] Since the new species is formed in the presence of protons following the generation of the **$BPDE^{2-}$**, we hypothesize that the catalytically active species under photo-Birch conditions is a two electron, one proton activated closed shell reductant **[BP-H]⁻**. Similar hydride complexes can be seen in a napthalene monoimide species which was recently reported by Rieth *et al.*[20]

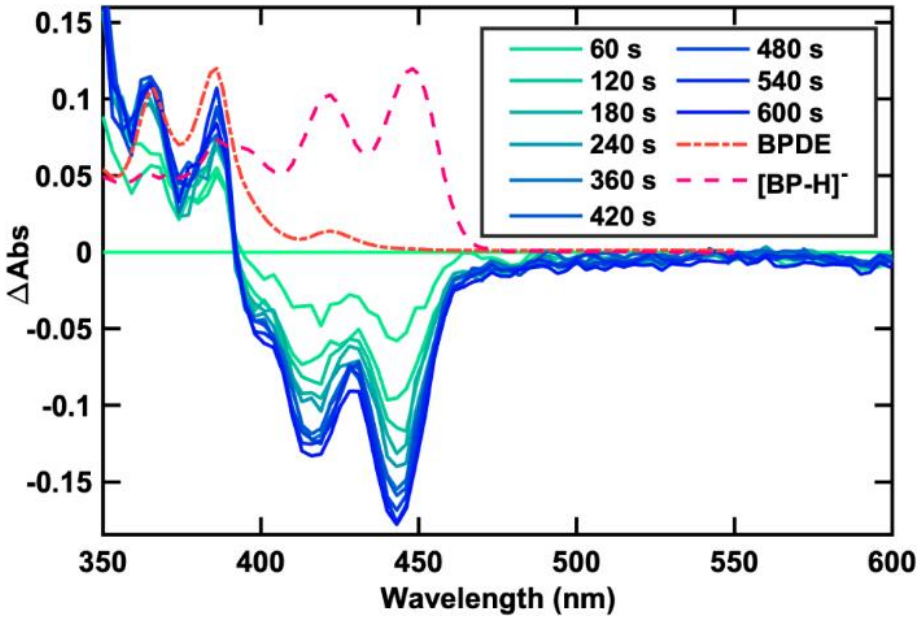

Figure 3.5. Spectroelectrochemistry of [BP-H]⁻, shown as a delta absorbance, highlighting spectral changes in the vibronic progression when held at potential at –0.4 V vs Fc^+/Fc. The applied potential oxidizes [BP-H]⁻ seen from the gradual decrease in the 420-450 nm vibronic progression. However, a simultaneous growth of a blue shifted vibronic progression that matches the absorption of BPDE indicated that upon oxidation [BP-H]⁻ undergoes structural changes to reform benzoperylene. The ground state BPDE and [BP-H]⁻ absorbance spectra are included for comparison.

The anodic current wave that emerges at –1.00 V vs Fc^+/Fc thus appears to involve oxidation of **[BP-H]⁻**. To explore this further, changes to the electrochemically generated **[BP-H]⁻** were monitored via spectroelectrochemistry in THF after shifting the transparent working electrode potential to –0.4 V vs Fc^+/Fc. As seen in Figure 3.5, the vibronic features associated with **[BP-H]⁻** (420nm and 450nm) decrease in intensity, while features associated with ground state **BPDE** reappear. There is no spectral evidence of any other intermediates within 300-1000nm spectral window during the conversion. This observation leads us to the conclusion that at potentials appropriate for oxidation, **[BP-H]⁻** undergoes structural rearrangements needed to re-aromatize back to **BPDE**. The observation is consistent with one-electron oxidation of **[BP-H]⁻** followed by spontaneous loss of a second electron and a proton at this potential. This in turn is consistent with

the expected ~ 2 V driving force for oxidation of **BPDE**$^{\cdot-}$ given that the **BPDE**/**BPDE**$^{\cdot-}$ couple is at -2.22 V vs Fc^{+}/Fc V (Figure 4A). A similar observation using electrochemistry was made in the case of $[NMI(H)]^{-}$ as well.[20]

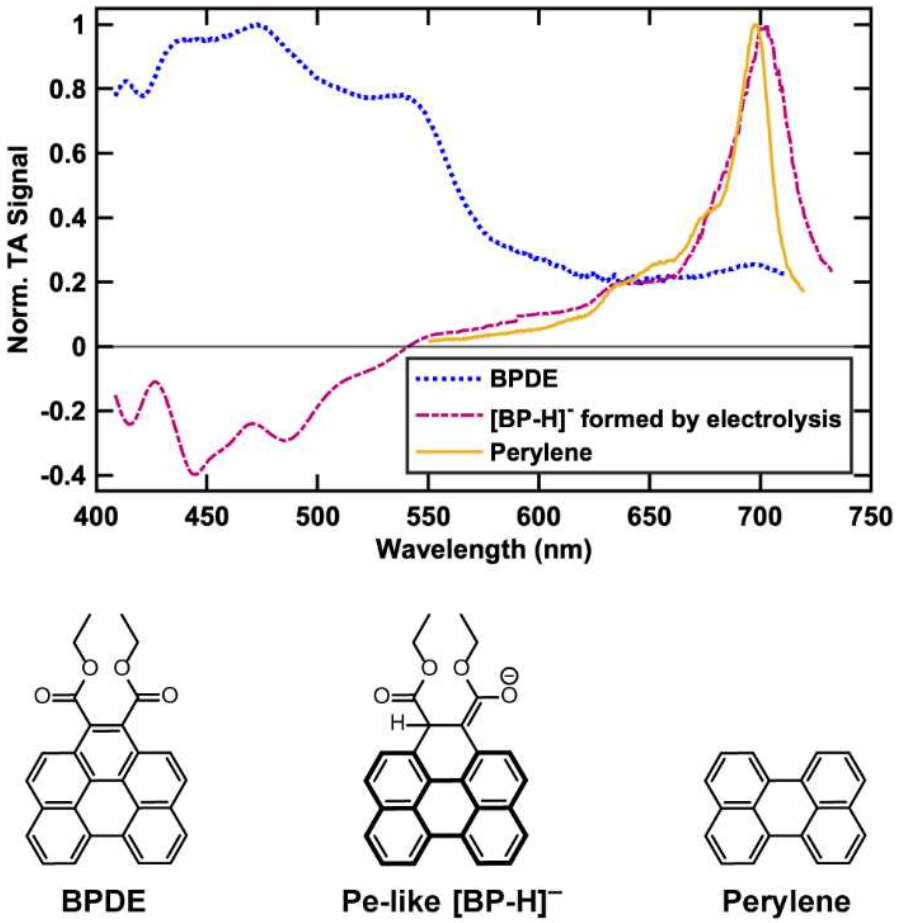

Figure 3.6. Comparison of TA spectra obtained for BPDE with that of the [BP-H]− species formed by bulk electrolysis. All the spectra were collected by exciting the sample at 398 nm and taking a spectral slice 100 ps after the pump excitation. Since the [BP-H]− species is electrochemically generated, there is a small amount of BPDE present in the solution. However, given the stark difference in their spectra profiles we estimate the contribution from BPDE to be very minimal. The excited state absorption (ESA) of pure perylene (Pe) in EtOH is plotted for comparison. The Pe like polyaromatic core of [BP-H]– is high-lighted for clarification.

*Computational and spectral indications for the formation of perylene-like **[BP-H]⁻**:* We turn to the question of the likely structure of **[BP-H]⁻**, envisioning the gain of two electrons and one proton as effectively a hydride transfer to **BPDE** in order to propose a possible set of isomers. These structures are shown in Fig. S3.51, although a single chromophore is expected on the basis of the single photoluminescence decay constant (~7 ns) observed for **[BP-H]⁻** in both the electrolysis (Fig. S3.25) and photolysis experiments (Fig. S3.21) in the presence of a proton source (vide supra). Our intuition at the outset was that a perylene-like structure (isomer *AA* in Fig. S3.51) was most likely to form, generated from a dianion where the negative charges lie towards the ester head, followed by protonation then tautomerization (see scheme of anticipated events in Fig. S3.13). An extensive thermochemical computational exploration that is also summarized within Fig. S3.51 (see S.I. for further details) supports a perylene structure with the energy of *AA* being the lowest of these isomers by a substantial amount in most cases and 7.8 kcal/mol for the closest isomer (*G*) which is represented by hydride transfer to a benzoperylene bay position. Furthermore, our calculations reveal a one-electron redox potential of -1.27 ± 0.29 V vs Fc^+/Fc for the *AA* isomer (Fig. S3.49). This value aligns well with the partially reversible wave at -1.10 V Fc^+/Fc for the cathodic current observed in the CV measurements (Fig. S3.10). It is noted that the polyaromatic hydrocarbon (PAH) core of isomer *AA* resembles perylene (Pe), to be contrasted with other PAH forms including benzo[e]pyrene, pyrene, phenanthrene, oxidized olympicene, and others. All photophysical data that we have collected is in support of a closed-shell Pe-like species. For example, the absorption spectrum of **[BP-H]⁻** is red-shifted into the visible region with the 0-0 peak of the vibronic progression at 442 nm, only 8 nm relative to pure Pe in EtOH where the peak is at 434 nm (Fig. S3.24). The emission spectrum of **[BP-H]⁻** is also similar to Pe, although the Stokes shift for **[BP-H]⁻** at 17 nm is larger than its PAH parent (4 nm, Fig. S3.24) suggesting more

reorganization within the **[BP-H]**$^-$ singlet excited state prior to emission, perhaps as a result of inclusion of partial charge-transfer character involving the enolate substituent. The high emission quantum yield of **[BP-H]**$^-$ is consistent with Pe. Finally, we were able to interrogate the transient absorption characteristics of **[BP-H]**$^-$. As shown in Figure 3.6, it exhibits an intense excited-state absorption at ~700 nm with a bluer shoulder at 635 nm. These same qualities are also characteristic of Pe.

Stern-Volmer like fluorescence quenching using electrochemically generated **[BP-H]**$^-$ and its unusual dependence on hydroxide concentration: Having identified the most likely structure of **[BP-H]**$^-$, we return to explorations of photoluminescence as a function of added substrate, recalling our earlier observation that emission intensity is diminished in the presence of benzene. As was noted, those preliminary studies involved chromophores generated non-quantitatively under photolysis conditions in the presence of excess TMAOH. Here, we rely on the bulk electrolysis procedures developed above to produce **[BP-H]**$^-$ more cleanly, without inclusion of hydroxide, for systematic interrogation. **BPDE** was electrolyzed in a THF/tAmOH/MeOH mixed solvent system using 0.1 M $TBAPF_6$ as supporting electrolyte to form **[BP-H]**$^-$; subsequently, a small amount of this solution was diluted with 2:1 THF/MeOH to prepare samples. Substrate was then added in varying amounts (i.e., [Q]) and the integrated emission intensity (F) relative to the case where [Q] = 0 (i.e., F_0) is used to obtain the Stern-Volmer quenching constant K_{SV} (Eq S3.1).

We first considered the Pe-like emission intensity of **[BP-H]**$^-$ as a function of benzene concentration in the absence of hydroxide. In these experiments, emission intensity quenching is minimal (see black circles of Figure 3.7A in Stern-Volmer plots). Additionally, we do not observe a meaningful decrease in the emission intensity with the addition of more easily reducible substrate 4-fluorobenzonitrile (Fig. S3.30B). This led us to consider the role of hydroxide since it is present

in excess when **[BP-H]**$^{-}$ is produced under photolysis conditions. Benzene was chosen as the quencher for these studies as it is considered to be very inert and difficult to reduce. Interestingly, the Stern-Volmer constant (K_{SV}) dramatically rises from 0.06 M^{-1} to 0.37 M^{-1} (a 517% enhancement) as the concentration of TMAOH is increased from 0 to 185 mM (Figure 3.7A). It is noted that with additional increases in concentration from here, the changes to K_{SV} appear muted. At 320 mM added TMAOH, K_{SV} = 0.42 M^{-1}, representing only a 13% increase. The potential relevance of the tetramethylammonium cation, as opposed to the hydroxide, is ruled out in studies using added TMACl, where minimal quenching is observed (see Fig. S3.33 for details).

Having identified the relevance of OH^{-}, we next considered emission quenching with different substrates, keeping the concentration of TMAOH constant at 300 mM. As shown in Figure 7B, K_{SV} varies substantially. The smallest value of 0.39 M^{-1} (consistent with Figure 3.7A) is achieved for benzene and this increases to 0.52 M^{-1} for fluorobenzene, to 1.55 M^{-1} for 4-fluorobenzonitrile, and to 3.95 M^{-1} for methyl 4-fluorobenzoate. This quenching constant increase correlates with reduction potential: the more easily reduced substrates 4-fluorobenzonitrile (E_{red} = -2.38 V vs SCE[34]) and methyl 4-fluorobenzoate (E_{red} = -2.28 V vs SCE[35]) quench the **[BP-H]**$^{-}$ emission more efficiently, while the less easily reduced substrates fluorobenzene (E_{red} = -2.97 V vs SCE[36]) and ultimately benzene (E_{red} = -3.48 V vs SCE[37]) are successively less efficient. This correlation with substrate reduction potential is evidence that the mode of quenching is electron transfer initiated by photoexcited **[BP-H]**$^{-}$, in line with our expectations given final Birch reduction and dehalogenation products for this model catalyst.

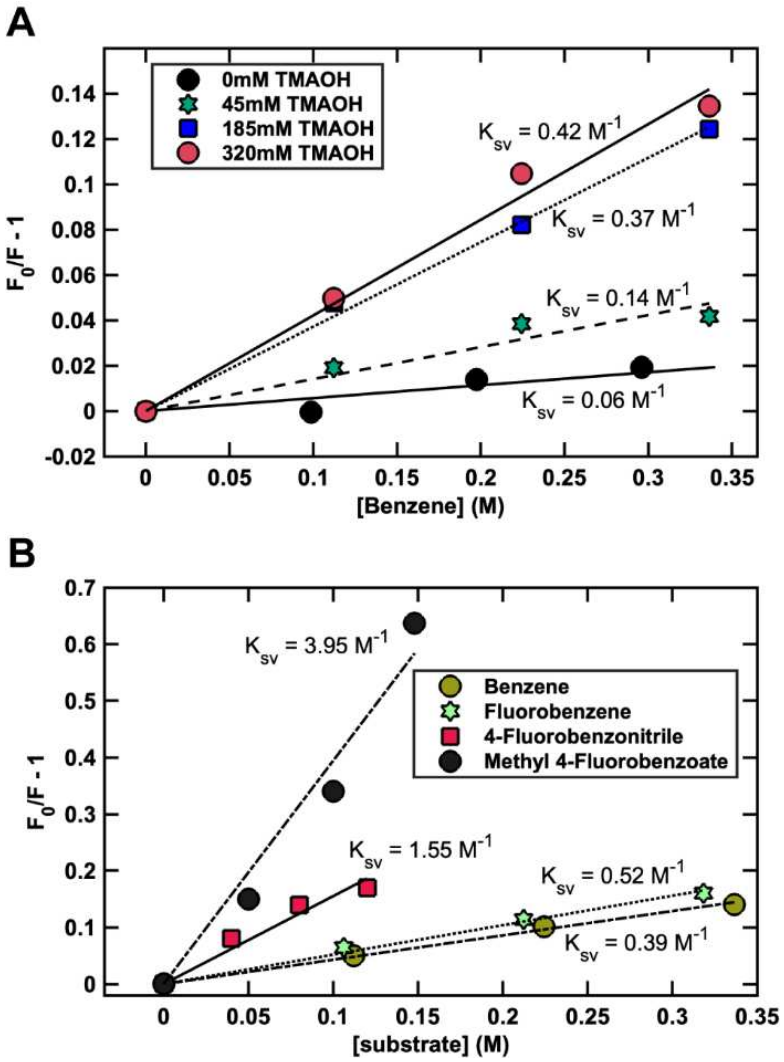

Figure 3.7. (A) Effect of TMAOH concentration in determining the Stern-Volmer rate constant with benzene as the quencher. (B) Stern-Volmer quenching rates for four different substrates with varying reduction potentials in presence of 300 mM TMAOH. Both experiments were done with the electrochemically generated [BP-H]⁻ species in a 2:1 THF:MeOH solvent system.

Electron transfer from photoexcited [BP-H]⁻ to inert arenes requires a proton coordinate:

While quenching efficiency correlates with reduction potential, the functional relationship is not yet identified. There are several complications to elucidating this relationship. For example, with benzene the reaction product from quenching is expected to be the benzene radical anion whereas for the fluorinated substrates, oxidative quenching of photoexcited **[BP-H]⁻** is anticipated to then couple with bond-dissociation, leading to an aryl radical and fluoride. The reorganization energy

associated with either dissociative electron transfer for aryl fluorides or loss of aromaticity for substrates such as benzene are both expected to be large with significant impacts on the rate constant for quenching. However, the details will be case specific making comparisons difficult. Interestingly, throughout Stern-Volmer studies used to quantify the quenching process, we see no evidence for significant life-time variation (Fig. S3.34) as a function of quencher concentration among any of the tested substrates which span 1.2 eV of driving force for photoinduced ET. These experiments indicate that quenching is induced by a pre-association between the closed-shell species **[BP-H]**$^-$ and the substrate. Such pre-association controlled by binding equilibria would complicate the identification of the functional form for KSV's driving force dependence.

The balance of observations uncovers an unusual confluence of factors that enable **[BP-H]**$^-$ – or related species in this catalyst class – to act as excited-state super-reductants. Due to the outcome of Birch chemistry, one such case being benzene to cyclohexadiene, there is an obvious draw to invoke a $2e^-/1H^+$ reduction of pre-associated arenes directly from photoexcited **[BP-H]**$^-$. However, photoinduced single electron transfer (SET) reactivity is sufficient to explain the initial steps in Birch chemistry, and equally as important, also within arene dehalogenation reactivity where SET is expected. Furthermore, the method of the reduction from the **[BP-H]**$^-$ to the substrate does not address the observed reliance on the presence of base (OH^-). We posit that proton-coupled electron transfer (PCET) or related proton transfer (PT) / electron transfer (ET) is an operative pathway (PT/ET). Namely, the relatively long-lived perylene-like singlet excited state of **[BP-H]**$^-$ engages in SET to the arene substrate, but this is accompanied by proton transfer to hydroxide. The end result is the formation of an arene radical anion (or an aryl radical plus a halide in the case of dehalogenation), and water.

While we do not yet have direct evidence for the order of PT and ET events in this system, the electrochemical evidence suggests that proton motions are a key ingredient needed to trigger reduction events, either through PT/ET or through PCET. First, it is noted that for **[BP-H]**$^-$, no emission peak shifts are observed in the presence of base. In other words, the Pe-like chromophore stores 2.76 eV of energy during its 7 ns lifetime (this corresponds to E_{00} taken as the average of the 0-0 peaks in the absorption and emission measurements; see Figure 4D). In the absence of base, the oxidation of **[BP-H]**$^-$ occurs at ~ –1.0 V vs Fc^+/Fc. Combining these photophysical and electrochemical data, the singlet excited state of **[BP-H]**$^-$ can act as a reductant with –3.76 V of potential ($E_{ox} – E_{00}$) vs Fc^+/Fc. This is po-tent, approximately 660 meV higher in energy than the recently reported napthalene monoimide derived closed shell photo-reductant $[NMI(H)]^-$ (-3.1 V vs Fc^+/Fc), but still likely insufficient for SET to substrates such as benzene ($E_{1/2}$ = –3.88 V vs Fc^+/Fc). At the other extreme, full deprotonation of **[BP-H]**$^-$ - would produce $BPDE^{2-}$, a species whose one electron oxidation occurs at –2.61 V vs Fc^+/Fc such that an excited state storing ~1.75 eV (estimated from the prominent 710 nm absorbance peak; see Figure 3.4C) could, in principle, function as a reductant with a remarkable –4.36 V of potential vs Fc^+/Fc. In practice, we do not imagine full deprotonation as the 710 nm absorption feature characteristic of $BPDE^{2-}$ is not observed even in the presence of excess TMAOH. Rather, we envision **[BP-H]**$^-$ as a weak acid where fluctuations on a proton transfer coordinate trigger electron transfer events for those **[BP-H]**$^-$ species coordinated with a substrate (Scheme 3.1). The relevance of base in a related context has recently been described by Bortolato et al. for dihydroacridine photocatalysts with excited-state oxidation potentials up to 3.21 V vs Fc^+/Fc.[38] This notion of a weak acid in the presence of a strong base is consistent with observations described above involving a rapid increase in KSV with added OH^- followed by a more muted response with additional OH^-, reflecting reactivity in

what would be a buffer region for the system. This overall model, where both substate binding and acid/base interactions are governed by equilibria, is consistent with the lack of observation of dynamic quenching. The probability of simultaneous collisions among three species (**[BP-H]**$^{-}$, substrate, and OH^{-}) leading to a favorable geometry, necessary for the needed PT

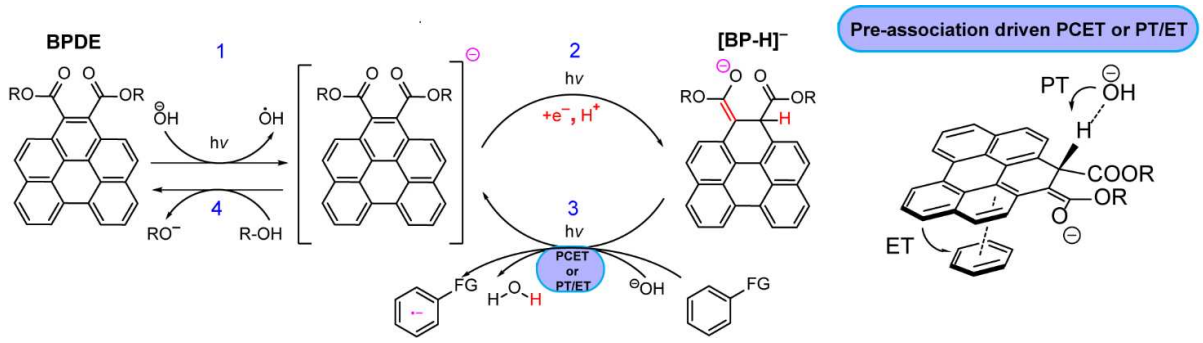

Scheme 3.1. Proposed catalytic cycle for BPDE driven reductive transformations involving proton-coupled electron transfer (PCET). (1) Photoinduced electron transfer from hydroxide, acting as the sacrificial reductant, to BPDE to form radical anion, BPDE•–.[39] *(2) An effective e– , H+ reduction of BPDE•– : a) a direct hydrogen atom transfer (HAT) from THF to BPDE•–* or b) hydroxide oxidation by BPDE•–* followed by a proton transfer from alcoholic solvent generating [BP-H]– in both cases (3) photoinduced electron trans-fer from [BP-H]– to substrate, along with proton transfer to hydroxide to form water. Pre-association is necessary for the connected PT and ET events to take place. (4) Oxidation of BPDE radical anion to neutral BPDE.*

and ET motions, is low, and as a result the fluorescence lifetime of the **[BP-H]**$^{-}$ complex remains unaffected even while static quenching can be observed. We expect the binding interaction to be weak with only a minor population of **[BP-H]**$^{-}$ being pre-associated. This limits our ability to detect a change in UV-Vis spectrum as a result of the substrate binding event. We also speculate that reorganization energy following SET from **[BP-H]**$^{-}$ is substantial, perhaps being coupled to proton loss and subsequent delocalization of the radical in the product $BPDE^{\bullet-}$. This could then slow down SET in collisional settings with any emission quenching requiring the interconnected PT and ET events and with them the need for substrate binding equilibria and an environment inclusive of proton-accepting basic sites.

CONCLUSION

In this work, we first acknowledged the standing limitations of the photo-Birch system which includes multiple catalyst loadings and long reaction times. The key findings are that the benzo[ghi]perylene monoimide (BPI) photocatalyst family is subject to ring opening during the photo-Birch reaction conditions. Additionally, BPI-P•- demonstrated a short excited-state lifetime (10 ps) and that a doublet open shell species is an unlikely photoactive intermediate in this system. Discovery of the ring-opening led us to prepare and study a diester-functionalized benzo[ghi]perylene model system BPDE, which has proved useful in spectroscopy, electrochemistry, and computational studies to understand how this new photocatalyst family can achieve challenging reduction chemistries. There are two main interrelated findings within this work. The first centers around formation and function of an active perylene-like **[BP-H]**$^-$ that is generated as a $2e^-/1H^+$ product from BPDE. The second centers around how that chromophore [BP-H]– is able to achieve remarkable potency as an excited state reductant.

During catalysis we have found a reliance on the presence of OH^- in excess and the studies herein indicate that it functions in dual roles. The first role is described in this paragraph and the second role in the paragraph that follows. Hydroxide first serves as an electron donor, acting to produce BPDE$^{\bullet-}$ from photoexcited BPDE* (Scheme 3.1, (1)).[40, 41] Following a second photon absorption event, BPDE$^{\bullet-*}$ could a) abstract a hydrogen atom from THF[42] to form **[BP-H]**$^-$ or b) undergo a second oxidization of hydroxide,43 transiently producing $BPDE^{2-}$ which in an alcoholic environment would abstract a proton to also form **[BP-H]**$^-$ (Scheme 3.1, (2)). **[BP-H]**$^-$ exhibits privileged properties relative to its precursors. For example, its absorption spectrum is red-shifted relative to BPDE and its S1 excited-state lifetime is lengthened by almost three orders of magnitude relative to BPI-P$^{\bullet-*}$ (7 ns compared to ~ 10 ps). The emergent properties of **[BP-H]**$^-$

are made possible by the structure of the starting BPDE. For example, the pi-system supports the first reduction generating the radical anion, while the ester functionalities can accommodate additional reduction through enol tautomerization. Most importantly, rehybridization of a benzo-ring carbon atom from sp^2 to sp^3 results in an effective indirect hydride addition ($2e^-/1H^+$), forming the stable closed shell molecule **[BP-H]**$^-$ that exhibits a perylene chromophore core. Rehybridization would presumably be hindered by strain in systems with intact ring structures such as benzo[ghi]perylene imides or an-hydrides.

As an electron-rich chromophore, **[BP-H]**$^-$ is poised to function as an excited state reductant. Its ground state oxidation – that we observe as a byproduct in the electrochemical experiments – is relatively facile. This, coupled with a 7 ns storage of 2.76 eV of S1 energy typical for a perylene core, means that **[BP-H]**$^{-*}$ is potent with -3.76 V (vs Fc^+/Fc) of reducing power. However, this is still thermodynamically insufficient to reduce benzene and suggests the second role played by OH-, now acting as a base rather than a reductant. We envision those fluctuations on a proton-transfer coordinate – involving the same H-atom added during protonation of $BPDE^{2-}$ – enervates the excited chromophore for challenging reduction events. Once the electron tunnels, the proton can fully transfer to hydroxide generating water and $BPDE^{\bullet-}$ (Scheme 3.1, (3)), thus insulating against non-productive back electron transfer events. Finally, $BPDE^{\bullet-}$ can oxidize back to BPDE through reduction of alcohols, present in excess in the reaction mixture (Scheme 3.1, (4)), or reenter the catalytic cycle by reforming **[BP-H]**$^-$ following another photoinduced reduction and proton addition.

To our knowledge no other excited state species, to date, has been reported to be quenched by a substrate as inert as benzene, discovering a new mode to perform challenging reductions without the need of solvated electrons, as previously pro-posed in the BPI system.[14] To this end

[BP-H]$^{-}$ should find utility in designing highly potent PCs to harvest multiphoton energies. The fact that the overall photo-Birch yield by the BPDE system is reduced compared to the original catalyst (BPI-P) could be related to a few things: a difference in the reorganization energy associated with ET to the substrate, a higher rate of back electron transfer from the reduced substrate, or weaker binding between the substrate and the non-core extended **[BP-H]**$^{-}$**.** Although BPDE is not a high performing photocatalyst in its own right, it provides mechanistic clarity. The uncovered mode of operation – electron transfer to inert substrates originating from a photoexcited $2e^{-}/1H^{+}$ species and involving a proton transfer coordinate – can be readily transferred to other diester functionalized polyaromatic hydrocarbon motifs. We envision these future diester based PCs to demonstrate improved reactivity and overcome the limitations of the original BPI based photo-Birch work with lower PC loadings and faster reaction times towards new and improved synthetic methodology.

REFERENCES

1. Romero, N. A.; Nicewicz, D. A., Organic Photoredox Catalysis. *Chem. Rev.* **2016,** *116* (17), 10075-10166.
2. Corbin, D. A.; Swisher, N. A.; Miyake, G. M., Fundamentals of Photochemical Redox Reactions. In *Organic Redox Chemistry: Chemical, Photochemical and Electrochemical Syntheses*, 2021; pp 45-102.
3. Chan, A. Y.; Perry, I. B.; Bissonnette, N. B.; Buksh, B. F.; Edwards, G. A.; Frye, L. I.; Garry, O. L.; Lavagnino, M. N.; Li, B. X.; Liang, Y., Metallaphotoredox: the merger of photoredox and transition metal catalysis. *Chem. Rev.* **2021,** *122* (2), 1485-1542.
4. McAtee, R. C.; McClain, E. J.; Stephenson, C. R., Illuminating photoredox catalysis. *Trends Chem.* **2019,** *1* (1), 111-125.
5. Bell, J. D.; Murphy, J. A., Recent advances in visible light-activated radical coupling reactions triggered by (i) ruthenium,(ii) iridium and (iii) organic photoredox agents. *Chem. Soc. Rev.* **2021,** *50* (17), 9540-9685.
6. Skubi, K. L.; Blum, T. R.; Yoon, T. P., Dual catalysis strategies in photochemical synthesis. *Chem. Rev.* **2016,** *116* (17), 10035-10074.
7. Ghosh, I.; Ghosh, T.; Bardagi, J. I.; König, B., Reduction of aryl halides by consecutive visible light-induced electron transfer processes. *Science* **2014,** *346* (6210), 725-728.
8. Glaser, F.; Kerzig, C.; Wenger, O. S., Multi-Photon Excitation in Photoredox Catalysis: Concepts, Applications, Methods. *Angew. Chem. Int. Ed. Engl.* **2020,** *59* (26), 10266-10284.
9. MacKenzie, I. A.; Wang, L.; Onuska, N. P. R.; Williams, O. F.; Begam, K.; Moran, A. M.; Dunietz, B. D.; Nicewicz, D. A., Discovery and characterization of an acridine radical photoreductant. *Nature* **2020,** *580* (7801), 76-80.
10. Zeman, C. J. t.; Kim, S.; Zhang, F.; Schanze, K. S., Direct Observation of the Reduction of Aryl Halides by a Photoexcited Perylene Diimide Radical Anion. *J. Am. Chem. Soc.* **2020,** *142* (5), 2204-2207.
11. Cowper, N. G. W.; Chernowsky, C. P.; Williams, O. P.; Wickens, Z. K., Potent Reductants via Electron-Primed Photoredox Catalysis: Unlocking Aryl Chlorides for Radical Coupling. *J. Am. Chem. Soc.* **2020,** *142* (5), 2093-2099.
12. Kim, H.; Kim, H.; Lambert, T. H.; Lin, S., Reductive Electrophotocatalysis: Merging Electricity and Light To Achieve Extreme Reduction Potentials. *J. Am. Chem. Soc.* **2020,** *142* (5), 2087-2092.
13. Glaser, F.; Wenger, O. S., Red Light-Based Dual Photoredox Strategy Resembling the Z-Scheme of Natural Photosynthesis. *JACS Au* **2022,** *2* (6), 1488-1503.
14. Cole, J. P.; Chen, D. F.; Kudisch, M.; Pearson, R. M.; Lim, C. H.; Miyake, G. M., Organocatalyzed Birch Reduction Driven by Visible Light. *J. Am. Chem. Soc.* **2020,** *142* (31), 13573-13581.
15. Chatterjee, A.; Konig, B., Birch-Type Photoreduction of Arenes and Heteroarenes by Sensitized Electron Transfer. *Angew. Chem. Int. Ed. Engl.* **2019,** *58* (40), 14289-14294.
16. Goez, M.; Hussein, B. H. M., Photoionization of xanthone via its triplet state or via its radical anion. *Phys. Chem. Chem. Phys.* **2004,** *6* (24), 5490-5497.
17. Fujita, M.; Ishida, A.; Majima, T.; Takamuku, S., Lifetimes of Radical Anions of Dicyanoanthracene, Phenazine, and Anthraquinone in the Excited State from the Selective Electron-Transfer Quenching. *J. Phys. Chem.* **1996,** *100* (13), 5382-5387.

18. Gosztola, D.; Niemczyk, M. P.; Svec, W.; Lukas, A. S.; Wasielewski, M. R., Excited Doublet States of Electrochemically Generated Aromatic Imide and Diimide Radical Anions. *J. Phys. Chem. A* **2000,** *104* (28), 6545-6551.
19. Fujitsuka, M.; Majima, T., Reaction dynamics of excited radical ions revealed by femtosecond laser flash photolysis. *J. Photochem. Photobiol. C* **2018,** *35*, 25-37.
20. Rieth, A. J.; Gonzalez, M. I.; Kudisch, B.; Nava, M.; Nocera, D. G., How Radical Are "Radical" Photocatalysts? A Closed-Shell Meisenheimer Complex Is Identified as a Super-Reducing Photoreagent. *J. Am. Chem. Soc.* **2021,** *143* (35), 14352-14359.
21. Li, H.; Wenger, O. S., Photophysics of Perylene Diimide Dianions and Their Application in Photoredox Catalysis. *Angew. Chem. Int. Ed. Engl.* **2022,** *61* (5), e202110491.
22. Emmett, P.; Skau, N., The catalytic hydrogenation of benzene over metal catalysts. *J. Am. Chem. Soc.* **1943,** *65* (6), 1029-1035.
23. Birch, A., The Birch Reduction. *J. Chem. Soc* **1944,** *430*, 436.
24. Kwon, Y.; Lee, J.; Noh, Y.; Kim, D.; Lee, Y.; Yu, C.; Roldao, J. C.; Feng, S.; Gierschner, J.; Wannemacher, R., Formation and degradation of strongly reducing cyanoarene-based radical anions towards efficient radical anion-mediated photoredox catalysis. *Nat. Commun.* **2023,** *14* (1), 92.
25. Marchini, M.; Gualandi, A.; Mengozzi, L.; Franchi, P.; Lucarini, M.; Cozzi, P. G.; Balzani, V.; Ceroni, P., Mechanistic insights into two-photon-driven photocatalysis in organic synthesis. *Phys. Chem. Chem. Phys.* **2018,** *20* (12), 8071-8076.
26. Han, X.; Li, H.-M.; Xu, C.; Xiao, Z.-Q.; Wang, Z.-Q.; Fu, W.-J.; Hao, X.-Q.; Song, M.-P., Water-soluble palladacycles containing hydroxymethyl groups: synthesis, crystal structures and use as catalysts for amination and Suzuki coupling of reactions. *Transition Met. Chem.* **2016,** *41* (4), 403-411.
27. Manning, S. J.; Bogen, W.; Kelly, L. A., Synthesis, characterization, and photophysical study of fluorescent N-substituted benzo[ghi]perylene "swallow tail" monoimides. *J. Org. Chem.* **2011,** *76* (15), 6007-13.
28. Bowden, K.; P. Hiscocks, S.; Perjéssy, A., Ring–chain tautomerism. Part 9.1 2-Acylbenzamides, 8-acyl-1-naphthamides and 5-acyl-4-phenanthramides. *J. Chem. Soc., Perkin Trans. 2* **1998,** (2), 291-296.
29. Clar, E.; Ironside, C. T.; Zander, M., Annellation effects in the perylene and coronene series. *Tetrahedron* **1966,** *22* (10), 3527-3533.
30. Guha, S.; Goodson, F. S.; Corson, L. J.; Saha, S., Boundaries of anion/naphthalenediimide interactions: from anion-pi interactions to anion-induced charge-transfer and electron-transfer phenomena. *J. Am. Chem. Soc.* **2012,** *134* (33), 13679-91.
31. Saha, S., Anion-Induced Electron Transfer. *Acc. Chem. Res.* **2018,** *51* (9), 2225-2236.
32. Shida, T.; Iwata, S., Electronic spectra of ion radicals and their molecular orbital interpretation. III. Aromatic hydrocarbons. *J. Am. Chem. Soc.* **1973,** *95* (11), 3473-3483.
33. Thielen, D.; Anderson, L., Electrochemical irreducibility of the cyclooctatetraene radical anion. *J. Am. Chem. Soc.* **1972,** *94* (7), 2521-2523.
34. Muthukrishnan, A.; Sangaranarayanan, M. V., Electrochemical reduction of carbon–fluorine bond in 4-fluorobenzonitrile – Mechanistic analysis employing Marcus–Hush quadratic activation-driving force relation. *Chem. Phys. Lett.* **2007,** *446* (4), 297-303.
35. Muthukrishnan, A.; Sangaranarayanan, M. V., Analysis of C–F bond cleavages in methylfluorobenzoates—Fragmentation and dimerization of anion radicals using convolution potential sweep voltammetry. *Electrochim. Acta* **2010,** *55* (5), 1664-1669.

36. Andrieux, C. P.; Blocman, C.; Savéant, J. M., Characterization of electrochemical reactions hidden in the background discharge the redox catalyzed reduction of fluorobenzene. *J. Electroanal. Chem. Interfacial Electrochem.* **1979,** *105* (2), 413-417.
37. Mortensen, J.; Heinze, J., The Electrochemical Reduction of Benzene—First Direct Determination of the Reduction Potential. *Angew. Chem., Int. Ed. Engl.* **1984,** *23* (1), 84-85.
38. Bortolato, T.; Simionato, G.; Vayer, M.; Rosso, C.; Paoloni, L.; Benetti, E. M.; Sartorel, A.; Leboeuf, D.; Dell'Amico, L., The Rational Design of Reducing Organophotoredox Catalysts Unlocks Proton-Coupled Electron-Transfer and Atom Transfer Radical Polymerization Mechanisms. *J. Am. Chem. Soc.* **2023,** *145* (3), 1835-1846.
39. Another slightly more complex mechanism is also possible that we cannot rule out at this time. As argued in the text and reiterated in this caption regarding Step 2 of the mechanism, HAT from THF could play a role producing $[BP\text{-}H]^-$. It is also possible that HAT plays a role in Step 1. Therein, HAT from THF to BPDE* would produce a transient product $[BPDE\text{-}H]^\bullet$ (and a THF radical). With hydroxide present, $[BPDE\text{-}H]^\bullet$ could then deprotonate leading to $BPDE^{\bullet-}$ plus water.
40. Based on the $E_{0,0}$ value of 2.86 eV (i.e., the amount of energy stored in the relaxed BPDE S_1 state as determined from the intersection between the absorption and emission spectra), along with BPDE's first reduction potential (-2.22 V vs Fc^+/Fc), we estimate the redox potential available for hydroxide oxidation to be 0.64 V vs Fc^+/Fc by BPDE* in its S_1 excited state. While we were unable to find an oxidation potential of OH^- in a THF/MeOH mixture, our solvent system, the reported value of 0.28 V vs Fc^+/Fc in MeCN (c.f. 41) would suggest that BPDE* is indeed capable of oxidizing OH^-. We do acknowledge that this number is not a true rep-resentative of OH^- oxidation potential in our system due to presence of protic MeOH in the solvent mixture. However, we feel that it is indeed reasonable to expect that the oxidation potential would still be within a range accessible by BPDE*.
41. Sawyer, D. T.; Roberts Jr, J. L., Hydroxide ion: an effective one-electron reducing agent? *Acc. Chem. Res.* **1988,** *21* (12), 469-476.
42. Jing, L.; Nash, J. J.; Kenttämaa, H. I., Correlation of hydrogen-atom abstraction reaction efficiencies for aryl radicals with their vertical electron affinities and the vertical ionization energies of the hydrogen-atom donors. *J. Am. Chem. Soc.* **2008,** *130* (52), 17697-17709.
43. In terms of the second hydroxide oxidation event, it is noted that it is challenging to estimate $E_{0,0}$ for the lowest excited doublet state of $BPDE^{\bullet-}$ because that species is non-emissive. Since we are able to detect weak absorption of $BPDE^{\bullet-}$ to the red at ~1000 nm, it can be argued that its D_1 state stores approximately ~1.2 eV of energy. With this number and given that $BPDE^{\bullet-} + e^- \rightleftharpoons BPDE^{2-}$ (-2.61 V vs Fc^+/Fc) couple takes place only 390 meV higher than the first reduction $BPDE + e^- \rightleftharpoons BPDE^{\bullet-}$ (-2.22 V vs Fc^+/Fc; see Fig. 4a in the main text), the potential for oxidation of OH- by $BPDE^{\bullet-*}$ is estimated to be 0.85 V vs Fc^+/Fc. This represents an excited state potential with a greater driving force than what was estimated in the first case discussed above involving BPDE*.

[3]CHAPTER 4 – SPECTROSCOPICALLY GUIDED DISCOVERY OF PHOTOANNULATION IN BAY-SUBSTITUTED BENZO[GHI]PERYLENE UNLOCKS UNPRECEDENTED PHOTO-BIRCH REDUCTIONS.

OVERVIEW

A general protocol based on a single photoredox catalyst capable of accomplishing the reduction of electron-deficient to electron-rich arenes has proven to be challenging. Herin, we report spectroscopically guided discovery of photoannulation (light-induced cyclization) in bay-substituted benzo[ghi]perylene diester, which led us to prepare and study diester-functionalized benzo[a]coronene model system as a new class of strongly reducing photocatalysts (PC). The catalytic efficiency of the photocatalyst has been evidenced through the notable photo-Birch reductions of the plethora of electron-deficient to electron-rich arenes with varying electronic nature at ambient temperature driven by visible light from commercially available LEDs. Furthermore, the efficacy of this developed protocol has been validated through its application in the multistep synthesis of pharmaceutical lead compounds. Mechanistic experiments suggest a two-electron, one-proton closed-shell species as a super-reductant, which after visible photon absorption, unlocks unprecedented photo-Birch reductions. Using time-resolved emission and transient absorption spectroscopy unambiguously reveals the outstanding excited state potential of our best-performing catalyst (-3.56 V vs SCE), which corroborates well with its strong reducing behavior and provides evidence for mechanistic key steps and intermediates. The present strategy

[3] *Author contributions. A.K.B and A.S contributed equally. A.K.B., A.S., A.R.G., N.H.D and G.M.M. conceived the idea. A.K.B, L.F.P., A.M.W. and A.R.G. executed the catalyst design, synthesis, and reaction development. A.S. contributed to all the electrochemistry and spectroscopic investigations. G.H., B.P, and R.S.P. performed DFT calculations. A.K.B. wrote the manuscript. All authors read and edited the manuscript.*

will broaden the chemical toolbox for the straightforward synthesis of complex organic compounds and will further translate into solving challenging photochemical processes.

INTRODUCTION

The direct reduction of benzene and its derivatives to introduce value added sp^3-hybridized carbon centers is a challenging and synthetically useful transformation. The conversion of readily available two-dimensional (2D) planar aromatic feedstocks into three-dimensional (3D) C(sp^3)-rich ring derivatives not only fosters the expansion of chemical diversity but also holds significant promise within the domain of medicinal chemistry and the pharmaceutical industry. A recent meta-analysis investigating biologically active molecules advancing through clinical trials has unveiled a compelling association between the efficacy of these candidates and their degree of 3D complexity. The Birch reduction is a key reaction in organic synthesis that has paved the way for straightforward access to value-added sp^3-hybridized carbon centers starting from planar aromatic feedstocks.[7,8] A classical Birch reduction requires two electrons and two protons to form a 1,4-cyclohexadiene derivative from arenes. The traditional Birch reductions pose extremely demanding reaction conditions, such as using pyrophoric metals under cryogenic conditions.[1] The harsh reaction conditions are an obvious disadvantage to this to this classic reaction and other transformations using these conditions at scale,[3] however other metal based methods have been shown to improve conditions for solvated electrons.[2] To mitigate the hazardous conditions of traditional Birch chemistry ammonia/metal-free[9], electrochemical[4], and photochemical[10] methods have been developed.

Driven by the continuous demand for sustainable organic synthesis, photochemistry serves as a valuable tool where photons translated to electron mobility serve as a sustainable and inherently safe redox reagent, providing an advantageous opportunity for generating various radical and radical ion species through single-electron transfer (SET).[4] However, the range of chemical transformations of unactivated arenes using these catalytic platforms is fundamentally limited by the energetics of visible photons. For instance, a photon with a wavelength of 400 nm imparts 3.1 electron volts (eV) of energy, establishing the maximal thermodynamic impetus for reactions facilitated by visible light.[6] Moreover, for photocatalysts (PCs) orchestrating reductive transformations, consideration must be given to the oxidation potential of the PC and energy loss before efficient electron transfer to a substrate, attributable to non-radiative intra-PC phenomena. In practice, reductive transformations requiring more negative than approximately -2.00 V cannot proceed without harnessing the combined energies of multiple photons. To overcome the insufficient energy input for arene reduction, strategies have been developed to harness the energy of two visible-light photons. Light driven Birch reductions (photo-Birch) offers advantages in terms of selectivity and control over the substrates. A handful of examples exist of photo-Birch reduction of planar aromatic feedstocks. However, such systems have been constrained to substrates (e.g., low triplet energy arenes)[13a], shows only moderate reactivity[13b] (no example of the electron-deficient substrate such as aryl benzoic acid and electron-rich substrate such as toluene, anisole, p-cymene, 4-tert-butyl anisole, 1,3-, and 1,4-dimethoxybenzene), and requires prolonged reaction times[13c], and require high energy UV light[13d] (Figure 4.1B).

A barrier inherent to the reduction of electron-rich and electron-deficient substrates is the requirement for both a sufficiently reducing and photostable redox catalyst. To overcome this challenge and transform a range of electron-rich and electron-deficient arenes, a high

thermodynamic driving force and strong single electron transfer capability are required in the photoredox catalyst system. Hence, the motivation of this work is to design a robust, photo-Birch strategy that is fast and effective for a wide range of arenes and encompassing both electron-rich and poor substrates. Herin, we report spectroscopically guided discovery of photoannulation in bay-substituted benzo[ghi]perylene diester, which led us to prepare and study diester-functionalized benzo[a]coronene model system as a new class of strongly reducing photocatalysts (Figure 4.1C, 4.1D). The catalytic reactivity of the photocatalyst has been demonstrated by successful photo-Birch reductions of a plethora of electron-deficient to electron-rich arenes with varying electronic nature at ambient temperature driven by visible light from commercially available LEDs (Figure 4.1E). While the substrate scope and regioselectivity closely resemble the classic Birch reduction, this new method is operationally straightforward and offers higher chemoselectivity without over-reducing the target product. Mechanistic experiments suggest a two-electron, one-proton closed-shell species as a super-reductant. The excited state potential is calculated as -3.56 V vs SCE, corroborating well with its strong reducing behavior (Figure 4.1E). The present strategy will broaden the chemical toolbox for the straightforward synthesis of complex organic compounds and will further translate into solving challenging photochemical processes.

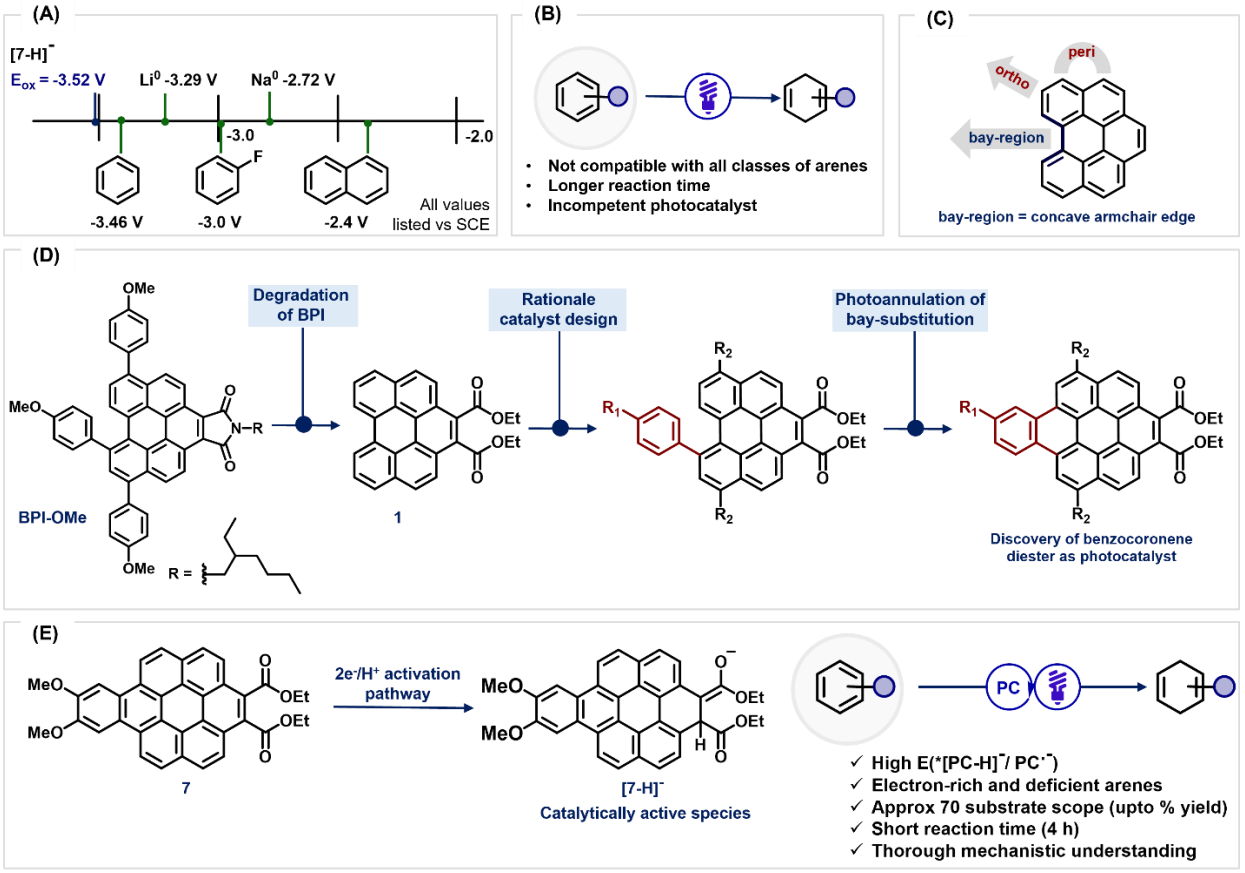

Fig 4.1. (A) Excited [7-H]- as a potent reductant, (B) Limitation of literature approaches, (C) Specific positions of benzo(ghi)perylene, (D) Design of spectroscopically guided discovery of benzo[a]coronene diester, (E) Overview of present work with simplified activation scheme towards the catalytically active PC, and highlights of the reactivity from the investigated active PC.

RESULTS AND DISCUSSION

Design and Characterization of the Photocatalyst Redox System: As reported in a recent study[11], benzo[ghi]perylene monoimide (BPI) photocatalyst family is subject to ring opening under the photo-Birch reaction conditions, which results in poor reactivity, prolonged reaction time, and limiting practical applicability. The degradation studies led us to prepare and study a diester-functionalized benzo[ghi]perylene model system, 1, which has proved useful in spectroscopy, electrochemistry, and computational studies, to understand how this new photocatalyst family can achieve challenging reduction chemistries.[13] Despite gaining a deeper

mechanistic understanding of PC 1 as a potent photo reductant, the synthetic utility was limited due to poor yields (6% on benzene to cyclohexadiene in 24 hours). In the present work, we leverage the mechanistic insights from the previous study to develop a functionally improved photocatalyst, using 1 as a template aiming to overcome the limitations of the previous photo-Birch system.

In prior work among the BPI family, the best performing photocatalyst was the tris phenylmethoxy (p-OMePh) substituted (6, 8, and 11-core positions) BPI (BPI-OMe, Figure 1D).[12] Consequently, we hypothesized that p-OMePh substitution on the benzo[ghi]perylene core of 1 will improve its reactivity towards benzene by driving the formation of the active species, monitored via UV-Vis. To test this hypothesis, we synthesized a family of BPDEs with mono (2), bis (3), and tris p-OMePh substitutions (4-OMe) (Figure 4.2A). Each successive p-OMePh substitution resulted in a red-shift (~8-9 nm per substitution) and broadening of the UV-Visible spectra, with all PCs exhibiting strong visible-light absorption (Section 4.14, SI). To benchmark the success of these PCs in the transformation of benzene to 1,4-cyclohexadiene the reaction was examined employing PC (2.0 mol%), tetramethylammonium hydroxide (TMAOH, 25 wt% in MeOH) as sacrificial reductant in mixed THF and tert-amyl alcohol (tAmylOH) as the solvent and H+ source irradiating with a 405 nm LED for 24 hours. The photo-Birch reactivity of all the new PCs was monitored via 1H NMR Spectroscopy (Figure 2A). PCs 2 and 3 exhibited marginal improvement in conversion of benzene to 1,4-cyclohexadiene (7% and 11% respectively) over 1 (6%), whereas 4-OMe outperformed them significantly with 88% conversion after 15 hours in optimized conditions. Additionally, 4-OMe exhibited versatile reactivity towards various substrates (Section 9a, SI). We synthesized two more tris substituted BPDEs: 4-H and 4-CF_3 to probe how possessing electron-neutral, and -withdrawing core substitution would affect the conversion of benzene. Under similar reaction conditions, good conversions of benzene to 1,4-

cyclohexadiene were obtained for both (73% for 4-H and 78% for 4-CF_3) after 15 hours, however 4-OMe remained the best performer (Figure 4.2A).

Our observation of tris-substituted BPDEs outperforming the original BPI system without the need for successive catalyst additions in less than half of the time prompted us to investigate the nature of the photoactive species in this catalyst family. It was previously established that following a 2e-, 1H+ activation of 1, the polyaromatic core of $[1\text{-H}]^-$, spectroscopically strongly resembled that of perylene[15]. Our investigation commenced by performing the same experiment and monitoring reactivity 2, and 3 in presence of excess TMAOH under photolysis conditions. As anticipated, the vibronic absorption peaks of 2, 3 in 370-390 nm region (originating from the benzo[ghi]perylene core) diminish over time, concomitant with the appearance of two new peaks at 420 and 450 nm that resemble a new redshifted vibronic progression (Figure 4.2B, Figure S4.38, S4.39). The shifts in absorption are consistent with a red-shifted perylene absorption resulting from the p-OMePh substitutions. Observation of an isosbestic point at 415 nm suggests a 1-to-1 conversion from 2, 3 to new species. However, when a similar experiment was performed on 4-OMe under identical photolysis conditions different spectroscopic findings were observed. Upon addition of TMAOH to a solution of 4-OMe in THF and irradiating with 405 nm light for 18 s, 4-OMe rapidly transformed into a new species wherein the broad 420 nm absorption band was rapidly lost, and the emerged spectrum does not resemble perylene nor do any of the new peaks appear at redder wavelengths which was observed in PCs 1, 2, and 3 (Figure 4.2C, 4.2D). Notably, this change persists, suggesting that the catalyst has undergone a light-driven structural change with the introduction of a p-OMePh group at the bay position, and we no longer generate a perylene-like [PC-H]- species with 4-OMe. Attempts to isolate the intermediates proved challenging since 4-OMe undergoes two sequential transformations in presence of TMAOH. As

two sequential transformations were occurring, we opted to switch to F- as the sacrificial reductant instead of OH-, hoping that F- which is relatively weaker reductant in comparison to OH- will facilitate solely the first transformation.[14] In a THF:tAmOH solvent, a mixture of 4-OMe and TBAF (tetra-nbutylammonium fluoride) was irradiated with a 405 nm LED, and the changes were monitored with UV-visible spectroscopy. The observation of an isosbestic point at 385 nm indicated conversion of 4-OMe into a single new species. The transformed absorption spectrum closely resembled that of the 4-OMe + TMAOH solution after brief irradiation (9s of irradiation, Figure S4.44) suggesting that F- can efficiently facilitate the first transformation to the PC but not the second one observed with TMAOH. Utilizing this method allowed for isolation of the first intermediate.

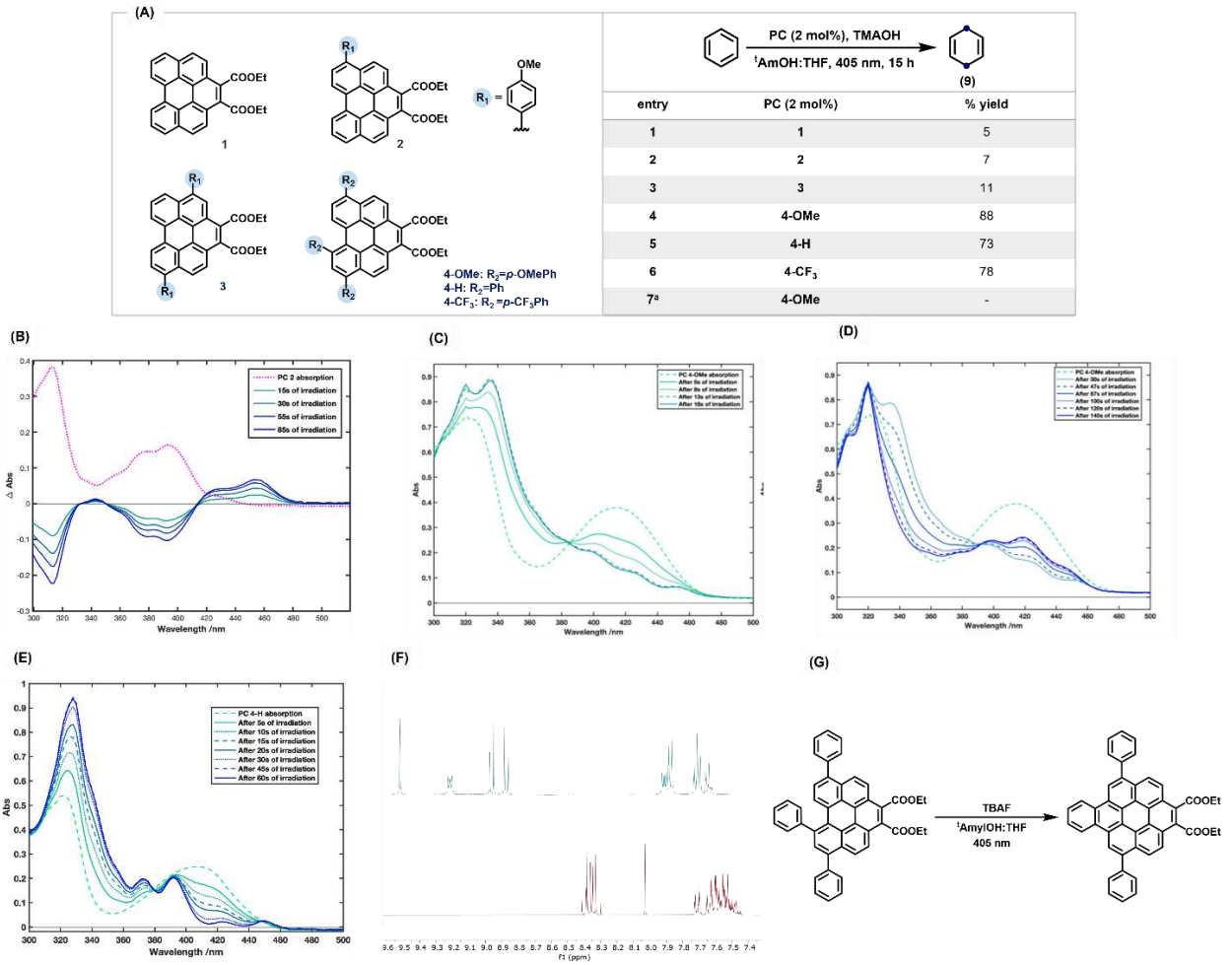

entry	PC (2 mol%)	% yield
1	1	5
2	2	7
3	3	11
4	4-OMe	88
5	4-H	73
6	4-CF_3	78
7[a]	4-OMe	-

Figure 4.2. (a) Optimization table for photo-Birch reduction using tris-substituted BPDEs, (B) UV-Vis spectra of 2 before and after irradiation with a 405 nm LED in presence of 225 µL TMAOH in the THF:MeOH (2:1) solvent system, (C) and (D) UV-Vis spectra of 4-OMe before and after irradiation with a 405 nm LED in presence of 225 µL TMAOH in the THF:MeOH (2:1) solvent system, (E) UV-Vis spectra of 4-H before and after irradiation with a 405 nm LED in presence of 225 µL TMAOH in the THF:MeOH (2:1) solvent system, (F) Stacked ^{1}H NMRs of photo cyclized product of 4-H with 6, (G) Schematic outline of photocyclization of tris-core extended diester (4-H).

The ^{1}H NMR spectrum showed that the aromatic resonances were significantly altered compared to those of 4-OMe. To support these findings with 4-OMe, the same UV-vis experiment was performed on 4-H, given its similar electronic and photocatalytic properties to 4-OMe (Figure 4.2E) and simpler spectral features. In contrast to the previous case, the ^{1}H NMR spectrum of the transformed species obtained from 4-H exhibited remarkable symmetry. While 4-H possesses

asymmetry inherent to bay substitution (like 4-OMe), the new species exhibited a new plane of symmetry NMR. The observed symmetry suggests that the phenyl ring at the bay position undergoes a photoinduced cyclization with the benzo[ghi]perylene core to yield a benzo[a]coronene moiety (5) (Figure 4.2G). These results support post synthetic in situ annulation of the benzo perylene core, which is a strategy used for structural modification.[15] We likely did not observe a symmetric spectrum with p-OMePh because the OMe substitution on the benzo[a]coronene core introduced asymmetry. Further characterization via 2D NMR (COSY) and high-resolution mass spectrometry (HRMS) of 4-OMe and 4-H consistently indicated the associated structural changes with in-situ transformation of the tris-phenyl-benzo[ghi]perylene moieties into π-conjugated bi-phenyl-benzo[a]coronene systems.[16] Additionally, we synthesized a model non-core substituted benzo[a]coronene diester (6) to validate the efficacy of cyclization between the core extensions and the benzo perylene core. The key feature of the benzo[a]coronene precisely overlapped with those of the photocyclized product (Figure 4.2F), supporting a photoinduced cyclization to a benzo[a]coronene moiety. As a control experiment, we irradiated two solutions of 4-OMe dissolved in a THF: tAmOH (1:1) mixture with a 405 nm LED with and without TBAF. Interestingly, the rate of change to the starting material was found to be at least four-times slower in the absence of TBAF. Based on these observations, we propose the following mechanism to generate a coronene based PC in situ: first, the photoexcited 4-OMe oxidizes F- (or OH-) generating a radical anion (shown in figure 4.2B). Following a second 405 nm photon absorption event, a C-C bond is formed between a carbon on the bay-substituted phenyl ring and the other bay carbon on benzo[ghi]perylene that are spatially close. We hypothesize that because the transition state must disrupt the aromaticity of the benzo[ghi]perylene core, we reason that it must be sufficiently high in energy and photoannulation of 4-H only proceeds through an

electronically excited state, as cyclization does not occur in the dark. A subsequent dehydrogenation event from proposed oxidant then restores π-aromaticity, generating a benzo[a]coronene radical anion which can be quenched by tAmOH resulting in a neutral benzo[a]coronene diester.

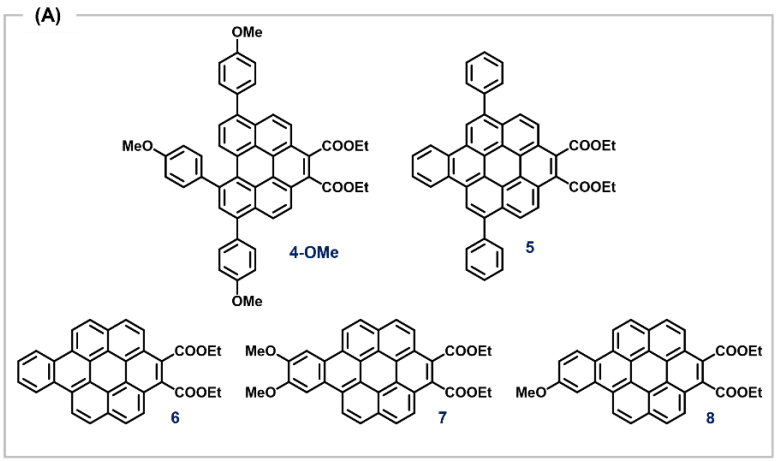

entry	PC	% yield (4 h)
1	4-OMe	-
2	5	65
3	6	45
4	8	55
5	7	72

*Fig 4.3. (A) Visible light driven photo-Birch reduction using a new class of organic photocatalyst benzo(a)coronene diester, (B) Optimizing reaction conditions with benzo[a]coronene diesters (**5**, **6**, **7** and **8**).*

Motivation for synthesis of diester-functionalized benzo[a]coronene model system as a new class of strongly reducing photocatalysts:

Having identified the structure of 5 with the help of various spectroscopic analysis. Next, we examined its ability to reduce benzene, noting that the reactions proceeded under the same conditions previously used with 4-OMe. Monitored by ^{1}H NMR spectroscopy, a 78% conversion to 1,4-cyclohexadiene was obtained in just 6 hours. This stands in stark comparison to the 15 hours required for a similar conversion with 4-OMe (88%). Recognizing that a benzo[a]coronene diester would represent one of the simplest proxies for 5, we synthesized 6, 7 and 8 using a one-pot benzyne reaction between 1 and substituted 2-(trimethylsilyl) phenyl trifluoromethanesulfonate (Figure 4.3A). Given that 4-OMe excelled in the BPDE family, we synthesized both bis- and

mono-methoxy substituted BCDEs (7 and 8). During optimization, we observed that 7 outperforms the all-other PCs tested in the conversion of benzene to 1,4-cyclohexadiene when the reaction time was reduced to 4 hours (72%, 9, Figure 4.3B). Additionally, experiments were carried out using 1,4-cyclohexadiene as the substrate to evaluate the possibility of its over-reduction under our improved conditions. Encouragingly, no over-reduced product was identified via 1H spectroscopy. This outcome confirms that the current protocol demonstrates excellent chemoselectivity, ensuring the target product is not over-reduced. The conversion profile of the reaction was monitored by tracking the product growth by ^{1}H NMR spectroscopy (see supplementary information for details, Section 4.4.2).

Mechanistic Investigations: The general function of 7 as a photocatalyst in effectively reducing benzene, combined with the simplicity and symmetry of the compound, motivated us to explore how this model PC functions during photocatalysis. Our investigation into the mechanism commenced by monitoring 7 reactivity with excess TMAOH in the dark via UV−visible spectroscopy in a THF/MeOH solvent system. The absorption spectrum of 7 remains the same upon the introduction of OH^- other than the expected dilution effect due to the added MeOH. Next, we sought to explore if photoexcited 7 would react with TMAOH. This reaction was performed by irradiating 7 in the presence of TMAOH inside a photoreactor fitted with two 385 nm LEDs. The vibronic absorption peaks of 7 in 340-380 nm region diminish over minutes, concomitant with the appearance of two new peaks at 320 and 410 nm that resemble a new redshifted vibronic progression. Observation of an isosbestic point at 390 nm suggests a 1-to-1 conversion from 7 to new species. During this absorption spectrum sequence, photoluminescence spectra were also collected after each period of irradiation by exciting the sample at 420 nm. As can be seen in Figure 4.4B, a bright vibronically resolved spectrum emerges that is distinct from

the fluorescence spectrum of 7 where the 0-0 peak is ~20 nm blue shifted, within 35 s of irradiation. Time-correlated single photon counting (TCSPC) showed a mono-exponential decay, indicating a single emitting chromophore is formed. The fluorescence lifetime of the newly formed species (~7.2 ns), which is shorter compared to that of 7 (~33.7 ns) (Figure S4.47, SI). At the same time, the newly formed species was found to be tolerant to air exposure even after 24 h, which, along multinanoseconds lifetime, suggests that it is not an open-shelled radical anion. These observations support our previous observation with 1 that under irradiation 1 underwent TMAOH-driven $2e^-$, $1H^+$ reduction to form $[1\text{-}H]^-$.

In order to probe the feasibility of a $2e^-$, $1H^+$ chemical reduction of 7, we turned to electrochemistry, replacing the chemical reductant with an electrode. Cyclic voltammetry studies of 7 are shown in Figure 4.4A. In the first scan, where the applied negative potential was strictly kept below –2.45 V vs Fc^+/Fc, the reversible first redox event was observed with a half-wave potential of –2.18 V vs Fc^+/Fc. This event corresponds to $7 + e^- \rightleftharpoons 7^{\bullet-}$. When scanning into more negative potentials, a second redox event is observed with a half-wave potential of −2.58 V vs Fc^+/Fc that corresponds to the dianion formation $7^{\bullet-} + e^- \rightleftharpoons 7^{2-}$. However, this redox event displays an apparent diminished return current (anodic peak) of the first reduction (see Figure 4.4A), and likely second reduction, and is accompanied by the appearance of a new anodic-current feature seen at approximately −1.00 V vs Fc^+/Fc. These observations together suggest that a chemical product formed at negative potentials capable of dianion formation (more negative than −2.59 V vs Fc^+/Fc), then requires a substantively positive potential (more positive than ~ -1.00 V vs Fc^+/Fc) to return 7. A similar observation was made with 1 as well, suggesting a similar pathway to generate a $2e^-$, $1H^+$ complex formation.

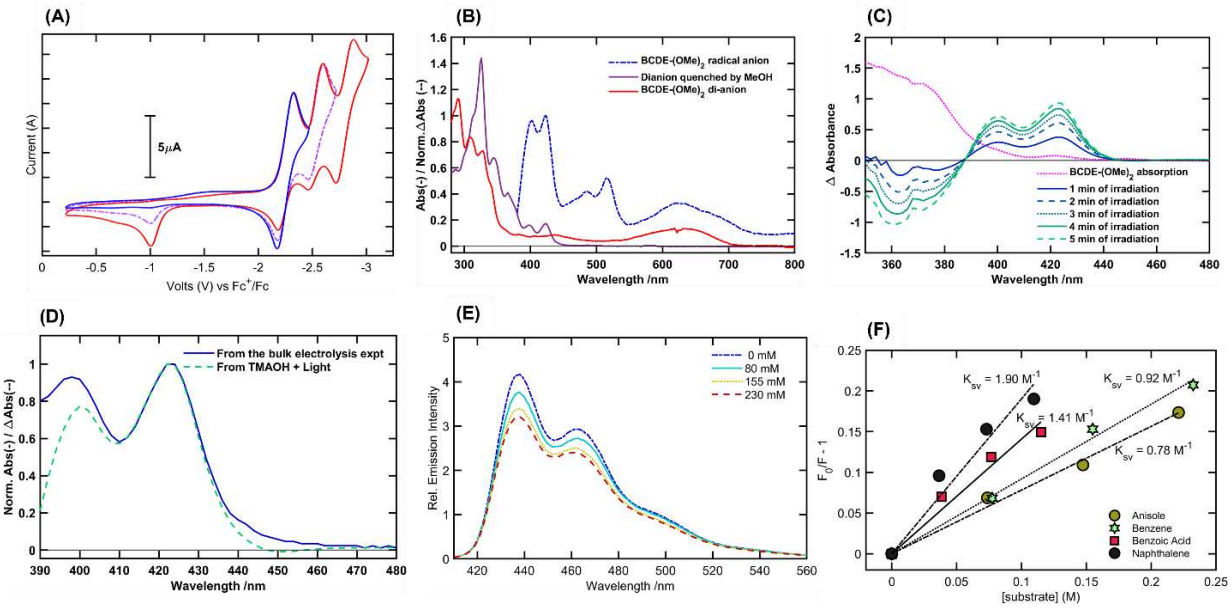

Fig 4.4. (A) Cyclic voltammogram of 1.0 mM 7 in 0.1 M TBAPF6 THF solution, scanning at 100 mV s-1 from 0 to –2.5 V (blue trace) and 0 to –3.0 V (dashed purple trace) vs Fc+/Fc using a Pt disk working electrode, Pt wire counter electrode, and leak-free Ag/AgNO3 reference electrode. (B) Absorbance spectrum of 7 after 4 hours of bulk electrolysis at -2.85 V vs Fc+/Fc in THF (red), bulk electrolyzed solution following addition of tAmOH (purple), and the solution after continued; Absorbance spectra of BPDE after 4 h of bulk electrolysis at −2.85 V vs Fc+/Fc in THF (blue), the bulk electrolyzed solution following the addition of tAmOH (dashed pink), and the solution after continued bulk electrolysis at −2.85 V vs Fc+/Fc in a 2:0.5:0.5 THF/MeOH/tAmOH solvent system (red). (C) Changes in the absorption spectrum of 35 μM 7 under irradiation in presence of 180 mM TMAOH in a 2:1 THF:MeOH solvent system. The emission spectra were collected by exciting the sample at 420 nm. (D) Comparing the absorption spectra of the electrochemically formed [7-H]- species to that formed by the reaction of 7, irradiation 405 nm for 200 s, and TMAOH. (E) Steady-state fluorescence quenching of [7-H]- in the presence of benzene as the quencher. (F) Stern- Volmer quenching rates for four different substrates with varying reduction potentials in presence of 300 mM TMAOH. The experiments were done with the electrochemically generated [7-H - species in a 2:1 THF:MeOH solvent system.

To support whether OH– was driving the $2e^{-}$, 1H+ reduction of 7, a bulk electrolysis experiment was performed where a concentrated solution of 7 in THF (with 0.1 M $TBAPF_6$) was electrolyzed at −2.45 V vs Fc+/Fc for 3 h. The UV−vis absorption spectrum of an aliquot taken from the H-cell is shown in the red trace and indicates the emergence of new absorption features, including a broad band at ~650 nm and an intense peak at 350 nm, which are assigned to 7^{2-}. Next, we then considered spectral changes upon addition of 100 μL of MeOH to the dianion solution,

guided by the fact that the reaction conditions rely on inclusion of tert-amyl alcohol (tAmOH) or MeOH environments. As can be seen in the dashed purple trace (Figure 4.4C), addition of 100 μL of MeOH leads to the loss of the prominent ~ 650 nm features. Importantly, we observe the emergence of a pair of peaks at ~ 400 and 420 nm suggestive of a second vibronic progression. These are effectively coincident with the peaks observed when 7 is irradiated in the presence of TMAOH in a THF/MeOH mixture (Figure 4.4A). The spectral similarity highlights that the same product is emerging in both electrochemical and photolysis experiments, supporting the idea that hydroxide can act as a sacrificial electron donor to 7 (Figure 4.4D). Additionally, without TMAOH, 7 upon irradiation shows no changes, as monitored by UV−vis, suggesting that TMAOH is needed to generate $[7\text{-H}]^-$ (Figure 4.4C).

We turn to the question of the likely structure of $[7\text{-H}]^-$, envisioning the gain of two electrons and one proton as effectively a hydride transfer to 7 to propose a possible set of isomers. Although a single chromophore is expected on the basis of the single photoluminescence decay constant (~7 ns) observed for $[7\text{-H}]^-$ in 7 photolysis experiments (Figure S4.22). An extensive thermochemical computational exploration that is also supports a naphthoperylene-like structure with the energy of AA being the lowest of these isomers by a substantial amount in most cases and 7.8 kcal/mol for the closest isomer (G), which is represented by hydride transfer to a benzocoronene bay position. To confirm that $2e^-$,$1H^+$ activation of 7 would be transformed into naphthoperylene-like species, we synthesized dimethoxy substituted naphthoperylene (7a) by reacting perylene with a dimethoxy benzyne intermediate. All photophysical data that we have collected are in support of a closed-shell naphthoperylene-like species. For example, the absorption spectrum of [7-H]− is red-shifted into the visible region with the 0−0 peak of the vibronic progression at 425 nm. We suggest the observed ~8 nm shift between their 0-0 absorption

peaks was due to the enolate group present in conjugation with naphthoperylene core. The emission spectrum of $[7\text{-H}]^-$ is also similar to 7a, although the Stokes shift for $[7\text{-H}]^-$ at 17 nm is larger than that for its 7a parent (4 nm, Figure S4.25), suggesting more reorganization within the $[7\text{-H}]^-$ singlet excited state prior to emission, perhaps as a result of inclusion of partial charge-transfer character involving the enolate substituent. After establishing the identity of the newly formed species as $[7\text{-H}]^-$ (Figure 4.5E), we investigated whether $[7\text{-H}]^-$ was the photoactive species engaged in electron transfer to the substrates from its excited state. To understand the role played by this new species within catalysis, photoluminescence spectra were recorded in the presence of substrate. When no TMAOH was added to the electrochemically generated $[7\text{-H}]^-$ solution, the emission intensity remained almost constant even after addition of benzene (Figure S4.49). These observations support our previous observation with 1 where we observed a strong dependence on the presence of TMAOH for the quenching occur. However, when the experiment was repeated in presence of 300 mM TMAOH, the fluorescence intensity of $[7\text{-H}]^-$ is found to be diminished as a function of benzene concentration (Figure 4.4E). Furthermore, the quenching rates (Stern−Volmer quenching constant, K_{SV}) were found to be dependent on the substrate (Figure 4.4F). A slightly lower K_{SV} was measured with electron rich anisole, whereas increased K_{SV} values were observed with electron poor benzoic acid and polycyclic naphthalene. This correlation with substrate reduction potential is evidence that the mode of quenching is electron transfer initiated by photoexcited $[7\text{-H}]^-$, in line with our expectations given the final Birch reduction and dehalogenation products for this model catalyst.

Along with the steady-state emission intensity, we also monitored the fluorescence lifetime of the $[7\text{-H}]^-$ complex during the quenching studies. With benzene as the quencher, (Equation S4.1, SI) fluorescence lifetime found to decrease minimally (even with [benzene] = 0.3 M) while the

emission intensity was diminished by more than 25%, indicating the mode of fluorescence quenching to be primarily static. We had previously reasoned that the requirement of a base such as OH^- and lack of dynamic quenching indicate that proton-coupled electron transfer (PCET) or related proton transfer (PT)/electron transfer (ET) is an operative pathway. Briefly, OH^- was deprotonating excited $[BP\text{-}H]^-$, transiently giving access to $BPDE^{2-*}$ which has the required driving force to reduce an inert substrate like benzene. Interestingly, dynamic quenching could be seen with the easier-to-reduce substrates benzoic acid and naphthalene. However, the overall quenching determined from the steady-state emission intensity quenching experiments was found to be greater than the dynamic quenching determined from the change in fluorescence lifetime. These observations support our previous observation with 1, where minimal dynamic quenching was observed with 1, which we attribute to the large reorganizational energy associated with $[1\text{-}H]^-$ reconverting to 1. Similarly, the dynamic quenching observed in this case would support that hypothesis, and that with a larger π-framework from $[7\text{-}H]^-$, the lowered reorganization energy supports why benzo[a]coronene diester performs better as strongly reducing photocatalysts.

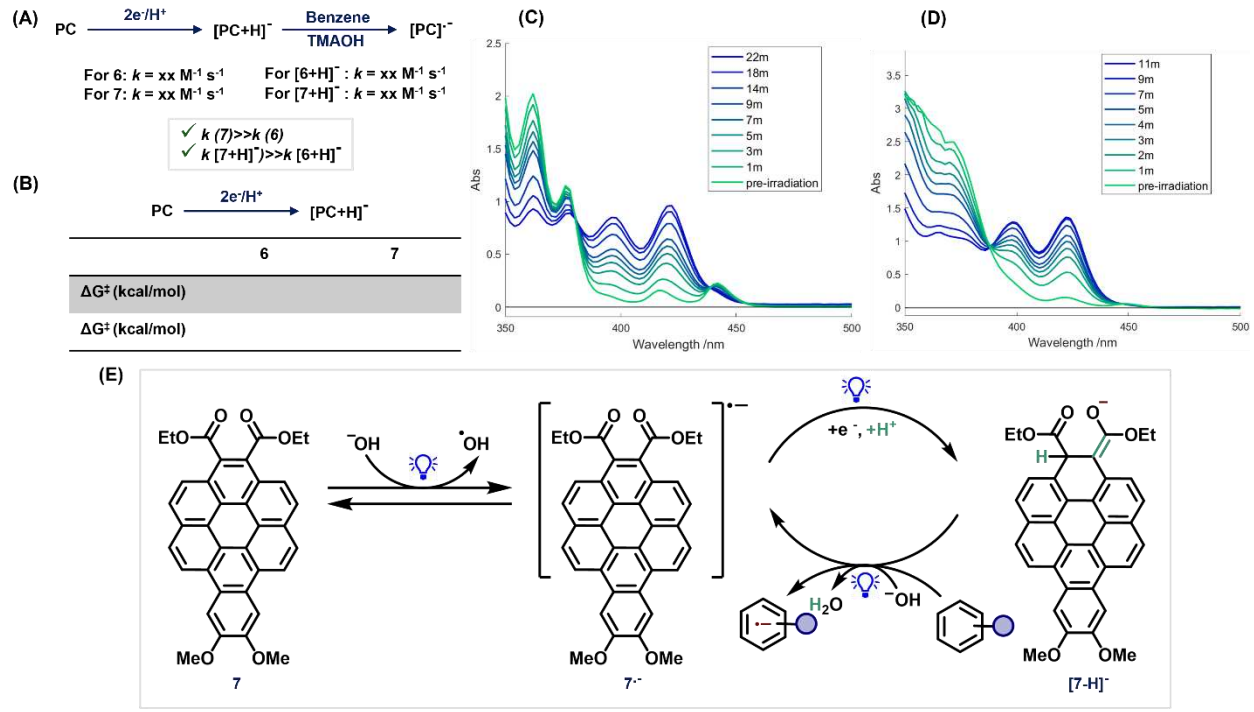

Fig 4.5. (A) Placeholder for rate constant for formation of [7-H]− and quenching rate constant for [7-H]−, (B) Placeholder for activation energies (ΔG‡), by DFT calculation studies, (C) UV-Vis spectra of formation of [7-H]− by irradiation 6 with a 405 nm LED in presence of 225 µL TMAOH in the THF:MeOH (2:1) solvent system, (D) UV-Vis spectra of formation of [7-H]− by irradiation 7 with a 405 nm LED in presence of 225 µL TMAOH in the THF:MeOH (2:1) solvent system, (E) Proposed Catalytic Cycle for 7 Driven Reductive Transformations Involving Proton-Coupled Electron Transfer (PCET) (1) Photoinduced electron transfer from hydroxide, acting as the sacrificial reductant, to BPDE to form a radical anion, 7•−, (2) An effective e−, H+ reduction of 7•− (a) a direct hydrogen atom transfer (HAT) from THF to 7•− or (b) hydroxide oxidation by 7•−* followed by a proton transfer from alcoholic solvent. [7-H]− is generated in both cases. (3) Photoinduced electron transfer from [7-H]−* to the substrate, along with proton transfer to hydroxide to form water. Pre-association is necessary for the connected PT and ET events to take place. (4) Oxidation of 7•−to neutral 7.*

We conducted mechanistic studies to understand the origin of the high activity of 7. First, we investigated the rate of formation of $2e^-/1H^+$ for both 6 and 7 by spectroscopically monitoring the formation of $[6\text{-H}]^-$, and $[7\text{-H}]^-$ in the presence of excess TMAOH under photolysis conditions (Figure 4.5A, 4.5C and 4.5D). Currently, our labs are undergoing kinetic experiments and computational DFT calculations to probe the rate of the catalytically active species $[6\text{-H}]^-$ and $[7\text{-H}]^-$ is formed as the major species to reduce our arenes.

Reductive Photocatalysis by Tailored Photocatalysts: arenes with varying electronic nature: With the suitable reaction condition, we first turned our attention to electron-deficient arene, specifically aryl carboxylic acids, as our substrate. To the best of our knowledge, these substrates have remained beyond the scope of previously of previously reported photochemical reducing protocols. Gratifyingly, all three benzoic acid derivatives, which are of significant interest in organic synthesis were reduced in good yields (10 (61%), 11 (55%), and 12 (52%)). Additionally, the reduction of $PhCO_2H$ was coupled with a sequential alkylation step by including methyl iodide in the same reaction mixture, producing 1-methylcyclohexa-2,5-diene-1-carboxylic acid in 45% yield (Section 9d, SI). We next evaluated a series of electron-rich arenes. Notably, some of the previous photo-Birch methodology proved ineffective in the reduction of electron-rich arenes. Encouragingly, substrates such as toluene, anisole, p-cymene, 4-tert-butyl anisole, 1,3-, and 1,4-dimethoxybenzene readily undergo photo-Birch reduction with our protocol to give corresponding 1,4-cyclohexadiene 13-18 in 59-80% yields (Figure 4.6). The protocol also exhibited tolerance towards amines, as evidenced by the reduction of phenethylamine to 19 in 66% yield. Furthermore, alcohols such as p-methoxybenzyl alcohol, 4-phenylbutan-2-ol, and 3-phenylpropan-1-ol were reduced, producing 20, 1, and 22 with good yields (67%, 81%, and 76%, respectively), without sacrificing the benzylic hydroxy group. Functional groups, such as carboxylic acid (24 and 25) are well tolerated. Remarkably, the cyclic ether motif was preserved in the high-yielding reduction of isochroman and isobenzofuran (26 and 27), while under conventional Birch conditions using lithium, exclusive benzyl C−O bond cleavage occurs. Additionally, naphthalene was reduced to triene 28 in 75% yield. Delightfully, the current protocol is operationally straightforward and offers good chemoselectivity without over-reducing the target product.

Next, when the optimized condition was applied to reductions of substrates such as carbocycles, heterocycles, and activated alkenes/alkynes along with the target product, we observed an over-reduced product as well. We assumed further optimization for reductions of these substrates would decrease the formation of over-reduced product. By monitoring the reduction of N-methyl indole to N-methyl indoline, it was determined that lowering the catalyst loading to 1 mol% along with a reaction time of 3 hours proved to be optimal for achieving the desired selective reduction with a minimal amount of over-reduced products (Section 8, SI). Employing the optimized conditions, we expanded the scope and observed the selectively reduced products 32-48 in excellent yield (Figure 4.6). Again, specific reductions/hydrogenations have previously been done by using metal complexes with high-bar pressure of hydrogen at elevated temperatures, thus limiting the opportunity for the synthesis of diverse alkaloids in large-scale applications.[28] To further demonstrate the utility of this catalytic system, we scaled up the reactions, achieving gram-scale reductions for both anisole and N-methyl indole, resulting in yields of 55% and 74% for products 11 and 39, respectively. Scale-up required minimal optimization - the same reactant stoichiometry was used in a larger reactor using four (instead of two) 405 nm LEDs, and the reaction was run for 20 hours. The present scope corroborates well with the strong reducing behavior of our best-performing catalyst 7 (E_{ox}= -3.56 V vs SCE). It demonstrates comparable reactivity to classical Birch reaction conditions that use sodium or lithium metal in liquid ammonia. Under these prescribed reaction conditions, this methodology proved ineffective in the reduction of alkyl halides, and nitrogen-containing heterocycles.[17]

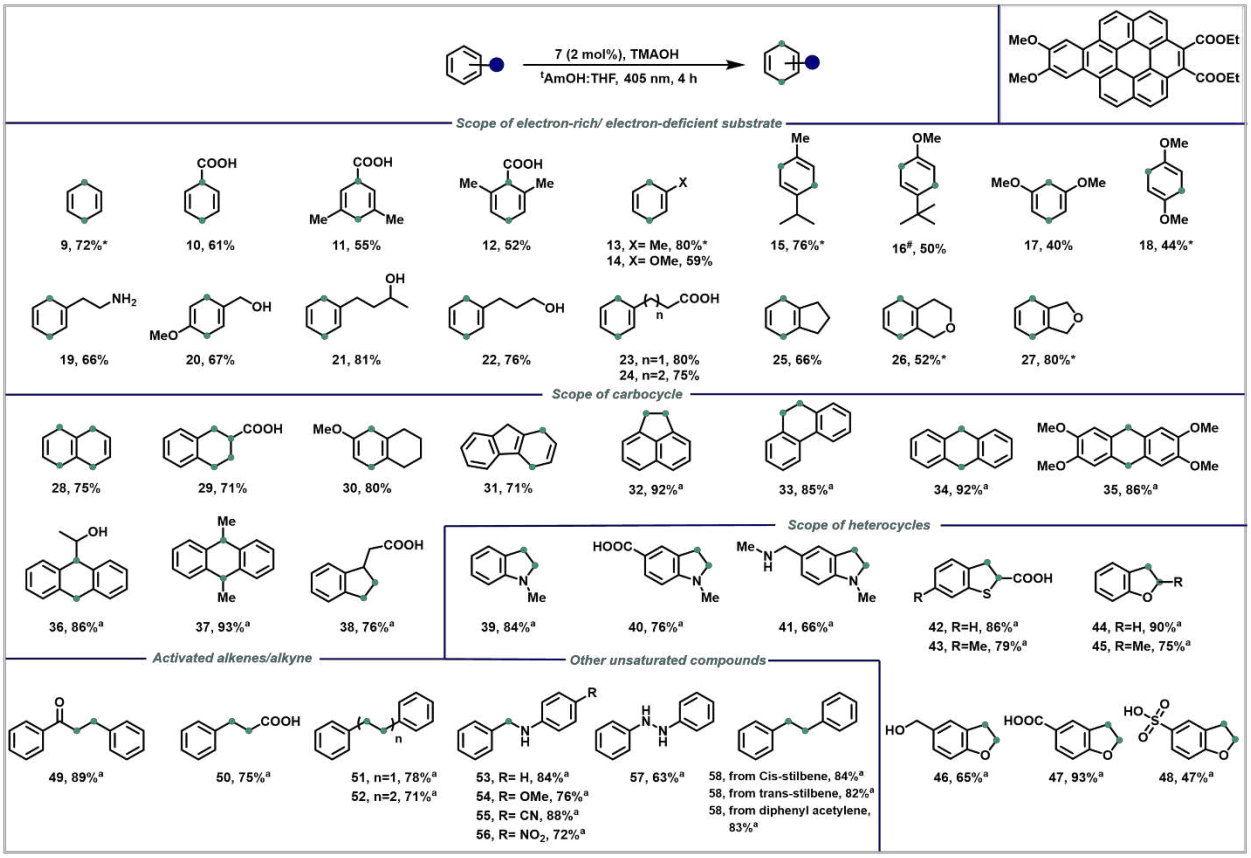

*Fig 4.6. Substrate scope for photocatalyzed Birch reduction. Reaction Conditions: 7 (2 mol%), substrate (0.25 mmol), 1 mL (11 equiv) of TMAOH (25% solution in MeOH), 405 nm LEDs (2 lights), isolated yield, *: NMR yield with mesitylene as internal standard, #: % conversion, a: 7 (1 mol%), reaction time- 3 h.*

To demonstrate the true potential of this new versatile catalytic paradigm, we next sought to reduce the complex natural product estrone-3-methyl ether with our optimized reaction conditions. The desired product 61 was obtained in 46% yield (Figure 4.7A), a precursor to synthetic androgenic hormone 9-Nortestosterone. Moreover, 7 allows late-stage functionalization of bioactive molecules, which include pharmaceutical and hormone derivatives, to the corresponding products (59, 60) in 64 and 66% yield (Figure 4.7B). Tailoring reaction conditions are of tremendous value in designing targeted synthesis routes for specific molecules, active pharmaceutical ingredients (APIs), and materials. Application of the current protocol in selective reduction was shown to be effective by manipulating the catalyst loading and reaction time.

Employing optimized conditions, fluorenone underwent tandem reductive deoxygenation and Birch reduction to afford 4,9-dihydro-1H-fluorene 31 in 52% yield. Subsequently, by reducing the catalyst loading (7, 1 mol%) and reaction time (3 h), 9H-fluorene (62) was selectively obtained from fluorenone by selective reductive deoxygenation in 72% yield, which was then further reduced to give 31 in 71% yield (Figure 4.7). A similar pattern was observed with trans-2-phenylcyclopropane-1-carboxylic acid, where ring opening occurred in the first reduction to yield 63 at a 73% yield, while its complete reduction provided 24 in 64% yield. Similar transformations can be observed for 3-(4-fluorophenyl)propan-1-ol and 4-phenylbut-3-yn-2-ol as well. Furthermore, the current protocol was extended to a wide range of reductive transformations, such as detosylations, ether debenzylation, defuntionalization of phosphates, hydrodefluorination, and cleavage of sulfones (Section 9c, SI). It also extends to the degradation of quaternary ammonium salts, considered to be an environmental pollutant.[22] Additionally, trans-1,2-diol 72, a motif central to the pradimicin and benanomicin antibiotic classes, was obtained in 86% through pinacol cyclization of biphenyl-2,2'-dicarbaldehyde. Lastly, we sought to apply our optimized reaction conditions to the fragmentation of oxidized lignin model substrates. The organocatalytic photochemical fragmentation of 2-phenoxy-1-phenylethanol proceeded by C−O bond cleavage, yielding the fragmentation products 75 and 76 in good yields of 92% and 89%, respectively. The current protocol demonstrates the potential applicability in various reductive organic transformations.

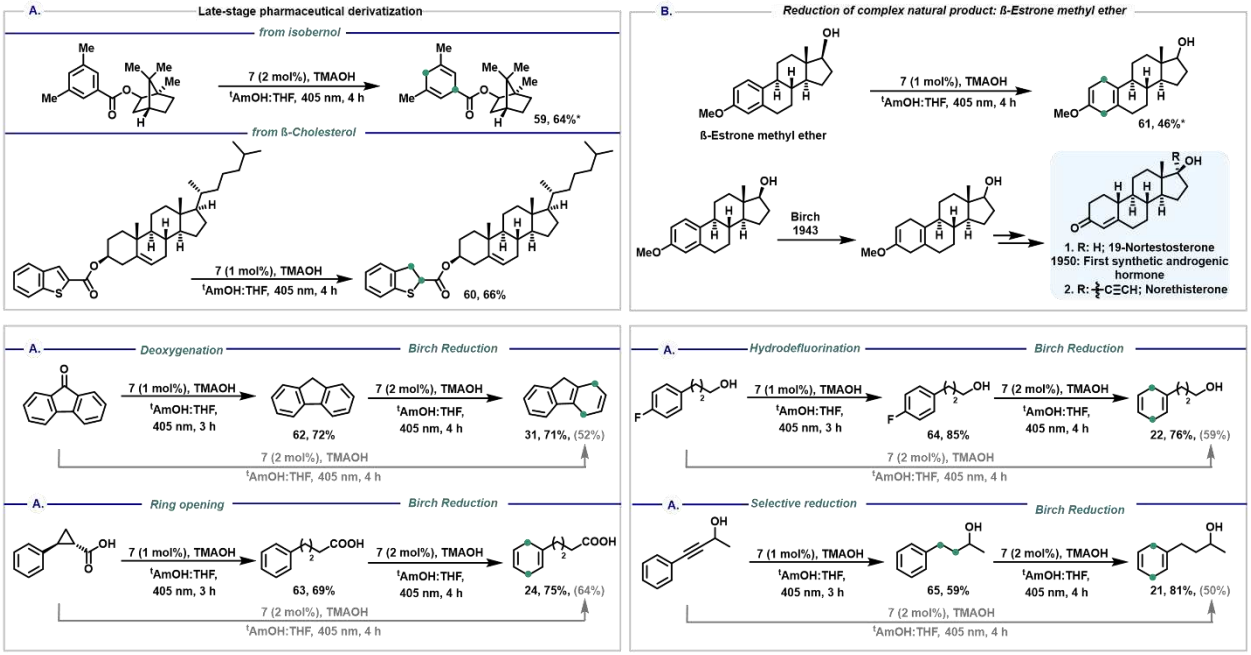

Fig 4.7. Substrate scope of complex moities for photocatalyzed Birch reduction. Reaction conditions are shown in each section and vary on reaction.

CONCLUSION

In summary, rational catalyst design based on mechanistic work of benzoperylene diesters, led to core extended BPDEs which showed improved reactivity of reducing/dearomatizing arenes with varying electronic nature. Extensive control experiments, and spectroscopic analysis helped us discover photoannulation in bay-substituted benzo[ghi]perylene of core extended which led us to prepare and study diester-functionalized benzo[a]coronene model system as a new class of strongly reducing photocatalysts (PC). The catalytic efficiency of the photocatalyst has been demonstrated by successful photoreduction of electron-poor and electron-rich arenes possessing different functional groups (e.g., alcohol, a carboxylic acid, unprotected amines, and cyclic ether motif), at ambient temperature driven by visible light in 4 hours. Thorough mechanistic understanding reveals a two electron, one-proton closed-shell species as super-reductant with excited state potential -3.56 V vs SCE which corroborates well with its strong reducing behavior.

REFERENCES

1. A. J. Birch, J. Chem. Soc. 430−436 (1944); b) A. J. Birch, Pure Appl. Chem. 68, 553−556 (1996); c) J. Burrows, S. Kamo, K. Koide, Science 374, 741−746 (2021)

2. P. Emmett, N. Skau, J. Am. Chem. Soc. 65, 1029-1035 (1943); b) Z. X. Giustra, J. S. A. Ishibashi, S. Y. Liu, Coord. Chem. Rev. 314, 134 –181 (2016); c) B. I. Yoo, Y. J. Kim, Y. You, J. W. Yang, S. W. Kim, J. Org. Chem. 83, 13847–13853 (2018).

3. a) A. J. Birch, Nature 158, 60−6 (1946); b) B. K. Peters, K. X. Rodriguez, S. H.Reisberg, S. B. Beil, D. P. Hickey, Y. Kawamata, M. Collins, J. Starr, L. Chen, S. Udyavara, K. Klunder, T. J. Gorey, S. L. Anderson, M. Neurock, S. D. Minteer, P. S. Baran Science 363, 838−845 (2019); c) K. E. Swenson, D. Zemach, C. Nanjundiah, E. Kariv-Miller, J. Org. Chem. 48, 1777–1779 (1983); d) R. A. Benkeser, E. M. Kaiser, J. Am. Chem. Soc. 85, 2858–2859 (1963); e) M. Bordeau, C. Biran, P. Pons, M. P. Leger-Lambert, J. Dunogues, J. Org. Chem. 57, 4705–4711 (1992); f) M. Ishifune, H. Yamashita , Y. Kera, N. Yamashita, K. Hirata, H. Murase, S. Kashimura Electrochim. Acta 48, 2405–2409 (2003).

4. a) J. M. R. Narayanam, C. R. Stephenson, Chem. Soc. Rev. 40, 102−113 (2011); b) C. K. Prier, D. A. Rankic, D. W. MacMillan Chem. Rev. 113, 5322−5363 (2013); c) D. M. Schultz, T. P. Yoon Science 343, 1239176 (2014); d) N. A. Romero, D. A. Nicewicz Chem. Rev. 116, 10075−10166 (2016); e) D. A. Corbin, N. A. Swisher, G. M. Miyake, Fundamentals of Photochemical Redox Reactions. In Organic Redox Chemistry: Chemical, Photochemicalnand Electrochemical Syntheses, 2021; pp 45-102; f) J. D. Bell, J. A. Murphy Chem. Soc. Rev. 50, 9540-9685 (2021); b) K. L. Skubi, T. R. Blum, T. P. Yoon, Chem. Rev. 116, 10035-10074 (2016).

5. J. Mortensen, J. Heinze, Angew. Chem., Int. Ed. 23, 84−85 (1984).

6. F. Glaser, C. Kerzig, O. S. Angew. Chem., Int. Ed. 59, 10266 (2020).

7. S. P. Roche, J. A. Porco, Angew. Chem. Int. Ed. 50, 4068 – 4093 (2011).

8. W. C. Wertjes, E. H. Southgate, D. Sarlah, Chem. Soc. Rev. 47, 7996–8017 (2018).

9. P. Lei, Y. Ding, X. Zhang, A. Adijiang, H. Li, Y. Ling, Org. Lett. 20, 3439−3442 (2018).

10. a) A. Chatterjee, B. Konig Angew. Chem., Int. Ed. 58, 14289−14294 (2019); b) S. Wu, F. Schiel, P. Melchiorre Angew. Chem. Int. Ed. 2023, 62, e20230636; c) J. P. Cole, D. F. Chen, M. Kudisch, R. M. Pearson, C. H. Lim, G. M. Miyake, J. Am. Chem. Soc. 142, 13573-13581 (2020); d) M. Yasuda, C. Pac, H. Sakurai, J. Org. Chem. 46, 788−792 (1981); K. Mizuno, H. Okamoto, C. Pac, H. Sakurai, J. Chem. Soc. Chem. Commun. 839 –840 (1975); M. Yasuda, C. Pac, H. Sakurai, J. Org. Chem. 46, 788–792 (1981); Y. Yoshimi, A. Ishise, H. Oda, Y. Moriguchi, H. Kanezaki, Y. Nakaya, K. Katsuno, T. Itou, S. Inagaki, T. Morita, M. Hatanaka, Tetrahedron Lett. 49, 3400–3404 (2008); T. McCallum, S. P. Pitre, M. Morin, J. C. Scaiano, L. Barriault, Chem. Sci. 8, 7412–7418 (2017)

11. J. C. Theriot, C. H. Lim, H. Yang, M. D. Ryan, C. B. Musgrave, G. M. Miyake, Science 352, 1082−1086 (2016); b) R. M. Pearson, C. H. Lim, B. G. McCarthy, C. B. Musgrave, G. M.

Miyake, J. Am. Chem. Soc. 138, 11399−11407 (2016); c) B. L. Buss, C. L. Lim, G. M. Miyake, Angew. Chem., Int. Ed. 59, 3209−3217 (2020)

12. Cole, J. P.; Chen, D. F.; Kudisch, M.; Pearson, R. M.; Lim, C. H.; Miyake, G. M., Organocatalyzed Birch Reduction Driven by Visible Light. *J. Am. Chem. Soc.* 2020, *142* (31), 13573-13581.

13. A. Sau, N. F. Pompetti, A. R. Green, M. V. Popescu, R. S. Paton, G. M. Miyake, N. H. D. ACS Catal. 2024, 14, 4, 2252–2263.

14. S. Guha, F. S. Goodson, L. J. Corson, S. Saha, J. Am. Chem. Soc. 134, 13679−13691 (2012); b) S. Saha, Acc. Chem. Res. 51, 2225−2236 (2018); c) F. S. Goodson, D. K. Panda, S. Ray, A. Mitra, S. Guha, S. Saha, Org. Biomol. Chem. 11, 4797−4803 (2013)

15. H. Ito, Y. Segawa, K. Murakami, K. Itami J. Am. Chem. Soc. 141, 3-10 (2019); H. Ito, K. Ozaki, K. Itami Angew. Chem. Int. Ed. 56, 11144-11164 (2017).

16. S. Kumar, Y. T. Tao, Chem. Asian J. 16, 621−647 (2021)

17. A. J. Birch, J. Chem. Soc. 809–813 (1945); H. Iio, M. Isobe, T. Kawai, T. Goto, Tetrahedron 35, 941–948 (1979); R. A. Archer, W. B. Blanchard, W. A. Day, D. W. Johnson, E. R. Lavagnino, C. W. Ryan, J. E. Baldwin J. Org. Chem. 42, 2277–2284 (1977).

18. J. Almena, F. Foubelo, M. Yus, Tetrahedron 51, 3365−3374 (1995).

19. c b) F. Zhang, H. S. Sasmal, C. G. Daniliuc, F. Glorius J. Am. Chem. Soc. 145, 15695-15701 (2023); c) W. Chen, Z. Yao, W. Chen, Q. Shen, D. Yuan, C. Zhang, Y. Zhu, H. W. Liang, Y. G. Wang, W. Song, C. Cao ACS Catal. 13, 12153−12162 (2023)

20. A. L. Wilds, N. A. Nelson J. Am. Chem. Soc. 75, 5366–5369 (1953)

21. S. Simić, E. Zukić, L. Schmermund, K. Faber, C. K. Winkler, W. Kroutil Chem. Rev. 122, 1052–1126 (2022)

22. U. Tezel, S. G. Pavlostathis Curr. Opin. Biotechnol. 33, 296−304 (2015)

APPENDIX A: SUPPLEMENTARY INFORMATION FOR CHAPTER 2

1. General experimental details

All experiments were performed under nitrogen atmosphere by using standard Schlenk technique or in a glove box, if not stated otherwise. All air- and moisture-insensitive reactions were carried out under ambient atmosphere and monitored by thin-layer chromatography (TLC). Concentration under reduced pressure was performed by rotary evaporation at 25–40 °C at an appropriate pressure. Purified compounds were further dried under a high vacuum. Yields refer to purified and spectroscopically pure compounds. All air- and moisture-sensitive manipulations were performed using oven-dried glassware (120 °C for a minimum of 24 hours) and standard Schlenk techniques under an atmosphere of nitrogen.

Photoreactor and light sources:

The photoreactor used was custom designed and built by our lab and the specifications have been published previously.[1] All light-emitting diodes (LEDs) used were purchased from LED Engin and full emission spectra, as well as peak wavelength shift vs. temperature data, are available online in the respective manufacturer datasheets. In the photoreactor, blue LEDs run at 700mA and a forward voltage of 13.5V. The mini fan (Manufacturer Product Number: THA0412AD) from Delta Electronics, Inc. The rest of the materials were produced in our laboratory using a 3D printer. The distance from the LED emitter surface to the vial is 5.0 mm (small scale reaction) and 10.0 mm (large-scale reaction).

Please see the datasheet for more details:

https://media.osram.info/media/img/osram-dam-5412925/LED_Engin_Datasheet_LuxiGen_LZ4-00UB00_rev1.pdf

Table S2.1. Light source specifications

LED peak wavelength	Luminous Flux	Manufacturer
365 nm	3.3 W @ 700 mA, 15.5 V	LED Engin
395 nm	4.1 W @ 700 mA, 15.5 V	LED Engin
405 nm	4.1 W @ 700 mA, 13.5 V	LED Engin
456 nm	4.1 W @ 700 mA, 13.5 V	LED Engin
Cool White	4.1 W @ 700 mA, 13.5 V	LED Engin
523 nm	4.1 W @ 700 mA, 13.5 V	LED Engin

Table S2.2. Photoreactor specifications

Photoreactor part	Specifications	Manufacturer
60 mm fan	51.7 cfm airflow at 750 mA, 12 V	Delta Electronics
40 mm fan	20.56 cfm airflow at 430 mA, 12 V	Delta Electronics
Fan power supply	12 V, 240 W, switching	Mean Well
LED power supply	18 V, 150 W, switching	Cincon
LED driver	Output: Input V – 2.5 V, 700 mA	LEDdynamics
Heatsink	2.75'' diameter, 3'' thick aluminum	Wakefield
Reaector chambor	Fits 40 mm fan, 65 mm heatsink	3D-Printed
Vial Holder	3D-printed N/A, 0.5 dram, 1.5 dram, or 20mL	3D-Printed

Solvent:

Tetrahydrofuran (THF), dimethylformamide (DMF), dichloromethane (DCM), and toluene were dried using a solvent purification system from MBRAUN Inertgas-Systeme GmbH. Dry dimethylacetamide (DMac), acetonitrile (MeCN), dimethyl sulfoxide (DMSO), acetone, methanol (MeOH), ethyl acetate (EtOAc), ethanol (EtOH), isopropyl alcohol (*i*PrOH), pyridine, *tert*-Amyl alcohol (*tert*-AmylOH), toluene and *n*-Hexane were purchased from Acros Organics, degassed, and purged with argon prior to use. All solvents are stored in the glovebox. Deuterated solvents were ordered from Oakwood Chemical and stored over molecular sieves.

Photoredox catalysts:

The photoredox catalysts **MesAcr(BF$_4$)**, **Fluorescein-Na**, **[Ir(dtbbpy)(ppy)$_2$]PF$_6$**, **[Ru(bpy)$_3$]Cl$_2$**, **Eosin Y** and **Rose Bengal** were used as received from commercial suppliers. The photoredox catalysts (**PDI**[2], **NpMI**[3], **BPI**[1] and **4CzIPN**[4]) were prepared according to the literature procedures.

Starting materials:

All substrates and reagents were used as received from commercial suppliers or prepared according to published procedures, respectively, unless otherwise stated. *Tetra*-methylammonium hydroxide (Me_4NOH), *tetra*-nbutylammonium fluoride (nBu_4NF), *tetra*-nbutylammonium chloride (nBu_4NCl), *tetra*-nbutylammonium bromide (nBu_4NBr), *tetra*-ethylammonium fluoride (Et_4NF), *tetra*-methylammonium fluoride (Me_4NF) and *tert*-Amyl alcohol (*tert*-AmylOH) were stored in the glovebox. Diethylaminosulfur trifluoride (DAST) was stored in refrigerator in the glovebox. Fluorinated polymers were synthesized using known literature procedures.[5-8]

Chromatography:

Analytical thin layer chromatography (TLC) was performed using pre–coated Merck glass backed silica gel plates (Silicagel 60 F254). Visualization was achieved using ultraviolet light (254 nm) and chemical staining with ceric ammonium molybdate or basic potassium permanganate solutions as appropriate. Flash column chromatography was undertaken on Fluka or Material Harvest silica gel (230–400 mesh) under a positive pressure of air. Flash chromatography purification system (Combiflash® Rf 150) was also used to purify the products.

Spectroscopy and Instruments:

Chemical shifts are reported in ppm relative to the deuterated solvent. Coupling constants are expressed in Hertz (Hz). The following abbreviations are used: s= singlet, d= doublet, t= triplet, q= quartet, h= heptet, br= broad and m= multiplet. NMR spectra were recorded at ambient temperature on either a Bruker Ultrashield-400 (400 MHz) spectrometer, a Varian 400 MR (400 MHz) spectrometer or an Agilent Inova 400 (400 MHz) spectrometer in the Colorado State University Analytical Resources Core (ARC). Gas chromatography (GC) analyses were performed on a Trace 1310 chromatograph with a 29 m HP5 column. The reported GC yields, and conversions are based on a calibrated area of mesitylene as the internal standard. The reported ^{1}H-NMR yields and conversions are based on a calibrated area of 1,3,5-trimethoxybenzene as internal standard. High Resolution Mass spectroscopy (HRMS) analysis was performed on a 6224 Time-of-Flight LC/MS (Agilent) at Colorado State University Central Instrument Facility. Ultraviolet-visible (UV-Vis) spectroscopy was performed on a Cary 5000 spectrophotometer. All samples were analyzed in 1.0 cm pathlength quartz cuvettes. Emission spectra were collected on an SLM 8000C fluorimeter. Emission spectra are affected by the instrumental setup in addition to the signal from the molecule alone. Because of this, the collected data was corrected for the instrument-specific response by application of a correction file associated with a specific configuration of the fluorimeter. Most of the data collected herein utilized a configuration in which the slits before and after each monochromator were set to 2 nm, and so a correction file generated under those conditions was used to correct the data. TCSPC measurements were made using a DeltaFlex Modular Fluorescence Lifetime System from Horiba Scientific. A Horiba NanoLED-405L was used as the excitation source (402 nm center-wavelength [CWL], c. 220 ps full-width at half maximum [FWHM]). Temperatures were measured with a built-in digital temperature sensor in the Horiba device. Temperature was controlled by a Quantum Northwest TC-1 temperature control

unit coupled with an aquarium pump submerged in a reservoir, and a jacketed sample holder. Cyclic voltammograms were obtained using a Gamry electrochemical analyzer with an $Ag/AgNO_3$ (0.01 M in acetonitrile) reference electrode and tetrabutylammonium hexafluorophosphate ($TBAPF_6$) (0.1 M in DMAc) as the electrolyte for the working electrode. All samples were analyzed in DMAc at a concentration between 0.06 mM and 1 mM (depending on solubility) at a total volume of 25.0 mL and were sparged with nitrogen for 15 minutes before data collection. Platinum was used for the working and counter electrodes. Analysis was conducted at scan rates of 100 mV/s, 80 mV/s, 50 mV/s, and 20 mV/s with 7 cycles each. Data from the 6^{th} cycle was analyzed unless otherwise noted. All voltammograms were corrected using the $E_{1/2}$ of ferrocene as a reference. Molecular weights were determined by Gel Permeation Chromatography (GPC) coupled with multi-angle light scattering (MALS) using an Agilent HPLC fitted with one guard column, three PL-gel 5 μm MIXED-C gel permeation columns, a Wyatt Technology TrEX differential refractometer, and a Wyatt Technology mini-DAWN TREOS light scattering detector (MALS).

2. Pictures of photoreactor set-up

(1) Small-scale photoreactor (0.2 mmol and 0.5 mmol)

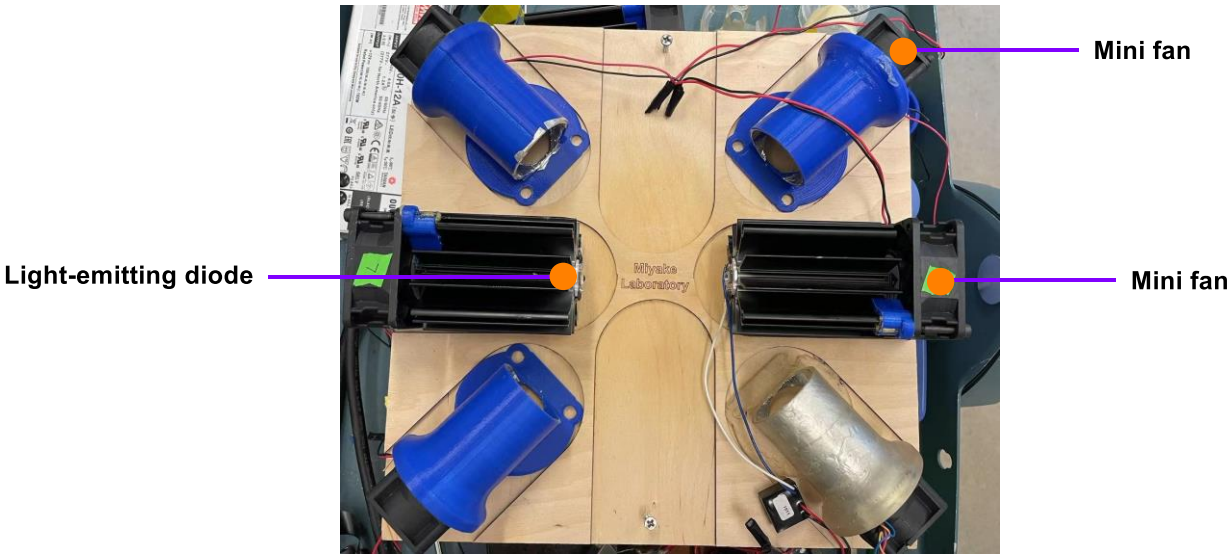

(2) Large-scale photoreactor (2.0 mmol and 10.0 mmol)

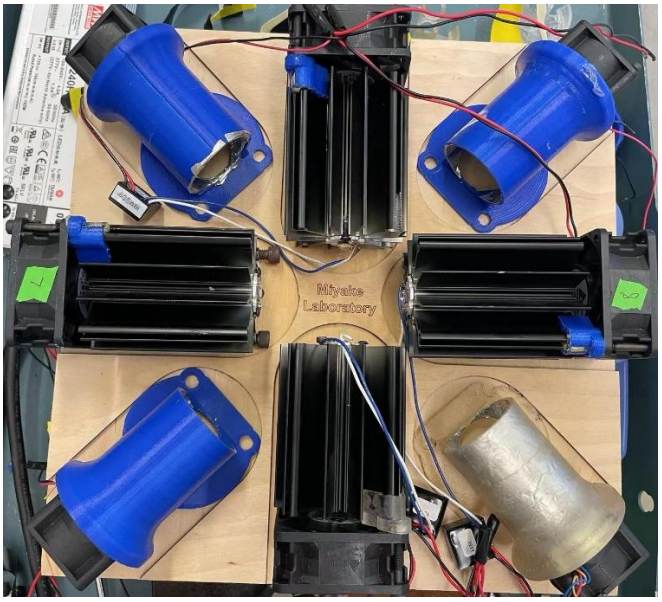

(3) Reaction set-up for irradiation of mixtures with blue LEDs

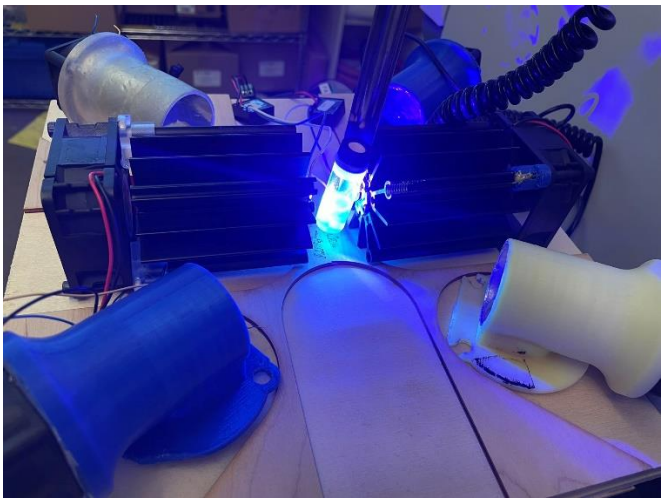

Table S2.3. The temperature of vial during the reaction

	without irradiation	with irradiation	
		20 min	60 min
IKA electronic contact thermometer	20.1 ºC	22.1 ºC	23.2 ºC
IR thermometer	21.7 ºC	22.4 ºC	22.7 ºC

***NOTE**: The temperature in the lab was 19.7 ºC when testing the vial's temperature.*

3. Hydrodefluoronation of aryl and alkyl fluorides

3.1 Reaction optimization

General procedure for optimization studies

In a glovebox, a 5 mL glass vial containing a stirring bar was sequentially charged with photocatalyst (2.5 μmol, 0.5 mol%), electron donor (1.5 mmol, 3.0 equiv.), and solvent (1.5 mL).

The mixture was stirred for 20 minutes at 23 °C. Subsequently, the starting materials (0.5 mmol) and *tert*-AmylOH (2.5 mmol, 5.0 equiv.) were added in one portion. The glass vial was placed into the light reactor and stirred for 16 h. The temperature was kept at approximately 23 °C through cooling with six mini fans. After the specified time, the mixture was diluted with ethyl acetate and analyzed by GC using mesitylene as the internal standard.

Table S2.4. Hydrodefluoronation of fluorobenzene 1 with different photoredox catalysts.

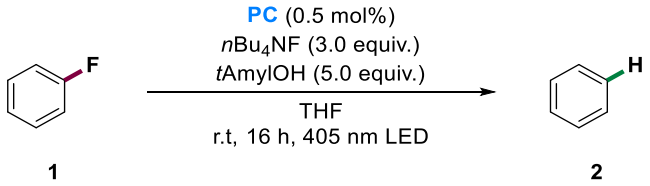

entry	**PC** (0.5 mol%)	conversion of **1** (%)	yield of **2** (%)
1	**PDI**	0	0
2	**NpMI**	12	7
3	**BPI**	99	88
4	**MesAcr(BF$_4$)**	0	0
5	**Fluorescein-Na**	0	0
6	**[Ir(dtbbpy)(ppy)$_2$]PF$_6$**	0	0
7	**[Ru(bpy)$_3$]Cl$_2$**	0	0
8	**4CzIPN**	0	0
9	**Eosin Y**	0	0
10	**Rose Bengal**	0	0

*Reaction conditions: **1** (0.5 mmol), **PC** (0.5 mol%), nBu$_4$NF (1.5 mmol, 1.5 mL, 1.0M in THF), tert-AmylOH (2.5 mmol, 5.0 equiv.), r.t (23 °C), 16 h, THF, 405 nm LED. The conversion and yields were determined by GC using mesitylene as the internal standard.*

Table S2.5. Hydrodefluoronation of fluorobenzene 1 with different light sources.

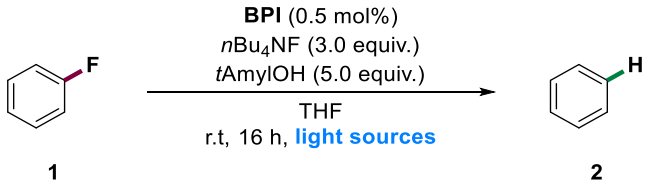

entry	light source	conversion of **1** (%)	yield of **2** (%)
1	365 nm	5	4
2	395 nm	99	87
3	405 nm	99	88
4	427 nm[a]	40	17
5	456 nm	57	45
6	Cool White	0	0
7	523 nm	0	0

*Reaction conditions: **1** (0.5 mmol), **BPI** (0.5 mol%), nBu$_4$NF (1.5 mmol, 1.5 mL, 1.0M in THF), tert-AmylOH (2.5 mmol, 5.0 equiv.), r.t (23 °C), 16 h, light source. The conversion and yields were determined by GC using mesitylene as the internal standard. [a] Kessil LED lights was used.*

***Note:** Kessil LED lights as a well-used light source in photocatalytic reaction, do not perform well in our system.*

Table S2.6. Hydrodefluoronation of fluorobenzene 1 with different hydrogen sources.

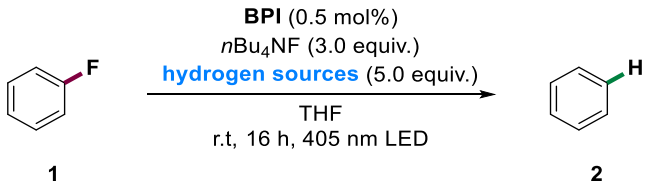

entry	hydrogen source	conversion of **1** (%)	yield of **2** (%)
1	-	21	17
2	H_2O (15.2 equiv.)	0	0
3	$HSCH_2CO_2Me$ (5.0 equiv.)	0	0
4	DMF (12.5 equiv.)	16	14
5	DMSO (12.3 equiv.)	0	0
6	MeOH (5.0 equiv.)	37	33
7	EtOH (5.0 equiv.)	57	42
8	*i*PrOH (5.0 equiv.)	68	65
9	*tert*-AmylOH (5.0 equiv.)	99	88
10	Glycerol (5.0 equiv.)	20	17
11	Benzyl alcohol (5.0 equiv.)	19	11
12	MeOH (14.8 equiv.)	98	85
13	MeOH (10.0 equiv.)	96	81
14	EtOH (10.0 equiv.)	99	84
15	*i*PrOH (10.0 equiv.)	>99	83

*Reaction conditions: **1** (0.5 mmol), **BPI** (0.5 mol%), nBu4NF (1.5 mmol, 1.5 mL, 1.0M in THF), hydrogen source, r.t (23 °C), 16 h, 405 nm LED. The conversion and yields were determined by GC using mesitylene as the internal standard.*

Table S2.7. Hydrodefluoronation of fluorobenzene 1 with different electron donors

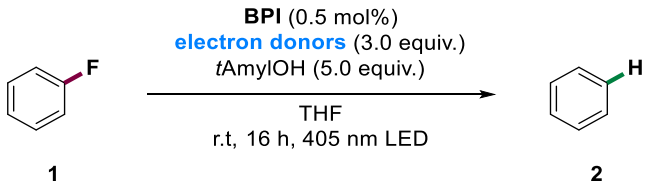

entry	electron donors (3.0 equiv.)	conversion of **1** (%)	yield of **2** (%)
1	Et_3N (soluble)	0	0
2	iPr_2NEt (soluble)	0	0
3	DIPEA (soluble)	0	0
4	DABCO (soluble)	0	0
5	nBu_4NF (soluble)	99	88
6	nBu_4NCl (slightly soluble)	<5	3
7	nBu_4NBr (insoluble)	0	0
8	nBu_4NI (insoluble)	0	0
9	nBu_4NPF_6 (insoluble)	0	0
10	$nBu_4N(HSO_4)$ (insoluble)	0	0
11	$nBu_4NF(OCOCH_3)$ (insoluble)	0	0
12	$nBu_4N(SCN)$ (insoluble)	0	0
13	$nBu_4N(OCOC_6H_5)$ (insoluble)	0	0
14	$nBu_4N(CF_3SO_3)$ (insoluble)	0	0
15	Et_4NF (soluble)	80	67
16	Me_4NF (insoluble)	11	<3
17	Me_4NOH (soluble)	77	56

*Reaction conditions: **1** (0.5 mmol), **BPI** (0.5 mol%), electron donors (1.5 mmol, 3.0 equiv.), tert-AmylOH (2.5 mmol, 5.0 equiv.), THF (1.5 mL), r.t (23 °C), 16 h, 405 nm LED. The conversion and yields were determined by GC using mesitylene as the internal standard.*

Table S2.8. Hydrodefluoronation of fluorobenzene 1 with different fluoride sources

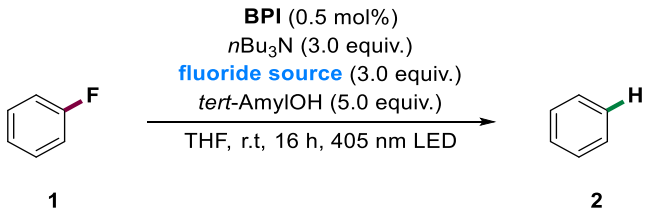

entry	fluoride sources	conversion of **1** (%)	yield of **2** (%)
1	KF (insoluble)	0	0
2	KHF_2 (insoluble)	0	0
3	CsF (insoluble)	0	0
4	CuF_2 (insoluble)	0	0
5	LiF (insoluble)	0	0
6	NaF (insoluble)	0	0
7	$LiPF_6$ (soluble)	0	0
8	Me_4NF (insoluble)	0	0

*Reaction conditions: **1** (0.5 mmol), **BPI** (0.5 mol%), nBu_3N (1.5 mmol, 3.0 equiv.), fluoride source (1.5 mmol, 3.0 equiv.), tert-AmylOH (2.5 mmol, 5.0 equiv.), THF (1.5 mL), r.t (23 °C), 16 h, 405 nm LED. The conversion and yields were determined by GC using mesitylene as the internal standard.*

3.2 Substrate scope for organic fluorides

General procedure for the dehalogenation of alkyl and aryl fluorides (**GP-1**)

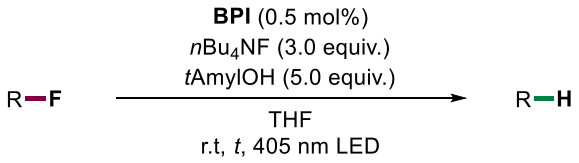

In a glovebox, a 5 mL glass vial containing a stirring bar was sequentially charged with **BPI** (2.5 μmol, 0.5 mol%) and *n*Bu_4NF (1.5 mmol, 1.5 mL, 3.0 equiv., 1.0M in THF). The mixture was stirred for 20 minutes at 23 °C, and the color changes from orange to light green. Subsequently, the organic fluorides (0.5 mmol) and *tert*-AmylOH (2.5 mmol, 5.0 equiv.) were added in one portion. The glass vial was placed into the light reactor and stirred for corresponding time. The temperature was kept at approximately 23 °C through cooling with six mini fans. After reaction, the crude mixture was purified by column chromatography on silica gel to afford the desired products.

Note: 1) Highly volatile or lower boiling point fluorinated substrates were added outside the glove box using a syringe; 2) CombiFlash Rf Flash Chromatography System was used to purify the product (40 g HP Silica was used).

Benzene (2)

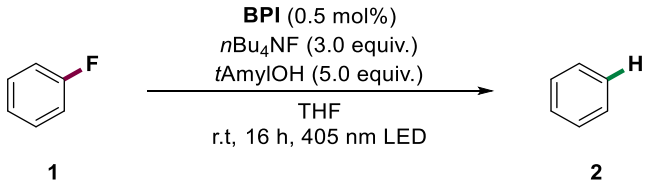

According to the **GP-1**, **BPI** (1.9 mg, 0.5 mol%), fluorobenzene (48 mg, 0.50 mmol), *n*Bu$_4$NF (1.5 mmol, 1.5 mL, 3.0 equiv., 1.0M in THF) and *tert*-AmylOH (2.5 mmol, 5.0 equiv.) were converted. After being stirred for 16 h, mesitylene (60 mg, 0.5 mmol) was added as internal standard. The yield of the title compound **2** was determined by GC using mesitylene as the internal standard (88.2% yield).

***N,N*-dimethyl-aniline (3)**

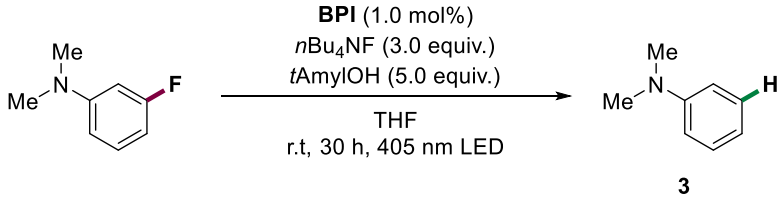

According to the **GP1**, **BPI** (3.9 mg, 1.0 mol%), *N*,*N*-dimethyl 3-fluoroaniline (75 mg, 0.50 mmol), *n*Bu$_4$NF (1.5 mmol, 1.5 mL, 3.0 equiv., 1.0M in THF) and *tert*-AmylOH (2.5 mmol, 5.0 equiv.) were converted. After being stirred for 30 h, the reaction mixture was purified by chromatography on silica gel eluting with *n*-hexane/ ethyl acetate (50: 1) to afford **3** (33.4 mg, 55.2% yield) as a colorless oil.

^{1}H-NMR (400 Hz, $CDCl_3$, 25 °C) δ= 7.40 – 7.30 (m, 2H), 6.92 – 6.76 (m, 3H), 3.04 (s, 6H) ppm.

^{13}C-NMR (101 Hz, $CDCl_3$, 25 °C) δ= 150.74, 129.14, 116.70, 112.73, 40.66 ppm.

The spectroscopic data corresponds to those reported in literature.[9]

Benzonitrile (4)

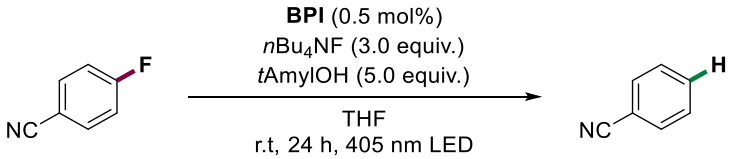

4

According to the **GP1**, **BPI** (1.9 mg, 0.5 mol%), 4-fluorobenzonitrile (60.5 mg, 0.500 mmol), *n*Bu$_4$NF (1.5 mmol, 1.5 mL, 3.0 equiv., 1.0M in THF) and *tert*-AmylOH (2.5 mmol, 5.0 equiv.) were converted. After being stirred for 24 h, mesitylene (60 mg, 0.5 mmol) was added as internal standard. The yield of the title compound **4** was determined by GC relative to the internal standard (73.4% yield).

Methyl benzoate (5)

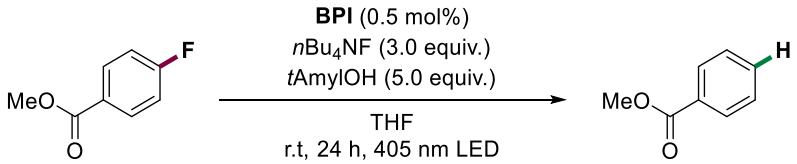

5

According to the **GP1**, **BPI** (1.7 mg, 0.5 mol%), methyl 4-flurobenzoate (77 mg, 0.50 mmol), *n*Bu$_4$NF (1.5 mmol, 1.5 mL, 3.0 equiv., 1.0M in THF) and *tert*-AmylOH (2.5 mmol, 5.0 equiv.) were converted. After being stirred for 24 h, the reaction mixture was purified by chromatography on silica gel eluting with *n*-hexane/ ethyl acetate (50: 1) to afford **5** (47.7 mg, 70.2% yield) as a colorless oil.

^{1}H-NMR (400 Hz, $CDCl_3$, 25 °C) δ= 8.10 – 8.00 (m, 2H), 7.60 – 7.52 (m, 1H), 7.49 – 7.40 (m, 2H), 3.92 (s, 3H) ppm.

^{13}C-NMR (101 Hz, $CDCl_3$, 25 °C) δ= 167.27, 133.05, 130.32, 129.72, 128.50, 52.25 ppm.

The spectroscopic data corresponds to those reported in literature.[10]

Methylbenzene (6-a)

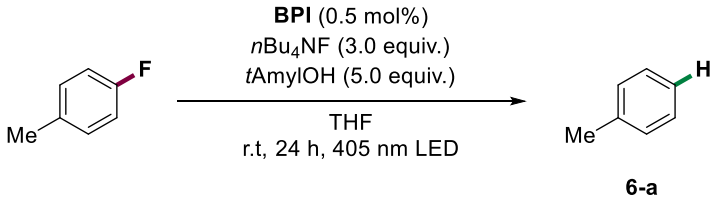

6-a

According to the **GP1**, **BPI** (1.9 mg, 0.5 mol%), 4-methylfluorobenzene (55 mg, 0.50 mmol), *n*Bu$_4$NF (1.5 mmol, 1.5 mL, 3.0 equiv., 1.0M in THF) and *tert*-AmylOH (2.5 mmol, 5.0 equiv.) were converted. After being stirred for 24 h, mesitylene (60 mg, 0.5 mmol) was added as internal standard. The yield of the title compound **6-a** was determined by GC relative to the internal standard (71.2% yield).

Methylbenzene (6-b)

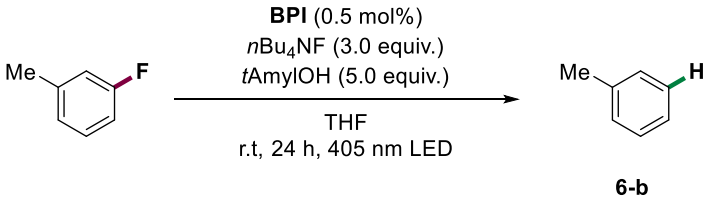

6-b

According to the **GP1**, **BPI** (1.9 mg, 0.5 mol%), 3-methylfluorobenzene (55 mg, 0.50 mmol), *n*Bu$_4$NF (1.5 mmol, 1.5 mL, 3.0 equiv., 1.0M in THF) and *tert*-AmylOH (2.5 mmol, 5.0 equiv.) were converted. After being stirred for 24 h, mesitylene (60 mg, 0.5 mmol) was added as internal standard. The yield of the title compound **6-b** was determined by GC relative to the internal standard (52.6% yield).

Methylbenzene (6-c)

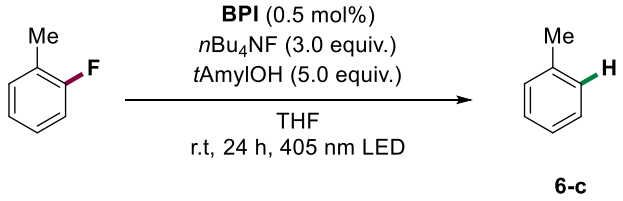

6-c

According to the **GP1**, **BPI** (1.8 mg, 0.5 mol%), 2-methylfluorobenzene (55 mg, 0.50 mmol), *n*Bu$_4$NF (1.5 mmol, 1.5 mL, 3.0 equiv., 1.0M in THF) and *tert*-AmylOH (2.5 mmol, 5.0 equiv.) were converted. After being stirred for 24 h, mesitylene (60 mg, 0.5 mmol) was added as internal standard. The yield of the title compound **6-c** was determined by GC relative to the internal standard (39.7% yield).

2-Phenylethanol (7)

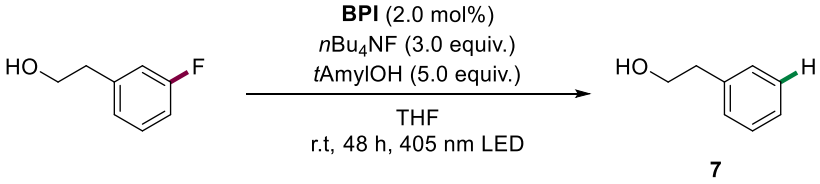

7

According to the **GP1**, **BPI** (7.6 mg, 2.0 mol%), 2-(3-fluorophenyl)ethanol (70 mg, 0.50 mmol), *n*Bu$_4$NF (1.5 mmol, 1.5 mL, 3.0 equiv., 1.0M in THF) and *tert*-AmylOH (2.5 mmol, 5.0 equiv.) were converted. After being stirred for 48 h, the reaction mixture was purified by chromatography

on silica gel eluting with *n*-hexane/ ethyl acetate (20: 1) to afford **7** (36.7 mg, 60.2% yield) as a colorless oil.

^{1}H-NMR (400 Hz, $CDCl_3$, 25 °C) δ= 7.33 (m, 2H), 7.28 – 7.19 (m, 3H), 3.87 (t, *J* = 6.8 Hz, 2H), 2.88 (t, *J* = 6.6 Hz, 2H), 1.50 (brs, 1H) ppm.

^{13}C-NMR (101 Hz, $CDCl_3$, 25 °C) δ= 138.61, 129.16, 128.72, 126.61, 63.81, 39.33 ppm.

The spectroscopic data corresponds to those reported in literature.[11]

3-Phenylpropionic acid (8)

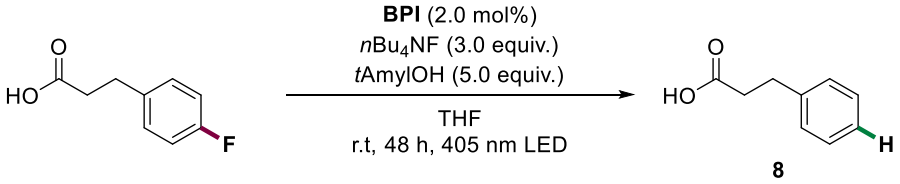

According to the **GP1**, **BPI** (7.6 mg, 2.0 mol%), 4-fluorophenylpropionic acid (84 mg, 0.50 mmol), *n*Bu_4NF (1.5 mmol, 1.5 mL, 3.0 equiv., 1.0M in THF) and *tert*-AmylOH (2.5 mmol, 5.0 equiv.) were converted. After being stirred for 48 h, the reaction mixture was purified by chromatography on silica gel eluting with *n*-hexane/ ethyl acetate (20: 1) to afford **8** (46.6 mg, 62.1% yield) as a colorless oil.

^{1}H-NMR (400 Hz, $CDCl_3$, 25 °C) δ= 11.68 (brs, 1H), 7.33 (m, 2H), 7.25 (m, 3H), 3.00 (t, *J* = 7.8 Hz, 2H), 2.72 (t, *J* = 7.8 Hz, 2H) ppm.

^{13}C-NMR (101 Hz, $CDCl_3$, 25 °C) δ= 179.63, 140.27, 128.69, 128.39, 126.51, 35.77, 30.69 ppm.

The spectroscopic data corresponds to those reported in literature.[12]

1-Indanone (9)

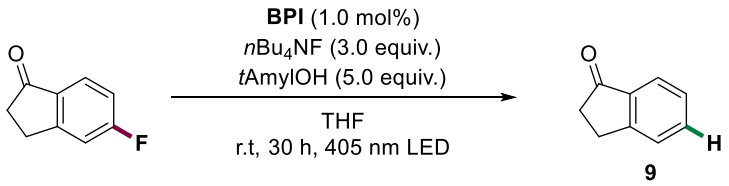

According to the **GP1**, **BPI** (3.9 mg, 1.0 mol%), 5-fluoro-1-indanone (75 mg, 0.50 mmol), nBu$_4$NF (1.5 mmol, 1.5 mL, 3.0 equiv., 1.0M in THF) and *tert*-AmylOH (2.5 mmol, 5.0 equiv.) were converted. After being stirred for 30 h, the reaction mixture was purified by chromatography on silica gel eluting with *n*-hexane/ ethyl acetate (50: 1) to afford **9** (34.9 mg, 52.9% yield) as a colorless oil.

^{1}H-NMR (400 Hz, $CDCl_3$, 25 °C) δ= 7.76 (d, *J* = 7.7 Hz, 1H), 7.62 – 7.57 (m, 1H), 7.53 – 7.44 (m, 1H), 7.38 – 7.35 (m, 1H), 3.18 – 3.13 (m, 2H), 2.72 – 2.67 (m, 2H) ppm.

^{13}C-NMR (101 Hz, $CDCl_3$, 25 °C) δ= 207.22, 155.31, 137.26, 134.74, 127.44, 126.85, 123.88, 36.37, 25.96 ppm.

The spectroscopic data corresponds to those reported in literature.[13]

Pyridine (10)

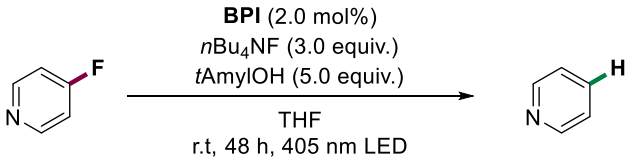

10

According to the **GP1**, **BPI** (7.6 mg, 2.0 mol%), 4-fluoropyridine (48.5 mg, 0.500 mmol), *n*Bu$_4$NF (1.5 mmol, 1.5 mL, 3.0 equiv., 1.0M in THF) and *tert*-AmylOH (2.5 mmol, 5.0 equiv.) were converted. After being stirred for 48 h, mesitylene (60 mg, 0.5 mmol) was added as internal standard. The yield of the title compound **10** was determined by GC relative to the internal standard (30.8% yield).

Adamantane (11)

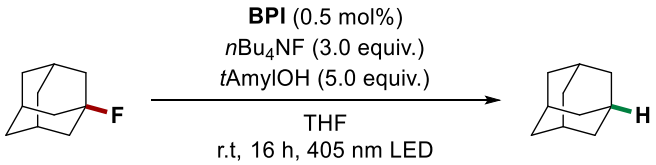

11

According to the **GP1**, **BPI** (1.9 mg, 0.5 mol%), 1-fluoroadamantane (77 mg, 0.50 mmol), *n*Bu$_4$NF (1.5 mmol, 1.5 mL, 3.0 equiv., 1.0M in THF) and *tert*-AmylOH (2.5 mmol, 5.0 equiv.) were converted. After being stirred for 16 h, mesitylene (60 mg, 0.5 mmol) was added as internal standard. The yield of the title compound **11** was determined by GC relative to the internal standard (81.0% yield).

***tert*-Butyl piperidinecarboxylate (12)**

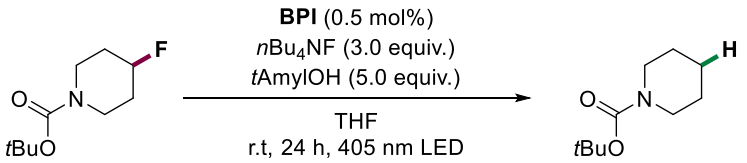

12

According to the **GP1**, **BPI** (1.9 mg, 0.5 mol%), *tert*-butyl 4-fluoropiperidine-1-carboxylate (102 mg, 0.500 mmol), nBu$_4$NF (1.5 mmol, 1.5 mL, 3.0 equiv., 1.0M in THF) and *tert*-AmylOH (2.5 mmol, 5.0 equiv.) were converted. After being stirred for 24 h, the reaction mixture was purified by chromatography on silica gel eluting with *n*-hexane/ ethyl acetate (10: 1) to afford **12** (78.8 mg, 81.9% yield) as a colorless oil.

^{1}H-NMR (400 Hz, $CDCl_3$, 25 °C) δ= 3.25 (m, 4H), 1.44 (m, 6H), 1.37 – 1.31 (s, 9H) ppm.

^{13}C-NMR (101 Hz, $CDCl_3$, 25 °C) δ= 154.82, 78.94, 44.59 (brs), 28.40, 25.69, 24.45 ppm.

The spectroscopic data corresponds to those reported in literature.[14]

The starting materials (*tert*-butyl 4-fluoropiperidine-1-carboxylate) were prepared according to literature procedures using standard Schlenk technique.[15]

1-Piperidinoethanol (13)

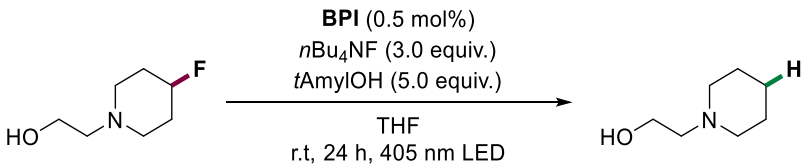

13

According to the **GP1**, **BPI** (1.9 mg, 0.5 mol%), 2-(4-fluoropiperidin-1-yl)ethanol (74 mg, 0.50 mmol), nBu$_4$NF (1.5 mmol, 1.5 mL, 3.0 equiv., 1.0M in THF) and *tert*-AmylOH (2.5 mmol, 5.0

equiv.) were converted. After being stirred for 24 h, the reaction mixture was purified by chromatography on silica gel eluting with DCM/ methanol (10: 1) to afford **13** (45.3 mg, 70.2 % yield) as a colorless oil.

^{1}H-NMR (400 Hz, $CDCl_3$, 25 °C) δ= 3.57 (t, *J* = 5.5 Hz, 2H), 3.15 (d, *J* = 10.0 Hz, 1H), 2.47 (t, *J* = 5.5 Hz, 2H), 2.41 (d, *J* = 5.9 Hz, 4H), 1.56 (p, *J* = 5.6 Hz, 4H), 1.44 (q, *J* = 6.0 Hz, 2H) ppm.

^{13}C-NMR (101 Hz, $CDCl_3$, 25 °C) δ= 60.06 57.88, 54.45, 26.19, 24.49 ppm.

The spectroscopic data corresponds to those reported in literature.[16]

The starting materials [2-(4-fluoropiperidin-1-yl)ethanol] were prepared according to literature procedures using standard Schlenk technique.[17]

1-Benzyloxycarbonyl piperidine (14)

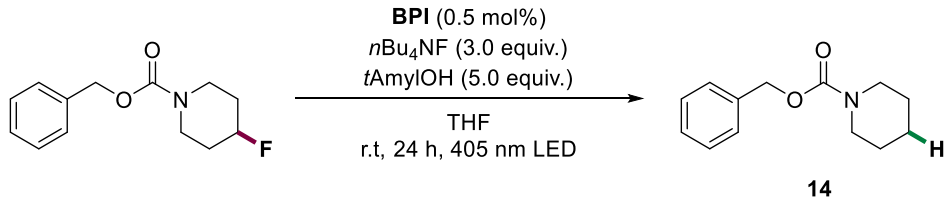

14

According to the **GP1**, **BPI** (1.9 mg, 0.5 mol%), benzyl 4-fluoro-1-piperidinecarboxylate (118 mg, 0.500 mmol), *n*Bu_4NF (1.5 mmol, 1.5 mL, 3.0 equiv., 1.0M in THF) and *tert*-AmylOH (2.5 mmol, 5.0 equiv.) were converted. After being stirred for 24 h, the reaction mixture was purified by chromatography on silica gel eluting with *n*-hexane/ ethyl acetate (10: 1) to afford **14** (69.0 mg, 63.1% yield) as white solid.

^{1}H-NMR (400 Hz, $CDCl_3$, 25 °C) δ= 7.33 (m, 5H), 5.13 (s, 2H), 3.45 (t, *J* = 5.3 Hz, 4H), 1.59 (m, 6H) ppm.

^{13}C-NMR (101 Hz, $CDCl_3$, 25 °C) δ= 155.35, 137.09, 128.48, 127.90, 127.82, 66.90, 44.90, 25.72, 24.41 ppm.

The spectroscopic data corresponds to those reported in literature.[18]

The starting materials (benzyl 4-fluoro-1-piperidinecarboxylate) were prepared according to literature procedures using standard Schlenk technique.[19]

2-Methylnaphthalene (15)

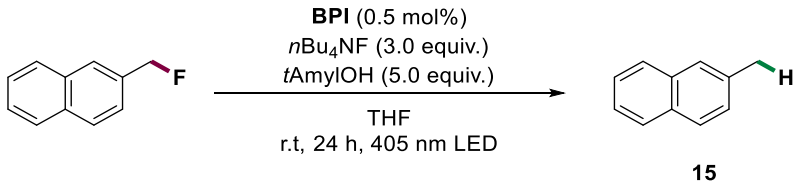

According to the **GP1**, **BPI** (1.8 mg, 0.5 mol%), 2-fluoromethylnaphthalene (80 mg, 0.50 mmol), *n*Bu_4NF (1.5 mmol, 1.5 mL, 3.0 equiv., 1.0M in THF) and *tert*-AmylOH (2.5 mmol, 5.0 equiv.) were converted. After being stirred for 24 h, the reaction mixture was purified by chromatography on silica gel eluting with *n*-hexane/ ethyl acetate (100: 1) to afford **15** (37.9 mg, 53.4% yield) as a colorless oil.

^{1}H-NMR (400 Hz, $CDCl_3$, 25 °C) δ= 7.98 – 7.82 (m, 3H), 7.74 (s, 1H), 7.58 – 7.55 (m, 2H), 7.46 (s, 1H), 2.65 (s, 3H) ppm.

^{13}C-NMR (101 Hz, $CDCl_3$, 25 °C) δ= 135.51, 133.81, 131.84, 128.22, 127.81, 127.72, 127.36, 126.96, 125.97, 125.06, 21.80 ppm.

The spectroscopic data corresponds to those reported in literature.[20]

Phenylpropane (16)

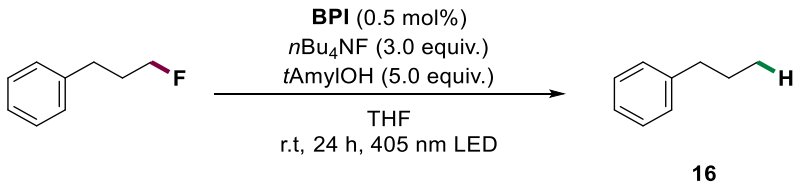

16

According to the **GP1**, **BPI** (1.9 mg, 0.5 mol%), 1-fluoro-3-phenylpropane (69 mg, 0.50 mmol), *n*Bu$_4$NF (1.5 mmol, 1.5 mL, 3.0 equiv., 1.0M in THF) and *tert*-AmylOH (2.5 mmol, 5.0 equiv.) were converted. After being stirred for 24 h, mesitylene (60 mg, 0.5 mmol) was added as internal standard. The yield of the title compound **16** was determined by GC relative to the internal standard (42.2% yield).

The starting materials (1-fluoro-3-phenylpropane) were prepared according to literature procedures using standard Schlenk technique.[19]

4-Methylanisole (17)

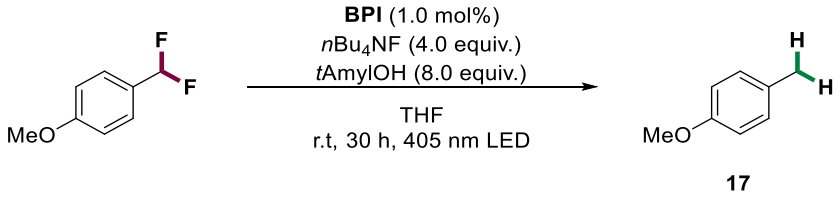

17

According to the **GP1**, **BPI** (3.9 mg, 1.0 mol%), 1-(difluoromethyl)-4-methoxybenzene (79 mg, 0.50 mmol), *n*Bu$_4$NF (2.0 mmol, 2.0 mL, 4.0 equiv., 1.0M in THF) and *tert*-AmylOH (4.0 mmol, 8.0 equiv.) were converted. After being stirred for 30 h, the reaction mixture was purified by chromatography on silica gel eluting with *n*-hexane/ ethyl acetate (30: 1) to afford **17** (42.1 mg, 69.0% yield) as a colorless oil.

^{1}H-NMR (400 Hz, $CDCl_3$, 25 °C) δ= 7.13 – 7.07 (m, 2H), 6.86 – 6.77 (m, 2H), 3.79 (s, 3H), 2.30 (s, 3H) ppm.

^{13}C-NMR (101 Hz, $CDCl_3$, 25 °C) δ= 157.61, 130.02, 113.83, 55.41, 20.58 ppm.

The spectroscopic data corresponds to those reported in literature.[21]

4-Methylbenzonitrile (18)

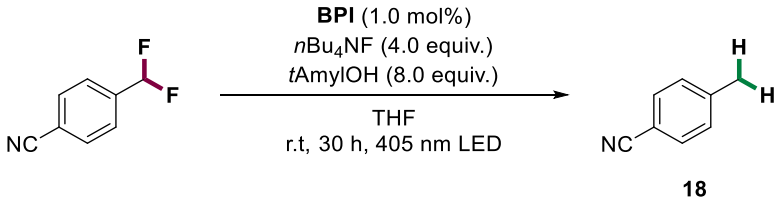

18

According to the **GP1**, **BPI** (3.8 mg, 1.0 mol%), 4-(difluoromethyl)-benzonitrile (76.5 mg, 0.500 mmol), *n*Bu_4NF (2.0 mmol, 2.0 mL, 4.0 equiv., 1.0M in THF) and *tert*-AmylOH (4.0 mmol, 8.0 equiv.) were converted. After being stirred for 30 h, the reaction mixture was purified by chromatography on silica gel eluting with *n*-hexane/ ethyl acetate (10: 1) to afford **18** (47.5 mg, 81.2% yield) as a colorless oil.

^{1}H-NMR (400 Hz, $CDCl_3$, 25 °C) δ= 7.52 – 7.50 (m, 2H), 7.24 – 7.21 (m, 2H), 2.41 (s, 3H) ppm.

^{13}C-NMR (101 Hz, $CDCl_3$, 25 °C) δ= 144.07, 132.37, 130.19, 119.50, 109.63, 22.17 ppm.

The spectroscopic data corresponds to those reported in literature.[22]

3-Methylbenzonitrile (19)

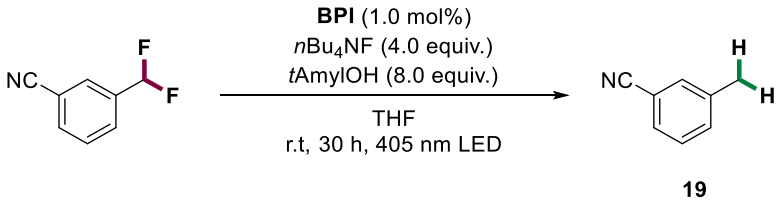

19

According to the **GP1**, **BPI** (3.8 mg, 1.0 mol%), 3-(difluoromethyl)benzonitrile (76.5 mg, 0.500 mmol), *n*Bu$_4$NF (2.0 mmol, 2.0 mL, 4.0 equiv., 1.0M in THF) and *tert*-AmylOH (4.0 mmol, 8.0 equiv.) were converted. After being stirred for 30 h, mesitylene (60 mg, 0.5 mmol) was added as internal standard. The yield of title compound **19** was determined by GC relative to the internal standard (68.3% yield).

2-Methylbenzonitrile (20)

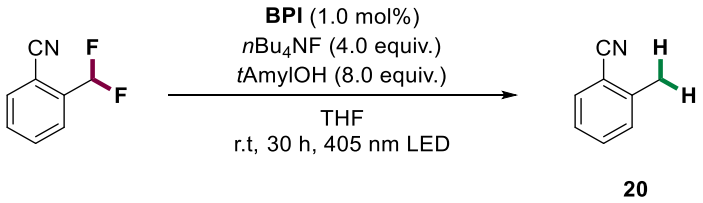

20

According to the **GP1**, **BPI** (3.9 mg, 1.0 mol%), 2-(difluoromethyl)benzonitrile (76.5 mg, 0.500 mmol), *n*Bu$_4$NF (2.0 mmol, 2.0 mL, 4.0 equiv., 1.0M in THF) and *tert*-AmylOH (4.0 mmol, 8.0 equiv.) were converted. After being stirred for 30 h, mesitylene (60 mg, 0.5 mmol) was added as internal standard. The yield of the title compound **20** was determined by GC relative to the internal standard (39.2% yield).

Methylenedioxybenzene (21)

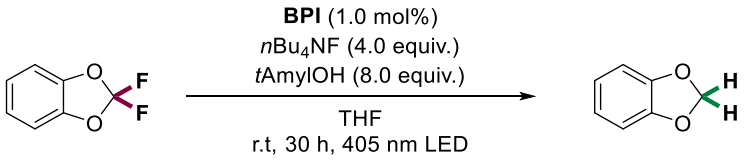

21

According to the **GP1**, **BPI** (3.9 mg, 1.0 mol%), 2,2-difluoro-1,3-benzodioxole (79 mg, 0.50 mmol), *n*Bu$_4$NF (2.0 mmol, 2.0 mL, 4.0 equiv., 1.0M in THF) and *tert*-AmylOH (4.0 mmol, 8.0 equiv.) were converted. After being stirred for 30 h, the reaction mixture was purified by chromatography on silica gel eluting with *n*-hexane/ ethyl acetate (25: 1) to afford **21** (22.7 mg, 37.3% yield) as a colorless oil.

^{1}H-NMR (400 Hz, $CDCl_3$, 25 °C) δ= 6.84 – 6.83 (m, 4H), 5.95 (d, *J* = 1.1 Hz, 2H) ppm.

^{13}C-NMR (101 Hz, $CDCl_3$, 25 °C) δ= 147.54, 121.77, 108.81, 100.74 ppm.

The spectroscopic data corresponds to those reported in literature.[23]

4-Methyl-benzoic acid methyl ester (22)

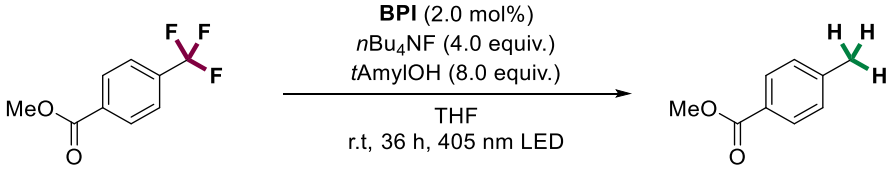

22

According to the **GP1**, **BPI** (7.6 mg, 2.0 mol%), methyl 4-(trifluoromethyl)benzoate (102 mg, 0.500 mmol), *n*Bu$_4$NF (2.0 mmol, 2.0 mL, 4.0 equiv., 1.0M in THF) and *tert*-AmylOH (4.0 mmol, 8.0 equiv.) were converted. After being stirred for 36 h, the reaction mixture was purified by chromatography on silica gel eluting with *n*-hexane/ ethyl acetate (50: 1) to afford **22** (53.0 mg, 70.7% yield) as a colorless oil.

^{1}H-NMR (400 Hz, $CDCl_3$, 25 °C) δ= 7.97 – 7.89 (m, 2H), 7.25 – 7.20 (m, 2H), 3.90 (s, 3H), 2.40 (s, 3H) ppm.

^{13}C-NMR (101 Hz, $CDCl_3$, 25 °C) δ= 167.33, 143.69, 129.75, 129.22, 127.59, 52.08, 21.79 ppm.

The spectroscopic data corresponds to those reported in literature.[24]

(4-methylphenyl)Acetonitrile (23)

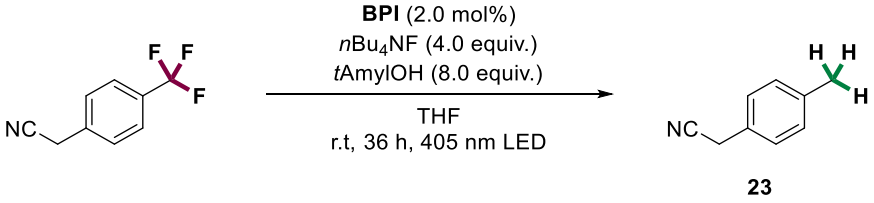

23

According to the **GP1**, **BPI** (7.6 mg, 2.0 mol%), 4-(trifluoromethyl)phenylacetonitrile (92.5 mg, 0.500 mmol), *n*Bu_4NF (2.0 mmol, 2.0 mL, 4.0 equiv., 1.0M in THF) and *tert*-AmylOH (4.0 mmol, 8.0 equiv.) were converted. After being stirred for 36 h, the reaction mixture was purified by chromatography on silica gel eluting with *n*-hexane/ ethyl acetate (50: 1) to afford **23** (37.4 mg, 57.1% yield) as a colorless oil.

^{1}H-NMR (400 Hz, $CDCl_3$, 25 °C) δ= 7.25 – 7.13 (m, 4H), 3.70 (s, 2H), 2.36 (s, 3H) ppm.

^{13}C-NMR (101 Hz, $CDCl_3$, 25 °C) δ= 137.60, 129.54, 127.57, 126.62, 117.87, 22.97, 20.81 ppm.

The spectroscopic data corresponds to those reported in literature.[25]

tert-Butyl pyrrolidine-1-carboxylate (24)

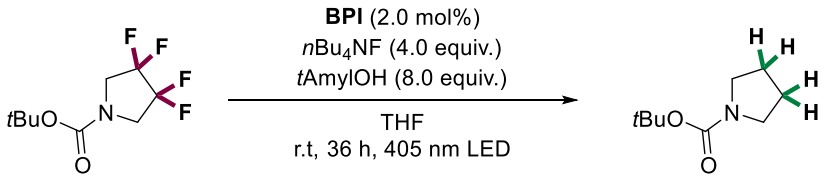

24

According to the **GP1**, **BPI** (7.6 mg, 2.0 mol%), *tert*-butyl 3,3,4,4-tetrafluoropyrrolidine-1-carboxylate (121 mg, 0.500 mmol), nBu$_4$NF (2.0 mmol, 2.0 mL, 5.0 equiv., 1.0M in THF) and *tert*-AmylOH (4.0 mmol, 8.0 equiv.) were converted. After being stirred for 36 h, mesitylene (60 mg, 0.5 mmol) was added as internal standard. The yield of title compound **24** was determined by GC relative to the internal standard (51.8% yield).

6-O-benzyl-1,2:3,4-di-O-isopropylidene-α-D-galactopyranos (25)

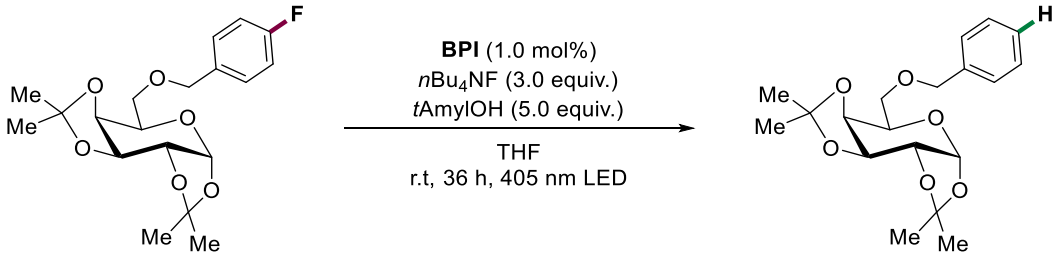

25

According to the **GP1**, **BPI** (3.8 mg, 1.0 mol%), 6-O-(4-fluorobenzyl)-1,2,3,4-di-O-isopropylidene-α-D-galactopyranoside (184 mg, 0.500 mmol), nBu$_4$NF (1.5 mmol, 1.5 mL, 3.0 equiv., 1.0M in THF) and *tert*-AmylOH (2.5 mmol, 5.0 equiv.) were converted. After being stirred for 36 h, the reaction mixture was purified by chromatography on silica gel eluting with *n*-hexane/ ethyl acetate (20: 1) to afford **25** (156 mg, 44.6% yield) as a colorless oil.

^{1}H-NMR (400 Hz, $CDCl_3$, 25 °C) δ= 7.42 – 7.30 (m, 5H), 5.55 (d, J = 5.0 Hz, 1H), 4.63 (d, J = 12.3 Hz, 1H), 4.61 – 4.58 (m, 1H), 4.56 (d, J = 9.0 Hz, 1H), 4.32 (dt, J = 4.2, 1.7 Hz, 1H), 4.28

(dd, J = 8.0, 1.8 Hz, 1H), 4.02 (t, *J* = 6.4 Hz, 1H), 3.71 (dd, *J* = 10.2, 5.9 Hz, 1H), 3.64 (dd, *J* = 10.2, 6.6 Hz, 1H), 1.45 (s, 3H), 1.34 (d, *J* = 3.1 Hz, 6H) ppm.

^{13}C-NMR (101 Hz, $CDCl_3$, 25 °C) δ= 138.46, 128.42, 127.82, 127.64, 109.31, 108.64, 96.49, 73.42, 71.30, 70.77, 70.72, 68.98, 26.22, 26.11, 25.06, 24.57 ppm.

The spectroscopic data corresponds to those reported in literature.[26]

The starting materials (6-O-(4-fluorobenzyl)-1,2,3,4-di-O-isopropylidene-α-D-galactopyranoside) were prepared according to literature procedures using standard Schlenk technique.[27]

2-(isopropyl)-5-Methylphenyl benzyl ether (26)

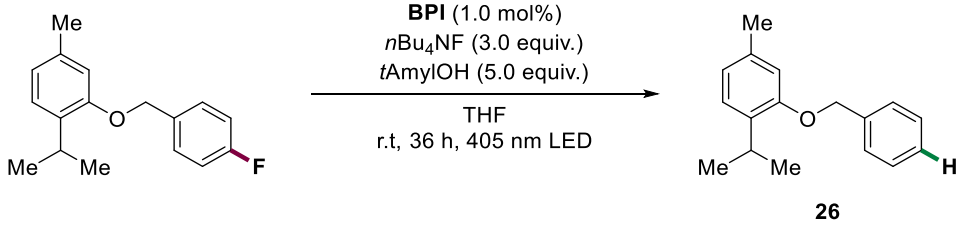

26

According to the **GP1**, **BPI** (3.9 mg, 1.0 mol%), 2-((4-fluorobenzyl)oxy)-1-isopropyl-4-methylbenzene (129 mg, 0.500 mmol), *n*Bu_4NF (1.5 mmol, 1.5 mL, 3.0 equiv., 1.0M in THF) and *tert*-AmylOH (2.5 mmol, 5.0 equiv.) were converted. After being stirred for 36 h, the reaction mixture was purified by chromatography on silica gel eluting with *n*-hexane/ ethyl acetate (25: 1) to afford **26** (84.2 mg, 70.2% yield) as white solid.

^{1}H-NMR (400 Hz, $CDCl_3$, 25 °C) δ= 7.54 – 7.51 (m, 2H), 7.47 – 7.45 (m, 2H), 7.40 – 7.38 (m, 1H), 7.20 (s, 1H), 6.89 – 6.79 (m, 2H), 5.13 (s, 2H), 3.46 – 3.43 (m, 1H), 2.40 (s, 3H), 1.31 (d, *J* = 6.9 Hz, 6H) ppm.

^{13}C-NMR (101 Hz, $CDCl_3$, 25 °C) δ= 155.97, 137.80, 136.44, 134.49, 128.63, 127.80, 127.23, 126.09, 121.58, 112.80, 70.06, 26.74, 22.96, 21.50 ppm.

The spectroscopic data corresponds to those reported in literature.[28]

The starting materials (2-((4-fluorobenzyl)oxy)-1-isopropyl-4-methylbenzene) were prepared according to literature procedures using standard Schlenk technique.[29]

***N*-benzyl-*N*-methyl-2-(pyridin-2-yl)ethanamine (27)**

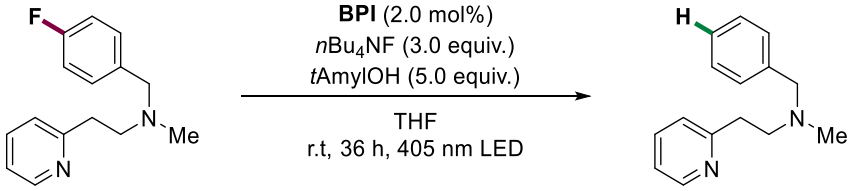

27

According to the **GP1**, **BPI** (7.6 mg, 2.0 mol%), *N*-[(4-fluorophenyl)methyl]-*N*-methyl-2-pyridin-2-ylethanamine (122 mg, 0.500 mmol), *n*Bu_4NF (1.5 mmol, 1.5 mL, 3.0 equiv., 1.0M in THF) and *tert*-AmylOH (2.5 mmol, 5.0 equiv.) were converted. After being stirred for 36 h, the reaction mixture was purified by chromatography on silica gel eluting with *n*-hexane/ ethyl acetate (20: 1) to afford **27** (58.4 mg, 51.7% yield) as white solid.

^{1}H-NMR (400 Hz, $CDCl_3$, 25 °C) δ= 8.51 – 8.49 (m, 1H), 7.57 – 7.55 (m, 1H), 7.32 – 7.20 (m, 5H), 7.15 – 7.13 (m, 1H), 7.11 – 7.05 (m, 1H), 3.56 (s, 2H), 3.01 (s, 2H), 2.84 – 2.79 (m, 2H), 2.27 (s, 3H) ppm.

^{13}C-NMR (101 Hz, $CDCl_3$, 25 °C) δ= 160.52, 149.15, 138.95, 136.26, 129.00, 128.19, 126.94, 123.25, 121.11, 62.17, 57.31, 42.05, 36.17 ppm.

The spectroscopic data corresponds to those reported in literature.[30]

Estrone 3-benzoate (28)

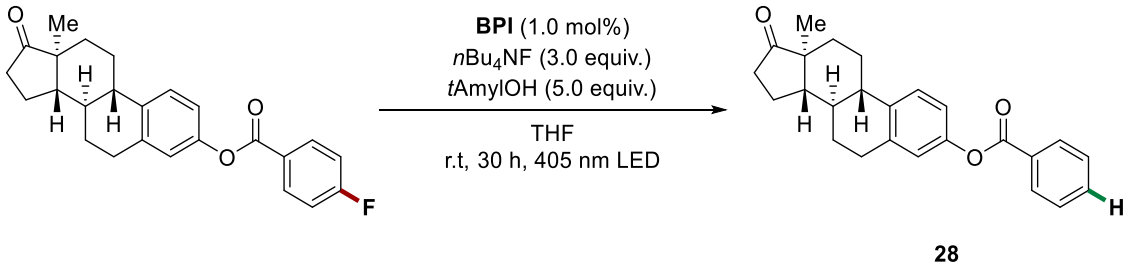

28

According to the **GP1**, **BPI** (3.9 mg, 1.0 mol%), estrone *p*-fluorobenzoate (196 mg, 0.500 mmol), *n*Bu_4NF (1.5 mmol, 1.5 mL, 3.0 equiv., 1.0M in THF) and *tert*-AmylOH (2.5 mmol, 5.0 equiv.) were converted. After being stirred for 30 h, the reaction mixture was purified by chromatography on silica gel eluting with *n*-hexane/ ethyl acetate (10: 1) to afford **28** (120 mg, 64.3% yield) as white solid.

^{1}H-NMR (400 Hz, $CDCl_3$, 25 °C) δ= 8.30 – 8.11 (m, 2H), 7.63 (t, *J* = 7.5 Hz, 1H), 7.51 (t, *J* = 7.6 Hz, 2H), 7.34 (d, *J* = 8.5 Hz, 1H), 7.06 – 6.89 (m, 2H), 2.95 (m, 2H), 2.61 – 2.38 (m, 2H), 2.32 (m, 1H), 2.21 – 1.95 (m, 4H), 1.70 – 1.44 (m, 6H), 0.93 (s, 3H) ppm.

^{13}C-NMR (101 Hz, $CDCl_3$, 25 °C) δ= 220.81, 165.51, 148.94, 138.17, 137.53, 133.61, 130.23, 129.75, 128.64, 126.56, 121.80, 118.97, 50.53, 48.04, 44.27, 38.12, 35.95, 31.66, 29.53, 26.46, 25.88, 21.69, 13.94 ppm.

The spectroscopic data corresponds to those reported in literature.[31]

The starting materials (estrone *p*-fluorobenzoate) were prepared according to literature procedures using standard Schlenk technique.[32]

3.3 Failed and low yielding substrates

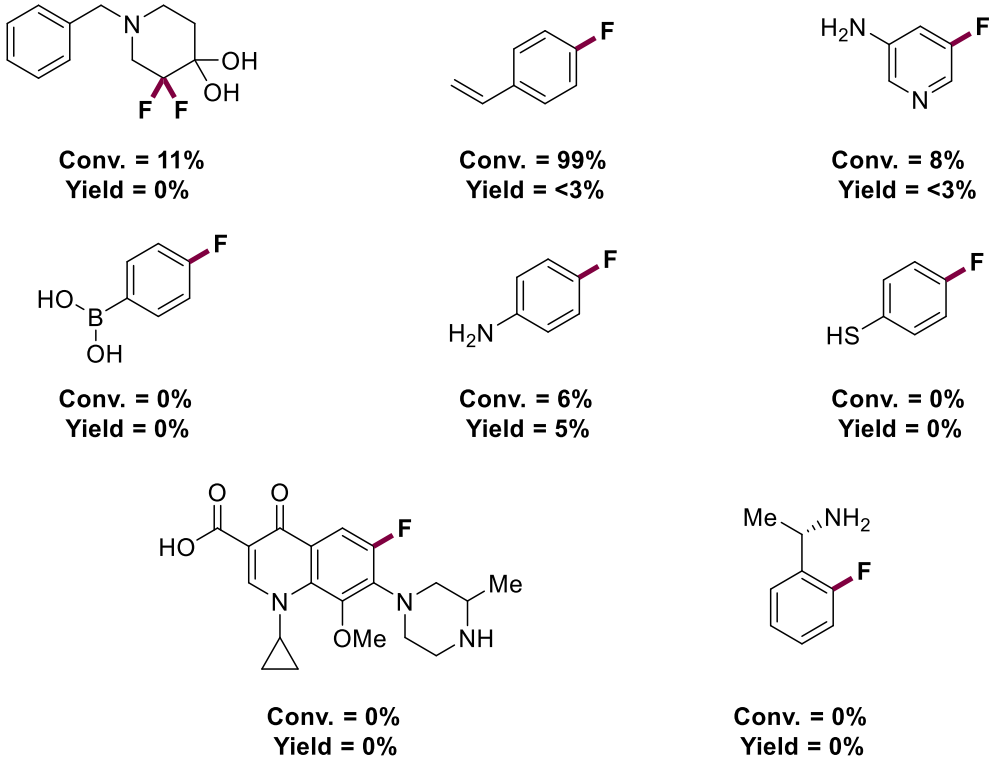

Figure. S2.1. Failed and low yielding substrates in dehalogenation reaction. Reaction conditions: BPI (1.5 mol%), organic fluorides (0.5 mmol), nBu$_4$NF (1.5 mmol, 1.5 mL, 3 equiv., 1.0M in THF), tert-AmylOH (2.5 mmol, 5.0 equiv.), r.t (23 °C), 36 h, 405 nm LED. The conversions were determined by GC using mesitylene as the internal standard.

3.4 Substrate scope for other organic halides

N-benzylpropanamide (29)

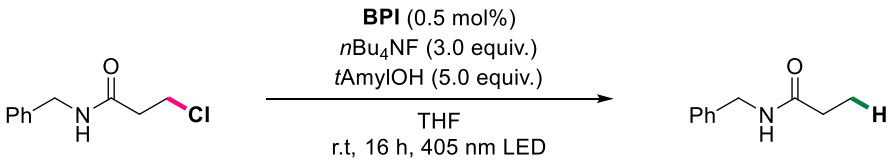

29

According to the **GP1**, **BPI** (1.9 mg, 0.5 mol%), beclamide (98.5 mg, 0.500 mmol), *n*Bu$_4$NF (1.5 mmol, 1.5 mL, 3.0 equiv., 1.0M in THF) and *tert*-AmylOH (2.5 mmol, 5.0 equiv.) were converted.

After being stirred for 16 h, the reaction mixture was purified by chromatography on silica gel eluting with *n*-hexane/ ethyl acetate (25: 1) to afford **29** (60.3 mg, 74.0% yield) as white solid.

^{1}H-NMR (400 Hz, $CDCl_3$, 25 °C) δ= 7.33 – 7.27 (m, 2H), 7.24 (d, *J* = 12.9 Hz, 3H), 6.33 (s, 1H), 4.37 (d, *J* = 5.8 Hz, 2H), 2.20 (q, *J* = 7.6 Hz, 2H), 1.13 (t, *J* = 8.4 Hz, 3H) ppm.

^{13}C-NMR (101 Hz, $CDCl_3$, 25 °C) δ= 173.58, 138.24, 128.29, 127.40, 127.03, 43.13, 29.27, 9.60 ppm.

The spectroscopic data corresponds to those reported in literature.[33]

Impramine (30)

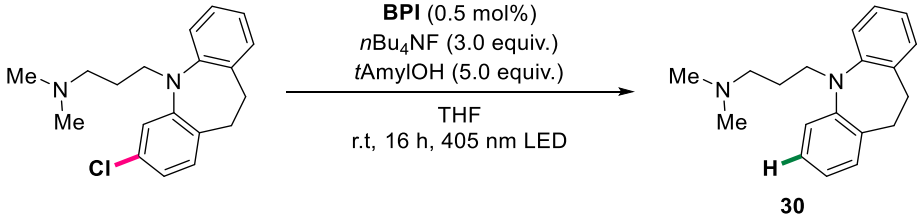

30

According to the **GP1**, **BPI** (1.8 mg, 0.5 mol%), clomipramine (157 mg, 0.500 mmol), nBu$_4$NF (1.5 mmol, 1.5 mL, 3.0 equiv., 1.0M in THF) and *tert*-AmylOH (2.5 mmol, 5.0 equiv.) were converted. After being stirred for 16 h, the reaction mixture was purified by chromatography on silica gel eluting with *n*-hexane/ ethyl acetate (20: 1) to afford **30** (42.6 mg, 60.8% yield) as white solid.

^{1}H-NMR (400 Hz, $CDCl_3$, 25 °C) δ= 7.19 – 6.99 (m, 6H), 6.91 (t, *J* = 7.3 Hz, 2H), 3.77 (t, *J* = 7.0 Hz, 2H), 3.16 (s, 4H), 2.31 (t, *J* = 7.3 Hz, 2H), 2.15 (s, 6H), 1.73 (p, *J* = 7.1 Hz, 2H) ppm.

^{13}C-NMR (101 Hz, $CDCl_3$, 25 °C) δ= 148.48, 134.37, 129.90, 126.48, 122.51, 120.16, 57.85, 49.03, 45.68, 32.36, 26.37 ppm.

The spectroscopic data corresponds to those reported in literature.[34]

(4-(isopropoxy) phenyl)(phenyl)Methanone (31)

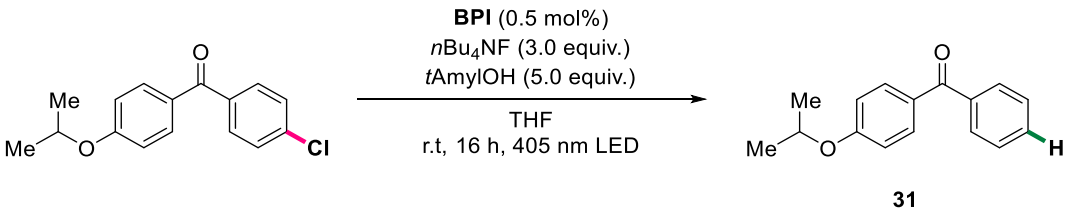

31

According to the **GP1**, **BPI** (1.8 mg, 0.5 mol%), 4-chloro-4'-isopropoxybenzophenone (137 mg, 0.500 mmol), *n*Bu$_4$NF (1.5 mmol, 1.5 mL, 3.0 equiv., 1.0M in THF) and *tert*-AmylOH (2.5 mmol, 5.0 equiv.) were converted. After being stirred for 16 h, the reaction mixture was purified by chromatography on silica gel eluting with *n*-hexane/ ethyl acetate (40: 1) to afford **31** (90.2 mg, 75.2% yield) as white solid.

^{1}H-NMR (400 Hz, $CDCl_3$, 25 °C) δ= 7.85 – 7.78 (m, 2H), 7.78 – 7.72 (m, 2H), 7.61 – 7.52 (m, 1H), 7.48 – 7.45 (m, 2H), 6.96 – 6.91 (m, 2H), 4.69 – 4.65 (m, 1H), 1.38 (d, *J* = 5.9 Hz, 6H) ppm.

^{13}C-NMR (101 Hz, $CDCl_3$, 25 °C) δ= 195.69, 161.91, 138.54, 132.77, 131.95, 129.86, 128.31, 115.08, 70.27, 22.09 ppm.

The spectroscopic data corresponds to those reported in literature.[35]

2-Phenoxyphenol (32)

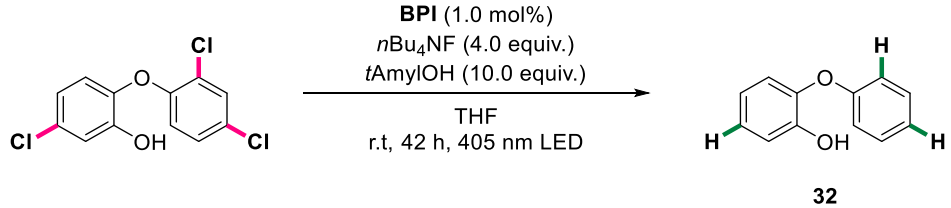

32

According to the **GP1**, **BPI** (3.8 mg, 1.0 mol%), triclosan (145 mg, 0.500 mmol), *n*Bu$_4$NF (2.0 mmol, 2.0 mL, 4.0 equiv., 1.0M in THF) and *tert*-AmylOH (5.0 mmol, 10.0 equiv.) were converted. After being stirred for 42 h, the reaction mixture was purified by chromatography on silica gel eluting with *n*-hexane/ ethyl acetate (10: 1) to afford **32** (52.7 mg, 56.7% yield) as white solid.

^{1}H-NMR (400 Hz, $CDCl_3$, 25 °C) δ= 7.40 – 7.31 (m, 2H), 7.13 (t, *J* = 7.4 Hz, 1H), 7.09 – 6.99 (m, 4H), 6.94 – 6.81 (m, 2H), 5.60 (s, 1H) ppm.

^{13}C-NMR (101 Hz, $CDCl_3$, 25 °C) δ= 156.90, 147.64, 143.61, 130.02, 124.91, 123.75, 120.77, 119.02, 118.14, 116.32 ppm.

The spectroscopic data corresponds to those reported in literature.[36]

1,1'-Ethylidenebis-benzene (33)

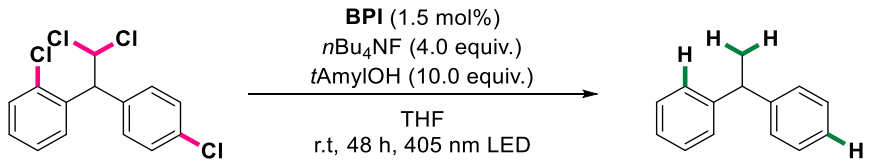

33

According to the **GP1**, **BPI** (5.7 mg, 1.5 mol%), mitotane (160 mg, 0.500 mmol), *n*Bu$_4$NF (2.0 mmol, 2.0 mL, 4.0 equiv., 1.0M in THF) and *tert*-AmylOH (5.0 mmol, 10.0 equiv.) were converted. After being stirred for 48 h, the reaction mixture was purified by chromatography on silica gel eluting with *n*-hexane/ ethyl acetate (50: 1) to afford **33** (37.5 mg, 41.2% yield) as white solid.

^{1}H-NMR (400 Hz, $CDCl_3$, 25 °C) δ= 7.36 – 7.29 (m, 4H), 7.29 – 7.19 (m, 6H), 4.20 (q, *J* = 7.2 Hz, 1H), 1.69 (d, *J* = 7.2 Hz, 3H) ppm.

^{13}C-NMR (101 Hz, $CDCl_3$, 25 °C) δ= 146.51, 128.50, 127.77, 126.16, 44.91, 22.00 ppm.

The spectroscopic data corresponds to those reported in literature.[37]

Phenyl acetonitrile (34)

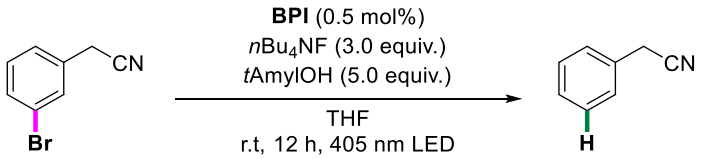

34

According to the **GP1**, **BPI** (1.9 mg, 0.5 mol%), 3-bromophenylacetonitrile (98 mg, 0.50 mmol), *n*Bu_4NF (1.5 mmol, 1.5 mL, 3.0 equiv., 1.0M in THF) and *tert*-AmylOH (2.5 mmol, 5.0 equiv.) were converted. After being stirred for 12 h, the reaction mixture was purified by chromatography on silica gel eluting with *n*-hexane/ ethyl acetate (50: 1) to afford **34** (49.5 mg, 84.6% yield) as white solid.

^{1}H-NMR (400 Hz, $CDCl_3$, 25 °C) δ= 7.43 – 7.36 (m, 2H), 7.36 – 7.30 (m, 3H), 3.76 (s, 2H) ppm.

^{13}C-NMR (101 Hz, $CDCl_3$, 25 °C) δ= 130.04, 129.28, 128.20, 128.06, 117.99, 23.76 ppm.

The spectroscopic data corresponds to those reported in literature.[38]

Benzophenone (35)

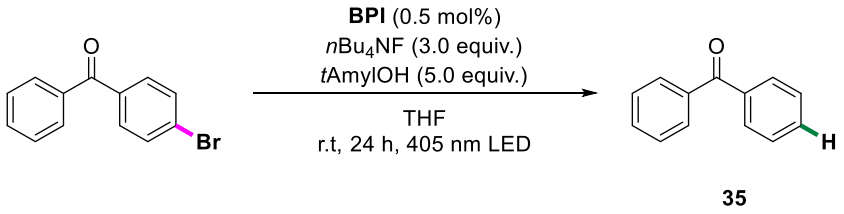

35

According to the **GP1**, **BPI** (1.9 mg, 0.5 mol%), 4-bromobenzophenone (130 mg, 0.500 mmol), *n*Bu$_4$NF (1.5 mmol, 1.5 mL, 3.0 equiv., 1.0M in THF) and *tert*-AmylOH (2.5 mmol, 5.0 equiv.) were converted. After being stirred for 24 h, the yield of title compound **35** was determined by GC relative to the internal standard (73.4% yield).

4. Hydrodefluoronation of per- and polyfluoroalkyl substances (PFAS)

4.1 General procedure

General procedure for the hydrodefluoronation of PFAS (**GP-2**)

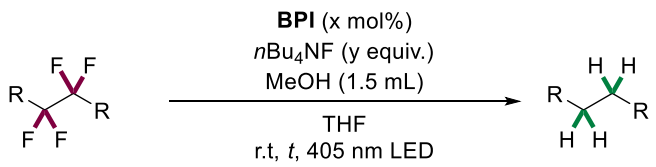

In a glovebox, a 5 mL glass vial containing a stirring bar was sequentially charged with **BPI** (catalyst was used according to the fluorine atom in the compounds, each fluorine atom corresponds to 0.5 mol% catalyst), *n*Bu$_4$NF (the amount of electron donor was adjusted for different types of substrates) and MeOH (1.5 mL). The mixture was stirred for 20 minutes at 23 °C, and the color changes from orange to light green. Subsequently, the PFAS (0.2 mmol) were added outside the glovebox. The glass vial was placed into the light reactor and stirred for corresponding time. The temperature was kept at approximately 23 °C through cooling with six mini fans. After reaction, the mixture was diluted with acetone and analyzed by GC using mesitylene as internal standard. The high boiling point product 4-butylbenzonitrile **41** and butyl octanoate **44** can be purified by column chromatography on silica gel.

Note 1: Highly volatile or lower boiling point PFAS were added outside the glove box using a syringe under nitrogen. 4-(perfluorobutyl)benzonitrile and perfluorooctanoic acid (PFOA) can be added in the glovebox.

Note 2: Due to the solubility of the **BPI** catalyst, the amount of methanol added cannot be higher than THF, otherwise the catalyst will be precipitated.

Note 3: Because our system has an excess of nBu$_4$NF, it is hard to determine the non-complete defluorinated product by ^{19}F-NMR.

Since the determination of yield using GC requires the corresponding product as a standard. We cannot determine the specific structure of partially hydrodefluorination products, so at this stage we mainly detect completely hydrodefluorination products.

Hexan-1-ol (36)

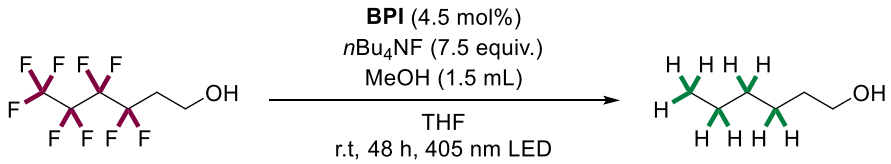

36

According to the **GP-2**, **BPI** (7.1 mg, 4.5 mol%), 1H,1H,2H,2H-nonafluoro-1-hexanol (52.8 mg, 0.200 mmol), *n*Bu$_4$NF (1.5 mmol, 1.5 mL, 7.5 equiv., 1.0M in THF) and MeOH (1.5 mL) were converted. After being stirred for 48 h, mesitylene (24 mg, 0.2 mmol) was added as internal standard. The yield of the title compound **36** was determined by GC relative to the internal standard (63.7% yield).

Butan-1-ol (37)

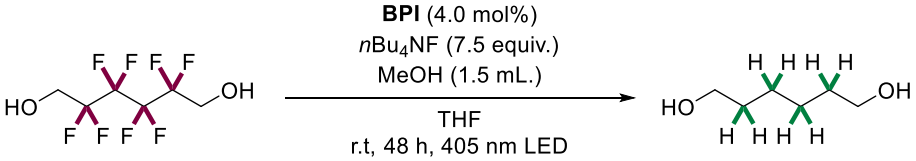

37

According to the **GP-2**, **BPI** (6.2 mg, 4.00 mol%), 2,2,3,3,4,4,5,5-octafluoro-1,6-hexanediol (52 mg, 0.20 mmol), *n*Bu$_4$NF (1.5 mmol, 1.5 mL, 7.5 equiv., 1.0M in THF) and MeOH (1.5 mL.) were converted. After being stirred for 48 h, mesitylene (24 mg, 0.2 mmol) was added as internal standard. The yield of the title compound **37** was determined by GC relative to the internal standard (49.6% yield).

Methyl butyrate (38)

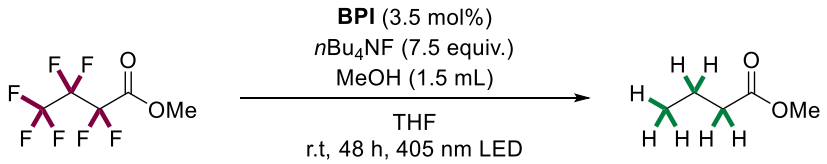

38

According to the **GP-2**, **BPI** (5.5 mg, 3.50 mol%), methyl perfluorobutyrate (45.6 mg, 0.200 mmol), *n*Bu$_4$NF (1.5 mmol, 1.5 mL, 7.5 equiv., 1.0M in THF) and MeOH (1.5 mL) were converted. After being stirred for 48 h, mesitylene (24 mg, 0.2 mmol) was added as internal standard. The yield of the title compound **38** was determined by GC relative to the internal standard (70.4% yield).

Methyl pentanoate (39)

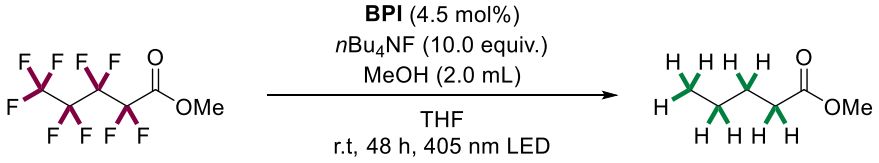

39

According to the **GP-2**, **BPI** (7.0 mg, 4.50 mol%), methyl perfluoropentanoate (55.6 mg, 0.200 mmol), *n*Bu$_4$NF (2.0 mmol, 2.0 mL, 10.0 equiv., 1.0M in THF) and MeOH (2.0 mL) were converted. After being stirred for 48 h, mesitylene (24 mg, 0.2 mmol) was added as internal standard. The yield of the title compound **39** was determined by GC relative to the internal standard (63.2% yield).

Methyl hexanoate (40)

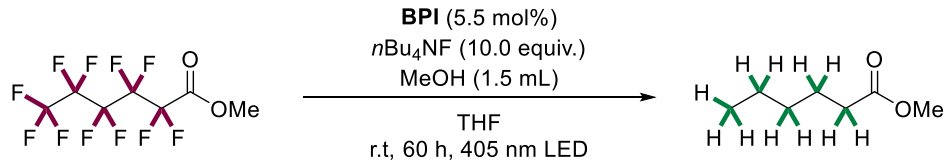

40

According to the **GP-2**, **BPI** (8.6 mg, 5.50 mol%), methyl perfluorohexanoate (65.6 mg, 0.200 mmol), nBu$_4$NF (2.0 mmol, 2.0 mL, 10.0 equiv., 1.0M in THF) and MeOH (1.5 mL) were converted. After being stirred for 60 h, mesitylene (24 mg, 0.2 mmol) was added as internal standard. The yield of the title compound **40** was determined by GC relative to the internal standard (58.1% yield).

4-Butylbenzonitrile (41)

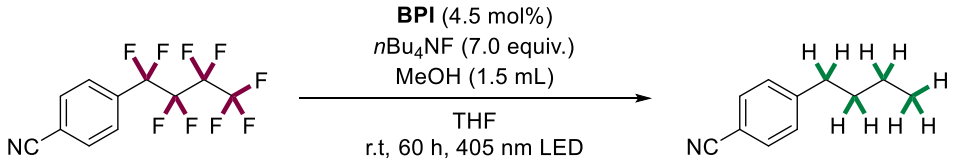

41

According to the **GP-2**, **BPI** (17.3 mg, 4.50 mol%), 4-(perfluorobutyl)benzonitrile (160 mg, 0.50 mmol), nBu$_4$NF (3.5 mmol, 3.5 mL, 7.0 equiv., 1.0M in THF) and MeOH (1.5 mL) were converted. After being stirred for 60 h, the reaction mixture was purified by chromatography on silica gel eluting with *n*-hexane/ ethyl acetate (50: 1) to afford **41** (50.1 mg, 63.3% yield) as colorless oil.

^{1}H-NMR (400 Hz, $CDCl_3$, 25 °C) δ= 7.60 – 7.56 (m, 2H), 7.29 (d, J = 7.4 Hz, 2H), 2.69 (t, J = 7.8 Hz, 2H), 1.65 – 1.60 (m, 2H), 1.39 – 1.36 (m, 2H), 0.95 (t, J = 7.3 Hz, 3H) ppm.

^{13}C-NMR (101 Hz, $CDCl_3$, 25 °C) δ= 148.71, 132.24, 129.33, 119.34, 109.62, 35.94, 33.22, 22.38, 13.99 ppm.

The spectroscopic data corresponds to those reported in literature.[39]

Methyl octanoate (43) and butyl octanoate (44)

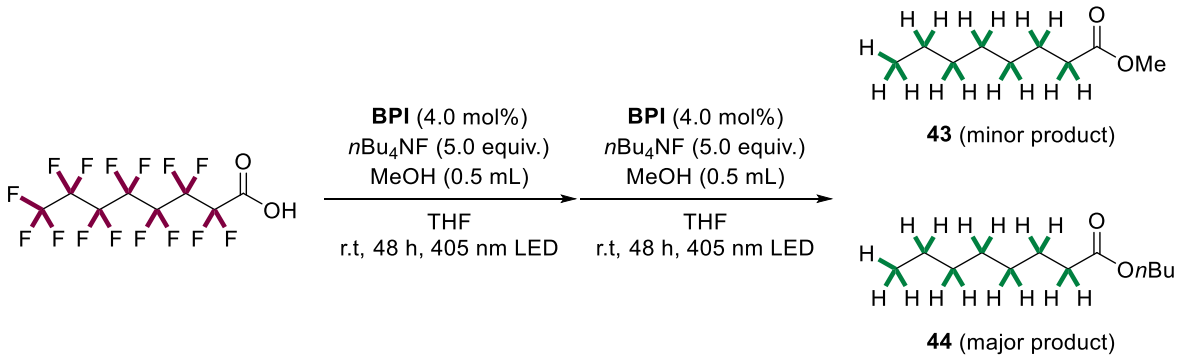

According to the **GP-2**, **BPI** (15.2 mg, 4.0 mol%), perfluorooctanoic acid (207 mg, 0.5 mmol), *n*Bu$_4$NF (2.5 mmol, 2.5 mL, 5.0 equiv., 1.0M in THF) and MeOH (0.5 mL) were reacted. After being stirred for 48 h, the reaction mixture was moved back into the glovebox, where more BPI (15.2 mg, 4.0 mol%), *n*Bu$_4$NF (2.5 mmol, 2.5 mL, 5.0 equiv., 1.0M in THF) and MeOH (0.5 mL) were added. The vial was then removed from the glovebox and placed back into the light reactor. After the reaction, mesitylene (60 mg, 0.5 mmol) was added as internal standard. The yield of the title compound **43** and **44** was determined by GC relative to the internal standard (3.6% yield of **43** and 45.3 % yield of **44**). Then, the reaction mixture was purified by chromatography on silica gel eluting with *n*-hexane/ ethyl acetate (50: 1) to afford **44** (30.7 mg, 30.7% yield) as colorless oil.

NMR for butyl octanoate (**44**)

^{1}H-NMR (400 Hz, $CDCl_3$, 25 °C) δ= 4.06 (t, *J* = 6.7 Hz, 2H), 2.28 (t, *J* = 7.5 Hz, 2H), 1.71 – 1.52 (m, 4H), 1.44 – 1.35 (m, 2H), 1.36 – 1.28 (m, 8H), 0.93 (t, *J* = 7.4 Hz, 3H), 0.87 (t, *J* = 6.5 Hz, 3H) ppm.

^{13}C-NMR (101 Hz, $CDCl_3$, 25 °C) δ= 174.17, 64.23, 34.56, 31.81, 30.86, 29.26, 29.07, 25.17, 22.74, 19.30, 14.20, 13.85 ppm.

The spectroscopic data corresponds to those reported in literature.[40]

Note 1: Large-scale photoreactor was used for this reaction.

Note 2: The butyl group of **44** comes from nBu$_4$NF (see Figure. S2 for details).

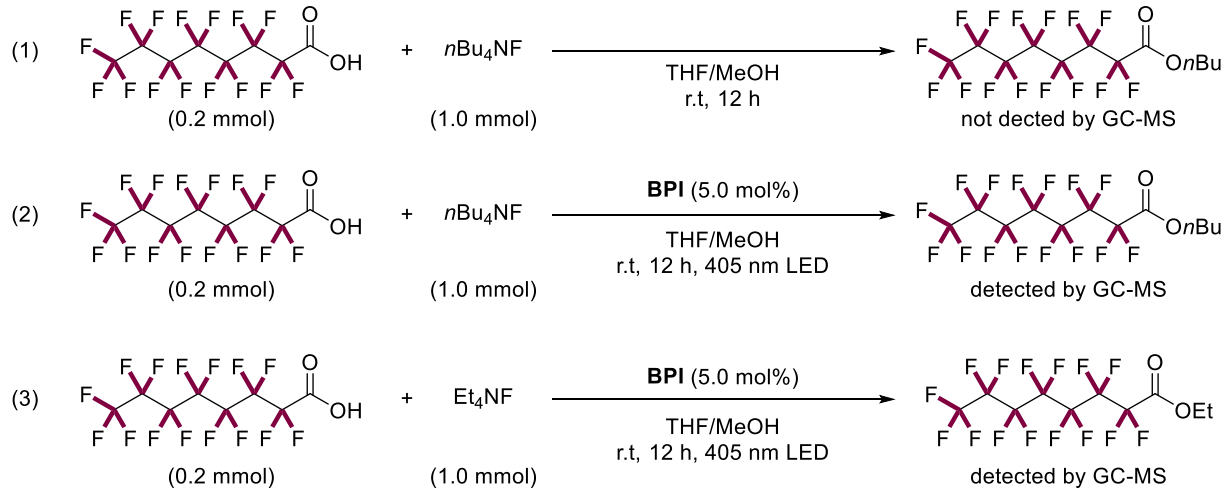

Figure S2.2. Control experiments of pentadecafluoro-octanoic acid butyl ester formation.

4.2 Kinetic profile of the hydrodefluorination of PFAS

Methyl perfluorohexanoate:

In a glovebox, a 5 mL glass vial containing a stirring bar was sequentially charged with **BPI** (20.9 mg, 5.50 mol%), and nBu$_4$NF (1.5 mmol, 1.5 mL, 7.5 equiv., 1.0M in THF). The mixture was stirred for 20 minutes at 23 °C, and the color changes from orange to light green. Subsequently, methyl perfluorohexanoate (65.6 mg, 0.200 mmol), and MeOH (1.5 mL) were added in one portion. The glass vial was placed into the light reactor and stirred for corresponding time. The

temperature was kept at approximately 23 °C through cooling with six mini fans. The conversion and yield were analyzed by GC using mesitylene as internal standard.

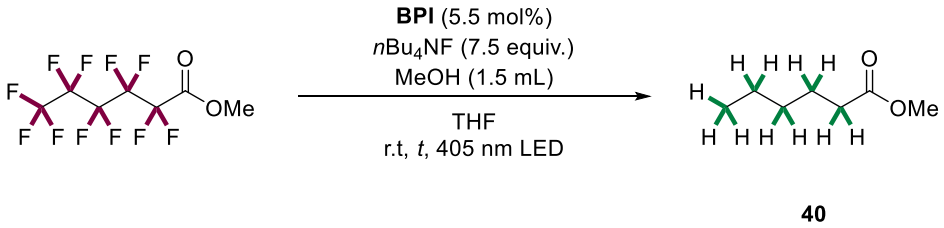

40

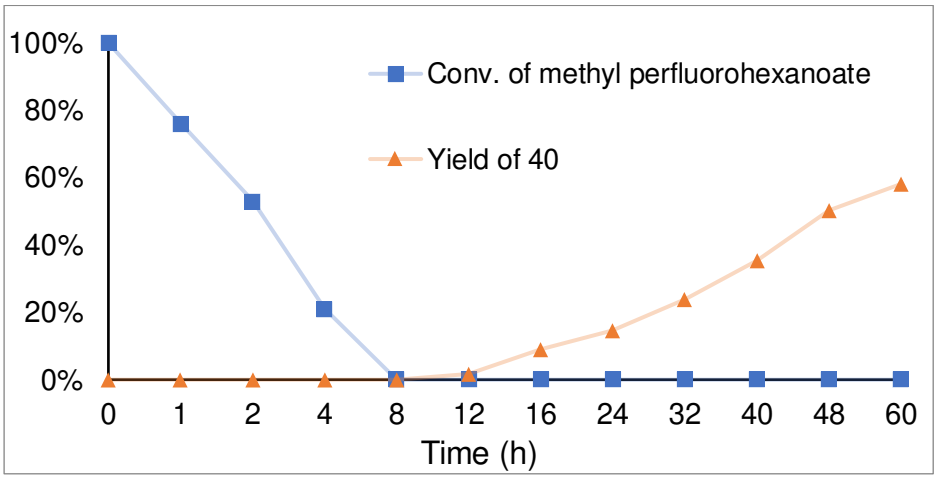

Figure S2.3. Kinetic profile of the hydrodefluorination of methyl perfluorohexanoate.

2,2,3,3,4,4,5,5-octafluoro-1,6-hexanediol:

In a glovebox, a 5 mL glass vial containing a stirring bar was sequentially charged with **BPI** (15.4 mg, 5.50 mol%), and *n*Bu$_4$NF (1.5 mmol, 1.5 mL, 7.5 equiv., 1.0M in THF). The mixture was stirred for 20 minutes at 23 °C, and the color changes from orange to light green. Subsequently, 2,2,3,3,4,4,5,5-octafluoro-1,6-hexanediol (65.6 mg, 0.200 mmol), and MeOH (1.5 mL) were added in one portion. The glass vial was placed into the light reactor and stirred for corresponding time. The temperature was kept at approximately 23 °C through cooling with six mini fans. The conversion and yield were analyzed by GC using mesitylene as internal standard.

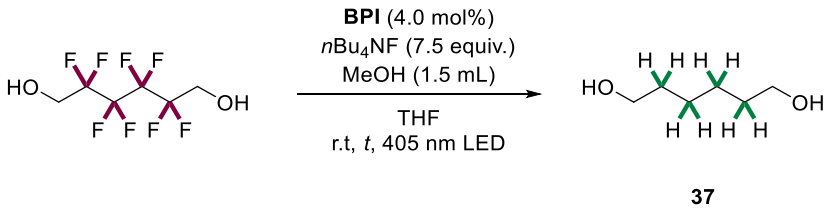

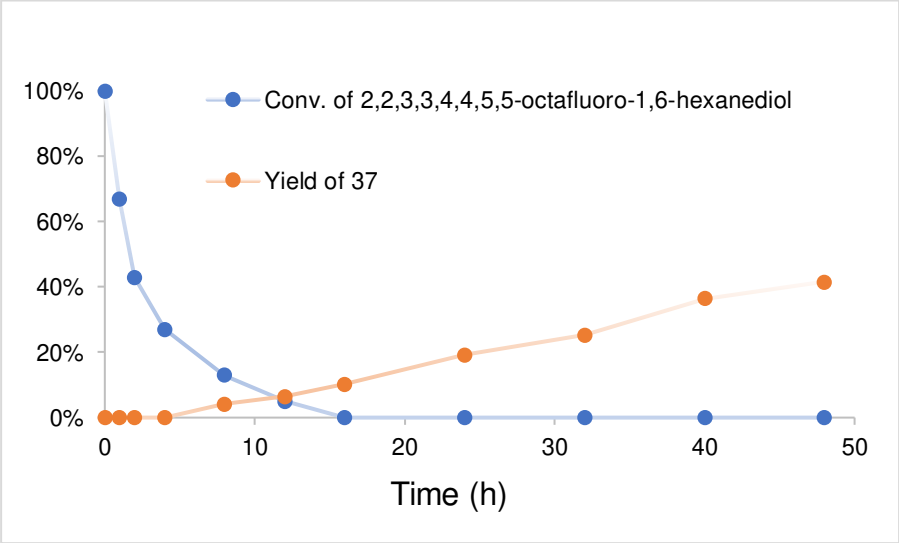

Figure S2.4. Kinetic profile of the hydrodefluorination of 2,2,3,3,4,4,5,5-octafluoro-1,6-hexanediol.

4.3 Failed and low yielding substrates

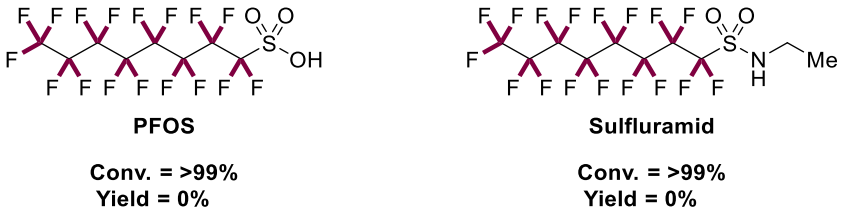

Figure. S2.5. Failed and low yielding substrates in hydrodefluorination of PFAS. Reaction conditions: BPI (7.0 mol%), PFAS (0.2 mmol), nBu$_4$NF (1.5 mmol, 1.5 mL, 7.5 equiv., 1.0M in THF), MeOH (1.5 mL), r.t (23 °C), 36 h, 405 nm LED. The conversions were determined by GC using mesitylene as the internal standard.

Note: Complete hydrodefluorination products and desulfonation products were not detected.

From the known literature (Science, 2022, 377, 839–845), defluorination of PFOA will be followed by chain-shortening via decarboxylation, and the decarboxylation has been proven to be the rate-limiting step. Because our system can desulfonation (see figure below), therefore, we hypothesized that PFOS might be reduced to light alkanes in our system.

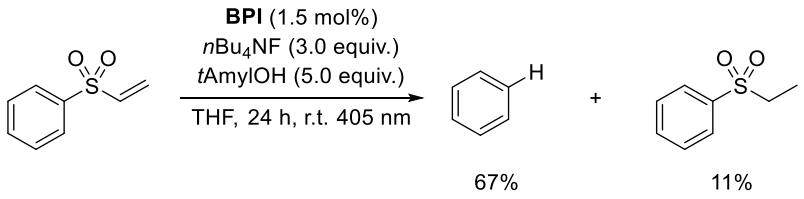

5. Hydrodefluoronation of fluorinated polymers

5.1 General procedure

General procedure for the hydrodefluoronation of fluorinated polymers (**GP-3**)

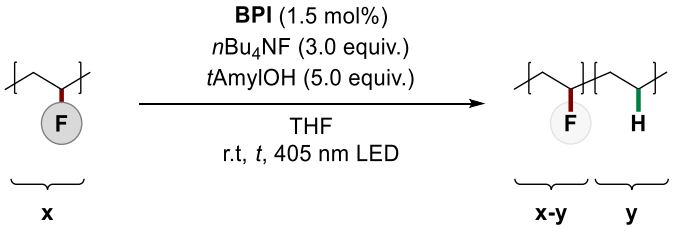

In a glovebox, a 5 mL glass vial containing a stirring bar was sequentially charged with **BPI** (5.0 μmol, 1.0 mol%) and *n*Bu$_4$NF (1.5 mmol, 1.5 mL, 3.0 equiv., 1.0M in THF). The mixture was stirred for 20 minutes at 23 °C, and the color changes from orange to light green. Subsequently, the fluorinated polymer (0.5 mmol, substrate was used according to the repeating unit of polymers) and *tert*-AmylOH (2.5 mmol, 5.0 equiv.) were added in one portion. The glass vial was placed into the light reactor and stirred for the corresponding time. The temperature was kept at approximately 23 °C through cooling with six mini fans. After reaction, the solution was pipetted into stirring methanol to precipitate polymer and collected via Büchner filtration with nylon filter paper to yield the dehalogenation polymers. Collected polymer is placed on high vacuum overnight before characterization. The ratio of the product units was determined by ^{19}F-NMR.

5.1 Substrate scope

Hydrodefluoronation of poly(4-fluorostyrene) (Large-scale reaction)

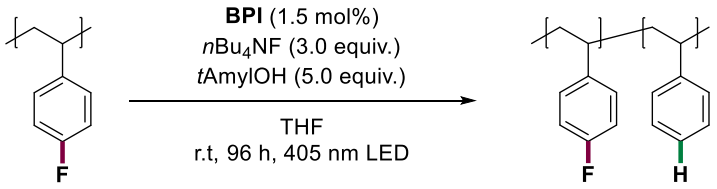

45 **46**

According to the **GP-3**, **BPI** (116 mg, 1.50 mol%), poly(4-fluorostyrene) **45** (1.22 g, 10.00 mmol), *n*Bu$_4$NF (30 mmol, 30 mL, 3.0 equiv., 1.0M in THF) and *tert*-AmylOH (2.5 mmol, 5.0 equiv.) were converted. After being stirred for 30 h, the solution was pipetted into stirring acetone to precipitate polymer and collected via Büchner filtration with nylon filter paper to yield the dehalogenation fluorinated polymers. Collected polymer is placed on high vacuum overnight before characterization. The ratio of the product units was determined by ^{19}F-NMR using 2-fluoropyridine as the internal standard.

The characterization of the starting materials [poly(4-fluorostyrene) **45**]:

^{1}H-NMR (400 Hz, $CDCl_3$, 25 °C) δ= 6.65 (bs), 6.42 (bs), 1.67 (bs), 1.39 (bs) ppm.

GPC (Chloroform): M_n = 27.6 kDa, M_w/M_n = 1.17.

The characterization of product **46**:

^{1}H-NMR (400 Hz, $CDCl_3$, 25 °C) δ= 7.09 (bs), 6.61(bs), 6.49 (bs), 1.62 (bs), 1.33 (bs) ppm.

GPC (Chloroform): M_n = 23.5 kDa, M_w/M_n = 1.24.

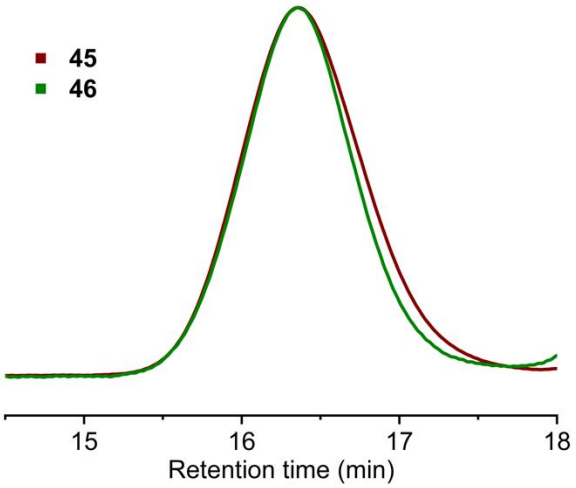

Hydrodefluoronation of poly(3-fluorostyrene)

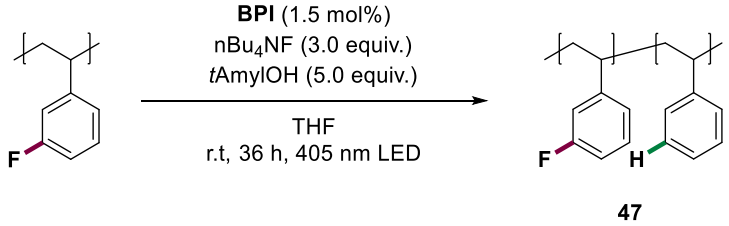

47

According to the **GP-3**, **BPI** (5.7 mg, 1.5 mol%), poly(3-fluorostyrene) (0.50 mmol, substrate was used according to the repeating unit of polymers), *n*Bu$_4$NF (1.5 mmol, 1.5 mL, 3.0 equiv., 1.0M in THF) and *tert*-AmylOH (2.5 mmol, 5.0 equiv.) were converted. After being stirred for 36 h, the solution was pipetted into stirring acetone to precipitate polymer and collected via Büchner filtration with nylon filter paper to yield the dehalogenation fluorinated polymers. Collected polymer is placed on high vacuum overnight before characterization. The ratio of the product units was determined by ^{19}F-NMR using 2-fluoropyridine as the internal standard.

The characterization of the starting materials [poly(3-fluorostyrene)]:

^{1}H-NMR (400 Hz, $CDCl_3$, 25 °C) δ= 7.02 (bs), 6.69 (bs), 6.34 (bs), 1.58 (bs), 1.36 (bs) ppm.

GPC (Chloroform): M_n = 35.3 kDa, M_w/M_n = 1.72.

The characterization of product **47**:

^{1}H-NMR (400 Hz, $CDCl_3$, 25 °C) δ= 7.05 (bs), 6.62 (bs), 6.54 (bs), 1.51 (bs), 1.39 (bs) ppm.

GPC (Chloroform): M_n = 28.7 kDa, M_w/M_n = 1.45.

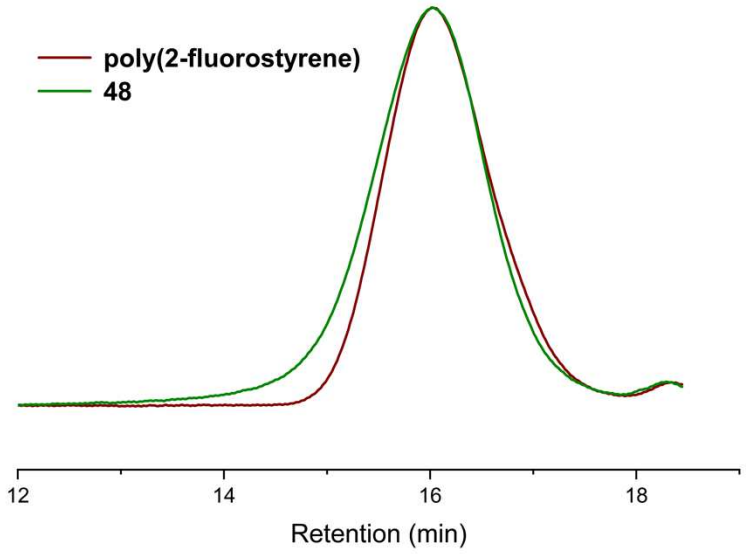

Hydrodefluoronation of poly(2-fluorostyrene)

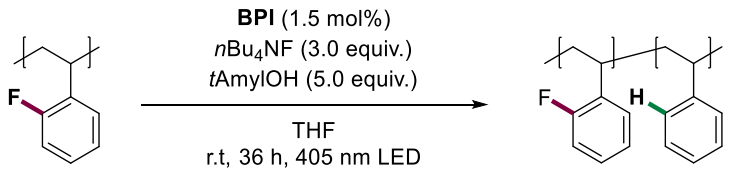

48

According to the **GP-3**, **BPI** (5.7 mg, 1.5 mol%), poly(2-fluorostyrene) (0.50 mmol, substrate was used according to the repeating unit of polymers), nBu$_4$NF (1.5 mmol, 1.5 mL, 3.0 equiv., 1.0M in THF) and *tert*-AmylOH (2.5 mmol, 5.0 equiv.) were converted. After being stirred for 30 h, the solution was pipetted into stirring acetone to precipitate polymer and collected via Büchner filtration with nylon filter paper to yield the dehalogenation fluorinated polymers. Collected polymer is placed on high vacuum overnight before characterization. The ratio of the product units was determined by ^{19}F-NMR using 2-fluoropyridine as the internal standard.

The characterization of the starting materials [(poly(2-fluorostyrene)]:

^{1}H-NMR (400 Hz, $CDCl_3$, 25 °C) δ= 6.98 (bs), 6.75 (bs), 6.54 (bs), 2.20 (bs), 1.53 (bs) ppm.

GPC (Chloroform): M_n = 28.3 kDa, M_w/M_n = 1.84.

The characterization of product **48**:

^{1}H-NMR (400 Hz, $CDCl_3$, 25 °C) δ= 6.96 (bs), 6.74 (bs), 6.53 (bs), 2.20 (bs), 1.46 (bs) ppm.

GPC (Chloroform): M_n = 30.1 kDa, M_w/M_n = 1.33.

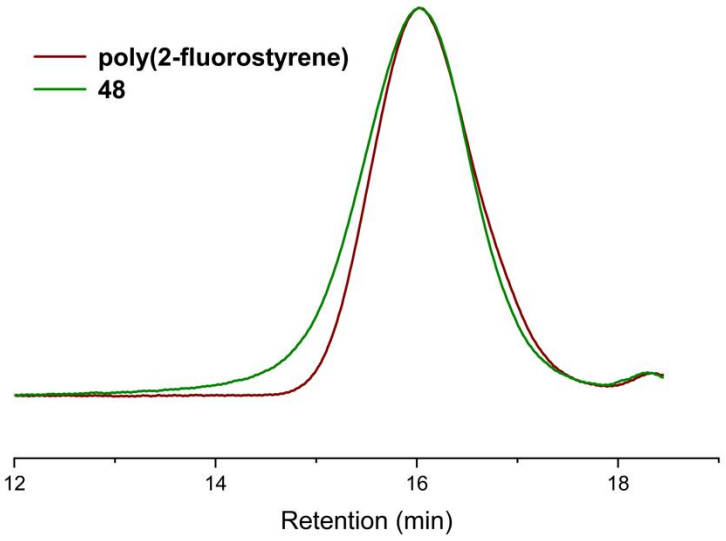
poly(2-fluorostyrene)
48
12
14
16
18
Retention (min)

Hydrodefluoronation of poly(2,2,2-trifluoroethyl acrylate)

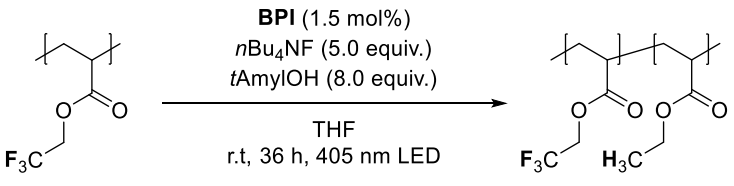

49

According to the **GP-3**, **BPI** (5.7 mg, 1.5 mol%), poly(2,2,2-trifluoroethyl acrylate) (0.50 mmol, substrate was used according to the repeating unit of polymers), *n*Bu$_4$NF (2.5 mmol, 2.5 mL, 5.0 equiv., 1.0M in THF) and *tert*-AmylOH (4.0 mmol, 8.0 equiv.) were converted. After being stirred for 36 h, the solution was pipetted into stirring acetone to precipitate polymer and collected via Büchner filtration with nylon filter paper to yield the dehalogenation fluorinated polymers. Collected polymer is placed on high vacuum overnight before characterization. The ratio of the product units was determined by ^{19}F-NMR using 2-fluoropyridine as the internal standard.

The characterization of the starting materials [poly(2,2,2-trifluoroethyl acrylate)]:

^{1}H-NMR (400 Hz, $CDCl_3$, 25 °C) δ= 4.47 (bs), 2.46 (bs), 2.03 (bs), 1.67 (bs), 1.49 (bs) ppm.

GPC (THF): M_n = 9.93 kDa, M_w/M_n = 1.67.

The characterization of product **49**:

^{1}H-NMR (400 Hz, $CDCl_3$, 25 °C) δ= 3.28 (bs), 1.47 (bs), 1.38 (bs), 0.96 (bs) ppm.

GPC (THF): M_n = 9.12 kDa, M_w/M_n = 1.52.

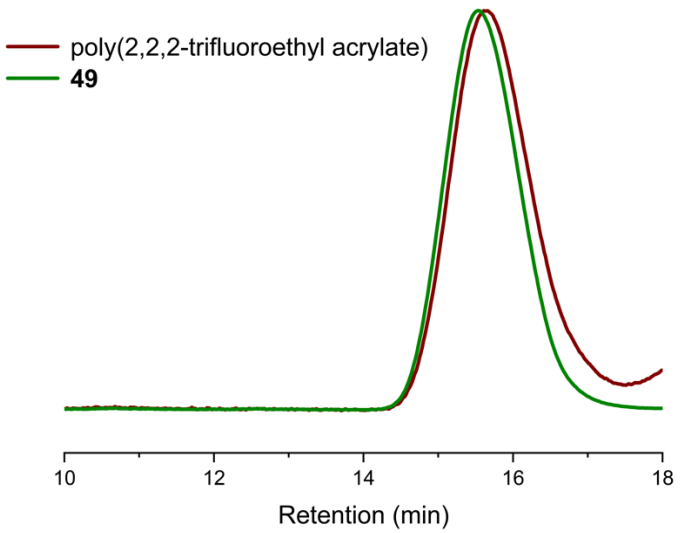
poly(2,2,2-trifluoroethyl acrylate)
49
10
12
14
16
18
Retention (min)

Hydrodefluoronation of poly(4-fluorostyrene-co-acrylonitrile)

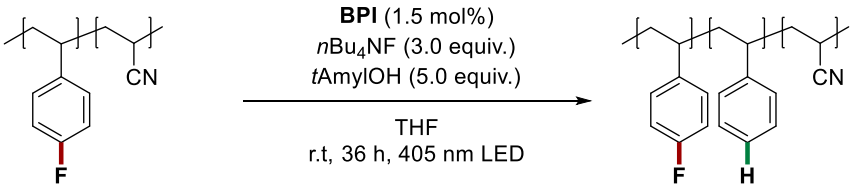

50

According to the **GP-3**, **BPI** (5.7 mg, 1.5 mol%), poly(4-fluorostyrene-co-acrylonitrile) (0.5 mmol, substrate was used according to the repeating unit of polymers), *n*Bu_4NF (1.5 mmol, 1.5 mL, 3.0 equiv., 1.0M in THF) and *tert*-AmylOH (2.5 mmol, 5.0 equiv.) were converted. After being stirred for 36 h, the solution was pipetted into stirring acetone to precipitate polymer and collected via Büchner filtration with nylon filter paper to yield the dehalogenation fluorinated polymers. Collected polymer is placed on high vacuum overnight before characterization. The ratio of the product units was determined by ^{19}F-NMR using 2-fluoropyridine as the internal standard.

The characterization of the starting materials [poly(4-fluorostyrene-co-acrylonitrile)]:

^{1}H-NMR (400 Hz, $CDCl_3$, 25 °C) δ= 6.79 (bs), 2.76 (bs), 1.70 (bs) ppm.

GPC (THF): M_n = 10.4 kDa, M_w/M_n = 1.54.

The characterization of product **50**:

^{1}H-NMR (400 Hz, $CDCl_3$, 25 °C) δ= 6.83 (bs), 2.60 (bs), 1.64 (bs) ppm.

GPC (THF): M_n = 13.1 kDa, M_w/M_n = 1.27

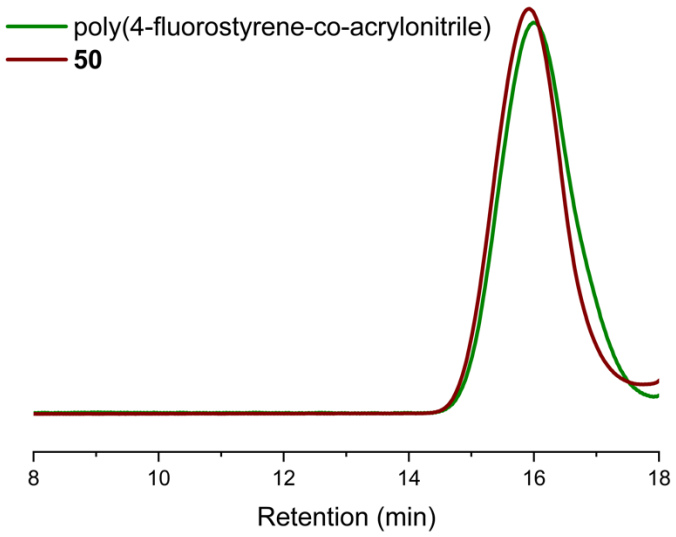
poly(4-fluorostyrene-co-acrylonitrile)
50
8
10
12
14
16
18
Retention (min)

Hydrodefluoronation of poly(4-fluorostyrene-co-ester)

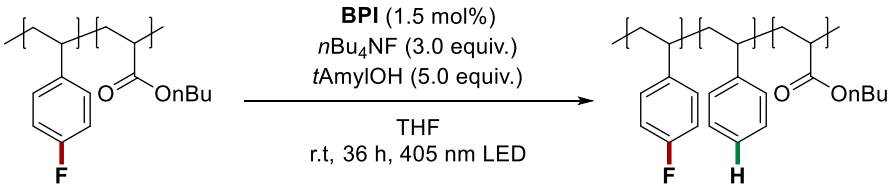

51

According to the **GP-3**, **BPI** (5.7 mg, 1.5 mol%), poly(4-fluorostyrene-co-ester) (0.5 mmol, substrate was used according to the repeating unit of polymers), *n*Bu$_4$NF (1.5 mmol, 1.5 mL, 3.0 equiv., 1.0M in THF) and *tert*-AmylOH (2.5 mmol, 5.0 equiv.) were converted. After being stirred for 36 h, the solution was pipetted into stirring acetone to precipitate polymer and collected via Büchner filtration with nylon filter paper to yield the dehalogenation fluorinated polymers. Collected polymer is placed on high vacuum overnight before characterization. The ratio of the product units was determined by ^{19}F-NMR using 2-fluoropyridine as the internal standard.

The characterization of the starting materials [poly(4-fluorostyrene-co-ester)]:

^{1}H-NMR (400 Hz, $CDCl_3$, 25 °C) δ= 6.76 (bs), 3.73 (bs), 2.31 (bs), 1.56 (bs), 0.95 (bs) ppm.

GPC (Chloroform): M_n = 12.6 kDa, M_w/M_n = 1.33

The characterization of product **51**:

^{1}H-NMR (400 Hz, $CDCl_3$, 25 °C) δ= 7.17 (bs), 6.72 (bs), 3.61 (bs), 2.28 (bs), 1.49 (bs), 0.89 (bs) ppm.

GPC (Chloroform): M_n = 9.28 kDa, M_w/M_n = 1.75

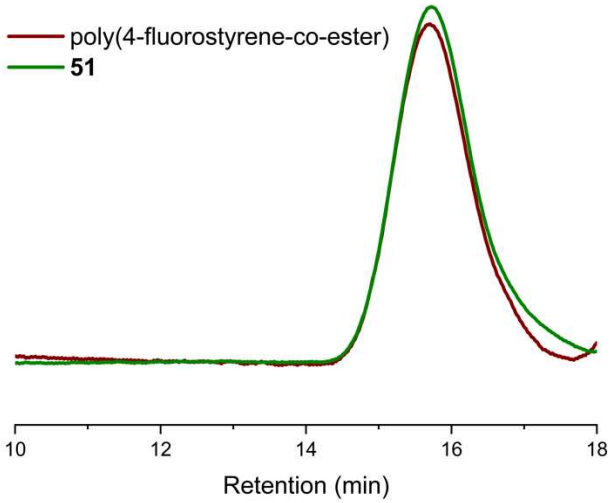

5.2 Kinetic studies of dehalogenation of fluorinated polymers

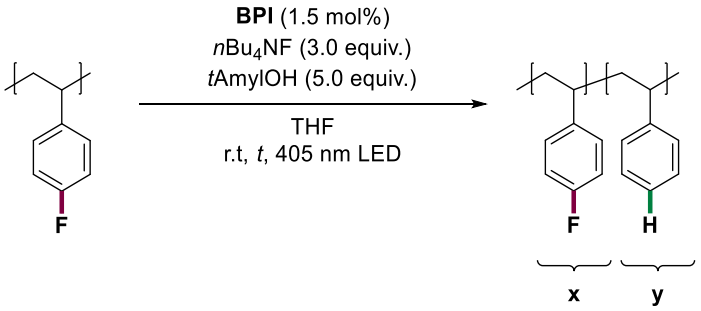

In a glovebox, a 5 mL glass vial containing a stirring bar was sequentially charged with **BPI** (5.7 mg, 1.5 mol%) and *n*Bu$_4$NF (1.5 mmol, 1.5 mL, 3.0 equiv., 1.0M in THF). The mixture was stirred for 20 minutes at 23 °C, and the color changes from orange to light green. Subsequently, poly(4-fluorostyrene) (0.5 mmol, substrate was used according to the repeating unit of polymers) and *tert*-AmylOH (2.5 mmol, 5.0 equiv.) were added in one portion. The glass vial was placed into the light reactor and stirred for corresponding time. The temperature was kept at approximately 23 °C through cooling with six mini fans. The ratio of the product units was determined by ^{19}F-NMR.

Table S2.9. Kinetic profile of the hydrodefluoronation of poly(4-fluorostyrene) 45

Time	4 h	8 h	16 h	24 h	32 h	40 h
F unit (%)	83	71	57	32	21	8
H unit (%)	17	29	43	68	79	92

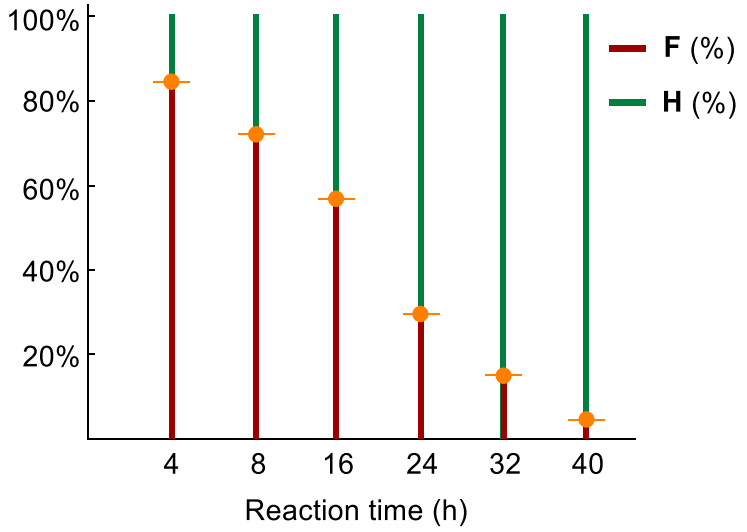

Figure S2.6. Kinetic profile of the hydrodefluorination of poly(4-fluorostyrene) 45.

6. Borylation reaction

6.1 Reaction optimization

General procedure for optimization studies

In a glovebox, a 5 mL glass vial containing a stirring bar was sequentially charged with **BPI** (7.5 μmol, 1.5 mol%) and *n*Bu$_4$NF (y equiv., 1.0M in THF). The mixture was stirred for 20 minutes at 23 °C, and the color changes from orange to light green. Subsequently, fluorobenzene **1** (48 mg, 0.5 mmol) and B_2Pin_2 (x equiv.) were added in one portion. The glass vial was placed into the light reactor and stirred for 30 h. The temperature was kept at approximately 23 °C through cooling with six mini fans. After reaction, the mixture was diluted with ethyl acetate and analyzed by GC using mesitylene as internal standard.

Table S2.10. Evaluation of reaction conditions for borylation of fluorobenzene 1.

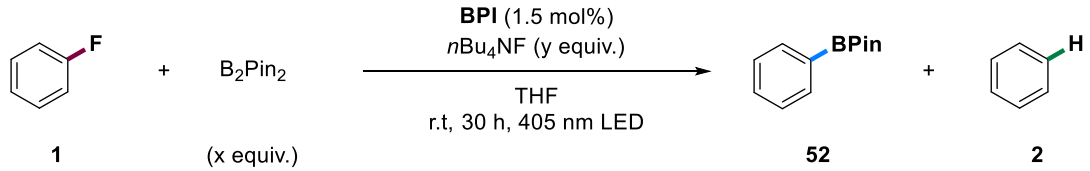

1 (x equiv.) **52** **2**

entry	B_2Pin_2 (x equiv.)	*n*Bu$_4$NF (y equiv.)	conv. of **1** (%)	yield of **52** (%)	yield of **2** (%)
1	1.0	2.0	58	18	23
2	1.5	2.0	64	30	25
3	2.0	2.0	70	35	21
4	2.5	2.0	77	49	17

5	3.0	2.0	73	46	19
6	2.5	1.0	56	35	12
7	2.5	3.0	96	74	22
8	2.5	4.0	98	57	31

Reaction conditions: 1 (0.50 mmol), BPI (1.5 mol%), B_2Pin_2 (x equiv.), nBu_4NF (y equiv., 1.0M in THF), r.t (23 °C), 30 h, 405 nm LED. The conversion and yields were determined by GC using mesitylene as the internal standard.

6.2 Substrate scope for aryl fluorides

General procedure for the dehalogenation of aryl fluorides (**GP-4**)

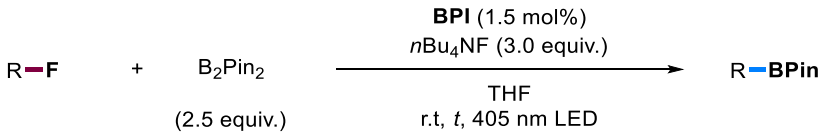

In a glovebox, a 5 mL glass vial containing a stirring bar was sequentially charged with **BPI** (7.5` μmol, 1.5 mol%) and nBu$_4$NF (1.5 mmol, 1.5 mL, 3.0 equiv., 1.0M in THF). The mixture was stirred for 20 minutes at 23 °C, and the color changes from orange to light green. Subsequently, the aryl fluorides (0.5 mmol) and B_2Pin_2 (2.5 equiv.) were added in one portion. The glass vial was placed into the light reactor and stirred for corresponding time. The temperature was kept at approximately 23 °C through cooling with six mini fans. After reaction, the crude mixture was purified by column chromatography on silica gel to afford the desired products.

Note: Highly volatile or lower boiling point fluorinated substrates were added outside the glove box by using a syringe.

Phenylboronic acid pinacol ester (52)

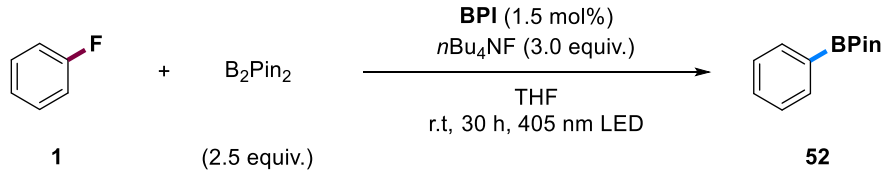

1 52

According to the **GP-4**, **BPI** (5.7 mg, 1.5 mol%), fluorobenzene (48 mg, 0.50 mmol), *n*Bu_4NF (1.5 mmol, 1.5 mL, 3.0 equiv., 1.0M in THF) and B_2Pin_2 (318 mg, 2.50 equiv.) were converted. After being stirred for 30 h, the reaction mixture was purified by chromatography on silica gel eluting with *n*-hexane/ ethyl acetate (10: 1) to afford **52** (72.0 mg, 70.6% yield) as white solid.

^{1}H-NMR (400 Hz, $CDCl_3$, 25 °C) δ= 7.85 – 7.78 (m, 2H), 7.50 – 7.43 (m, 1H), 7.38 –7.34 (m, 2H), 1.35 (s, 12H) ppm.

^{13}C-NMR (101 Hz, $CDCl_3$, 25 °C) δ= 134.89, 131.39, 127.85, 83.91, 25.02 ppm.

The spectroscopic data corresponds to those reported in literature.[41]

4-Methylphenylboronic acid pinacol ester (53)

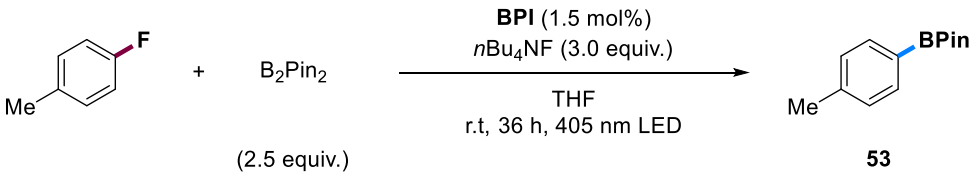

53

According to the **GP-4**, **BPI** (5.7 mg, 1.5 mol%), 4-methylfluorobenzene (55 mg, 0.5 mmol), *n*Bu_4NF (1.5 mmol, 1.5 mL, 3.0 equiv., 1.0M in THF) and B_2Pin_2 (318 mg, 2.50 equiv.) were

converted. After being stirred for 36 h, mesitylene (60 mg, 0.50 mmol) was added as internal standard. The yield of title compound **53** was determined by GC relative to the internal standard (51.8% yield).

4-Methoxyphenylboronic acid pinacol ester (54)

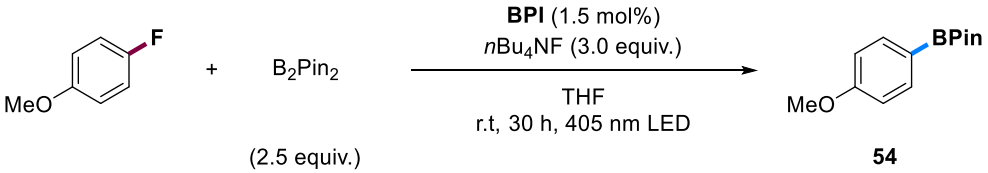

According to the **GP-4**, **BPI** (5.8 mg, 1.5 mol%), 1-fluoro-4-methoxybenzene (63 mg, 0.5 mmol), *n*Bu_4NF (1.5 mmol, 1.5 mL, 3.0 equiv., 1.0M in THF) and B_2Pin_2 (319 mg, 2.50 equiv.) were converted. After being stirred for 30 h, the reaction mixture was purified by chromatography on silica gel eluting with *n*-hexane/ ethyl acetate (10: 1) to afford **54** (69.8 mg, 59.7% yield) as white solid.

^{1}H-NMR (400 Hz, $CDCl_3$, 25 °C) δ= 8.21 – 8.01 (m, 2H), 7.33 – 7.11 (m, 2H), 4.16 (s, 3H), 1.69 (s, 12H) ppm.

^{13}C-NMR (101 Hz, $CDCl_3$, 25 °C) δ= 162.25, 136.61, 113.39, 83.60, 55.13, 24.94 ppm.

The spectroscopic data corresponds to those reported in literature.[41]

4-Methoxycarbonylphenylboronic acid pinacol ester (55)

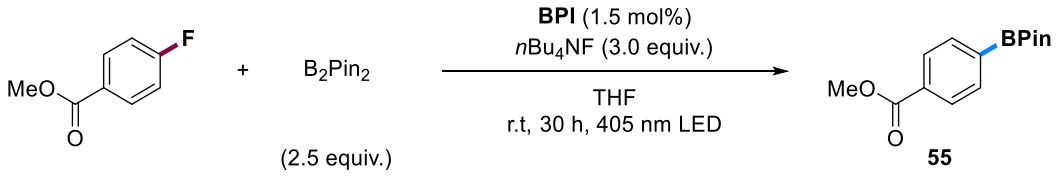

According to the **GP-4**, **BPI** (5.7 mg, 1.5 mol%), methyl 4-flurobenzoate (77 mg, 0.5 mmol), *n*Bu_4NF (1.5 mmol, 1.5 mL, 3.0 equiv., 1.0M in THF) and B_2Pin_2 (317 mg, 2.50 equiv.) were converted. After being stirred for 30 h, the reaction mixture was purified by chromatography on silica gel eluting with *n*-hexane/ ethyl acetate (25: 1) to afford **55** (110.8 mg, 84.60% yield) as white solid.

^{1}H-NMR (400 Hz, $CDCl_3$, 25 °C) δ= 8.02 (d, *J* = 7.7 Hz, 2H), 7.87 (d, *J* = 7.6 Hz, 2H), 3.92 (s, 3H), 1.36 (s, 12H) ppm.

^{13}C-NMR (101 Hz, $CDCl_3$, 25 °C) δ= 167.13, 134.65, 132.30, 128.58, 84.17, 52.14, 24.87 ppm.

The spectroscopic data corresponds to those reported in literature.[41]

4-Cyanophenylboronic acid pinacol ester (56)

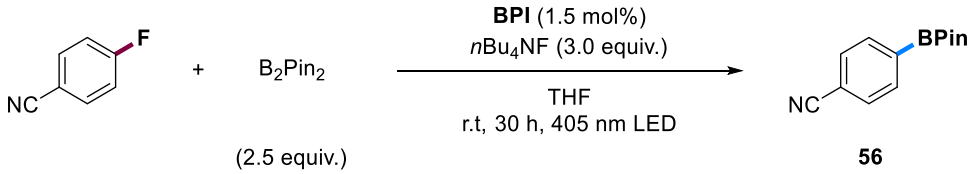

According to the **GP-4**, **BPI** (5.6 mg, 1.5 mol%), 4-fluorobenzonitrile (60.5 mg, 0.500 mmol), *n*Bu_4NF (1.5 mmol, 1.5 mL, 3.0 equiv., 1.0M in THF) and B_2Pin_2 (317 mg, 2.50 equiv.) were converted. After being stirred for 30 h, the reaction mixture was purified by chromatography on silica gel eluting with *n*-hexane/ ethyl acetate (20: 1) to afford **56** (84.8 mg, 73.7% yield) as white solid.

^{1}H-NMR (400 Hz, $CDCl_3$, 25 °C) δ= 7.88 (d, *J* = 7.6 Hz, 2H), 7.64 (d, *J* = 7.7 Hz, 2H), 1.35 (s, 12H) ppm.

^{13}C-NMR (101 Hz, $CDCl_3$, 25 °C) δ= 135.24, 131.28, 119.02, 114.69, 84.64, 25.01 ppm.

The spectroscopic data corresponds to those reported in literature.[41]

3-Cyanophenylboronic acid pinacol ester (57)

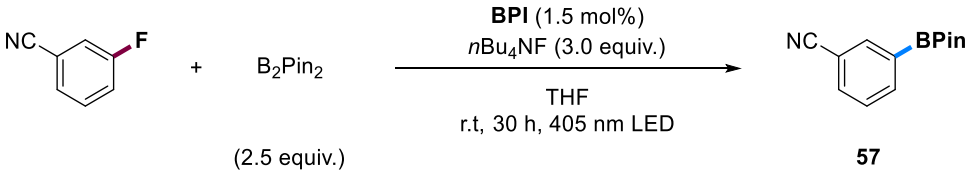

According to the **GP-4**, **BPI** (5.7 mg, 1.5 mol%), 3-fluorobenzonitrile (60.5 mg, 0.500 mmol), *n*Bu_4NF (1.5 mmol, 1.5 mL, 3.0 equiv., 1.0M in THF) and B_2Pin_2 (317 mg, 2.50 equiv.) were converted. After being stirred for 30 h, the reaction mixture was purified by chromatography on silica gel eluting with *n*-hexane/ ethyl acetate (20: 1) to afford **57** (54.6 mg, 47.7% yield) as white solid.

^{1}H-NMR (400 Hz, $CDCl_3$, 25 °C) δ= 8.09 – 8.07 (m, 1H), 8.00 (d, *J* = 7.5Hz, 1H), 7.72 (d, *J* = 7.8 Hz, 1H), 7.46 (t, *J* = 7.6 Hz, 1H), 1.35 (s, 12H) ppm.

^{13}C-NMR (101 Hz, $CDCl_3$, 25 °C) δ= 138.88, 138.55, 134.54, 128.53, 118.98, 112.22, 84.63, 25.00 ppm.

The spectroscopic data corresponds to those reported in literature.[41]

2-(4-(4,4,5,5-tetramethyl-1,3,2-dioxaborolan-2-yl)benzyl)-1,2,3,4-tetrahydroisoquinoline (58)

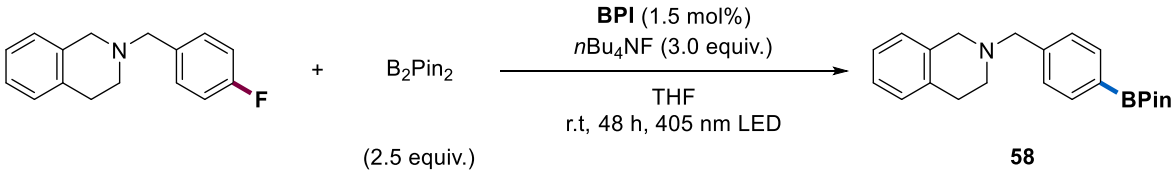

According to the **GP-4**, **BPI** (5.8 mg, 1.5 mol%), 2-(4-fluoro-benzyl)-1,2,3,4-tetrahydro-isoquinoline (220 mg, 0.500 mmol), *n*Bu_4NF (1.5 mmol, 1.5 mL, 3.0 equiv., 1.0M in THF) and B_2Pin_2 (317 mg, 2.50 equiv.) were converted. After being stirred for 48 h, the reaction mixture was purified by chromatography on silica gel eluting with *n*-hexane/ ethyl acetate (20: 1) to afford **58** (92.6 mg, 53.1% yield) as white solid.

^{1}H-NMR (400 Hz, $CDCl_3$, 25 °C) δ= 7.80 (d, *J* = 7.5 Hz, 2H), 7.43 (d, *J* = 7.5 Hz, 2H), 7.13 – 7.10 (m, 3H), 7.00 – 6.97 (m, 1H), 3.71 (s, 2H), 3.64 (s, 2H), 2.90 (t, *J* = 6.0 Hz, 2H), 2.74 (t, *J* = 5.9 Hz, 2H), 1.36 (s, 12H) ppm.

^{13}C-NMR (101 Hz, $CDCl_3$, 25 °C) δ= 141.89, 135.03, 134.95, 134.49, 128.83, 128.57, 126.73, 126.21, 125.69, 83.87, 62.97, 56.31, 50.79, 29.26, 25.01 ppm.

HRMS (ESI) Calculated for $C_{22}H_{29}BNO_2^+$ $[M+H]^+$ (**58**): 350.2286, measured: 350.2289

The starting materials (2-(4-Fluoro-benzyl)-1,2,3,4-tetrahydro-isoquinoline) were prepared according to literature procedures using standard Schlenk technique.[42]

4,4,5,5-tetramethyl-2-[4-(2-phenoxyethoxy)phenyl][1,3,2]dioxaborolane (59)

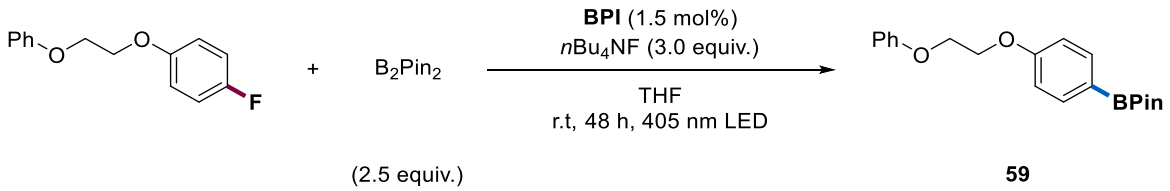

According to the **GP-4**, **BPI** (5.8 mg, 1.5 mol%), 1-p-Fluorphenoxy-2-phenoxyaethan (60.5 mg, 0.500 mmol), *n*Bu_4NF (1.5 mmol, 1.5 mL, 3.0 equiv., 1.0M in THF) and B_2Pin_2 (317 mg, 2.50 equiv.) were converted. After being stirred for 48 h, the reaction mixture was purified by chromatography on silica gel eluting with *n*-hexane/ ethyl acetate (10: 1) to afford **59** (82.1 mg, 48.3% yield) as white solid.

^{1}H-NMR (400 Hz, $CDCl_3$, 25 °C) δ= 7.85 – 7.77 (m, 2H), 7.33 – 7.30 (m, 2H), 7.02 – 6.95 (m, 5H), 4.37 – 4.32 (m, 4H), 1.37 (s, 12H) ppm.

^{13}C-NMR (101 Hz, $CDCl_3$, 25 °C) δ= 160.99, 158.37, 136.33, 129.27, 120.89, 114.47, 113.77, 83.34, 66.12, 66.04, 24.65 ppm.

HRMS (ESI) Calculated for $C_{20}H_{26}BO_4^+$ $[M+H]^+$ (**59**): 341.1919, measured: 341.1928

The starting materials (1-p-Fluorphenoxy-2-phenoxyaethan) were prepared according to literature procedures using standard Schlenk technique.[42]

4,4,5,5-tetramethyl-4-[2-(naphthalen-2-ylsulfanylmethyl)phenyl]-1,3,2-dioxaborolane (60)

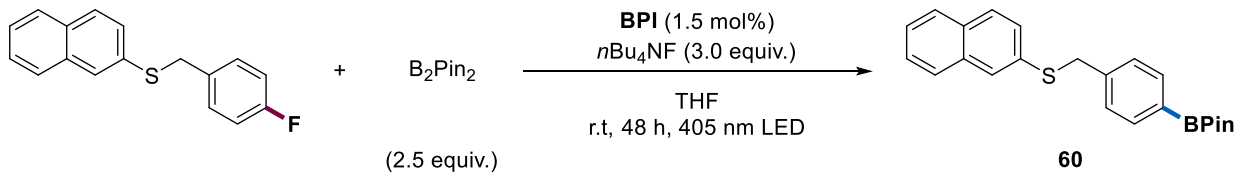

According to the **GP-4**, **BPI** (5.7 mg, 1.5 mol%), 2-(4-fluorobenzylthio)naphthalene (134 mg, 0.500 mmol), *n*Bu_4NF (1.5 mmol, 1.5 mL, 3.0 equiv., 1.0M in THF) and B_2Pin_2 (317 mg, 2.50 equiv.) were converted. After being stirred for 48 h, the reaction mixture was purified by chromatography on silica gel eluting with *n*-hexane/ ethyl acetate (10: 1) to afford **60** (112 mg, 59.6% yield) as white solid.

^{1}H-NMR (400 Hz, $CDCl_3$, 25 °C) δ= 7.87 – 7.69 (m, 6H), 7.55 – 7.35 (m, 5H), 4.25 (s, 2H), 1.39 (s, 12H) ppm.

^{13}C-NMR (101 Hz, $CDCl_3$, 25 °C) δ= 140.68, 135.11, 133.88, 133.77, 131.94, 128.39, 128.30, 127.75, 127.73, 127.71, 127.23, 126.53, 83.82, 39.04, 24.94 ppm.

HRMS (ESI) Calculated for $C_{23}H_{26}BO_2S^+$ $[M+H]^+$ (**60**): 377.1741, measured:377.1762

The starting materials (2-(4-fluorobenzylthio)naphthalene) were prepared according to literature procedures using standard Schlenk technique.[43]

4-methyl-7-[4-(4,4,5,5-tetramethyl-[1,3,2] dioxaborolan-2-yl)-benzyloxy]-chromen-2-one (61)

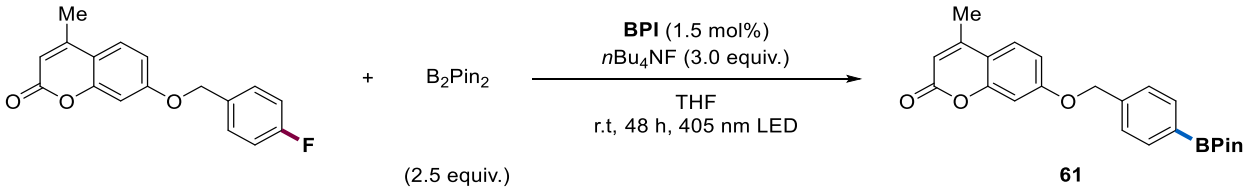

According to the **GP-4**, **BPI** (5.9 mg, 1.5 mol%), 7-(4-fluorobenzyloxy)-4-methylcoumarin (142 mg, 0.500 mmol), *n*Bu_4NF (1.5 mmol, 1.5 mL, 3.0 equiv., 1.0M in THF) and B_2Pin_2 (317 mg, 2.50 equiv.) were converted. After being stirred for 48 h, the reaction mixture was purified by

chromatography on silica gel eluting with *n*-hexane/ ethyl acetate (5: 1) to afford **61** (91.7 mg, 46.8% yield) as white solid.

^{1}H-NMR (400 Hz, $CDCl_3$, 25 °C) δ= 7.83 (d, J = 7.5 Hz, 2H), 7.49 (d, J = 8.9 Hz, 1H), 7.43 (d, J = 7.5 Hz, 2H), 6.92 (d, J = 8.8 Hz, 1H), 6.88 – 6.86 (m, 1H), 6.13 (s, 1H), 5.17 – 5.14 (m, 2H), 2.39 (s, 3H), 1.35 (s, 12H) ppm.

^{13}C-NMR (101 Hz, $CDCl_3$, 25 °C) δ= 161.75, 161.38, 155.33, 152.61, 139.02, 135.32, 126.70, 125.69, 113.95, 113.05, 112.24, 102.17, 84.03, 70.49, 25.00, 18.80 ppm.

The spectroscopic data corresponds to those reported in literature.[44]

The starting materials (7-(4-fluorobenzyloxy)-4-methylcoumarin) were prepared according to literature procedures using standard Schlenk technique.[45]

Benzene-1,4-diboronic acid bispinacol ester (62)

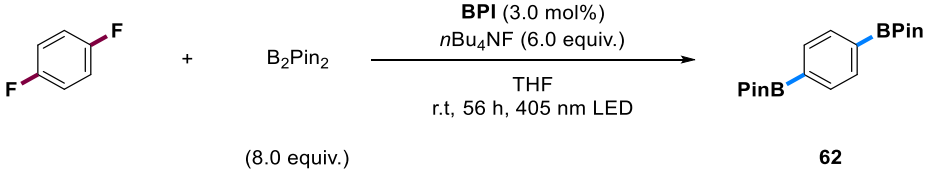

According to the **GP-4**, **BPI** (11.6 mg, 3.0 mol%), 1,4-difluorobenzene (57 mg, 0.50 mmol), *n*Bu_4NF (3.0 mmol, 3.0 mL, 6.0 equiv., 1.0M in THF) and B_2Pin_2 (1.01 g, 8.00 equiv.) were converted. After being stirred for 56 h, the reaction mixture was purified by chromatography on silica gel eluting with *n*-hexane/ ethyl acetate (10: 1) to afford **62** (73.7 mg, 44.7% yield) as white solid.

^{1}H-NMR (400 Hz, $CDCl_3$, 25 °C) δ= 7.80 (s, 4H), 1.35 (s, 24H) ppm.

^{13}C-NMR (101 Hz, $CDCl_3$, 25 °C) δ= 134.03, 84.00, 25.02 ppm. (the signals for the carbons that are attached to the boron atoms were not observed)

The spectroscopic data corresponds to those reported in literature.[41]

4-(4,4,6,6-tetramethyl-1,3,2-dioxaborinan-2-yl) benzonitrile (63)

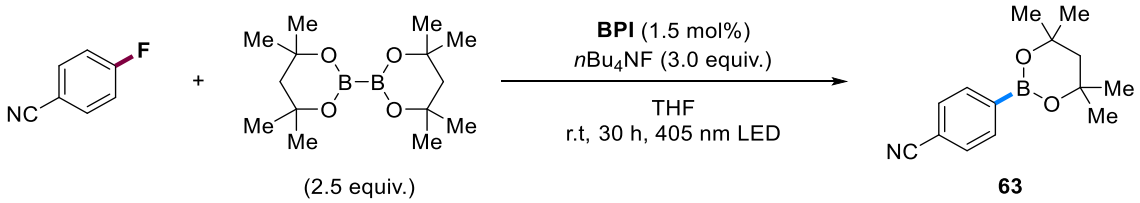

According to the **GP-4**, **BPI** (5.7 mg, 1.5 mol%), 4-fluorobenzonitrile (60.5 mg, 0.500 mmol), *n*Bu_4NF (1.5 mmol, 1.5 mL, 3.0 equiv., 1.0M in THF) and bis(2,4-dimethylpentane-2,4-glycolato)diboron (353 mg, 2.50 equiv.) were converted. After being stirred for 30 h, the reaction mixture was purified by chromatography on silica gel eluting with *n*-hexane/ ethyl acetate (10: 1) to afford **63** (70.8 mg, 58.3% yield) as white solid.

^{1}H-NMR (400 Hz, $CDCl_3$, 25 °C) δ= 7.90 (d, *J* = 7.6 Hz, 1H), 7.66 (d, *J* = 7.7 Hz, 1H), 7.60 (d, *J* = 7.6 Hz, 1H), 7.48 (d, *J* = 7.6 Hz, 1H), 1.93 (s, 1H), 1.79 (s, 1H), 1.43 (s, 6H), 1.33 (s, 6H) ppm.

^{13}C-NMR (101 Hz, $CDCl_3$, 25 °C) δ= 134.36, 132.92, 132.32, 131.03, 129.27, 71.57, 69.54, 49.63, 49.02, 32.06, 31.88 ppm.

HRMS (ESI) Calculated for $C_{14}H_{19}BNO_2^+$ $[M+H]^+$ (**63**): 244.1504, measured: 244.1527

5,5-Dimethyl-2-phenyl-1,3,2-dioxaborinane (64)

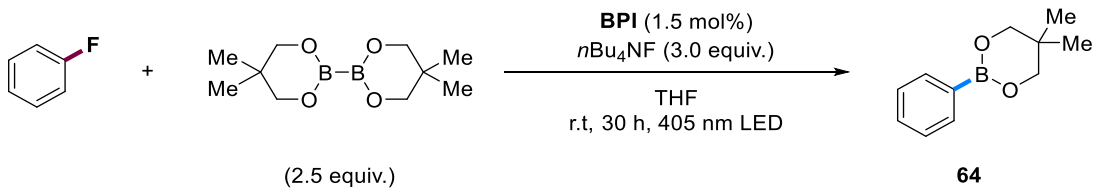

According to the **GP-4**, **BPI** (5.7 mg, 1.5 mol%), fluorobenzene (48 mg, 0.50 mmol), nBu$_4$NF (1.5 mmol, 1.5 mL, 3.0 equiv., 1.0M in THF) and $B_2(neop)_2$ (282 mg, 2.50 equiv.) were converted. After being stirred for 30 h, the reaction mixture was purified by chromatography on silica gel eluting with *n*-hexane/ ethyl acetate (10: 1) to afford **64** (37.6 mg, 39.6% yield) as white solid.

^{1}H-NMR (400 Hz, $CDCl_3$, 25 °C) δ= 7.86 – 7.80 (m, 2H), 7.48 – 7.42 (m, 1H), 7.40 – 7.35 (m, 2H), 3.79 (s, 4H), 1.04 (s, 6H) ppm.

^{13}C-NMR (101 Hz, $CDCl_3$, 25 °C) δ= 133.95, 130.80, 127.70, 72.43, 32.00, 22.03 ppm.

The spectroscopic data corresponds to those reported in literature.[46]

(1S,2R,5S)-2-Isopropyl-5-methylcyclohexyl 4-(4,4,5,5-tetramethyl-1,3,2-dioxaborolan-2-yl)benzoat (65)

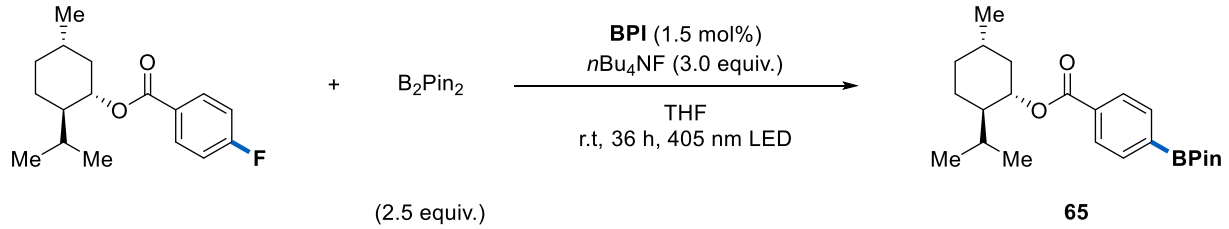

According to the **GP-4**, **BPI** (5.8 mg, 1.5 mol%), 2-isopropyl-5-methylcyclohexyl 4-fluorobenzoate (139 mg, 0.500 mmol), *n*Bu_4NF (1.5 mmol, 1.5 mL, 3.0 equiv., 1.0M in THF) and B_2Pin_2 (318 mg, 2.50 equiv.) were converted. After being stirred for 36 h, the reaction mixture was purified by chromatography on silica gel eluting with *n*-hexane/ ethyl acetate (20: 1) to afford **65** (116.2 mg, 60.20% yield) as white solid.

^{1}H-NMR (400 Hz, $CDCl_3$, 25 °C) δ= 8.02 (d, *J* = 7.7 Hz, 2H), 7.86 (d, *J* = 7.7 Hz, 2H), 4.94 (td, *J* = 10.9, 4.4 Hz, 1H), 2.22 – 2.06 (m, 1H), 1.94 – 1.92 (m, 1H), 1.77 – 1.69 (m, 2H), 1.61 – 1.52 (m, 2H), 1.35 (s, 12H), 1.14 – 1.11 (m, 2H), 0.94 – 0.91 (m, 7H), 0.79 (d, *J* = 6.9 Hz, 3H) ppm.

^{13}C-NMR (101 Hz, $CDCl_3$, 25 °C) δ= 166.24, 134.76, 133.18, 128.70, 84.25, 75.05, 47.38, 41.08, 34.46, 31.59, 26.66, 25.03, 24.96, 23.82, 22.18, 20.87, 16.69 ppm.

The spectroscopic data corresponds to those reported in literature.[47]

The starting materials (2-isopropyl-5-methylcyclohexyl 4-fluorobenzoate) were prepared according to literature procedures using standard Schlenk technique.[32]

(*E*)-3,7-dimethylocta-2,6-dien-1-yl 4-(4,4,5,5-tetramethyl-1,3,2-dioxaborolan-2-yl)benzoate (66)

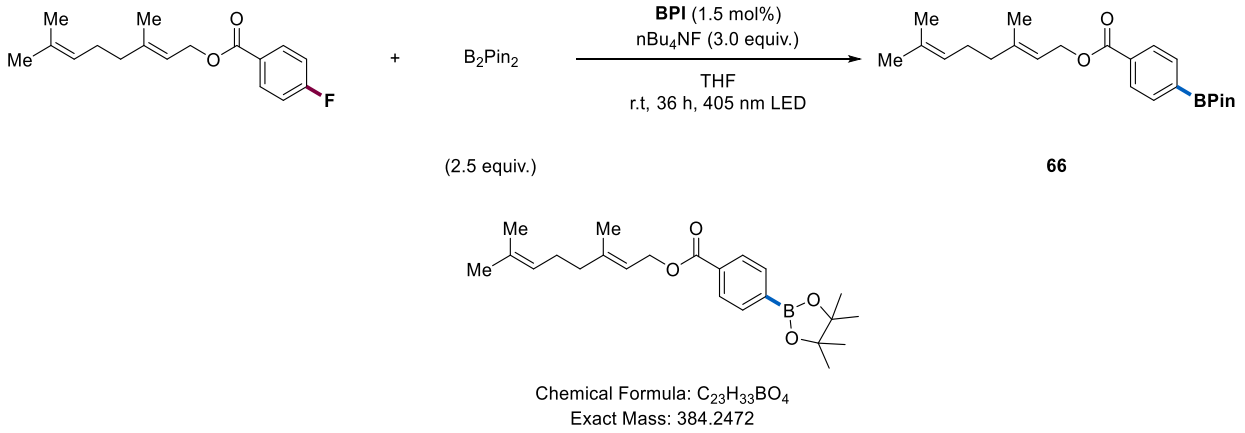

According to the **GP-4**, **BPI** (5.9 mg, 1.5 mol%), neryl 4-fluorobenzoate (138 mg, 0.500 mmol), nBu_4NF (1.5 mmol, 1.5 mL, 3.0 equiv., 1.0M in THF) and B_2Pin_2 (319 mg, 2.50 equiv.) were converted. After being stirred for 36 h, the reaction mixture was purified by chromatography on silica gel eluting with *n*-hexane/ ethyl acetate (10: 1) to afford **66** (98.3 mg, 51.2% yield) as white solid.

^{1}H-NMR (400 Hz, $CDCl_3$, 25 °C) δ= 8.05 – 7.99 (d, *J* = 7.6 Hz, 2H), 7.86 (d, *J* = 7.7 Hz, 2H), 5.47 (t, *J* = 7.2 Hz, 1H), 5.09 (t, *J* = 6.7 Hz, 1H), 4.84 (d, *J* = 7.0 Hz, 2H), 2.13 – 2.10 (m, 4H), 1.74 (s, 3H), 1.67 (s, 3H), 1.60 (s, 3H), 1.35 (s, 12H) ppm.

^{13}C-NMR (101 Hz, $CDCl_3$, 25 °C) δ= 166.83, 142.47, 134.74, 132.84, 131.98, 128.75, 123.88, 118.53, 84.29, 62.13, 39.69, 26.43, 25.82, 25.02, 17.84, 16.70 ppm.

HRMS (ESI) Calculated for $C_{23}H_{34}BO_4^+$ $[M+H]^+$ (**66**): 385.2545, measured: 385.2549

The starting materials (neryl 4-fluorobenzoate) were prepared according to literature procedures using standard Schlenk technique.[48]

1,3,3-Trimethylbicyclo[2.2.1]heptan-2-yl 4-(4,4,5,5-tetramethyl-1,3,2-dioxaborolan-2-yl)benzoate (67)

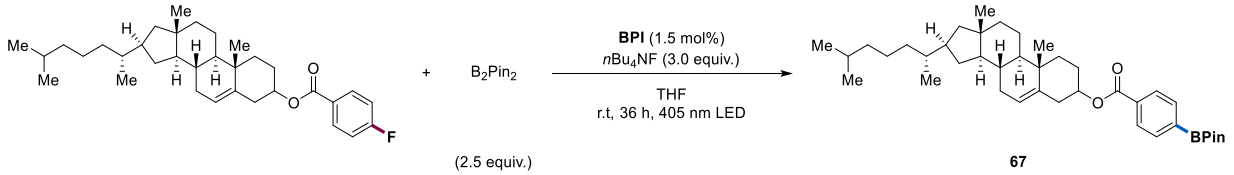

According to the **GP-4**, **BPI** (5.7 mg, 1.5 mol%), cholesterol *p*-fluorobenzoate (254 mg, 0.500 mmol), nBu$_4$NF (1.5 mmol, 1.5 mL, 3.0 equiv., 1.0M in THF) and B_2Pin_2 (319 mg, 2.50 equiv.) were converted. After being stirred for 30 h, the reaction mixture was purified by chromatography on silica gel eluting with *n*-hexane/ ethyl acetate/ DCM (50: 1: 1) to afford **67** (125.6 mg, 40.80% yield) as white solid.

^{1}H-NMR (400 Hz, $CDCl_3$, 25 °C) δ= 8.01 (d, J = 8.1 Hz, 2H), 7.89 – 7.83 (m, 2H), 5.43 – 5.41 (m, 1H), 4.88 – 4.86 (m, 1H), 2.48 – 2.45 (m, 2H), 2.07 – 1.46 (m, 14H), 1.36 (s, 12H), 1.27 – 0.99 (m, 15H), 0.92 (d, J = 6.4 Hz, 3H), 0.87 (s, 6H), 0.69 (s, 3H) ppm.

^{13}C-NMR (101 Hz, $CDCl_3$, 25 °C) δ= 166.15, 139.81, 134.72, 133.17, 128.69, 122.91, 84.27, 74.81, 56.84, 56.28, 50.19, 42.47, 39.89, 39.67, 38.35, 37.19, 36.80, 36.33, 35.94, 32.08, 32.03, 28.38, 28.16, 28.01, 25.02, 24.44, 23.98, 22.97, 22.71, 21.20, 21.18, 19.53, 18.87, 12.01 ppm.

The spectroscopic data corresponds to those reported in literature.[49]

The starting materials (cholesterol *p*-fluorobenzoate) were prepared according to literature procedures using standard Schlenk technique.[50]

6.3 Failed and low yielding substrates

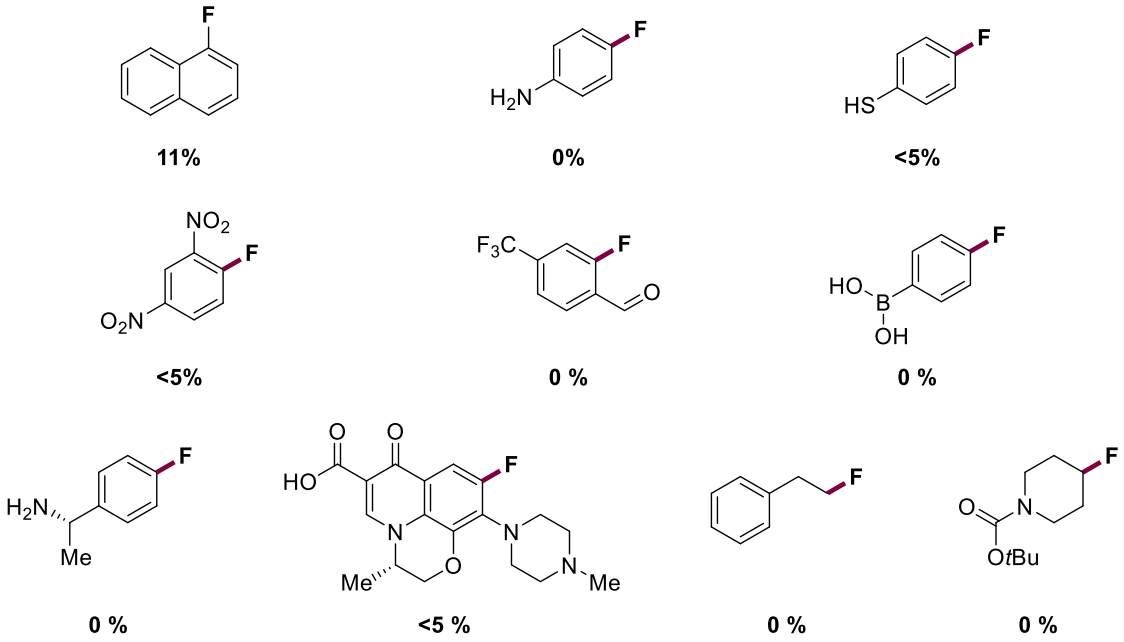

Figure. S2.7. Failed and low yielding substrates in borylation reactions. Reaction conditions: BPI (1.5 mol%), organofluorides (0.5 mmol), nBu_4NF (1.5 mmol, 3.0 equiv., 1.0M in THF), B_2Pin_2 (2.5 equiv.), r.t (23 °C), 36 h, 405 nm LED. The conversions were determined by GC using mesitylene as the internal standard.

6.4 Substrate scope for other aryl halides

9-(3-(4,4,5,5-tetramethyl-1,3,2-dioxaborolan-2-yl)Phenyl)carbazole (68)

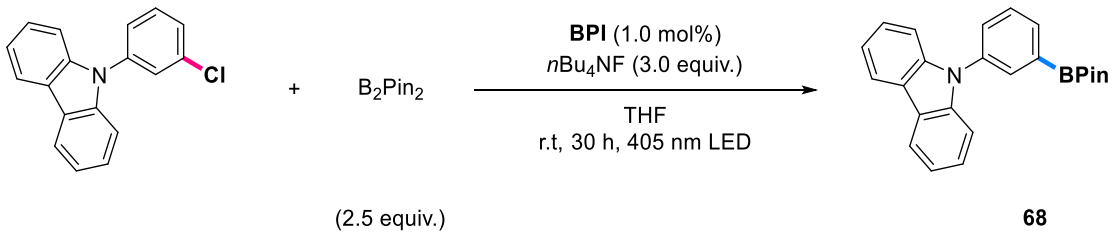

According to the **GP-4**, **BPI** (3.8 mg, 1.0 mol%), 9-(3-chlorophenyl)-9H-carbazole (139 mg, 0.500 mmol), nBu$_4$NF (1.5 mmol, 1.5 mL, 3.0 equiv., 1.0M in THF) and B_2Pin_2 (318 mg, 2.50 equiv.)

were converted. After being stirred for 30 h, the reaction mixture was purified by chromatography on silica gel eluting with *n*-hexane/ ethyl acetate (40: 1) to afford **68** (108 mg, 58.5% yield) as white solid.

^{1}H-NMR (400 Hz, $CDCl_3$, 25 °C) δ= 8.15 (d, *J* = 7.7 Hz, 2H), 8.00 (s, 1H), 7.92 (d, *J* = 6.9 Hz, 1H), 7.69 – 7.51 (m, 2H), 7.49 – 7.34 (m, 4H), 7.30 – 7,27 (m, 2H), 1.36 (s, 12H) ppm.

^{13}C-NMR (101 Hz, $CDCl_3$, 25 °C) δ= 141.22, 137.39, 133.97, 133.67, 130.27, 129.44, 125.99, 123.44, 120.38, 119.91, 109.98, 84.25, 25.04. ppm.

The spectroscopic data corresponds to those reported in literature.[51]

2-(biphenyl-4-yl)-4,4,5,5-Tetramethyl-1,3,2-dioxaborolane (69)

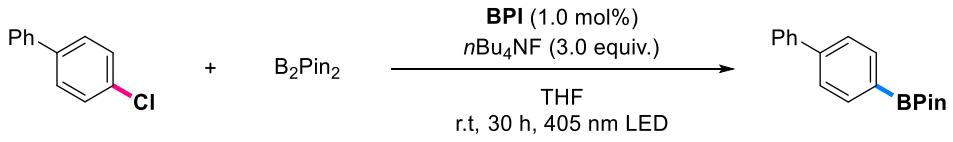

According to the **GP-4**, **BPI** (3.8 mg, 1.0 mol%), 4-chlorobiphenyl (94.0 mg, 0.498 mmol), *n*Bu_4NF (1.5 mmol, 1.5 mL, 3.0 equiv., 1.0M in THF) and B_2Pin_2 (318 mg, 2.50 equiv.) were converted. After being stirred for 30 h, the reaction mixture was purified by chromatography on

silica gel eluting with *n*-hexane/ ethyl acetate (25: 1) to afford **69** (88.3 mg, 63.1% yield) as white solid.

^{1}H-NMR (400 Hz, $CDCl_3$, 25 °C) δ= 7.93 – 7.86 (m, 2H), 7.65 – 7.60 (m, 4H), 7.51 – 7.41 (m, 2H), 7.40 – 7.32 (m, 1H), 1.37 (s, 12H) ppm.

^{13}C-NMR (101 Hz, $CDCl_3$, 25 °C) δ= 144.03, 141.17, 135.40, 128.91, 127.70, 127.38, 126.61, 83.96, 25.03 ppm.

The spectroscopic data corresponds to those reported in literature.[41]

7. Phosphonylation reaction

7.1 Reaction optimization

General procedure for optimization studies

In a glovebox, a 5 mL glass vial containing a stirring bar was sequentially charged with **BPI** (10 μmol, 2.0 mol%) and *n*Bu_4NF (y equiv., 1.0M in THF). The mixture was stirred for 20 minutes at 23 °C, and the color changes from orange to light green. Subsequently, fluorobenzene (48 mg, 0.5 mmol), $P(OEt)_3$ (x equiv.) and co-solvent (1.0 mL) were added in one portion. The glass vial was placed into the light reactor and stirred for 30 h. The temperature was kept at approximately 23 °C through cooling with six mini fans. After reaction, the mixture was diluted with ethyl acetate and analyzed by GC using mesitylene (0.5 mmol) as internal standard.

Table S2.11. Evaluation of reaction conditions for phosphonylation of fluorobenzene 1.

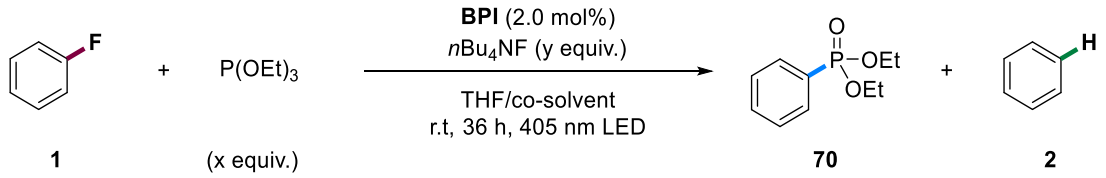

entry	$P(OEt)_3$ (x eq.)	nBu_4NF (y eq.)	co-solvent (1.0 mL)	yield of **70** (%)	yield of **2** (%)
1	5.0	3.0	–	13	<3
2	7.5	3.0	–	11	<3
3	2.5	3.0	–	<3	0
4	5.0	1.0	–	5	<3
5	5.0	3.0	DMF	17	11
6	5.0	3.0	DMSO	22	14
7	5.0	3.0	MeCN	55	11
8	5.0	3.0	DMac	15	19
9	5.0	3.0	*n*-hexane	0	0

*Reaction conditions: **1** (0.5 mmol), **BPI** (2.0 mol%), $P(OEt)_3$ (x equiv.), nBu_4NF (y equiv., 1.0M in THF), co-solvent (1.0 mL), r.t (23 °C), 30 h, 405 nm LED. The conversion and yields were determined by GC using mesitylene as the internal standard.*

7.2 Substrate scope for aryl fluorides

General procedure for the dehalogenation of aryl fluorides (**GP-5**)

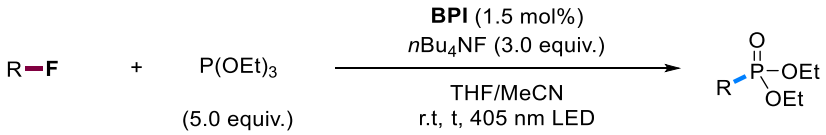

In a glovebox, a 5 mL glass vial containing a stirring bar was sequentially charged with **BPI** (5.0 μmol, 1.0 mol%) and *n*Bu$_4$NF (1.5 mmol, 1.5 mL, 3.0 equiv., 1.0M in THF). The mixture was stirred for 20 minutes at 23 °C, and the color changes from orange to light green. Subsequently, the aryl fluorides (0.5 mmol), P(OEt)$_3$ (5.0 equiv.) and MeCN (1.0 mL) were added in one portion. The glass vial was placed into the light reactor and stirred for corresponding time. The temperature was kept at approximately 23 °C through cooling with six mini fans. After reaction, the crude mixture was purified by column chromatography on silica gel to afford the desired products.

Diethyl phenylphosphonate (70)

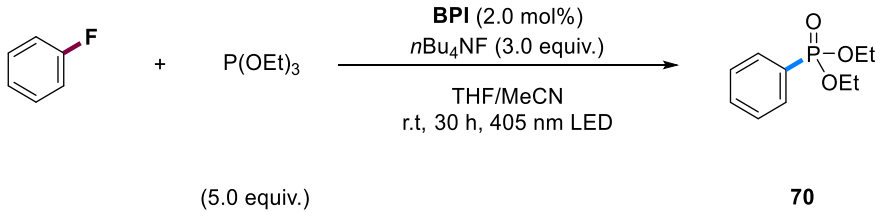

According to the **GP-5**, **BPI** (7.6 mg, 2.0 mol%), fluorobenzene (48 mg, 0.500 mmol), *n*Bu$_4$NF (1.5 mmol, 1.5 mL, 3.0 equiv., 1.0M in THF), P(OEt)$_3$ (415 mg, 5.00 equiv.) and MeCN (1.0 mL) were converted. After being stirred for 30 h, the reaction mixture was purified by chromatography on silica gel eluting with DCM/ methanol (100: 0 to 95: 5) to afford **70** (50.0 mg, 46.8% yield) as colorless oil.

^{1}H-NMR (400 Hz, $CDCl_3$, 25 °C) δ= 7.81 – 7.78 (m, 2H), 7.56 – 7.53 (m, 1H), 7.46 – 7.42 (m, 2H), 4.20 – 4.00 (m, 4H), 1.31 (t, *J* = 7.1 Hz, 6H) ppm.

^{13}C-NMR (101 Hz, $CDCl_3$, 25 °C) δ= 132.49, 132.46, 131.93, 131.83, 129.43, 128.64, 128.49, 127.57, 62.23, 62.18, 16.47, 16.40 ppm.

^{31}P-NMR (162 MHz, $CDCl_3$, 25 °C) δ= 18.79 ppm.

The spectroscopic data corresponds to those reported in literature.[2]

Diethyl 4-methoxyphenylphosphonate (71)

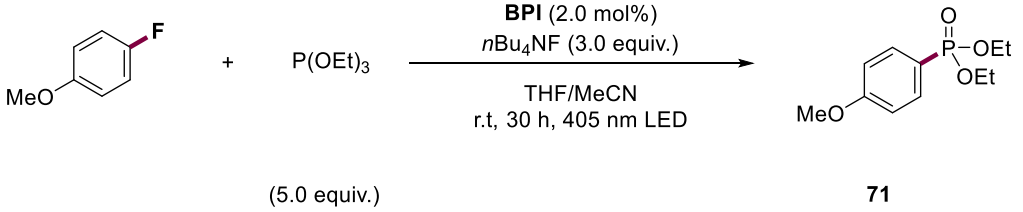

(5.0 equiv.) **71**

According to the **GP-5**, **BPI** (7.6 mg, 2.0 mol%), 1-fluoro-4-methoxybenzene (63 mg, 0.500 mmol), *n*Bu$_4$NF (1.5 mmol, 1.5 mL, 3.0 equiv., 1.0M in THF), P(OEt)$_3$ (415 mg, 5.00 equiv.) and MeCN (1.0 mL) were converted. After being stirred for 30 h, the reaction mixture was purified by chromatography on silica gel eluting with DCM/ methanol (100: 0 to 95: 5) to afford **71** (47.7 mg, 39.1% yield) as light-yellow oil.

^{1}H-NMR (400 Hz, $CDCl_3$, 25 °C) δ= 8.15 – 7.91 (m, 2H), 7.27 – 7.24 (m, 2H), 4.45 – 4.29 (m, 4H), 4.13 (s, 3H), 1.59 (t, *J* = 7.1 Hz, 6H) ppm.

^{13}C-NMR (101 Hz, $CDCl_3$, 25 °C) δ= 162.98, 162.94, 133.95, 133.84, 120.65, 118.71, 114.20, 114.04, 62.04, 61.99, 55.44, 16.48, 16.41 ppm.

^{31}P-NMR (162 MHz, $CDCl_3$, 25 °C) δ= 19.72 ppm.

The spectroscopic data corresponds to those reported in literature.[2]

Diethyl (m-tolyl)phosphonate (72)

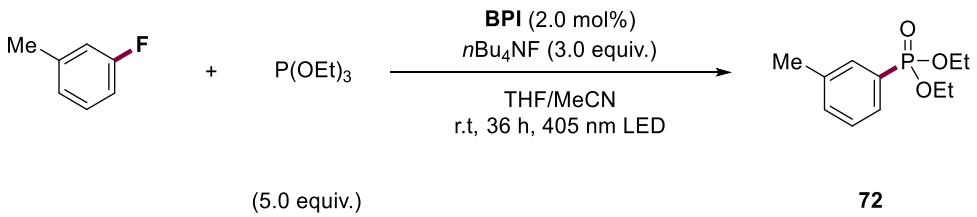

(5.0 equiv.) **72**

According to the **GP-5**, **BPI** (5.7 mg, 1.5 mol%), *m*-fluorotoluene (55 mg, 0.500 mmol), nBu$_4$NF (1.5 mmol, 1.5 mL, 3.0 equiv., 1.0M in THF), P(OEt)$_3$ (415 mg, 5.00 equiv.) and MeCN (1.0 mL) were converted. After being stirred for 36 h, the reaction mixture was purified by chromatography on silica gel eluting with DCM/ methanol (100: 0 to 95: 5) to afford **72** (41.5 mg, 36.4% yield) as light-yellow oil.

^{1}H-NMR (400 Hz, $CDCl_3$, 25 °C) δ= 7.65 – 7.42 (m, 2H), 7.34 – 7.15 (m, 2H), 4.04 – 4.01 (m, 4H), 2.39 – 2.18 (m, 3H), 1.24 (s, 6H) ppm.

^{13}C-NMR (101 Hz, $CDCl_3$, 25 °C) δ= 138.24, 138.10, 133.07, 133.05, 132.24, 132.14, 128.99, 128.73, 128.64, 128.38, 128.22, 127.14, 61.94, 61.89, 21.20, 21.15, 16.27, 16.21 ppm.

^{31}P-NMR (162 MHz, $CDCl_3$, 25 °C) δ= 19.18 ppm.

The spectroscopic data corresponds to those reported in literature.[2]

Methyl 4-(diethoxyphosphoryl)benzoate (73)

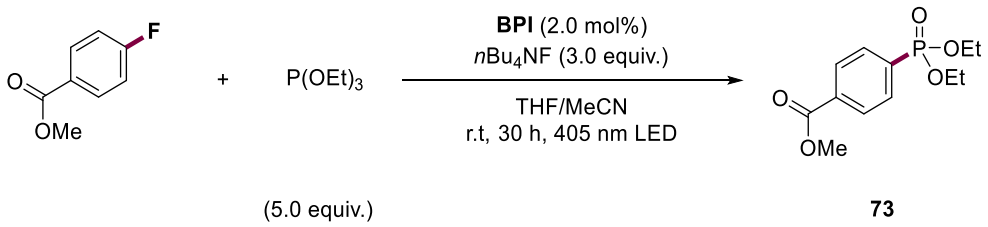

73

According to the **GP-5**, **BPI** (7.6 mg, 2.0 mol%), methyl 4-flurobenzoate (77 mg, 0.500 mmol), nBu$_4$NF (1.5 mmol, 1.5 mL, 3.0 equiv., 1.0M in THF), P(OEt)$_3$ (415 mg, 5.00 equiv.) and MeCN (1.0 mL) were converted. After being stirred for 30 h, the yield of title compound **73** was determined by GC relative to the internal standard (48.6% yield).

8. Hetero arylation reaction

8.1 Reaction optimization

General procedure for optimization studies

In a glovebox, a 5 mL glass vial containing a stirring bar was sequentially charged with **BPI** (10 μmol, 2.0 mol%) and *n*Bu$_4$NF (y equiv., 1.0M in THF). The mixture was stirred for 20 minutes at 23 °C, and the color changes from orange to light green. Subsequently, fluorobenzene (48 mg, 0.5 mmol), *N*-methylpyrrole (x equiv.) and co-solvent (1.0 mL) were added in one portion. The glass vial was placed into the light reactor and stirred for 30 h. The temperature was kept at approximately 23 °C through cooling with six mini fans. After reaction, the mixture was diluted with ethyl acetate and analyzed by GC using mesitylene (0.5 mmol) as internal standard.

Table S12. Evaluation of reaction conditions for arylation of fluorobenzene 1.

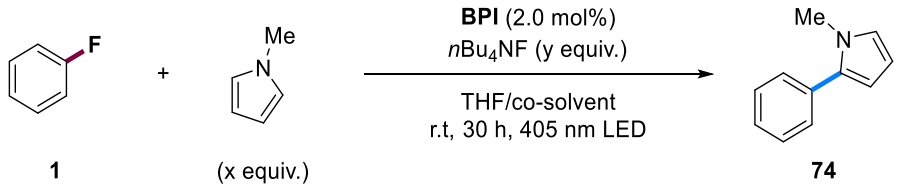

1 (x equiv.) **74**

entry	*N*-methylpyrrole (x eq.)	*n*Bu$_4$NF (y eq.)	co-solvent (1.0 mL)	yield of **74** (%)
1	5.0	3.0	–	6
2	10	3.0	–	12
3	15	3.0	–	20
4	20	3.0	–	36
5	25	3.0	–	37
6	20	2.0	–	31

7	20	3.0	MeCN	29
8	20	3.0	DMac	18
9	20	3.0	DMF	33
10	20	3.0	DMSO	71
11	20	3.0	*n*-hexane	19

Reaction conditions: 1 (0.5 mmol), BPI (2.0 mol%), N-methylpyrrole (x equiv.), nBu$_4$NF (y equiv., 1.0M in THF), co-solvent (1.0 mL), r.t (23 °C), 30 h, 405 nm LED. The conversion and yields were determined by GC using mesitylene as the internal standard.

8.2 Substrate scope for (hetero) arylation reaction

General procedure for the dehalogenation of aryl fluorides (**GP-6**)

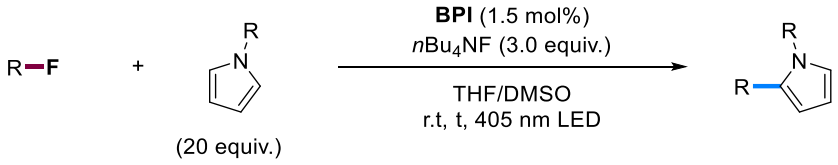

In a glovebox, a 5 mL glass vial containing a stirring bar was sequentially charged with **BPI** (7.5 μmol, 1.5 mol%) and *n*Bu$_4$NF (1.5 mmol, 1.5 mL, 3.0 equiv., 1.0M in THF). The mixture was stirred for 20 minutes at 23 °C, and the color changes from orange to light green. Subsequently, the aryl fluorides (0.5 mmol), heteroarene (20.0 equiv.) and DMSO (1.0 mL) were added in one portion. The glass vial was placed into the light reactor and stirred for corresponding time. The temperature was kept at approximately 23 °C through cooling with six mini fans. After reaction, the crude mixture was purified by column chromatography on silica gel to afford the desired products.

1-Methyl-2-phenylpyrrole (74)

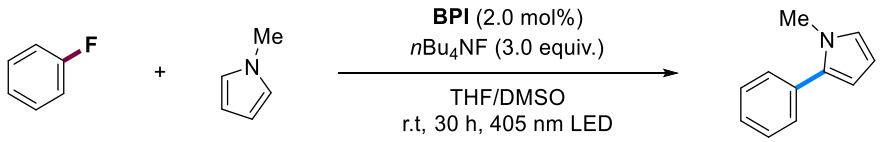

(20 equiv.) **74**

According to the **GP-6**, **BPI** (7.6 mg, 2.0 mol%), fluorobenzene (48 mg, 0.50 mmol), *n*Bu$_4$NF (1.5 mmol, 1.5 mL, 3.0 equiv., 1.0M in THF), *N*-methylpyrrole (20.0 equiv.) and DMSO (1.0 mL) were converted. After being stirred for 30 h, mesitylene (60 mg, 0.5 mmol) was added as internal standard. The yield of the title compound **74** was determined by GC relative to the internal standard (70.8% yield).

1-Methyl-2-(4-cyanophenyl)pyrrole (75)

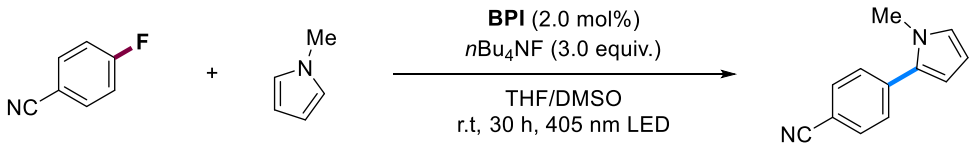

(20 equiv.) **75**

According to the **GP-6**, **BPI** (7.6 mg, 2.0 mol%), 4-fluorobenzonitrile (60.5 mg, 0.500 mmol), *n*Bu$_4$NF (1.5 mmol, 1.5 mL, 3.0 equiv., 1.0M in THF), *N*-methylpyrrole (20.0 equiv.) and DMSO (1.0 mL) were converted. After being stirred for 30 h, the reaction mixture was purified by chromatography on silica gel eluting with *n*-hexane/ ethyl acetate (9: 1) to afford **75** (47.0 mg, 51.7% yield) as light-yellow oil.

^{1}H-NMR (400 Hz, $CDCl_3$, 25 °C) δ= 7.73 – 7.62 (m, 2H), 7.56 – 7.46 (m, 2H), 6.80 – 6.77 (m, 1H), 6.36 (dd, *J* = 3.7, 1.8 Hz, 1H), 6.24 (dd, *J* = 3.7, 2.7 Hz, 1H), 3.72 (s, 3H) ppm.

^{13}C-NMR (101 Hz, $CDCl_3$, 25 °C) δ= 137.75, 132.65, 132.31, 128.31, 125.94, 119.11, 110.82, 109.69, 108.64, 35.52 ppm.

The spectroscopic data corresponds to those reported in literature.[2]

1-Methyl-2-(3-methylphenyl)-1H-pyrrole (76)

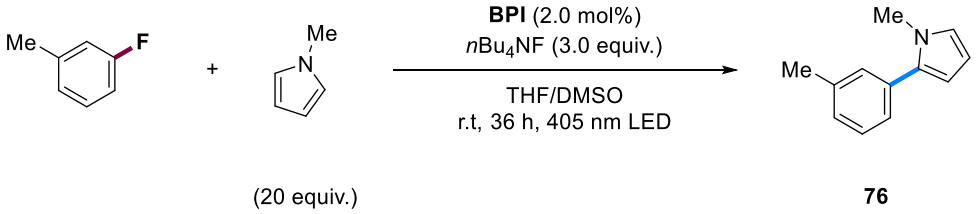

According to the **GP-6**, **BPI** (7.6 mg, 2.0 mol%), *m*-fluorotoluene (55 mg, 0.50 mmol), nBu$_4$NF (1.5 mmol, 1.5 mL, 3.0 equiv., 1.0M in THF), *N*-methylpyrrole (20 equiv.) and DMSO (1.0 mL) were converted. After being stirred for 36 h, mesitylene (60 mg, 0.5 mmol) was added as internal standard. The yield of title compound **76** was determined by ^{1}H-NMR relative to the internal standard (39.3% yield).

2-(1-methyl-1H-pyrrol-2-yl) Benzonitrile (77)

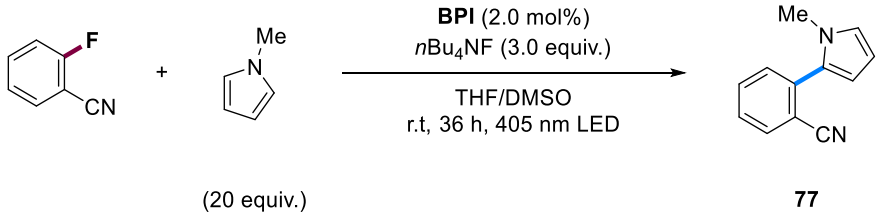

According to the **GP-6**, **BPI** (7.6 mg, 2.0 mol%), 2-fluorobenzonitrile (60.5 mg, 0.500 mmol), nBu$_4$NF (1.5 mmol, 1.5 mL, 3.0 equiv., 1.0M in THF), *N*-methylpyrrole (20 equiv.) and DMSO (1.0 mL) were converted. After being stirred for 36 h, the reaction mixture was purified by chromatography on silica gel eluting with *n*-hexane/ ethyl acetate (10: 1) to afford **77** (34.3 mg, 37.7% yield) as light-yellow oil.

^{1}H-NMR (400 Hz, $CDCl_3$, 25 °C) δ= 7.75 – 7.72 (m, 1H), 7.63 – 7.61 (m, 1H), 7.51 – 7.35 (m, 2H), 6.80 (dd, *J* = 2.7, 1.8 Hz, 1H), 6.48 – 6.37 (m, 1H), 6.26 (dd, *J* = 3.7, 2.7 Hz, 1H), 3.62 (s, 3H) ppm.

^{13}C-NMR (101 Hz, $CDCl_3$, 25 °C) δ= 136.92, 133.55, 132.41, 132.40, 130.89, 129.95, 127.46, 124.86, 118.68, 112.82, 111.47, 108.32, 34.85 ppm.

The spectroscopic data corresponds to those reported in literature.[52]

1-(4-(1-methyl-1H-pyrrol-2-yl) Phenyl)ethan-1-one (78)

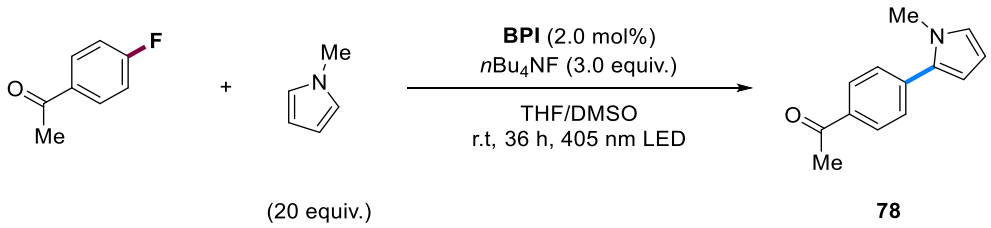

According to the **GP-6**, **BPI** (7.6 mg, 2.0 mol%), 1-(4-Fluorophenyl)ethanone (69 mg, 0.50 mmol), *n*Bu_4NF (1.5 mmol, 1.5 mL, 3.0 equiv., 1.0M in THF), *N*-methylpyrrole (20 equiv.) and DMSO (1.0 mL) were converted. After being stirred for 36 h, the reaction mixture was purified by chromatography on silica gel eluting with *n*-hexane/ ethyl acetate (10: 1) to afford **78** (35.9 mg, 31.6% yield) as light-yellow oil.

^{1}H-NMR (400 Hz, $CDCl_3$, 25 °C) δ= 8.01 – 7.96 (m, 2H), 7.50 (d, *J* = 8.2 Hz, 2H), 6.77 (t, *J* = 2.3 Hz, 1H), 6.35 – 6.33 (m, 1H), 6.23 (q, *J* = 3.7 Hz, 1H), 3.72 (s, 3H), 2.63 (d, *J* = 2.8 Hz, 3H) ppm.

^{13}C-NMR (101 Hz, $CDCl_3$, 25 °C) δ= 197.74, 138.07, 135.09, 128.74, 128.11, 125.46, 110.37, 108.51, 35.59, 26.73 ppm.

The spectroscopic data corresponds to those reported in literature.[52]

1,2-Diphenylpyrrole (79)

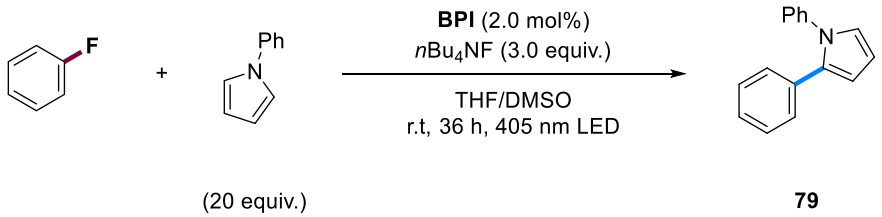

According to the **GP-6**, **BPI** (7.6 mg, 2.0 mol%), fluorobenzene (48 mg, 0.500 mmol), *n*Bu$_4$NF (1.5 mmol, 1.5 mL, 3.0 equiv., 1.0M in THF), 1-phenylpyrrole (20 equiv.) and DMSO (1.0 mL) were converted. After being stirred for 36 h, mesitylene (60 mg, 0.5 mmol) was added as internal standard. The yield of title compound **79** was determined by GC relative to the internal standard (51.8% yield).

1-Benzyl-2-phenyl-1H-pyrrole (80)

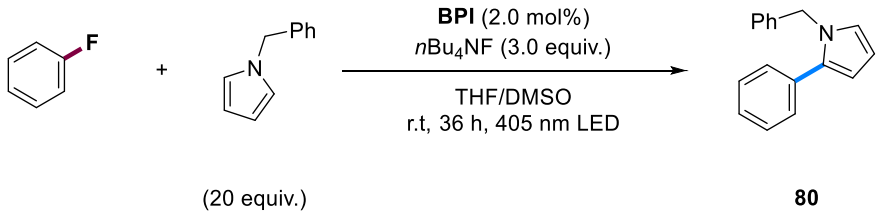

According to the **GP-6**, **BPI** (7.6 mg, 2.0 mol%), fluorobenzene (48 mg, 0.500 mmol), *n*Bu$_4$NF (1.5 mmol, 1.5 mL, 3.0 equiv., 1.0M in THF), 1-benzyl-1H-pyrrole (20 equiv.) and DMSO (1.0 mL) were converted. After being stirred for 36 h, the reaction mixture was purified by chromatography on silica gel eluting with *n*-hexane/ ethyl acetate (10: 1) to afford **80** (69.5 mg, 49.6% yield) as light-yellow oil.

^{1}H-NMR (400 Hz, $CDCl_3$, 25 °C) δ= 7.38 – 7.35 (m, 4H), 7.34 – 7.28 (m, 4H), 7.08 – 7.03 (m, 2H), 6.80 – 6.77 (m, 1H), 6.32 (d, *J* = 2.3 Hz, 2H), 5.19 (s, 2H) ppm.

^{13}C-NMR (101 Hz, $CDCl_3$, 25 °C) δ= 138.97, 135.11, 133.41, 129.02, 128.80, 128.50, 127.44, 127.10, 126.59, 123.02, 109.01, 108.63, 50.78 ppm.

The spectroscopic data corresponds to those reported in literature.[53]

9. Sulfuration & Selenization reaction

9.1 Reaction optimization

General procedure for optimization studies

In a glovebox, a 5 mL glass vial containing a stirring bar was sequentially charged with **BPI** (7.5 μmol, 1.5 mol%) and *n*Bu$_4$NF (y equiv., 1.0M in THF). The mixture was stirred for 20 minutes at 23 °C, and the color changes from orange to light green. Subsequently, fluorobenzene (48 mg, 0.50 mmol), dimethyldisulfide (x equiv.) and co-solvent (1.0 mL) were added in one portion. The glass vial was placed into the light reactor and stirred for 30 h. The temperature was kept at approximately 23 °C through cooling with six mini fans. After reaction, the mixture was diluted with ethyl acetate and analyzed by GC using mesitylene (0.5 mmol) as internal standard.

Table S2.13. Evaluation of reaction conditions for sulfuration of fluorobenzene 1.

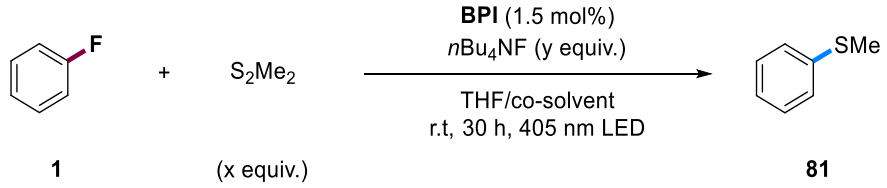

entry	S_2Me_2 (x eq.)	*n*Bu$_4$NF (y eq.)	co-solvent (1.0 mL)	yield of **81** (%)
1	3.0	3.0	–	75
2	2.0	3.0	–	52
3	1.0	3.0	–	33
4	3.0	2.0	–	53
5	3.0	1.0	–	27

6	3.0	3.0	toluene	31
7	3.0	3.0	MeCN	69
8	3.0	3.0	DMac	48
9	3.0	3.0	DMF	53
10	3.0	3.0	DMSO	41
11	3.0	3.0	*n*-hexane	39

Reaction conditions: ***1*** *(0.5 mmol),* ***BPI*** *(1.5 mol%), dimethyldisulfide (x equiv.), nBu_4NF (y equiv., 1.0M in THF), co-solvent (1.0 mL), r.t (23 °C), 30 h, 405 nm LED. The conversion and yields were determined by GC using mesitylene as the internal standard.*

9.2 Substrate scope for sulfuration & Selenization

General procedure for the dehalogenation of aryl fluorides (**GP-7**)

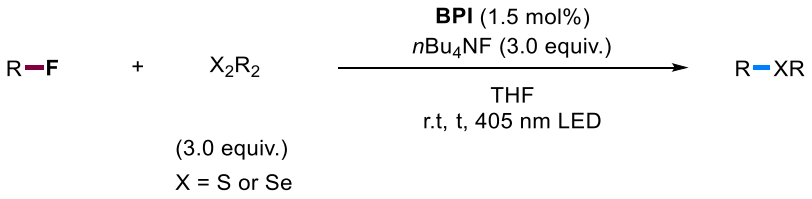

In a glovebox, a 5 mL glass vial containing a stirring bar was sequentially charged with **BPI** (7.5 μmol, 1.5 mol%) and *n*Bu$_4$NF (1.5 mmol, 1.5 mL, 3.0 equiv., 1.0M in THF). The mixture was stirred for 20 minutes at 23 °C, and the color changes from orange to light green. Subsequently, the aryl fluorides (0.5 mmol) and coupling partner (3.0 equiv.) were added in one portion. The glass vial was placed into the light reactor and stirred for corresponding time. The temperature was kept at approximately 23 °C through cooling with six mini fans. After reaction, the crude mixture was purified by column chromatography on silica gel to afford the desired products.

Thioanisole (81)

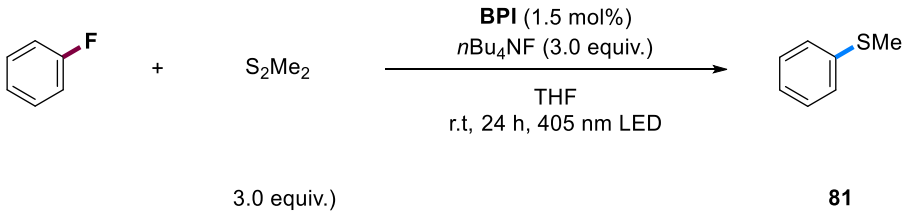

According to the **GP-7**, **BPI** (5.7 mg, 1.5 mol%), fluorobenzene (48 mg, 0.50 mmol), *n*Bu$_4$NF (1.5 mmol, 1.5 mL, 3.0 equiv., 1.0M in THF) and S_2Me_2 (3.0 equiv.) were converted. After being stirred for 24 h, mesitylene (60 mg, 0.5 mmol) was added as internal standard. The yield of title compound **81** was determined by GC relative to the internal standard (71.7% yield).

4-Methylphenyl methylsulfide (82)

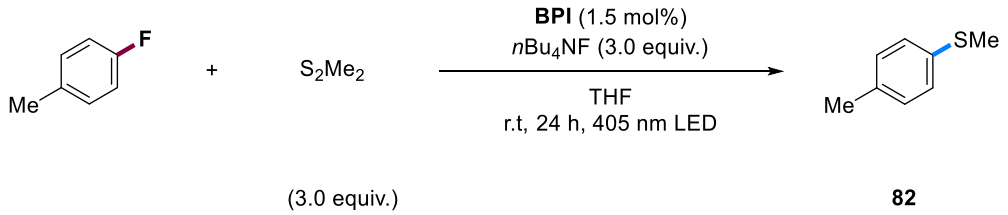

According to the **GP-5**, **BPI** (5.7 mg, 1.5 mol%), 4-fluorotoluene (55 mg, 0.50 mmol), nBu$_4$NF (1.5 mmol, 1.5 mL, 3.0 equiv., 1.0M in THF) and S_2Me_2 (3.0 equiv.) were converted. After being stirred for 24 h, the reaction mixture was purified by chromatography on silica gel eluting with *n*-hexane/ ethyl acetate (50: 1) to afford **82** (36.7 mg, 53.2% yield) as light-yellow oil.

^{1}H-NMR (400 Hz, $CDCl_3$, 25 °C) δ= 7.21 – 7.16 (m, 2H), 7.13 – 7.08 (m, 2H), 2.47 (s, 3H), 2.32 (s, 3H) ppm.

^{13}C-NMR (101 Hz, $CDCl_3$, 25 °C) δ= 135.22, 134.83, 129.75, 127.46, 21.06, 16.70 ppm.

The spectroscopic data corresponds to those reported in literature.[54]

4-Methoxythioanisole (83)

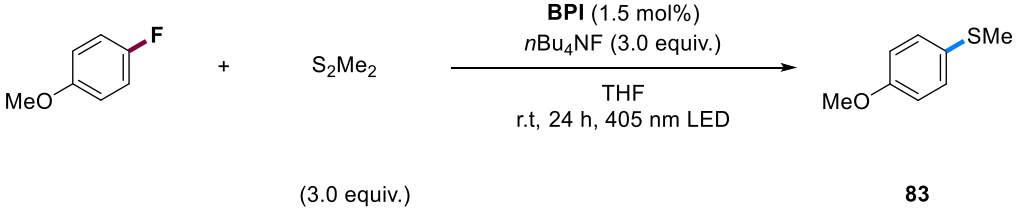

According to the **GP-7**, **BPI** (5.8 mg, 1.5 mol%), 4-fluoroanisole (63 mg, 0.50 mmol), *n*Bu$_4$NF (1.5 mmol, 1.5 mL, 3.0 equiv., 1.0M in THF) and S_2Me_2 (3.0 equiv.) were converted. After being stirred for 24 h, the reaction mixture was purified by chromatography on silica gel eluting with *n*-hexane/ ethyl acetate (50: 1) to afford **83** (46.3 mg, 61.2% yield) as light-yellow oil.

^{1}H-NMR (400 Hz, $CDCl_3$, 25 °C) δ= 7.30 (dd, *J* = 8.7, 1.9 Hz, 2H), 6.92 – 6.83 (m, 2H), 3.82 (d, *J* = 1.0 Hz, 3H), 2.47 (s, 3H) ppm.

^{13}C-NMR (101 Hz, $CDCl_3$, 25 °C) δ= 158.02, 130.02, 128.58, 114.43, 55.18, 17.90 ppm.

The spectroscopic data corresponds to those reported in literature.[54]

3-Methoxythioanisole (84)

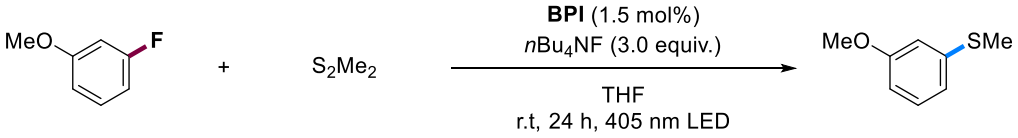

According to the **GP-7**, **BPI** (5.8 mg, 1.5 mol%), 3-fluoroanisole (63 mg, 0.50 mmol), *n*Bu$_4$NF (1.5 mmol, 1.5 mL, 3.0 equiv., 1.0M in THF) and S_2Me_2 (3.0 equiv.) were converted. After being stirred for 24 h, the reaction mixture was purified by chromatography on silica gel eluting with *n*-hexane/ ethyl acetate (50: 1) to afford **84** (29.3 mg, 38.1% yield) as light-yellow oil.

^{1}H-NMR (400 Hz, $CDCl_3$, 25 °C) δ= 7.20 (t, *J* = 8.0 Hz, 1H), 6.88 – 6.78 (m, 2H), 6.68 (d, *J* = 8.2, 1H), 3.80 (s, 3H), 2.48 (s, 3H) ppm.

^{13}C-NMR (101 Hz, $CDCl_3$, 25 °C) δ= 160.03, 139.98, 129.79, 118.91, 112.26, 110.73, 55.38, 15.86 ppm.

The spectroscopic data corresponds to those reported in literature.[54]

2-Methoxythioanisole (85)

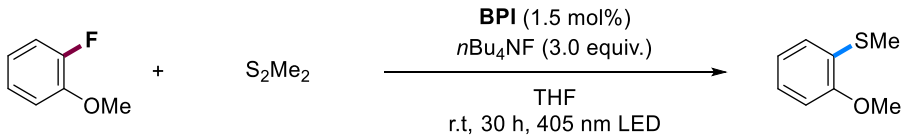

(3.0 equiv.) **85**

According to the **GP-7**, **BPI** (5.9 mg, 1.5 mol%), 2-fluoroanisole (63 mg, 0.50 mmol), nBu$_4$NF (1.5 mmol, 1.5 mL, 3.0 equiv., 1.0M in THF) and S_2Me_2 (3.0 equiv.) were converted. After being stirred for 30 h, the reaction mixture was purified by chromatography on silica gel eluting with *n*-hexane/ ethyl acetate (50: 1) to afford **85** (25.1 mg, 32.6% yield) as light-yellow oil.

^{1}H-NMR (400 Hz, $CDCl_3$, 25 °C) δ= 7.21 – 7.10 (m, 2H), 6.96 (d, J = 7.5 Hz, 1H), 6.84 (d, J = 8.1 Hz, 1H), 3.90 (s, 3H), 2.44 (s, 3H) ppm.

^{13}C-NMR (101 Hz, $CDCl_3$, 25 °C) δ= 156.45, 126.35, 126.07, 121.32, 110.21, 55.90, 14.90 ppm.

The spectroscopic data corresponds to those reported in literature.[54]

Butyl(phenyl)selane (86)

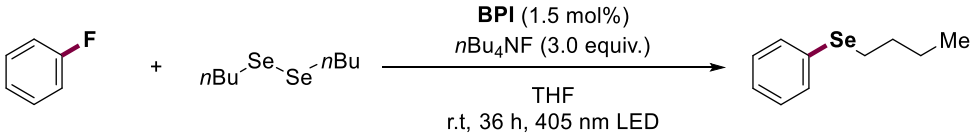

(3.0 equiv.) **86**

According to the **GP-5**, **BPI** (5.8 mg, 1.5 mol%), fluorobenzene (48 mg, 0.500 mmol), nBu$_4$NF (1.5 mmol, 1.5 mL, 3.0 equiv., 1.0M in THF) and Se_2nBu$_2$ (3.0 equiv.) were converted. After being

stirred for 36 h, the reaction mixture was purified by chromatography on silica gel eluting with *n*-hexane/ ethyl acetate (10: 1) to afford **86** (52.8 mg, 49.6% yield) as colorless oil.

^{1}H-NMR (400 Hz, $CDCl_3$, 25 °C) δ= 7.54 – 7.49 (m, 2H), 7.31 – 7.24 (m, 3H), 3.01 – 2.86 (m, 2H), 1.73 – 1.71 (m, 2H), 1.47 – 1.45 (m, 2H), 0.94 (t, *J* = 7.3 Hz, 3H) ppm.

^{13}C-NMR (101 Hz, $CDCl_3$, 25 °C) δ= 132.48, 130.83, 129.10, 126.70, 32.38, 27.75, 23.09, 13.70 ppm.

The spectroscopic data corresponds to those reported in literature.[55]

10. Diversification of 1,4-fluorobenzene

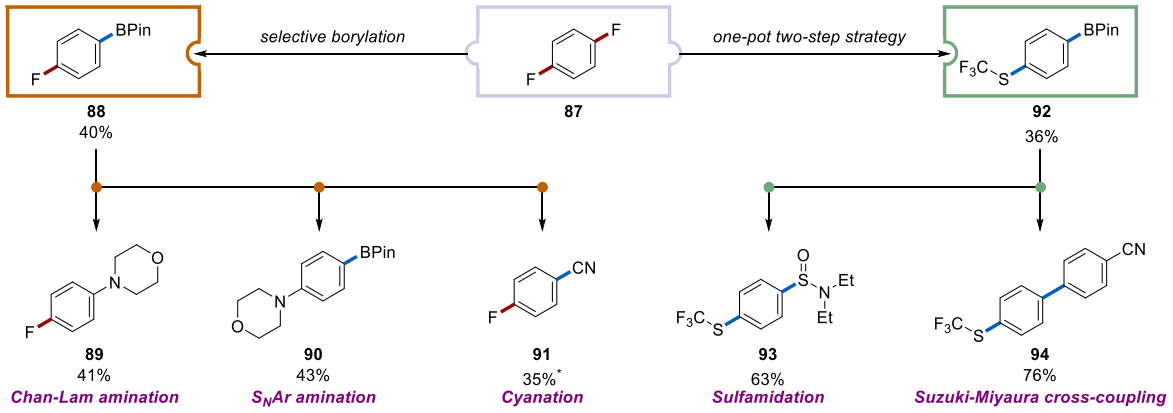

Figure. S2.8. Diversification of 1,4-difluorobenzene.

10.1 Selective borylation

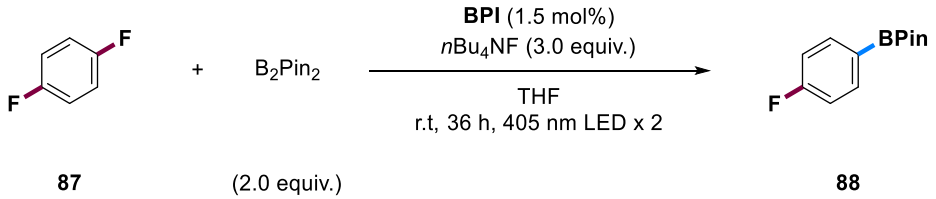

87 (2.0 equiv.) **88**

In glovebox, **BPI** (5.7 mg, 1.5 mol%), 1,4-fluorobenzene (57 mg, 0.50 mmol), *n*Bu_4NF (1.5 mmol, 1.5 mL, 3.0 equiv., 1.0M in THF) and B_2Pin_2 (254 mg, 2.00 equiv.) were converted. After being stirred for 36 h, the reaction mixture was purified by chromatography on silica gel eluting with *n*-hexane/ ethyl acetate (10: 1) to afford **88** (45.0 mg, 40.4% yield) as white solid.

^{1}H-NMR (400 Hz, $CDCl_3$, 25 °C) δ= 7.84 – 7.76 (m, 2H), 7.09 – 7.00 (m, 2H), 1.34 (s, 12H) ppm.

^{13}C-NMR (101 Hz, $CDCl_3$, 25 °C) δ= 165.35 (d, *J* = 249.9 Hz), 137.12 (d, *J* =7.2 Hz), 115.01 (d, *J* = 20.3 Hz), 84.06, 25.00 ppm. (the signal for the carbon that is attached to the boron atom was not observed)

^{19}F-NMR (376 MHz, $CDCl_3$, 25 °C) δ= -108.44 ppm.

The spectroscopic data corresponds to those reported in literature.[56]

10.2 Chan-Lam amination

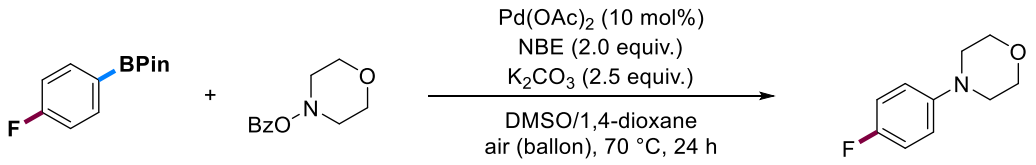

88 **89**

A 25 mL of oven-dried Schlenk tube equipped with a stir bas was charged with 2-(4-fluorophenyl)-4,4,5,5-tetramethyl-1,3,2-dioxaborolane (0.5 mmol, 1.0 equiv.), 4-(benzoyloxy)morpholine (1.0 mmol, 2.0 equiv.), $Pd(OAc)_2$ (0.05 mmol, 10mol%), NBE (1.0 mmol), K_2CO_3 (1.25 mmol), DMSO (0.8 mL) and 1,4-dioxane (2.0 mL). The reaction was stirred at 70 °C under air (ballon) for 24 h. The reaction mixture was purified by chromatography on silica gel eluting with *n*-hexane/ ethyl acetate (20: 1) to afford **89** (37.4 mg, 41.3% yield) as white solid.

^{1}H-NMR (400 Hz, $CDCl_3$, 25 °C) δ= δ 7.04 – 6.96 (m, 2H), 6.92 – 6.85 (m, 2H), 3.94 – 3.83 (m, 4H), 3.17 – 3.02 (m, 4H) ppm.

^{13}C-NMR (101 Hz, $CDCl_3$, 25 °C) δ= 158.41 (d, *J*= 240.0 Hz), 148.04, 117.64 (d, *J*= 7.0 Hz), 115.73 (d, *J*= 21.2 Hz), 67.07, 50.49 ppm.

The spectroscopic data corresponds to those reported in literature.[57]

10.3 SNAr amination

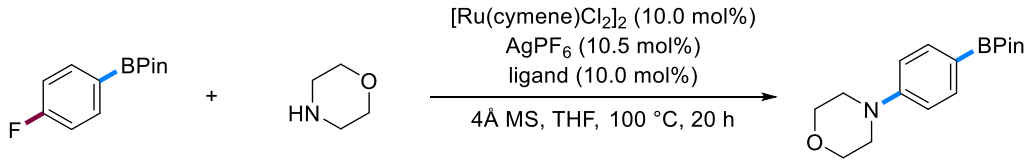

88 **90**

A 10 mL of oven dried Schlenk tube equipped with a stir bas was charged with $[Ru(cymene)Cl_2]_2$ (0.010 mmol) and $AgPF_6$ (0.042 mmol) were stirred in acetone (1.0 mL) at room temperature for 15 minutes. The formed AgCl precipitate was filtered off and acetone solution was

transferred to a 4 mL vial which contained ligand (0.040 mmol). Then acetone was excluded under reduced pressure, affording the catalyst as yellow foam. Then, the prepared catalyst was mixed with 4Å MS (20 mg), **88** (0.4 mmol) and amine (1.20 mmol) under N_2 atmosphere, and then 0.1 mL THF was added. The reaction was heated to 100 °C and stirred for 20 hours. The reaction mixture was purified by chromatography on silica gel eluting with *n*-hexane/ ethyl acetate (20: 1) to afford **90** (62.5 mg, 43.2% yield) as white solid.

^{1}H-NMR (400 Hz, $CDCl_3$, 25 °C) δ= 7.79 – 7.66 (m, 2H), 6.93 – 6.84 (m, 2H), 3.88 – 3.83 (m, 4H), 3.25 – 3.19 (m, 4H), 1.33 (s, 12H) ppm.

^{13}C-NMR (101 Hz, $CDCl_3$, 25 °C) δ= 153.52, 136.31, 114.24, 83.56, 66.94, 48.52, 25.00 ppm.

The spectroscopic data corresponds to those reported in literature.[58]

The ligand was prepared according to literature procedures using standard Schlenk technique.[58]

10.4 Cyanation

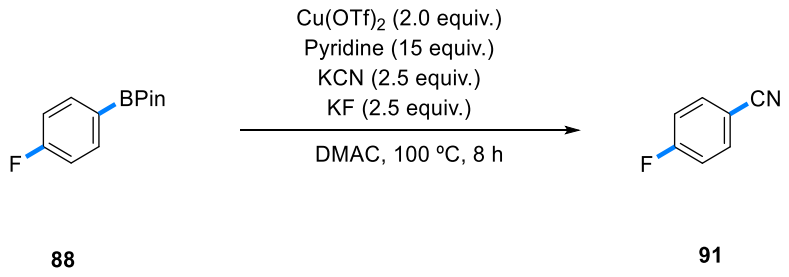

88 **91**

A 5 mL glass vial containing a stirring bar was sequentially charged with $Cu(OTf)_2$ (2.0 equiv.), pyridine (15.0 equiv.), KF (2.5 equiv.), KCN (2.5 equiv.), **88** (0.5 mmol) and DMAC (2.5 mL). The mixture was stirred at 100 °C for 8 h. After reaction, mesitylene (60 mg, 0.5 mmol) was added as internal standard. The yield of title compound **91** was determined by GC relative to the internal standard (35.1% yield).

10.5 One-pot two step strategy

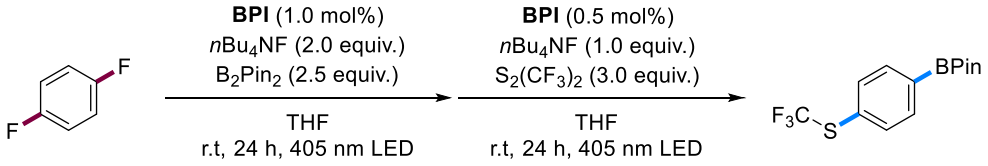

87 **92**

In a glovebox, a 5 mL glass vial containing a stirring bar was sequentially charged with **BPI** (3.8 mg, 1.0 mol%), 1,4-fluorobenzene **87** (57 mg, 0.50 mmol), *n*Bu_4NF (1.5 mmol, 1.5 mL, 3.0 equiv., 1.0M in THF) and B_2Pin_2 (254 mg, 2.00 equiv.) were converted. After being stirred for 24 h, the reaction was moved back into the glovebox, where more catalyst (1.9 mg, 0.5 mol %), *n*Bu_4NF (0.5 mmol, 0.5 mL, 1.0 equiv., 1.0M in THF) and $S_2(CF_3)_2$ (3.0 equiv.) were added. The vial was then removed from the glovebox and placed back into the light reactor. After reaction for another 24 h, the reaction mixture was purified by chromatography on silica gel eluting with *n*-hexane/ ethyl acetate (10: 1) to afford **92** (54.0 mg, 35.6% yield) as white solid.

^{1}H-NMR (400 Hz, $CDCl_3$, 25 °C) δ= 7.88 – 7.80 (m, 2H), 7.68 – 7.58 (m, 2H), 1.35 (s, 12H) ppm.

^{13}C-NMR (101 Hz, $CDCl_3$, 25 °C) δ= 135.77, 135.27, 131.24, 128.18, 127.64, 127.62, 84.39, 25.02 ppm. (the signal for the carbon that is attached to the boron atom was not observed)

^{19}F-NMR (376 MHz, $CDCl_3$, 25 °C) δ= -42.28 ppm.

The spectroscopic data corresponds to those reported in literature.[59]

10.6 Sulfinamidation

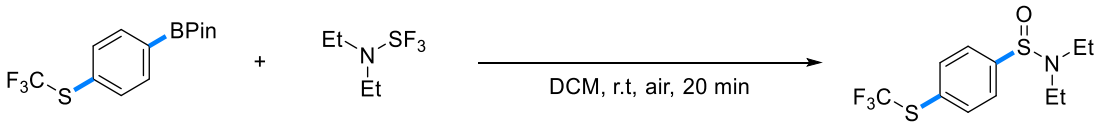

92 **93**

A 5 mL glass vial containing a stirring bar was sequentially charged with **88** (152 mg, 0.5 mmol) and DCM (2.5 mL). Under open air, diethylaminosulfur trifluoride (DAST) (161 mg, 1.0 mmol) was added to the mixture. Then, the solution mixture was stirred at room temperature for 20 min. After reaction, the mixture was purified by chromatography on silica gel eluting with *n*-hexane/ ethyl acetate (3: 1) to afford **93** (93.8 mg, 63.2% yield) as light oil.

^{1}H-NMR (400 Hz, $CDCl_3$, 25 °C) δ= 7.81 – 7.68 (m, 4H), 3.14 (q, *J* = 7.2 Hz, 4H), 1.13 (t, *J* = 7.2 Hz, 6H) ppm.

^{13}C-NMR (101 Hz, $CDCl_3$, 25 °C) δ= 147.73, 136.25, 129.59, 127.58, 42.41, 14.51 ppm.

^{19}F-NMR (376 MHz, $CDCl_3$, 25 °C) δ= -42.13 ppm

HRMS (ESI) Calculated for $C_{11}H_{15}F_3NOS_2^+$ $[M+H]^+$ (**93**): 298.0542, measured: 298.0549

10.7 Suzuki-Miyaura cross-coupling

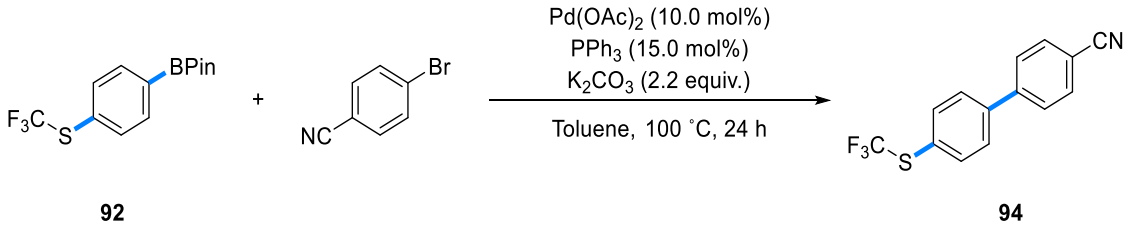

92 **94**

A 10 mL glass vial containing a stirring bar was sequentially charged with **92** (152 mg, 0.5 mmol), 4-bromobenzonitrile (0.6 mmol), $Pd(OAc)_2$ (10.0 mol%), PPh_3 (15.0 mol%), K_2CO_3 (2.2 equiv.) and toluene (4.0 mL). After stirring at 100 °C for 24 h, the solvent was removed by evaporation, 20 ml water was added, and the mixture was extracted with DCM (20.0 mL). The organic layer was purified by chromatography on silica gel eluting with n-hexane/ ethyl acetate (20: 1) to afford **94** (106 mg, 76.1% yield) as light oil.

^{1}H-NMR (400 Hz, $CDCl_3$, 25 °C) δ= 7.81 – 7.74 (m, 4H), 7.73 – 7.70 (m, 2H), 7.69 – 7.62 (m, 2H) ppm.

^{13}C-NMR (101 Hz, $CDCl_3$, 25 °C) δ= 144.18, 141.80, 136.96, 132.88, 131.13, 128.36, 127.99, 125.03 (q, J = 294.0 Hz), 118.72, 112.02 ppm.

^{19}F-NMR (376 MHz, $CDCl_3$, 25 °C) δ= -42.42 ppm

HRMS (ESI) Calculated for $C_{14}H_9F_3NS^+$ $[M+H]^+$ (**94**): 280.0403, measured: 280.0410

11. Troubleshooting: frequently questions

Question 1:

Will excess H_2O affect the progress of the reaction?

Answer:

In the presence of trace amounts of H_2O, the reaction with F^- produces a small quantity of OH^-, which can hydrolyze the catalyst (**BPI**), leading to the formation of open-ring intermediate (**BPI-RO**). However, excess H_2O reacts with fluoride ions, leading to the rapid formation of the thermodynamically stable bifluoride anion (HF_2^-) (refer to the figure below). HF_2^- is not an effective electron donor.

$$F^- + H_2O \rightleftharpoons HF + OH^-$$

$$F^- + HF \rightleftharpoons HF_2^-$$

Notably, when nBu$_4$NF•3H$_2$O reacts with **BPI**, ring-open products **BPI-RO** can also be obtained. But the hydrodefluoriantion yield is very low (see Figure below).

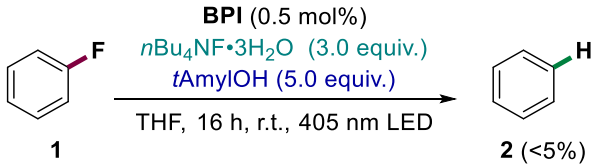

Question 2:

Is it possible to perform this reaction at high temperature? If this is feasible, more fluoropolymers can be incorporated into the system such as polyvinylidene difluoride (PVDF).

Answer:

We conducted hydrodefluorination experiments on PVDE at 60 and 90 °C but did not observe any corresponding products. This is likely because our reaction system includes alcohols, and PVDF is challenging to dissolve, even at elevated temperatures. Additionally, the solubility of **BPI** in common photocatalytic solvents such as MeCN, DMF, DMSO, and DMac is limited (refer to the

table below). Our research group is currently exploring structural modifications to **BPI** to enhance its solubility.

	THF	DMSO	MeCN	DMF	DMac	DCM	MeOH	toluene
BPI	✓	+	✗	+	+	✓	✗	✓

✓ = good soluble + = slightly soluble ✗ = insoluble

Question 3:

Can you separate a mixture of hydrodefluorination product and starting material from this system?

Answer:

Indeed, while it is feasible, the separation process, particularly when starting with aryl fluorides, can be quite challenging. The most practical approach for separation in these cases is to employ an automated column machine, adjusting to a lower flow rate for optimal performance.

Question 4:

Is a glovebox necessary?

Answer:

No! In the absence of a glove box, adding all chemicals under nitrogen protection still yields corresponding results (see figure below).

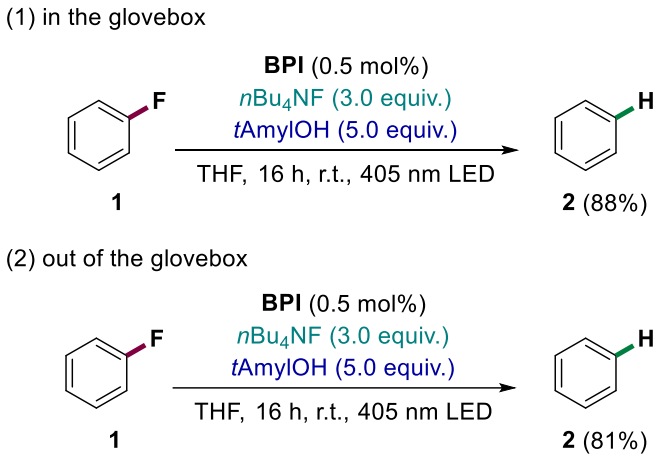

Question 5:

How to obtain nBu_4NF with low H_2O content?

Answer: Here

Here we introduce two methods of drying nBu$_4$NF.

Method A: nBu$_4$NF•3H$_2$O was heated in a round-bottomed flask with magnetic stirring at 50 ºC under vacuum. After 4-5 h, the sample liquified. Then, keep heating for another 24 h until the sample lost 20% of its original weight. The resulting "dried" nBu$_4$NF contained 0.2-0.3 equiv. of H$_2$O (determined by ^{1}H-NMR) and 10% of nBu$_4$NHF$_2$ (δ= -146 ppm in the ^{19}F-NMR). The signal of "dried" nBu$_4$NF at δ= -100 ppm in the ^{19}F-NMR. The dry nBu$_4$NF must be used immediately with THF.

More synthesis details and spectroscopic data, please check the literature.[61]

Method B: Purchase nBu$_4$NF from the supplier and confirm its purity through ^{19}F-NMR after picking it up. If the content of nBu$_4$NHF$_2$ (δ= -146 ppm in the ^{19}F-NMR) is less than 20%, then

add 4Å molecular sieves and keep it in the refrigerator. After 48 hours, the nBu$_4$NF solution contained 0.3-0.4 equiv. of H_2O (determined by ^{1}H-NMR). The dry nBu$_4$NF must be used immediately.

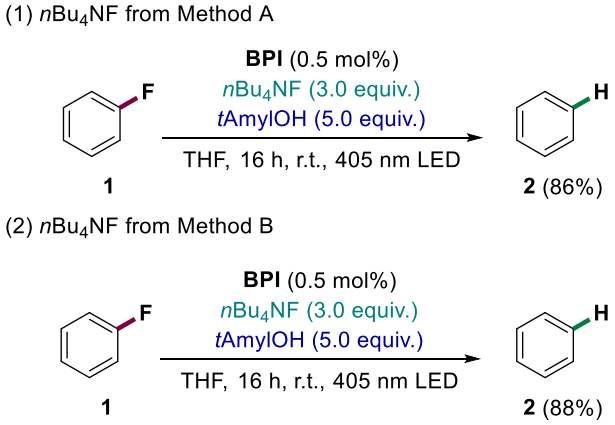

Question 6:

From the known literature, the dried nBu$_4$NF will decompose to tributylamine (nBu$_3$N) at room temperature. Does the presence of nBu$_3$N affect the progress of the reaction?

Answer:

We found that trace amounts of nBu$_3$N in TBAF do not affect the experimental results. However, adding an excess of amines (e.g., Et$_3$N, DIPEA, nBu3N, or Bn$_3$N) to the reaction system hinders its operation (see Table S14 below). Remarkably, the presence of excess nBu$_3$N would decompose the ring-open intermediate under irradiation (see Figure S53-S55).

Table S14. Hydrodefluoronation of benzofluorene 1 with different amines.

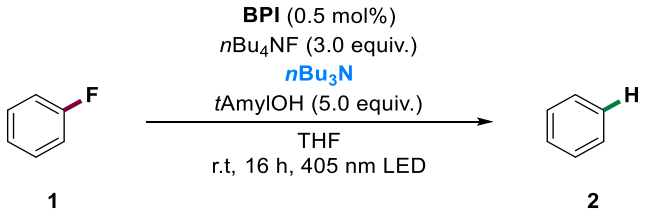

entry	***n*Bu$_3$N**	conversion of **1** (%)	yield of **2** (%)
1	1.0 equiv.	0	0
2	0.5 equiv.	0	0
3	0.1 equiv.	0	0
4	0.1 equiv.[a]	0	0
5	0.1 equiv.[b]	0	0
6	0.1 equiv.[c]	0	0

Reaction conditions: 1 (0.5 mmol), PC (0.5 mol%), nBu$_4$NF (1.5 mmol, 1.5 mL, 1.0M in THF), nBu$_3$N (x µL), tert-AmylOH (2.5 mmol, 5.0 equiv.), r.t (23 °C), 16 h, THF, 405 nm LED. The conversion and yields were determined by GC using mesitylene as the internal standard. [a] Et$_3$N instead of nBu$_3$N. [b] DIPEA instead of nBu$_3$N. [c] Bn$_3$N instead of nBu$_3$N.

12. Mechanistic investigation

12.1 Guidelines for mechanism studies

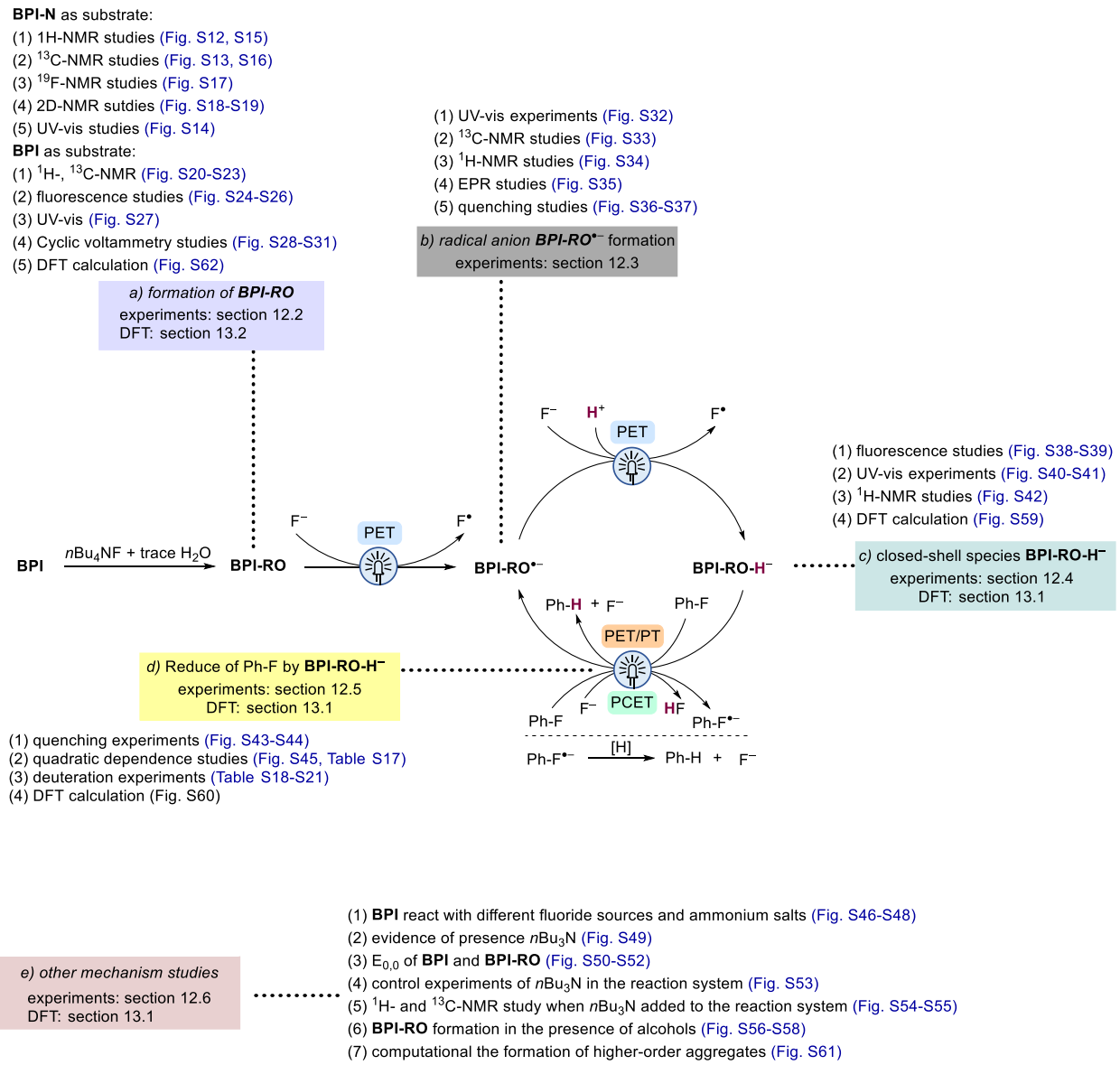

Figure. S2.9. Guidelines for the mechanism studies. The color-highlights call out sections (a)-(e) which are summarized below and then expanded upon in subsequent sections 12.2-12.6 and 13.1-13.2

General summary for each sub-section of experiments and computational arguments addressing specific mechanistic steps outlined with Figure S11:

(a) Formation of **BPI-RO** species (see section 12.2 for experiments details/protocols and 13.2 for DFT calculation)

From the known literature and our previously results,[1,62-64] the reactions involving imide-type compounds and *n*Bu$_4$NF can proceed through several pathways, as illustrated in Figure S10. These pathways include: (i) electron transfer from F^- to imide-type compounds in aprotic solvents leading to the formation of a radical anion or dianion, (ii) form anion–π complex between F^- and imide-type compounds, (iii) form fluoride adduct via nucleophilic attack of F^-, and (iv) hydrolysis of the imide ring.

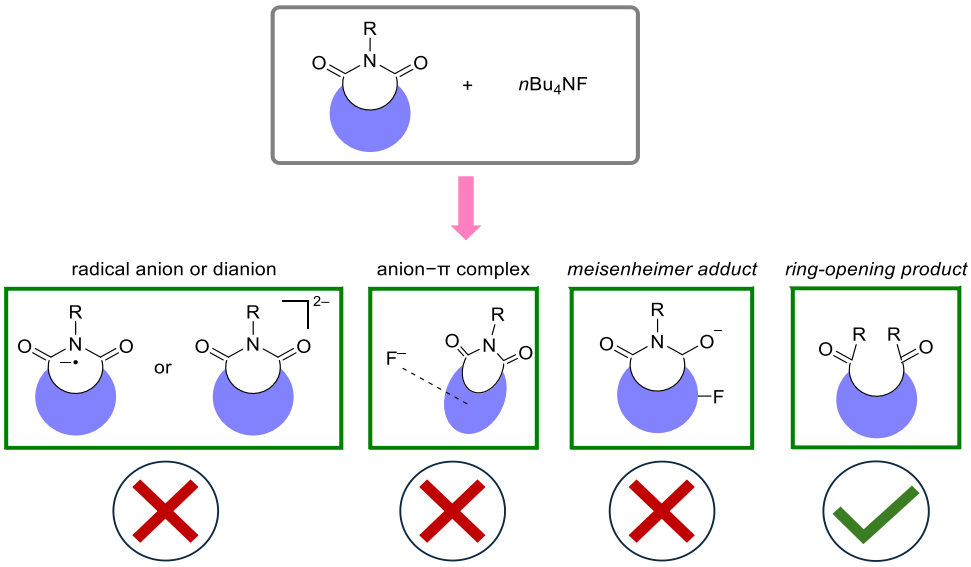

Figure S2.10. The possible reaction pathway between imide-type compounds with nBu$_4$NF.

*Spectroscopic investigations reveal that upon interacting with nBu$_4$NF, **BPI** undergoes an imide ring-opening. The ring-open species has been isolated by using the symmetric **BPI-N** and at the same time all the other spectroscopic data strongly argue against the other modes of interactions.*

For the hydrolysis of imide to ring-opening intermediate:

Using symmetric **BPI-N** as catalyst, we now have successfully isolated the ring-open product **BPI-N-RO** (see Figure S11) and have characterized it by ^{1}H-, ^{13}C-, ^{1}H COSY-NMR, and UV-vis (see Figure S12-S19).

The ^{1}H-, ^{13}C- and ^{19}F-NMR clearly show that the isolated product is a ring-open species (referred to as **BPI-N-RO)** where the imide ring has been hydrolyzed. Comparing the ^{1}H-, ^{13}C- NMR spectra as well as the UV-Vis spectra of the crude **BPI-N** + *n*Bu$_4$NF mixture with those of the isolated **BPI-N-RO** confirms that it is indeed the product that was formed in-situ.

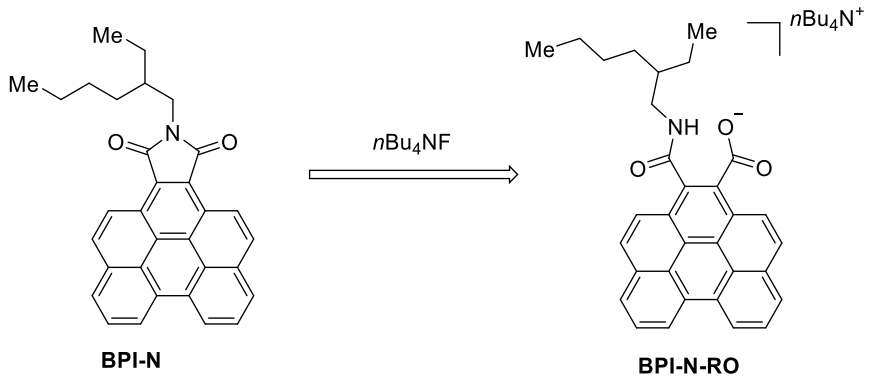

Figure S2.11. Isolated intermediate BPI-N-RO from the reaction mixture of BPI-N with nBu$_4$NF.

Furthermore, our mechanistic experiments do not support the formation of radical anion or dianion, anion−π complex, and fluoride adduct (for more detailed discussion corresponding to each form of interaction see below).

For the radical anion or dianion formation:

According to literature,[63] the F^- induced formation of radical anions can be detected by UV-vis, EPR and NMR spectra. The dianion formed via electron transfer from F^- can be observed by UV-vis.[63] Observing the UV-vis spectrum during titration, with increasing molar ratios of F^- relative to **BPI**, shows a decrease in **BPI** absorption bonds with increasing F^- in conjunction with the appearance of new absorbance features (λ_{abs}, max = 427 nm) (Figure S2.25-26). The UV-vis spectra of generated radical anion will show a red-shift, as opposed to the blue-shift observed in our UV-vis studies (Figure S2.27). Furthermore, we did not observe any potential radical anion or dianion signal generation between 450-600 nm. During the titration of **BPI** with F^-, all signals (^{1}H-, and ^{13}C-NMR) remain unbroadened, indicating no formation of **BPI**$^{\bullet-}$ radical anion (Figure S2.20-S2.23). The EPR spectrum of the F^- induced solution of **BPI** further confirms that there is no radical anion formation (Figure S2.35).

For the anion−π complex formation:

Prior to light absorption, the fluorescence spectra of **BPI** were found to blue-shift upon *n*Bu$_4$NF addition (see Figure S2.25-26), conforming interaction between the ground state **BPI** with F^-. It is relevant to note that information of an anion−π complex between anion and **NDIs** a red-shift was reported, as opposed to the blue-shift observed in our studies. According to literature,[65] the NMR signal shift of the anion–π interaction is very small due to the binding is too weak. In our NMR studies, the ^{1}H- and ^{13}C signal of **BPI** noticeably shift upon adding *n*Bu$_4$NF (Figure S20-S23). All of these results do not support an anion−π complex formation in our system.

For the fluoride adduct formation:

If diamagnetic fluoride adducts formation via nucleophilic attack of F^-, the ^{19}F-NMR should detect new signals during F^- titration. When using symmetric **BPI-N** as catalyst for ^{19}F-NMR studies, we

can obtain a new signal at -125.73 ppm. However, this signal is absent in the isolated intermediate **BPI-N-RO** (Figure S17). Additionally, the two-dimensional ^{13}C-^{19}F correlation NMR fails to detect any signals, further indicating the absence of fluorine atoms in the intermediate.

According to the known literature, the signals identified in ^{19}F-NMR are suggested to originate from fluoride ions interacting with the amide protons (–NH–, from the ring-opening product) through strong -NH•••F hydrogen bonding.

Other characterization:

Cyclic voltammetry suggests that the **BPI-RO** has stronger reduction potential ability (-1.84 V vs. SCE) than **BPI** (-1.24 V vs. SCE) (see Table S2.15-S2.16. Figure S2.28-S2.31).

(b) Radical anion **BPI-RO**$^{\bullet-}$ formation (see section 12.3 for experiments details/protocols)

Investigating the dark speciation and resting stat of **BPI-RO**, we next explored its reactivity under the light. Upon photon absorption, we propose that excited **BPI-RO** oxidizes F^-, forming the radical anion **BPI-RO**$^{\bullet-}$. Firstly, irradiating **BPI-RO** with a 405 nm LED reveals a new species observable via UV-vis at 546 nm (see Figure S2.32). Secondly, the broadening of ^{13}C- and ^{1}H-NMR signals also supports the formation of a radical anion (see Figure S2.33-S2.34). Lastly, the EPR detected radical anion signal from **BPI** with *n*Bu_4NF under irradiation, and we suggest the signal is **BPI-RO**$^{\bullet-}$ rather than **BPI**$^{\bullet-}$ (see Figure S2.35).

Before considering **BPI-RO**$^{\bullet-}$, we first explored the behavior of its precursor **BPI-RO** which is closed shell and emissive. For this species, we cannot observe any changes in the steady state emission intensity upon addition of fluorobenzene (see Figure. S2.36). This then suggests that photoexcited **BPI-RO** does not store an appropriate thermodynamic driving force for such a reduction and that the PC requires further reductive transformation made possible by PET in the

presence of excess nBu$_4$NF (see (b) above). The further converted **BPI-RO**$^{\bullet-}$ is expected to be a more powerful reductant from its excited state. Here, however, experimental challenges emerge. The solution of **BPI-RO** (under irradiation for 30 min) does produce emissive intermediates that can be explored in quenching studies (see Figure S2.37). But there are important caveats. Most importantly, the emission spectrum seen in Figure S2.37 cannot be attributed to **BPI-RO**$^{\bullet-}$ since that species has an open-shell doublet excited state as well as UV-Vis features tailing into the near IR and therefore red of the peak emission seen at 461 nm in Figure S2.37. Under these conditions it is unreasonable to assume that non-radiative decay does not substantially outcompete fluorescence from the doublet excited state of **BPI-RO**$^{\bullet-*}$. Figure S2.37 does show some diminution of emission intensity with added fluorobenzene. Here the emission is likely due to closed-shell PC impurities (see (c) and (d) below) generated in small amounts because of residual protons, with quenching arising from their photoreactivity.

(c) Closed-shell species **BPI-RO-H**$^-$ formation (see section 12.4 for experiments details/protocols and 13.1 for DFT calculation)

After introducing tAmylOH into the reaction mixture (containing **BPI** and nBu$_4$NF) and then irradiating it with a 405 nm LED (see section 12.4.1), both the absorption and fluorescence spectra show that **BPI-RO** was converted into a new species (Figures S2.38-S2.39). The emissive nature and multi-nanoseconds fluorescence lifetime of this new species strongly suggests that it is electronically closed shell. Based on the results obtained with a similar model photocatalyst (benzo[ghi]perylene diester: **BPDE**)[87], we hypothesize the converted species to be **BPI-RO-H**$^-$. The ^{1}H-NMR further supports a new species that has formed (Figure S2.42). The new species was able to exist in open air conditions for up to 4 hours, which can be seen in the proton NMR with no major change in features. According to DFT calculations, formal additional of a hydride can

occur at the a-position next to the carboxylate group or next to the amide group (Figure S2.59). As the thermodynamic diffraction between these two species is small, both species were considered for the calculation of their ground and excited state reduction potentials (see (e) below).

(e) Reduction of Ph-F by **BPI-RO-H**$^-$ (see section 12.5 for experiments details/protocols and 13.1 for DFT calculation)

Quenching experiments are consistent with **BPI-RO-H**$^-$ functioning as a potent excited state reductant. (see Figure S2.43 for experiments with fluorobenzene and S2.44 for experiments with 4-methylfluorobenzene). Moreover, our quadratic power dependence studies suggest that the catalytic cycle is based on the two-photon mechanism (see Figure S2.45 and Table S2.17). Deuteration-labeling experiments show that the proton source is *t*AmylOH, *n*Bu$_4$NF, and THF (Table S2.18-S2.21). To be thermodynamically viable, the bond dissociation free energies (BDFE) of the bonds breaking in the reactants should be lower than the BDFE of the bonds forming in the products. The BDFE of tertiary alcohols and THF are higher than that of the reduction products in the deuterium-labeling experiments. This raises a question: how does alcohol function as a hydrogen donor in our system? One hypothesis is that hydrogen atoms are transferred from the alcohol to the **BPI-RO**$^{\bullet-}$, forming a closed-shell species **BPI-RO-H**$^-$. This protonated **BPI-RO-H**$^-$ could then reduce the substrate via a photoinduced electron-transfer/proton-transfer (PET/PT) mechanism.

Computed thermochemistry and reduction potential indicate that the closed-shell species **BPI-RO-H**$^-$ is a stable intermediate, the redox potential of excited state **BPI-RO-H**$^{-*}$ up to -3.64 V vs. SCE.

(e) Other mechanism experiments (see section 12.6 for experiments details/protocols and 13.1 for DFT calculation)

Additional experiments were undertaken to support the proposed mechanism regarding different reductants, amines, and alcohols. For example, adding different fluoride sources and ammonium salts outside of nBu$_4$NF with **BPI** did not result in major feature changes in the emission intensity (see Figures S2.46-S2.48). The effect of nBu$_3$N and alcohol in our reductant solution was further studied, where we monitored the nBu$_3$N in proton NMR with irradiation of 405 nm for 1 hour, to see no increase inside products (see Figure S2.49). This is important, because any large amount of nBu$_3$N in our system negatively impacts yields (see Figure S2.53-S2.55). When comparing different alcohol sources, and the order of addition, it was shown that both methanol and tAmylOH cause slower formation of **BPI-RO** which emphasizes that the alcohols should be added sequentially with the substrate after **BPI-RO** is formed in THF alone (see Figure S2.56), Once **BPI-RO** has formed, the alcohol addiction does not change the emission intensity of that adduct (see Figure S2.57). These experiments in tandem with a control experiment with just **BPI** and alcohol showing no adduct formation (see Figure S2.58) put emphasis on when the alcohol should be introduced into the system. Additionally, the excited state energies were extrapolated for **BPI**, **BPI** with nBu$_4$NF, and **BPI** with Me$_4$NOH (see Figures S2.50-S2.52). The DFT calculations suggest that the formation of higher-order aggregates (e.g., with three molecules of tAmylOH) increases the ability to donate an electron compared to when a single molecule of alcohol is bound (-1.11 V vs. -0.76 V) (see Figure 2.61).

12.2 Formation of BPI-RO from BPI

12.2.1 ^{1}H- and ^{13}C-NMR spectroscopic studies on BPI-N + *n*Bu$_4$NF mixture

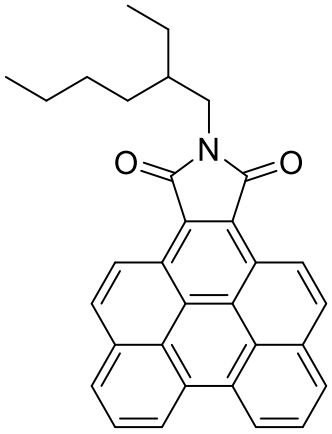

BPI-N

To structurally elucidate what happens when **BPI** reacts with *n*Bu$_4$NF, we employed its symmetric variant **BPI-N** as a model (as shown on the left). **BPI-N** was prepared according to the literature procedure [87].

Step 1: In glovebox, a dry NMR tube was charged with **BPI-N** (5.0 mg) and THF-d$_8$ (0.8 mL). ^{1}H and ^{13}C-NMR spectra were recorded.

Step 2: In the glovebox, **BPI-N** solution from step 1 was poured into a 2 mL glass vial containing a stirring bar and was then charged with 20 equivalents of *n*Bu$_4$NF (1.0 M in THF). The mixture was stirred inside the glove box for 60 min, then transferred to a dry NMR tube. ^{1}H and ^{13}C-NMR spectra were recorded.

Note: The number of scans of all ^{1}H-NMR is 128. Taken on a 400 MHz instrument.

^{1}H-NMR spectra:

***Step 2. BPI-N** with nBu$_4$NF (20 equiv.)*

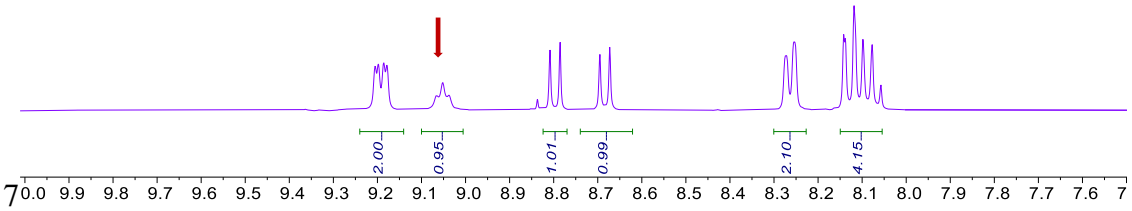

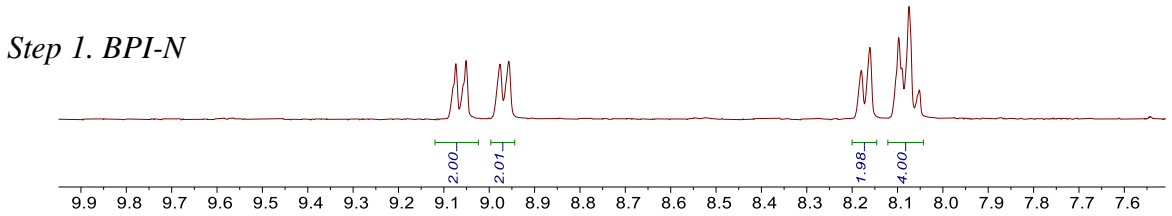

Figure S2.12. Comparing the aromatic region of BPI-N ^{1}H NMR spectrum before and after it reacts with 20 equivalents of nBu$_4$NF. Two things visibly stand out: a) appearance of two doublet peaks (~8.68 and 8.8 ppm) both integrating to one proton each. This indicates the introduction of an asymmetry in the structure. For comparison, in BPI-N all the peaks integrate to either 2 or 4 protons consistent with it having a plane of symmetry, b) a new triplet peak at ~9.05 ppm that corresponds to one proton. The total number of protons in the 7-10 ppm region in BPI-N with nBu$_4$NF mixture is 11 in contrast to 10 protons in the case of BPI-N.

^{13}C-NMR spectra:

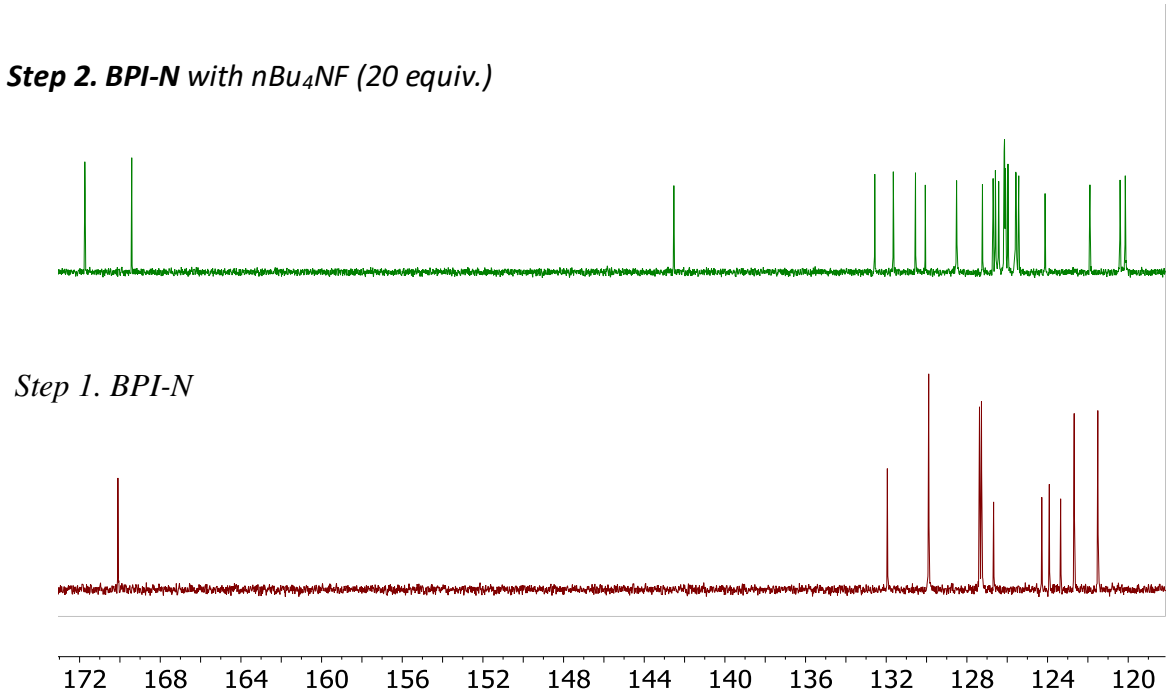

Figure S2.13. Comparing the 115-175 ppm region of BPI-N (^{13}C NMR spectrum before and after it reacts with 20 equivalents of nBu$_4$NF). A clear doubling of the number of resonances in the spectrum is visible after BPI-N reacts with nBu$_4$NF, especially in the carbonyl region where we now find two peaks. This further confirms that after reacting nBu$_4$NF, BPI-N no longer retains a plane of symmetry, consistent with the lack of symmetry previously seen in the ^{1}H spectrum (Figure S23).

12.2.2 Isolation and characterization of the ring-open product BPI-N-RO

Procedure for isolation: The crude reaction mixture of **BPI-N** and *n*Bu$_4$NF was subjected to an aqueous extraction (involving DCM and water) to remove all the excess fluoride salts, followed by brine wash and the product was then isolated with a basic alumina flash column (gradient of 10-50% methanol in THF).

UV-vis spectra:

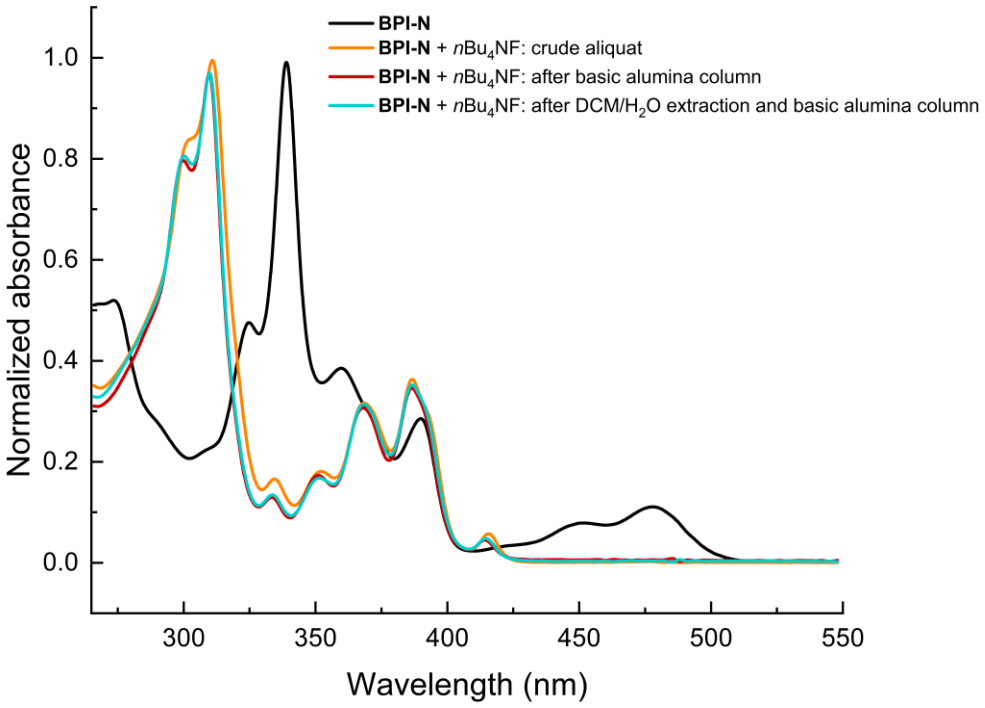

Figure S2.14. Comparing the UV-visible spectra of isolated BPI-N-RO (post basic alumina column with and without aqueous workup) with that of the crude BPI-N with nBu$_4$NF mixture. Absorption spectrum of BPI-N is shown for reference. There are no significant changes in the absorption spectrum of the BPI-N with nBu$_4$NF mixture even after it is pushed through a basic alumina column or extracted with DCM/Water suggesting that the BPI-N-RO species is stable and isolable.

^{1}H-NMR:

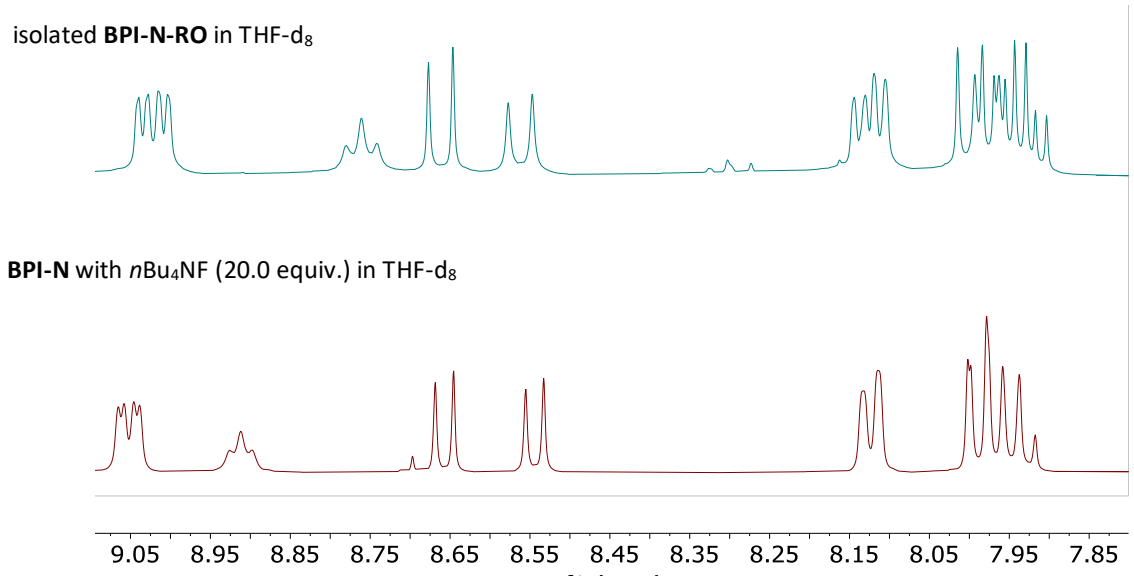

Figure S2.15. Comparing the ^{1}H-NMR spectrum of isolated BPI-N-RO with that of the crude BPI-N with nBu$_4$NF mixture.

^{13}C-NMR:

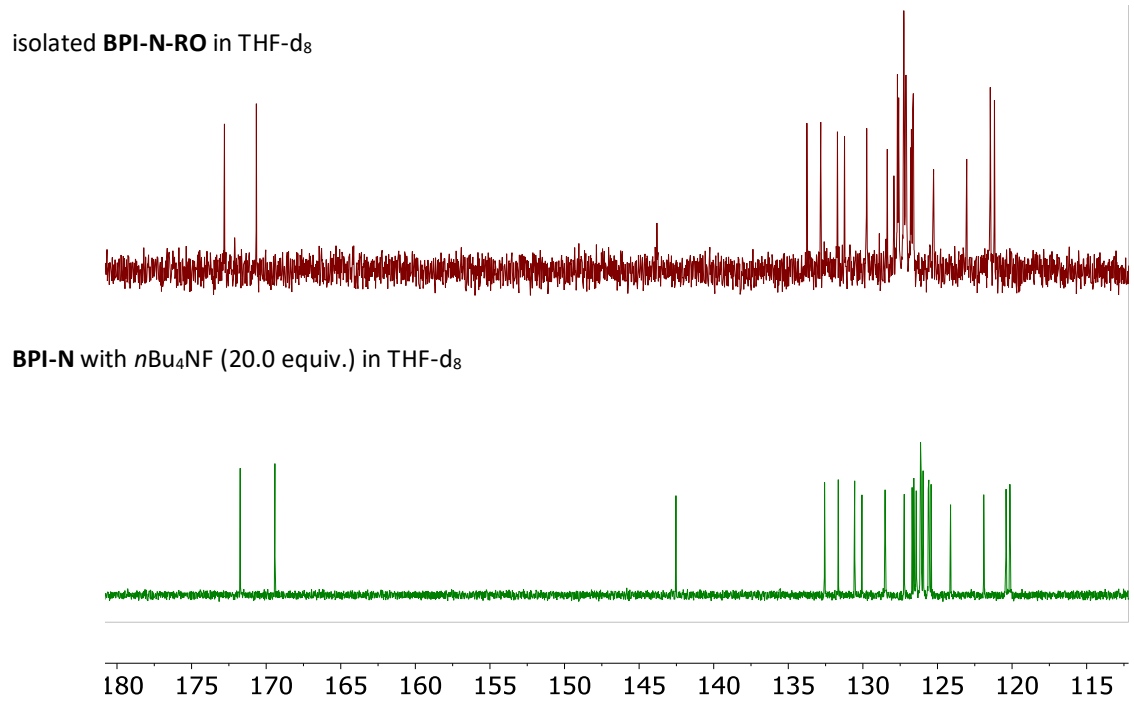

Figure S2.16. Comparing the ^{13}C-NMR spectrum of isolated BPI-N-RO with that of the crude BPI-N with nBu4NF mixture.

^{19}F-NMR:

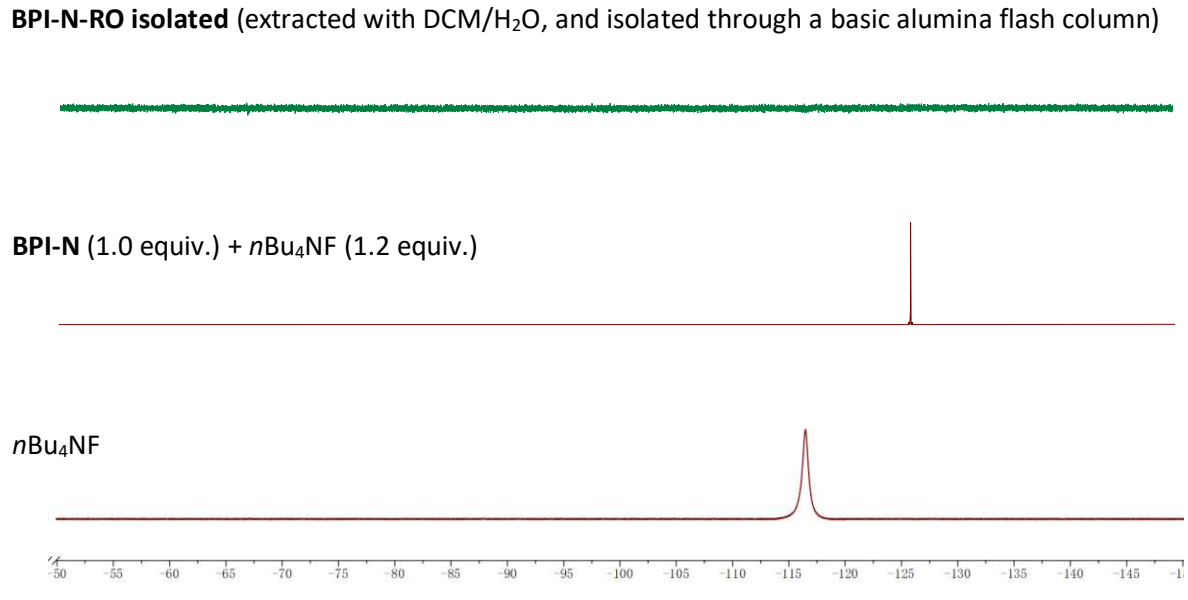

Figure S2.17. Comparing the ^{19}F-NMR spectra of isolated BPI-N-RO with that of the crude BPI-N with nBu_4NF mixture. All are collected in THF-d_8. Absence of any peak in the ^{19}F-spectrum of isolated BPI-N-RO confirms that there is no fluorine or fluoride bound to this species.

^{1}H-^{1}H COSYNMR:

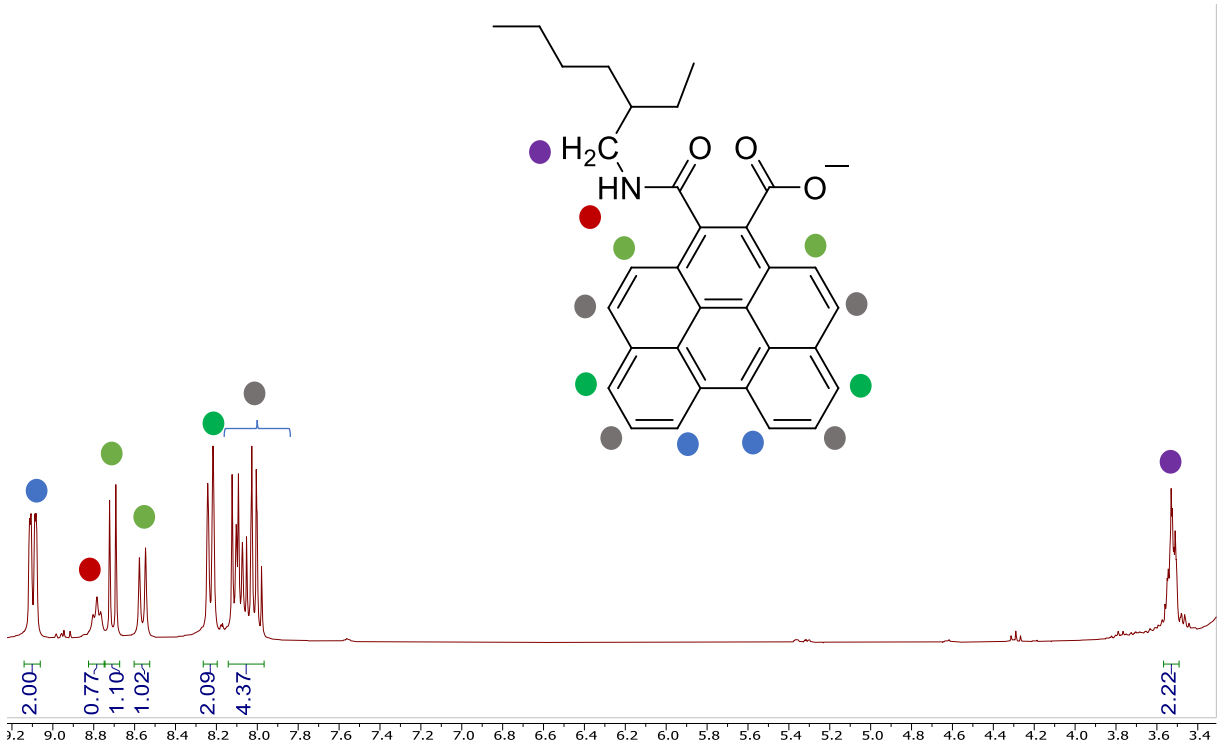

Figure S2.18. Assignment of the proton peaks in the ^{1}H spectrum (acetone-d_6, 300 MHz) of isolated BPI-N-RO based on the COSY data (see below, Figure S2.21).

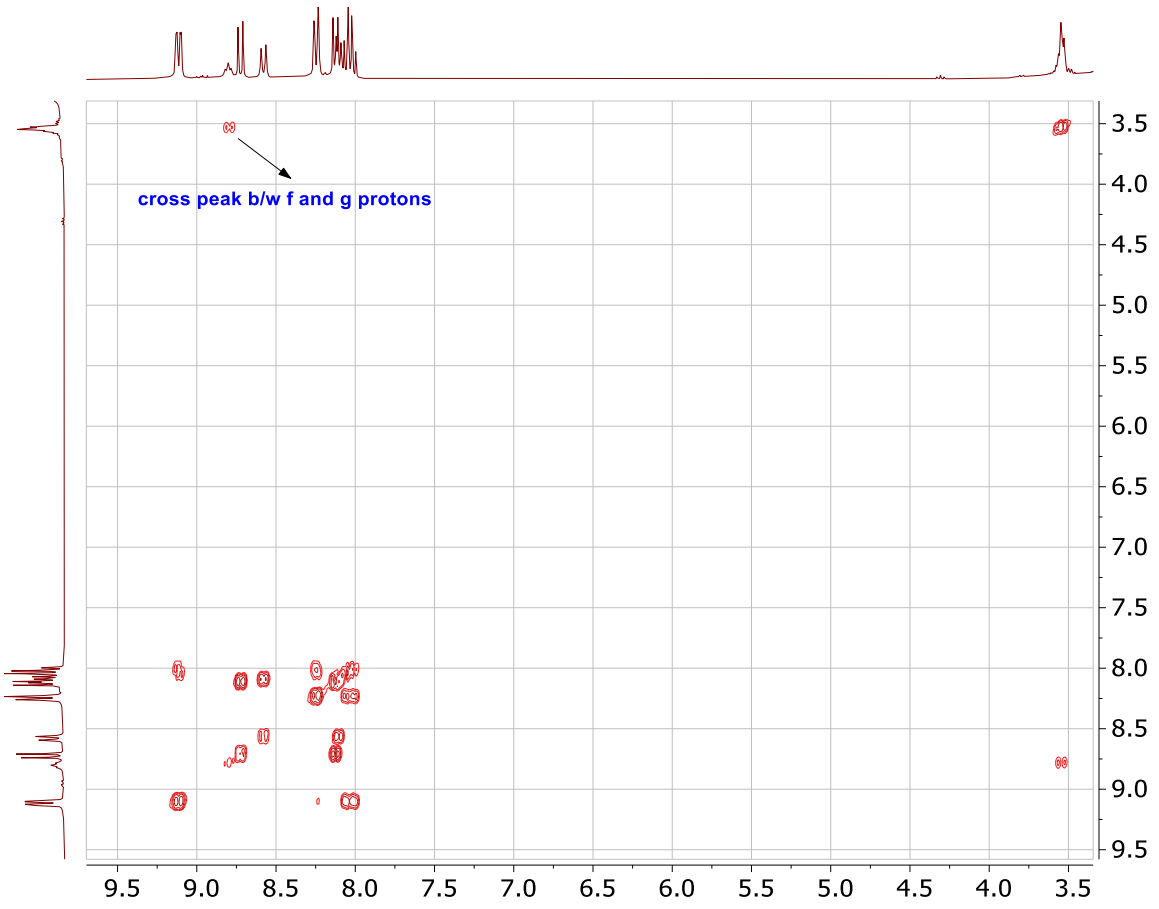

Figure S2.19. ^{1}H-^{1}H COSY of the isolated intermediate BPI-N-RO (Acetone-d_6, 300 MHz). Acetone was used to slow down the rate of exchange between the amide proton and protons from water. The cross peak (highlighted with an arrow) between the amide proton (marked f) and the CH_2 protons (marked g) stands out and further confirms the imide hydrolysis.

12.2.3 ^{1}H- and ^{13}C-NMR studies of BPI reacting with *n*Bu$_4$NF

^{1}H-NMR:

Step 1: In glovebox, a dry NMR tube was charged with **BPI** (5.0 mg) and THF-d$_8$ (0.8 mL). The ^{1}H-NMR spectrum was recorded.

Step 2: In glovebox, a 2 mL glass vial containing a stirring bar was sequentially charged with **BPI** (5.0 mg), *n*Bu$_4$NF (0.4 mL, 1.0 M in THF). The mixture was stirred in the glove box for 60 min, then transferred to a dry NMR tube. The ^{1}H-NMR spectrum was recorded.

Note: The number of scans of all ^{1}H-NMR is 128.

Upon the addition of *n*Bu$_4$NF (1.0 M in THF) to **BPI** solutions, a notable color change was observed, as depicted in Figure S22.

Figure S2.20. A color change when BPI reacts with nBu$_4$NF

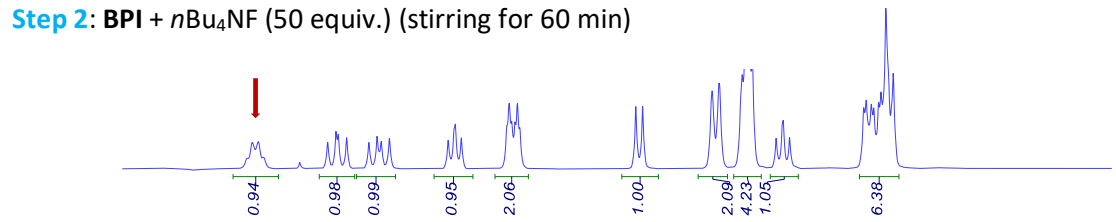

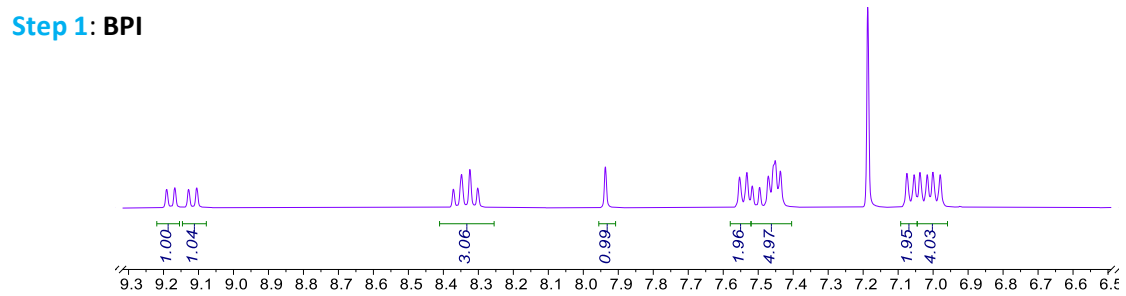

Figure S21. Comparing the aromatic region of BPI ^{1}H NMR spectrum before and after it reacts with 20 equivalents of nBu$_4$NF. Along with several changes in the splitting pattern and chemical shifts, the total number of protons in this region now integrates to 20 (as opposed to 19 in BPI). We posit the additional proton (highlighted with a red arrow) to be associated with the amide group formed due to hydrolysis of the imide ring.

^{13}C-NMR:

Step 1: In glovebox, a dry NMR tube was charged with **BPI** (8.0 mg) and THF-d$_8$ (0.8 mL). The ^{13}C-NMR spectrum was recorded.

Step 2: In glovebox, a 2.0 mL glass vial containing a stirring bar was sequentially charged with **BPI** (8.0 mg), *n*Bu$_4$NF (0.1 mL, 1.0 M in THF), and THF-d$_8$ (0.4 mL). The mixture was stirred in the glove box for 5 min, then transferred to a dry NMR tube. The ^{13}C-NMR spectrum was recorded.

Note: The number of scans of all ^{13}C-NMR is 3000.

Upon introducing *n*Bu$_4$NF (1.0 M in THF) into **BPI** solutions, two new signals were observed (δ = 173.4 and 170.6 ppm) in the downfield region, as shown in Figure S24 and S25.

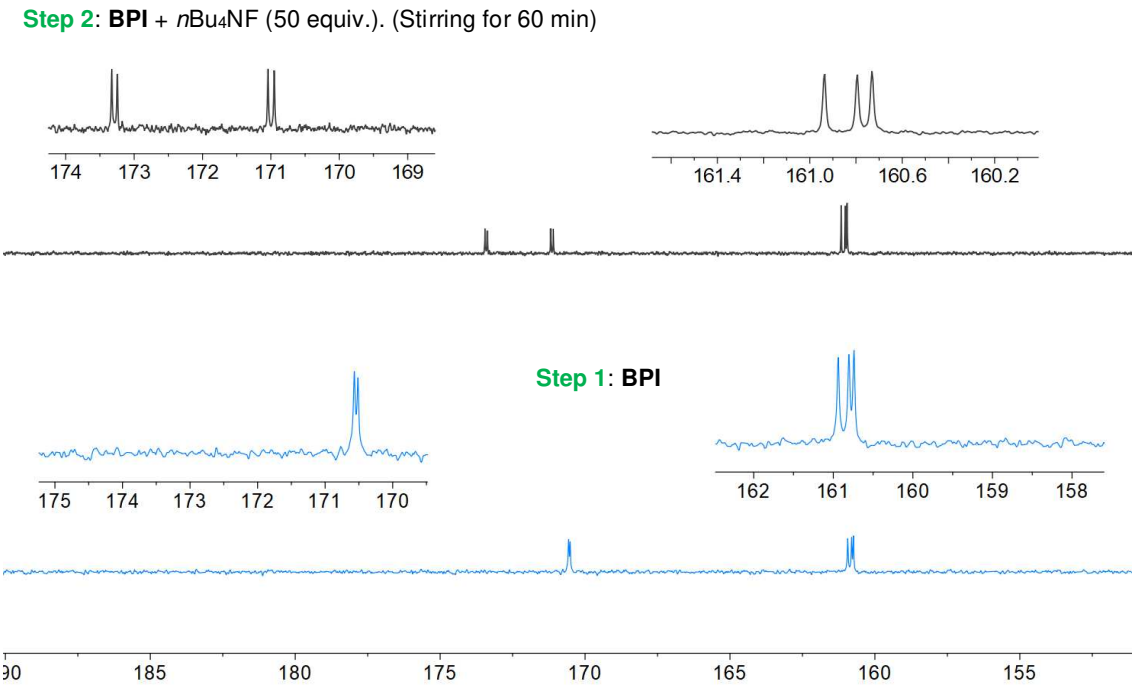

Figure S2.22. Partial ^{13}C-NMR of BPI and BPI with nBu$_4$NF at downfield.

Step 2: **BPI** + *n*Bu$_4$NF (50 equiv.). (Stirring for 60 min)

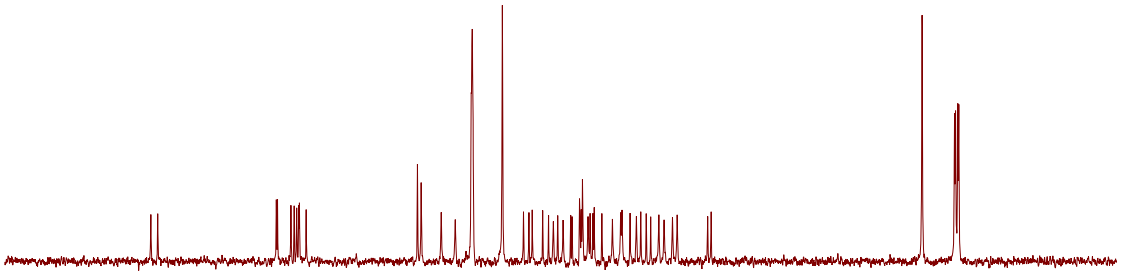

Step 1: **BPI**

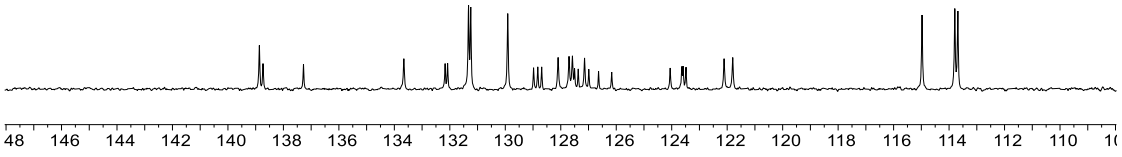

Figure S2.23. Partial ^{13}C-NMR of BPI and BPI with nBu$_4$NF at midfield.

12.2.4 Emission profiles for BPI and BPI-RO

Test sample preparation: **BPI**

In a glove box, a 50 mL glass vial containing a stirring bar was sequentially charged with **BPI** (1.5 mg) and THF (20 mL).

1) *Test sample preparation*: **BPI-RO**

In a glove box, a 5 mL glass vial containing a stirring bar was sequentially charged with **BPI** (1.5 mg), *n*Bu_4NF (1.0 mmol, 1 mL, 1.0 M in THF). The mixture was stirred in the glove box for 2 hours, and the color changed from yellow to light green. Then, transfer the mixture to a 50 mL glass vial and add degassed THF (19 mL) to dilute the **BP** to 1.0 x 10^{-4} M.

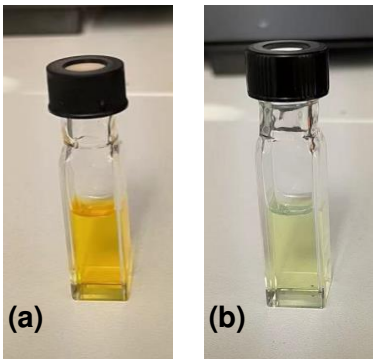

Figure S2.24. Picture demonstrating the color change of BPI in THF after stirring in the presence of nBu_4NF. (a) BPI (1.0 x 10^{-4} M) in degassed THF; (b) BPI with nBu_4NF (20 equiv. 1.0 M in THF) after 2 hours of stirring in degassed THF.

The emission of these mixtures clearly underwent a hypsochromic shift (from 565 to 461 nm, Figure. S25) resulted from the formation of a new species.

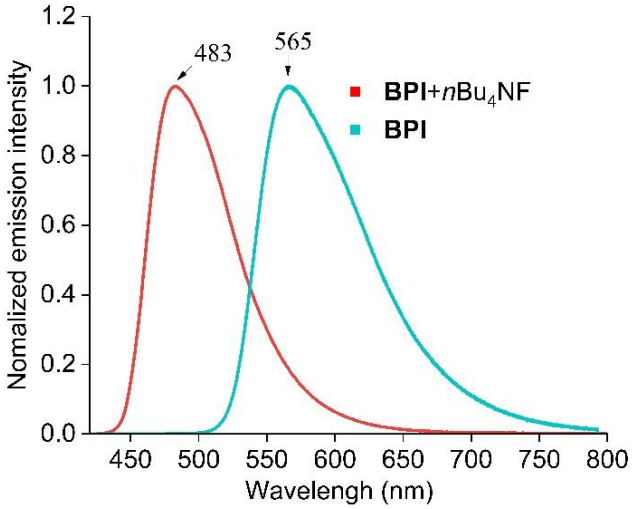

Figure S2.25. The normalized emission spectra for BPI and BPI with nBu_4NF (BPI-RO) after two hours of stirring in degassed THF. The samples were excited at 405nm.

Titrating **BPI** with increasing equivalents of *n*Bu$_4$NF. First, two stock solutions were prepared in THF: stock 1 of just **BPI** (25 µM) and stock 2 of **BPI** (25 µM) with 100 eq of *n*Bu$_4$NF (2.5 mM). Appropriate amounts of these two stock solutions were then mixed to reach the target equivalents in the following 4 steps.

Step 1: **BPI**: 2.5 mL of stock 1 + 0 mL of stock 2

Step 2: **BPI** + 3.0 eq of *n*Bu$_4$NF: 2.425 mL of stock 1 + 0.075 mL of stock 2

Step 3: **BPI** + 5.0 eq of *n*Bu$_4$NF: 2.375 mL of stock 1 + 0.125 mL of stock 2

Step 4: **BPI** + 10.0 eq of *n*Bu$_4$NF: 2.25 mL of stock 1 + 0.25 mL of stock 2

Monitoring fluorescence shows a diminishing of the **BPI** fluorescence (λ_{em}, max = 565 nm) with the appearance of emission from a new species (λ_{em}, max = 483 nm).

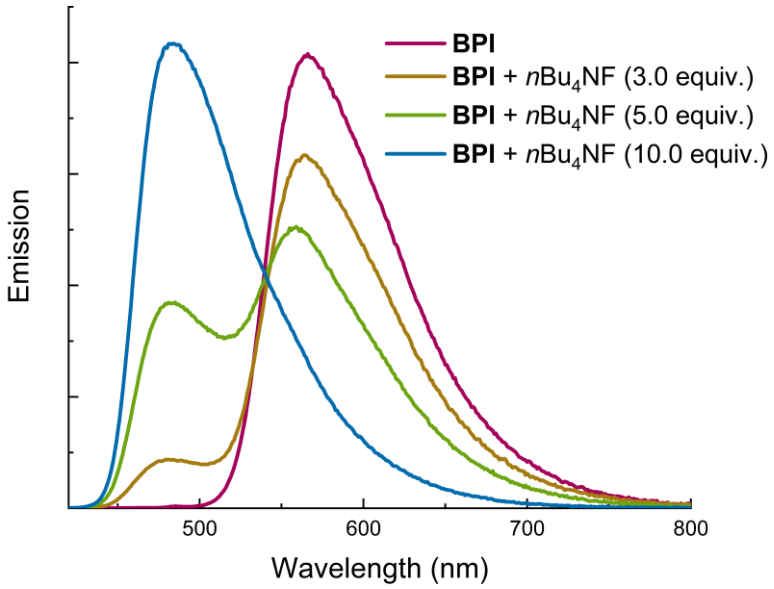

Figure S2.26. Fluorescence spectrum of 25 µM BPI in a THF solution in the presence of a varying equivalence of nBu$_4$NF in THF at room temperature within a 1cm cuvette.

12.2.5 Monitoring BPI and *n*Bu$_4$NF interaction via UV-vis spectroscopy

Titrating **BPI** with increasing equivalents of *n*Bu$_4$NF. First, two stock solutions were prepared in THF: stock 1 of **BPI** (25 μM) and stock 2 of **BPI** (25 μM) with 100 eq of *n*Bu$_4$NF (2.5 mM). Appropriate amounts of these two stock solutions were then mixed to reach the target equivalents in the following 6 steps.

Step 1: **BPI**: 2.5 mL of stock 1 + 0 mL of stock 2

Step 2: **BPI** + 1.0 eq of *n*Bu$_4$NF: 2.475 mL of stock 1 + 0.025 mL of stock 2

Step 3: **BPI** + 3.0 eq of *n*Bu$_4$NF: 2.425 mL of stock 1 + 0.075 mL of stock 2

Step 4: **BPI** + 5.0 eq of *n*Bu$_4$NF: 2.375 mL of stock 1 + 0.125 mL of stock 2

Step 5: **BPI** + 10.0 eq of *n*Bu$_4$NF: 2.25 mL of stock 1 + 0.25 mL of stock 2

Step 6: **BPI** + 100.0 eq of *n*Bu$_4$NF: 0 mL of stock 1 + 2.5 mL of stock 2

The absorption spectra of **BPI** were found to blue shift with *n*Bu$_4$NF addition, confirming interaction between the ground state **BPI** and F^-. When increasing molar ratios of F relative to **BPI** show a decrease in **BPI** absorption bands with increasing [F^-] in conjunction with the appearance of new absorbance features (λ_{abs}, max = 427 nm).

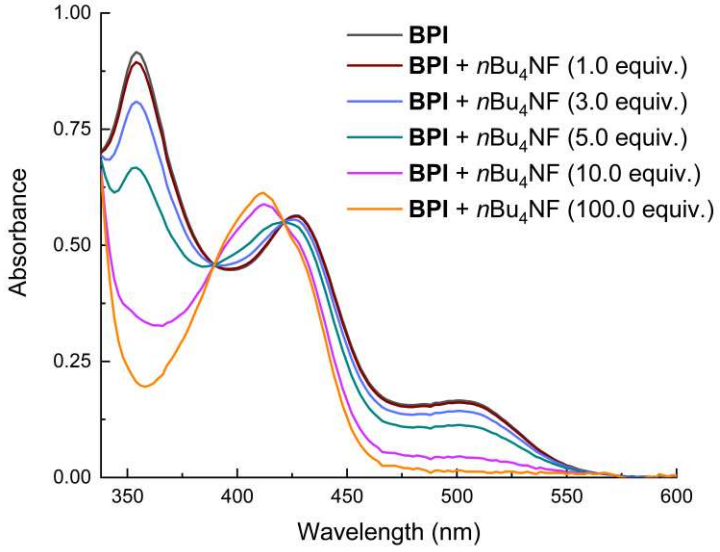

Figure S2.27. Absorption spectrum of 25 μM BPI in a THF solution in the presence of a varying equivalence of nBu4NF in THF at room temperature in a 1 cm cuvette.

12.2.6 Cyclic voltammetry of BPI and BPI with *n*Bu4NF

Cyclic voltammetry (CV) was performed with a potentiostat (Gamry Instruments) using a 3-electrode electrochemical cell with an $Ag/AgNO_3$ reference electrode consisting of Ag wire and an $AgNO_3$ solution (0.01 M) in MeCN or DMAc with $TBAPF_6$ electrolyte (0.100 M), separated by a frit from the analyte solution. The counter electrode was a Pt wire and was separated from the analyte solution by a Vycor frit for bulk electrolysis in the spectroelectrochemistry experiment and for CVs performed in THF. A Pt working electrode (Gamry Instruments) was used for CV characterization of catalysts. For spectroelectrochemistry, a 1 x 5 cm glassy carbon working electrode (IKA) was used. For other CVs in THF, a small glassy carbon working electrode (IKA) was used. $TBAPF_6$ in DMAc or THF (0.100 M) was used as the electrolyte in all analyte solutions. For spectroelectrochemistry, UV-vis spectra were recorded using the Cary 5000 equipped with a

fiber optic coupler (Harrick Scientific Fiber Mate) and probe that was placed in the analyte solution in the electrochemical cell. The cell and probe assembly were placed on a stir plate inside a light-tight box. For all experiments, solutions were degassed by sparging with N_2 through a Teflon tube for at least 15 minutes prior to starting the potentiostat. CV was performed with the tube pulled out of the solution and without stirring. For spectroelectrochemistry, the solution was stirred and sparged throughout the measurement.

Table S2.15. Summarized electrochemical data in THF.

PCs	E^0 ($PC/PC^{\bullet-}$) = vs. Fc^+/Fc	E^0 ($PC^{\bullet-}/PC^{2-}$) = vs. Fc^+/Fc	E^0 ($PC/PC^{\bullet-}$) = vs. SCE	E^0 ($PC^{\bullet-}/PC^{2-}$) = vs. SCE
BPI	-1.80	-2.43	-1.24	-1.87
BPI with nBu$_4$NF	-2.40	-2.85	-1.84	-2.29
Fc^+/Fc	0.22			

[a] *Conversion used for measurement of Fc^+/Fc vs. SCE in THF*

Table S2.16. Summary of redox potentials of well-known aryl imide photocatalysts

entry	PCs	E^0 ($PC/PC^{\bullet-}$) = vs. SCE	Ref.
1	BPI with nBu$_4$NF	-1.84 V	this work
2	NpDI	-1.52 V	*J. Am. Chem. Soc. 142*, 2093−2099 (2020)
3	NpMI	-1.42 V	*J. Am. Chem. Soc. 142*, 2093−2099 (2020)
4	nBuO-NpMI	-1.30 V	*Angew. Chem. Int. Ed.* 60*, 20817*–20825 (2021)

5	PhMI	-1.24 V	*J. Am. Chem. Soc.* 142, 2093−2099 (2020)
6	PDI	-0.40 V	*Science* 346, 725 (2014)

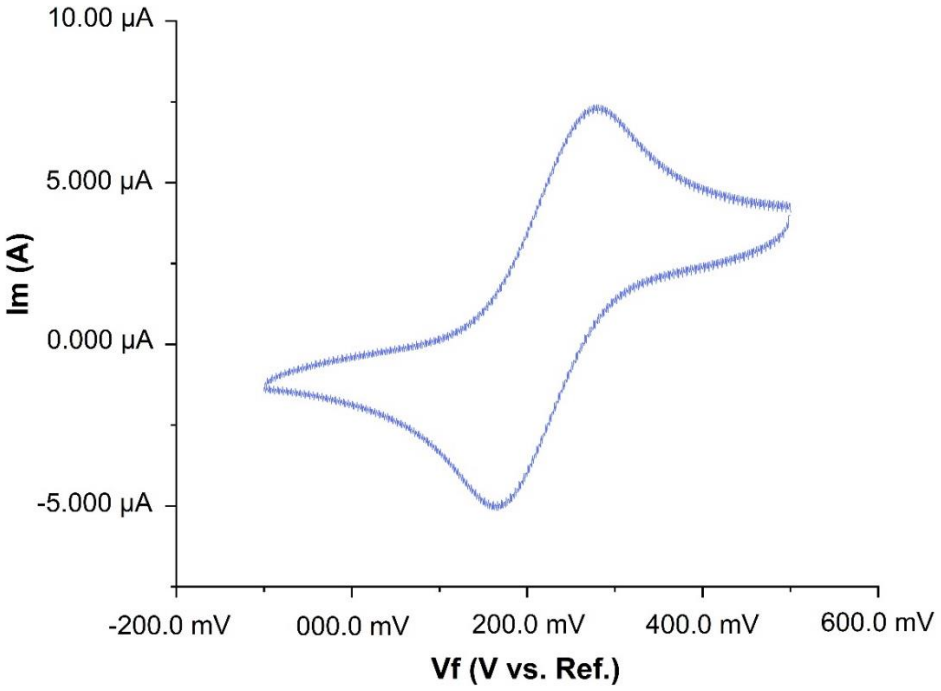

Figure S2.28. Cyclic voltammogram of Fc^+/Fc standard (1.0 mM in THF).

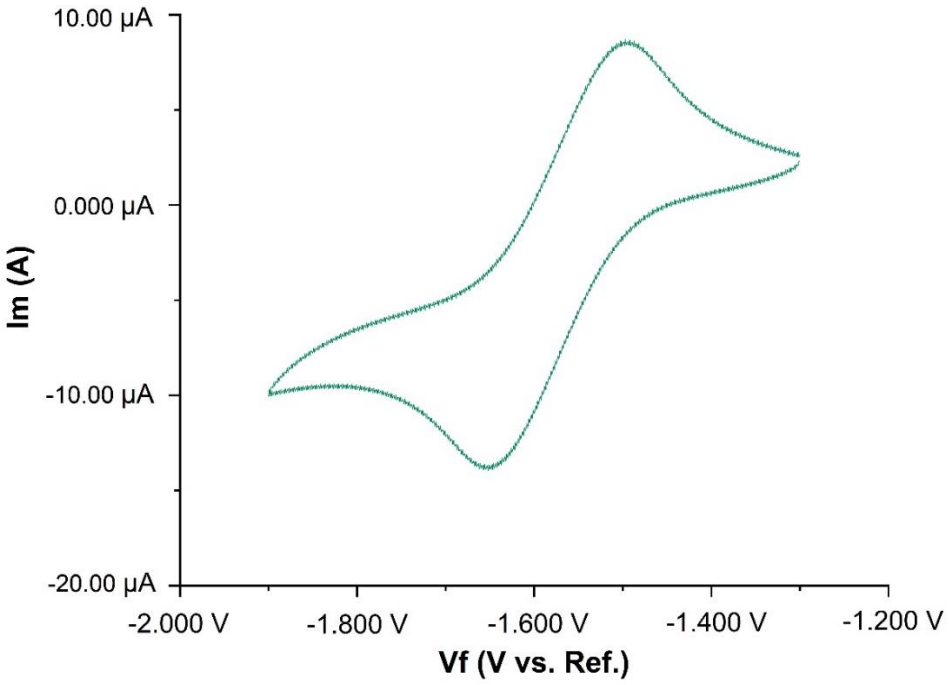

Figure S2.29. Cyclic voltammogram of BPI (1.0 mM in THF) showing the first reduction event.

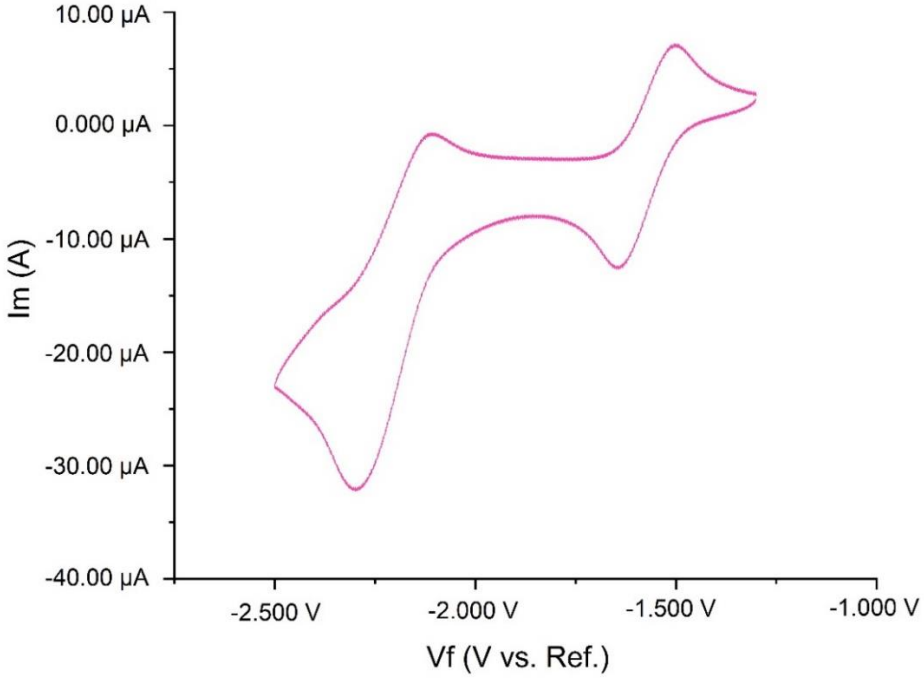

Figure S2.30. Cyclic voltammogram of BPI (1.0 mM in THF) showing two reduction events.

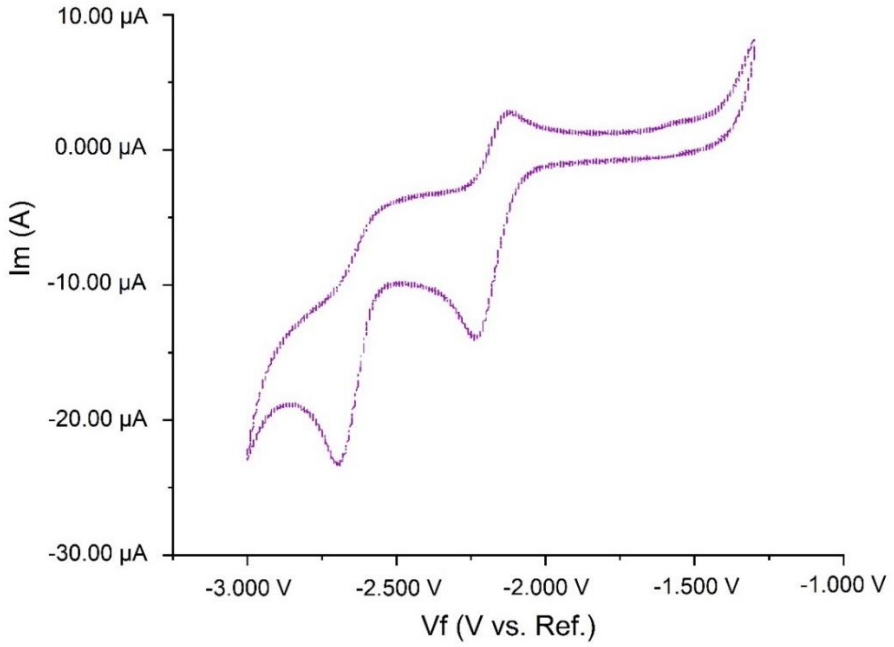

Figure S2.31. Cyclic voltammogram of BPI (1.0 mM in THF) with nBu_4NF (200 equiv.) showing two reduction events.

12.3 Radical anion BPI-RO$^{\bullet-}$ formation

12.3.1 Detection of BPI-RO$^{\bullet-}$ in the presence of a protic solvent via UV-vis spectroscopy

Test sample preparation: In a 1 cm cuvette with 2.5 mL THF, 25 µM solution of **BPI w**as prepared along with approximately 160 molar equivalences of *n*Bu$_4$NF (4 mM). An absorption spectrum of the solution was then collected before irradiation (black trace) and then periodically (time designated in the legend) after irradiation via a 405nm LED.

From the known literature[71], the radical anion formation can be obtained by UV-vis (λ_{abs}, max = 520-560 nm). In the absence of a proton source, the radical anion signal can be observed at 546 nm which suggests that the new species is **BPI-RO$^{\bullet-}$**.

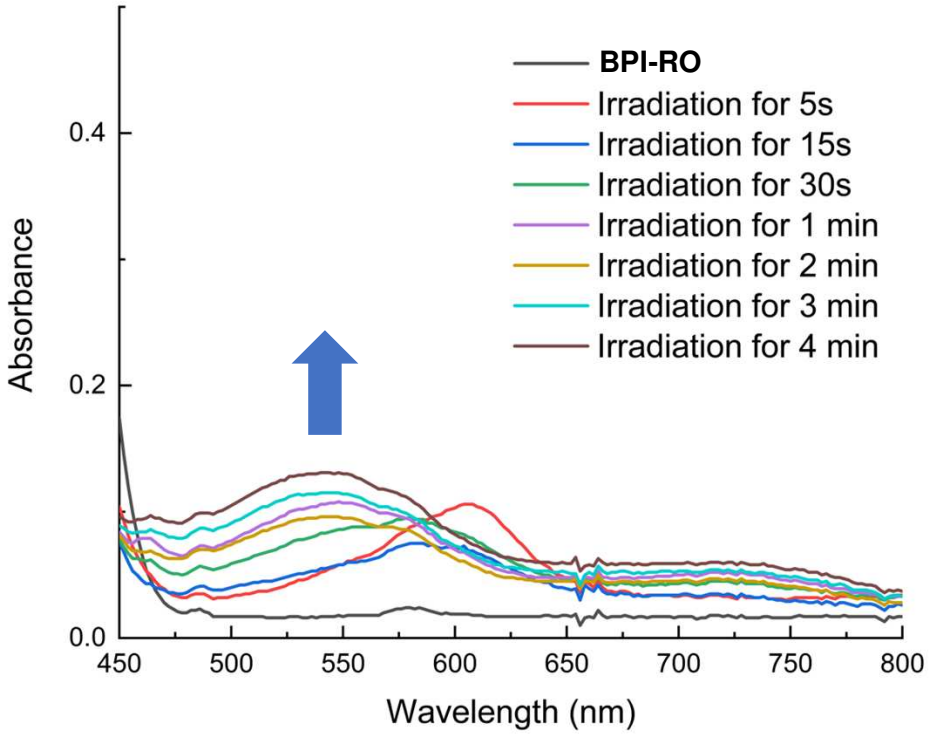

*Figure S2.32. The absorption spectrum of 25 µM **BPI** in THF solution, nBu$_4$NF (160 molarr equivalence) (1.0 M in THF) in a 1 cm cuvette pre and post 405nm irradiation. The amount of*

irradiation time applied to the cuvette and its corresponding absorption spectrum are designated in the legend.

12.3.2 ^{13}C-NMR spectroscopic evidence for BPI-RO$^{\bullet-}$ formation

Step 1: In glovebox, a 2.0 mL glass vial containing a stirring bar was sequentially charged with **BPI** (8.0 mg), *n*Bu$_4$NF (0.1 mL, 1.0 M in THF), and THF-d$_8$ (0.4 mL). The mixture was stirred in the glove box for 5 min, then transferred to a dry NMR tube. The ^{13}C-NMR spectrum was recorded.

Step 2: The solution (from step 2) was irradiated with 405 nm blue LED for 45 min. The ^{13}C-NMR spectrum was recorded.

Note: The number of scans of all ^{13}C-NMR is 3000.

Upon irradiating the BP solution, a noticeable broadening of the peaks is observed, as evidenced in Figure S35 and Figure S36. This broadening implies the formation of radical anions.

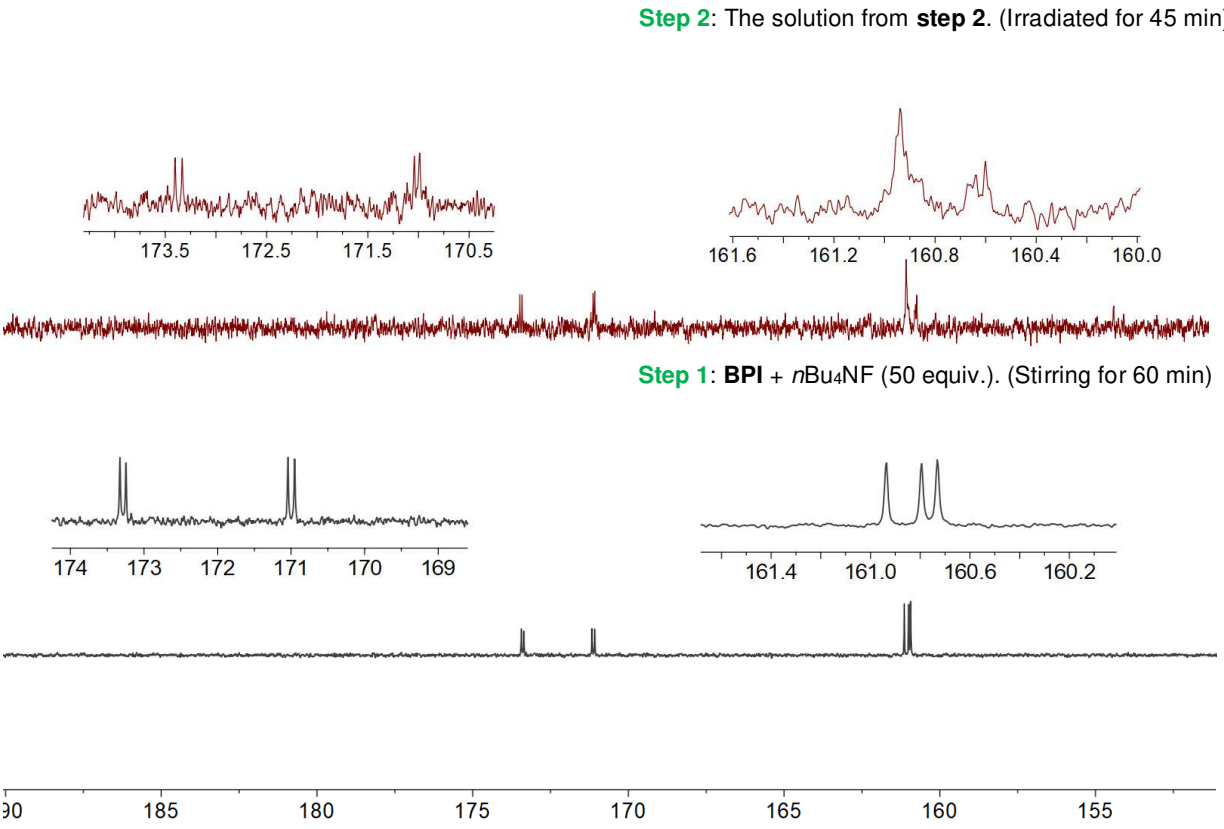

Figure S2.33. Partial ^{13}C-NMR of BPI-RO and BPI-RO under irradiation. The signal peak is between 150 – 190 ppm.

12.3.3 ^{1}H-NMR spectroscopic evidence for BPI-RO$^{\bullet-}$ formation

Step 1: In glovebox, a 2 mL glass vial containing a stirring bar was sequentially charged with **BPI** (5.0 mg), *n*Bu$_4$NF (0.4 mL, 1.0 M in THF). The mixture was stirred in the glove box for 60 min, then transferred to a dry NMR tube. The ^{1}H-NMR spectrum was recorded.

Step 2: The mixture (from step 1) was irradiated with 405 nm blue LED for 5 min. The ^{1}H-NMR spectrum was recorded.

Step 5: The solution (from step 2) was keep irradiated for another 40 min. The ^{1}H-NMR spectrum was recorded.

Step 6: The irradiated solution was kept at room temperature under argon conditions for 3 hours, then the ^{1}H NMR spectrum was recorded.

Note: The number of scans of all ^{1}H-NMR is 128.

When the **BPI-RO** solution is under irradiation, the signals have been broadening which suggests the radical anion formation (see Figure S32, steps 2-3). The radical anion **BPI-RO$^{\bullet-}$** is a stable intermediate which can keep for 3 h without any changes (see step 4).

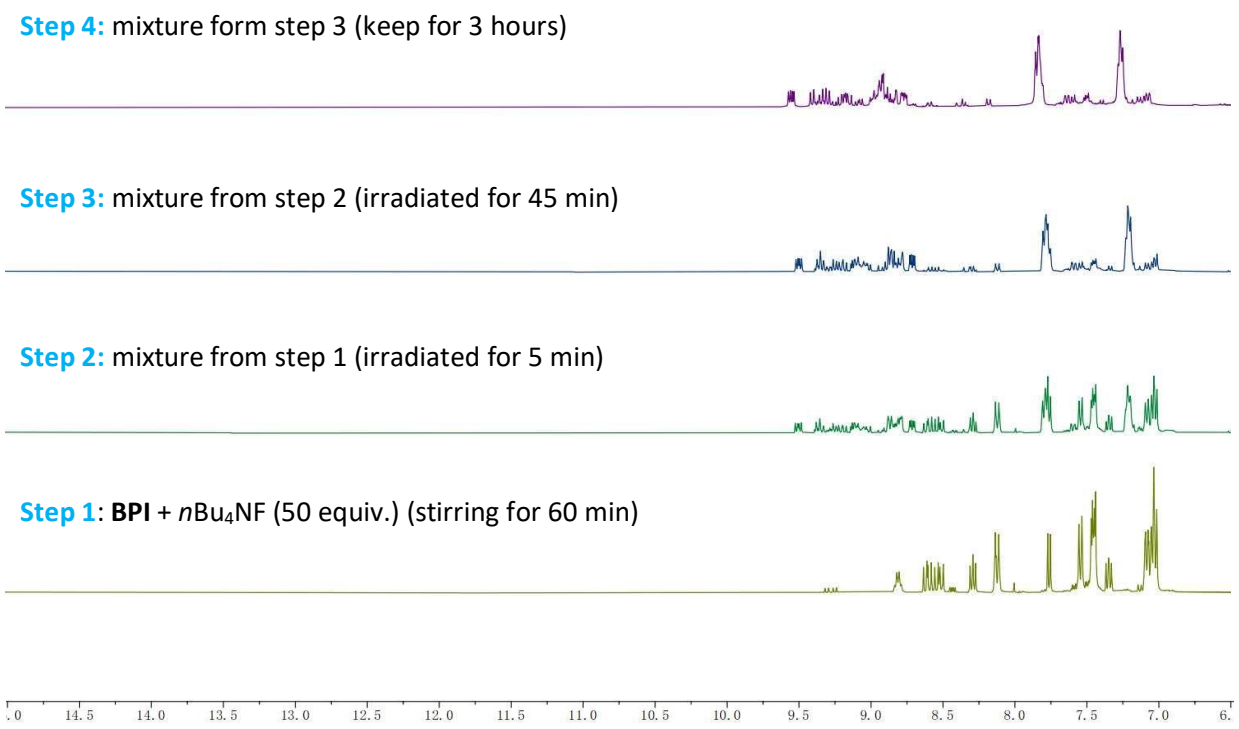

Figure S2.34. Evidence of the generation of BPI-RO$^{\bullet-}$ by ^{1}H-NMR measurement.

12.3.4 Electron paramagnetic resonance (EPR) characterization of BPI-RO$^{\bullet-}$

To verify that the species (**BPI-RO**) was the long-lived radical anion **BPI-RO**$^{\bullet-}$, electron paramagnetic resonance (EPR) spectroscopy was conducted.

Test sample preparation:

Step 1: In a glovebox, the solution of 6 mM **BPI** with *n*Bu$_4$NF 5 mM was stirred for 120 min under dark conditions. No EPR signal has been detected (see Figure S37, grey).

Step 2: In a glovebox, the solution of 6 mM **BPI** with *n*Bu$_4$NF 5 mM was stirred for 120 min under dark conditions. Then, the mixture was irradiated with 405 nm blue LED for 120 min at room temperature. No EPR signal has been detected (light blue).

Step 3: In a glovebox, the solution of 5 mM **BPI** with *n*Bu$_4$NF (50 equiv., 1.0 M in THF) was stirred for 120 min under dark conditions. No EPR signal has been detected (orange).

Step 4: In a glovebox, the solution of 5 mM **BPI** with *n*Bu$_4$NF (50 equiv., 1.0 M in THF) was stirred for 120 min. Then, the mixture was irradiated with 405 nm blue LED for 60 min at room temperature. The EPR Signals are recorded (dark green).

No signal has been observed when **BPI** reacts with *n*Bu$_4$NF under dark conditions (see Figure 37, step 1 and 3). Additionally, the reaction mixture from step 1 fails to exhibit any signal upon irradiation (refer to step 2). In contrast, the mixture from step 3 does display a signal indicative of radical anion formation under irradiation conditions (see step 4). Based on our intermediate studies, we suggest that the signal detected by EPR is **BPI-RO**$^{\bullet-}$ rather than **BPI**$^{\bullet-}$.

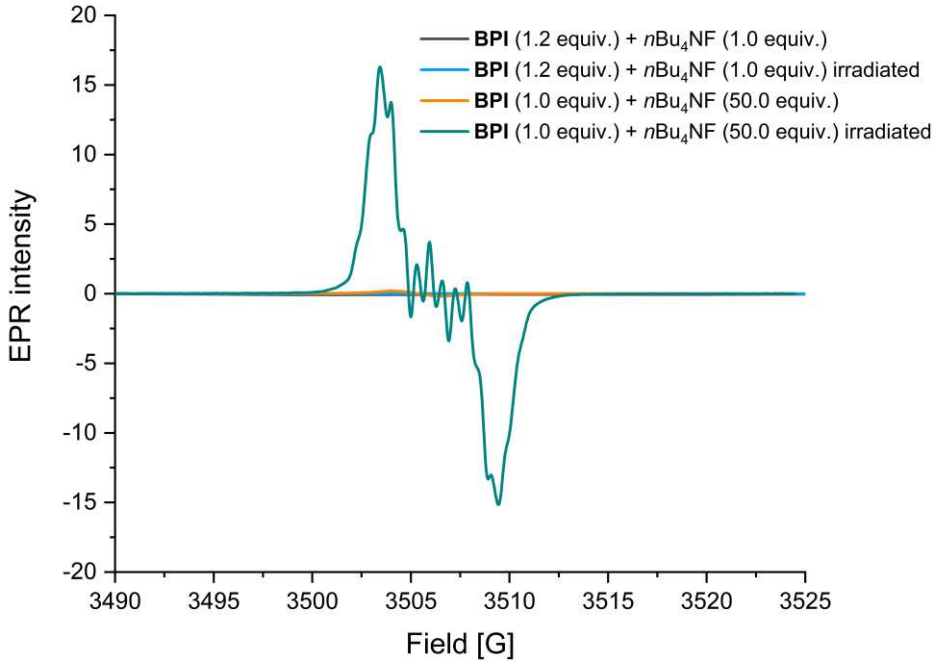

Figure S2.35. EPR spectrum to support the presence of BPI-RO$^{\bullet-}$.

12.3.5 Inconclusive experiments looking for reduction of Ph-F by BPI-RO$^{\bullet-}$

BPI-RO$^{\bullet-}$ exploration:

As was noted in the summary at the beginning of section 12.1, we first looked for quenching behavior in the presence of **BPI-RO$^{\bullet-}$**. The null results are shown below in Figure S38.

Stock solution preparation:

A stock solution of **BP** species was prepared by dissolving 1.0 mg of **BPI** in 1.0 mL of *n*Bu$_4$NF (1.0M in THF) which was then kept in dark inside a glovebox for 2 hours. This was to ensure complete conversion of **BPI** into **BP** (ring-opening product). After 2 hours, an aliquot of this stock solution was transferred into a cuvette and diluted with 2.5 mL THF, and an absorption spectrum was taken which confirmed that there was no **BPI** left.

Sample preparation:

For each sample, 8.0 µL of the stock solution was transferred into a 1cm cuvette fitted with a Kontes valve (in order ensure it remains air-free) inside a glovebox. To this, THF (1.9 mL), and *n*Bu$_4$NF (0.2 mL, 1.0M in THF) were added sequentially. Thus, the final concentration of the **BPI-RO** species became 4.0 µM. The extra *n*Bu$_4$NF was used to make the quenching conditions closely resemble the defluorination reaction condition. A steady state fluorescence spectrum was then collected by exciting the sample at 405 nm (same wavelength as the LED used for the reaction). The OD at this wavelength was ~0.045 which allowed us to avoid non-linear processes like self-absorption while measuring the emission.

*Absence of fluorescence quenching of **BPI-RO**:*

The same cuvette was used to collect the steady state fluorescence spectra of the new **BPI-RO** species in presence of increasing amounts of substrates. For fluorobenzene, an increment of 35 µL was used which resulted in substrate concentrations of 0.15, 0.30, and 0.45 M. The area under the fluorescence curve was integrated to calculate the total fluorescence.

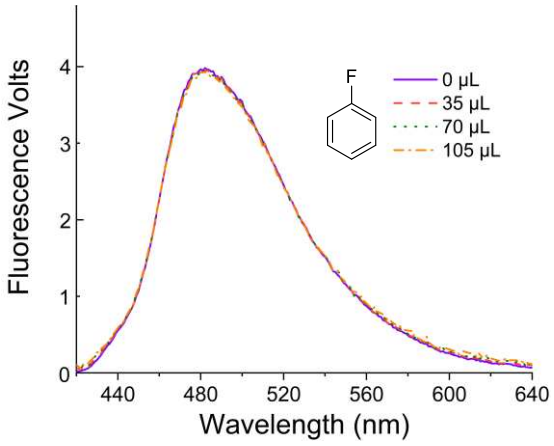

Figure S2.36. Steady state fluorescence spectra collected on BPI-RO (without tAmylOH and irradiation) solution with increasing amount of fluorobenzene.

The result above (see Figure. S2.36) suggests that photoexcited **BPI-RO** does not store the appropriate thermodynamic driving force for fluorobenzene reduction thereby requiring further reductive transformation. The radical **BPI-RO**$^{\bullet-}$ is expected to be a more powerful reductant from its excited state but exposes experimental challenges in its interrogation. As shown below, **BP** (under irradiation for 30 min) does produce emissive intermediates that can be explored in quenching studies (see Figure S2.37). However, these studies do not expose quenching behavior of **BPI-RO**$^{\bullet-}$.

BPI-RO conversion under irradiation for 30 min:

Sample preparation:

For each sample, 8.0 µL of the stock solution was transferred into a 1cm cuvette fitted with a Kontes valve (in order ensure it remains air-free) inside a glovebox. To this, THF (1.9 mL) and *n*Bu_4NF (0.2 mL, 1.0M in THF) were added sequentially. Thus, the final concentration of the **BPI-RO** species became 4.0 µM. The extra *n*Bu_4NF was used to make the quenching conditions closely resemble the defluorination reaction condition. The cuvette was then irradiated with a 405 nm LED briefly for 30 mins and an absorption spectrum was measured afterwards which showed that the **BPI-RO** was now converted into new species (see Figure 37, a). We suggest that changes include the formation of **BPI-RO**$^{\bullet-}$. Photoluminescence studies (see Figure S37, b) show that emissive intermediates are also formed but these are not attributed to **BPI-RO**$^{\bullet-}$. They are likely due to the presence of some residual protons.

Fluorescence of emission intermediate and diminution with added fluorobenzene:

The same cuvette was used to collect the steady state fluorescence spectra in the presence of increasing amounts of substrates. For fluorobenzene, an increment of 50 µL was used which resulted in substrate concentrations of 0.22, 0.44, and 0.66 M. The area under the fluorescence curve was integrated to calculate the total fluorescence.

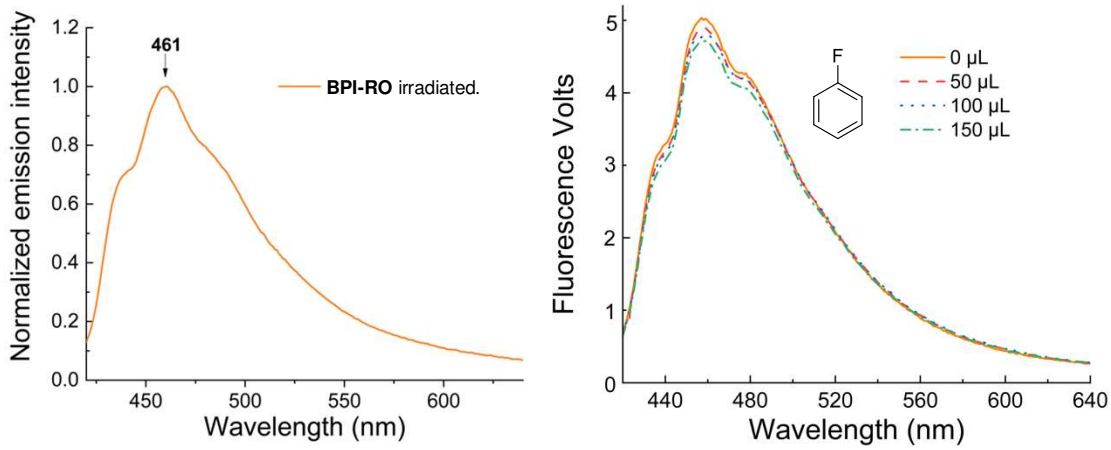

Figure S.37. a) Emission profile for intermediate produced when BPI-RO is irradiated for 30 min in THF in the presence of nBu_4NF but without an alcohol source. b) Steady state fluorescence spectra collected for this sample with increasing amounts of added fluorobenzene.

12.4 Closed-shell species BPI-RO-H$^-$ formation

12.4.1 Emission profiles for BPI-RO irradiated with *t*AmylOH

Test sample preparation: A stock solution of **BPI-RO** species was prepared by dissolving 1.0 mg of **BPI** in 1.0 mL of *n*Bu_4NF (1.0M in THF) which was then kept in dark inside a glovebox for 2 hours. This was to ensure complete conversion of **BPI** into **BPI-RO**. After 2 hours, an aliquot of this stock solution was transferred into a cuvette and diluted with 2.5 mL THF, and an absorption spectrum was taken which confirmed that there was no **BPI** left.

8.0 μL of the stock solution was transferred into a cuvette fitted with a Kontese valve inside the glovebox and was then diluted with 2.0 mL of THF and 0.5 mL of *tert*-AmylOH. A steady state fluorescence spectrum was collected by exciting the sample at 380 nm. The dilution made sure the optical density (OD) at 380 nm was <0.1, allowing us to avoid self-absorption and other non-linear effects. The cuvette was then irradiated for 5s inside the photoreactor fitted with a single 405 nm LED and another fluorescence spectrum was collected by exciting it at the same wavelength (380 nm). This was repeated 3 more times.

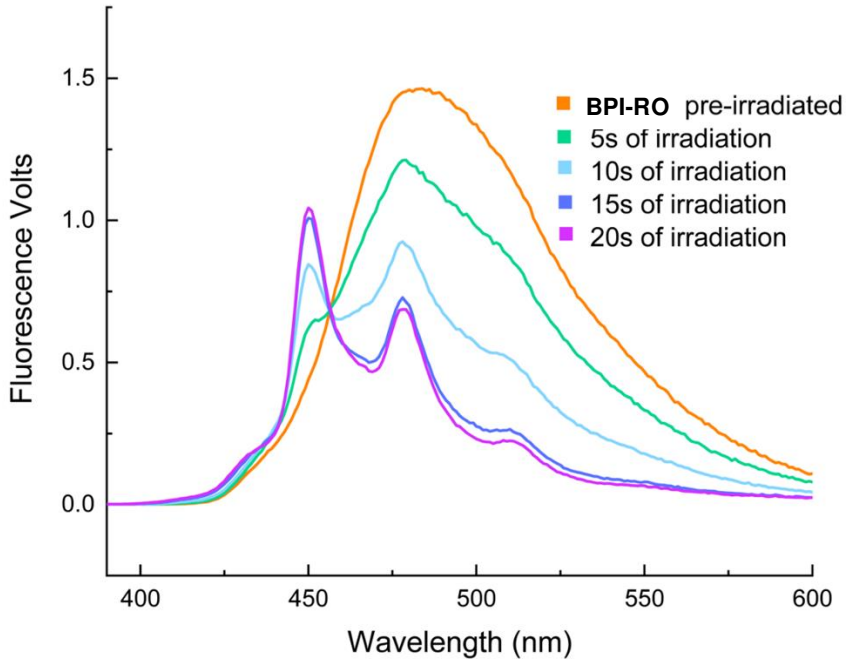

Figure S2.38. Fluorescence spectrum changes for BPI-RO in THF as a function of 405nm irradiation. The fluorescence spectra were collected by exciting the sample at 380nm. This data is presented within the main text as Figure 2c.

BPI-RO was generated within the glovebox by dissolving 1.0 mg of **BPI** in 1.0 mL of *n*Bu_4NF (1.0M in THF). This solution was allowed to sit for 1.5 h before 16 µL was taken from the solution and added to 1.9 mL of THF within a 1.0 cm Kontese cuvette. This was followed by the addition of 0.4 mL of *tert*-AmylOH then 0.2 mL of *n*Bu_4NF. The cuvette was sealed within the glovebox. An absorption and emission spectrum were immediately taken where the emission spectrum was obtained by irradiating the solution at 405nm, the same wavelength as the reaction conditions. After the air-free emission spectrum was collected, the solution was stirred open to air for 10 minutes. The solution was transferred back to the cuvette and an absorption/emission spectrum was again collected. The solution was allowed to sit under aerated conditions in the dark for a total of 8 hours with spectra being collected at the 3- and 8-hour mark. These spectra are shown below. There is about 20% emission quenching after initial exposure to air which is standard for oxygen

quenching[72]. After initial air exposure, very minimal fluorescence intensity is lost as well as virtually no change in the shape of the fluorescence spectrum.

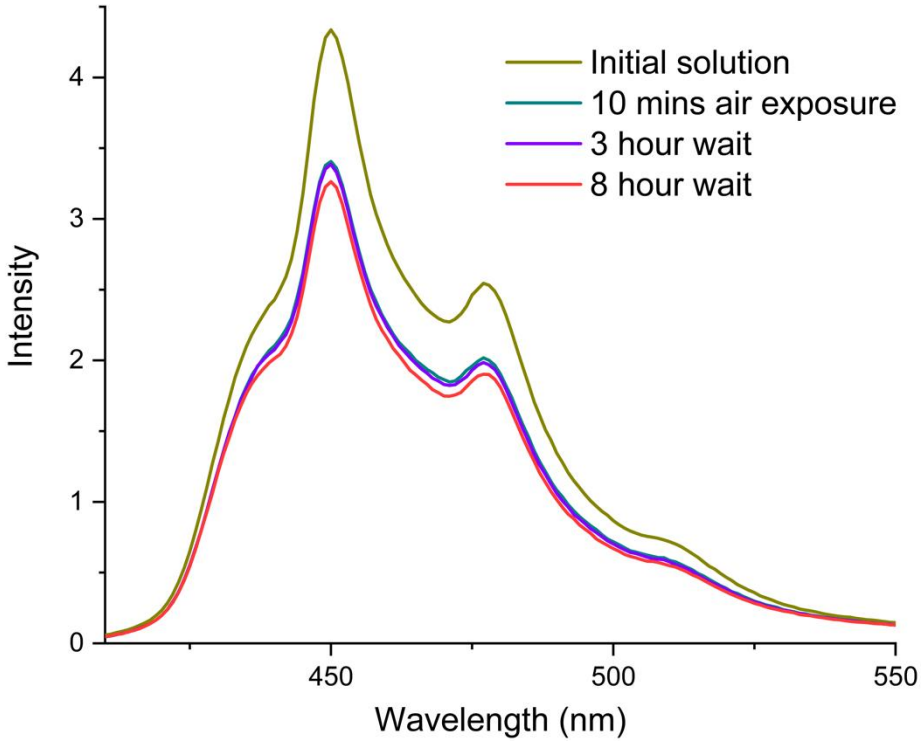

Figure S2.39. *Fluorescence of irradiated* ***BPI-RO*** *solution in 5:1 THF: tert-AmylOH initially under Ar then under aerated conditions.*

12.4.2 Monitoring the features of BPI-RO-H⁻ formation via UV-Vis as a function of *n*Bu$_4$NF concentration

Test sample preparation (high nBu$_4$NF concentration sample): In a 1 cm cuvette with 2.4 mL THF and 0.1 mL *t*AmylOH, 25 µM solution of **BPI** was prepared along with approximately 3300 molar equivalences of *n*Bu$_4$NF (83 mM). An absorption spectrum of the solution was then collected before irradiation (denoted **BPI-RO**) and then periodically (time designated in the legend) after irradiation via a 405nm LED. In 4s, **BPI-RO** is seen to be completely converted to **BPI-RO-H⁻**.

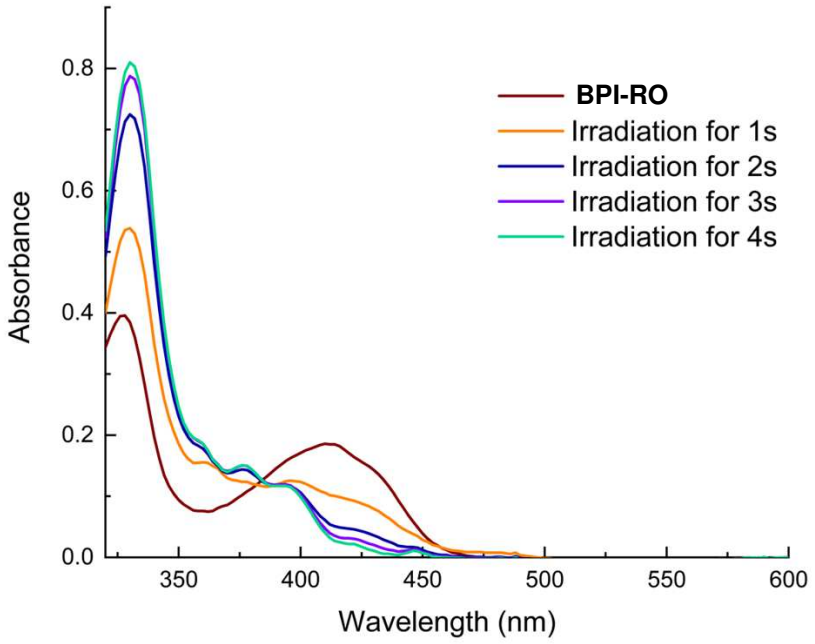

Figure S2.40. *The absorption spectrum of 25 μM* ***BPI*** *THF solution, nBu_4NF (3300 molar equivalence) (1.0 M in THF), and 0.1 mL of tAmylOH in a 1 cm cuvette pre and post 405nm irradiation. The amount of irradiation time applied to the cuvette and its corresponding absorption spectrum are designated in the legend.*

Test sample preparation (low nBu_4NF concentration sample): In a 1 cm cuvette with 2.4 mL THF and 0.1 mL *t*AmylOH, 25 μM solution of **BPI** was prepared along with approximately 130 molar equivalences of nBu$_4$NF (3.2 mM). An absorption spectrum of the solution was then collected before irradiation (denoted **BPI-RO**) and then periodically (time designated in the legend) after irradiation via a 405nm LED. Unlike the previous case where it took only 4s, this time the complete conversion from **BPI-RO** to **BPI-RO-H**$^-$ takes place over 20s.

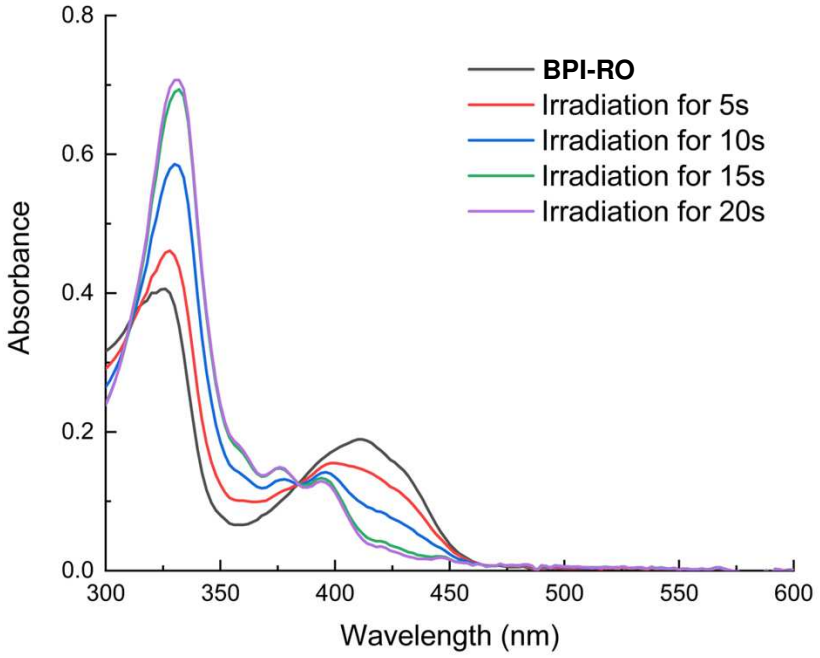

Figure S2.41. The absorption spectrum of 25 μM BPI solution, nBu$_4$NF (130 molar equivalence) (1.0 M in THF), and 0.1 mL of tAmylOH in a 1 cm cuvette pre and post 405nm irradiation. The amount of irradiation time applied to the cuvette and its corresponding absorption spectrum are designated in the legend.

12.4.3 ^{1}H-NMR evidence for the closed-shell species

Step 1: In a glovebox, a 2 mL glass vial containing a stirring bar was sequentially charged with **BPI** (8.0 mg), *n*Bu$_4$NF (0.1 mL, 1.0 M in THF), and THF-d$_8$ (0.8 mL). The mixture was stirred in the glove box for 30 min, then transferred to a dry NMR tube. The mixture in the tube was irradiated with 405 nm blue LED for 120 min. The ^{1}H-NMR spectrum was recorded.

Step 2: The solution (from step 1) was moved back to glovebox, then added 0.05 mL *tert*-AmylOH. Then, the mixture was irradiated for 60 min. The ^{1}H-NMR spectrum was recorded.

Step 3: The mixture (from step 2) is exposed to air conditions for 4 h. The ^{1}H-NMR spectrum was recorded.

Note: The number of scans of all ^{1}H-NMR is 128.

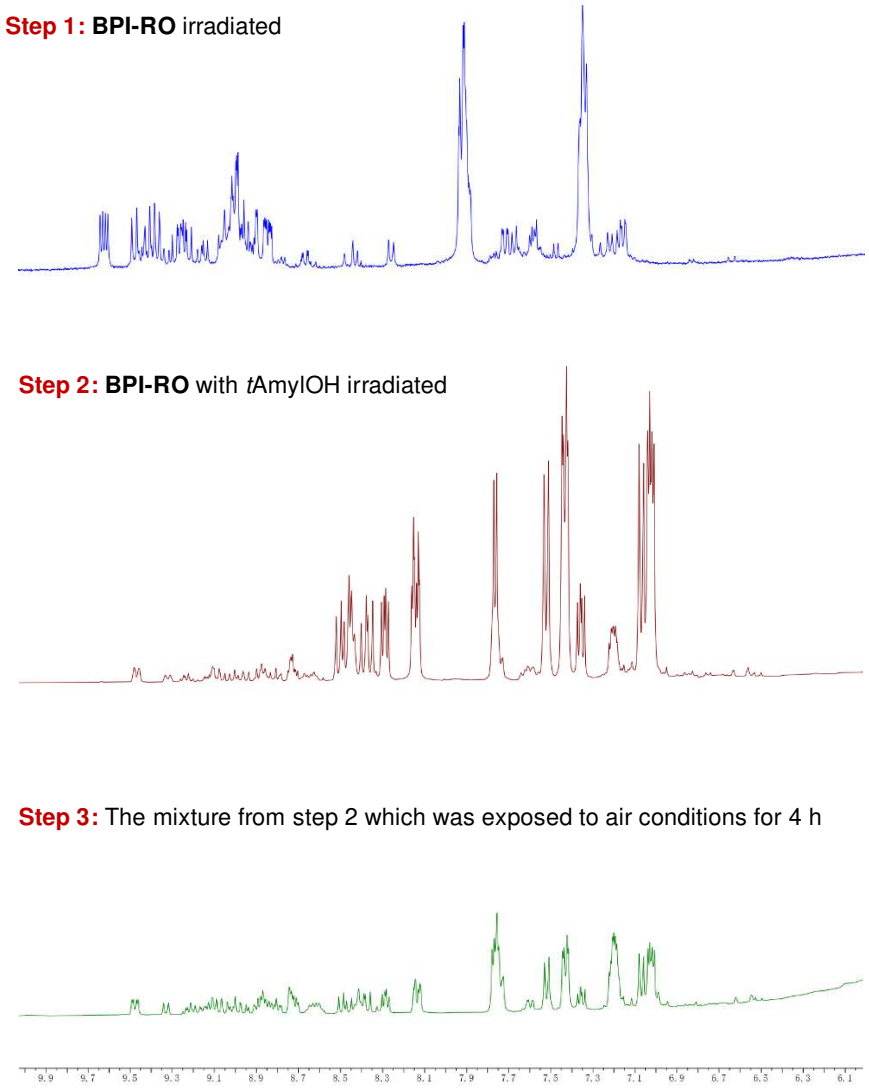

Figure S2.42. ^{1}H-NMR studies for support the presence of BPI-RO-H^{-}.

12.5 Reduction of Ph-F by BPI-RO-H$^-$

12.5.1 Quenching experiments

BPI-RO quenching reaction (with *t*AmylOH and irradiation):

Sample preparation:

For each sample, 8.0 μL of the stock solution was transferred into a 1cm cuvette fitted with a Kontes valve (in order ensure it remains air-free) inside a glovebox. To this, THF (1.9 mL), *tert*-AmylOH (0.4 ml) and *n*Bu_4NF (0.2 mL, 1.0M in THF) were added sequentially. Thus, the final concentration of the **BPI-RO** species became 4.0 μM. The extra *n*Bu_4NF was used to make the quenching conditions closely resemble the defluorination reaction condition. The cuvette was then irradiated with a 405 nm LED briefly for 3 seconds and an absorption spectrum was measured afterwards which showed that the **BPI-RO** was now converted into a new species. A steady state fluorescence spectrum was then collected by exciting the sample at 405 nm (same wavelength as the LED used for the reaction). The OD at this wavelength was ~0.045 which allowed us to avoid non-linear processes like self-absorption while measuring the emission.

Fluorescence Quenching:

The same cuvette was used to collect the steady state fluorescence spectra of the new **BPI-RO** species in presence of increasing amounts of substrates. For fluorobenzene, an increment of 35 µL was used which resulted in substrate concentrations of 0.15, 0.30, 0.45 and 0.60 M. The area under the fluorescence curve was integrated to calculate the total fluorescence.

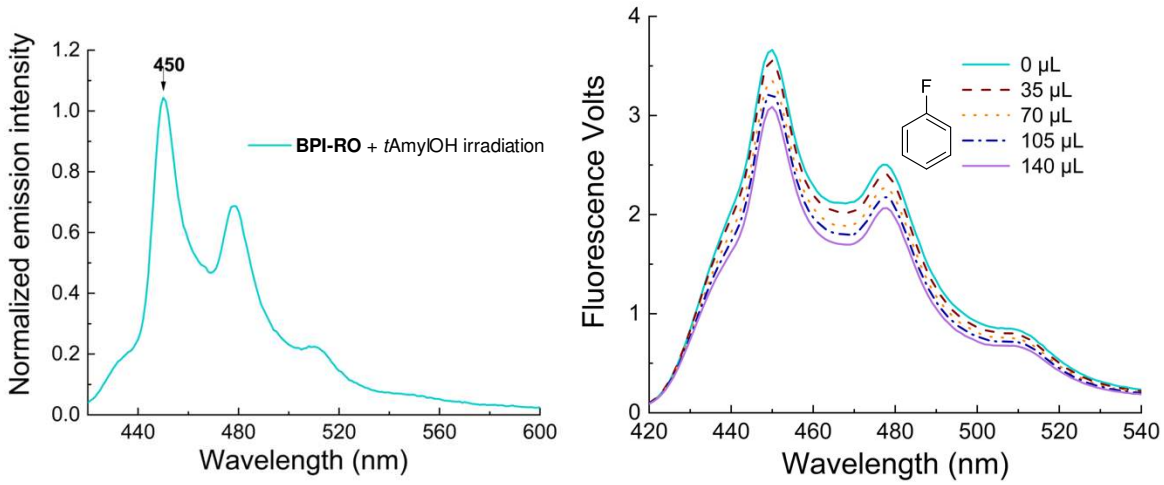

Figure S2.43. a) Emission profile of BPI-RO-H⁻ generated by irradiating by BPI and nBu_4NF in presence of tAmylOH under irradiation. b) Steady state fluorescence spectra collected on the irradiated BPI-RO (with tAmylOH) solution with increasing amount of fluorobenzene. Stern-Volmer plot using this data presented in Figure 2d.

For 4-methylfluorobenzoate, an increment of 30 µL was used which gave us concentrations of 0.09, 0.18. 0.27 and 0.36 M respectively.

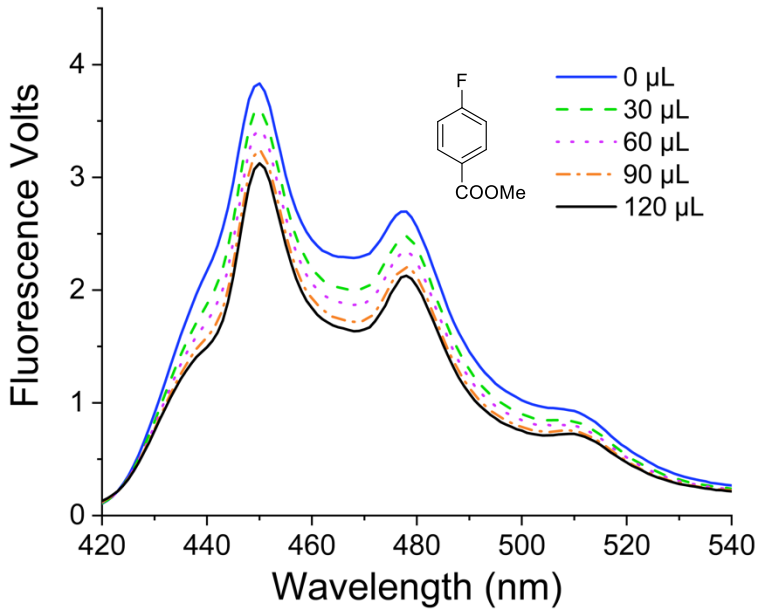

Figure S2.44. Steady state fluorescence spectra collected on the irradiated BPI-RO (with tAmylOH) solution with increasing amount of 4-methylfluorobenzoate. Stern-Volmer plot using this data presented in Figure 2d.

12.5.2 The quadratic dependence studies

Mechanistic insight into photoredox reactions that rely on multi-photon excitation can be gained by quadratic dependence studies. In the initial phase of a two-photon transfer reaction, the conversion is frequently expected to show a quadratic dependence on excitation power. Thus, doubling the excitation power will not simply result in a doubled yield for single-photon transfer reaction, but instead of a four-fold increase of the yield for a two-photon transfer reaction.[73]

Near quadratic dependency of the conversion of 4-fluorobenzonitrile on the irradiation density further supported that the aryl radical formation mechanism involves an overall two-photon excitation.[41, 74]

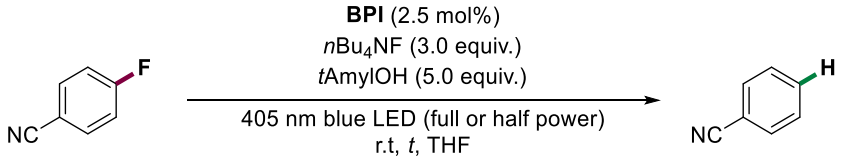

The irradiation power of blue LED (405 nm) was controlled by using multiple photo reactors (full or half power), as illustrated in the following picture.

Full power **Half power**

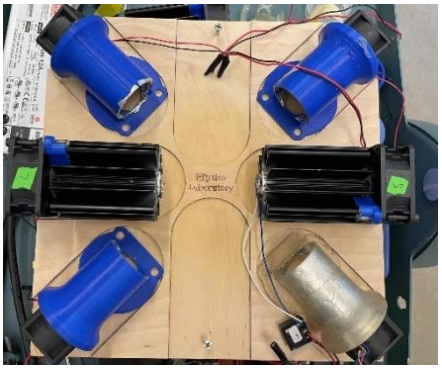

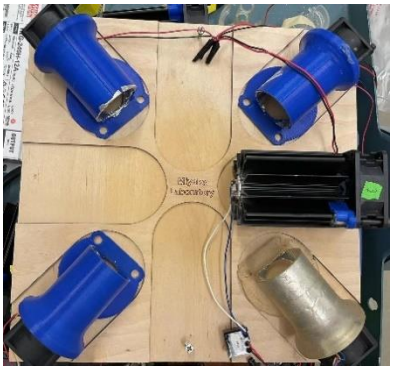

In a glovebox, a 5 mL glass vial containing a stirring bar was sequentially charged with **BPI** (25 μmol, 2.5 mol%), 4-fluorobenzonitrile (0.5 mmol), *n*Bu_4NF (1.5 mmol, 3.0 equiv., 1.0 M in THF), *t*AmylOH (0.5 mL). The glass vial was placed into the light reactor (single power or double power) and stirred for corresponding time. The temperature was kept at approximately 23 °C through cooling with four mini fans. After reaction, the conversion of 4-fluorobenzonitrile was calculated based on the ^{19}F-NMR analysis of the crude mixture (2-fluoropyridine was used as internal standard). Each of these reactions was conducted three times, the averaged conversion was shown in Table S2.17.

Table S2.17. Quadratic dependency of the conversion of 4-fluorobenzonitrile

time / conv. / ligh1t	0 min	20 min	40 min	60 min	80 min
single power	0%	0.9%	1.7%	3.0%	4.3%
double power	0%	3.8%	7.3%	12.4%	16.7%

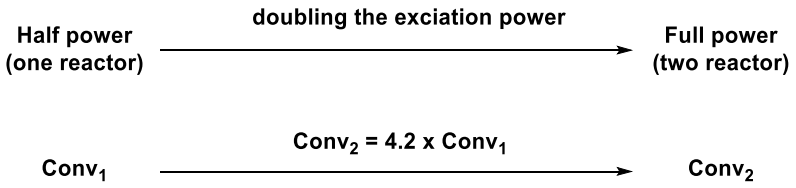

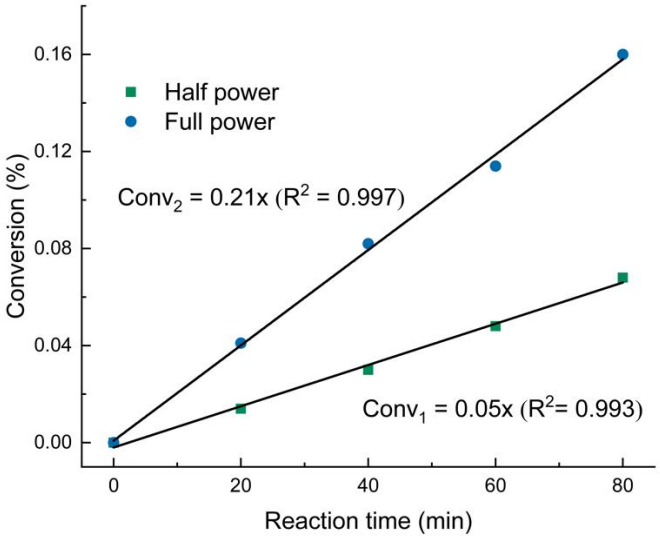

Figure S2.45. *Conversion dependency on the irradiation intensity. This data is presented in Figure 2e.*

In summary, depending on the actual two-photon mechanism, situations in between the linear and the quadratic power dependence can result.[64] Our quadratic dependence studies suggest that the closed-shell catalytic cycle has two-photon transfer processes.

12.5.3 Deuterium experiments

General procedure for deuterium-labeling experiments

In a glovebox, a 5 mL glass vial containing a stirring bar was sequentially charged with **BPI** (0.5 mol%), substrate (0.5 mmol), *n*Bu_4NF (1.0 mmol, 2.0 equiv., 1.0 M in THF) or *n*Bu_4NF (1.0 mmol, 2.0 equiv., 1.0 M in THF-d_8), and alcohols (5.0 equiv.). The glass vial was placed into the light reactor and stirred for 8 hours. The temperature was kept at approximately 23 °C through cooling with four mini fans. After reaction, the conversion was determined by GC using mesitylene as the internal standard. The ratio of H/D was determined by ^{1}H-NMR.

Synthesis of dry *n*Bu_4NF (1.0 in THF-d_8):

n$Bu_4NF{\bullet}3H_2O$ was heated in a round-bottomed flask with magnetic stirring at 50 ºC under vacuum. After 4-5 h, the sample liquified. Then, keep heating for another 24 h until the sample lost 20% of its original weight. The resulting "dried" *n*Bu_4NF contained 0.2-0.3 equiv. of H_2O (determined by ^{1}H-NMR) and 10% of *n*Bu_4NHF_2 (δ= -146 ppm in the ^{19}F-NMR). The signal of "dried" *n*Bu_4NF at δ= -100 ppm in the ^{19}F-NMR. The dry *n*Bu_4NF (1.0 mmol) was added to 1.0 mL THF-d_8, then the mixture was used for reaction.

Table S2.18. Deuterium-labeling experiments by using 4-trifluoromethylbenzonitrile as substrate.

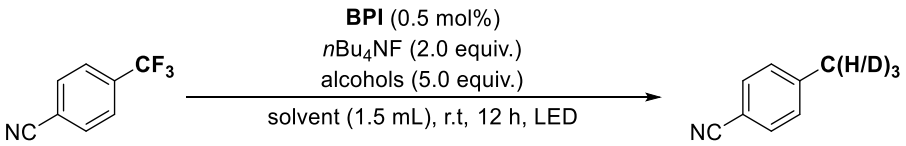

entry	solvent	alcohols	conv. (%)	H/D ratio
1	nBu$_4$NF (1.0 M in THF) + THF-d$_8$ (0.5 mL)	*tert*-AmylOH	21	100:0
2	dry nBu$_4$NF (2.0 equiv.) +THF-d$_8$ (1.5 mL)	*tert*-AmylOH	24	89:11
3	THF (1.5 mL)	methanol-d$_4$	15	83:17
4	THF (1.5 mL)	2-propanol-d$_8$	24	67:33
5	THF (1.5 mL)	*tert*-butanl-d$_{10}$	29	64:36

Reaction conditions: 4-trifluoromethylbenzonitrile (0.5 mmol), ***BPI*** *(0.5 mol%), dried nBu$_4$NF (1.0 mmol, 2.0 equiv.) (see section 11 for synthesis details), alcohol (2.5 mmol, 5.0 equiv.), solvent (0.5 mL), r.t (23 °C), 12 h, 405 nm LED. The ratio of H/D was determined by ^{1}H-NMR. The conversion was determined by GC using mesitylene as the internal standard. [a] 16 h reaction time.*

Table S2.19. Deuterium-labeling experiments by using 4-methylbenzotrifluoride as substrate.

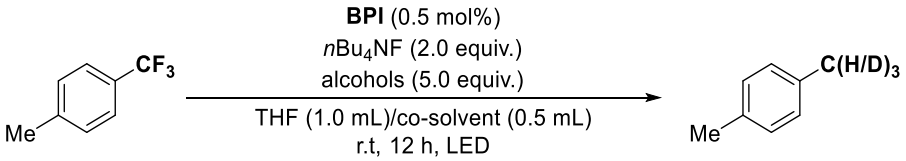

entry	Solvent	alcohols	conv. (%)	H/D ratio
1	THF (1.0 ml)/THF-d_8 (0.5 mL)[a]	-	<5	100:0
2	THF (1.0 mL)/THF-d_8 (0.5 mL)	*tert*-AmylOH	23	100:0
3	THF (1.5 mL)	methanol-d_4	9	85:15
4	THF (1.5 mL)	2-propanol-d_8	17	64:36
5	THF (1.5 mL)	*tert*-butanl-d_{10}	18	63:37

*Reaction conditions: 4-methylbenzotrifluoride (0.5 mmol), **BPI** (0.5 mol%), nBu_4NF (1.0 mmol, 2.0 equiv.), alcohol (2.5 mmol, 5.0 equiv.), THF (1.0 mL)/co-solvent (0.5 mL), r.t (23 °C), 12 h, 405 nm LED. The ratio of H/D was determined by ^{1}H-NMR. The conversion was determined by GC using mesitylene as the internal standard. [a] 16 h reaction time.*

***Table S2.20**. Deuterium-labeling experiments by using benzotrifluoride as substrate.*

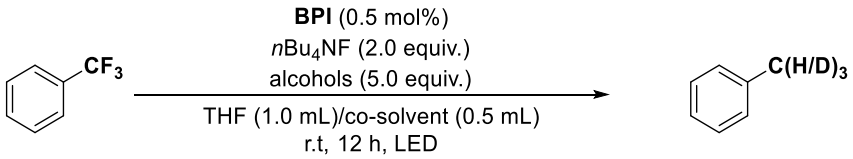

entry	solvent	alcohols	conv./%	H/D ratio
1	THF (1.0 ml)/THF-d_8 (0.5 mL)[a]	-	5	100:0
2	THF (1.0 mL)/THF-d_8 (0.5 mL)	*tert*-AmylOH	29	100:0
3	THF (1.5 mL)	methanol-d_4	18	79:21
4	THF (1.5 mL)	2-propanol-d_8	27	61:39
5	THF (1.5 mL)	*tert*-butanl-d_{10}	31	55:45

*Reaction conditions: benzotrifluoride (0.5 mmol), **BPI** (0.5 mol%), nBu4NF (1.0 mmol, 2.0 equiv.), alcohol (2.5 mmol, 5.0 equiv.), THF (1.0 mL)/co-solvent (0.5 mL), r.t (23 °C), 12 h, 405 nm LED. The ratio of H/D was determined by ^{1}H-NMR. The conversion was determined by GC using mesitylene as the internal standard. [a] 16 h reaction time.*

Table S2.21. Deuterium-labeling experiments by using 3-phenylpropyl fluoride as substrate.

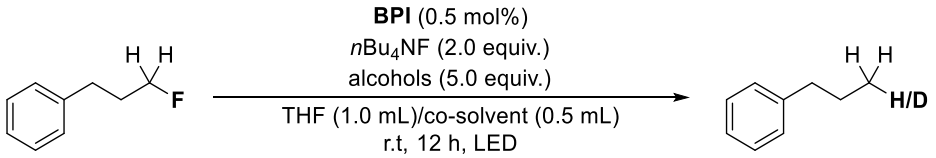

entry	solvent	alcohols	conv./%	H/D ratio
1	THF (1.0 ml)/THF-d_8 (0.5 mL)[a]	-	11	100:0
2	THF (1.0 mL)/THF-d_8 (0.5 mL)	*tert*-AmylOH	30	100:0
3	THF (1.5 mL)	methanol-d_4	20	87:13
4	THF (1.5 mL)	2-propanol-d_8	26	74:26
5	THF (1.5 mL)	*tert*-butanl-d_{10}	33	71:29

*Reaction conditions: 3-phenylpropyl fluoride (0.5 mmol), **BPI** (0.5 mol%), nBu4NF (1.0 mmol, 2.0 equiv.), alcohol (2.5 mmol, 5.0 equiv.), THF (1.0 mL)/co-solvent (0.5 mL), r.t (23 °C), 12 h, 405 nm LED. The ratio of H/D was determined by ^{1}H-NMR. The conversion was determined by GC using mesitylene as the internal standard. [a] 16 h reaction time.*

12.6 Other mechanism studies

12.6.1 BPI with different fluoride sources and ammonium salts

Test sample preparation: In a glovebox, a 5.0 mL glass vial equipped with stir bar was sequentially charged with **BPI** (7.50 mg), corresponding fluoride source (0.05 mmol), and THF (1.00 mL). The mixture was stirred in the glovebox for 2 hours. The mixture was then transferred to a 50 mL glass vial followed by the addition of degassed THF (19 mL) to dilute the mixture to a concentration of 5.0×10^{-4} M relative to **BPI**. Then, 2.2 mL of mixture was transferred into a 1 cm cuvette inside the glovebox. The cuvette was pumped out of the glove box and a fluorescence spectrum was immediately collected via 405nm excitation.

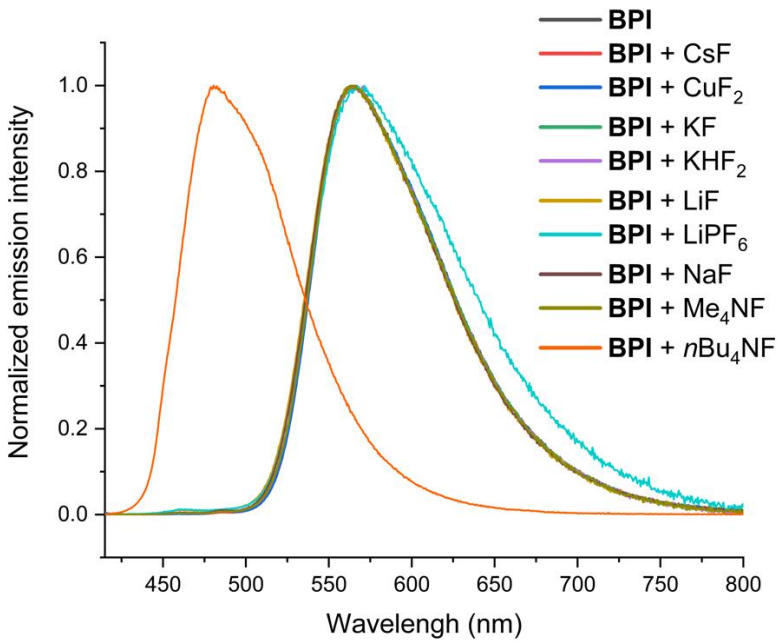

Figure S2.46. Fluorescence spectrum after 405 nm excitation of BPI in the presence of various fluoride sources. Aside from 405nm excitation during the experiment, light was excluded from the sample.

Test sample preparation: In a glovebox, a 5.0 mL glass vial was sequentially charged with **BPI** (7.50 mg), corresponding fluoride source (0.05 mmol), *n*Bu_3N (0.10 mmol), and THF (1.0 mL). The mixture was stirred in the glovebox for 2 hours. The mixture was then transferred to a 50 mL glass vial followed by the addition of degassed THF (19 mL) in order to dilute the mixture to 5.0 x 10^{-4} M. Then, 2.2 mL of mixture was transferred into a 1 cm cuvette inside the glovebox. The cuvette was pumped out of the glove box and a fluorescence spectrum was immediately collected via 405nm excitation.

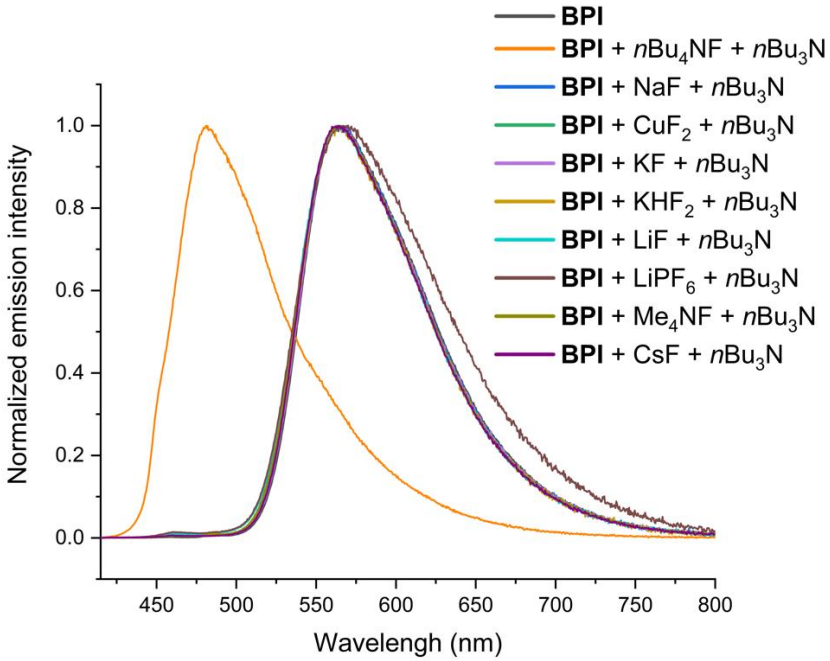

Figure S2.47. Fluorescence spectrum after 405 nm excitation of BPI in the presence of triethyl amine and various fluoride sources. Aside from 405nm excitation during the experiment, light was excluded from the sample.

Test sample preparation: In a glovebox, a 5.0 mL glass vial was sequentially charged with **BPI** (7.5 mg), corresponding ammonium salt (0.1 mmol), and THF (1.0 mL). The mixture was stirred in the glovebox for 2 hours. The mixture was then transferred to a 50 mL glass vial followed by the addition of degassed THF (19 mL) in order to dilute the mixture to 5.0 x 10^{-4} M. Then, 2.2 mL of mixture was transferred into a 1 cm cuvette inside the glovebox. The cuvette was pumped out of the glove box and a fluorescence spectrum was immediately collected via 405nm excitation.

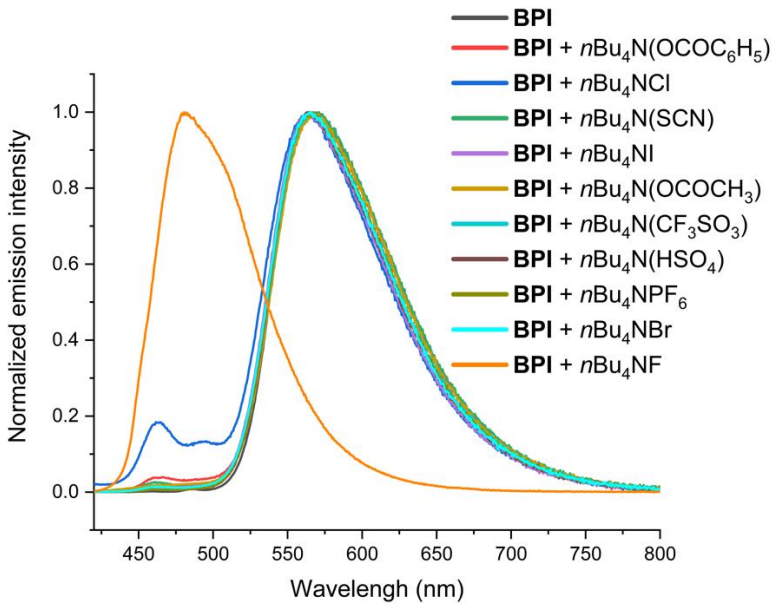

Figure S2.48. Fluorescence spectrum after 405 nm excitation of BPI in the presence of various ammonium salts. Aside from 405nm excitation during the experiment, light was excluded from the sample.

12.6.2 Evidence of presence *n*Bu$_3$N

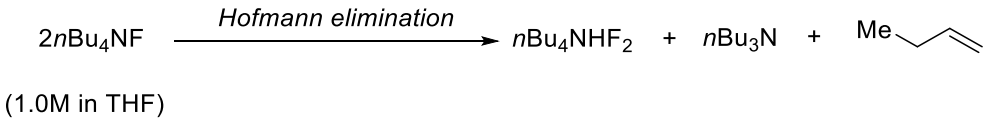

The dried tetrabutylammonium fluoride (*n*Bu$_4$NF, 1.0M in THF) is reported to decompose by Hofmann elimination at room temperature.[61,75] The salt isolated after dehydration is contaminated with copious amounts of *n*Bu$_4$NHF$_2$, tributylamine (*n*Bu$_3$N), and but-1-ene. Moreover, we found that the elimination process was not further promoted through 405nm irradiation.

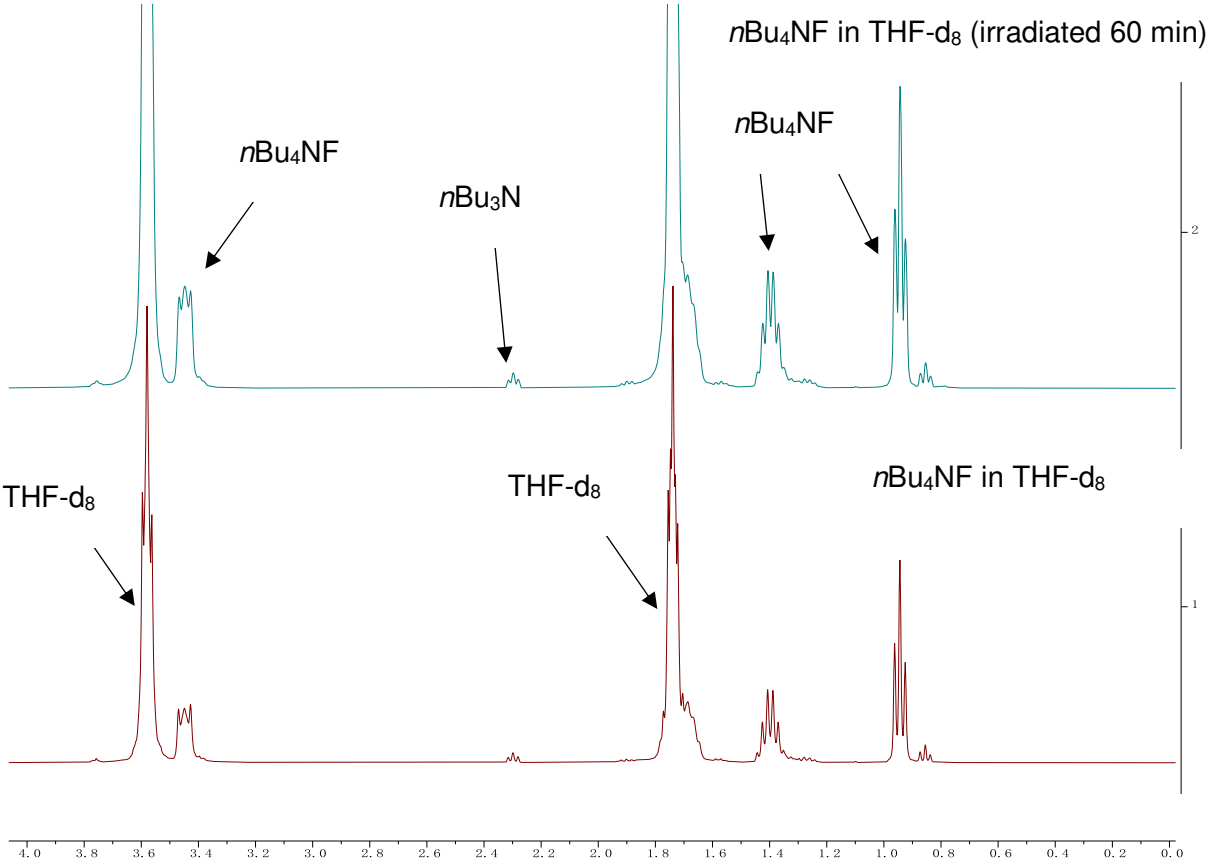

Figure S2.49. ^{1}H-NMR of nBu$_4$NF after dehydration before and after irradiation (60 min) with 405nm light.

12.6.3 Approximation of the lowest singlet excited state energy of BPI, BPI with *n*Bu$_4$NF, and BPI with Me$_4$NOH

The energy associated with the vibrationally cooled singlet excited state ($E_{0,0}$) was estimated by the point of intersection between the absorption spectrum (normalized to the peak of the lowest energy absorption band) and emission (normalized to the peak of the highest energy emission band). This value in units of wavelength was then converted to units of electron volts through the shown equation.

BPI:

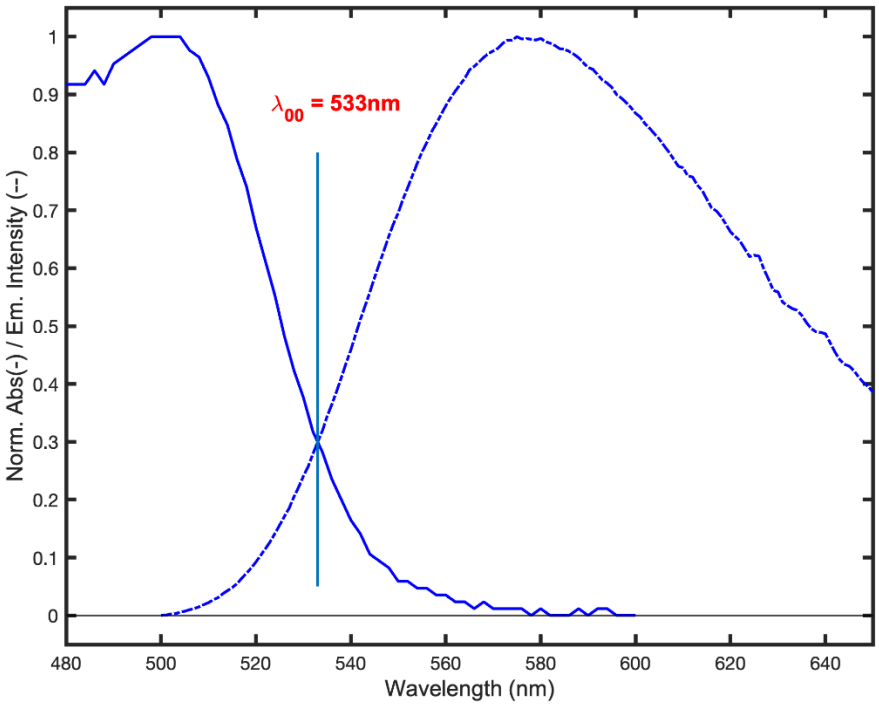

Figure S2.50. The zero-zero vibrational state excitation energy $E_{0,0}$ of BPI.

BPI with *n*Bu$_4$NF**:**

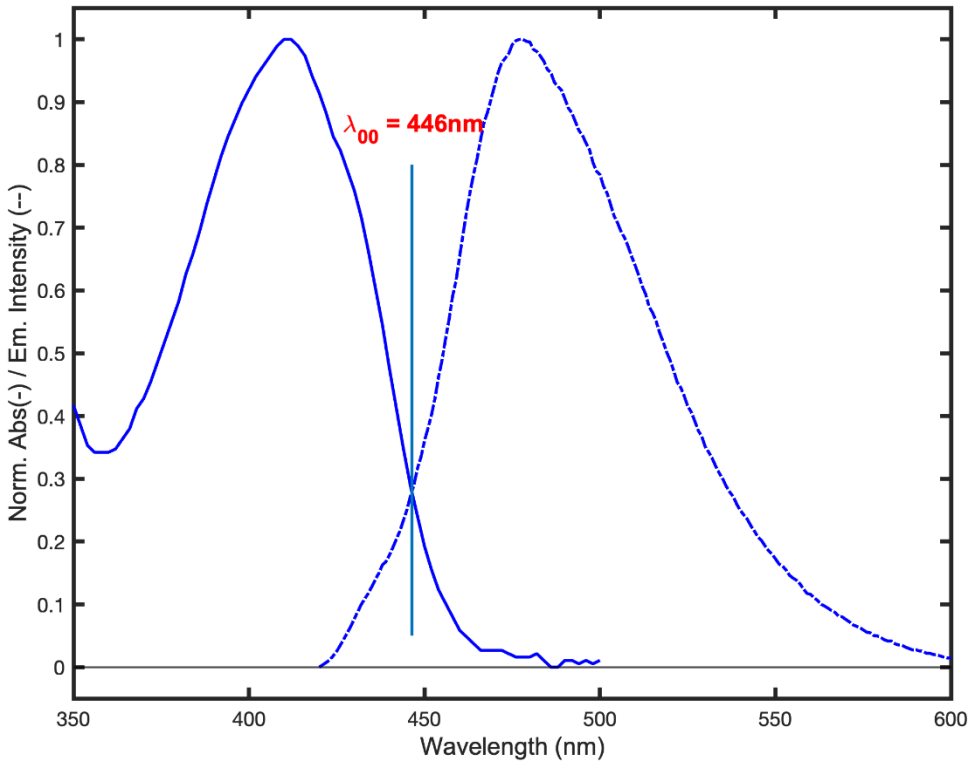

Figure S2.51. The zero-zero vibrational state excitation energy $E_{0,0}$ of BPI with nBu_4NF.

BPI with Me_4NOH

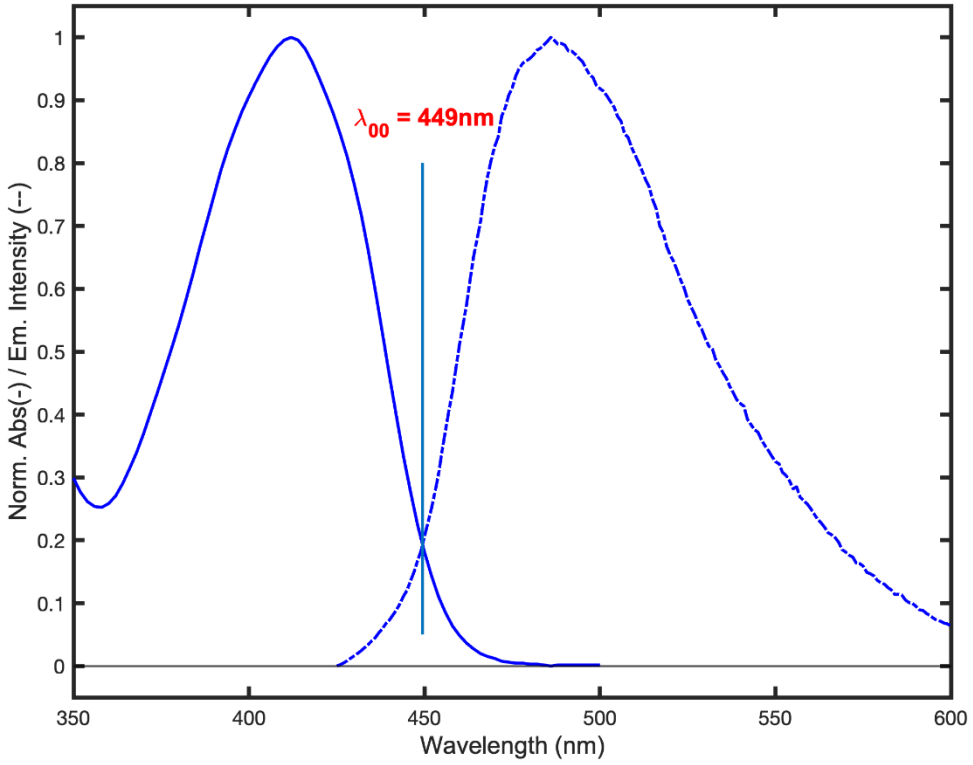

Figure S2.52. The zero-zero vibrational state excitation energy $E_{0,0}$ of BPI with Me4NOH.

12.6.4 Control experiments of *n*Bu$_3$N in the reaction system

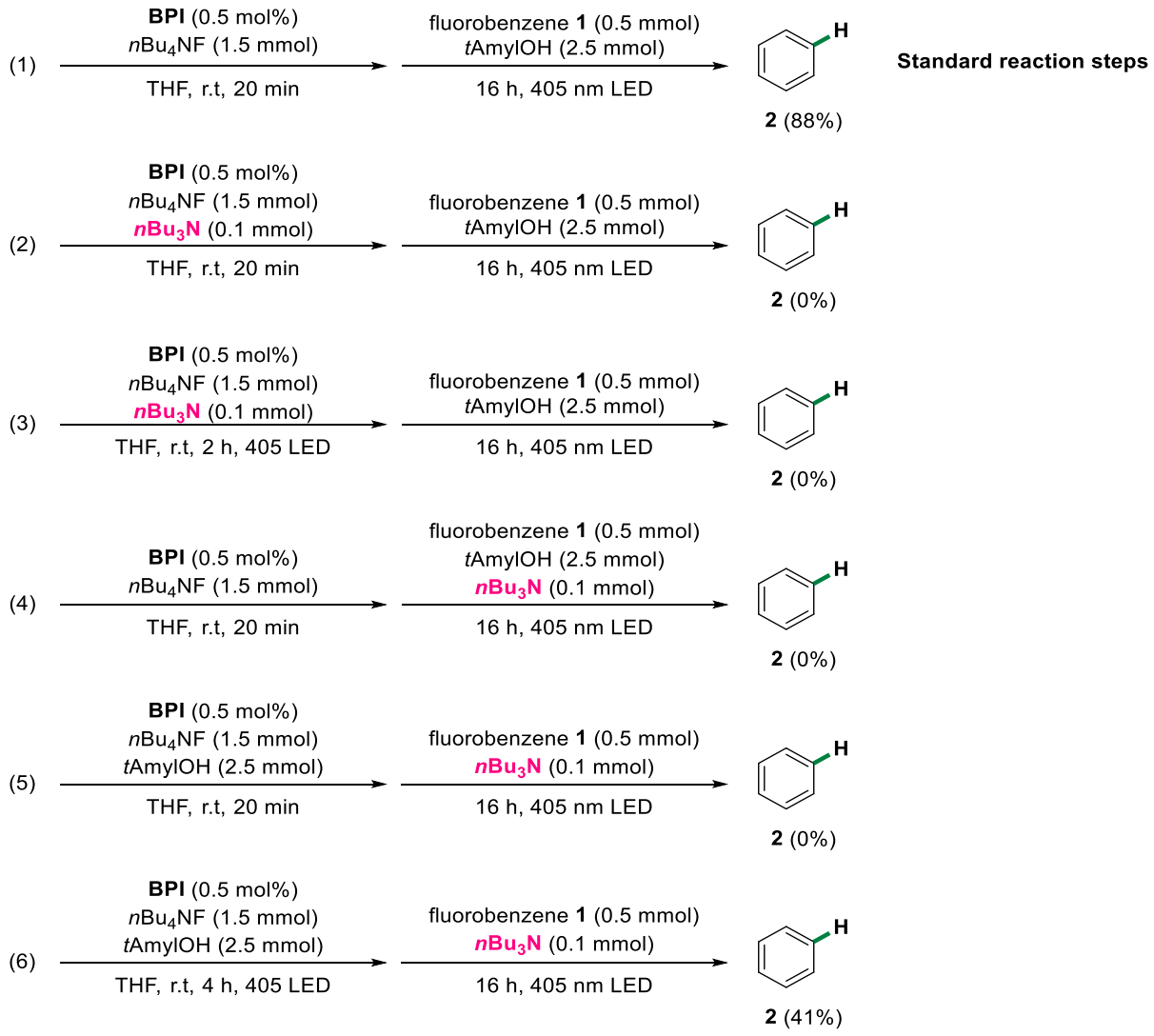

Figure S2.53. Control experiment of nBu$_3$N in the reaction system.

12.6.5 ^{1}H- and ^{13}C-NMR study when *n*Bu$_3$N added to the reaction system.

Step 1: In glovebox, a 4 mL glass vial containing a stirring bar was sequentially charged with **BPI** (7.7 mg), *n*Bu$_4$NF (0.1 mL, 1.0 M in THF) and THF-d$_8$ (0.3 mL). Then, transferred to a dry NMR tube. The ^{1}H-NMR spectrum was recorded.

Step 2: The mixture (from step.1) was irradiated with 405 nm LED for 5 min. The ^{1}H-NMR spectrum was recorded.

Step 3: The mixture (from step. 2) was irradiated with 405 nm blue LED for 45 min. The ^{1}H-NMR spectrum was recorded.

Step 4: The mixture (from step. 3) was irradiated with 405 nm blue LED for 180 min. The ^{1}H-NMR spectrum was recorded.

Step 5: The *n*Bu$_3$N (0.05 mL) was added to the mixture (from step 4). The ^{1}H-NMR spectrum was recorded.

Step 6: The mixture (from step.5) was irradiated with 405 nm blue LED for 45 min. The ^{1}H-NMR spectrum was recorded.

Note: The number of scans of all ^{1}H-NMR is 128.

Step.6: mixture from Step.5 (irradiated for 45 min)

Step.5: mixture from Step.4 (*n*Bu$_3$N was added)

Step.4: BPI + *n*Bu$_4$NF (irradiated for 180 min)

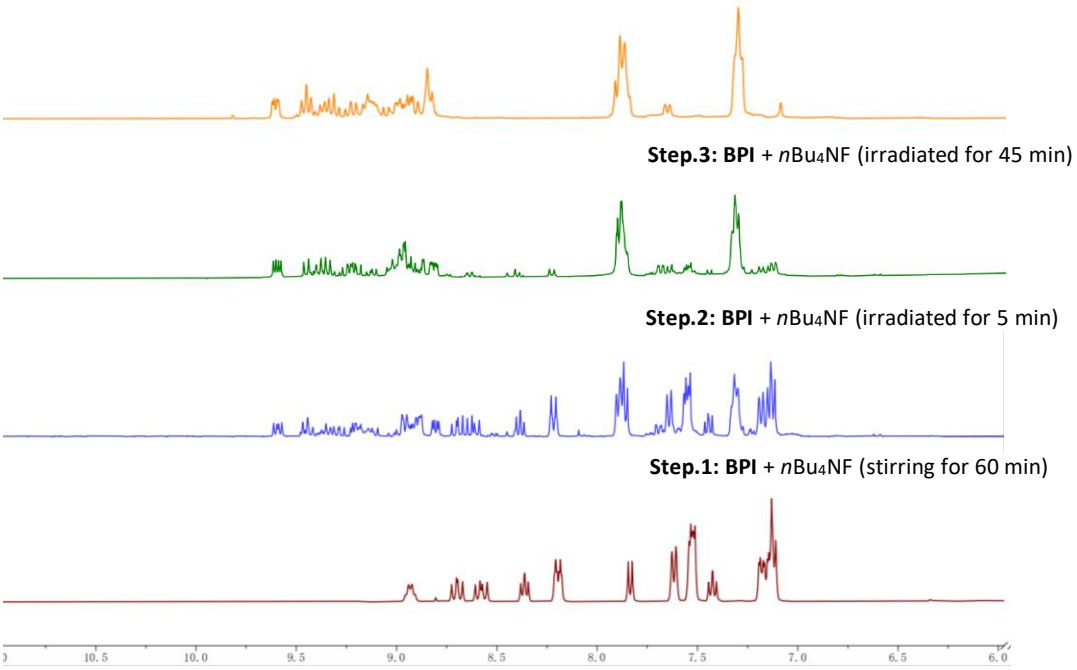

Figure S2.54. ^{1}H-NMR studies support that nBu_3N results in BPI-RO decomposition.

Step 1: In glovebox, a 4 mL glass vial containing a stirring bar was sequentially charged with **BPI** (7.7 mg), *n*Bu$_4$NF (0.1 mL, 1.0 M in THF) and THF-d$_8$ (0.3 mL). After the mixture stirred for 20 min, transferred to a dry NMR tube. The ^{13}C-NMR spectrum was recorded.

Step 2: In glovebox, a 4 mL glass vial containing a stirring bar was sequentially charged with **BPI** (7.7 mg), *n*Bu$_4$NF (0.1 mL, 1.0 M in THF) and THF-d$_8$ (0.3 mL). After the mixture stirred for 20 min, *n*Bu$_3$N (0.05 mL) was added and kept stirring for 10 min. Then, transferred to a dry NMR tube. The ^{13}C-NMR spectrum was recorded.

Step 3: The mixture (from step. 1) was irradiated with 405 nm blue LED for 60 min. The ^{13}C-NMR spectrum was recorded.

Step 4: The solution (from step. 2) was irradiated with 405 nm blue LED for 45 min. The ^{13}C-NMR spectrum was recorded.

Note: The number of scans of all ^{13}C-NMR is 3000.

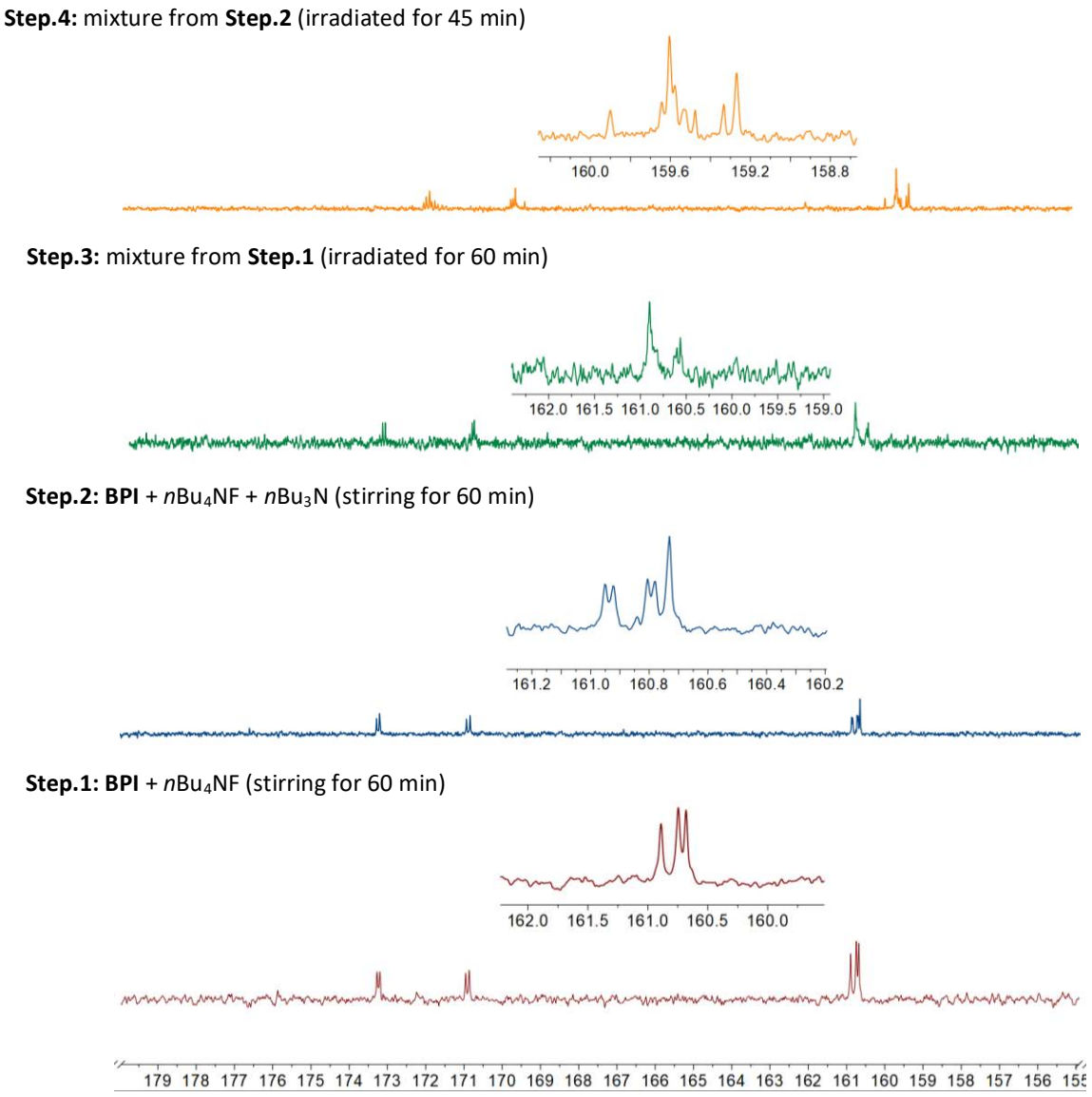

Figure S2.55. ^{13}C-NMR studies support that nBu$_3$N reacts with BPI-RO.

12.6.6 BPI-RO formation in the presence of alcohols

Sample preparation: A stock solution was prepared by dissolving 1.0 mg of **BPI** in 1.0 mL of *n*Bu$_4$NF (1.0M in THF) and corresponding alcohols (1.0 mL) which was then kept in dark inside

a glovebox for corresponding time. The fluorescence spectrum was collected at the same wavelength (405 nm).

The experimental results show that the addition of alcohol in advance will make the formation of **BPI-RO** very slow.

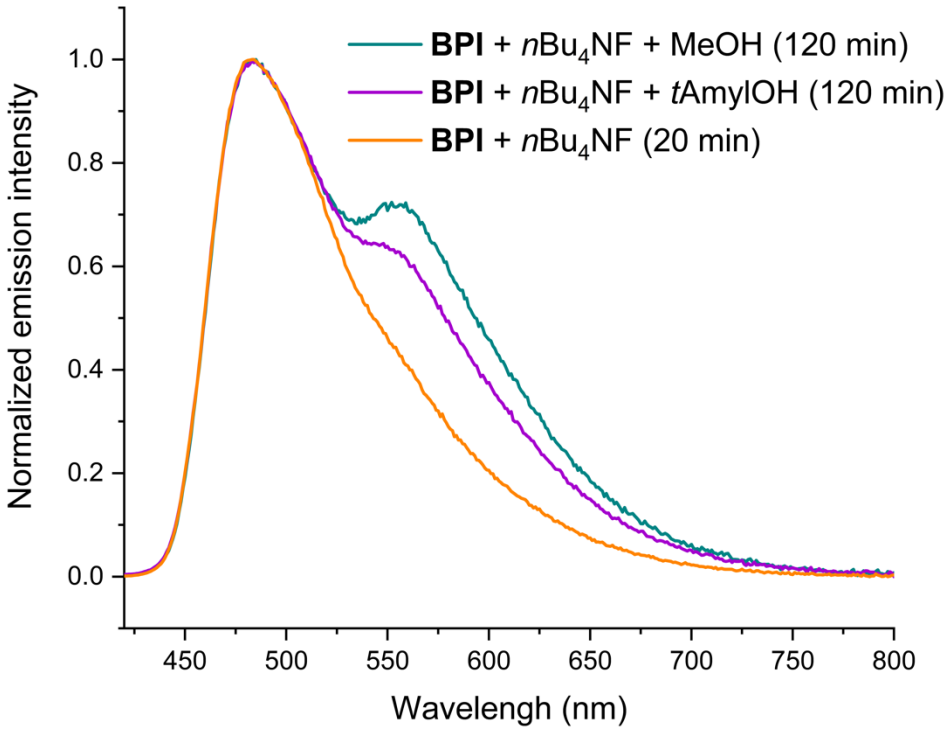

Figure S2.56. The formation of BPI-RO in the presence of alcohol.

Sample preparation: A stock solution was prepared by dissolving 1.0 mg of **BPI** in 1.0 mL of *n*Bu_4NF (1.0M in THF) which was then kept in dark inside a glovebox for 20 min. Then, alcohol (1.0 mL) was added into the reaction mixture. The fluorescence spectrum was collected at the same wavelength (405 nm).

The experimental results show that when **BPI-RO** is fully formed, the addition of alcohol will not affect its structure.

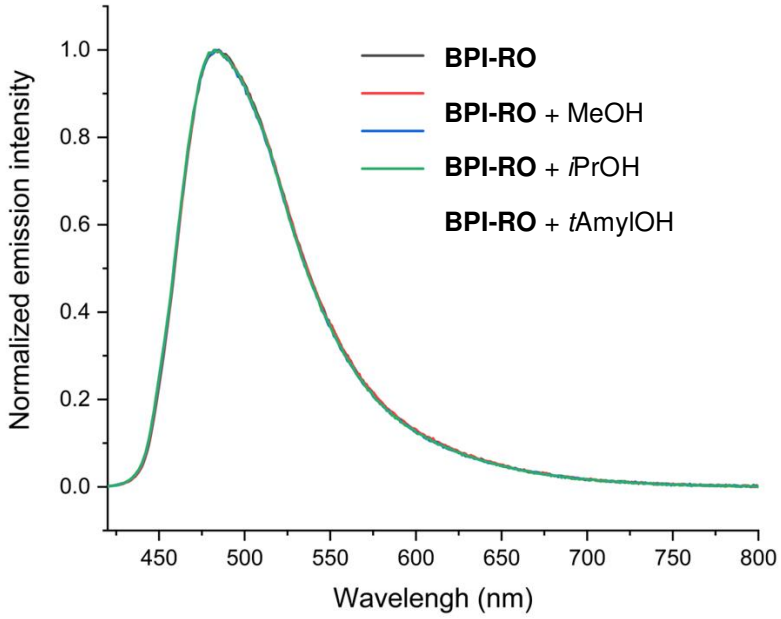

Figure S2.57. The BPI-RO solution with different alcohols.

Sample preparation: A stock solution was prepared by dissolving 1.0 mg of **BPI** in 1.0 mL of corresponding alcohols (1.0 mL) which was then kept in dark inside a glovebox for 1 hour. The fluorescence spectrum was collected at the same wavelength (405 nm).

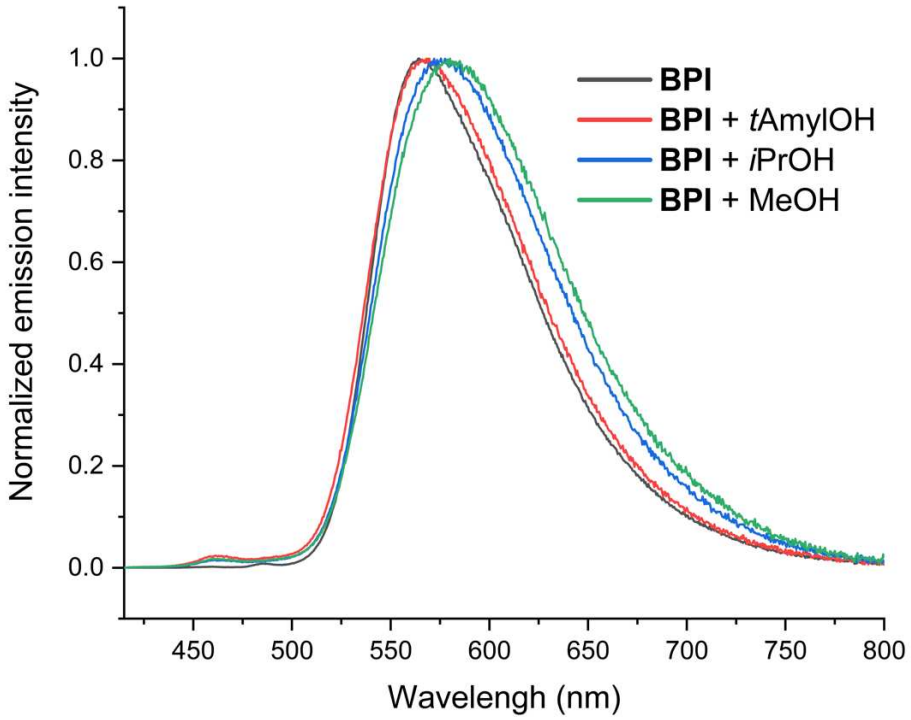

Figure S2.58. BPI-RO reacts with different alcohols.

13. Computational investigations

The meta-augmented hybrid functional M06-2X[1] in conjunction with Grimme's D3 dispersion correction[2] was used for the investigation of the hydrolysis mechanism. The double-z def2-SVP basis set was used for geometry optimization for C and H elements, while the triple-z including additional diffuse functions def2-TZVPD was used for all the electronegative elements N, O, and F.[3][4] The inclusion of a high-level basis set with dispersion correction was informed based on previous studies showing their necessity when studying reactions involving fluoride atoms. All calculations were performed in the presence of the continuous implicit solvation model SMD for tetrahydrofuran.[5]

Calculation of excited state reduction/oxidation potentials of the proposed catalytic species was performed using time-dependent density functional theory (TD-DFT) using the range-separated hybrid functional CAM-B3LYP,[6] in conjunction with the D3(BJ) dispersion correction.[7] The double-z def2-SVP basis set was used for geometry optimization for C and H elements, while the triple-z including additional diffuse functions def2-TZVPD was used for all the electronegative elements N, O, and F. Similarly, solvation effects were accounted for using the SMD solvation model for tetrahydrofuran.

All calculations were performed using Gaussian 16 version C01.[8] Vibrational frequency calculations were performed to verify that stationary points were either minima or first-order saddle points on the potential energy surface (PES) and to calculate thermal corrections to Gibbs free energies (G). The computed thermochemistry data were corrected following Grimme's quasi-harmonic (QHA) model for entropy with a frequency cut-off value of 100.0 cm^{-1} using the GoodVibes program at 273.15 K.[9][10] Also, we applied (i) 1 M standard concentration corrections

to all individual calculations to account for reactions in solution (change in standard concentration from 1 atm to 1 M).[11] Molecular graphics were generated using PyMol.[12]

13.1 Calculation of redox potentials

Previous work has shown that formation of the formation of the intermediate **BPI-RO-H**$^{-}$ of model systems of **BPI** catalysts proceeds preferentially with the formation of a new C–H bond adjacent to the carbonyl groups.[13] For the hydrolysis products, formal additional of a hydride can occur at the a-position next to the carboxylate group (**B**) or next to the amide group (**C**) (Figure S59). The thermochemistry computed thermochemistry at the CAM-B3LYP-D3(BJ)/def2-SVP[C;H]def2-TZVPD[N;O;F]-SMD(THF) level of theory suggests that the structure **B** is marginally thermodynamically more stable than **C** by 1.9 kcal/mol. As the thermodynamic diffraction between these two species is small, both species were considered for the calculation of their ground and excited state reduction potentials.

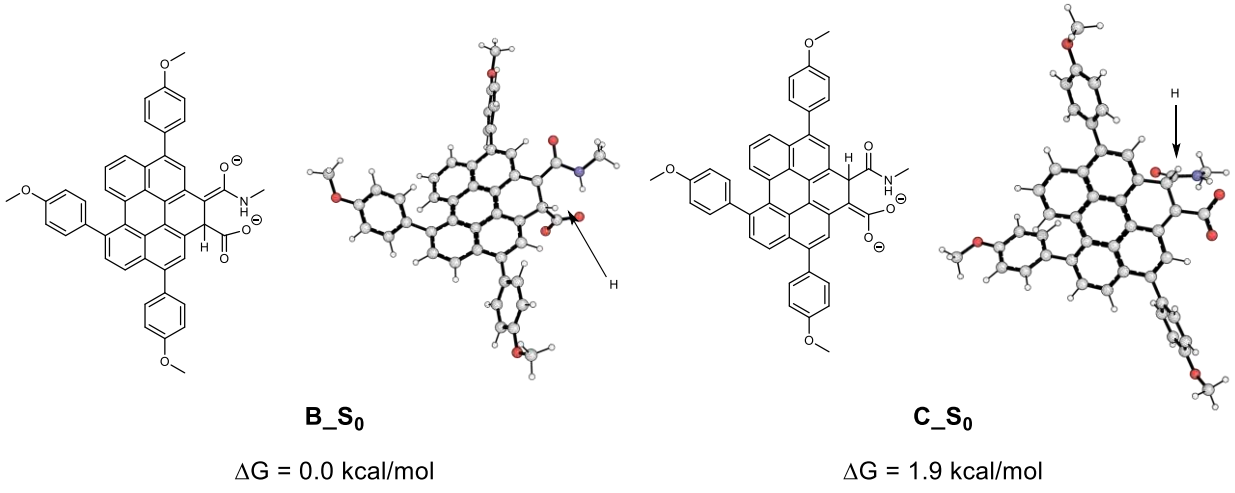

*Figure S2.59. Compute thermodynamics of isomeric form of the hydride adducts **B** and **C** at the CAM-B3LYP-D3(BJ)/def2-SVP[C;H]def2-TZVPD[N;O;F]-SMD(THF) level of theory.*

Calculation of reduction potentials of different speciation of the proposed photocatalytic systems were carried out using the CAM-B3LYP-D3(BJ)/def2-SVP[C;H]def2-TZVPD[N;O;F]-SMD(THF) level of theory (Figure SX). Using equation (eq.1),[14] the absolute reduction potentials computed directly from DFT were referenced against the standard calomel electrode. Previous studies have shown that liquid junction potential E_L is proportional to the dipole moment of the solvent.[15] As no experimental E_L values are available for THF, the potential of ethanol was used instead (E_L = 0.03 V), as it possesses a similar dipole moment to that of THF. For the calculation of the excited state potentials, the ΔG value between the S_1 optimized structures.

$$E_{1/2} = -\frac{\Delta G}{F} - E_{SCE}^{abs} + E_L \qquad [eq.1]$$

$E_{1/2}^{SCE}$: computed redox potential referenced vs SCE in V.

ΔG : computed Gibbs free energy for the reduction process in kcal mol^{-1}.

F : Faraday constant (23.061 kcal mol^{-1} V^{-1})

E_{SCE}^{abs} : absolute redox potential of SCE (4.52 V).

E_L : experimental liquid junction potential (0.03 V).

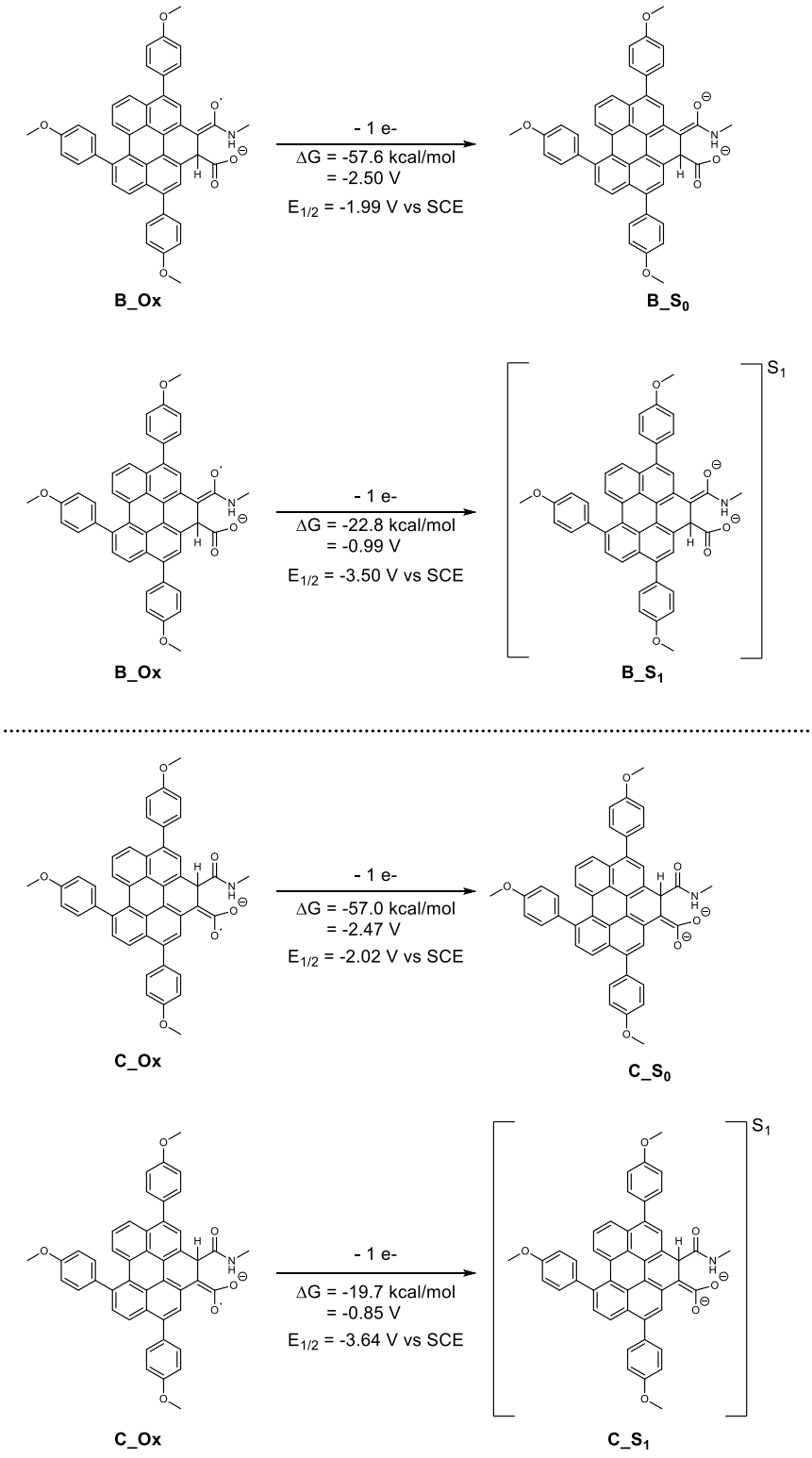

Figure S2.60. Computed reduction potentials for the proposed photocatalytic species catalytic species at the CAM-B3LYP-D3(BJ)/def2-SVP[C;H]def2-TZVPD[N;O;F]-SMD(THF)

Computations were also undertaken to assess the thermodynamic feasibility of various species in solution acting as electron-donor (Figure S61) using the protocol above. Computed standard oxidation potentials in THF suggest that the *t*AmylOH bound fluoride is a more favorable electron-donor compared to either t-amyl alkoxide or amine (in which n-butyl groups were modeled computationally as methyl) species. Hydrogen bonding of either alkoxide or amine to a molecule of alcohol reduces the favorability of these species acting as electron-donor. In the case of fluoride, the formation of higher-order aggregates (e.g., with three molecules of *t*AmylOH) increases the ability to donate an electron compared to when a single molecule of alcohol is bound (-1.11 V vs. -0.76 V).

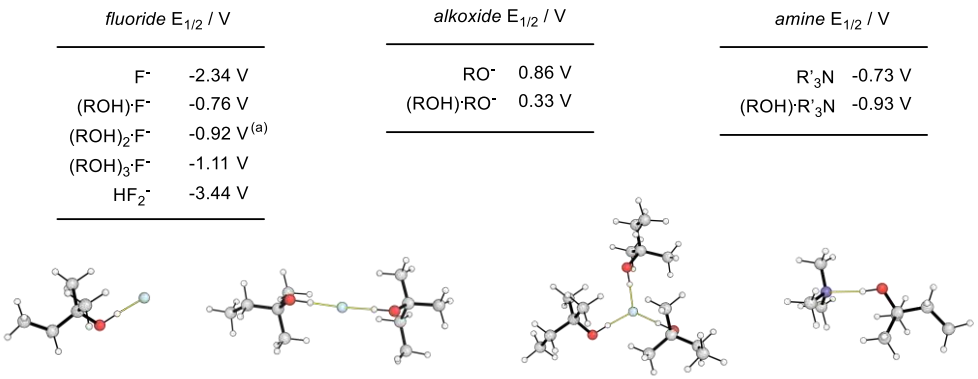

Figure S2.61. Computed oxidation potentials for the proposed photocatalytic species catalytic species at the CAM-B3LYP-D3(BJ)/def2-SVP[C;H]def2-TZVPD[N;O;F]-SMD(THF); (a) Note: "loose" optimization criteria were used for the anion optimization due to convergence difficulty.

13.2 Hydrolysis of BPI to BPI-RO

The hydrolysis of **BPI** was investigated computationally using a model system **C** without the core extended *p*-methoxy phenyl substituents and a truncated N-alkyl chain. The mechanism of

hydrolysis was initially investigated using free fluoride anions in the presence of trace water. Formation of the fluoride tetrahedral intermediate **D** was found to be 14.5 kcal/mol endergonic, via **TS-I** ($\Delta G^{\ddagger}$ = 15.7 kcal/mol). The subsequent collapse of the tetrahedral intermediate was found to require a very high effective activation barrier of 35.7 kcal/mol, to facilitate the formation of a putative acyl fluoride species **E**. Due to the prohibitively high barrier, it was hypothesized that fluoride may alternatively lead to the formation of free hydroxide through the reaction with water, which was computed to be a 16.2 kcal/mol endergonic process. The subsequent addition of hydroxide to imide **C** was found to have a low activation energy barrier of 4.5 kcal/mol (an effective barrier of 19.7 kcal/mol) via **TS-III**. This leads to the formation of tetrahedral intermediate **E**, which could then undergo collapse via **TS-IV** ($\Delta G^{\ddagger}$ = 11.2 kcal/mol) to form intermediate **F** which contains a deprotonated amide group. This can then readily undergo intramolecular proton transfer via **TS-V** ($\Delta G^{\ddagger}$ = 4.0 kcal/mol), to give the ring-opened product **G** in an overall -14.0 kcal/mol exergonic process.

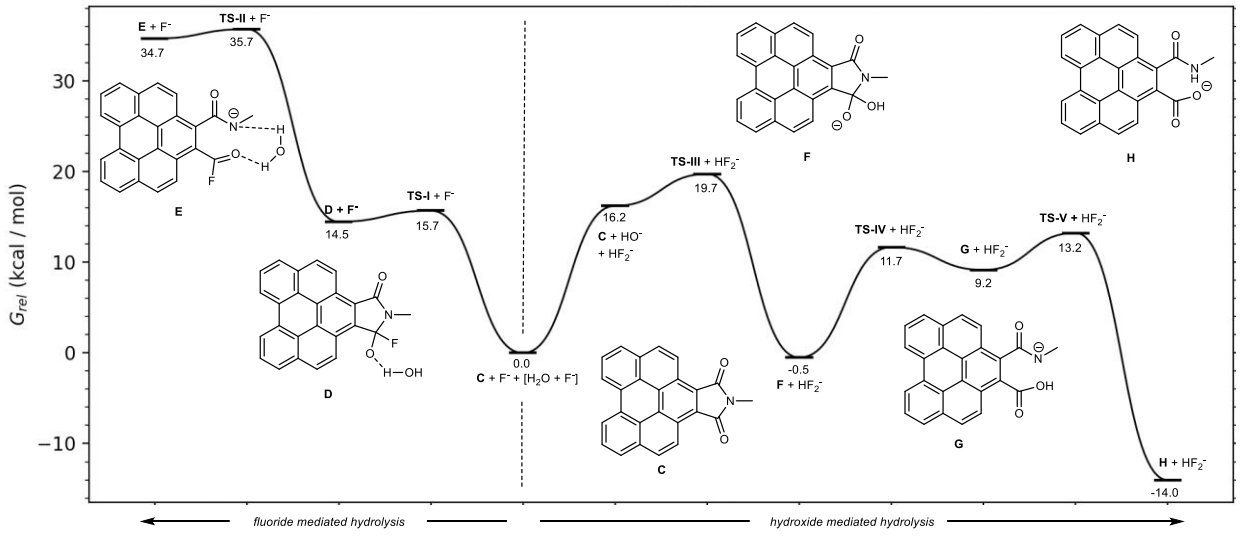

Figure S2.62. Computed hydrolysis mechanisms of model system C at the M06-2X-D3/def2-SVP[C;H]def2-TZVPD[N;O;F]-SMD(THF) level of theory

Table S2.22: *Computed relative thermochemistry for the hydrolysis mechanisms of model system* ***C*** *at the M06-2X-D3/def2-SVP[C;H]def2-TZVPD[N;O;F]-SMD(THF) level of theory in kcal/mol.*

Entry	ΔE	ΔZPE	ΔH	T.ΔS	T.qh-ΔS	Δ*G(298.15)*	*qh-*Δ*G(298.15)*
E + F^-	23.9	0.8	24.7	-9.2	-9.9	34.0	34.7
TS-II + F^-	24.7	0.5	24.8	-10.5	-10.9	35.3	35.7
D + F^-	2.7	1.5	4.0	-10.0	-10.5	14.0	14.5
TS-I + F^-	4.4	1.0	5.2	-9.9	-10.5	15.1	15.7
[F^- + H_2O] + **C** + F^-	0.0	0.0	0.0	0.0	0.0	0.0	0.0
HF_2^- + **C** + HO^-	18.7	-2.4	16.3	0.1	0.1	16.2	16.2
TS-III + HF_2^-	14.1	-1.5	11.8	-8.2	-7.9	20.0	19.7
F + HF_2^-	-8.2	0.2	-9.1	-8.6	-8.6	-0.5	-0.5
TS-IV + HF_2^-	4.4	-0.5	2.6	-9.0	-9.1	11.6	11.7
G + HF_2^-	1.9	0.0	0.9	-8.3	-8.3	9.2	9.2
TS-IV + HF_2^-	7.2	-1.2	5.0	-8.1	-8.2	13.1	13.2
H + HF_2^-	-21.9	0.7	-22.1	-8.0	-8.0	-14.1	-14.0

ΔE = change in energy; ΔZPE = change in zero point energy; ΔH = change in enthalpy; ΔS = change in entropy; qh-ΔS = change in quasi-harmonic corrected entropy; ΔG = change in Gibbs free energy; change in quasi-harmonic corrected Gibbs free Energy

13.3 Thermochemistry

Table S2.23. Computed thermochemistry using the M06-2X-D3 or CAM-B3LYP-D3(BJ) functions, in conjunction with def2-SVP[C;H]def2-TZVPD[N;O;F] and SMD(THF) solvation in Hartree; E = energy; ZPE = zero point energy; H = enthalpy; S = entropy; qh-S = quasi-harmonic corrected entropy; G = Gibbs free energy; qh-G = quasi-harmonic corrected Gibbs free energy; n_{imag} = imaginary frequency.

Structure	*E*	*ZPE*	*H*	*T.S*	*T.qh-S*	*G(298.15)*	*qh-G(298.15)*	n_{imag}
A_S0_CAM-B3LYP	-2277.087429	0.680675	-2276.363000	0.119286	0.109265	-2276.482286	-2276.472265	
A_S1_CAM-B3LYP	-2277.030135	0.678698	-2276.307597	0.118747	0.109132	-2276.426344	-2276.416729	
A_ox_CAM-B3LYP	-2276.994593	0.680893	-2276.269676	0.121584	0.110749	-2276.391259	-2276.380424	
B_S0_CAM-B3LYP	-2277.084344	0.680438	-2276.360223	0.118451	0.108946	-2276.478673	-2276.469169	
B_S1_CAM-B3LYP	-2277.023643	0.678890	-2276.301174	0.117939	0.108527	-2276.419113	-2276.409700	

B_ox_CAM-B3LYP	-2276.992713	0.681010	-2276.267756	0.12 1133	0.110 524	-2276.388888	-2276.378280
C_M06-2X	-1164.784517	0.314316	-1164.450353	0.06 3826	0.06 1715	-1164.514179	-1164.512068
D_M06-2X	-1341.206650	0.339554	-1340.843107	0.07 2533	0.06 9657	-1340.915640	-1340.912764
E_M06-2X	-1341.172894	0.338490	-1340.810044	0.07 3761	0.07 0526	-1340.883805	-1340.880570
F_H2O_anion_M06-2X	-176.426450	0.022908	-176.399130	0.02 4629	0.02 4631	-176.423759	-176.423761
F_M06-2X	-1240.721098	0.327288	-1240.372431	0.06 6539	0.06 4406	-1240.438971	-1240.436838
F_anion_1_tAmylOH_CAM-B3LYP	-372.762513	0.165542	-372.586570	0.04 1289	0.04 0759	-372.627859	-372.627329

F_anion_2_tAmylOH_CAM-B3LYP	-645.526469	0.331732	-645.174915	0.065198	0.061310	-645.240113	-645.236225
F_anion_3_tAmylOH_CAM-B3LYP	-918.292729	0.498392	-917.765160	0.086307	0.079858	-917.851467	-917.845018
F_anion_CAM-B3LYP	-99.998928	0.000000	-99.996568	0.013500	0.013500	-100.010068	-100.010068
F_anion_M06-2X	-99.977601	0.000000	-99.975240	0.013500	0.013500	-99.988741	-99.988741
F_radical_1_tAmylOH_CAM-B3LYP	-372.566091	0.163540	-372.391600	0.044334	0.042691	-372.435934	-372.434291
F_radical_2_tAmylOH_CAM-B3LYP	-645.323854	0.329317	-644.974016	0.068523	0.063530	-645.042539	-645.037546
F_radical_3_tAmylOH_CAM-B3LYP	-918.079367	0.494806	-917.554002	0.096085	0.085330	-917.650087	-917.639332

F_radical_CAM-B3LYP	-99.747355	0.000000	-99.744995	0.014155	0.014155	-99.759150	-99.759150
G_M06-2X	-1240.704967	0.326833	-1240.356492	0.067014	0.064959	-1240.423506	-1240.421451
H2O_M06-2X	-76.437361	0.023638	-76.409941	0.019794	0.019794	-76.429735	-76.429735
HF2_anion_CAM-B3LYP	-200.516503	0.010120	-200.502905	0.021079	0.021079	-200.523984	-200.523984
HF2_anion_M06-2X	-200.480611	0.010326	-200.466818	0.021714	0.021714	-200.488531	-200.488531
HF2_radical_CAM-B3LYP	-200.221943	0.010181	-200.206683	0.026218	0.025935	-200.232900	-200.232618
HO_anion_M06-2X	-75.893575	0.008696	-75.881574	0.016534	0.016534	-75.898108	-75.898108

H_M06-2X	-1240.742851	0.328074	-1240.393053	0.067503	0.065330	-1240.460556	-1240.458383	
Me3N_CAM-B3LYP	-174.311526	0.120480	-174.184720	0.030540	0.030550	-174.215260	-174.215270	
Me3N_ox_CAM-B3LYP	-174.116002	0.119181	-173.989547	0.034917	0.033854	-174.024464	-174.023401	
Me3N_tAmylOH_CAM-B3LYP	-447.074315	0.286817	-446.771724	0.054929	0.052285	-446.826653	-446.824009	
Me3N_tAmylOH_ox_CAM-B3LYP	-446.872822	0.285858	-446.570450	0.056619	0.054426	-446.627069	-446.624875	
TS_III_M06-2X	-1240.685561	0.324557	-1240.339061	0.067206	0.065513	-1240.406268	-1240.404574	-80.16
TS_II_M06-2X	-1341.171654	0.338069	-1340.809941	0.071664	0.068948	-1340.881606	-1340.878889	-109.97

TS_IV_M06-2X	-1240.700870	0.326059	-1240.353815	0.065853	0.063625	-1240.419669	-1240.417440	-133.59
TS_I_M06-2X	-1341.204001	0.338839	-1340.841229	0.072615	0.069586	-1340.913845	-1340.910816	-213.32
TS_V_M06-2X	-1240.696540	0.325017	-1240.349951	0.067291	0.064990	-1240.417242	-1240.414941	-486.34
tAmylO_anion_CAM-B3LYP	-272.210353	0.150335	-272.051480	0.036418	0.036080	-272.087898	-272.087560	
tAmylO_dimer_anion_CAM-B3LYP	-544.985813	0.314640	-544.653278	0.060639	0.056934	-544.713917	-544.710212	
tAmylO_dimer_radical_CAM-B3LYP	-544.834023	0.317343	-544.498187	0.063872	0.059139	-544.562058	-544.557325	
tAmylO_radical_CAM-B3LYP	-272.077073	0.151328	-271.917003	0.037748	0.037169	-271.954751	-271.954172	

13.4 XYZ Coordinates

86

A_S0_CAM-B3LYP

Eopt -2277.087429

C	3.617661	1.798070	0.137526
C	2.962238	0.541524	0.176383
C	1.535754	0.524816	0.255591
C	0.803230	1.754071	0.385598
C	1.483541	2.970551	0.215285
C	2.894224	2.960800	0.122526
C	0.830394	-0.722002	0.150465
C	-0.638374	1.665758	0.691057
C	-1.332028	0.432800	0.450675
C	-0.616913	-0.748140	0.144945
C	-2.762930	0.421931	0.542721
C	-3.438138	1.570686	0.985441
C	-2.738670	2.698160	1.377990
C	-1.349448	2.736080	1.227967
H	4.703084	1.837553	0.052681
H	3.412738	3.915090	0.004506
H	-4.526893	1.565017	1.039314
H	-3.266037	3.565595	1.780757
C	3.679248	-0.691269	0.061326
C	2.955571	-1.861440	-0.040250
C	1.550624	-1.905114	0.002966
H	3.497647	-2.806292	-0.131807
C	0.878889	-3.257191	-0.059722
C	-0.591368	-3.159876	-0.437840
C	-1.291156	-1.962152	-0.190269
C	-3.445287	-0.791048	0.155729
C	-2.732131	-1.886025	-0.237490

H	-3.259193	-2.790537	-0.530415	C	-7.033711	-1.360729	-0.961669
H	-0.821507	3.636709	1.530152	H	-5.102728	-1.361641	-1.903813
C	-1.213850	-4.345837	-0.997778	C	-7.043328	-0.853550	1.396410
O	-2.372380	-4.419741	-1.469143	H	-5.137788	-0.482475	2.299784
C	1.097582	-4.043962	1.281138	C	-7.739372	-1.175732	0.226480
O	0.943626	-3.432213	2.354652	H	-7.546002	-1.616935	-1.887947
N	-0.442536	-5.491270	-1.011144	H	-7.602703	-0.727165	2.325458
C	-1.038442	-6.732539	-1.427439	C	5.164501	-0.743610	0.027311
H	-1.911518	-7.017964	-0.814129	C	5.834223	-1.414494	-0.998810
H	-1.379033	-6.685943	-2.471897	C	5.949954	-0.174005	1.043482
H	-0.284341	-7.528710	-1.347511	C	7.225202	-1.521761	-1.029321
O	1.396639	-5.267580	1.152973	H	5.254116	-1.862932	-1.808140
H	0.323245	-5.563622	-0.339664	C	7.332456	-0.268498	1.028626
C	-4.931806	-0.887313	0.186437	H	5.461206	0.336841	1.875664
C	-5.645365	-1.215622	-0.967398	C	7.981856	-0.942223	-0.011808
C	-5.664618	-0.712651	1.371526	H	7.700471	-2.051777	-1.853557

H	7.932451	0.169821	1.828473
O	9.340606	-0.979517	0.050247
O	-9.090584	-1.290405	0.342674
C	-9.833300	-1.638717	-0.808997
H	-9.728306	-0.882603	-1.604136
H	-9.531802	-2.622427	-1.204059
H	-10.884971	-1.686097	-0.498322
C	10.038412	-1.666263	-0.970277
H	9.757689	-2.731360	-1.007775
H	9.862799	-1.211607	-1.958946
H	11.105308	-1.586482	-0.725443
C	0.828209	4.292467	0.000983
C	-0.071274	4.478248	-1.052283
C	1.142763	5.407368	0.788780
C	-0.663101	5.713055	-1.303940
H	-0.328167	3.629715	-1.689738
C	0.561529	6.646372	0.553236
H	1.842271	5.296003	1.620567
C	-0.350707	6.806470	-0.492668
H	-1.362065	5.808107	-2.133572
H	0.801197	7.506997	1.180781
O	-0.878393	8.051209	-0.648785
C	-1.816727	8.255332	-1.687327
H	-2.708101	7.619980	-1.559634
H	-2.118322	9.309113	-1.630846
H	-1.374467	8.061772	-2.678227
H	1.405264	-3.853637	-0.821386

86

A_S1_CAM-B3LYP

Eopt -2277.030135

C	3.636934	1.770878	0.158584
C	2.974772	0.517911	0.203669

C	1.547017	0.511451	0.290200	C	3.681363	-0.721305	0.091187
C	0.820626	1.745647	0.414302	C	2.948031	-1.888445	0.005986
C	1.509615	2.957181	0.235859	C	1.546166	-1.922209	0.059812
C	2.919423	2.937570	0.140315	H	3.482515	-2.839133	-0.078160
C	0.834414	-0.730395	0.195678	C	0.852440	-3.261919	0.030743
C	-0.622879	1.667097	0.712597	C	-0.585322	-3.139330	-0.461258
C	-1.321256	0.437587	0.473907	C	-1.286271	-1.947391	-0.205061
C	-0.609126	-0.746316	0.172989	C	-3.438774	-0.781417	0.154702
C	-2.753146	0.431323	0.548597	C	-2.728256	-1.872146	-0.251396
C	-3.427226	1.584092	0.976598	H	-3.258952	-2.771792	-0.553435
C	-2.725901	2.713542	1.367792	H	-0.809230	3.648925	1.529626
C	-1.336874	2.746505	1.232053	C	-1.199974	-4.284045	-1.114830
H	4.722038	1.805228	0.069671	O	-2.269342	-4.257993	-1.765262
H	3.443408	3.887880	0.013522	C	0.934849	-4.003376	1.405262
H	-4.516601	1.584163	1.019255	O	0.969576	-3.330019	2.451715
H	-3.254914	3.585867	1.757720	N	-0.503441	-5.464685	-1.034401

C	-1.066426	-6.665546	-1.590536
H	-2.038719	-6.934470	-1.141189
H	-1.228080	-6.567514	-2.674341
H	-0.366945	-7.496898	-1.422401
O	0.936366	-5.269474	1.330664
H	0.120717	-5.564344	-0.225644
C	-4.925334	-0.873277	0.188048
C	-5.644726	-1.201576	-0.961637
C	-5.651643	-0.692280	1.376472
C	-7.033730	-1.341060	-0.949461
H	-5.106659	-1.349224	-1.900524
C	-7.030714	-0.827056	1.407528
H	-5.119323	-0.457279	2.300356
C	-7.732989	-1.150583	0.241371
H	-7.551323	-1.596003	-1.873133
H	-7.586346	-0.693714	2.337904
C	5.165523	-0.788318	0.043405
C	5.817937	-1.469916	-0.986461
C	5.967811	-0.222861	1.049317
C	7.207772	-1.588790	-1.032504
H	5.225011	-1.917817	-1.786922
C	7.349213	-0.327871	1.018668
H	5.492937	0.296780	1.884046
C	7.980859	-1.011672	-0.026078
H	7.668723	-2.127549	-1.859185
H	7.962187	0.108904	1.809603
O	9.339933	-1.062878	0.023020
O	-9.084150	-1.259194	0.363736
C	-9.832969	-1.611321	-0.782742
H	-9.730070	-0.859511	-1.582243
H	-9.535403	-2.597650	-1.174364
H	-10.883297	-1.654700	-0.467068

C 10.020738 -1.752624 -1.006686

H 9.735336 -2.816668 -1.040145

H 9.833219 -1.297590 -1.993001

H 11.091271 -1.677331 -0.776635

C 0.862093 4.280093 0.007684

C -0.033002 4.461652 -1.050032

C 1.183502 5.401281 0.783940

C -0.613178 5.698500 -1.317870

H -0.292939 3.608936 -1.680604

C 0.613711 6.642558 0.532382

H 1.881838 5.294054 1.617251

C -0.293542 6.798504 -0.518523

H -1.307582 5.790513 -2.151732

H 0.860485 7.508769 1.149403

O -0.808395 8.046296 -0.692617

C -1.737389 8.246741 -1.740194

H -2.635800 7.621605 -1.611074

H -2.028967 9.304064 -1.699063

H -1.290207 8.036621 -2.725490

H 1.408893 -3.906647 -0.667495

86

A_ox_CAM-B3LYP

Eopt -2276.994593

C 3.636934 1.770878 0.158584

C 2.974772 0.517911 0.203669

C 1.547017 0.511451 0.290200

C 0.820626 1.745647 0.414302

C 1.509615 2.957181 0.235859

C 2.919423 2.937570 0.140315

C 0.834414 -0.730395 0.195678

C -0.622879 1.667097 0.712597

C -1.321256 0.437587 0.473907

C	-0.609126	-0.746316	0.172989
C	-2.753146	0.431323	0.548597
C	-3.427226	1.584092	0.976598
C	-2.725901	2.713542	1.367792
C	-1.336874	2.746505	1.232053
H	4.722038	1.805228	0.069671
H	3.443408	3.887880	0.013522
H	-4.516601	1.584163	1.019255
H	-3.254914	3.585867	1.757720
C	3.681363	-0.721305	0.091187
C	2.948031	-1.888445	0.005986
C	1.546166	-1.922209	0.059812
H	3.482515	-2.839133	-0.078160
C	0.852440	-3.261919	0.030743
C	-0.585322	-3.139330	-0.461258
C	-1.286271	-1.947391	-0.205061
C	-3.438774	-0.781417	0.154702
C	-2.728256	-1.872146	-0.251396
H	-3.258952	-2.771792	-0.553435
H	-0.809230	3.648925	1.529626
C	-1.199974	-4.284045	-1.114830
O	-2.269342	-4.257993	-1.765262
C	0.934849	-4.003376	1.405262
O	0.969576	-3.330019	2.451715
N	-0.503441	-5.464685	-1.034401
C	-1.066426	-6.665546	-1.590536
H	-2.038719	-6.934470	-1.141189
H	-1.228080	-6.567514	-2.674341
H	-0.366945	-7.496898	-1.422401
O	0.936366	-5.269474	1.330664
H	0.120717	-5.564344	-0.225644
C	-4.925334	-0.873277	0.188048

C	-5.644726	-1.201576	-0.961637	C	7.980859	-1.011672	-0.026078
C	-5.651643	-0.692280	1.376472	H	7.668723	-2.127549	-1.859185
C	-7.033730	-1.341060	-0.949461	H	7.962187	0.108904	1.809603
H	-5.106659	-1.349224	-1.900524	O	9.339933	-1.062878	0.023020
C	-7.030714	-0.827056	1.407528	O	-9.084150	-1.259194	0.363736
H	-5.119323	-0.457279	2.300356	C	-9.832969	-1.611321	-0.782742
C	-7.732989	-1.150583	0.241371	H	-9.730070	-0.859511	-1.582243
H	-7.551323	-1.596003	-1.873133	H	-9.535403	-2.597650	-1.174364
H	-7.586346	-0.693714	2.337904	H	-10.883297	-1.654700	-0.467068
C	5.165523	-0.788318	0.043405	C	10.020738	-1.752624	-1.006686
C	5.817937	-1.469916	-0.986461	H	9.735336	-2.816668	-1.040145
C	5.967811	-0.222861	1.049317	H	9.833219	-1.297590	-1.993001
C	7.207772	-1.588790	-1.032504	H	11.091271	-1.677331	-0.776635
H	5.225011	-1.917817	-1.786922	C	0.862093	4.280093	0.007684
C	7.349213	-0.327871	1.018668	C	-0.033002	4.461652	-1.050032
H	5.492937	0.296780	1.884046	C	1.183502	5.401281	0.783940

C	-0.613178	5.698500	-1.317870
H	-0.292939	3.608936	-1.680604
C	0.613711	6.642558	0.532382
H	1.881838	5.294054	1.617251
C	-0.293542	6.798504	-0.518523
H	-1.307582	5.790513	-2.151732
H	0.860485	7.508769	1.149403
O	-0.808395	8.046296	-0.692617
C	-1.737389	8.246741	-1.740194
H	-2.635800	7.621605	-1.611074
H	-2.028967	9.304064	-1.699063
H	-1.290207	8.036621	-2.725490
H	1.408893	-3.906647	-0.667495

86

B_S0_CAM-B3LYP

Eopt -2277.084344

C	3.504630	1.737724	-0.182402
C	2.848367	0.507136	-0.210739
C	1.411563	0.476562	-0.195758
C	0.692560	1.722046	-0.248429
C	1.396861	2.931603	-0.059165
C	2.796278	2.926235	-0.055120
C	0.724424	-0.757628	-0.136062
C	-0.746106	1.674870	-0.544979
C	-1.446402	0.434591	-0.398390
C	-0.710874	-0.770284	-0.140132
C	-2.869974	0.390685	-0.566457
C	-3.538542	1.565333	-0.996681
C	-2.830079	2.716895	-1.255135
C	-1.450824	2.778157	-1.031226
H	4.592640	1.769343	-0.216967
H	3.331499	3.867689	0.081561

H	-4.613634	1.537486	-1.170847
H	-3.346759	3.599431	-1.641754
C	3.555830	-0.764194	-0.281006
C	2.874331	-1.936994	-0.283778
C	1.432112	-2.027179	-0.138876
H	3.408235	-2.885260	-0.314208
C	0.782561	-3.244997	-0.003438
C	-0.697686	-3.248231	0.358515
C	-1.408804	-1.967795	0.022716
C	-3.558173	-0.851231	-0.370682
C	-2.804981	-1.978599	-0.095085
H	-3.324482	-2.928627	0.057677
H	-0.927982	3.701388	-1.263127
C	-0.882687	-3.635730	1.836050
O	-1.156344	-2.842782	2.733291
C	1.429601	-4.607411	-0.171804
O	2.669359	-4.734555	-0.310984
N	-0.733283	-4.949642	2.069841
C	-0.647267	-5.476861	3.409542
H	0.097127	-4.935261	4.015682
H	-1.611179	-5.416153	3.940465
H	-0.351275	-6.532833	3.358671
O	0.641382	-5.610569	-0.219556
H	-0.435493	-5.503592	1.255930
C	-5.036110	-0.969824	-0.463641
C	-5.627071	-1.947711	-1.268260
C	-5.899428	-0.155911	0.291302
C	-7.010787	-2.120931	-1.332764
H	-4.988017	-2.593828	-1.874275
C	-7.275476	-0.310375	0.237365
H	-5.477411	0.606221	0.949455
C	-7.842998	-1.295812	-0.578045

H	-7.420259	-2.896520	-1.978630	H	-9.508247	-3.378824	-1.073439
H	-7.934414	0.323322	0.834372	H	-10.899571	-2.261055	-1.217698
C	5.044033	-0.812131	-0.330988	C	9.912634	-1.647170	-1.415885
C	5.704688	-1.403818	-1.406811	H	9.634850	-2.707831	-1.527838
C	5.831254	-0.311906	0.718383	H	9.731528	-1.124494	-2.369330
C	7.097078	-1.501404	-1.454424	H	10.980480	-1.581701	-1.170598
H	5.117061	-1.801959	-2.237254	C	0.744442	4.235153	0.255329
C	7.214104	-0.399698	0.688955	C	1.027826	5.389336	-0.472879
H	5.343423	0.143437	1.582959	C	-0.121400	4.355592	1.354759
C	7.857788	-0.995602	-0.401362	C	0.456292	6.623207	-0.150976
H	7.568322	-1.972712	-2.315636	H	1.697282	5.327672	-1.333824
H	7.818410	-0.017328	1.513963	C	-0.692817	5.570255	1.691271
O	9.217566	-1.036575	-0.346544	H	-0.351263	3.470988	1.951932
O	-9.202411	-1.374992	-0.570408	C	-0.413020	6.714768	0.934171
C	-9.817683	-2.363815	-1.371705	H	0.696112	7.495913	-0.756787
H	-9.592758	-2.218297	-2.441015	H	-1.365092	5.655773	2.547223

O -1.025227 7.862768 1.332985

C -0.771236 9.045308 0.601188

H -1.090641 8.949419 -0.449387

H -1.356543 9.840273 1.080879

H 0.296068 9.319476 0.630158

H -1.172639 -4.063705 -0.206237

86

B_S1_CAM-B3LYP

Eopt -2277.023643

C 3.453059 1.708923 -0.205009

C 2.797591 0.477893 -0.213781

C 1.363408 0.449489 -0.154891

C 0.634747 1.688986 -0.206527

C 1.343748 2.901363 -0.043365

C 2.744595 2.893540 -0.066797

C 0.680822 -0.787339 -0.069122

C -0.810036 1.624755 -0.495958

C -1.496612 0.374734 -0.351737

C -0.752682 -0.812067 -0.060307

C -2.916231 0.299384 -0.544419

C -3.599009 1.462312 -0.981614

C -2.909030 2.629549 -1.218767

C -1.533509 2.717414 -0.978347

H 4.540559 1.743898 -0.272062

H 3.282027 3.836804 0.048229

H -4.670698 1.417162 -1.172221

H -3.438601 3.505198 -1.603517

C 3.504257 -0.788843 -0.317139

C 2.817992 -1.962231 -0.324152

C 1.385724 -2.048495 -0.123878

H 3.351444 -2.906349 -0.414652

C 0.727388 -3.261414 0.042339

C	-0.675918	-3.221377	0.628360	H	0.240246	-5.058602	1.942280
C	-1.432697	-2.018733	0.138667	C	-5.054394	-1.106253	-0.498729
C	-3.582870	-0.956289	-0.354298	C	-5.594893	-2.087305	-1.334020
C	-2.821696	-2.064440	-0.025220	C	-5.960718	-0.318527	0.232835
H	-3.330546	-3.018419	0.142781	C	-6.971614	-2.287849	-1.450705
H	-1.030529	3.654488	-1.195977	H	-4.920545	-2.713992	-1.921862
C	-0.639311	-3.267594	2.172254	C	-7.330463	-0.500174	0.127068
O	-1.028223	-2.347465	2.892819	H	-5.578138	0.444270	0.914019
C	1.340113	-4.610852	-0.186393	C	-7.847462	-1.487758	-0.718737
O	2.350895	-4.731846	-0.924491	H	-7.341275	-3.064785	-2.118598
N	-0.131860	-4.411655	2.656838	H	-8.023567	0.112856	0.706702
C	0.104464	-4.606452	4.062381	C	4.990168	-0.830256	-0.421364
H	0.808265	-3.862682	4.471695	C	5.609935	-1.443428	-1.510823
H	-0.827889	-4.532663	4.644096	C	5.819367	-0.309303	0.585321
H	0.529405	-5.606979	4.218539	C	6.998916	-1.539137	-1.613748
O	0.765638	-5.598024	0.389950	H	4.990501	-1.857642	-2.309296

C	7.200194	-0.394806	0.500238
H	5.368320	0.158964	1.462705
C	7.800766	-1.009905	-0.603760
H	7.435589	-2.025832	-2.484677
H	7.836924	0.004843	1.292048
O	9.161645	-1.046170	-0.605349
O	-9.204312	-1.594542	-0.760974
C	-9.770374	-2.592717	-1.586741
H	-9.512239	-2.437799	-2.647125
H	-9.449448	-3.602098	-1.281547
H	-10.858868	-2.513649	-1.469533
C	9.812212	-1.672376	-1.693426
H	9.534144	-2.735694	-1.775466
H	9.587606	-1.166400	-2.646648
H	10.889416	-1.599256	-1.495832
C	0.702160	4.213570	0.252663
C	0.992431	5.354387	-0.493949
C	-0.167225	4.355023	1.346549
C	0.425887	6.595804	-0.193816
H	1.663563	5.275478	-1.352159
C	-0.733599	5.577661	1.661692
H	-0.403473	3.481101	1.956924
C	-0.445809	6.708716	0.887556
H	0.671129	7.457448	-0.813117
H	-1.408157	5.680192	2.513987
O	-1.054893	7.865222	1.265391
C	-0.791734	9.035655	0.517422
H	-1.108990	8.926505	-0.532523
H	-1.373652	9.840772	0.984166
H	0.277105	9.303648	0.545410
H	-1.204959	-4.136026	0.323765
86			

B_ox_CAM-B3LYP

Eopt -2276.992713

C	3.453059	1.708923	-0.205009
C	2.797591	0.477893	-0.213781
C	1.363408	0.449489	-0.154891
C	0.634747	1.688986	-0.206527
C	1.343748	2.901363	-0.043365
C	2.744595	2.893540	-0.066797
C	0.680822	-0.787339	-0.069122
C	-0.810036	1.624755	-0.495958
C	-1.496612	0.374734	-0.351737
C	-0.752682	-0.812067	-0.060307
C	-2.916231	0.299384	-0.544419
C	-3.599009	1.462312	-0.981614
C	-2.909030	2.629549	-1.218767
C	-1.533509	2.717414	-0.978347
H	4.540559	1.743898	-0.272062
H	3.282027	3.836804	0.048229
H	-4.670698	1.417162	-1.172221
H	-3.438601	3.505198	-1.603517
C	3.504257	-0.788843	-0.317139
C	2.817992	-1.962231	-0.324152
C	1.385724	-2.048495	-0.123878
H	3.351444	-2.906349	-0.414652
C	0.727388	-3.261414	0.042339
C	-0.675918	-3.221377	0.628360
C	-1.432697	-2.018733	0.138667
C	-3.582870	-0.956289	-0.354298
C	-2.821696	-2.064440	-0.025220
H	-3.330546	-3.018419	0.142781
H	-1.030529	3.654488	-1.195977
C	-0.639311	-3.267594	2.172254

O	-1.028223	-2.347465	2.892819	H	-5.578138	0.444270	0.914019
C	1.340113	-4.610852	-0.186393	C	-7.847462	-1.487758	-0.718737
O	2.350895	-4.731846	-0.924491	H	-7.341275	-3.064785	-2.118598
N	-0.131860	-4.411655	2.656838	H	-8.023567	0.112856	0.706702
C	0.104464	-4.606452	4.062381	C	4.990168	-0.830256	-0.421364
H	0.808265	-3.862682	4.471695	C	5.609935	-1.443428	-1.510823
H	-0.827889	-4.532663	4.644096	C	5.819367	-0.309303	0.585321
H	0.529405	-5.606979	4.218539	C	6.998916	-1.539137	-1.613748
O	0.765638	-5.598024	0.389950	H	4.990501	-1.857642	-2.309296
H	0.240246	-5.058602	1.942280	C	7.200194	-0.394806	0.500238
C	-5.054394	-1.106253	-0.498729	H	5.368320	0.158964	1.462705
C	-5.594893	-2.087305	-1.334020	C	7.800766	-1.009905	-0.603760
C	-5.960718	-0.318527	0.232835	H	7.435589	-2.025832	-2.484677
C	-6.971614	-2.287849	-1.450705	H	7.836924	0.004843	1.292048
H	-4.920545	-2.713992	-1.921862	O	9.161645	-1.046170	-0.605349
C	-7.330463	-0.500174	0.127068	O	-9.204312	-1.594542	-0.760974

C	-9.770374	-2.592717	-1.586741
H	-9.512239	-2.437799	-2.647125
H	-9.449448	-3.602098	-1.281547
H	-10.858868	-2.513649	-1.469533
C	9.812212	-1.672376	-1.693426
H	9.534144	-2.735694	-1.775466
H	9.587606	-1.166400	-2.646648
H	10.889416	-1.599256	-1.495832
C	0.702160	4.213570	0.252663
C	0.992431	5.354387	-0.493949
C	-0.167225	4.355023	1.346549
C	0.425887	6.595804	-0.193816
H	1.663563	5.275478	-1.352159
C	-0.733599	5.577661	1.661692
H	-0.403473	3.481101	1.956924
C	-0.445809	6.708716	0.887556
H	0.671129	7.457448	-0.813117
H	-1.408157	5.680192	2.513987
O	-1.054893	7.865222	1.265391
C	-0.791734	9.035655	0.517422
H	-1.108990	8.926505	-0.532523
H	-1.373652	9.840772	0.984166
H	0.277105	9.303648	0.545410
H	-1.204959	-4.136026	0.323765

41

C_M06-2X Eopt -1164.784517

C	-2.832606	-3.540838	-0.056302
C	-1.608945	-2.846653	-0.055750
C	-1.610983	-1.421668	-0.029484
C	-2.847695	-0.712732	-0.003314
C	-4.036674	-1.446268	-0.005008

C	-4.029274	-2.844736	-0.031362	H	-0.384155	-4.646244	-0.102281
C	-0.357345	-0.719796	-0.032985	H	1.783659	-3.415855	-0.095197
C	-2.829952	0.759661	0.023142	C	2.061526	-0.725965	-0.075328
C	-1.576910	1.440691	0.015802	C	2.081502	0.646379	-0.061540
C	-0.338673	0.712031	-0.014225	C	0.892554	1.415754	-0.026572
C	-1.545295	2.864648	0.037249	C	-0.278080	3.541908	0.026463
C	-2.752687	3.586645	0.067826	H	-0.278083	4.633811	0.043268
C	-3.964600	2.917663	0.076239	C	0.893216	2.852207	-0.004819
C	-4.001914	1.519414	0.053826	H	1.855340	3.363096	-0.014322
H	-2.821926	-4.632433	-0.077295	H	-4.974441	1.028961	0.060553
H	-4.977132	-3.385338	-0.032594	H	-4.998077	-0.935010	0.013545
H	-2.716697	4.677833	0.084332	C	3.513463	1.103056	-0.090542
H	-4.900331	3.478410	0.099858	O	3.925055	2.261489	-0.095506
C	-0.357259	-3.554820	-0.082633	C	3.487021	-1.278139	-0.093026
C	0.828178	-2.890185	-0.083552	O	3.853547	-2.190309	0.681829
C	0.853957	-1.454300	-0.060028	N	4.268424	-0.010228	-0.093854

C 5.703186 -0.020099 -0.110239

H 6.099016 0.006678 -1.137212

H 6.088871 0.847330 0.440775

H 6.041903 -0.942238 0.379919

45

D_M06-2X Eopt -1341.206650

C -2.296897 3.968154 -0.041706

C -1.289511 2.986279 -0.059948

C -1.652759 1.608273 -0.039319

C -3.028531 1.236068 -0.001259

C -3.992397 2.247218 0.015683

C -3.630665 3.598225 -0.004163

C -0.618175 0.611448 -0.054252

C -3.384649 -0.192805 0.020081

C -2.345217 -1.169234 0.008318

C -0.962830 -0.778255 -0.026587

C -2.675480 -2.554676 0.032613

C -4.026388 -2.947055 0.065729

C -5.029149 -1.992742 0.075454

C -4.710856 -0.630689 0.053158

H -2.009784 5.021467 -0.056937

H -4.410234 4.361598 0.010676

H -4.268101 -4.011717 0.083886

H -6.076405 -2.297992 0.101238

C 0.100570 3.353954 -0.097765

C 1.078535 2.410389 -0.114243

C 0.739532 1.014847 -0.091439

H 0.351261 4.416610 -0.113091

H 2.135533 2.676429 -0.151488

C 1.723368 0.004404 -0.092192

C 1.395211 -1.327996 -0.061556

C 0.049979 -1.770972 -0.031881

C -1.621255 -3.530977 0.023700

H -1.897955 -4.587200 0.042772

C -0.313376 -3.160648 -0.006457

H 0.487927 -3.898660 -0.012020

H -5.527270 0.090268 0.062510

H -5.051755 1.996456 0.045750

C 2.665187 -2.132394 -0.064968

O 2.770428 -3.356919 -0.035585

C 3.241664 0.176906 -0.139813

O 3.795312 0.947786 -0.955908

F 3.555522 0.601857 1.312835

N 3.676552 -1.247448 -0.123201

C 5.066665 -1.601716 -0.154630

H 5.483955 -1.704072 0.859009

H 5.198002 -2.551275 -0.689319

H 5.607434 -0.807481 -0.685746

O 5.352807 2.818075 0.221215

H 4.852937 2.518168 -0.541534

H 5.145039 2.265255 0.978066

45

E_M06-2X Eopt -1341.172894

C -3.226393 -3.444990 -0.179617

C -1.991994 -2.771371 -0.221779

C -1.957005 -1.351651 -0.132567

C -3.174738 -0.623345 0.002750

C -4.376983 -1.333564 0.038982

C -4.403927 -2.729289 -0.051414

C -0.690416 -0.672967 -0.183078

C -3.125185 0.844290 0.101110

C -1.862402 1.502216 0.037055

C	-0.643444	0.753587	-0.114197
C	-1.800231	2.921570	0.127373
C	-2.986334	3.662295	0.280689
C	-4.207963	3.014636	0.344132
C	-4.276168	1.620476	0.255343
H	-3.238074	-4.534432	-0.250374
H	-5.362108	-3.250180	-0.019901
H	-2.925854	4.750185	0.349861
H	-5.127597	3.589347	0.464992
C	-0.759190	-3.492489	-0.360300
C	0.436377	-2.848170	-0.398876
C	0.507738	-1.414602	-0.303774
H	-0.801412	-4.580764	-0.436436
H	1.354953	-3.423468	-0.505909
C	1.742731	-0.701708	-0.361474
C	1.800484	0.678885	-0.314668
C	0.597191	1.429168	-0.186154
C	-0.522388	3.574472	0.064969
H	-0.494687	4.663203	0.142914
C	0.625279	2.864457	-0.087430
H	1.591371	3.363827	-0.148419
H	-5.255001	1.146580	0.311449
H	-5.324023	-0.804907	0.138310
C	3.158028	1.363423	-0.351339
O	3.356522	2.252517	-1.213822
C	3.014285	-1.474643	-0.458070
O	3.377834	-2.377716	0.223289
F	3.746819	-1.138907	-1.540270
N	3.987244	0.887100	0.548445
C	5.321503	1.445326	0.496880
H	5.815017	1.245621	-0.471917
H	5.326008	2.542169	0.627855

H 5.939036 1.003085 1.292386

O 2.914455 -1.882561 3.007679

H 2.801586 -2.763284 2.635055

H 3.685108 0.259490 1.489005

4

F_H2O_anion_M06-2X

Eopt -176.426450

F 1.399951 0.015839 -0.003007

O -1.421378 -0.111060 -0.002193

H 0.442123 -0.102350 0.041398

H -1.670658 0.848281 0.003204

43

F_M06-2X Eopt -1240.721098

C 2.754307 -3.658480 -0.015720

C 1.583915 -2.880472 -0.017706

C 1.682280 -1.459409 -0.009844

C 2.964419 -0.837965 0.000046

C 4.100180 -1.652586 0.001555

C 3.996866 -3.046198 -0.006224

C 0.479566 -0.672713 -0.012106

C 3.050636 0.629694 0.008254

C 1.850038 1.396883 0.005787

C 0.563718 0.756200 -0.004357

C 1.918343 2.819762 0.013513

C 3.171678 3.455518 0.023601

C 4.334100 2.702028 0.026068

C 4.273824 1.305885 0.018492

H 2.667850 -4.746715 -0.021796

H 4.904938 -3.650802 -0.004770

H 3.213083 4.546399 0.029466

H 5.306634 3.196256 0.033976

C	0.287486	-3.502022	-0.027631
C	-0.851902	-2.762942	-0.029800
C	-0.782127	-1.328296	-0.022107
H	0.239723	-4.592733	-0.033457
H	-1.832210	-3.237330	-0.037357
C	-1.925372	-0.504536	-0.023946
C	-1.844003	0.871167	-0.016512
C	-0.612327	1.555007	-0.006508
C	0.703460	3.588785	0.010931
H	0.783565	4.677590	0.016938
C	-0.514464	2.987929	0.001336
H	-1.432941	3.573344	-0.000576
H	5.209691	0.749342	0.020803
H	5.094694	-1.209291	0.008847
C	-3.239335	1.414135	-0.021104
O	-3.618907	2.562044	-0.017263
C	-3.375053	-0.883429	-0.033531
O	-3.643663	-1.544044	-1.070356
N	-4.082721	0.312661	-0.031154
C	-5.524005	0.420609	-0.038263
H	-5.869841	0.952241	0.857335
H	-5.860271	0.961779	-0.931792
H	-5.940324	-0.592325	-0.045907
O	-3.692666	-1.646111	1.133662
H	-4.541027	-2.078827	1.012667

19

F_anion_1_tAmylOH_CAM-B3LYP

Eopt -372.762513

O	0.881769	-0.000526	-0.997592
H	1.781917	-0.000542	-0.562434
C	-0.147278	0.000293	-0.006430
C	-1.458697	-0.002651	-0.822441

H -1.430659 -0.883151 -1.478975

H -1.431476 0.874221 -1.483848

C -0.031964 1.264772 0.863810

H -0.103657 2.164365 0.240087

H -0.814285 1.314748 1.630541

H 0.936977 1.285815 1.377920

C -0.029469 -1.260483 0.868796

H -0.812126 -1.309221 1.635257

H -0.098788 -2.162639 0.248514

H 0.939185 -1.277371 1.383593

C -2.769011 -0.000971 -0.029196

H -2.863196 0.886539 0.607647

H -3.626954 -0.003654 -0.712914

H -2.862141 -0.884537 0.613262

F 3.327729 -0.000681 -0.085017

37

F_anion_2_tAmylOH_CAM-B3LYP

Eopt -645.526469

F -0.092621 -1.707834 -0.668955

O 2.253380 -0.695667 -1.268797

H 1.368593 -1.077706 -1.036210

C 2.820533 -0.086087 -0.112158

C 4.159374 0.490425 -0.589005

H 3.940728 1.173907 -1.425810

H 4.740877 -0.342941 -1.016278

C 3.021478 -1.148149 0.970002

H 3.407950 -0.717940 1.906248

H 2.066731 -1.645452 1.194153

H 3.729655 -1.917317 0.624498

C 1.886758 1.015729 0.392159

H 2.253167 1.471557 1.324147

H 1.785252 1.808959 -0.364272

H 0.884663 0.607198 0.583571

C 4.995908 1.214463 0.457375

H 5.270604 0.554772 1.294698

H 5.933161 1.585950 0.015143

H 4.467971 2.083995 0.878036

O -1.689775 0.256002 -0.077522

H -1.111165 -0.521496 -0.294749

C -2.994916 -0.189682 0.264287

C -3.825981 1.071356 0.536947

H -3.352795 1.594941 1.383878

H -4.827807 0.763716 0.880077

C -2.928174 -1.039251 1.534351

H -3.924329 -1.401143 1.833823

H -2.280092 -1.914017 1.373761

H -2.508789 -0.452324 2.365499

C -3.581676 -1.016910 -0.881161

H -4.620662 -1.315642 -0.670429

H -3.565844 -0.452484 -1.823388

H -2.987877 -1.930648 -1.031576

C -3.951989 2.032684 -0.636375

H -4.470053 2.955673 -0.332903

H -2.959762 2.312000 -1.019397

H -4.523307 1.596813 -1.469908

55

F_anion_3_tAmylOH_CAM-B3LYP

Eopt -918.292729

O -2.354988 -1.849820 -0.497498

H -1.530461 -1.325581 -0.333620

C -3.375447 -1.459059 0.427028

C -4.556578 -2.426034 0.193848

H -5.349527 -2.188537 0.915988

H -4.204501 -3.438233 0.436397

C	-3.781772	0.005530	0.180473
H	-4.101993	0.151570	-0.857080
H	-4.606631	0.309093	0.838404
H	-2.934266	0.676681	0.365593
C	-2.866503	-1.622886	1.870222
H	-3.643848	-1.371108	2.602753
H	-2.550226	-2.657942	2.048464
H	-2.006414	-0.967878	2.056152
C	-5.134272	-2.429268	-1.225060
H	-5.898053	-3.210105	-1.328429
H	-5.608040	-1.473964	-1.479794
H	-4.349632	-2.623583	-1.963800
F	-0.023785	-0.629655	-0.216229
O	2.536034	-0.590503	-0.902375
H	1.597830	-0.638384	-0.585146
C	3.377450	-1.334236	-0.009749
C	4.792882	-1.178498	-0.604261
H	5.003234	-0.102224	-0.668491
H	4.755170	-1.547537	-1.638269
C	2.931159	-2.806279	0.007116
H	3.549490	-3.418193	0.674232
H	1.892924	-2.883655	0.352954
H	2.985672	-3.233887	-1.001525
C	3.289539	-0.734275	1.403802
H	3.913348	-1.278789	2.122256
H	3.609875	0.314592	1.396457
H	2.255657	-0.770753	1.768339
C	5.932846	-1.876085	0.144195
H	5.787742	-2.961613	0.194541
H	6.887056	-1.698055	-0.366727
H	6.038404	-1.504871	1.170377
O	-0.602933	1.872451	0.428823

H -0.331180 0.967487 0.127068

C -0.074222 2.862633 -0.461259

C -0.715624 4.203173 -0.042275

H -1.798641 4.113920 -0.204680

H -0.360106 4.987319 -0.724469

C -0.479590 2.539728 -1.909862

H -0.117809 3.304737 -2.608380

H -0.063605 1.574769 -2.224706

H -1.571350 2.483970 -1.998348

C 1.460487 2.904780 -0.345512

H 1.889400 3.689037 -0.982880

H 1.768232 3.098707 0.687963

H 1.895077 1.944056 -0.646888

C -0.465910 4.628286 1.408229

H -1.033663 5.536340 1.646531

H -0.778374 3.841808 2.103194

H 0.591694 4.845614 1.598418

1

F_anion_CAM-B3LYP

Eopt -99.998928

F 0.000000 0.000000 0.000000

1

F_anion_M06-2X Eopt -99.977601

F 0.000000 0.000000 0.000000

19

F_radical_1_tAmylOH_CAM-B3LYP

Eopt -372.566091

O -0.918372 0.229541 -0.831024

H -2.359734 -0.096206 -0.372376

C 0.164804 0.084838 0.013018

C 1.406581 -0.276902 -0.850090

H 1.474836 0.465101 -1.653882

H 1.193026 -1.243699 -1.323273

C -0.117804 -0.905209 1.150727

H -0.269918 -1.911860 0.744702

H 0.719389 -0.941079 1.853842

H -1.015332 -0.610232 1.704659

C 0.308120 1.548616 0.590771

H 1.143068 1.525521 1.297841

H 0.517779 2.260126 -0.210911

H -0.603022 1.839283 1.119341

C 2.736757 -0.362717 -0.097665

H 2.718572 -1.131769 0.682040

H 3.535683 -0.625619 -0.801003

H 3.010615 0.590129 0.368453

F -3.300971 -0.276420 -0.177978

37

F_radical_2_tAmylOH_CAM-B3LYP

Eopt -645.323854

O 2.629613 0.933065 0.567947

H 1.393619 1.752684 0.694795

C 2.807792 0.046364 -0.451677

C 2.133397 -1.313178 0.149893

H 2.230706 -2.003819 -0.696196

H 1.073276 -1.091174 0.297794

C 4.303748 -0.185238 -0.721766

H 4.443883 -1.039535 -1.391424

H 4.723755 0.704765 -1.204033

H 4.850470 -0.363495 0.207646

C 2.025035 0.419856 -1.721286

H 0.949608 0.470687 -1.524171

H 2.368943 1.392811 -2.090670

H 2.201391 -0.325387 -2.503845

C	2.769276	-1.882442	1.408754
H	2.685336	-1.198457	2.258752
H	2.245626	-2.810037	1.673320
H	3.825269	-2.132547	1.266545
F	0.597871	2.322148	0.862085
O	-1.101791	0.210610	-0.036118
H	-0.776128	1.045777	0.345339
C	-2.541890	0.182845	0.080870
C	-2.939097	-1.157012	-0.568143
H	-2.402994	-1.952837	-0.033900
H	-2.548537	-1.153763	-1.594525
C	-3.125479	1.384415	-0.675732
H	-2.750412	2.322959	-0.247256
H	-2.834327	1.351239	-1.732223
H	-4.219361	1.410481	-0.618946
C	-2.922091	0.237566	1.567230
H	-2.487104	-0.612281	2.106335
H	-2.543238	1.161433	2.023247
H	-4.008051	0.219798	1.711766
C	-4.436119	-1.479529	-0.592872
H	-4.604629	-2.449300	-1.076330
H	-4.859667	-1.539487	0.416345
H	-5.008279	-0.731138	-1.153380

55

F_radical_3_tAmylOH_CAM-B3LYP

Eopt -918.079367

O	2.376121	-0.922157	-0.118058
H	1.464760	-1.237739	0.006562
C	3.276431	-1.987364	0.254338
C	4.695858	-1.444088	-0.000700
H	5.415989	-2.198330	0.342389
H	4.831498	-0.565564	0.644461

C	2.969616	-3.234878	-0.587669
H	3.003573	-3.007445	-1.657975
H	3.685720	-4.039807	-0.382163
H	1.965889	-3.613982	-0.355098
C	3.101149	-2.300206	1.747919
H	3.787084	-3.091924	2.072897
H	3.295091	-1.406696	2.352759
H	2.077583	-2.638248	1.955025
C	5.006182	-1.054065	-1.449314
H	5.999589	-0.593990	-1.516220
H	5.002319	-1.921544	-2.119347
H	4.274499	-0.332183	-1.827295
F	-0.416565	-1.152729	0.503536
O	-0.641438	1.722999	0.417069
H	-0.271479	0.823206	0.402285
C	0.420895	2.661581	0.127889
C	-0.264850	4.036488	0.241705
H	-0.695966	4.106684	1.249317
H	-1.110468	4.042358	-0.459244
C	0.952801	2.395716	-1.287824
H	1.756661	3.090297	-1.556899
H	1.359671	1.378942	-1.354550
H	0.148660	2.496194	-2.026531
C	1.537651	2.482804	1.166428
H	2.359028	3.189982	1.004619
H	1.147217	2.633353	2.180015
H	1.954421	1.469986	1.099998
C	0.620746	5.258219	-0.020464
H	1.036548	5.253756	-1.034691
H	0.034932	6.178862	0.088507
H	1.457448	5.317850	0.685173
O	-2.616098	-1.476796	-0.575195

H -1.321035 -1.259633 0.099176

C -3.726759 -0.749137 -0.212736

C -5.016542 -1.518278 -0.587407

H -4.978497 -1.733815 -1.661597

H -5.866679 -0.846678 -0.419902

C -3.600687 0.516933 -1.170520

H -4.482845 1.129833 -0.957019

H -2.690708 1.074136 -0.937036

H -3.606614 0.206432 -2.217292

C -3.670399 -0.272201 1.247836

H -4.582483 0.282193 1.492158

H -3.592927 -1.125949 1.928733

H -2.811697 0.387021 1.409231

C -5.210002 -2.822200 0.194265

H -6.116615 -3.333438 -0.149295

H -4.364307 -3.503866 0.044248

H -5.317988 -2.644015 1.269781

1

F_radical_CAM-B3LYP

Eopt -99.747355

F 0.000000 0.000000 0.000000

43

G_M06-2X Eopt -1240.704967

C -3.304507 -3.311128 0.017931

C -2.024152 -2.727975 0.036931

C -1.893380 -1.310755 0.015044

C -3.060511 -0.493397 -0.029315

C -4.310591 -1.116234 -0.047069

C -4.432490 -2.509849 -0.023344

C -0.581931 -0.723894 0.038807

C -2.909313 0.971072 -0.056096

C	-1.600681	1.535245	-0.015280
C	-0.433708	0.696320	0.039878
C	-1.439687	2.949370	-0.031873
C	-2.575123	3.778274	-0.093305
C	-3.841972	3.221894	-0.137149
C	-4.006856	1.832878	-0.118203
H	-3.391762	-4.399352	0.036719
H	-5.425765	-2.961303	-0.037394
H	-2.439733	4.861626	-0.106544
H	-4.721941	3.865283	-0.186433
C	-0.839391	-3.538023	0.082766
C	0.398127	-2.976408	0.092701
C	0.565565	-1.547758	0.062171
H	-0.954580	-4.623362	0.110484
H	1.280170	-3.617029	0.130763
C	1.853093	-0.935718	0.084463
C	2.011432	0.435563	0.121218
C	0.855648	1.272710	0.092781
C	-0.115303	3.504295	0.012090
H	-0.010384	4.591066	-0.005764
C	0.982378	2.705968	0.076428
H	1.984013	3.132253	0.125382
H	-5.018732	1.431532	-0.154006
H	-5.220641	-0.518599	-0.078704
C	3.401227	1.052304	0.196175
O	3.644606	1.790165	1.190011
C	3.067587	-1.819651	0.109545
O	3.785306	-1.978880	1.064036
N	4.181644	0.726166	-0.801568
C	5.512925	1.287107	-0.698193
H	5.505731	2.391376	-0.636844
H	6.045241	0.937553	0.206646

H 6.111822 0.999907 -1.575402

O 3.230916 -2.501058 -1.035868

H 4.028123 -3.049180 -0.937966

3

H2O_M06-2X Eopt

-76.437361

O 0.000000 0.110851 -0.000001

H 0.783837 -0.443405 -0.000016

H -0.783837 -0.443405 0.000021

3

HF2_anion_CAM-B3LYP

Eopt -200.516503

F 0.000000 0.000000 1.143008

H 0.000000 0.000000 0.000000

F 0.000000 0.000000 -1.143008

3

HF2_anion_M06-2X

Eopt -200.480611

F 0.000000 0.000000 1.135037

H 0.000000 0.000000 -0.001323

F 0.000000 0.000000 -1.134890

3

HF2_radical_CAM-B3LYP

Eopt -200.221943

F 0.000000 0.000000 -1.552755

H 0.000000 0.000000 -0.615043

F 0.000000 0.000000 1.621093

2

HO_anion_M06-2X

Eopt -75.893575

O -0.000000 0.000000 0.106788

H 0.000000 -0.000000 -0.854304

43

H_M06-2X Eopt -1240.742851

C	-3.372555	-3.268215	-0.044385
C	-2.081256	-2.710501	-0.008876
C	-1.922796	-1.295946	-0.010509
C	-3.073479	-0.455413	-0.051481
C	-4.335277	-1.053397	-0.086056
C	-4.484423	-2.444563	-0.082205
C	-0.600381	-0.735201	0.030006
C	-2.893649	1.006049	-0.057225
C	-1.574602	1.543939	0.000012
C	-0.424575	0.681707	0.051481
C	-1.386028	2.954737	0.003859
C	-2.504688	3.806426	-0.053786
C	-3.781777	3.275551	-0.113676
C	-3.973766	1.889885	-0.114822
H	-3.481075	-4.354682	-0.041055
H	-5.486176	-2.876274	-0.109031
H	-2.348152	4.887003	-0.051298
H	-4.648720	3.936603	-0.159987
C	-0.912828	-3.544099	0.033782
C	0.335283	-3.006964	0.059673
C	0.530684	-1.581576	0.049760
H	-1.049303	-4.627254	0.045892
H	1.204422	-3.665142	0.094869
C	1.829679	-0.995146	0.089030
C	2.014384	0.372121	0.145659
C	0.875342	1.232028	0.120903
C	-0.051442	3.483036	0.064247
H	0.074713	4.567692	0.061982
C	1.030041	2.662622	0.125008
H	2.039406	3.068555	0.186555

H	-4.992985	1.508901	-0.162816
H	-5.233290	-0.437714	-0.115570
C	3.415381	0.960369	0.238421
O	3.665887	1.680555	1.243381
C	3.026617	-1.902789	0.110157
O	3.305613	-2.655690	1.008407
N	4.196506	0.631545	-0.757874
C	5.537765	1.164807	-0.638052
H	5.551792	2.268137	-0.562643
H	6.056559	0.793434	0.265951
H	6.137260	0.876949	-1.514640
O	3.725148	-1.858739	-1.035729
H	3.896917	0.067143	-1.527092

13

Me3N_CAM-B3LYP

Eopt -174.311526

N	-0.000010	0.000011	-0.381903
C	0.418479	1.325893	0.061859
H	1.419893	1.548393	-0.323783
H	-0.274360	2.082721	-0.323177
H	0.446992	1.415098	1.166953
C	-1.357561	-0.300563	0.061869
H	-2.050885	0.455221	-0.324372
H	-1.666230	-1.279305	-0.322711
H	-1.449275	-0.319837	1.166951
C	0.939073	-1.025355	0.061860
H	0.631031	-2.003792	-0.323930
H	1.940950	-0.803643	-0.323087
H	1.002010	-1.094780	1.166941

13

Me3N_ox_CAM-B3LYP

Eopt -174.116002

N	0.006314	-0.004430	-0.050517
C	1.405897	-0.301304	0.003824
H	1.582250	-1.361360	-0.202564
H	1.938305	0.334355	-0.716631
H	1.773929	-0.048104	1.014565
C	-0.439016	1.356158	0.006630
H	0.413937	2.040975	0.000536
H	-1.097161	1.547421	-0.853890
H	-1.035437	1.492976	0.924299
C	-0.965621	-1.055390	0.001456
H	-1.915183	-0.710184	-0.421146
H	-0.591242	-1.939351	-0.526271
H	-1.121160	-1.322506	1.063261

31

Me3N_tAmylOH_CAM-B3LYP

Eopt -447.074315

N	2.245752	0.004344	0.041081
C	2.191681	-0.692480	-1.246003
H	1.845940	-1.720742	-1.094297
H	1.487480	-0.183111	-1.912515
H	3.178962	-0.726683	-1.742950
C	2.640905	1.403866	-0.131920
H	1.932603	1.907453	-0.798576
H	2.626848	1.912876	0.837780
H	3.654669	1.500345	-0.562828
C	3.139829	-0.683880	0.975077
H	3.125554	-0.172333	1.943450
H	2.797305	-1.713837	1.121709
H	4.182934	-0.711020	0.609298
O	-0.336186	-0.056254	1.235406
H	0.565733	-0.034215	0.814535
C	-1.312750	-0.018609	0.203646

C	-1.186896	1.243177	-0.670230
H	-0.256468	1.220079	-1.198123
H	-1.994316	1.273196	-1.371709
H	-1.222460	2.112949	-0.048032
C	-1.238829	-1.253948	-0.712909
H	-1.321020	-2.142060	-0.121806
H	-2.040448	-1.221260	-1.420890
H	-0.303657	-1.256845	-1.232856
C	-2.700479	-0.000956	0.871101
H	-2.822249	-0.883183	1.464184
H	-2.784666	0.863424	1.496129
C	-3.791783	0.042385	-0.214614
H	-4.756144	0.045975	0.248952
H	-3.675233	0.928933	-0.802277
H	-3.702214	-0.817641	-0.844878

31

Me3N_tAmylOH_ox_CAM-B3LYP

Eopt -446.872822

N	-2.445994	0.004572	0.017428
C	-2.246162	-0.653935	1.299600
H	-1.855123	-1.659634	1.140750
H	-1.586813	-0.050344	1.924665
H	-3.241337	-0.715189	1.767265
C	-2.666484	1.442989	0.019712
H	-1.981932	1.919359	0.722001
H	-2.551527	1.833791	-0.991998
H	-3.703739	1.590749	0.359042
C	-3.044735	-0.770332	-1.059914
H	-2.904682	-0.248102	-2.007305
H	-2.613123	-1.771515	-1.075865
H	-4.119799	-0.833655	-0.829571
O	0.290899	-0.037741	-1.114493

H -0.578864 -0.023196 -0.673946

C 1.330472 -0.013662 -0.130922

C 1.254984 1.247359 0.749831

H 0.351898 1.228271 1.323391

H 2.096492 1.272039 1.410252

H 1.264114 2.117932 0.127802

C 1.306296 -1.272266 0.756169

H 1.357451 -2.144746 0.138867

H 2.144479 -1.256141 1.421067

H 0.400159 -1.290395 1.324930

C 2.658252 0.010320 -0.910681

H 2.693434 0.883346 -1.528328

H 2.727443 -0.863620 -1.524148

C 3.835814 0.035617 0.081442

H 4.758326 0.054116 -0.460341

H 3.765617 0.908620 0.696127

H 3.801674 -0.838309 0.697874

43

TS_III_M06-2X Eopt -1240.685561

C 2.879048 -3.598033 -0.045915

C 1.678955 -2.865013 -0.061919

C 1.724153 -1.440889 -0.046988

C 2.982470 -0.772120 -0.006240

C 4.147924 -1.543084 0.003946

C 4.097347 -2.940154 -0.016797

C 0.493308 -0.699341 -0.079459

C 3.012803 0.699003 0.022037

C 1.783862 1.420207 -0.017799

C 0.523672 0.731808 -0.073674

C 1.798684 2.844624 -0.000038

C 3.027076 3.526271 0.065351

C	4.216091	2.817748	0.110592
C	4.208208	1.419759	0.088040
H	2.833365	-4.688855	-0.058655
H	5.027614	-3.510348	-0.008535
H	3.026620	4.618016	0.081848
H	5.168297	3.347728	0.164922
C	0.406040	-3.533350	-0.092569
C	-0.758073	-2.833434	-0.119971
C	-0.741476	-1.397351	-0.123555
H	0.397952	-4.625213	-0.092050
H	-1.724532	-3.336164	-0.140020
C	-1.917286	-0.622757	-0.171297
C	-1.887740	0.751082	-0.188847
C	-0.681730	1.479767	-0.126150
C	0.555612	3.565149	-0.048922
H	0.592339	4.656348	-0.031559
C	-0.636161	2.915806	-0.113454
H	-1.578147	3.461868	-0.148180
H	5.163186	0.897589	0.127392
H	5.124722	-1.062154	0.026462
C	-3.299787	1.238717	-0.268566
O	-3.708582	2.382669	-0.254160
C	-3.349018	-1.056307	-0.259340
O	-3.807296	-2.170980	-0.377236
N	-4.087791	0.118209	-0.420581
C	-5.519646	0.136633	-0.281340
H	-5.787223	-0.002538	0.776762
H	-5.898550	1.100748	-0.638187
H	-5.955158	-0.671051	-0.881065
O	-3.307998	-0.402712	2.135885
H	-3.650972	-0.953698	2.846255

45

TS_II_M06-2X Eopt

-1341.171654

C	-3.177091	-3.521009	-0.046128
C	-1.958211	-2.820909	-0.099297
C	-1.957179	-1.398091	-0.060163
C	-3.193156	-0.694513	0.032704
C	-4.379280	-1.431033	0.080758
C	-4.372651	-2.829039	0.042297
C	-0.705958	-0.691438	-0.117265
C	-3.178911	0.776236	0.075492
C	-1.930508	1.461237	0.008501
C	-0.691639	0.737322	-0.095544
C	-1.904193	2.884030	0.047195
C	-3.110048	3.601271	0.150865
C	-4.317354	2.927350	0.216238
C	-4.350606	1.529729	0.179309
H	-3.162984	-4.612312	-0.076708
H	-5.318718	-3.371089	0.082497
H	-3.076118	4.692194	0.179797
H	-5.252426	3.483772	0.297938
C	-0.707687	-3.518995	-0.198587
C	0.473017	-2.849171	-0.246957
C	0.509895	-1.411465	-0.200158
H	-0.725365	-4.610026	-0.235638
H	1.408233	-3.402754	-0.321057
C	1.726550	-0.674528	-0.264513
C	1.751648	0.706242	-0.254975
C	0.535691	1.440420	-0.170081
C	-0.641026	3.564386	-0.015812
H	-0.640695	4.655673	0.022932
C	0.526859	2.878722	-0.121337
H	1.482892	3.395495	-0.182006

H -5.319057 1.034968 0.235489

H -5.339528 -0.921849 0.148712

C 3.127878 1.342112 -0.326864

O 3.314699 2.385131 -0.990819

C 3.026341 -1.418926 -0.360202

O 3.414367 -2.296754 0.348430

F 3.600281 -1.283404 -1.591386

N 4.014354 0.604479 0.312228

C 5.394731 0.984166 0.121062

H 5.681067 0.971297 -0.946355

H 5.603791 2.003545 0.490359

H 6.048925 0.284973 0.662538

O 3.530028 -0.601100 2.781389

H 3.369347 -1.502994 2.482623

H 3.682189 -0.124456 1.924541

43

TS_IV_M06-2X Eopt

-1240.700870

C 2.973653 -3.534735 -0.067602

C 1.757484 -2.828357 -0.047025

C 1.768070 -1.404766 -0.020621

C 3.011211 -0.707892 -0.010968

C 4.194207 -1.451133 -0.034450

C 4.176664 -2.849237 -0.062927

C 0.520421 -0.690215 -0.007335

C 3.005771 0.763413 0.024220

C 1.758370 1.454764 0.026948

C 0.510952 0.737529 0.001965

C 1.743251 2.877743 0.056948

C 2.957063 3.588746 0.085778

C 4.162878 2.908837 0.085224

C 4.185810 1.510814 0.054517

H	2.952185	-4.626226	-0.089181
H	5.120111	-3.397128	-0.081603
H	2.930501	4.680126	0.109212
H	5.104079	3.460474	0.108748
C	0.498004	-3.519618	-0.056232
C	-0.677938	-2.839934	-0.035816
C	-0.702430	-1.400820	-0.007426
H	0.507062	-4.611153	-0.082020
H	-1.622077	-3.385110	-0.047378
C	-1.921325	-0.669592	-0.003122
C	-1.944405	0.710768	-0.024296
C	-0.719373	1.442042	-0.011258
C	0.481081	3.562027	0.060132
H	0.487046	4.653758	0.091257
C	-0.694803	2.881809	0.023827
H	-1.651377	3.400130	0.010801
H	5.153042	1.010315	0.056643
H	5.159730	-0.947299	-0.033168
C	-3.331657	1.336872	-0.089544
O	-3.506304	2.480649	-0.581403
C	-3.220230	-1.448340	-0.043440
O	-3.721503	-1.860200	-1.074960
N	-4.226199	0.491525	0.354620
C	-5.606846	0.842688	0.150396
H	-5.897813	1.752324	0.706708
H	-5.837595	1.039558	-0.913299
H	-6.255175	0.020548	0.492577
O	-3.478285	-2.056202	1.145244
H	-4.232886	-2.645442	0.989952

45

TS_I_M06-2X Eopt

-1341.204001

C	-2.334181	3.923654	-0.134416	H	-4.159697	-4.082638	0.231528
C	-1.309885	2.959637	-0.144590	H	-5.997732	-2.400547	0.229963
C	-1.647879	1.576335	-0.089137	C	0.072584	3.351585	-0.205319
C	-3.015761	1.181030	-0.021063	C	1.067675	2.426372	-0.226404
C	-3.997641	2.174825	-0.016837	C	0.752849	1.025857	-0.184954
C	-3.660648	3.531004	-0.073075	H	0.304897	4.418078	-0.231728
C	-0.596065	0.597593	-0.103280	H	2.118386	2.716173	-0.265445
C	-3.345759	-0.252323	0.043559	C	1.747396	0.028420	-0.204647
C	-2.289868	-1.210478	0.040601	C	1.445348	-1.308474	-0.121379
C	-0.915828	-0.796745	-0.032577	C	0.112417	-1.773981	-0.032513
C	-2.594839	-2.600214	0.110461	C	-1.524283	-3.558892	0.111502
C	-3.937480	-3.014968	0.178172	H	-1.782169	-4.618395	0.168689
C	-4.956692	-2.078081	0.177534	C	-0.224050	-3.168115	0.044148
C	-4.663087	-0.712128	0.111593	H	0.588302	-3.894058	0.045815
H	-2.066211	4.981216	-0.175867	H	-5.491503	-0.005149	0.115458
H	-4.453786	4.280384	-0.066825	H	-5.052004	1.905940	0.032040

C	2.731594	-2.081692	-0.144328
O	2.884925	-3.290662	-0.048484
C	3.245528	0.188365	-0.340820
O	3.820839	1.048997	-1.003066
F	3.530072	0.588378	1.396642
N	3.724365	-1.170058	-0.309625
C	5.124759	-1.495727	-0.318387
H	5.498190	-1.672674	0.700922
H	5.297744	-2.393758	-0.924811
H	5.667302	-0.650411	-0.758467
O	4.674495	2.981178	0.893968
H	4.656384	2.750716	-0.044493
H	4.271385	2.166861	1.258412

43

TS_V_M06-2X Eopt

-1240.696540

C	-3.211080	-3.386068	0.015341
C	-1.949287	-2.764148	0.033328
C	-1.864112	-1.342826	0.018989
C	-3.055483	-0.561629	-0.018942
C	-4.285975	-1.222936	-0.034247
C	-4.363618	-2.619672	-0.016577
C	-0.572121	-0.714993	0.042483
C	-2.947063	0.906661	-0.044802
C	-1.655154	1.510289	-0.018519
C	-0.461889	0.708294	0.033882
C	-1.538721	2.928435	-0.046760
C	-2.699110	3.722546	-0.098426
C	-3.949046	3.128225	-0.122293
C	-4.070835	1.734947	-0.096179
H	-3.264758	-4.476548	0.027379
H	-5.342307	-3.101988	-0.029259

H	-2.596249	4.809371	-0.119638
H	-4.848786	3.744302	-0.162503
C	-0.740041	-3.539375	0.066505
C	0.479005	-2.939212	0.084394
C	0.597216	-1.505832	0.071908
H	-0.822646	-4.627953	0.077324
H	1.384048	-3.549626	0.110286
C	1.863055	-0.859606	0.097941
C	1.991333	0.515832	0.104901
C	0.813098	1.323108	0.070514
C	-0.231490	3.522524	-0.025947
H	-0.159763	4.611790	-0.057226
C	0.891899	2.760249	0.033262
H	1.880158	3.215842	0.066398
H	-5.070361	1.302972	-0.118253
H	-5.214806	-0.654639	-0.060420
C	3.387622	1.126952	0.163635
O	3.589473	2.059956	0.986302
C	3.101539	-1.711224	0.126816
O	3.703846	-1.988162	1.127500
N	4.242473	0.559008	-0.653990
C	5.589106	1.077655	-0.539497
H	5.643929	2.165956	-0.726841
H	6.014624	0.920669	0.469766
H	6.247819	0.576795	-1.265226
O	3.387864	-2.276337	-1.080039
H	4.289238	-2.002834	-1.314216

17

tAmylO_anion_CAM-B3LYP

Eopt -272.210353

O	1.468390	-0.000002	1.114608
C	0.543632	0.000000	0.145188

C -0.905710 0.000000 0.771906

H -0.945224 0.876694 1.437848

H -0.945224 -0.876694 1.437848

C 0.678780 -1.263351 -0.779400

H 0.548506 -2.172839 -0.173958

H -0.022775 -1.319170 -1.628345

H 1.699984 -1.293524 -1.186287

C 0.678782 1.263353 -0.779397

H -0.022774 1.319176 -1.628341

H 0.548511 2.172839 -0.173953

H 1.699985 1.293525 -1.186285

C -2.143135 0.000000 -0.138546

H -2.173012 -0.883891 -0.788998

H -3.076178 0.000002 0.444104

H -2.173011 0.883891 -0.788999

35

tAmylO_dimer_anion_CAM-B3LYP

Eopt -544.985813

O -1.155550 0.943835 -0.015084

C -2.185822 -0.008744 0.089748

C -3.482282 0.739408 -0.263012

H -3.349436 1.167331 -1.266333

H -3.559850 1.594128 0.431796

C -2.236743 -0.561894 1.515087

H -2.470404 0.241566 2.229235

H -2.989680 -1.358293 1.634668

H -1.250866 -0.975510 1.779723

C -1.928605 -1.155311 -0.898807

H -2.702099 -1.940641 -0.837526

H -1.906495 -0.774591 -1.933375

H -0.955824 -1.618470 -0.685808

C -4.777990 -0.065457 -0.221105

H -4.974712 -0.478263 0.781024

H -5.638868 0.568379 -0.485513

H -4.765935 -0.907878 -0.931892

H -0.211023 0.541760 0.284421

O 1.026819 0.003906 0.764299

C 2.166931 0.158032 -0.002048

C 3.344969 -0.536360 0.727938

C 2.501850 1.654831 -0.190371

C 1.977204 -0.479593 -1.393992

H 3.032370 -1.583627 0.894680

H 3.409414 -0.077565 1.729243

C 4.726284 -0.519167 0.072916

H 2.642561 2.132191 0.792336

H 3.409395 1.835402 -0.795384

H 1.663245 2.178287 -0.693276

H 2.838318 -0.339320 -2.069725

H 1.795077 -1.562810 -1.295106

H 1.089780 -0.035305 -1.879130

H 5.099602 0.510775 -0.071884

H 5.467235 -1.043932 0.690987

H 4.723272 -1.010009 -0.914999

35

tAmylO_dimer_radical_CAM-B3LYP

Eopt -544.834023

O 1.120556 -0.285437 -0.583813

C 2.340726 -0.053874 0.144834

C 3.430721 -0.048064 -0.945233

H 3.158736 0.725546 -1.675940

H 3.370194 -1.008657 -1.474375

C 2.546852 -1.194347 1.153852

H 2.595558 -2.159645 0.635906

H 3.466621 -1.067724 1.736032

H	1.709308	-1.230667	1.862265
C	2.247739	1.298599	0.868146
H	3.151602	1.518374	1.447496
H	2.094358	2.109754	0.146275
H	1.399644	1.298826	1.564547
C	4.867980	0.182363	-0.469011
H	5.198150	-0.594020	0.230993
H	5.556326	0.166468	-1.322693
H	4.985541	1.152849	0.027047
H	0.379146	-0.293091	0.054953
O	-1.320930	-0.060860	0.939443
C	-2.354800	-0.049265	0.019853
C	-3.709356	0.002965	0.770757
C	-2.232815	-1.243766	-0.946508
C	-2.081534	1.286791	-0.757917
H	-3.668376	0.856388	1.458918
H	-3.768823	-0.900460	1.392236
C	-4.964375	0.097837	-0.102244
H	-2.390018	-2.183722	-0.404730
H	-2.977426	-1.178974	-1.745949
H	-1.236672	-1.265982	-1.399194
H	-2.821370	1.366302	-1.560496
H	-2.175079	2.147833	-0.090326
H	-1.078431	1.268258	-1.191491
H	-5.068380	-0.767793	-0.765962
H	-5.857800	0.133480	0.532529
H	-4.966645	1.001607	-0.722255

17

tAmylO_radical_CAM-B3LYP

Eopt -272.077073

O	-1.355302	-0.000016	1.168533
C	-0.512888	-0.000001	0.080311

C	0.908109	-0.000005	0.780944
H	0.956087	-0.883634	1.426417
H	0.956085	0.883613	1.426432
C	-0.712150	1.277266	-0.758549
H	-0.528877	2.169629	-0.149842
H	-0.044587	1.299087	-1.626065
H	-1.743812	1.317830	-1.127231
C	-0.712143	-1.277251	-0.758578
H	-0.044577	-1.299050	-1.626092
H	-0.528869	-2.169626	-0.149889
H	-1.743803	-1.317812	-1.127263
C	2.088136	0.000003	-0.194863
H	2.094201	0.887757	-0.835588
H	3.021982	-0.000003	0.380867
H	2.094200	-0.887740	-0.835604

14. NMR spectra

14.1 NMR spectra for small molecule products

N,N-dimethyl-aniline (**3**) ^{1}H-NMR spectrum in $CDCl_3$

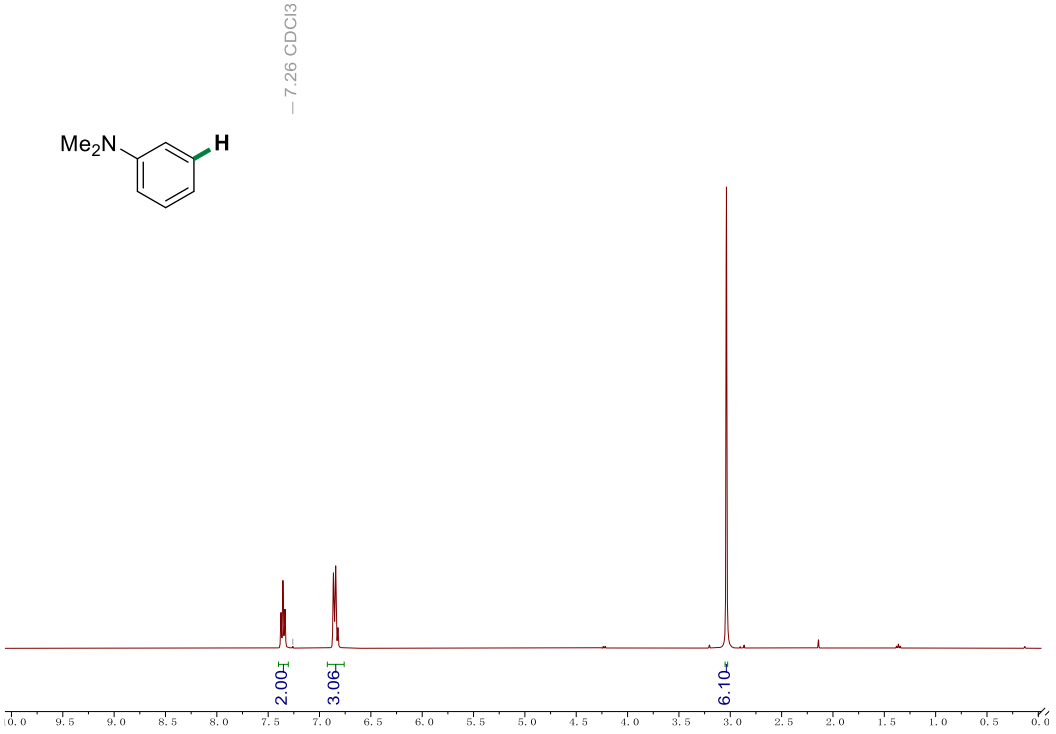

*N,N-dimethyl-aniline (**3**) ^{13}C-NMR spectrum in $CDCl_3$*

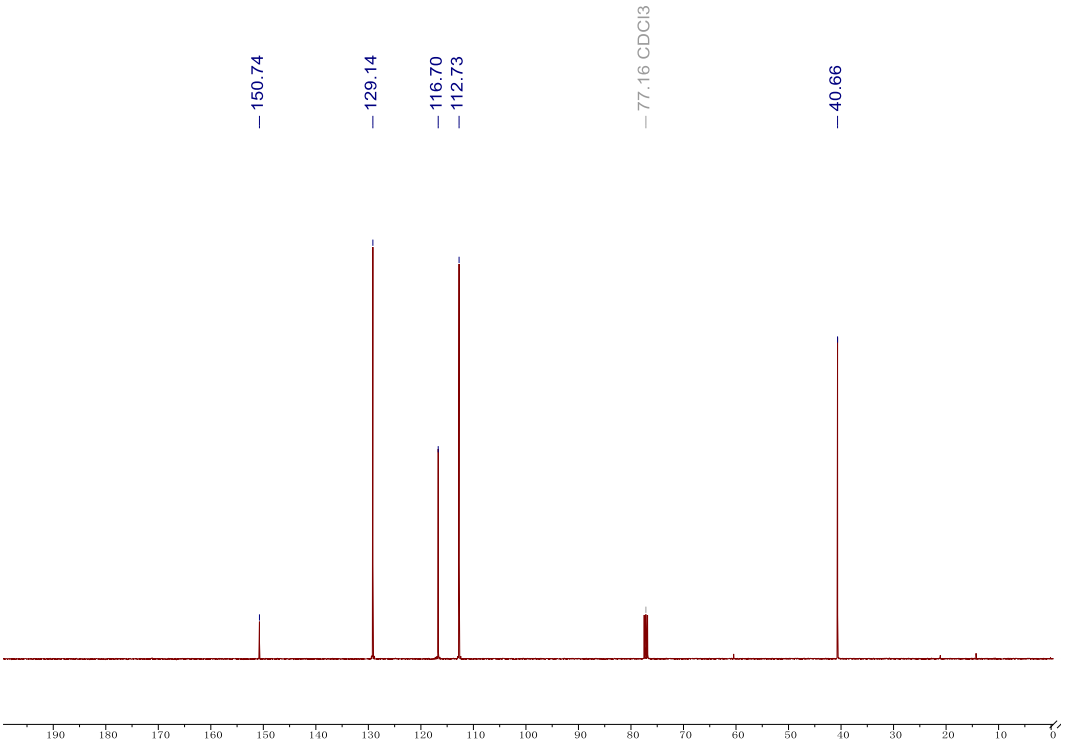

*Methyl benzoate (**5**) ^{1}H-NMR spectrum in $CDCl_3$*

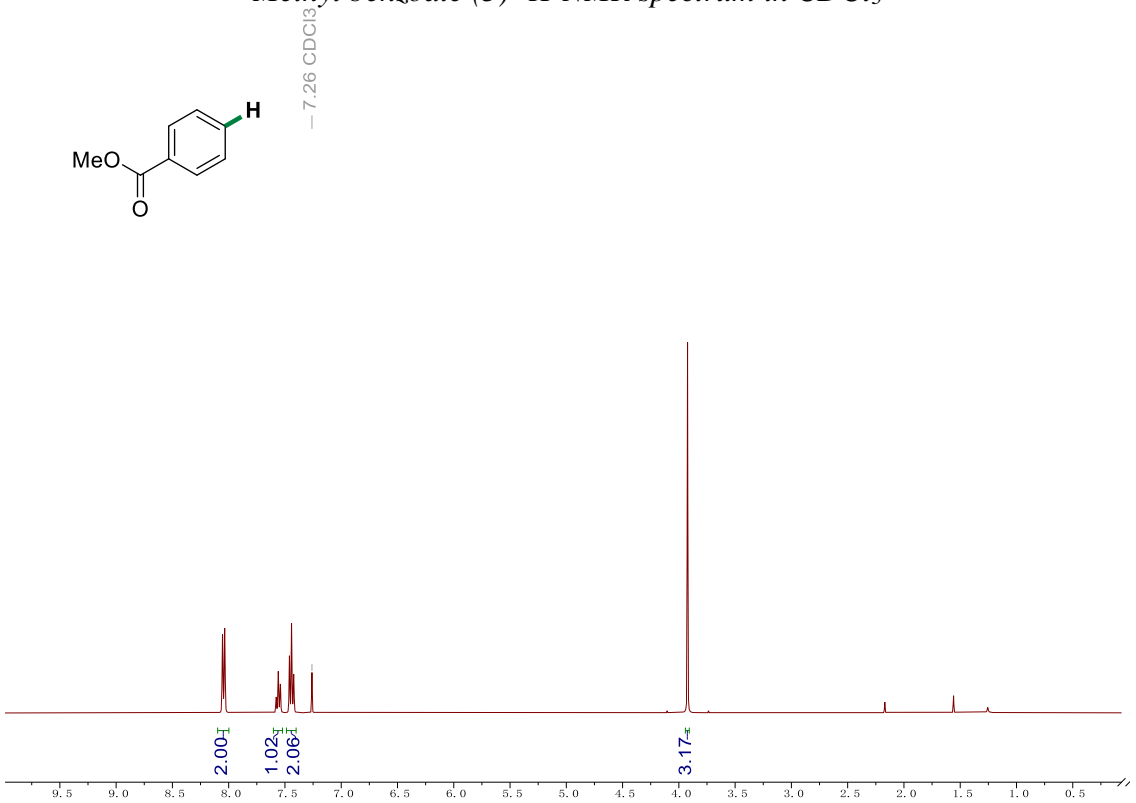

*Methyl benzoate (**5**) ^{13}C-NMR spectrum in $CDCl_3$*

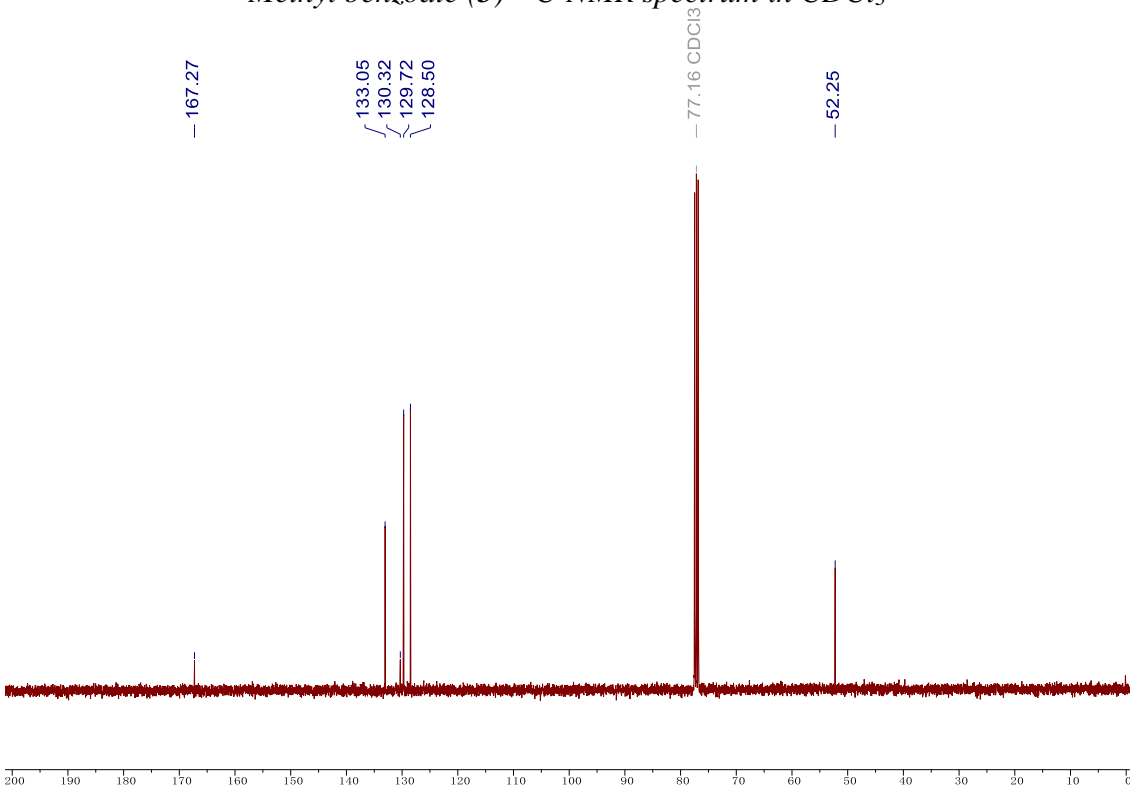

*2-Phenylethanol (**7**) ^{1}H-NMR spectrum in $CDCl_3$*

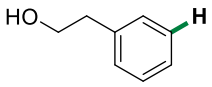

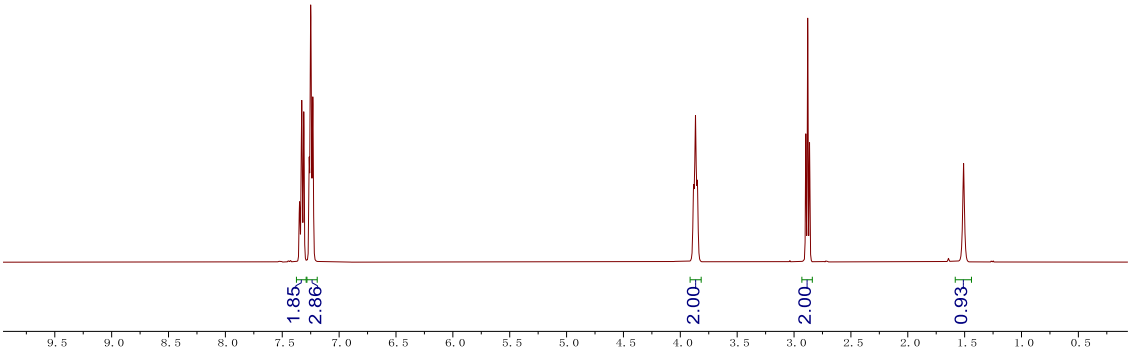

*2-Phenylethanol (**7**) ^{13}C-NMR spectrum in $CDCl_3$*

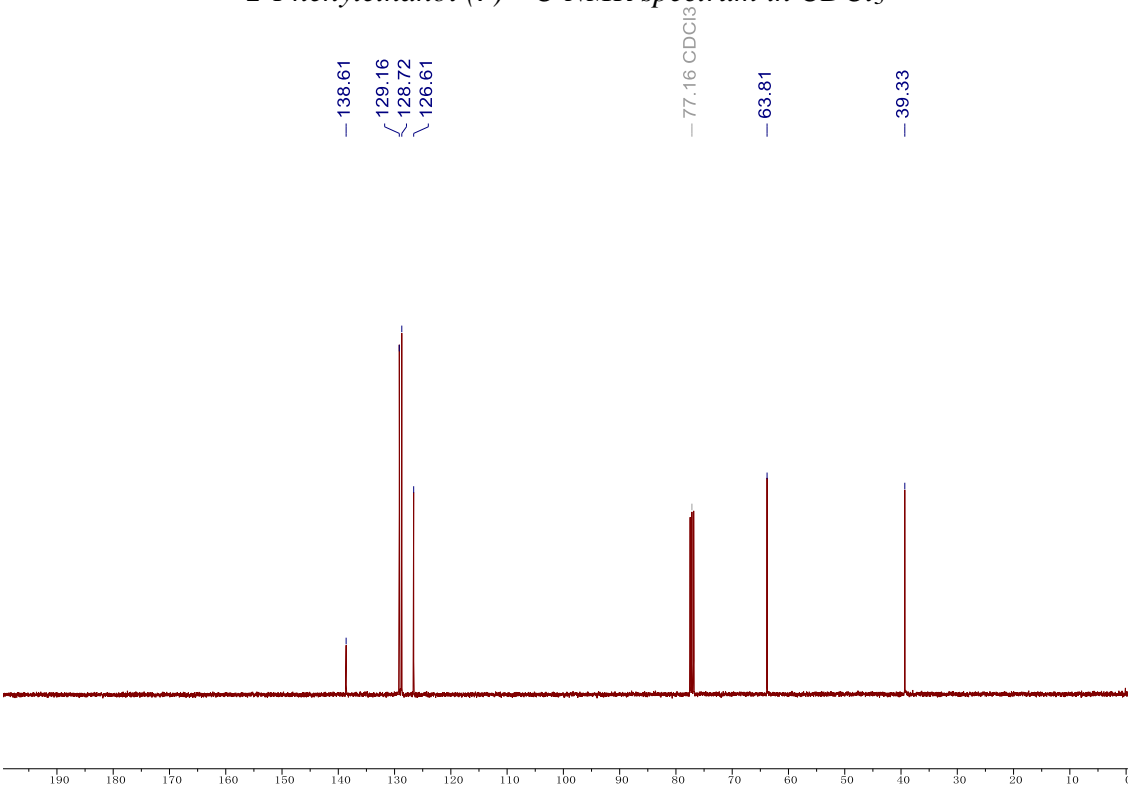

*3-Phenylpropionic acid (**8**) ^{1}H-NMR spectrum in $CDCl_3$*

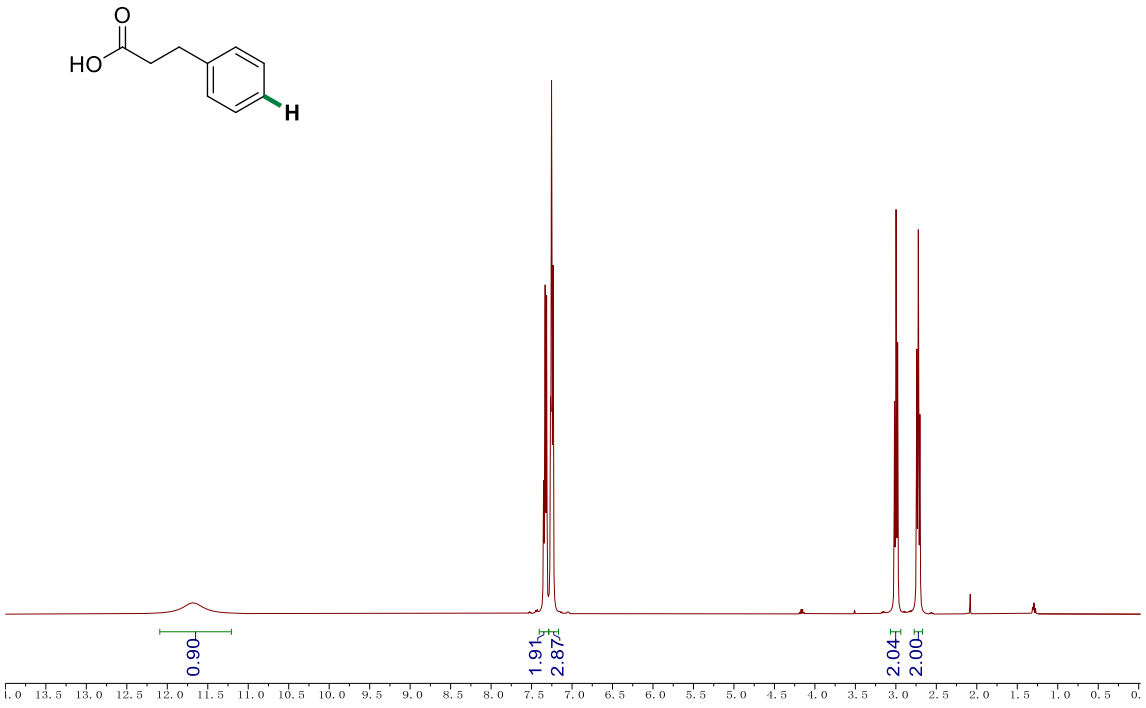

*3-Phenylpropionic acid (**8**) ^{13}C-NMR spectrum in $CDCl_3$*

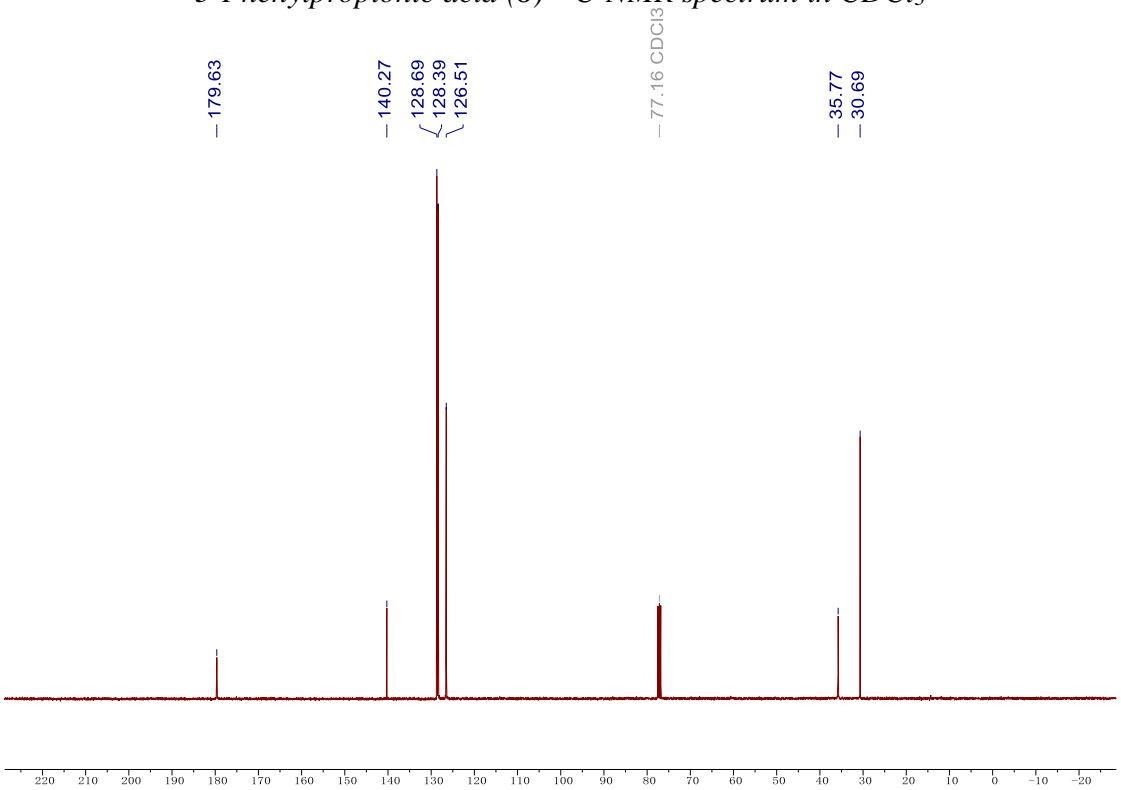

*1-Indanone (**9**) ^{1}H-NMR spectrum in $CDCl_3$*

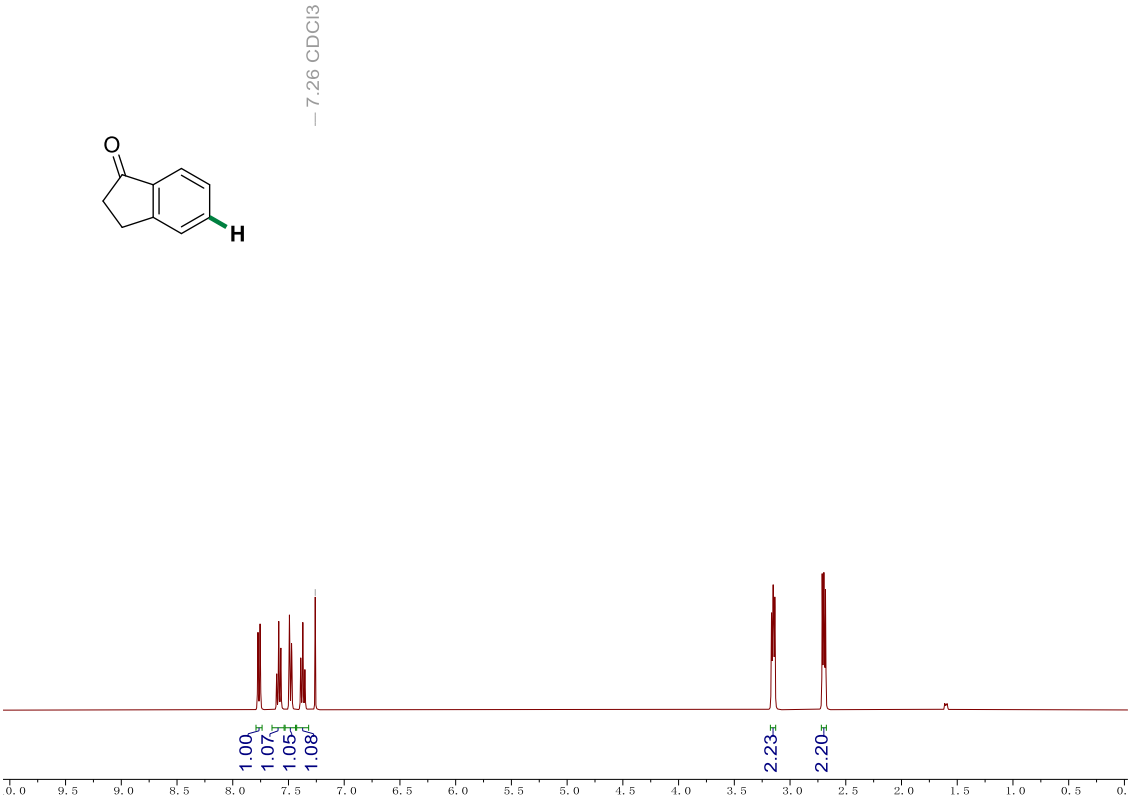

*1-Indanone (**9**) ^{13}C-NMR spectrum in $CDCl_3$*

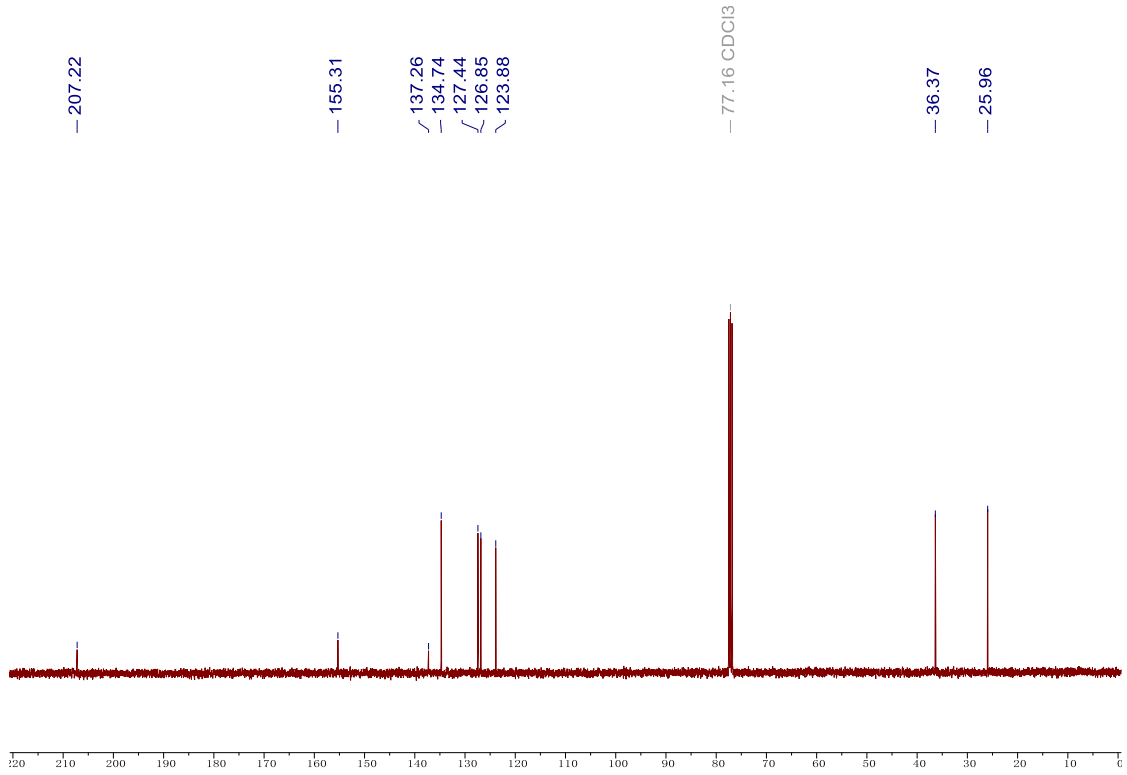

*tert-Butyl piperidinecarboxylate (**12**) ^{1}H-NMR spectrum in $CDCl_3$*

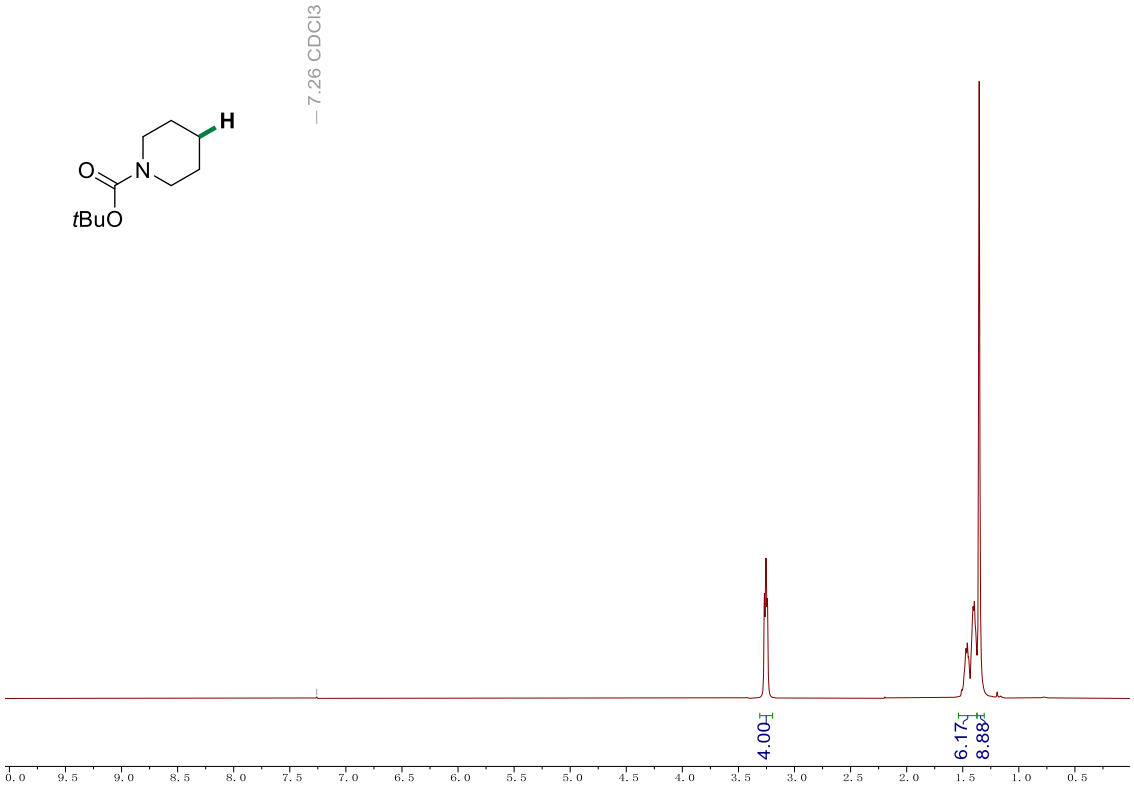

*tert-Butyl piperidinecarboxylate (**12**) ^{13}C-NMR spectrum in $CDCl_3$*

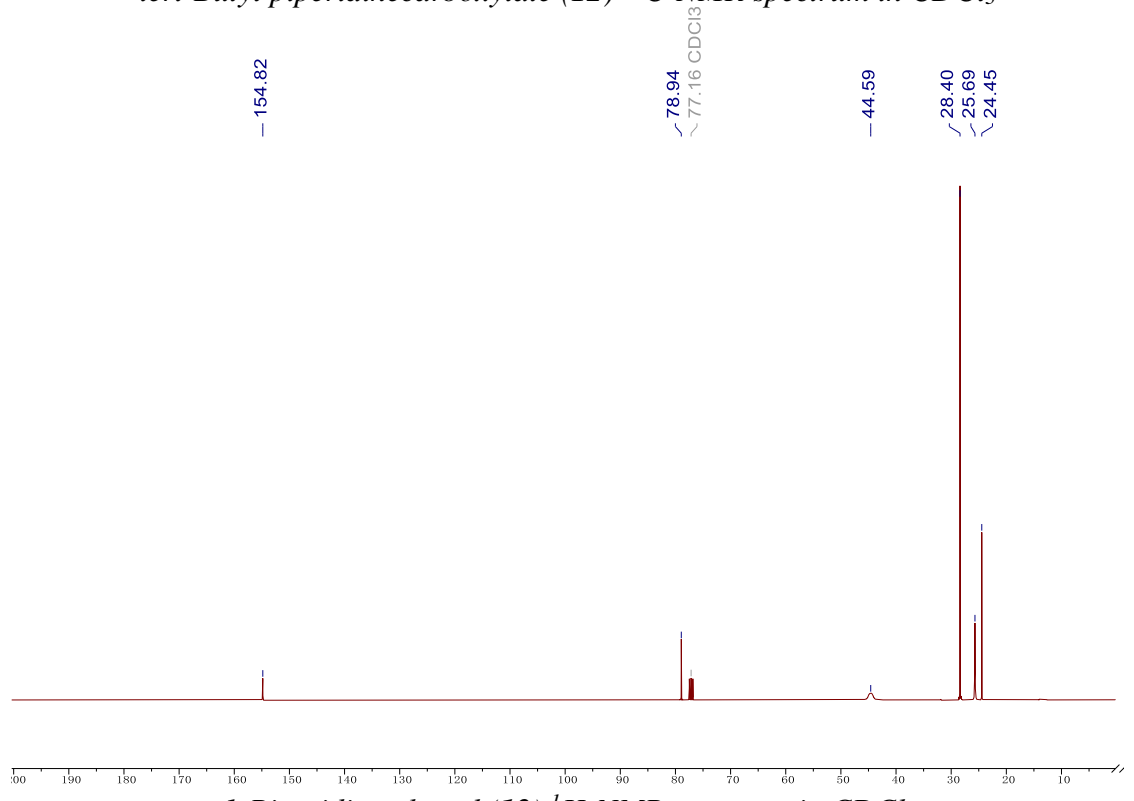

*1-Piperidinoethanol (**13**) ^{1}H-NMR spectrum in $CDCl_3$*

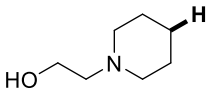

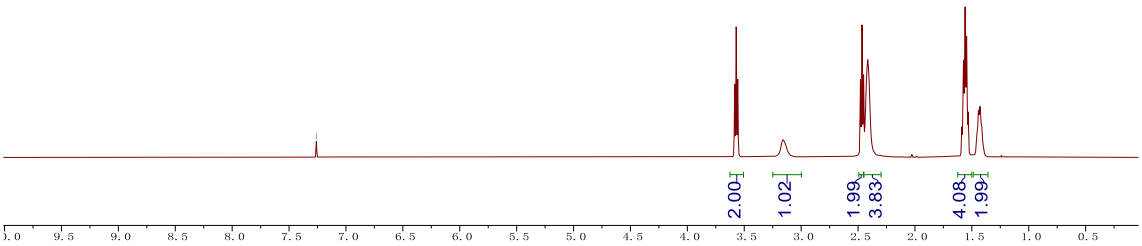

*1-Piperidinoethanol (**13**) ^{13}C-NMR spectrum in $CDCl_3$*

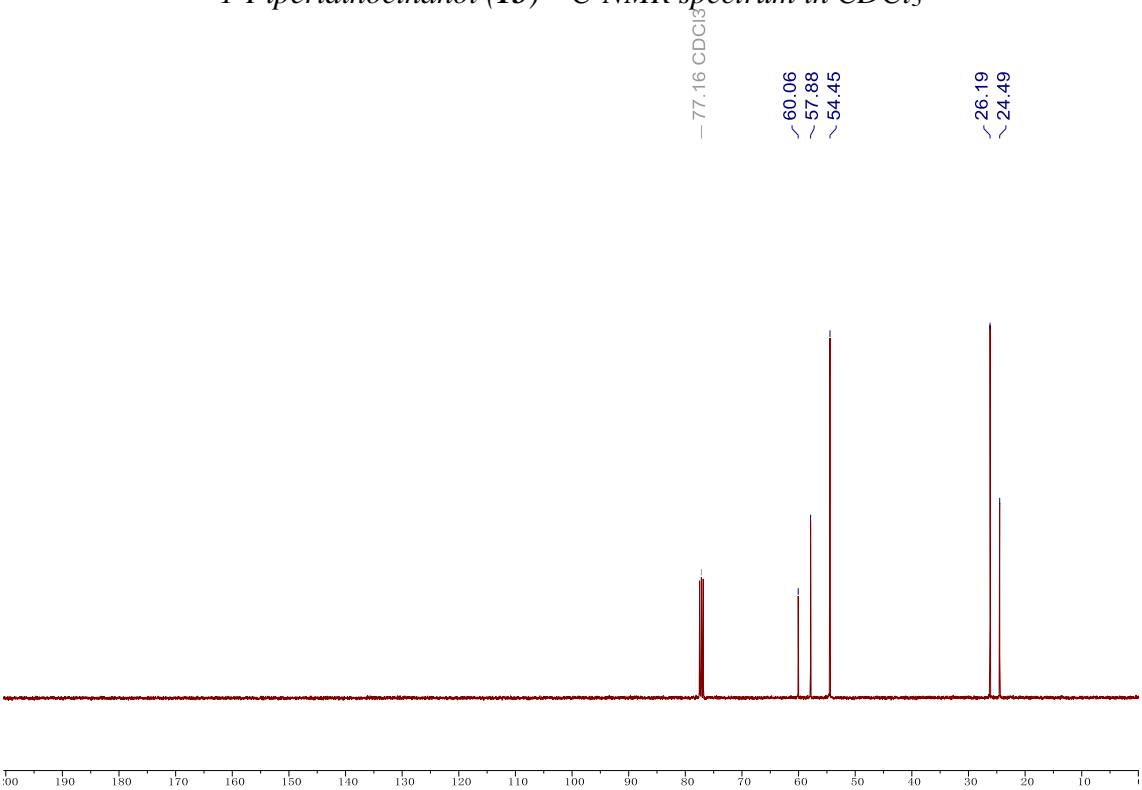

*1-Benzyloxycarbonyl piperidine (**14**) ^{1}H-NMR spectrum in $CDCl_3$*

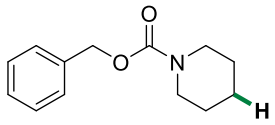

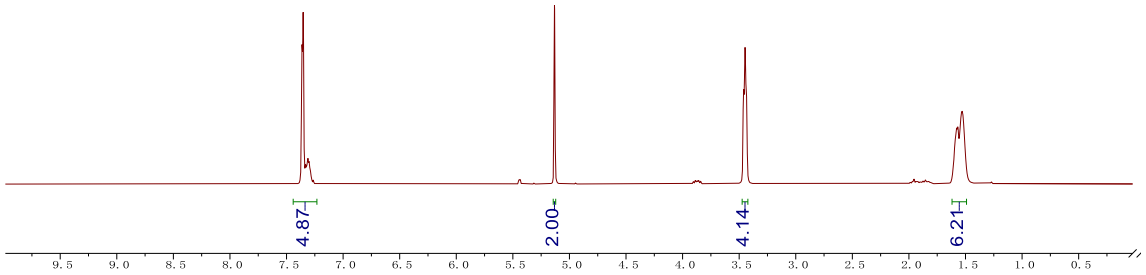

*1-Benzyloxycarbonyl piperidine (**14**) ^{13}C-NMR spectrum in $CDCl_3$*

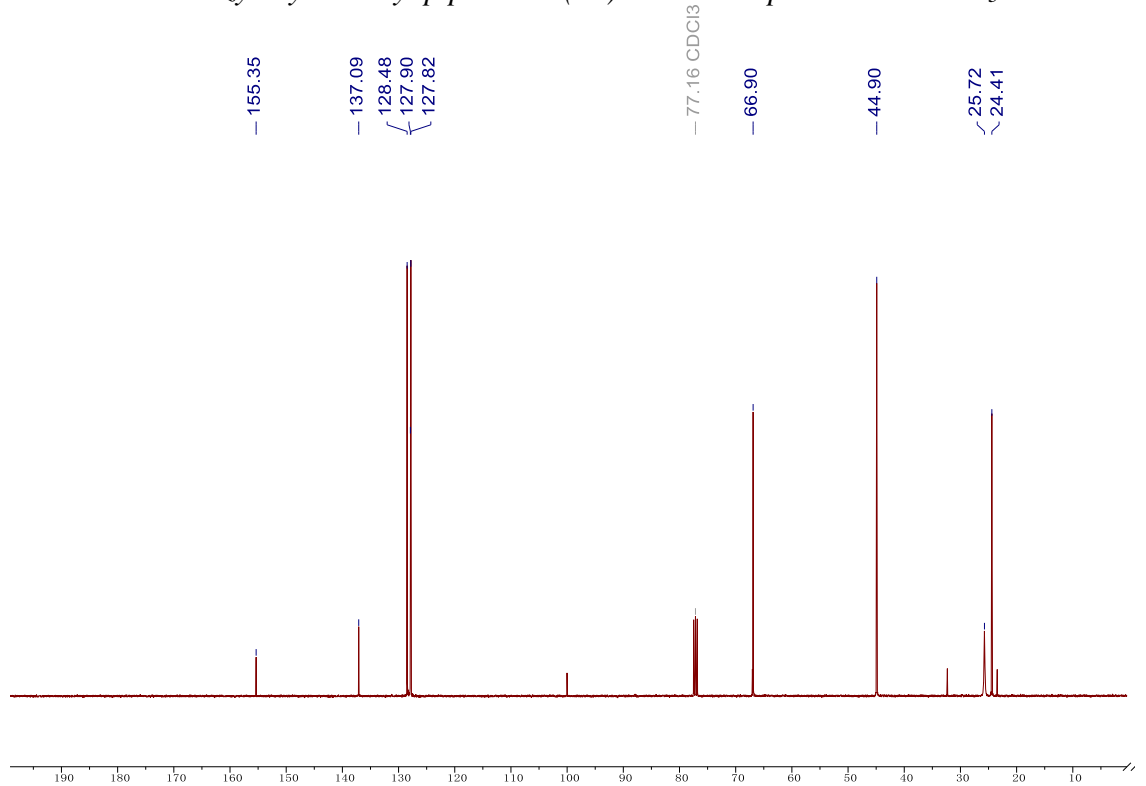

*2-Methylnaphthalene (**15**) ^{1}H-NMR spectrum in $CDCl_3$*

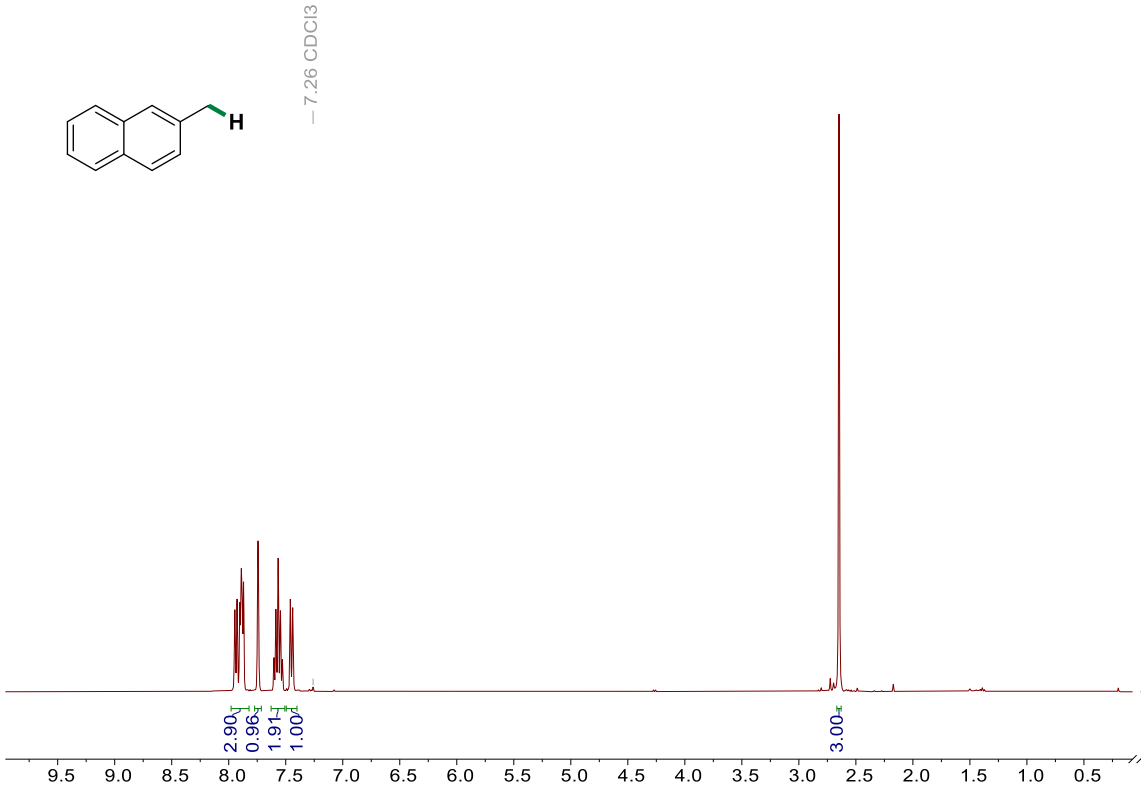

*2-Methylnaphthalene (**15**) ^{13}C-NMR spectrum in $CDCl_3$*

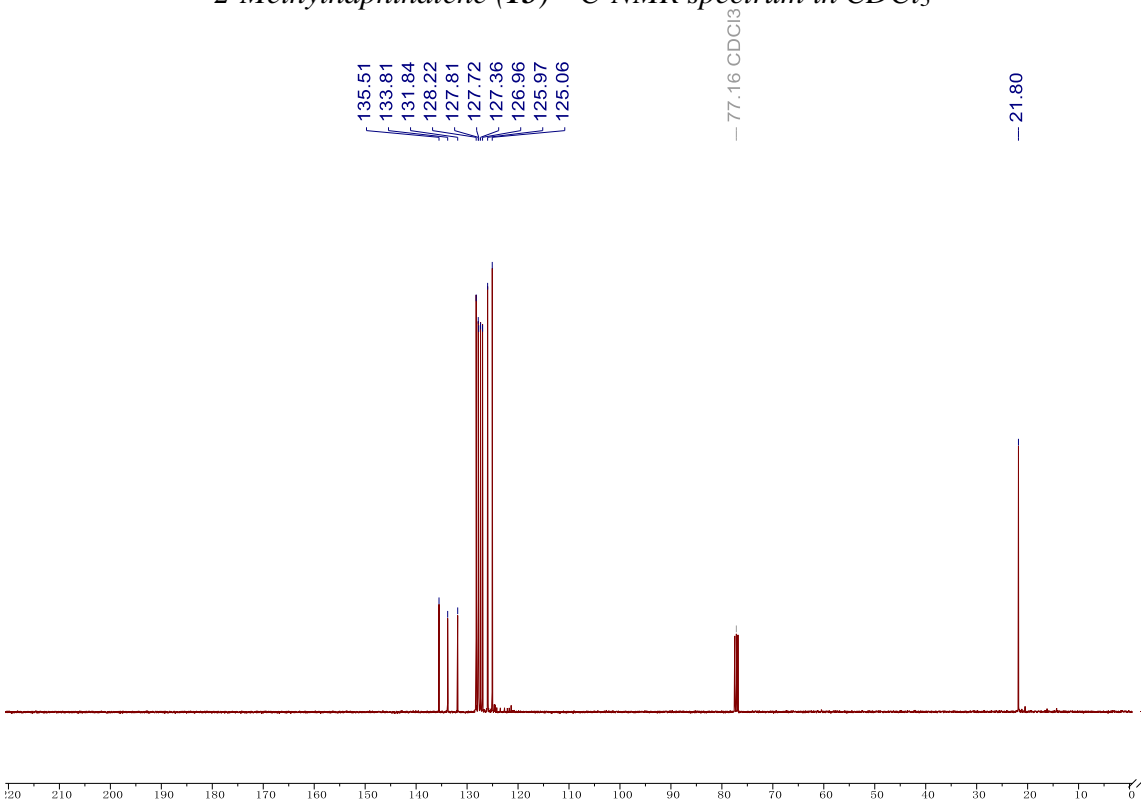

*4-Methylanisole (**17**) ^{1}H-NMR spectrum in $CDCl_3$*

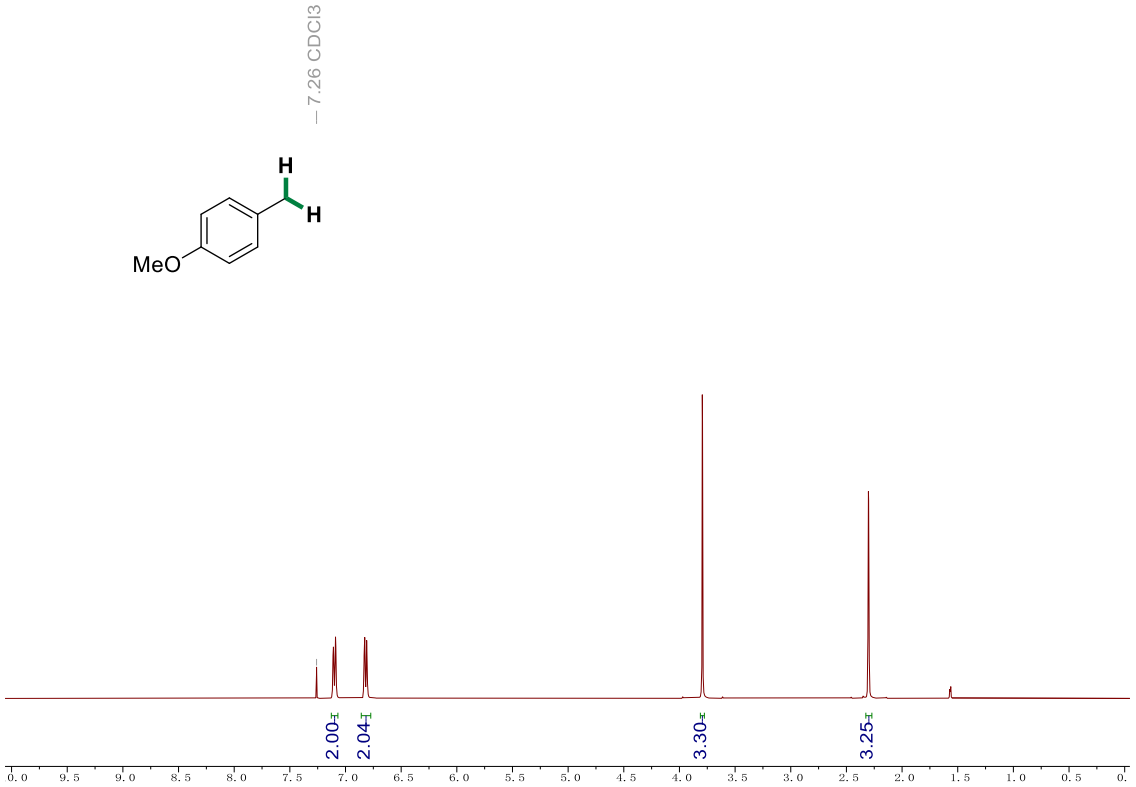

*4-Methylanisole (**17**) ^{13}C-NMR spectrum in $CDCl_3$*

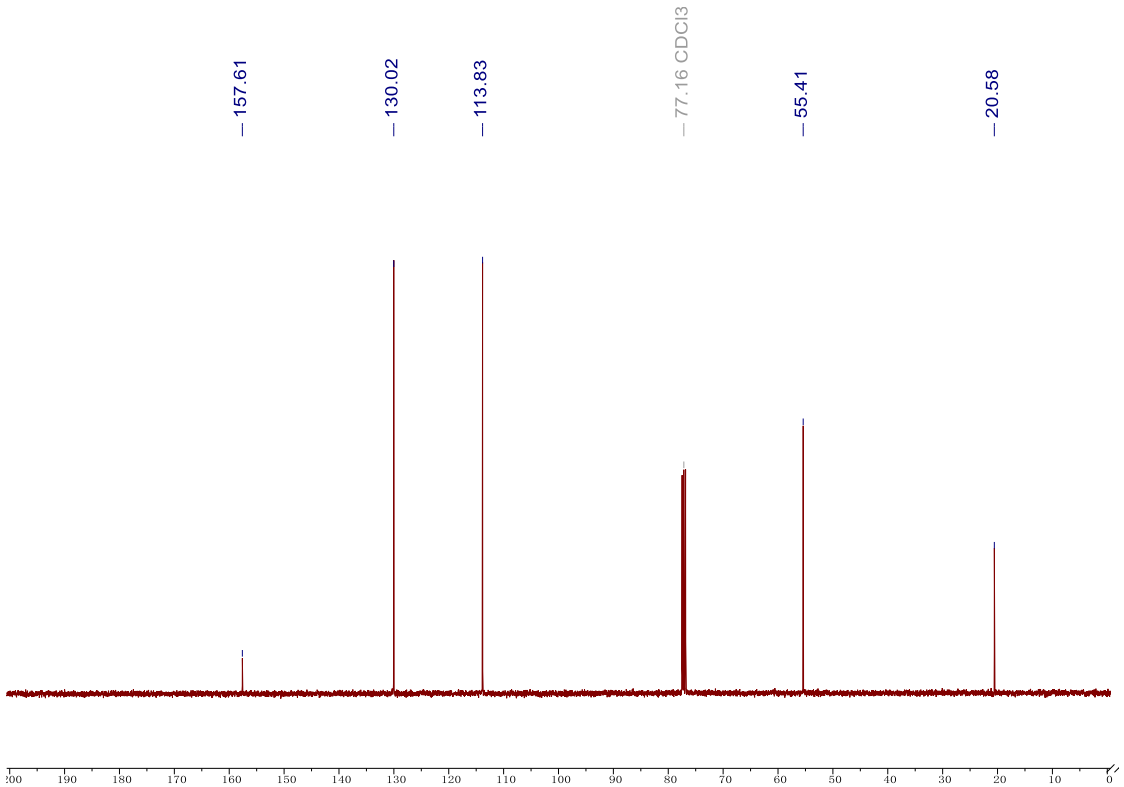

*4-methylbenzonitrile (**18**) ^{1}H-NMR spectrum in $CDCl_3$*

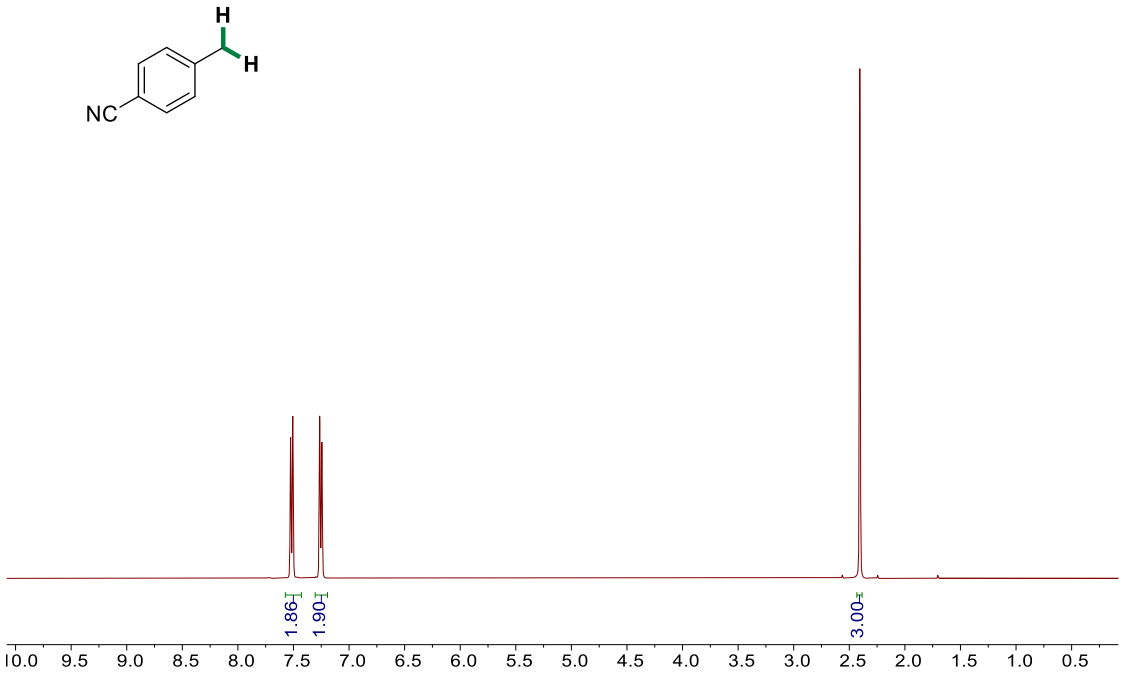

*4-methylbenzonitrile (**18**) ^{13}C-NMR spectrum in $CDCl_3$*

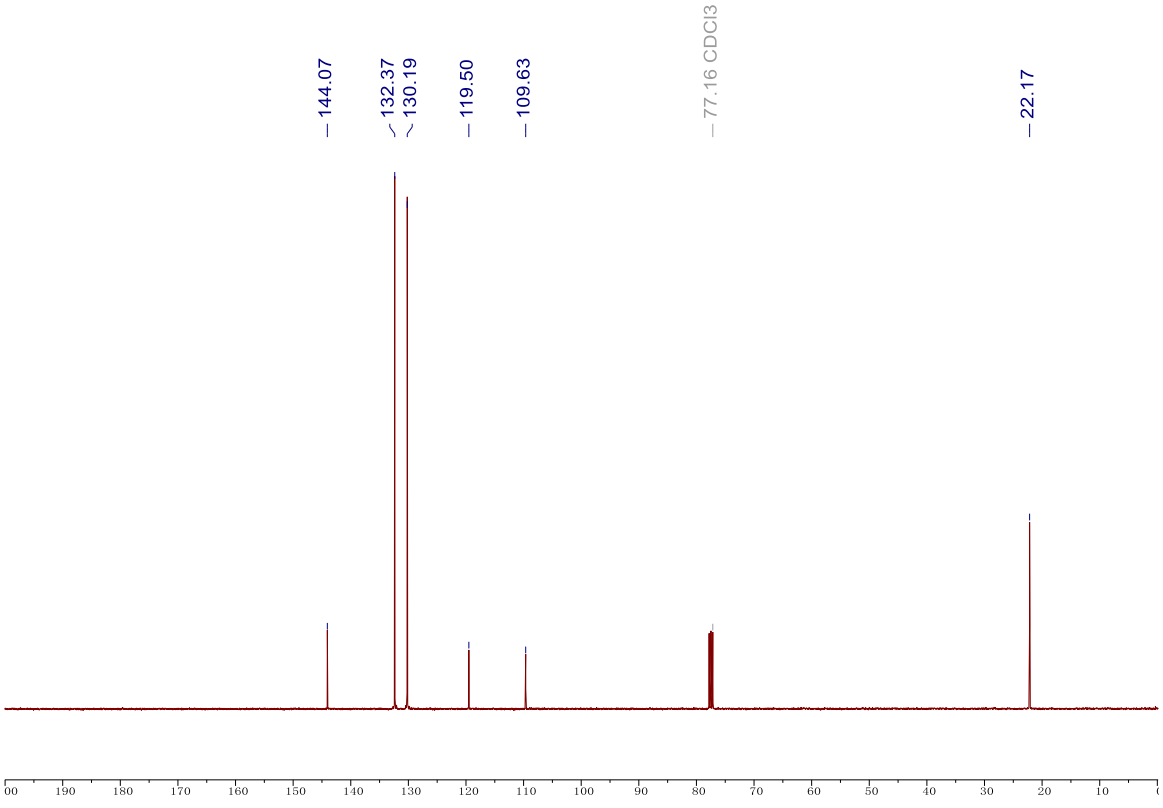

*Methylenedioxybenzene (**21**) ^{1}H-NMR spectrum in $CDCl_3$*

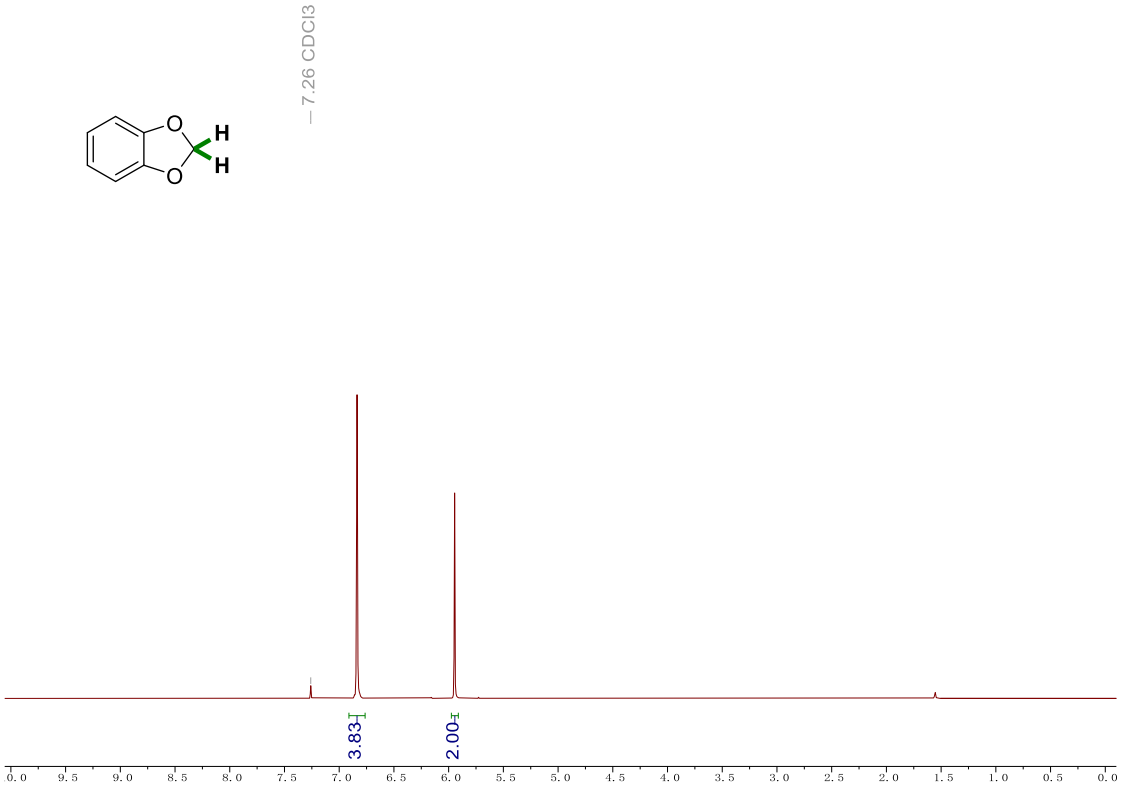

*Methylenedioxybenzene (**21**) ^{13}C-NMR spectrum in $CDCl_3$*

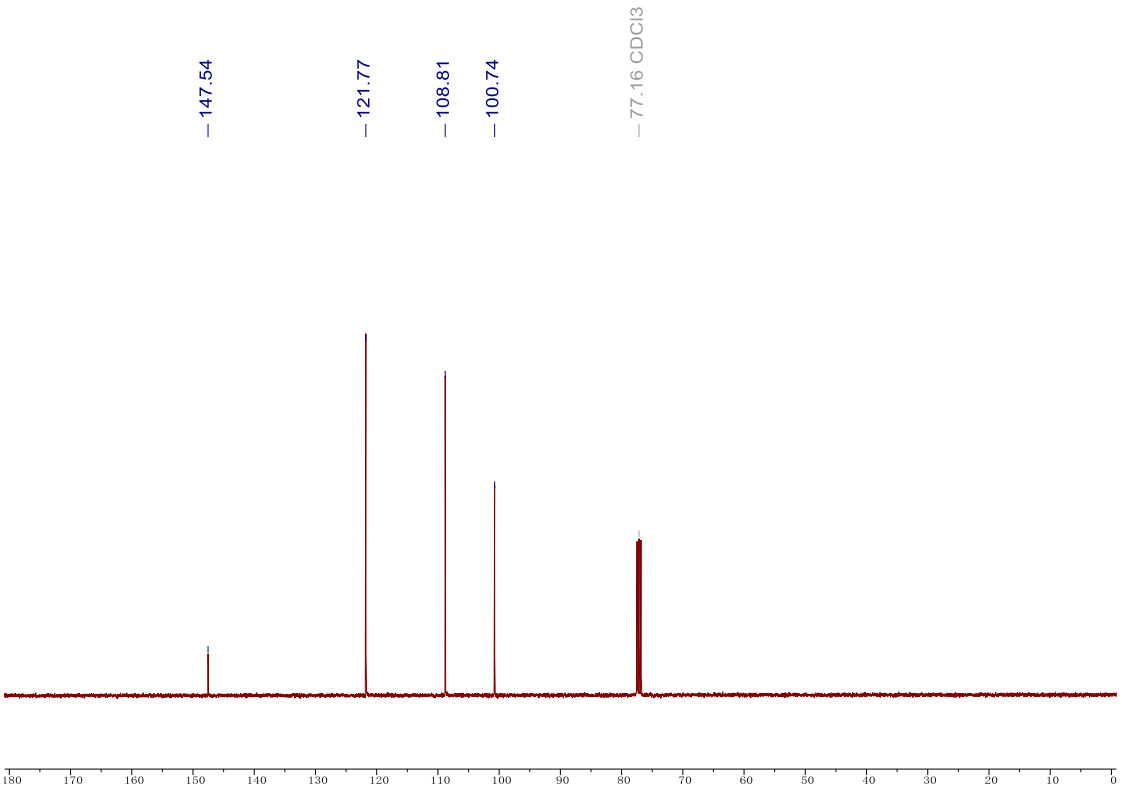

*4-Methyl-benzoic acid methyl ester (**22**) ^{1}H-NMR spectrum in $CDCl_3$*

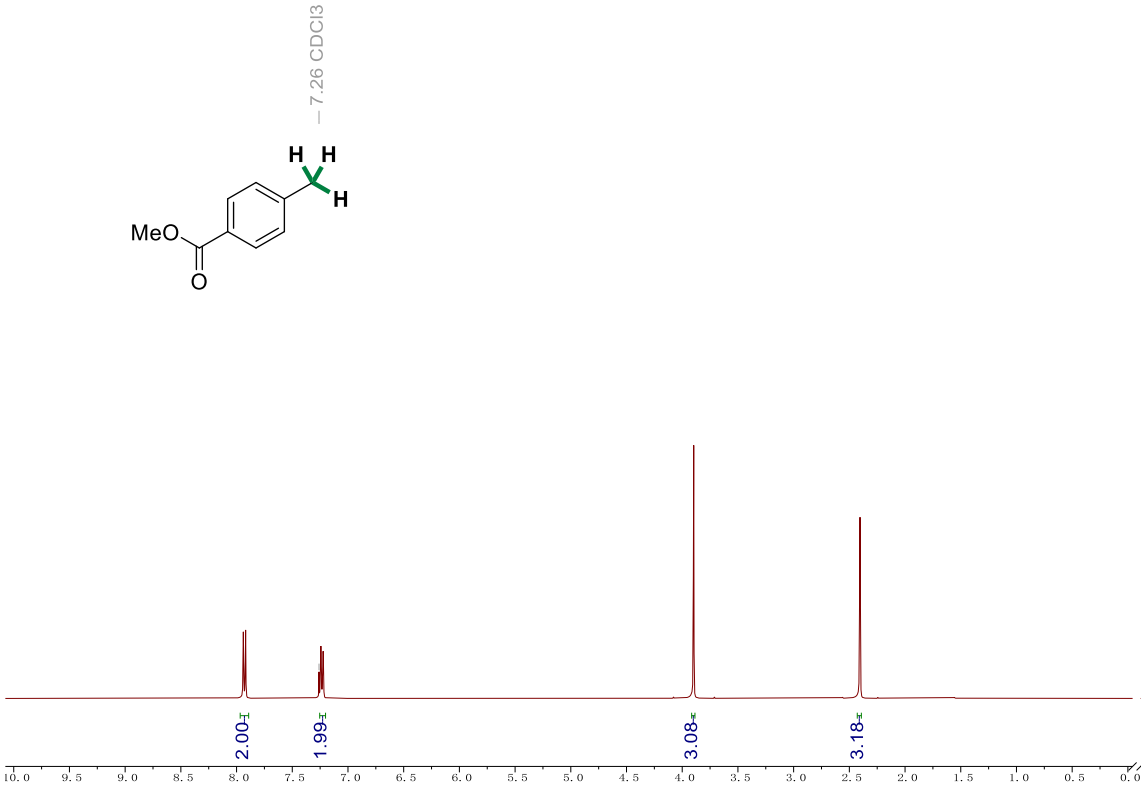

*4-Methyl-benzoic acid methyl ester (**22**) ^{13}C-NMR spectrum in $CDCl_3$*

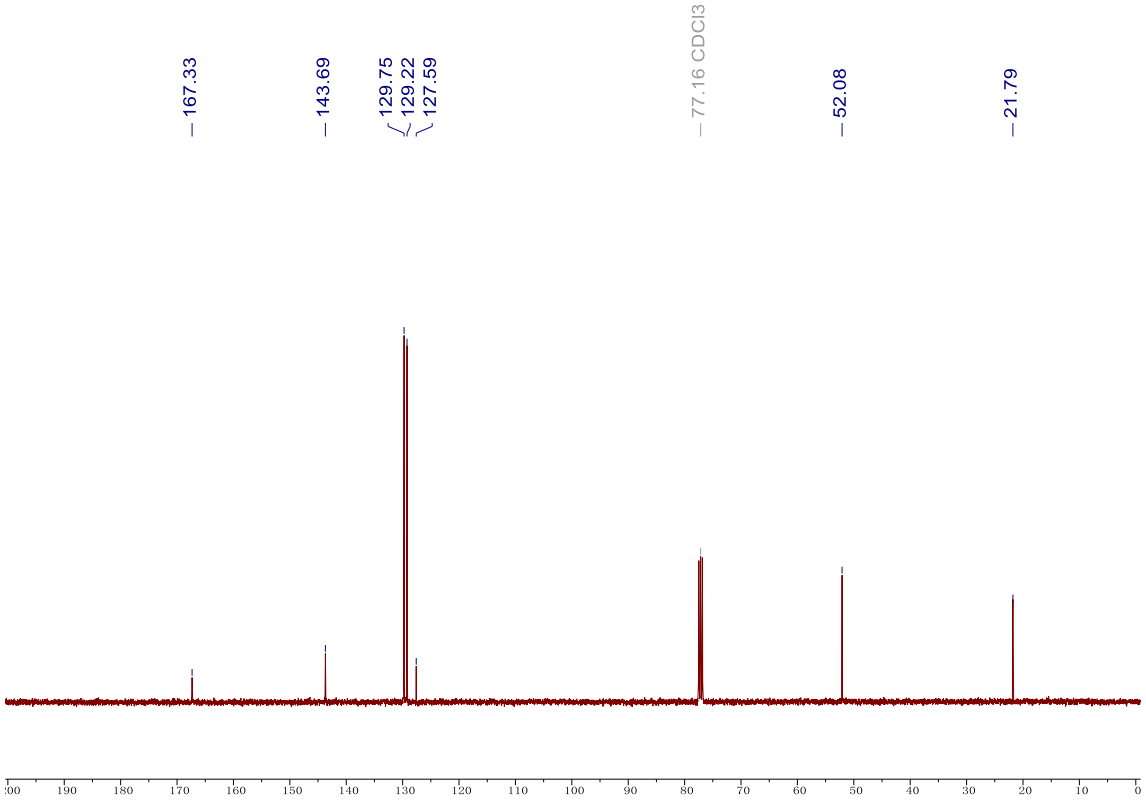

*(4-methylphenyl)Acetonitrile (**23**) ^{1}H-NMR spectrum in $CDCl_3$*

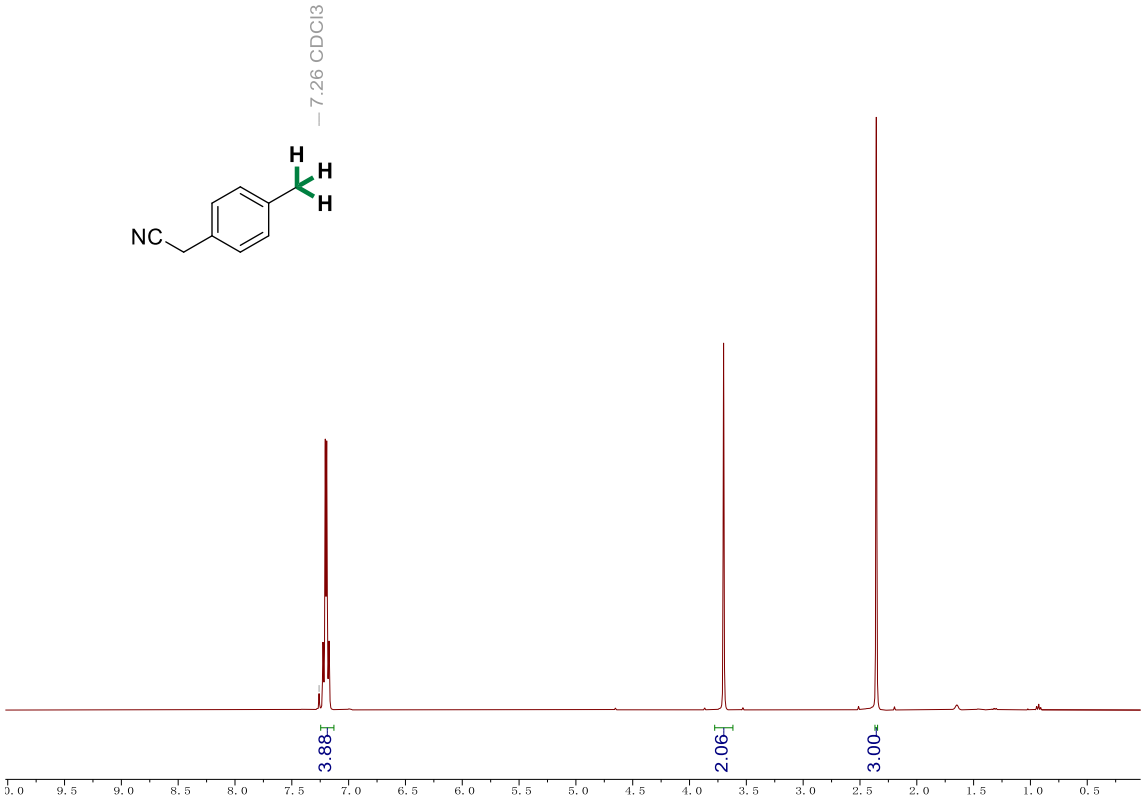

*(4-methylphenyl)Acetonitrile (**23**) ^{13}C-NMR spectrum in $CDCl_3$*

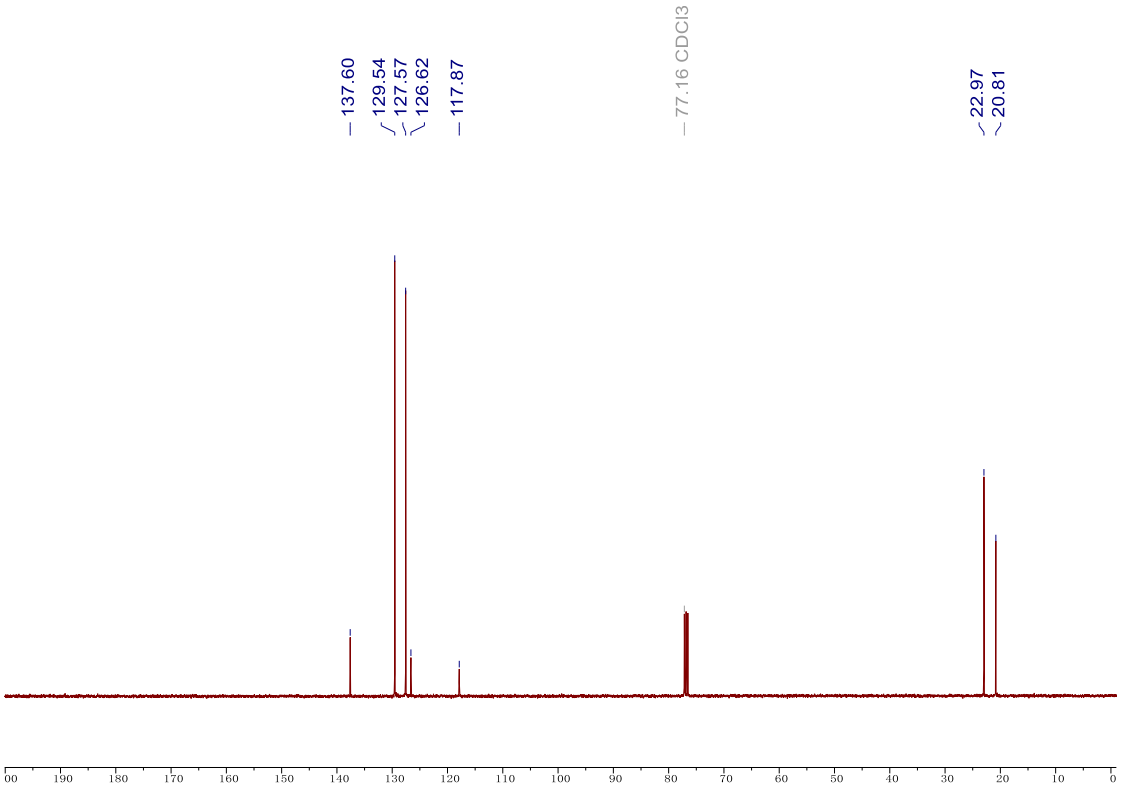

*6-O-benzyl-1,2:3,4-di-O-isopropylidene-α-D-galactopyranos (**25**) ^{1}H-NMR spectrum in $CDCl_3$*

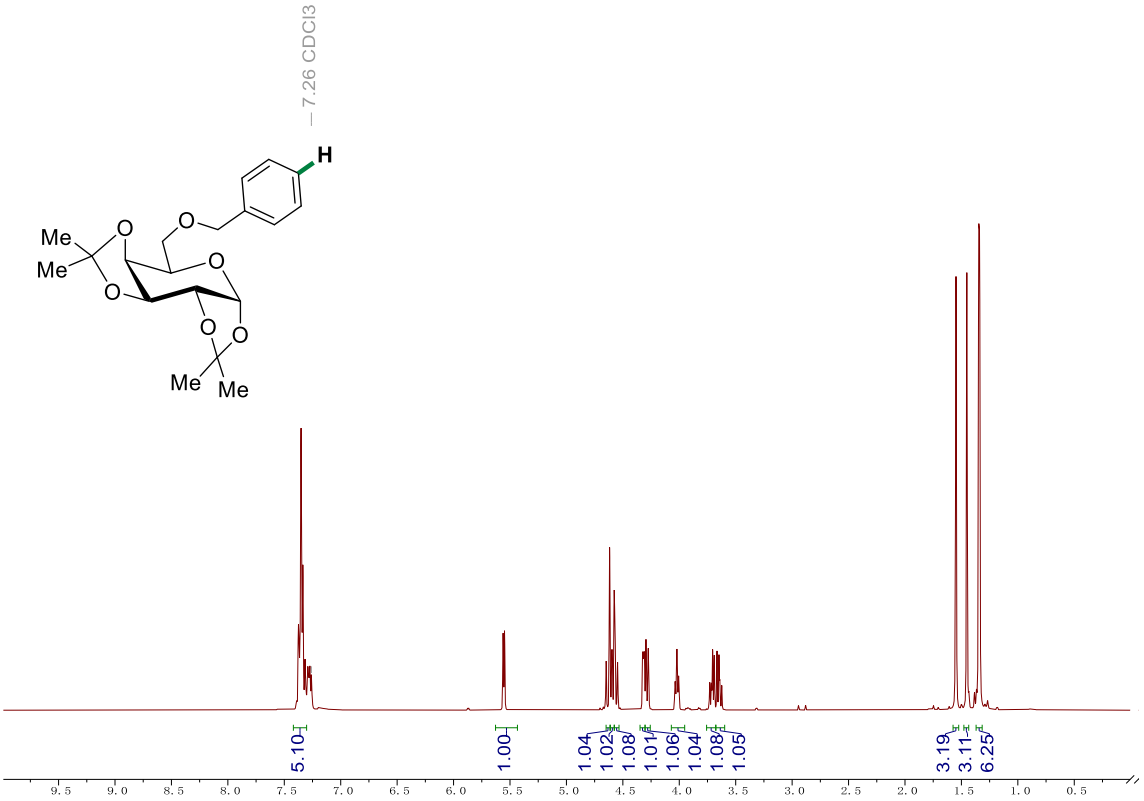

*6-O-benzyl-1,2:3,4-di-O-isopropylidene-α-D-galactopyranos (**25**) ^{13}C-NMR spectrum in $CDCl_3$*

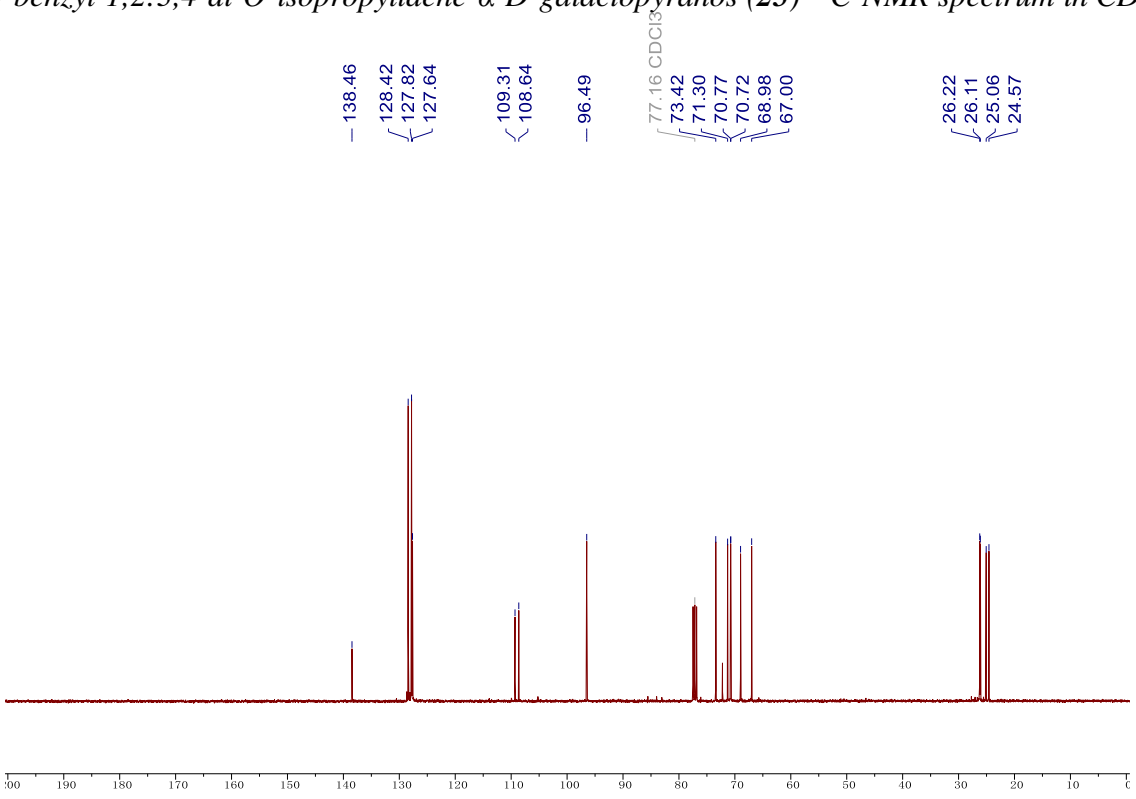

*2-(isopropyl)-5-Methylphenyl benzyl ether (**26**) ^{1}H-NMR spectrum in $CDCl_3$*

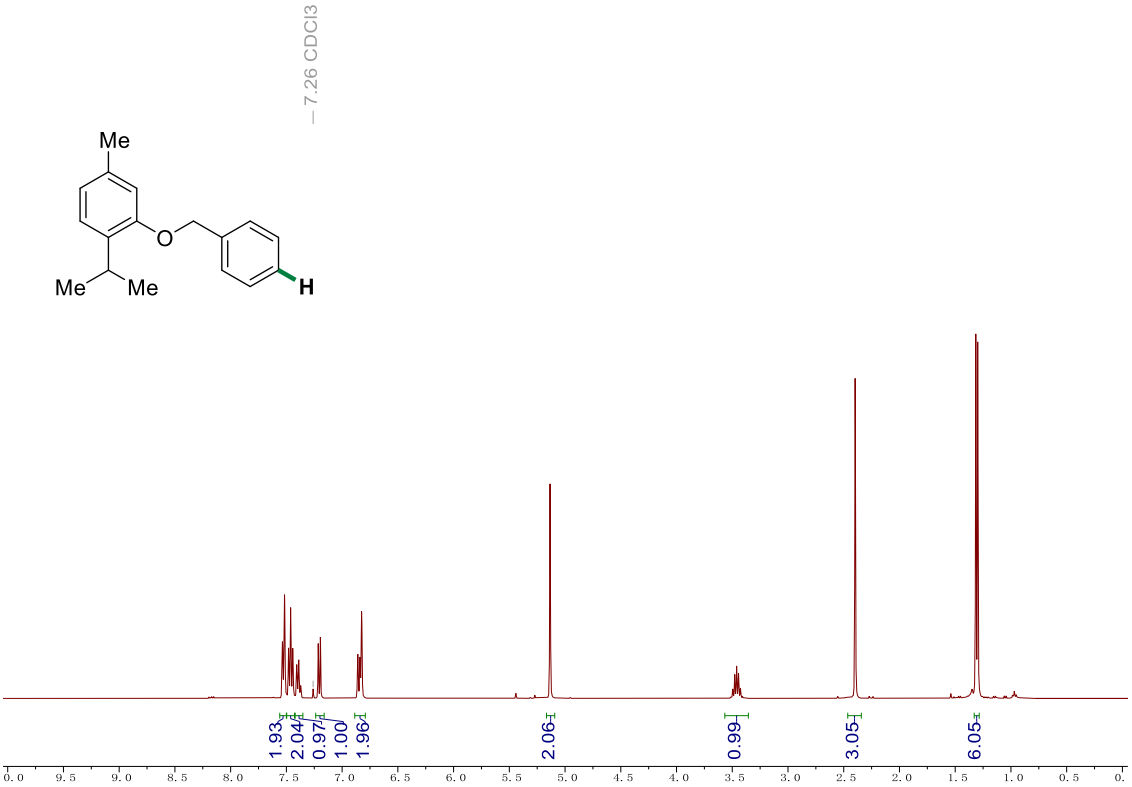

*2-(isopropyl)-5-Methylphenyl benzyl ether (**26**) ^{13}C-NMR spectrum in $CDCl_3$*

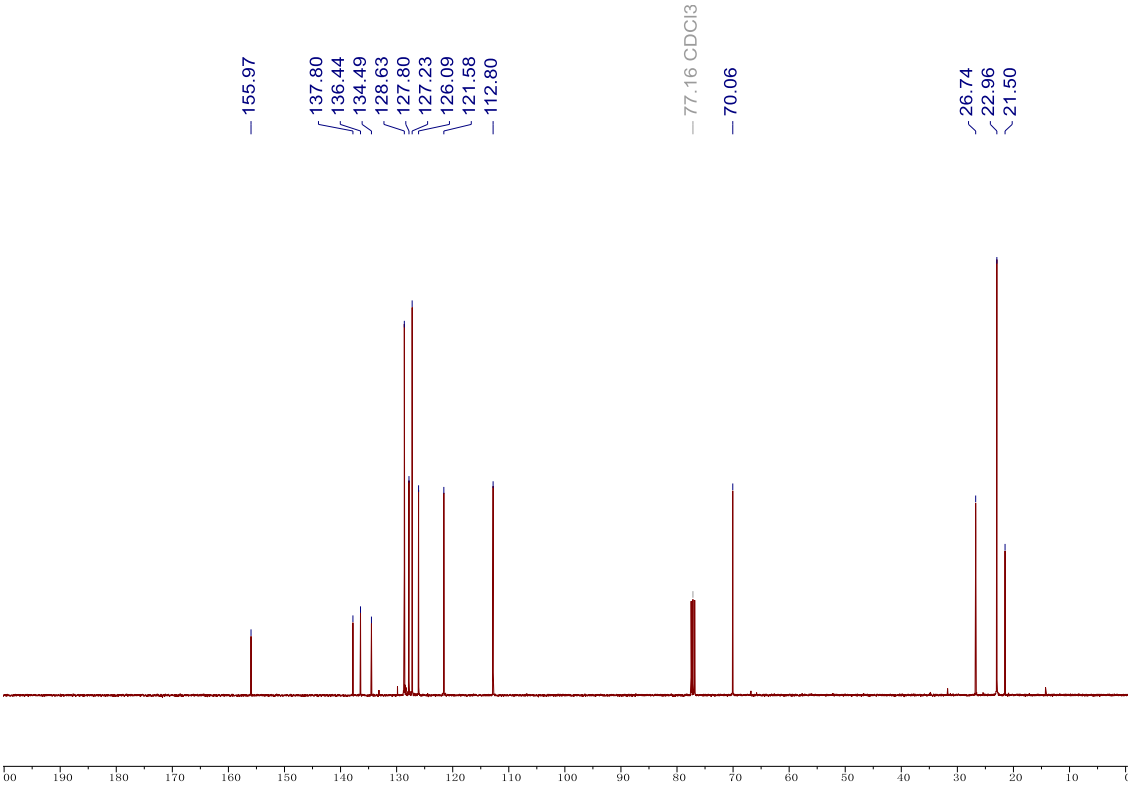

*N-benzyl-N-methyl-2-(pyridin-2-yl)ethanamine (**27**) ^{1}H-NMR spectrum in $CDCl_3$*

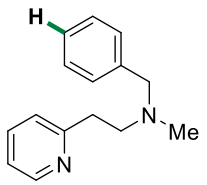

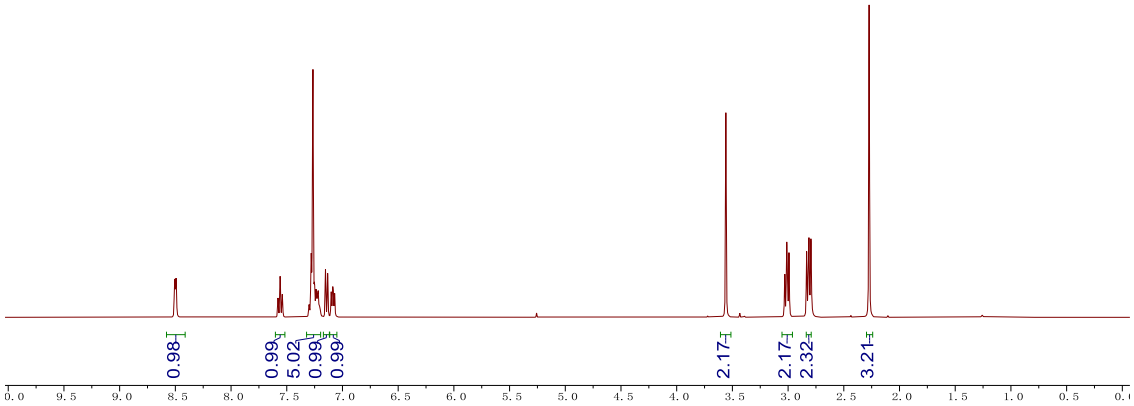

*N-benzyl-N-methyl-2-(pyridin-2-yl)ethanamine (**27**) ^{13}C-NMR spectrum in $CDCl_3$*

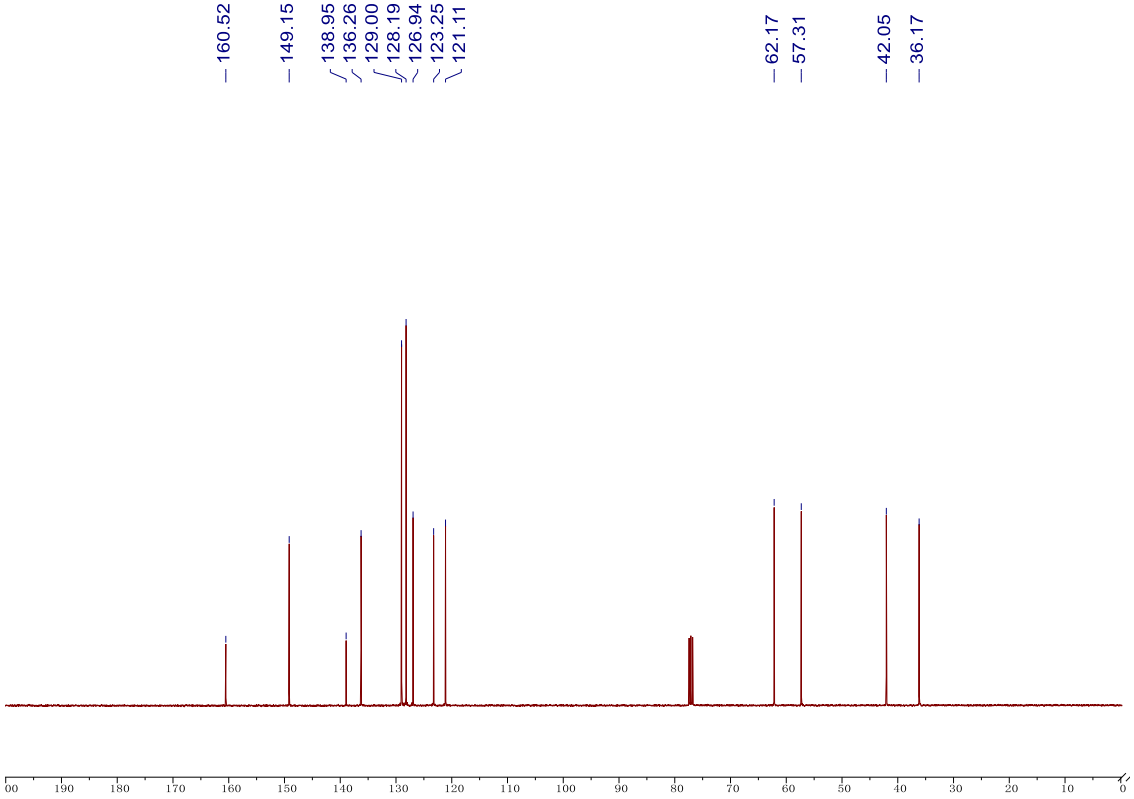

*Estrone 3-benzoate (**28**) ^{1}H-NMR spectrum in $CDCl_3$*

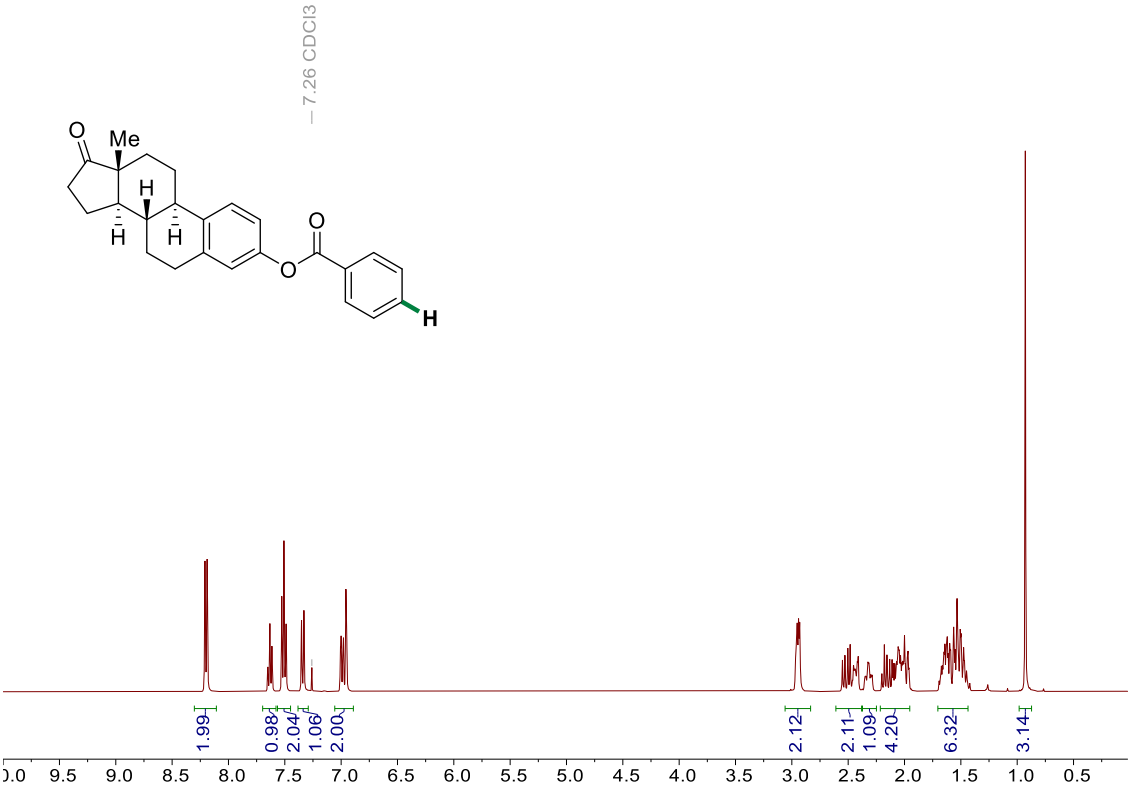

*Estrone 3-benzoate (**28**) ^{13}C-NMR spectrum in $CDCl_3$*

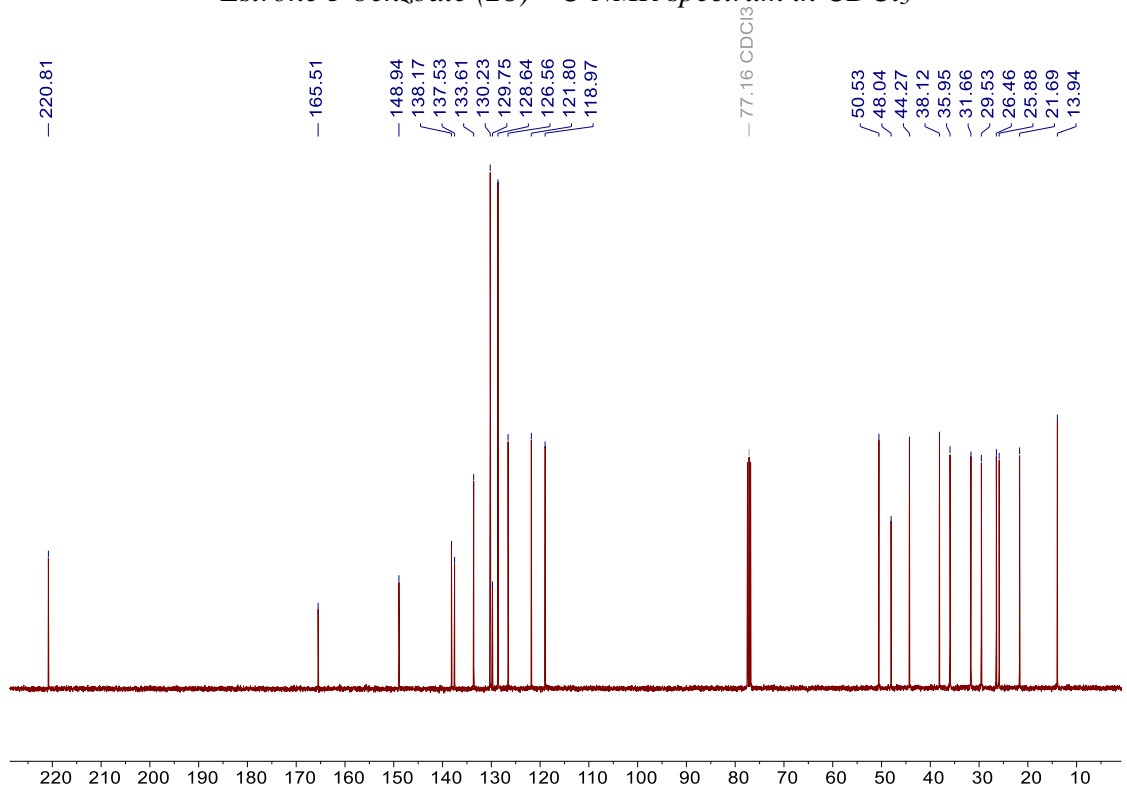

*N-benzylpropanamide (**29**) ^{1}H-NMR spectrum in $CDCl_3$*

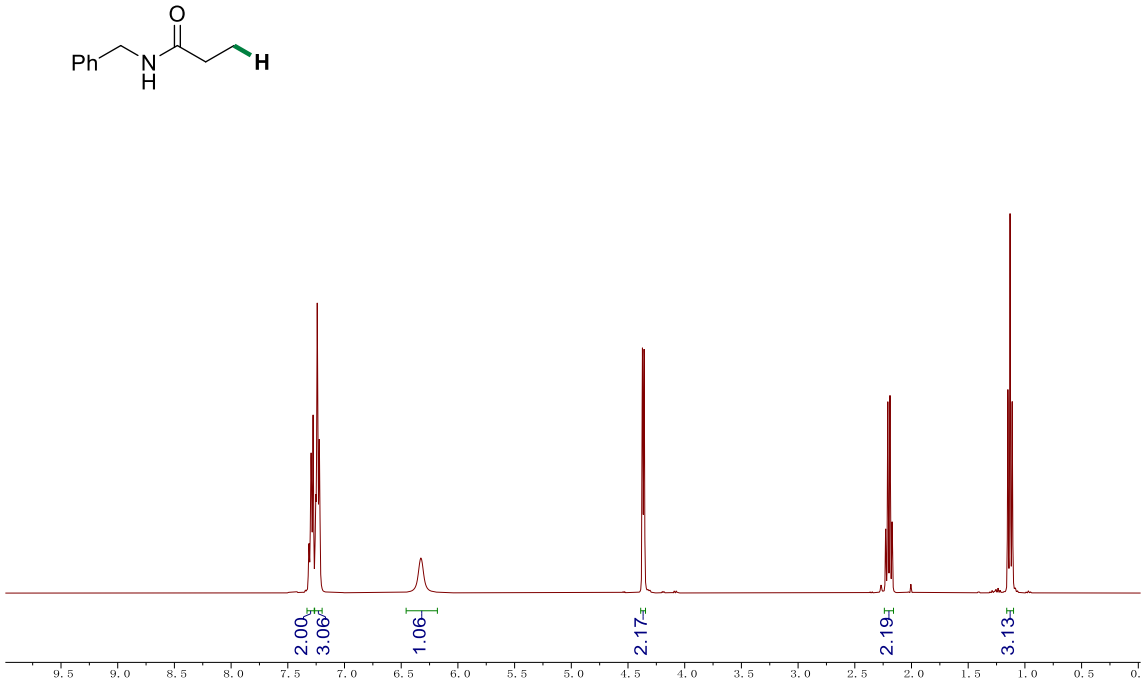

*N-benzylpropanamide (**29**) ^{13}C-NMR spectrum in $CDCl_3$*

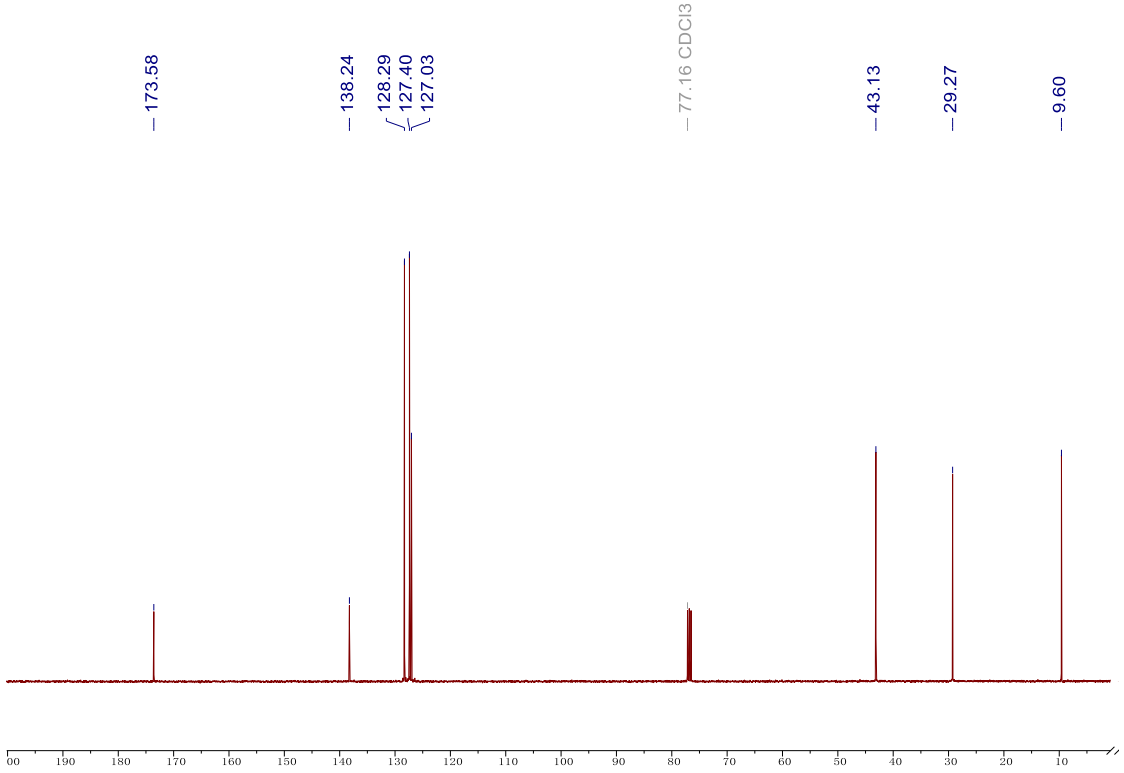

*Impramine (**30**) ^{1}H-NMR spectrum in $CDCl_3$*

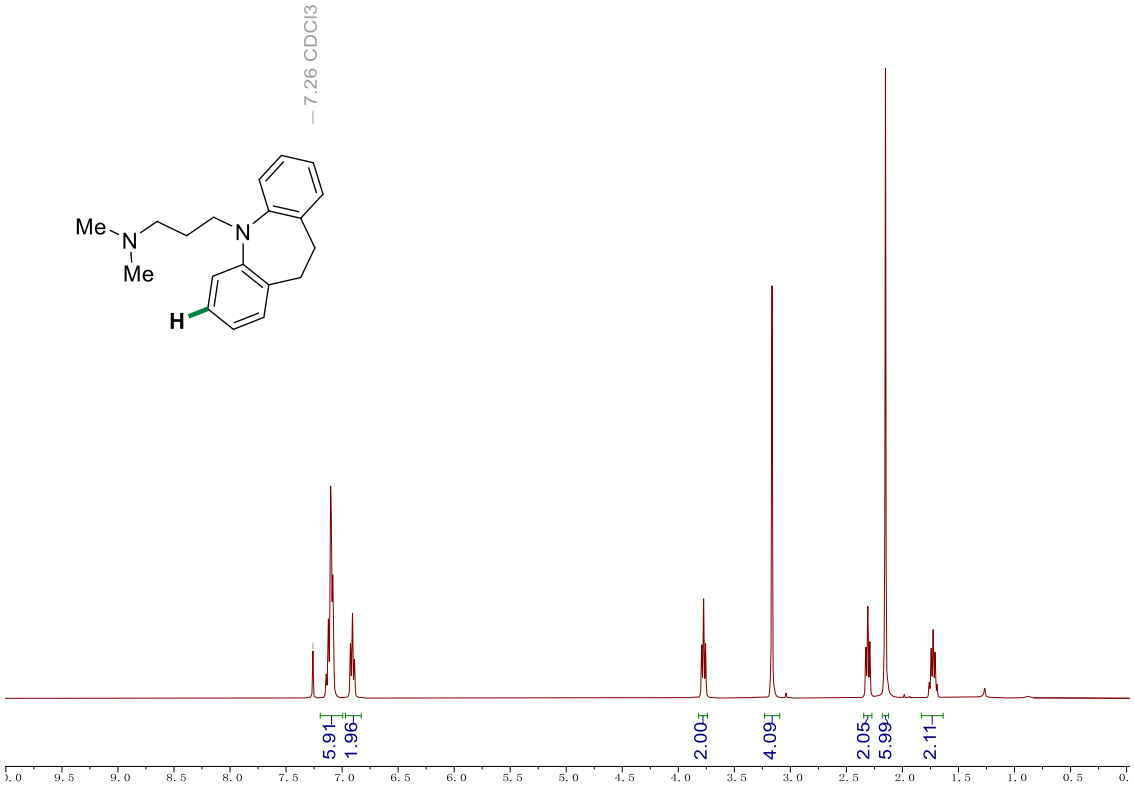

*Impramine (**30**) ^{13}C-NMR spectrum in $CDCl_3$*

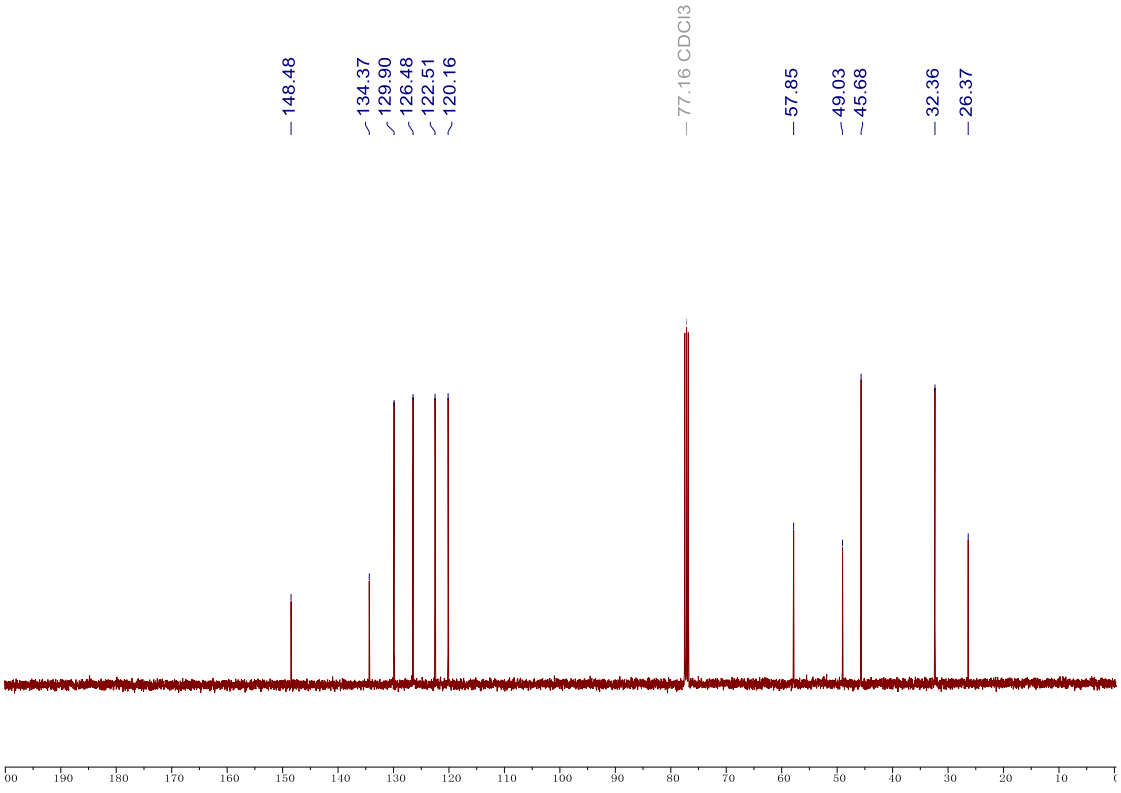

*(4-(isopropoxy)phenyl)(phenyl)Methanone (**31**) ^{1}H-NMR spectrum in $CDCl_3$*

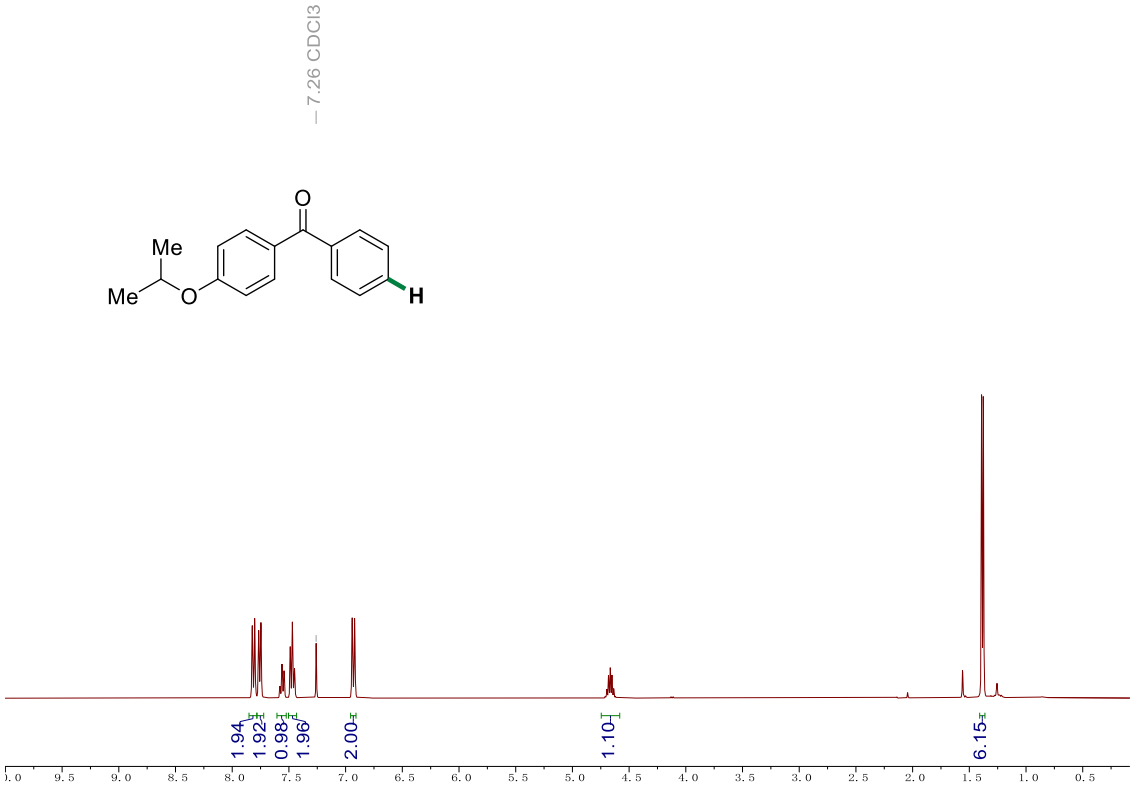

*(4-(isopropoxy)phenyl)(phenyl)Methanone (**31**) ^{13}C-NMR spectrum in $CDCl_3$*

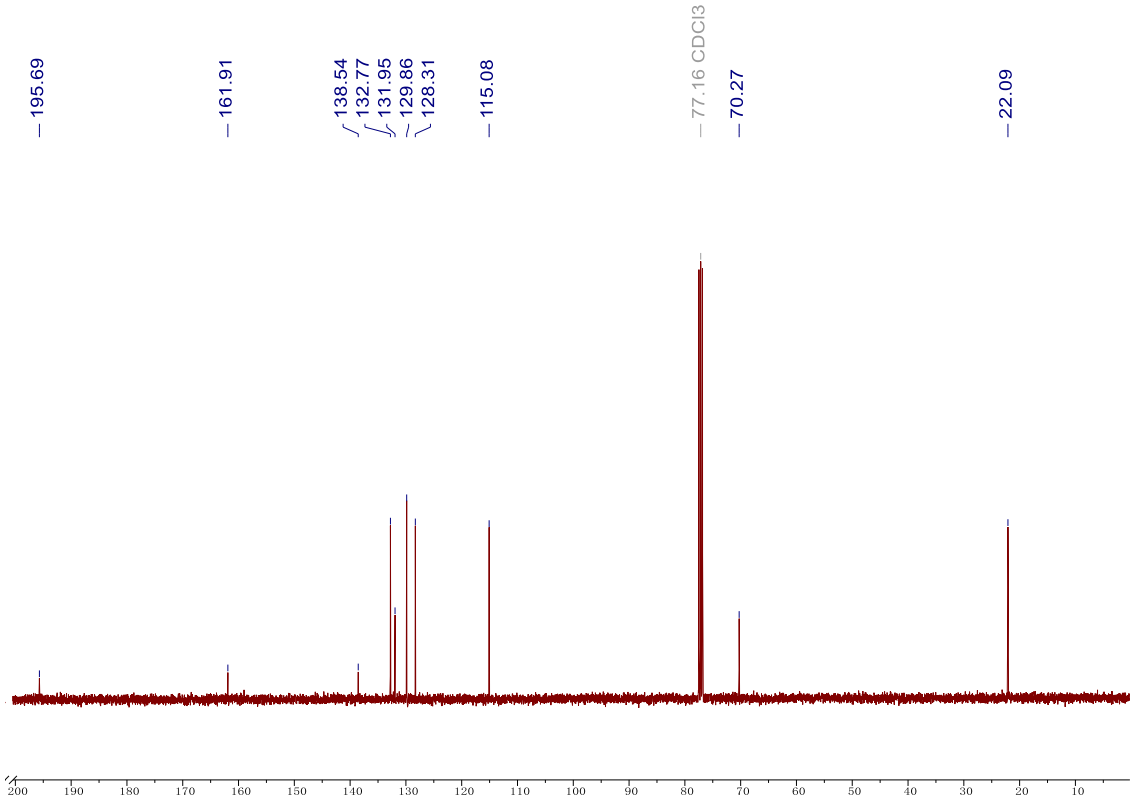

*2-Phenoxyphenol (**32**) ^{1}H-NMR spectrum in $CDCl_3$*

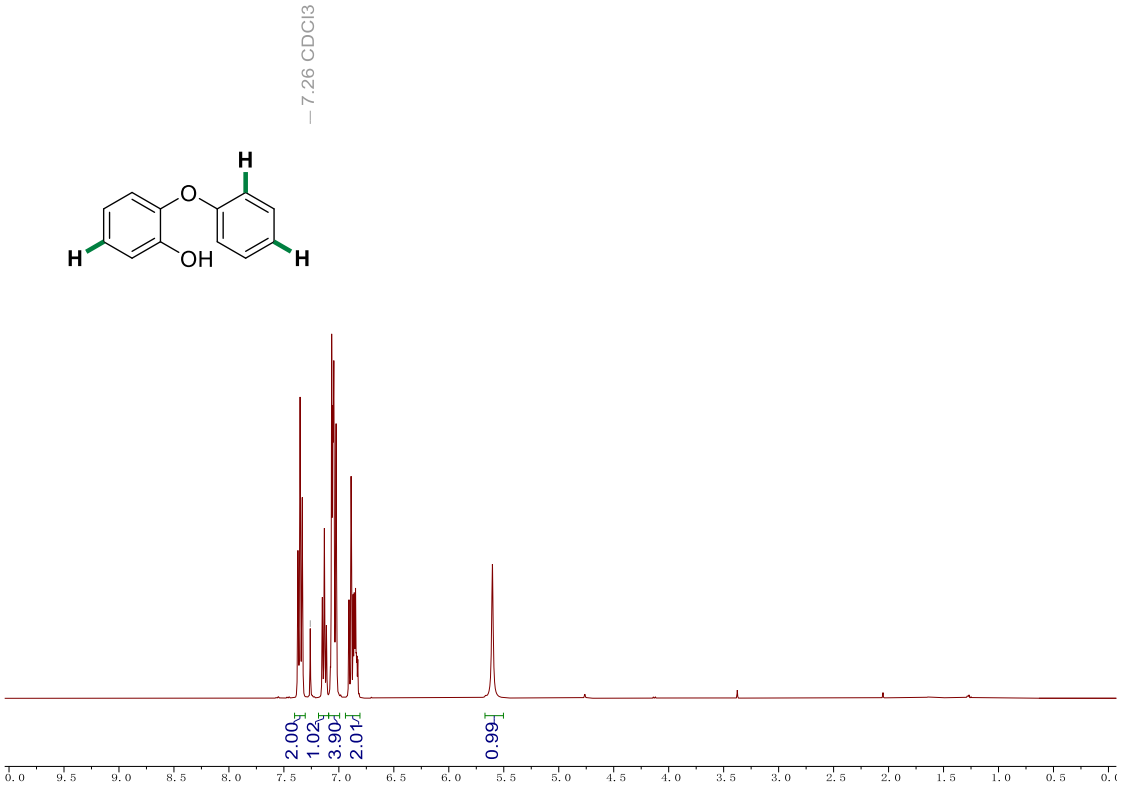

*2-Phenoxyphenol (**32**) ^{13}C-NMR spectrum in $CDCl_3$*

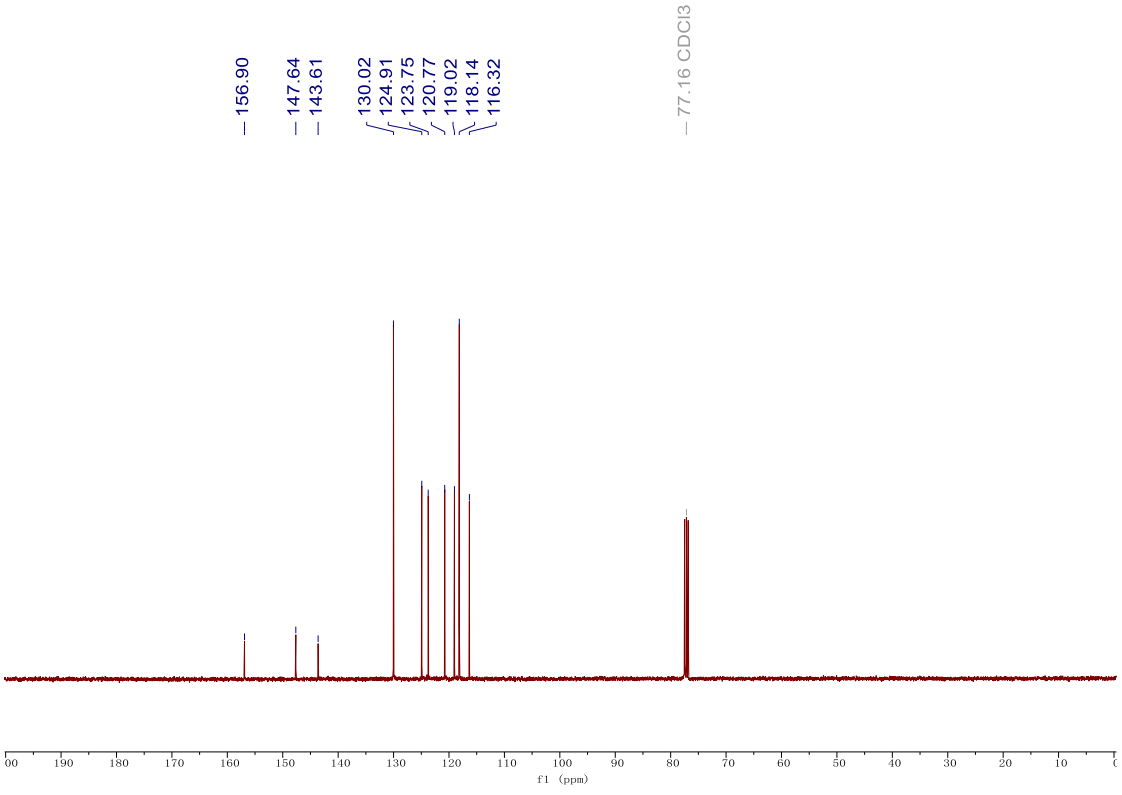

*1,1'-Ethylidenebis-benzene (**33**) ^{1}H-NMR spectrum in $CDCl_3$*

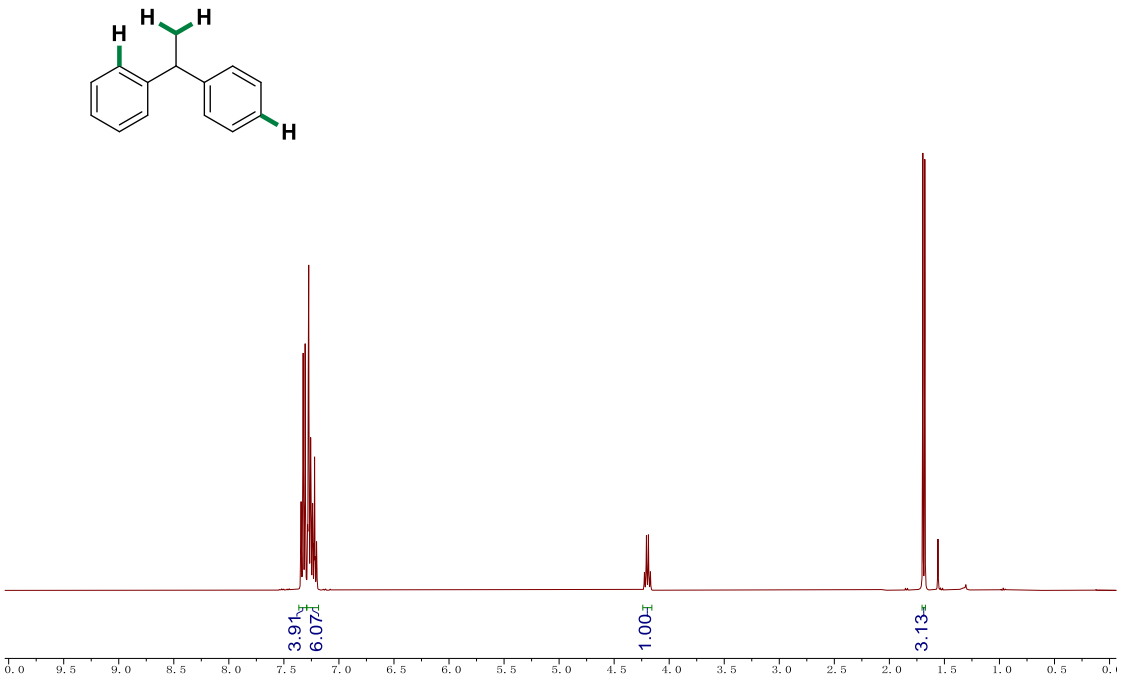

*1,1'-Ethylidenebis-benzene (**33**) ^{13}C-NMR spectrum in $CDCl_3$*

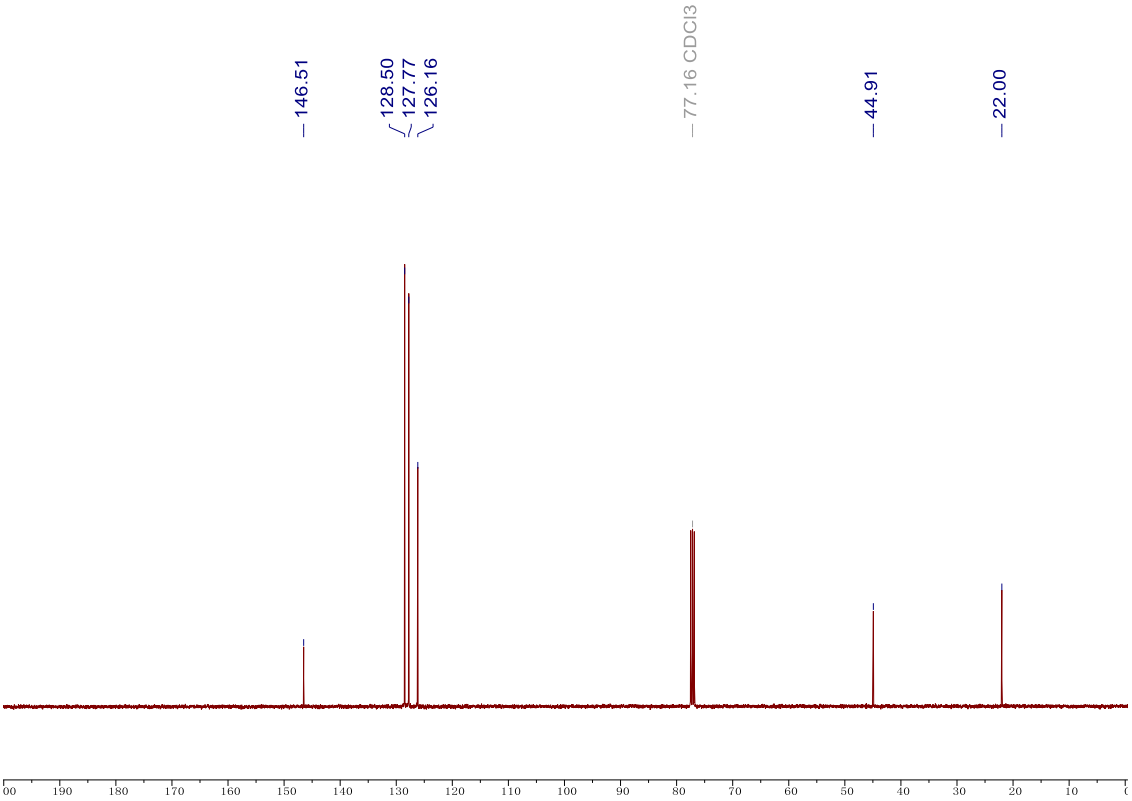

*Phenyl acetonitrile (**34**) ^{1}H-NMR spectrum in $CDCl_3$*

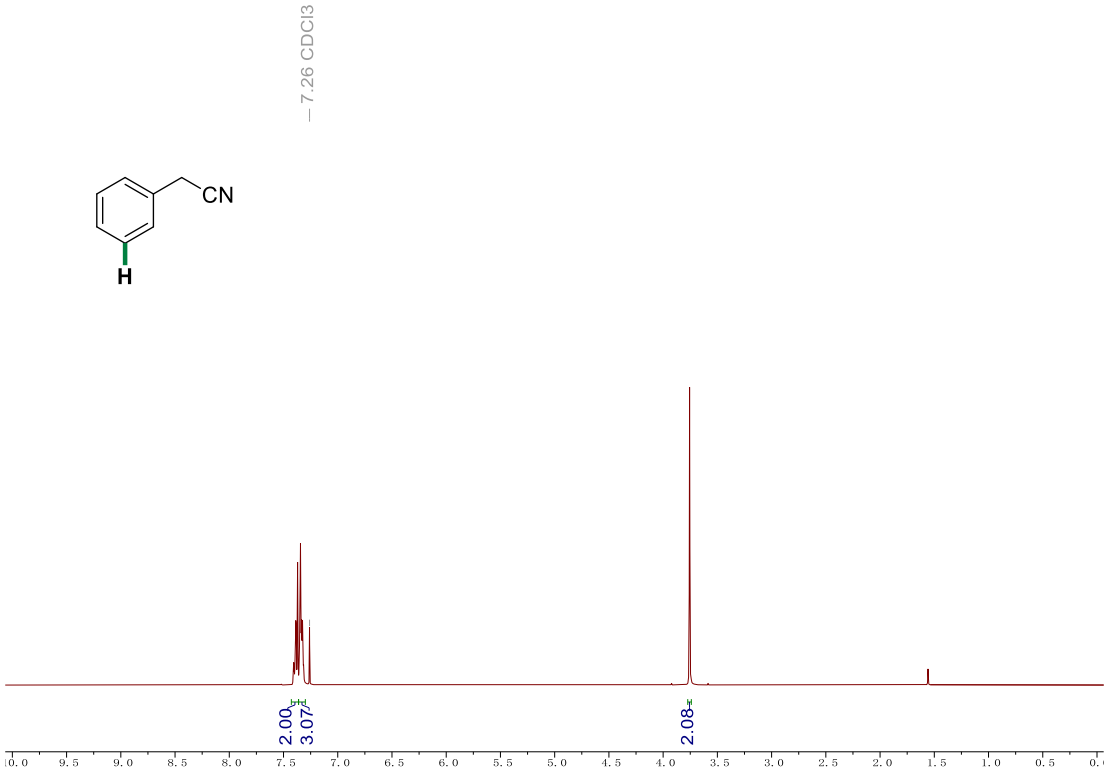

*Phenyl acetonitrile (**34**) ^{13}C-NMR spectrum in $CDCl_3$*

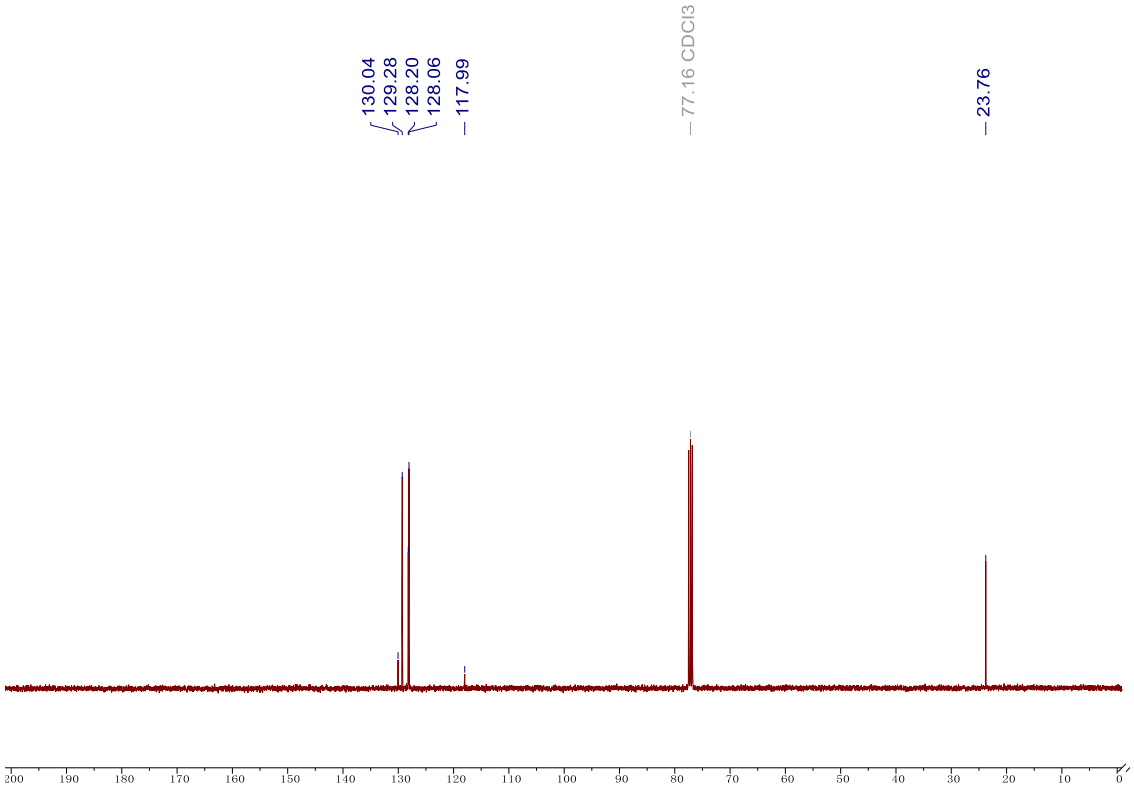

*Diphenylmethanone (**35**) ^{1}H-NMR spectrum in $CDCl_3$*

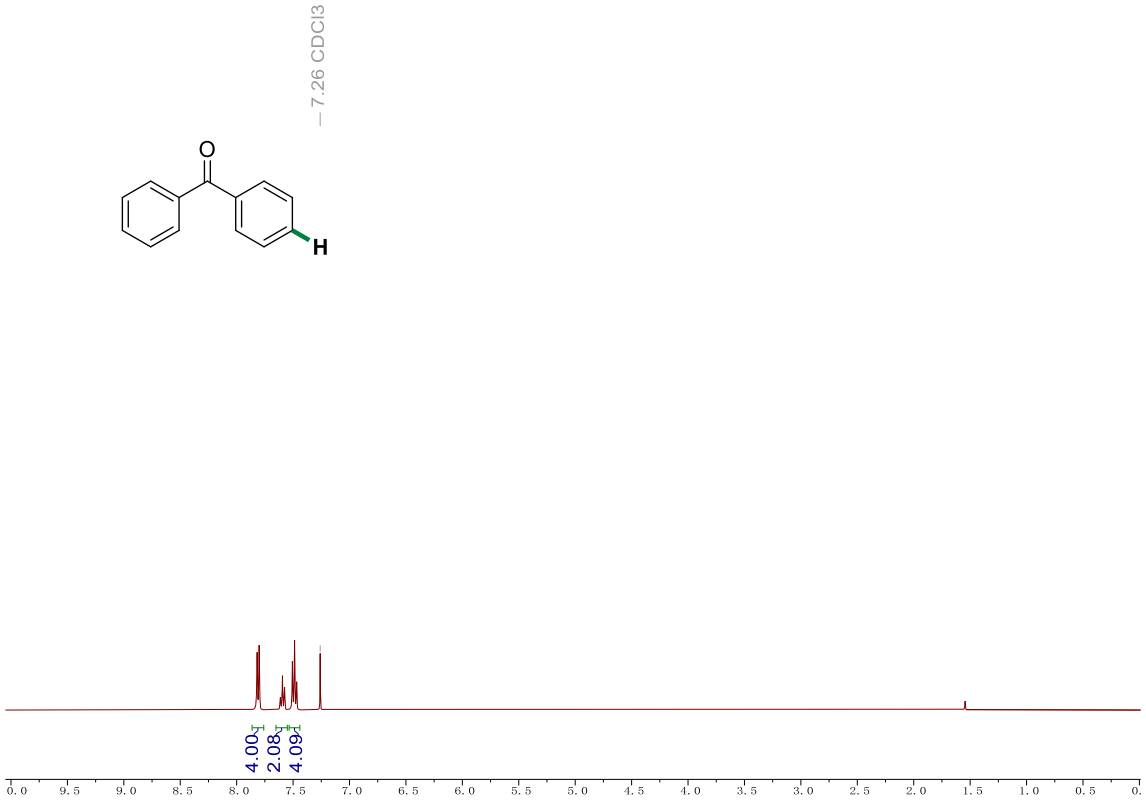

*Diphenylmethanone (**35**) ^{13}C-NMR spectrum in $CDCl_3$*

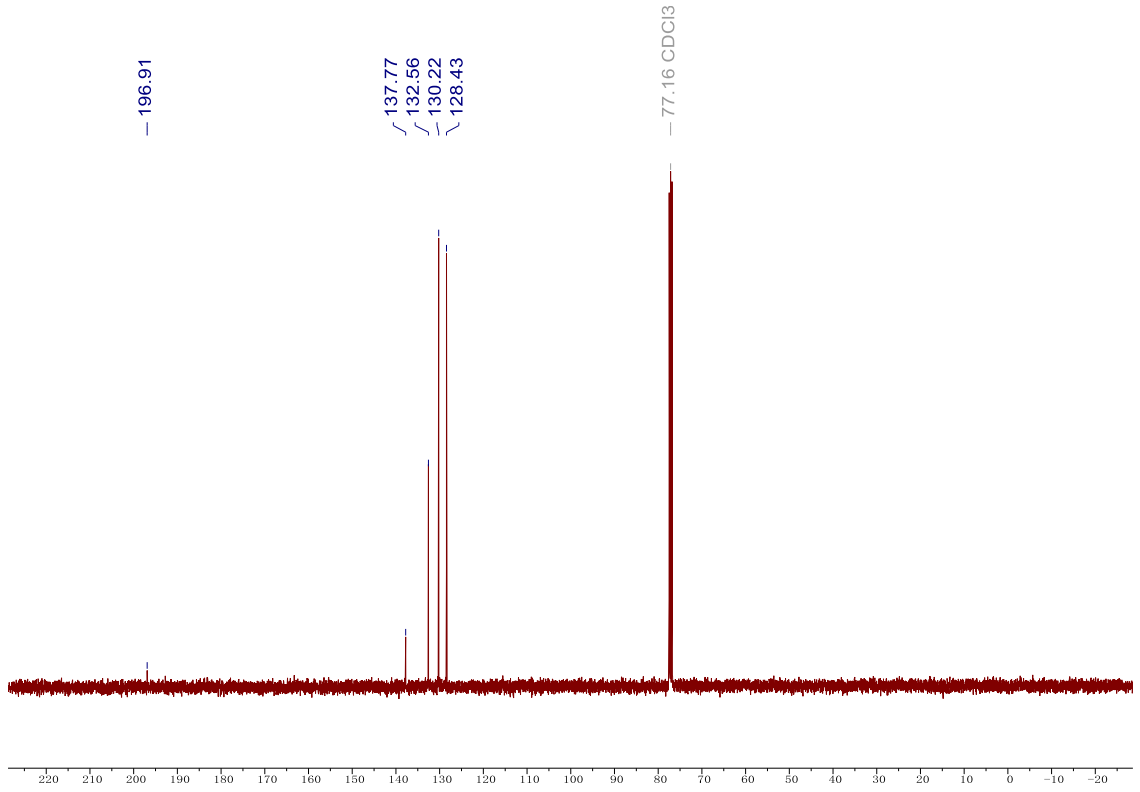

*4-Butylbenzonitrile **(41)** ^{1}H-NMR spectrum in $CDCl_3$*

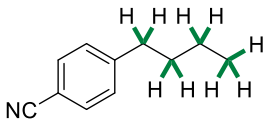

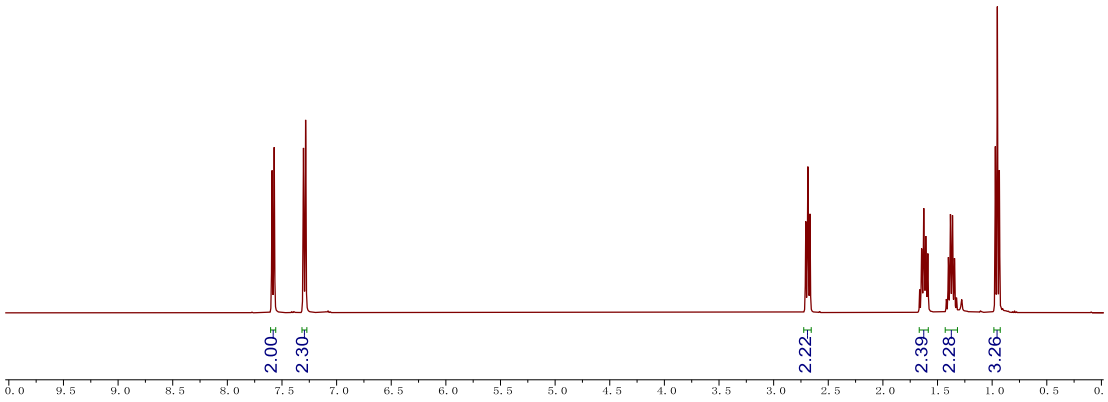

*4-Butylbenzonitrile (**41**) ^{13}C-NMR spectrum in $CDCl_3$*

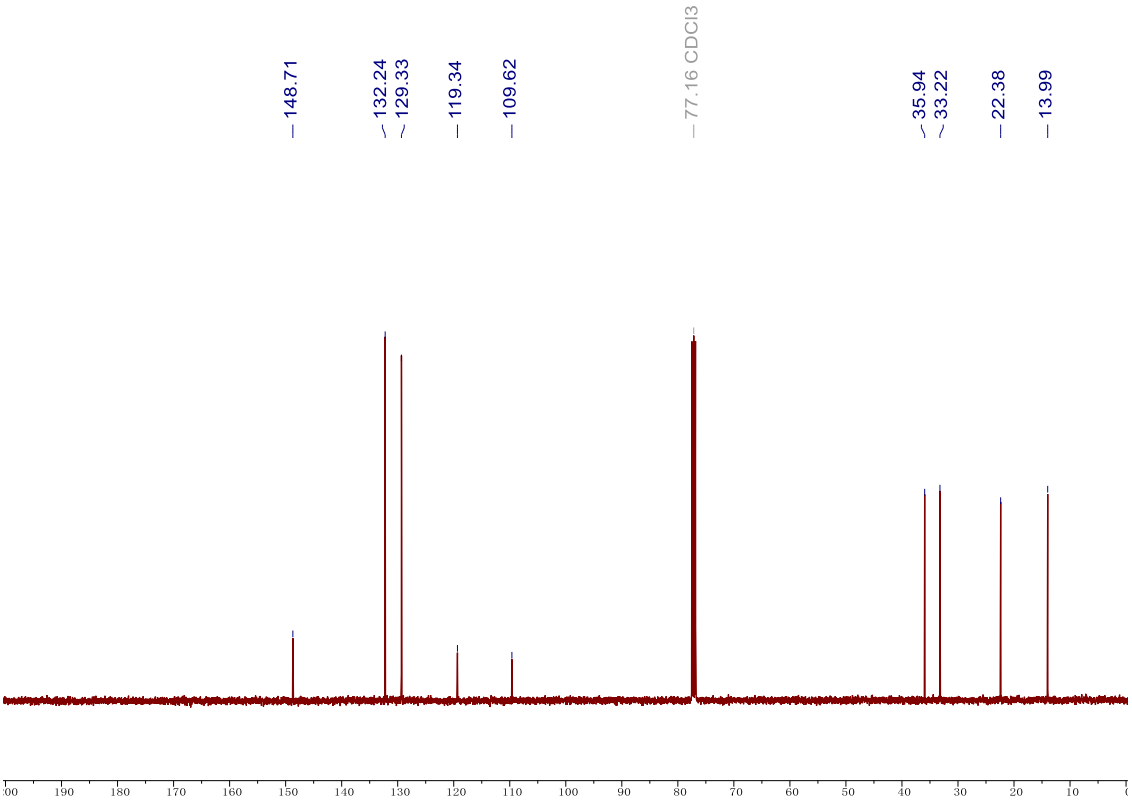

*Butyl octanoate (**44**) ^{1}H-NMR spectrum in $CDCl_3$*

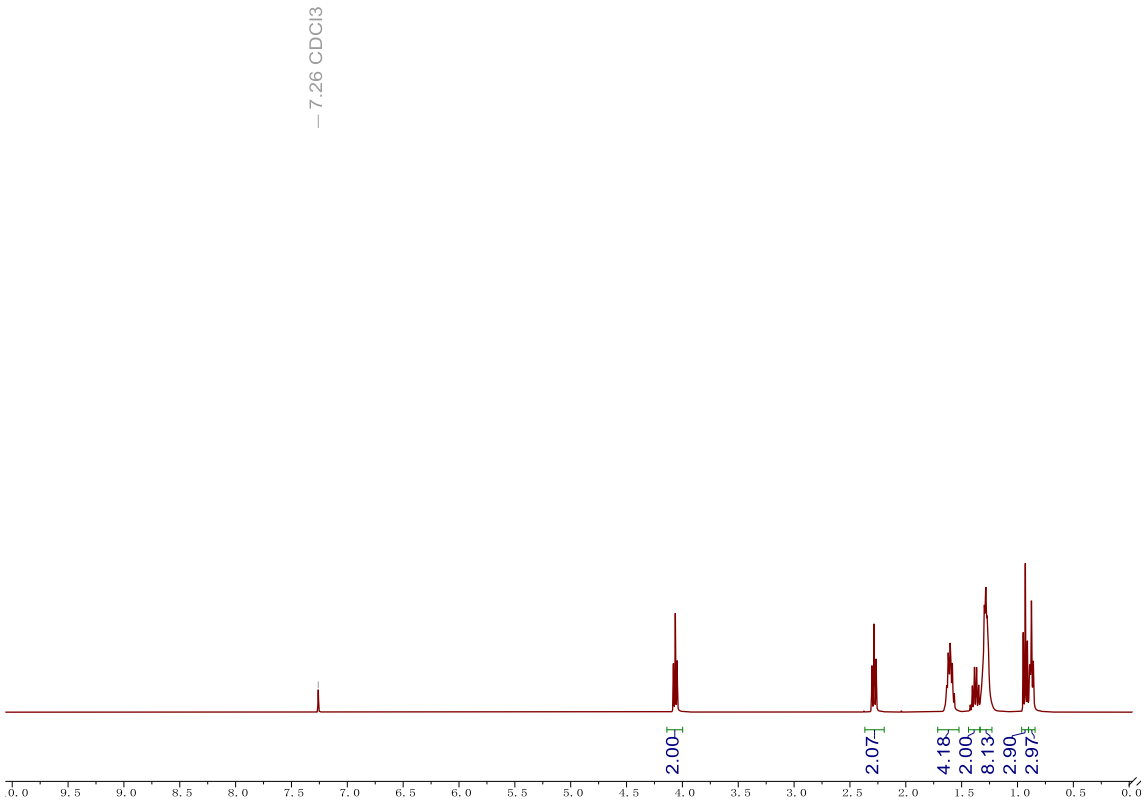

*Butyl octanoate (**44**) ^{13}C-NMR spectrum in $CDCl_3$*

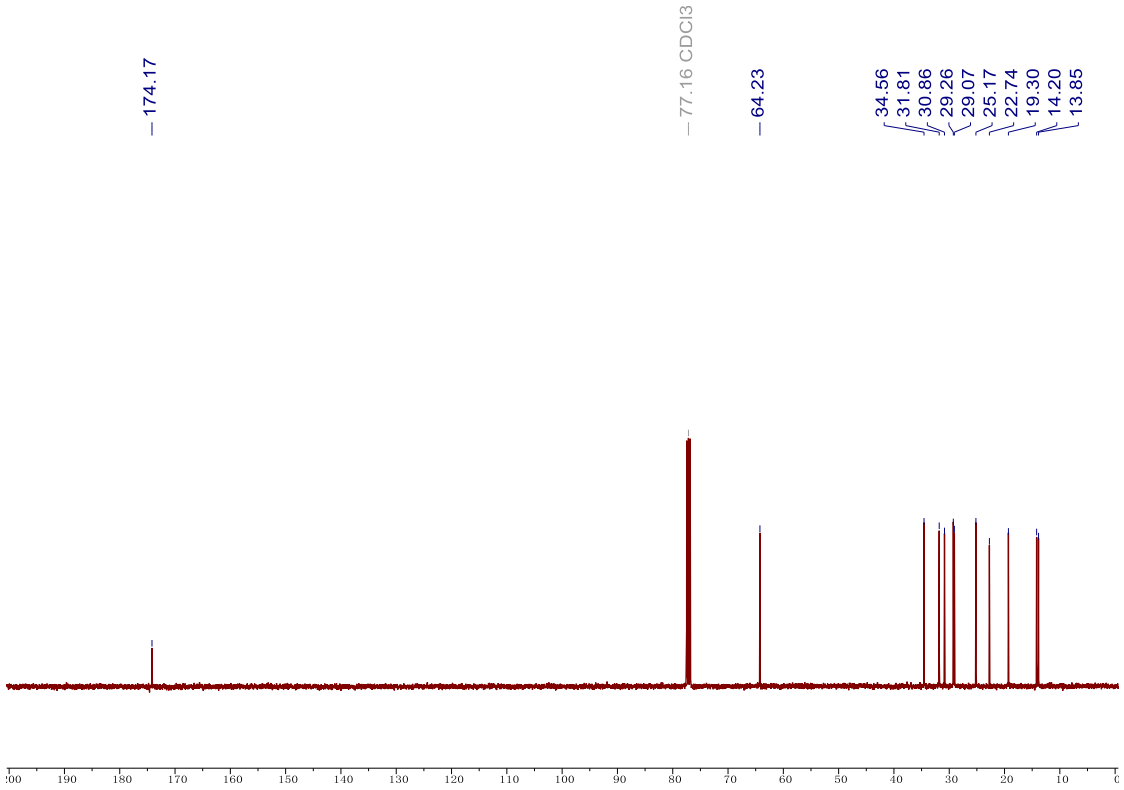

*Phenylboronic acid pinacol ester (**52**) ^{1}H-NMR spectrum in $CDCl_3$*

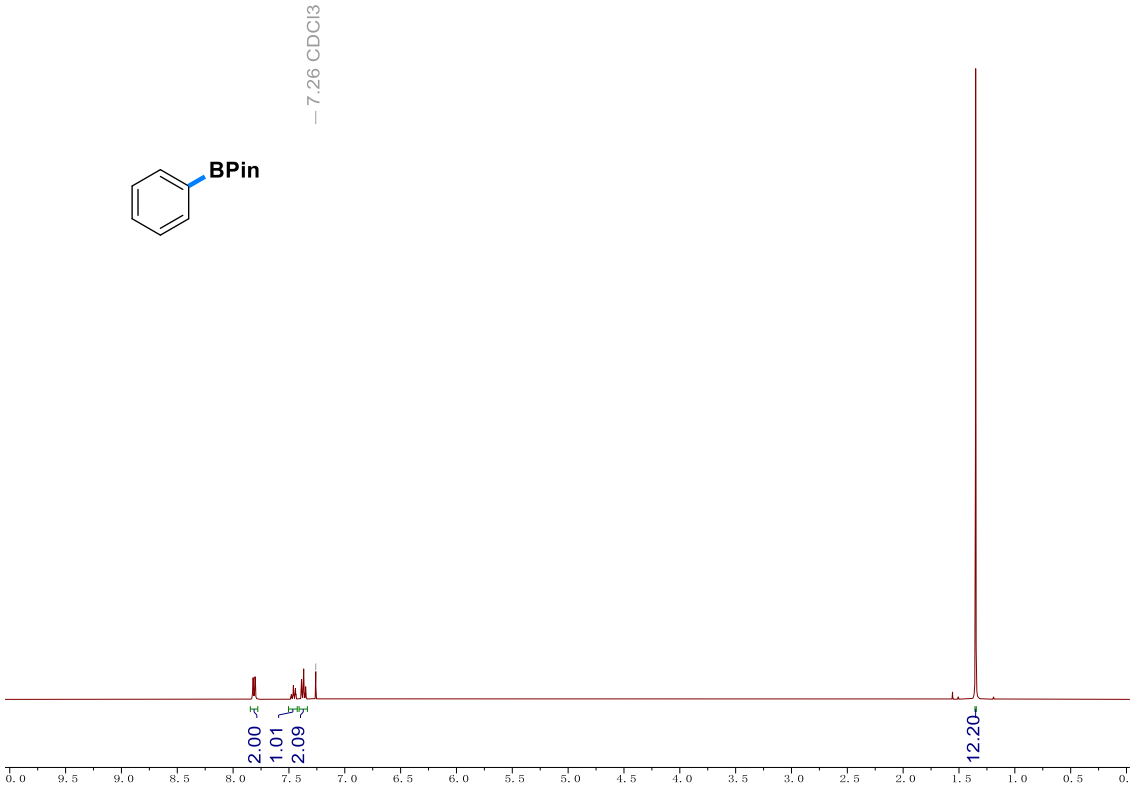

*Phenylboronic acid pinacol ester (**52**) ^{13}C-NMR spectrum in $CDCl_3$*

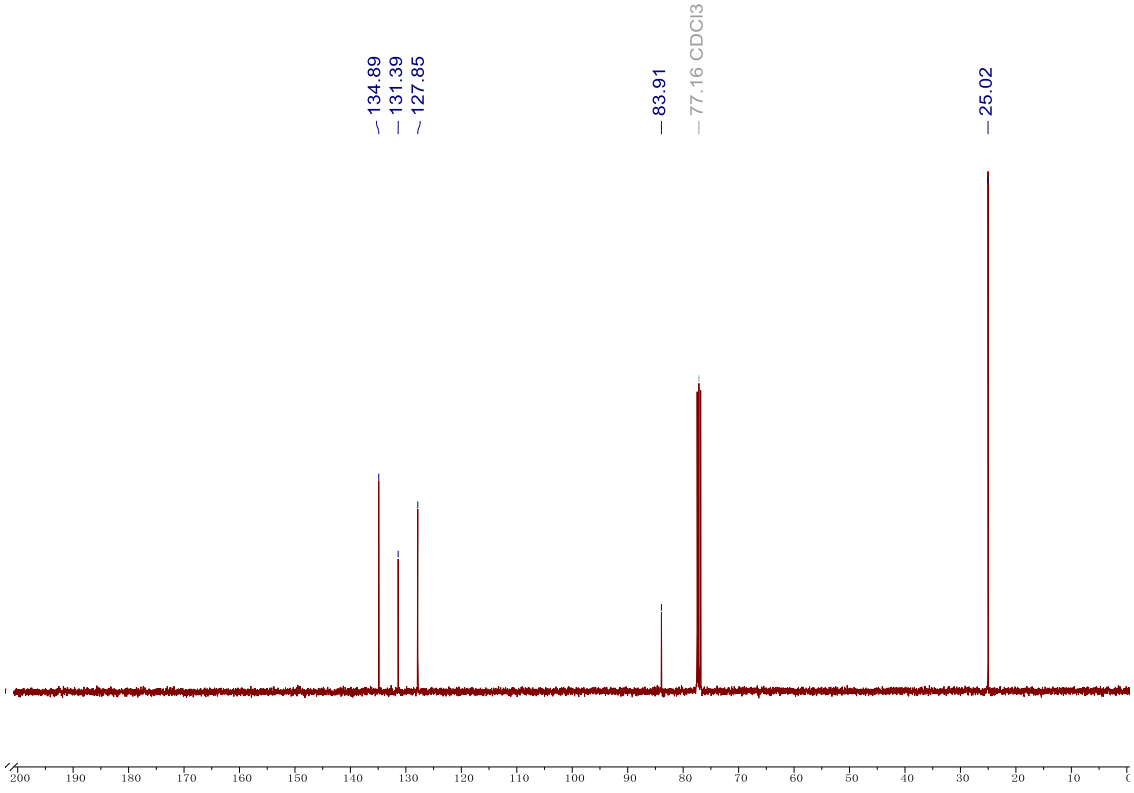

*4-Methoxyphenylboronic acid pinacol ester (**54**) ^{1}H-NMR spectrum in $CDCl_3$*

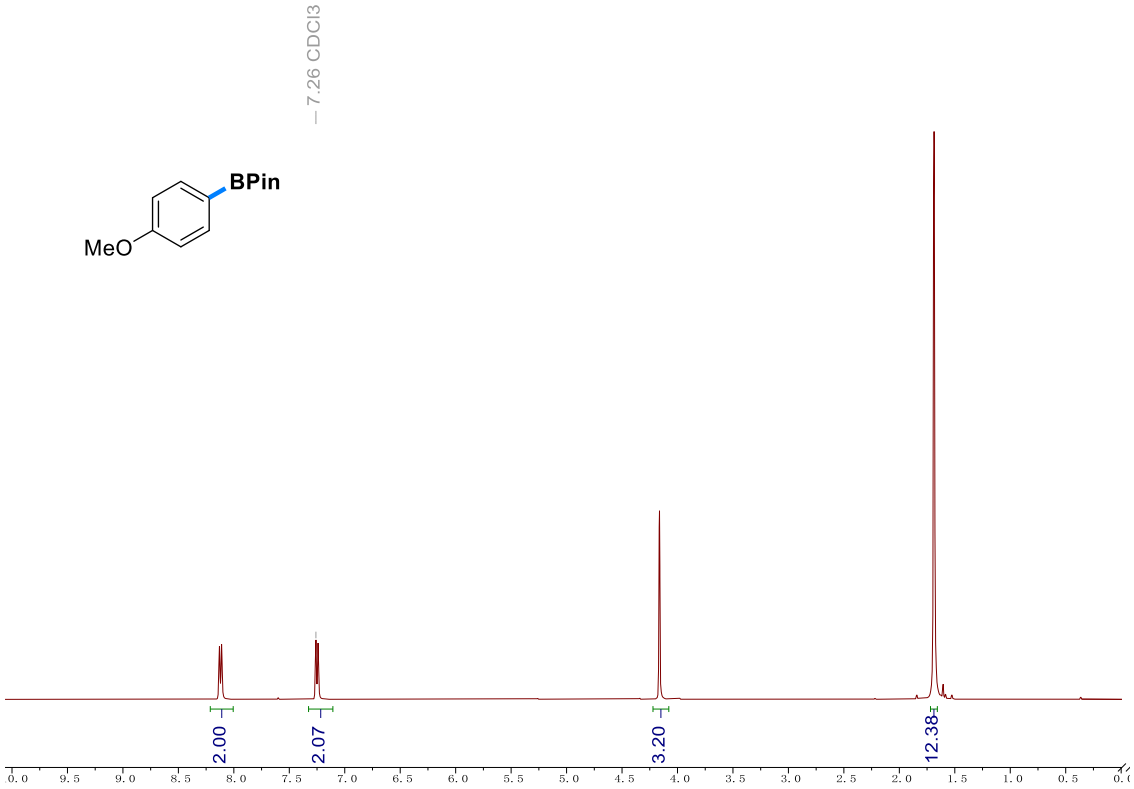

*4-Methoxyphenylboronic acid pinacol ester (**54**) ^{13}C-NMR spectrum in $CDCl_3$*

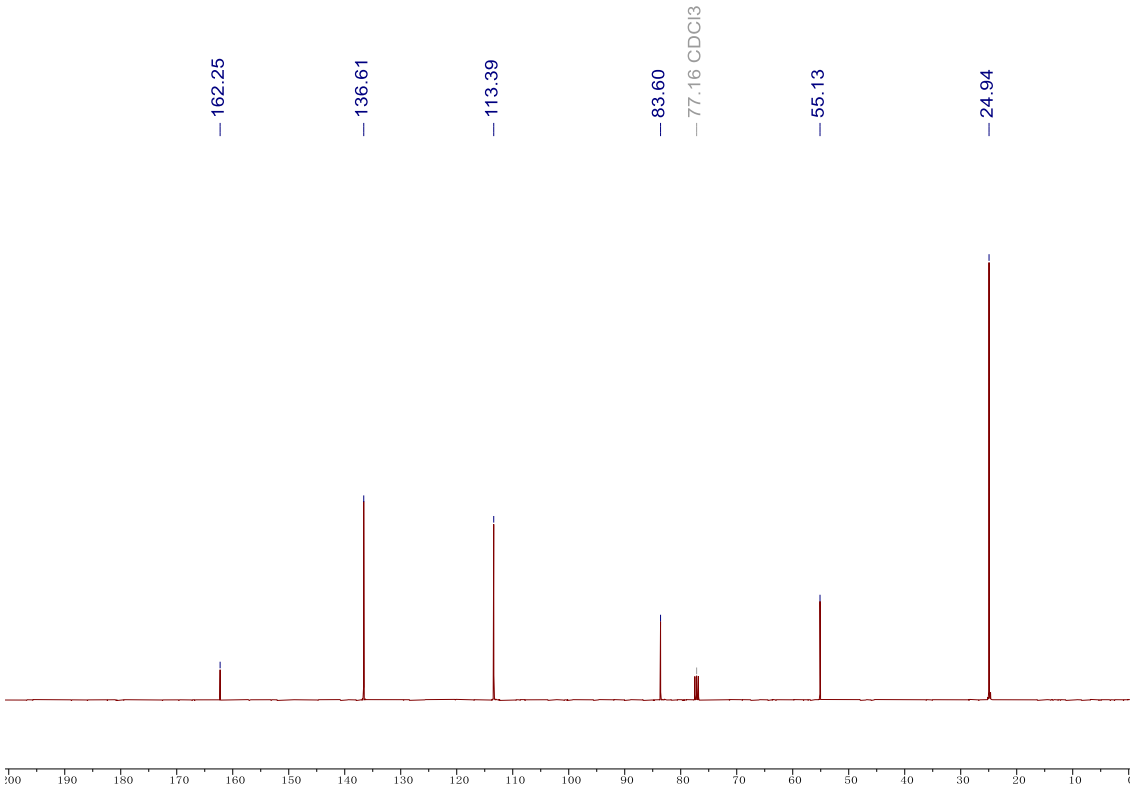

*4-Methoxycarbonylphenylboronic acid pinacol ester (**55**) ^{1}H-NMR spectrum in $CDCl_3$*

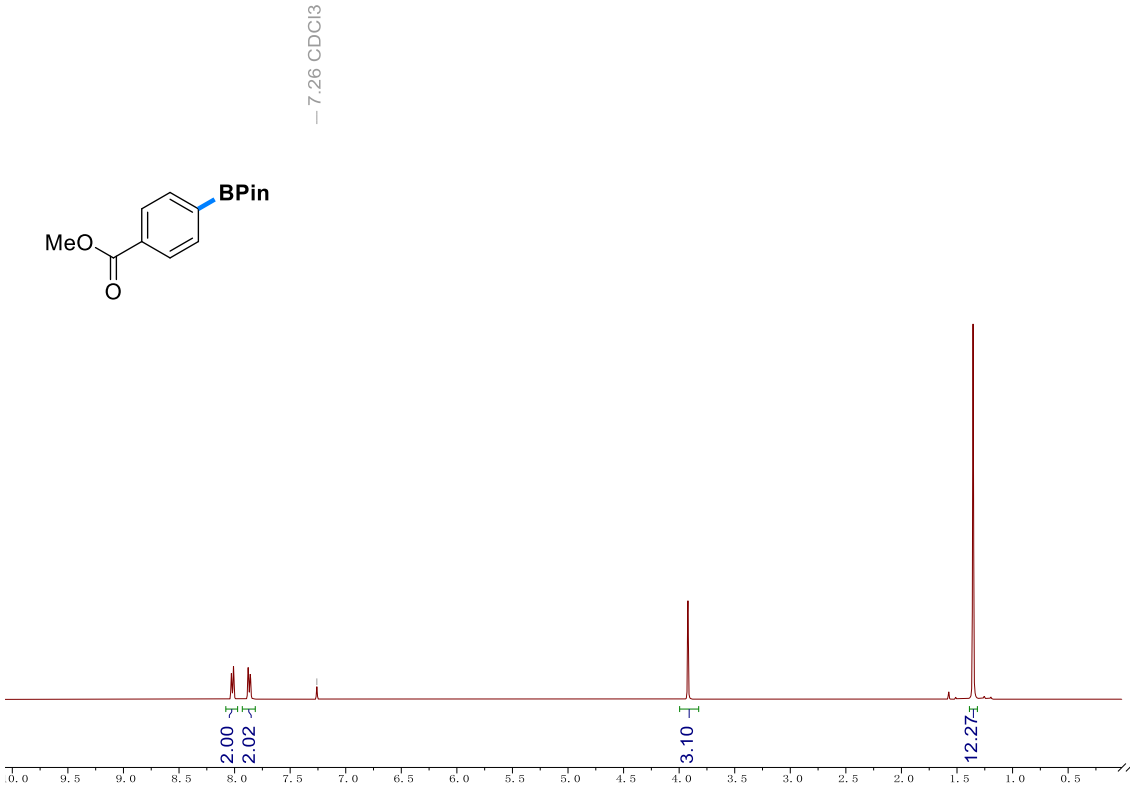

*4-Methoxycarbonylphenylboronic acid pinacol ester (**55**) ^{13}C-NMR spectrum in $CDCl_3$*

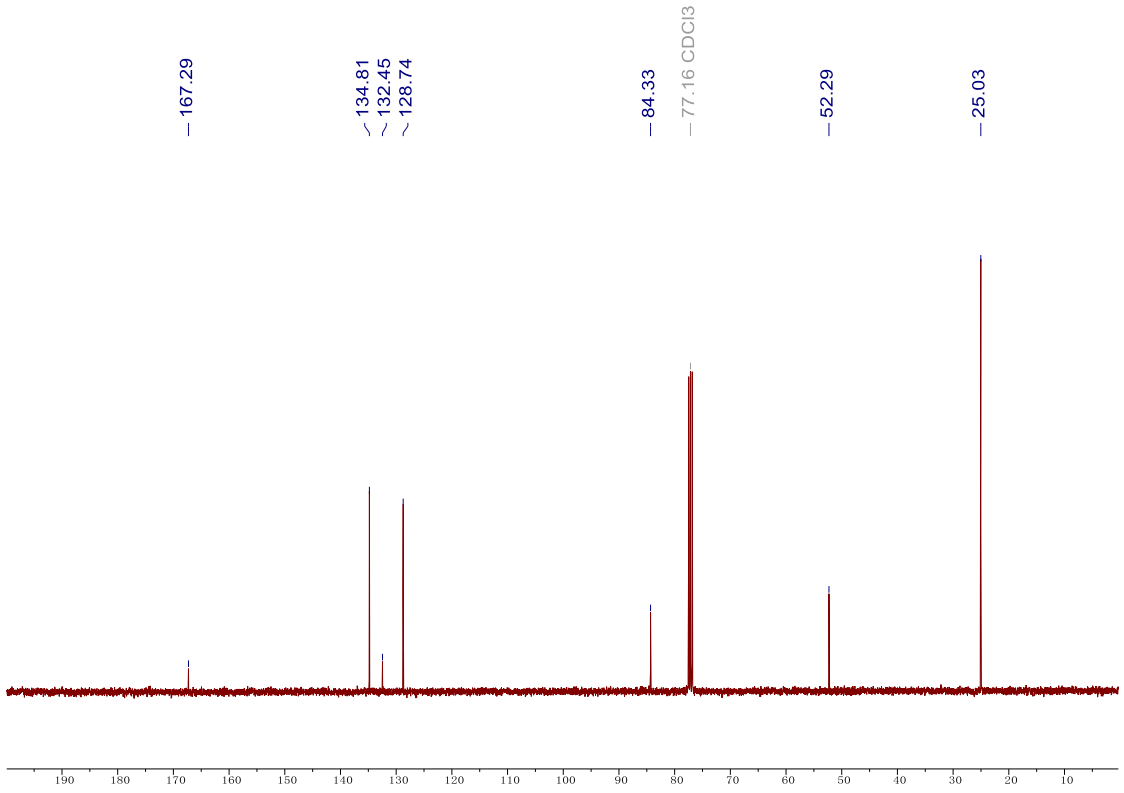

*4-Cyanophenylboronic acid pinacol ester (**56**) ^{1}H-NMR spectrum in $CDCl_3$*

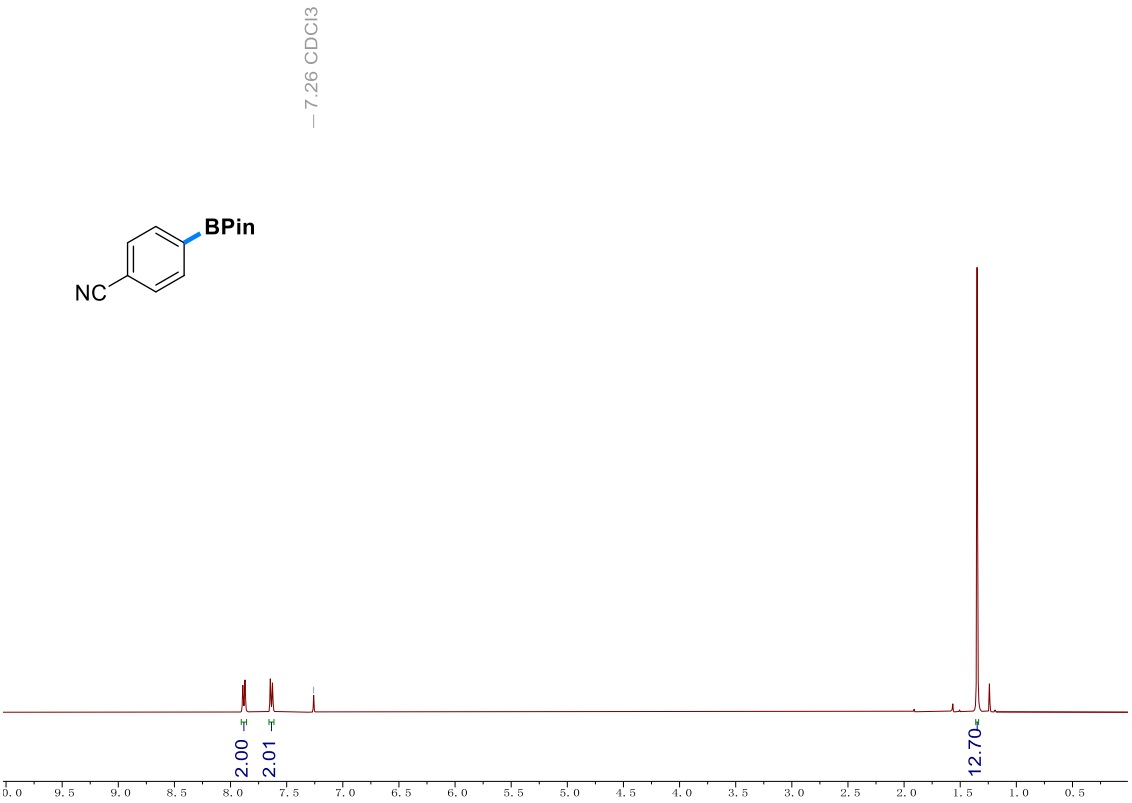

*4-Cyanophenylboronic acid pinacol ester (**56**) ^{13}C-NMR spectrum in $CDCl_3$*

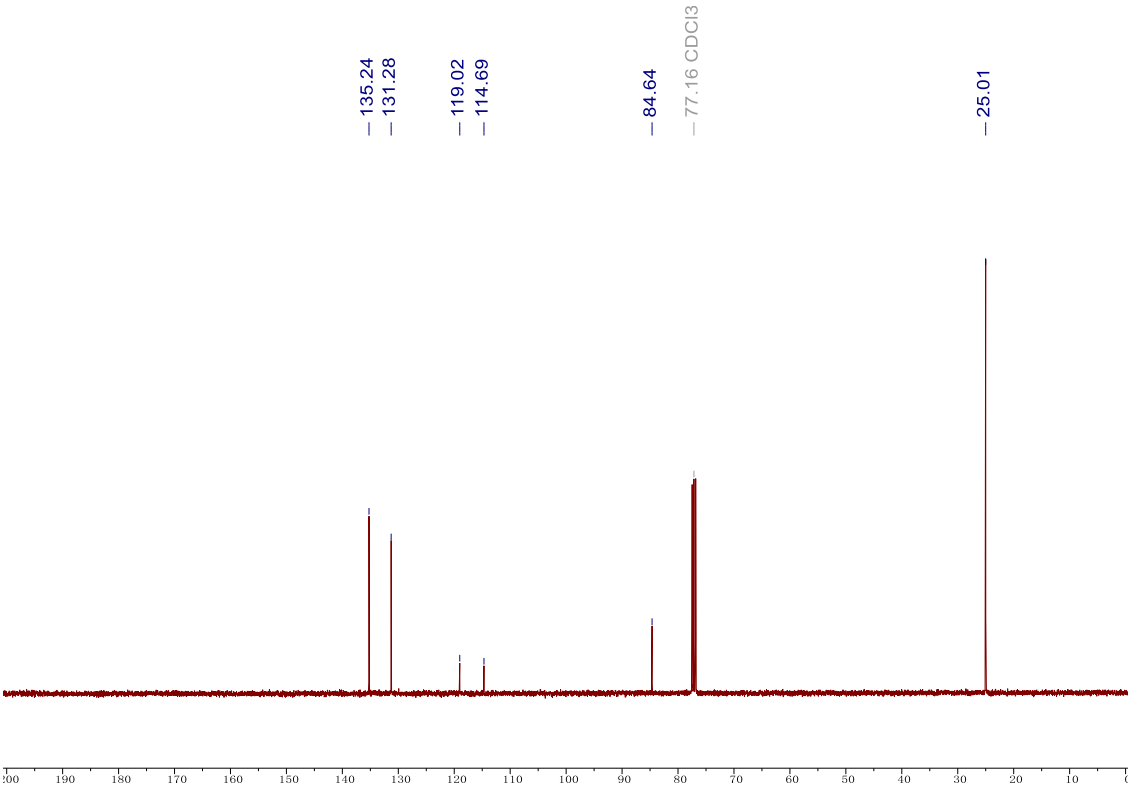

*3-Cyanophenylboronic acid pinacol ester (**57**) ^{1}H-NMR spectrum in $CDCl_3$*

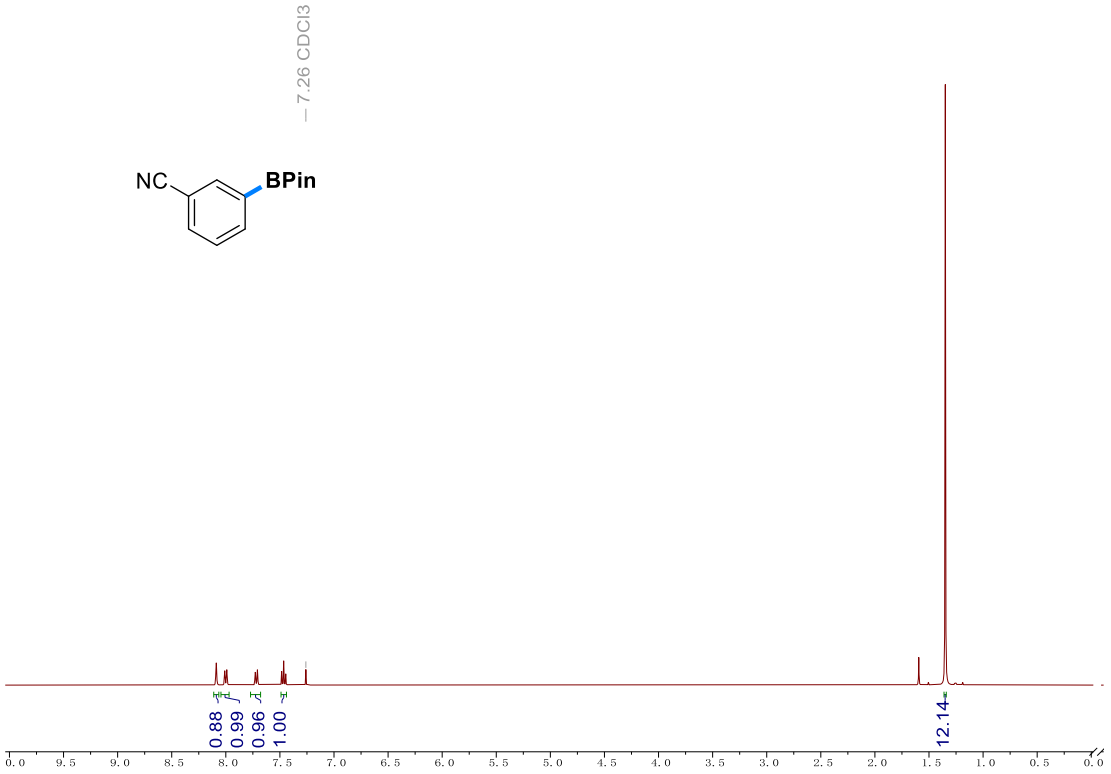

*3-Cyanophenylboronic acid pinacol ester (**57**) ^{13}C-NMR spectrum in $CDCl_3$*

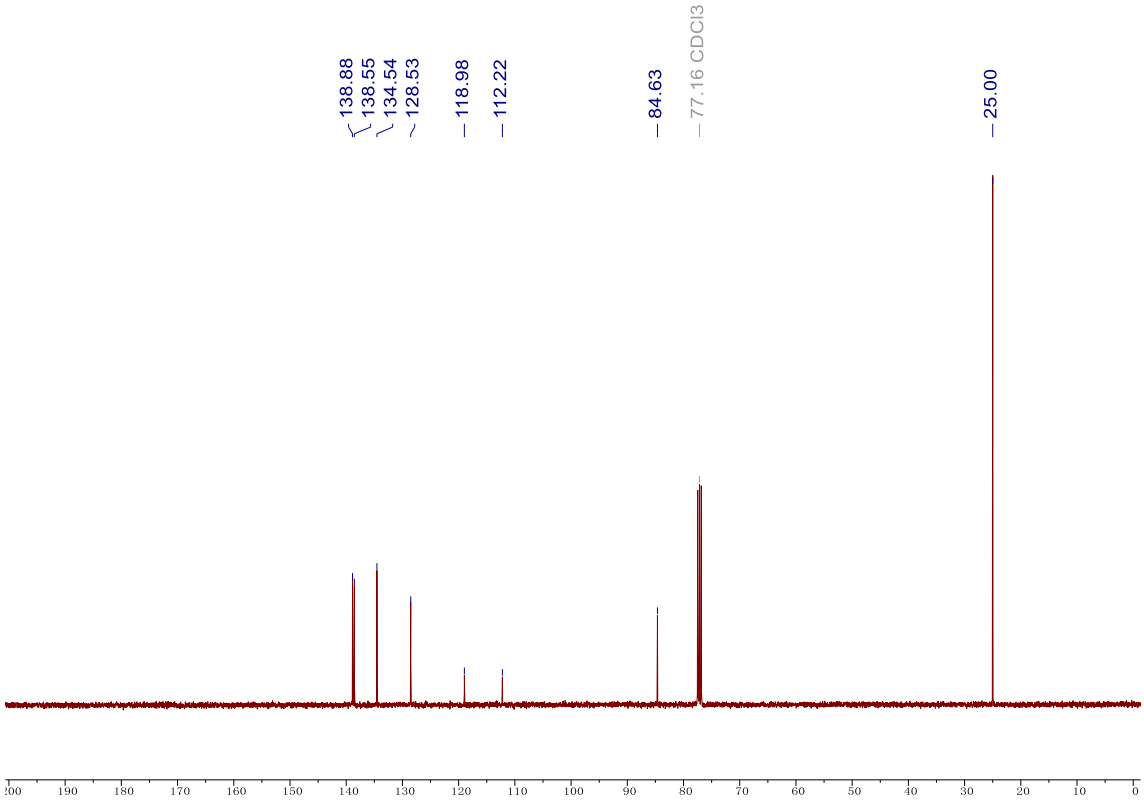

2-(4-(4,4,5,5-tetramethyl-1,3,2-dioxaborolan-2-yl)benzyl)-1,2,3,4-tetrahydroisoquinoline ***(58)***
^{1}H-NMR spectrum in $CDCl_3$

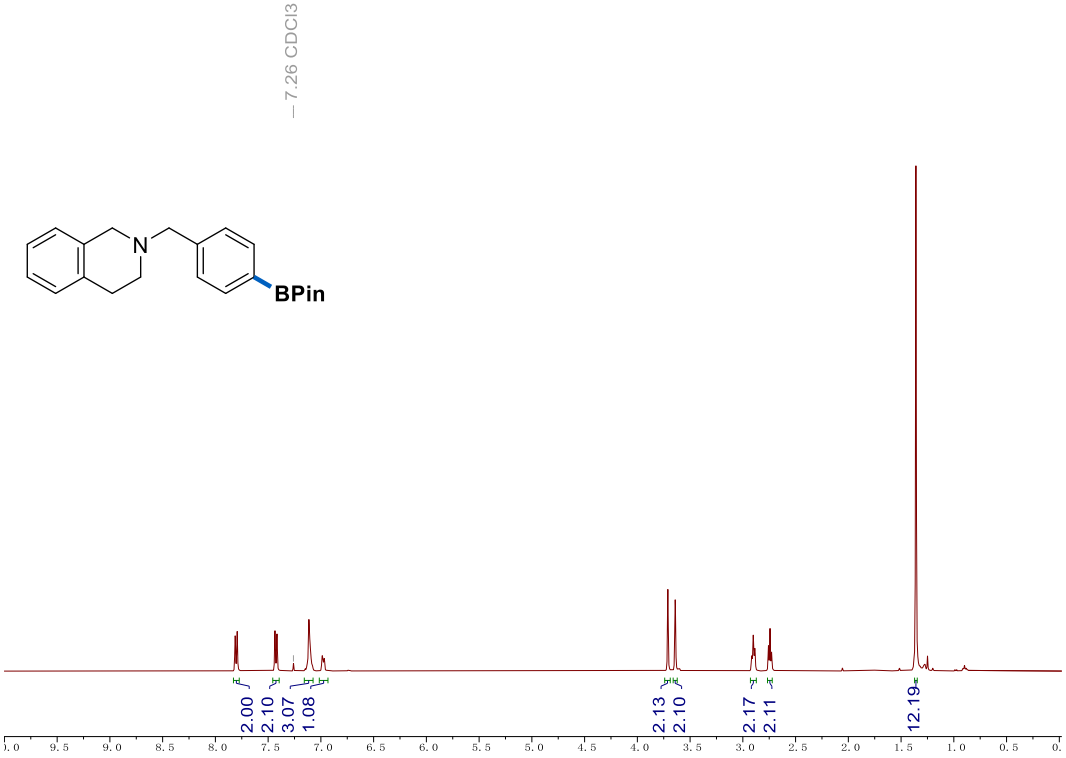

2-(4-(4,4,5,5-tetramethyl-1,3,2-dioxaborolan-2-yl)benzyl)-1,2,3,4-tetrahydroisoquinoline ***(58)***
^{13}C-NMR spectrum in $CDCl_3$

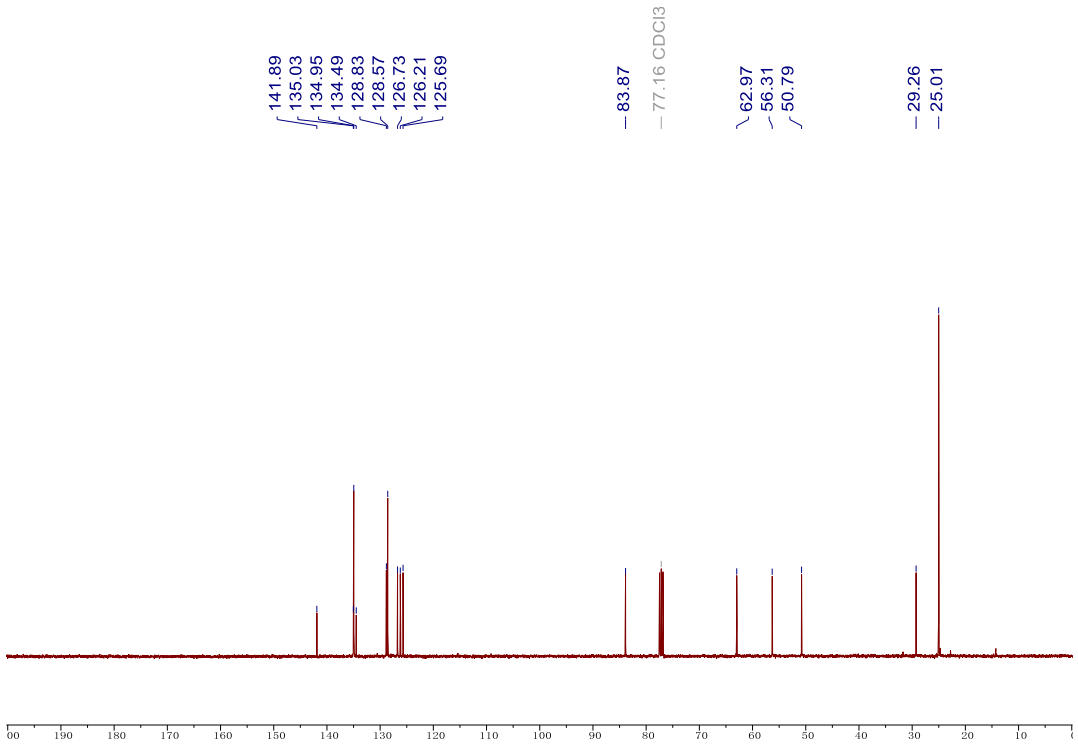

*4,4,5,5-tetramethyl-2-[4-(2-phenoxyethoxy)phenyl][1,3,2]dioxaborolane (**59**) ^{1}H-NMR spectrum in $CDCl_3$*

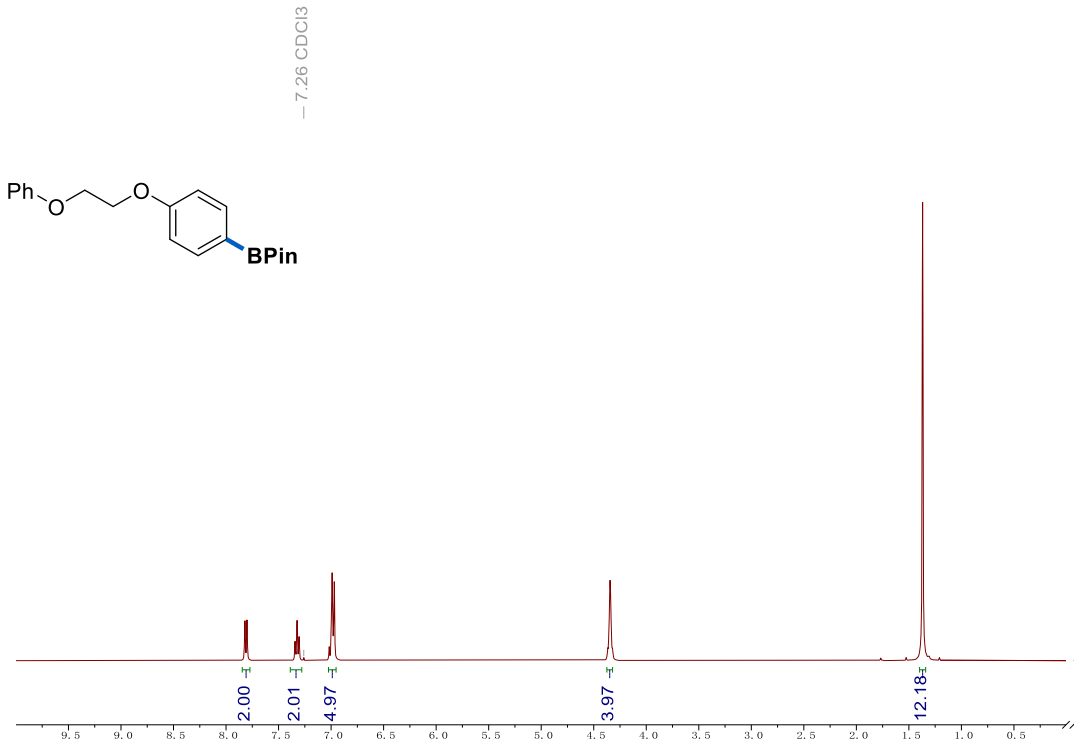

*4,4,5,5-tetramethyl-2-[4-(2-phenoxyethoxy)phenyl][1,3,2]dioxaborolane (**59**) ^{13}C-NMR spectrum in $CDCl_3$*

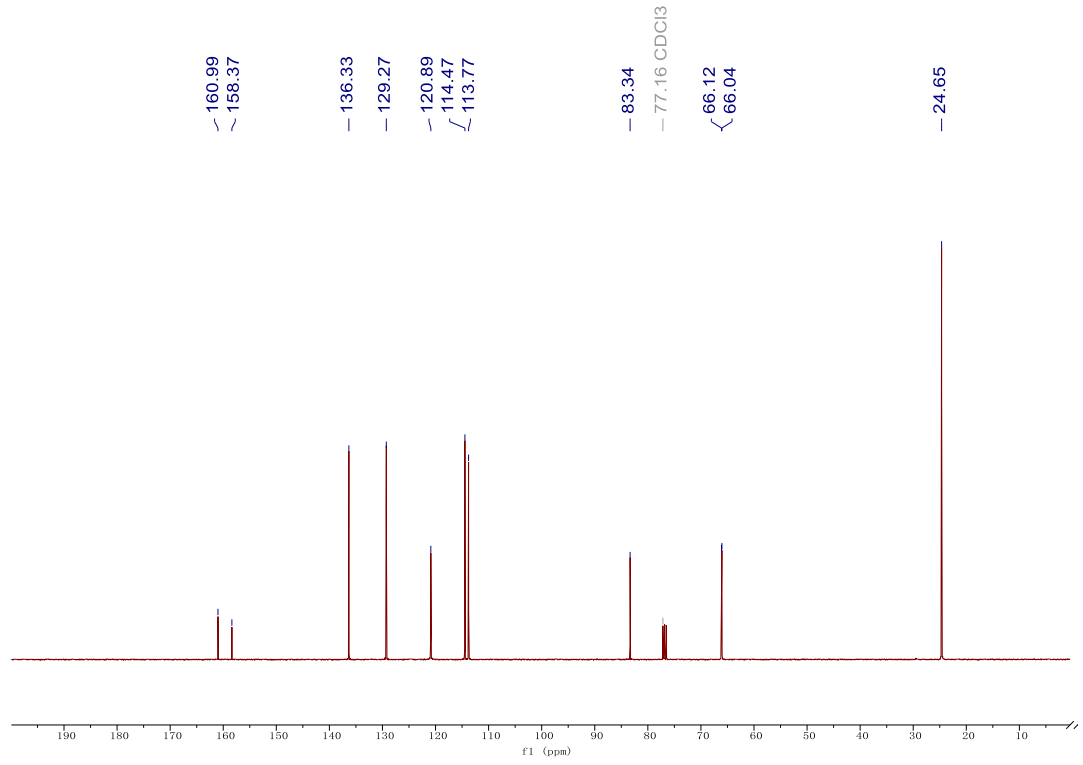

4,4,5,5-Tetramethyl-2-[4-(naphthalen-2-ylsulfanylmethyl)phenyl]-1,3,2-dioxaborolane ***(60)*** *^{1}H-NMR spectrum in $CDCl_3$*

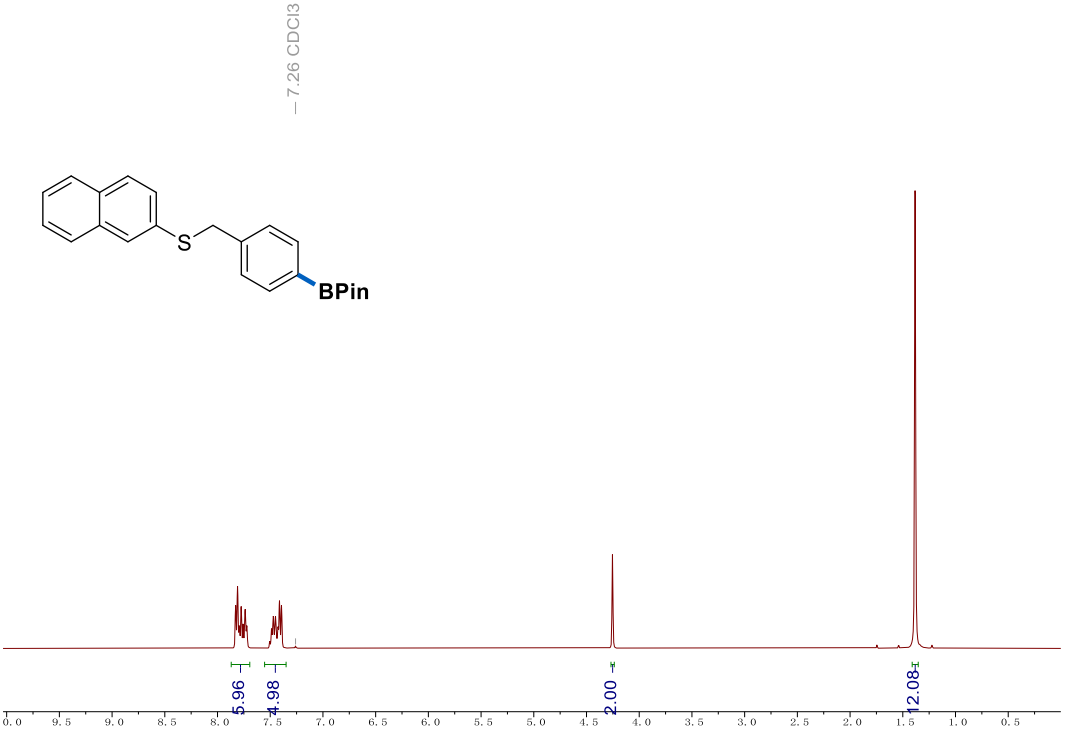

4,4,5,5-tetramethyl-2-[4-(naphthalen-2-ylsulfanylmethyl)phenyl]-1,3,2-dioxaborolane ***(60)*** *^{13}C-NMR spectrum in $CDCl_3$*

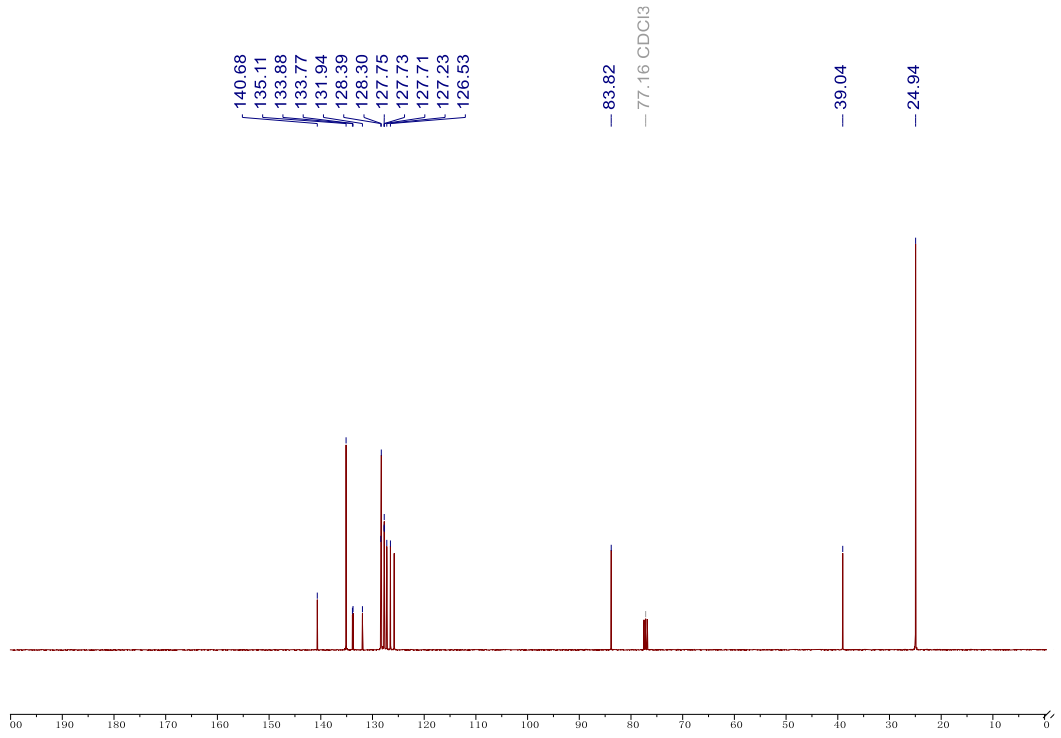

*4-Methyl-7-[4-(4,4,5,5-tetramethyl-[1,3,2] dioxaborolan-2-yl)-benzyloxy]-chromen-2-one (**61**)*
^{1}H-NMR spectrum in $CDCl_3$

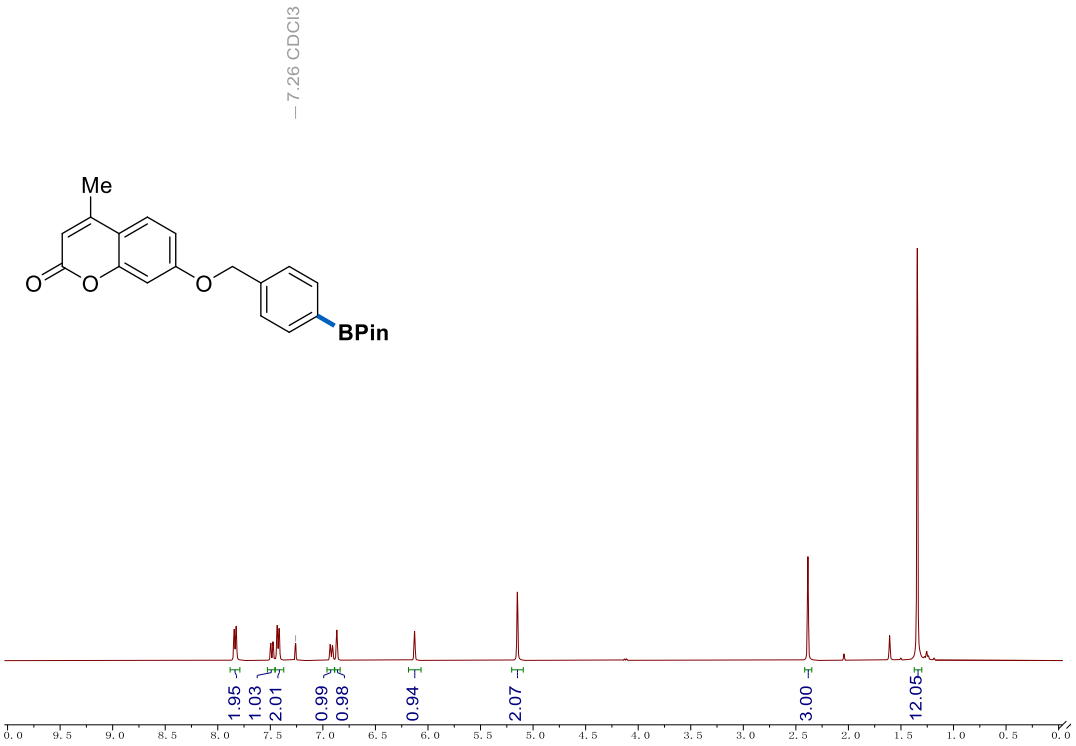

*4-methyl-7-[4-(4,4,5,5-tetramethyl-[1,3,2] dioxaborolan-2-yl)-benzyloxy]-chromen-2-one (**61**)*
^{13}C-NMR spectrum in $CDCl_3$

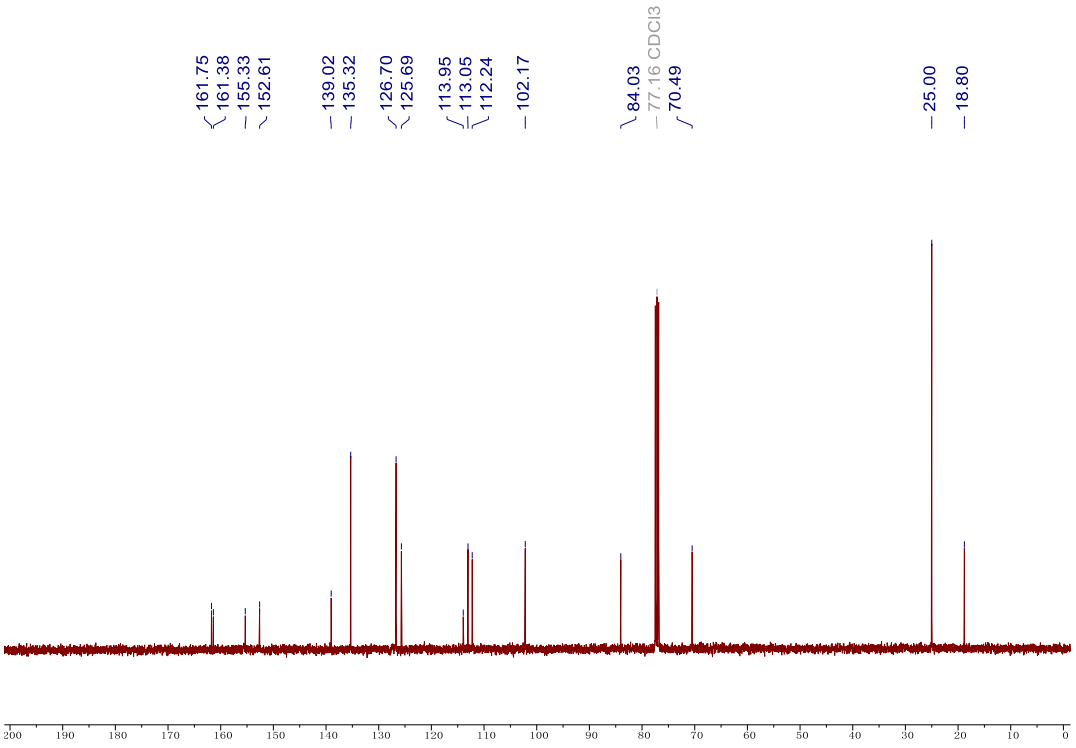

*Benzene-1,4-diboronic acid bispinacol ester (**62**) ^{1}H-NMR spectrum in $CDCl_3$*

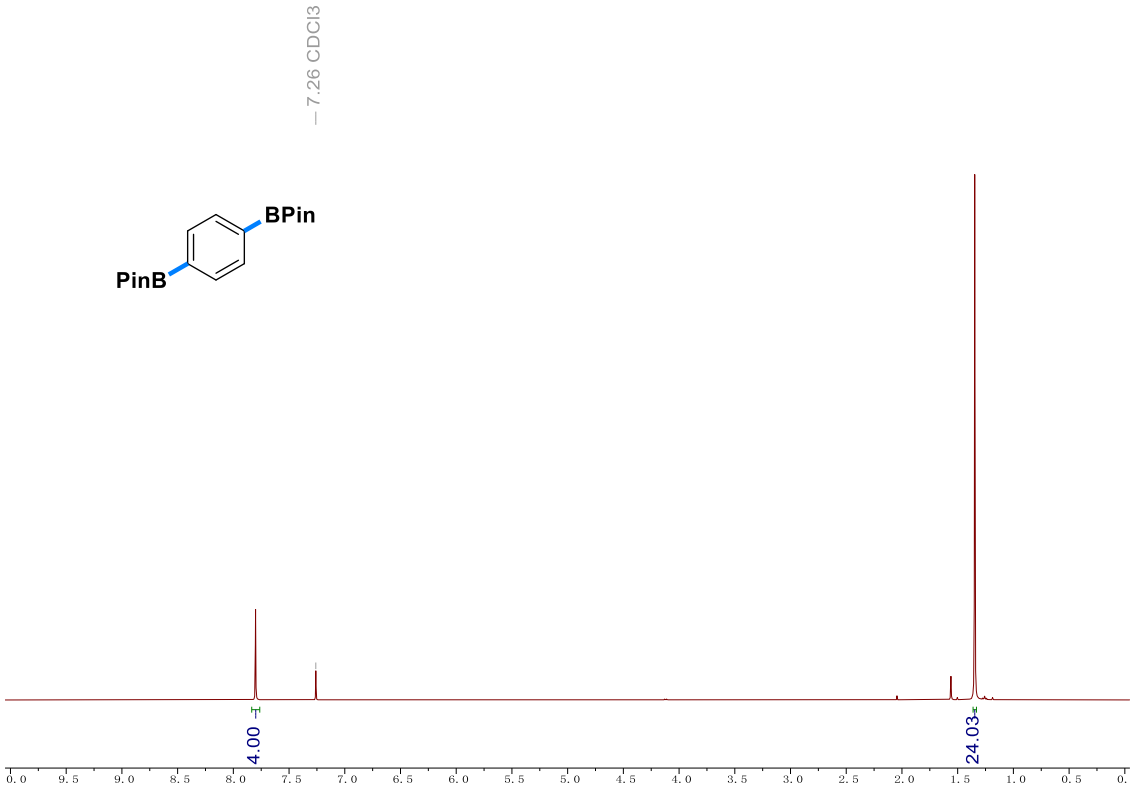

*Benzene-1,4-diboronic acid bispinacol ester (**62**) ^{13}C-NMR spectrum in $CDCl_3$*

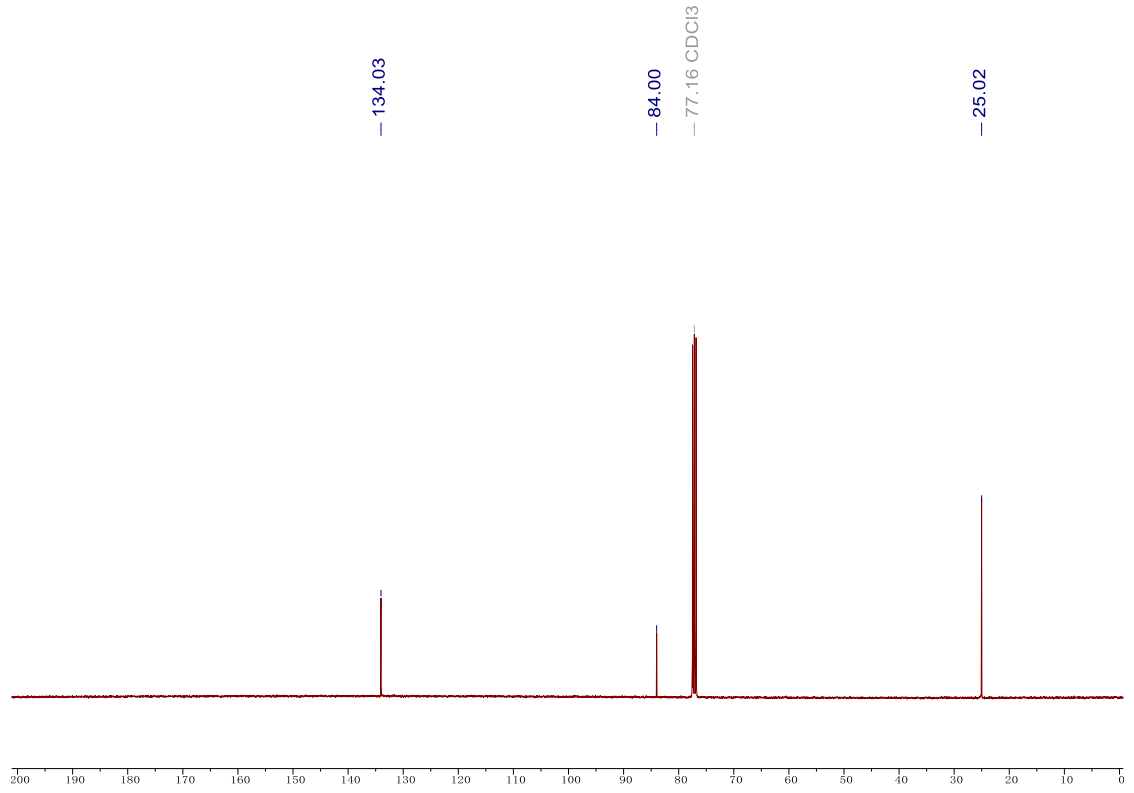

*4-(4,4,6,6-tetramethyl-1,3,2-dioxaborinan-2-yl) Benzonitrile (**63**) ^{1}H-NMR spectrum in $CDCl_3$*

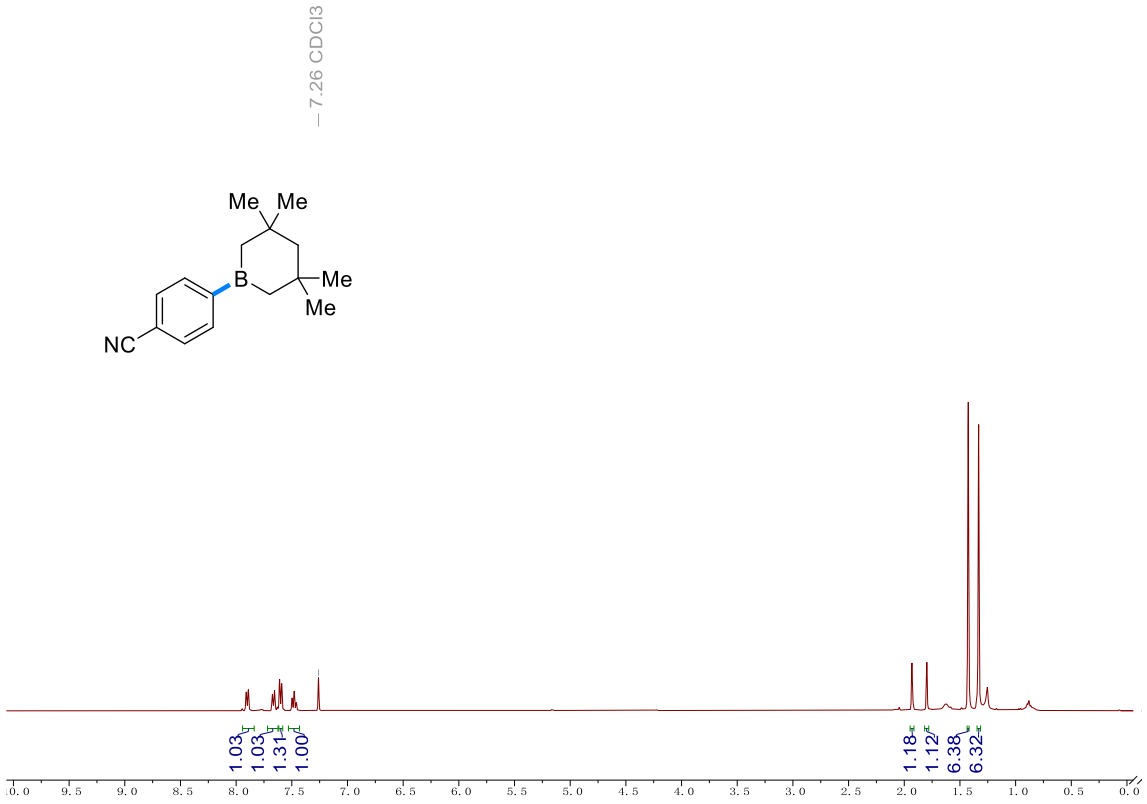

*4-(4,4,6,6-tetramethyl-1,3,2-dioxaborinan-2-yl) Benzonitrile (**63**) ^{13}C-NMR spectrum in $CDCl_3$*

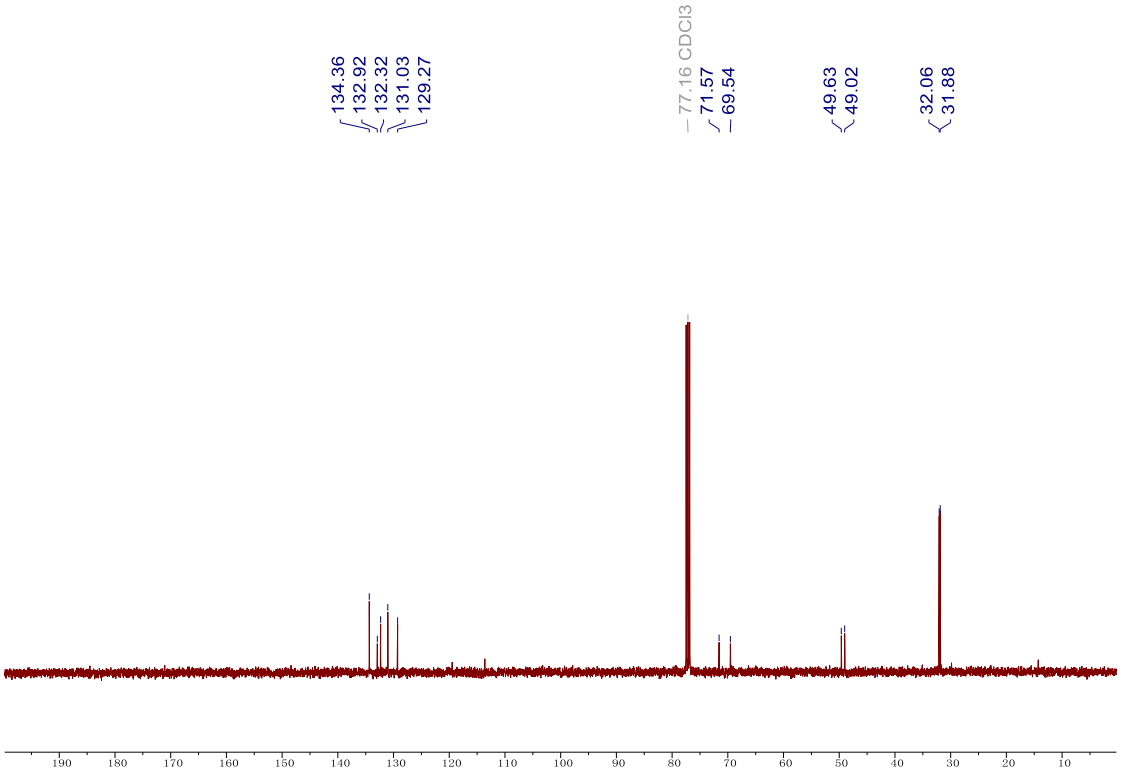

*5,5-Dimethyl-2-phenyl-1,3,2-dioxaborinane (**64**) ^{1}H-NMR spectrum in $CDCl_3$*

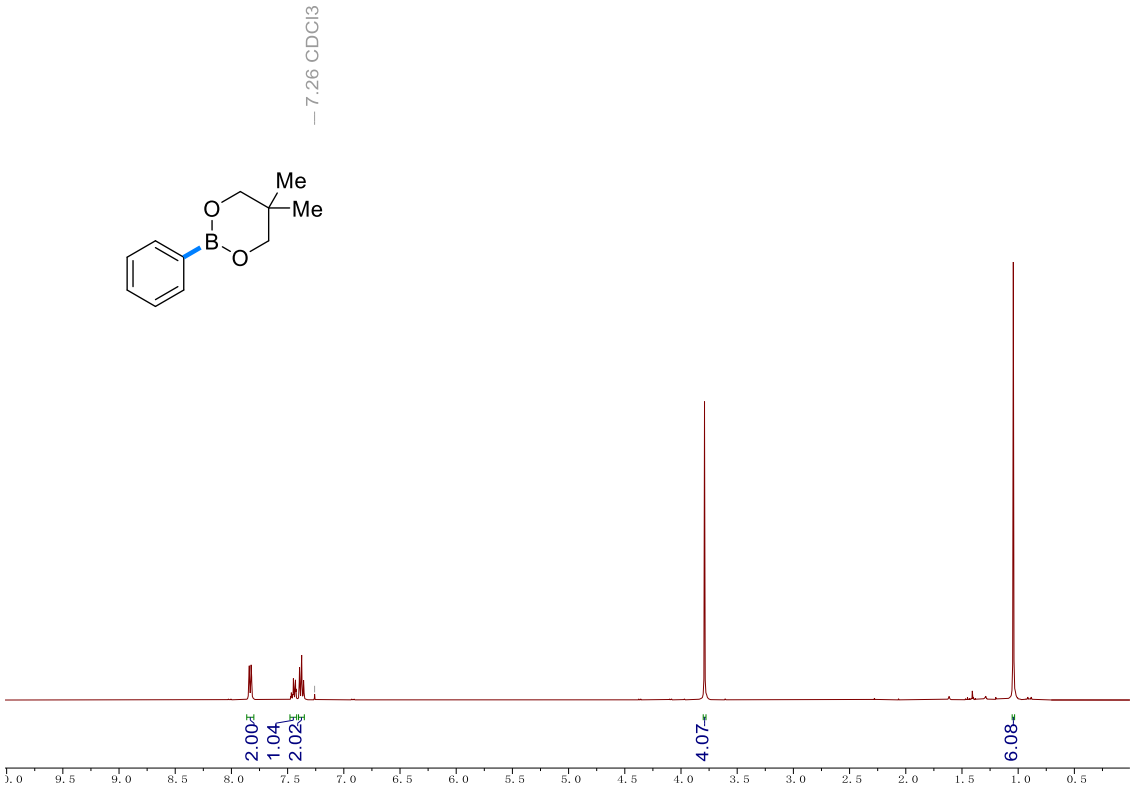

*5,5-Dimethyl-2-phenyl-1,3,2-dioxaborinane (**64**) ^{13}C-NMR spectrum in $CDCl_3$*

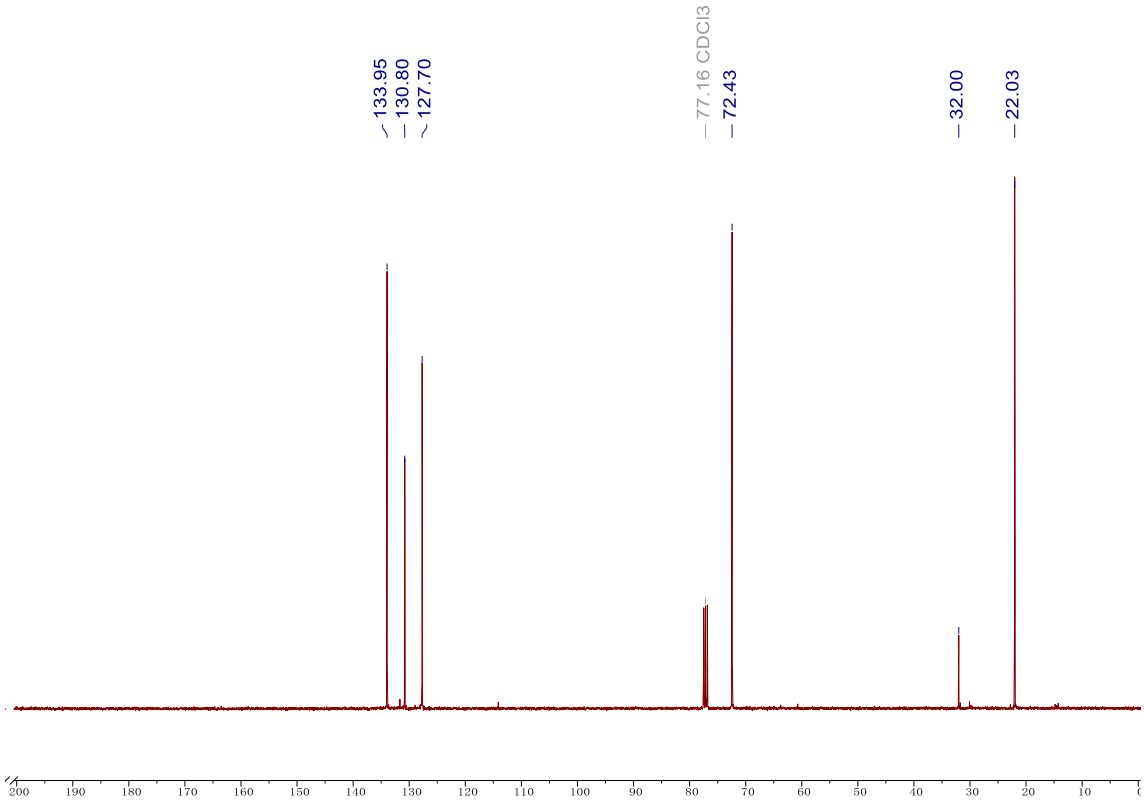

*(1S,2R,5S)-2-Isopropyl-5-methylcyclohexyl 4-(4,4,5,5-tetramethyl-1,3,2-dioxaborolan-2-yl)benzoat (**65**) ^{1}H-NMR spectrum in $CDCl_3$*

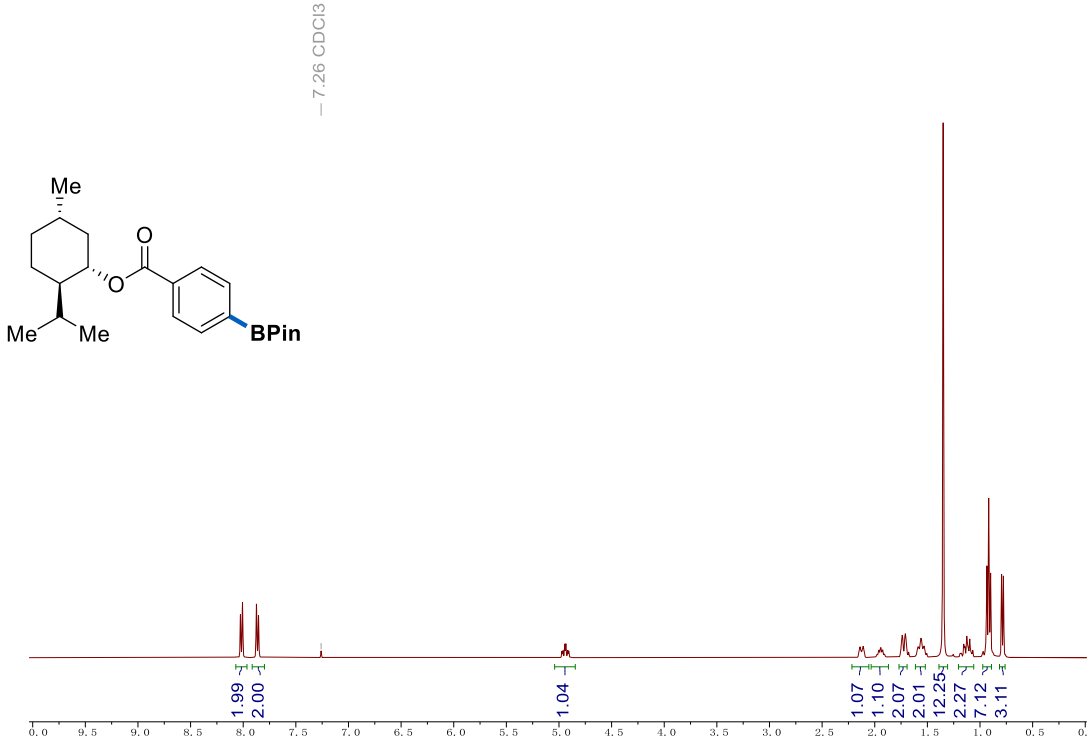

*(1S,2R,5S)-2-Isopropyl-5-methylcyclohexyl 4-(4,4,5,5-tetramethyl-1,3,2-dioxaborolan-2-yl)benzoat (**65**) ^{13}C-NMR spectrum in $CDCl_3$*

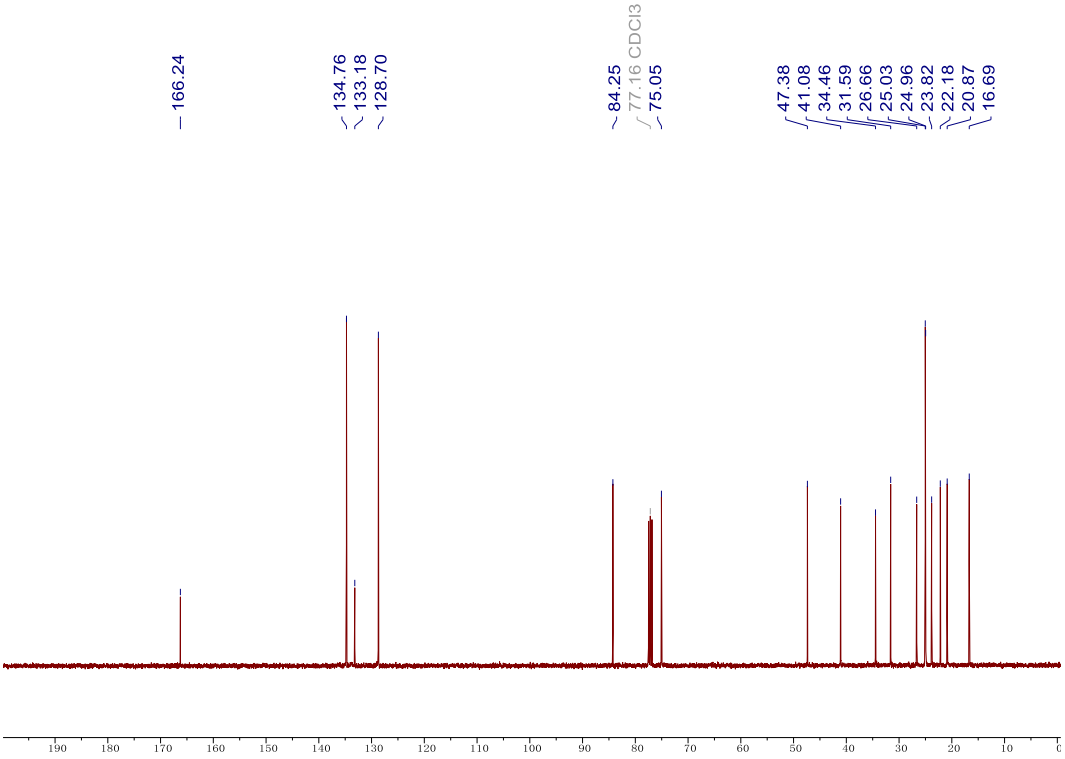

*(E)-3,7-Dimethylocta-2,6-dien-1-yl 4-(4,4,5,5-tetramethyl-1,3,2-dioxaborolan-2-yl)benzoate (**66**)*
^{1}H-NMR spectrum in $CDCl_3$

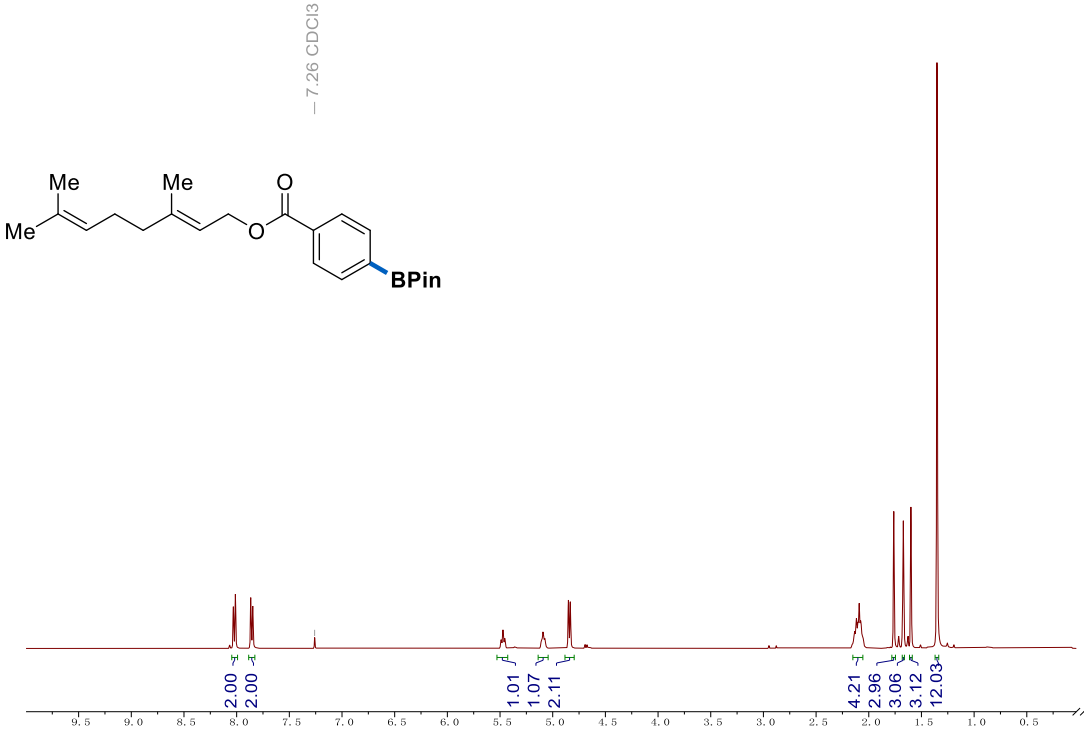

*(E)-3,7-Dimethylocta-2,6-dien-1-yl 4-(4,4,5,5-tetramethyl-1,3,2-dioxaborolan-2-yl)benzoate (**66**)*
^{13}C-NMR spectrum in $CDCl_3$

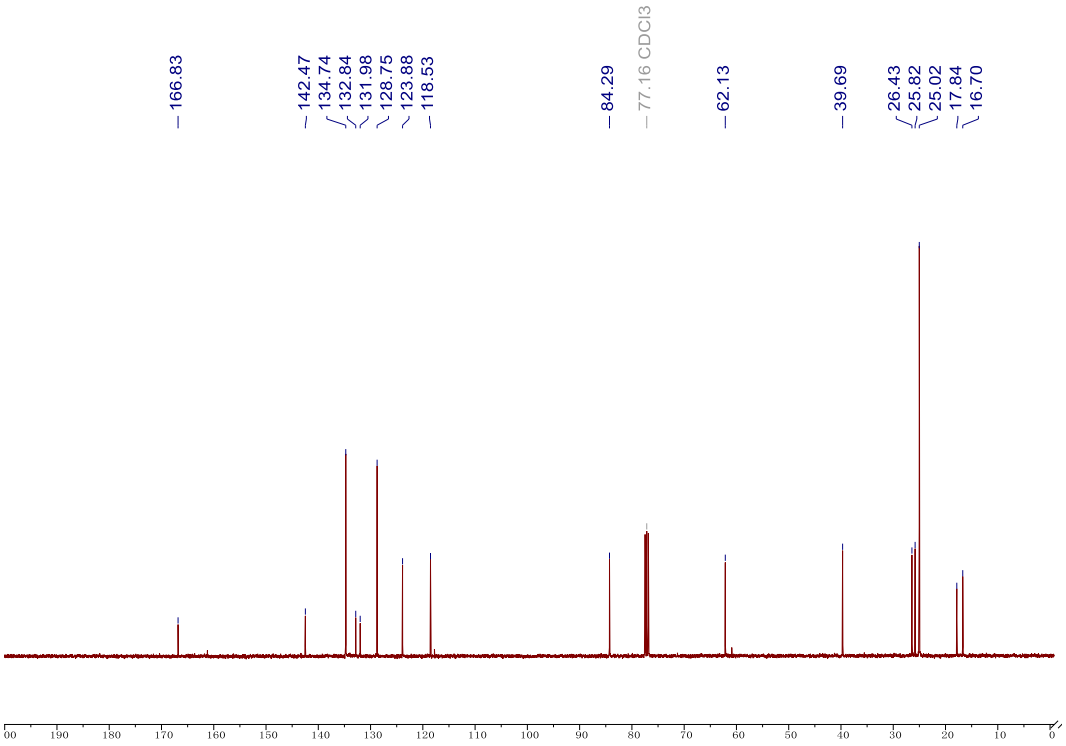

*1,3,3-Trimethylbicyclo[2.2.1]heptan-2-yl 4-(4,4,5,5-tetramethyl-1,3,2-dioxaborolan-2-yl)benzoate (**67**) ^{1}H-NMR spectrum in $CDCl_3$*

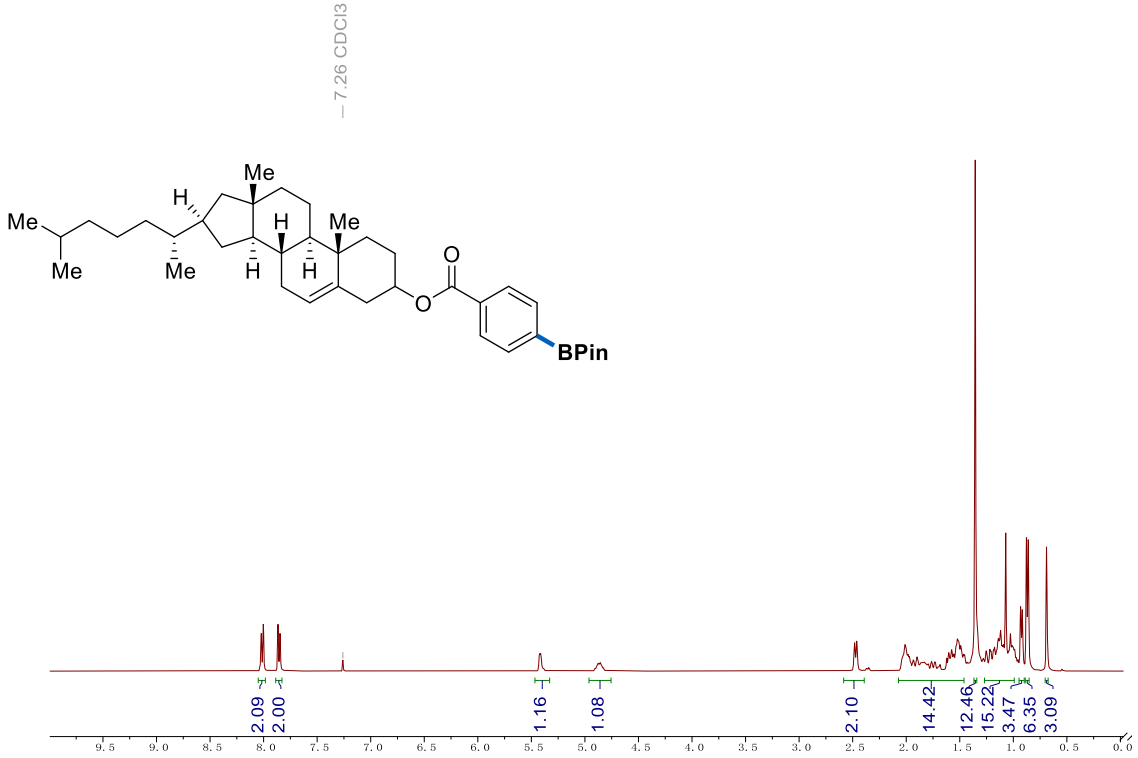

*1,3,3-Trimethylbicyclo[2.2.1]heptan-2-yl 4-(4,4,5,5-tetramethyl-1,3,2-dioxaborolan-2-yl)benzoate (**67**) ^{13}C-NMR spectrum in $CDCl_3$*

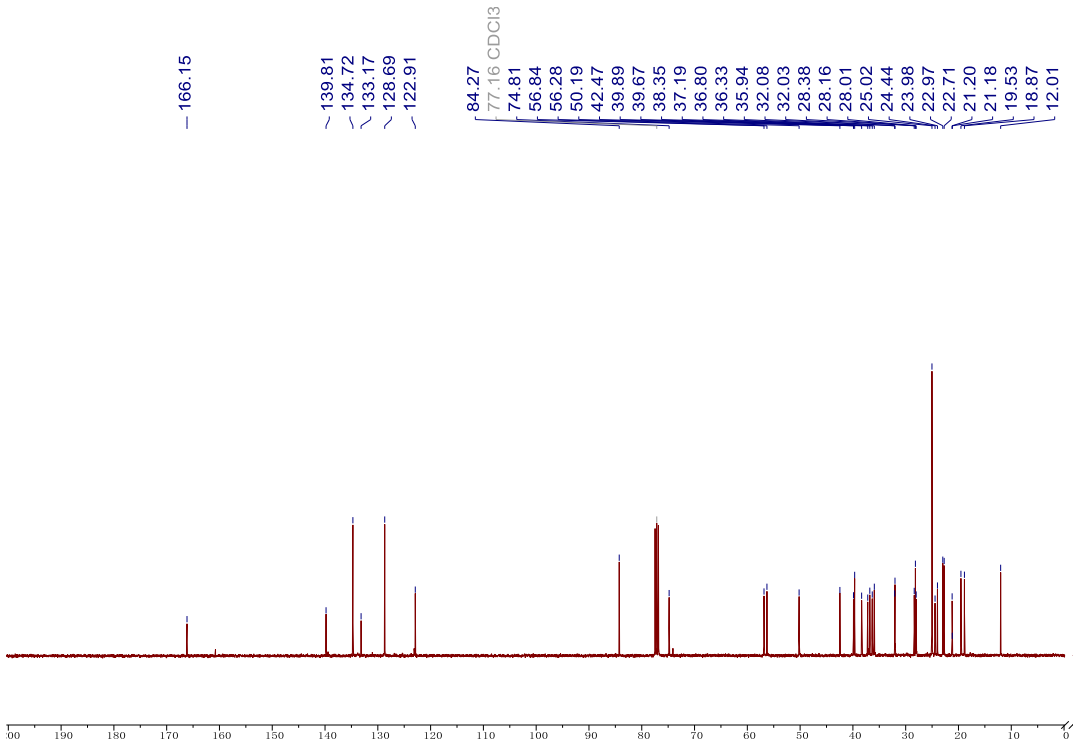

*9-(3-(4,4,5,5-tetramethyl-1,3,2-dioxaborolan-2-yl)phenyl)carbazole (**68**) ^{1}H-NMR spectrum in $CDCl_3$*

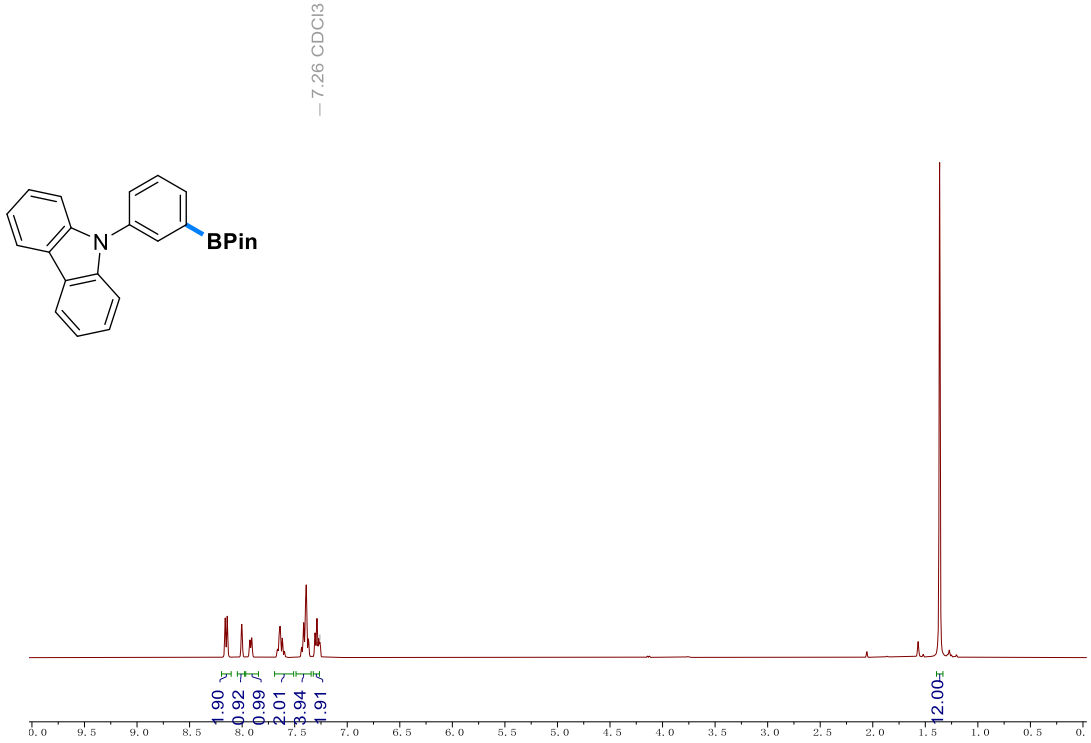

*9-(3-(4,4,5,5-tetramethyl-1,3,2-dioxaborolan-2-yl)phenyl)carbazole (**68**) ^{13}C-NMR spectrum in $CDCl_3$*

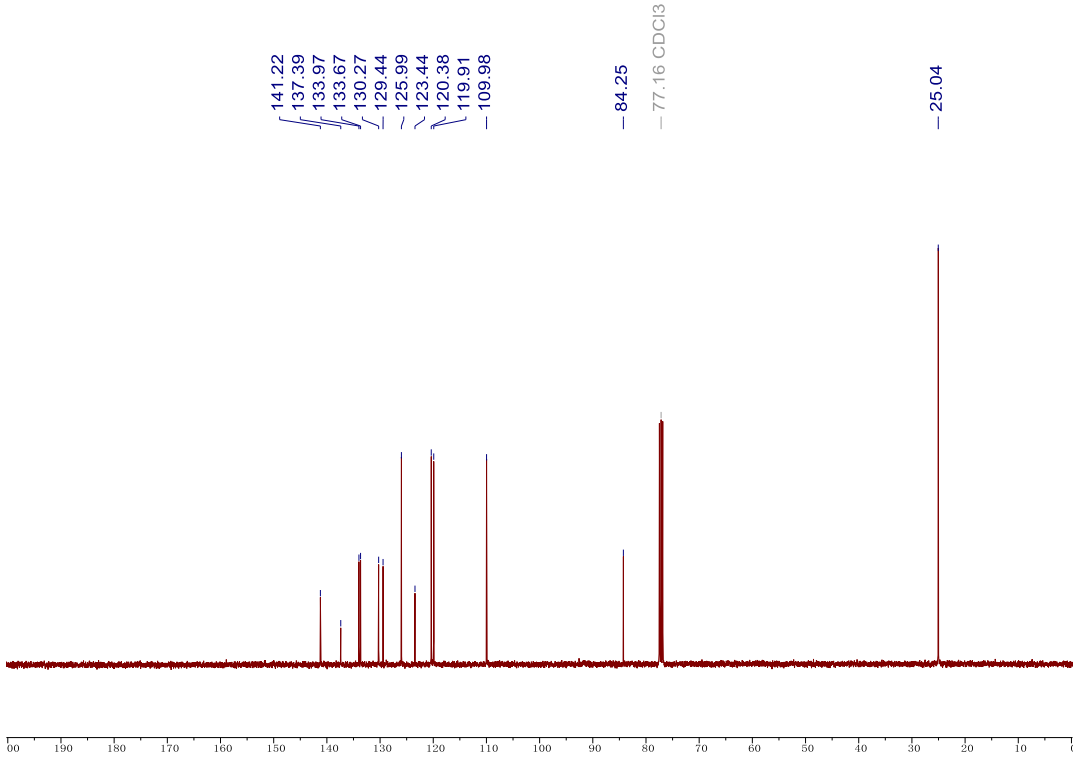

*2-(biphenyl-4-yl)-4,4,5,5-tetramethyl-1,3,2-dioxaborolane (**69**) ^{1}H-NMR spectrum in $CDCl_3$*

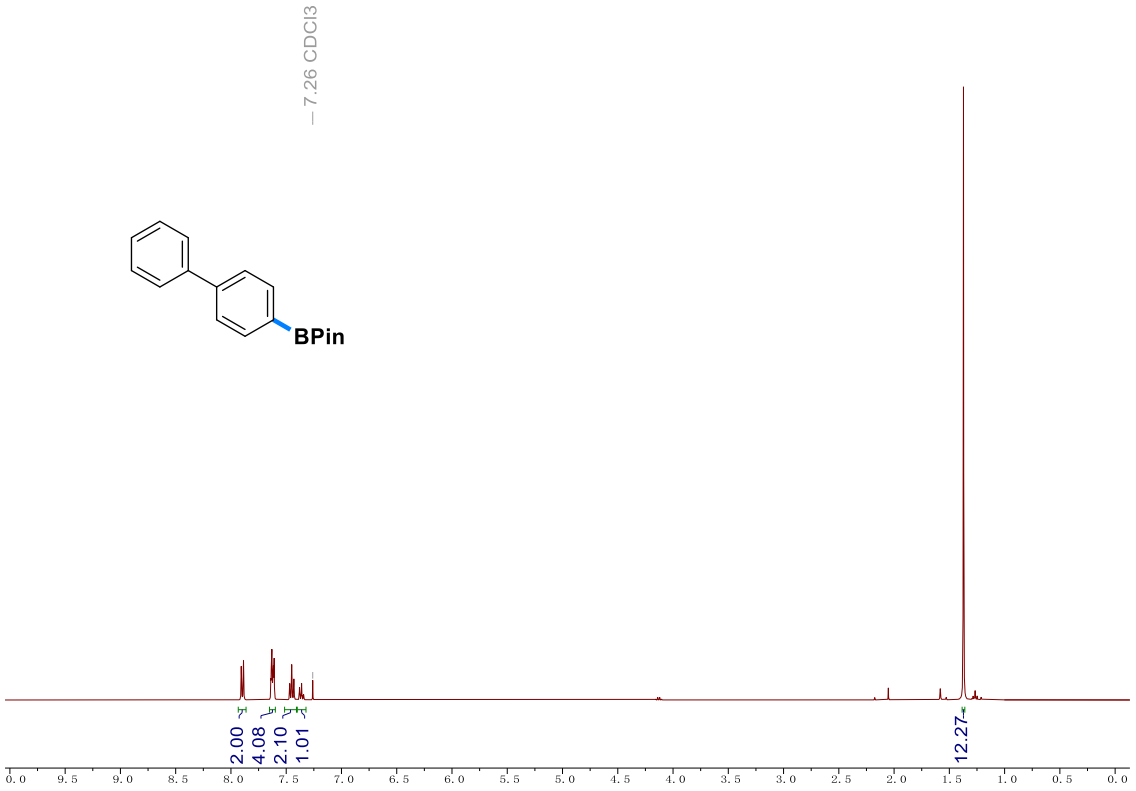

*2-(biphenyl-4-yl)-4,4,5,5-tetramethyl-1,3,2-dioxaborolane (**69**) ^{13}C-NMR spectrum in $CDCl_3$*

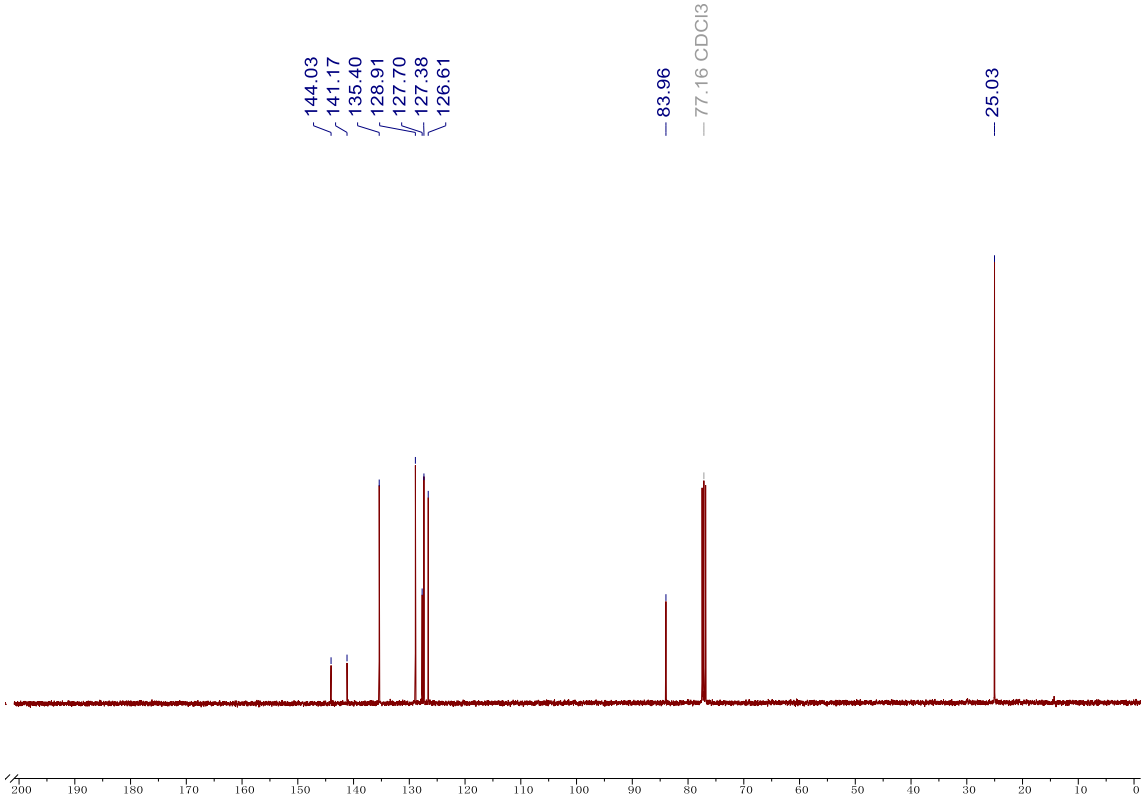

*Diethyl phenylphosphonate (**70**) ^{1}H-NMR spectrum in $CDCl_3$*

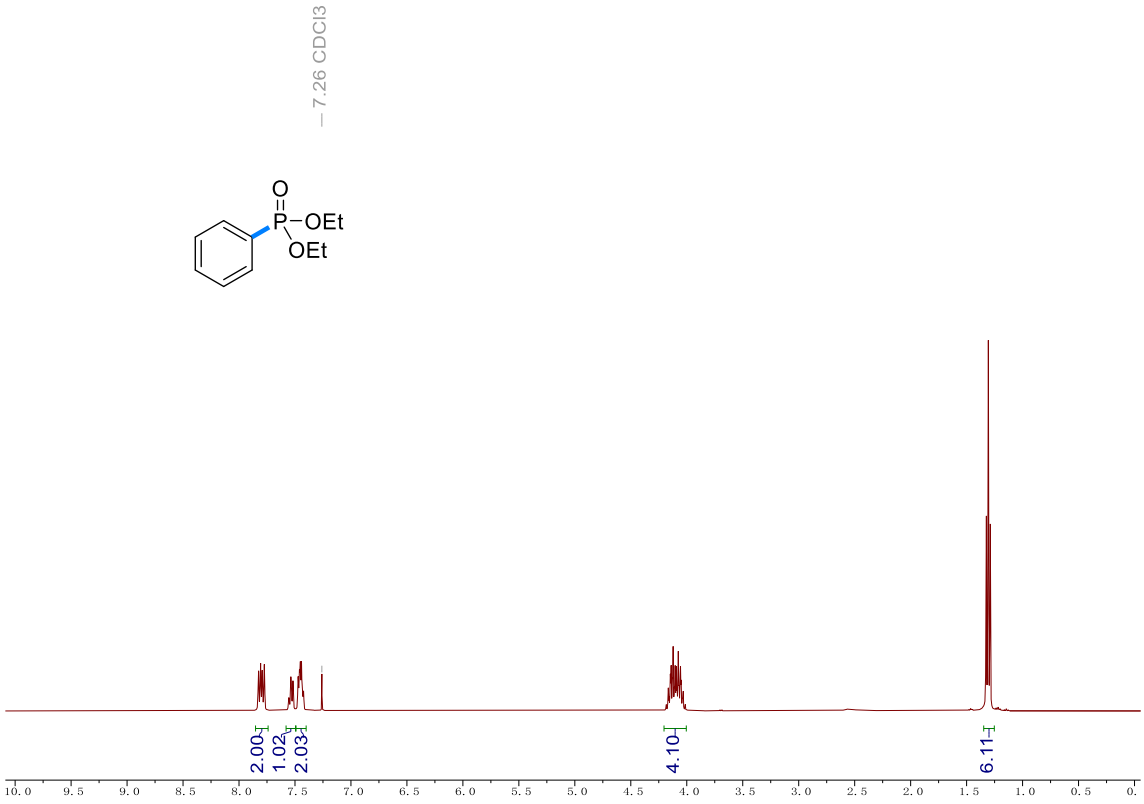

*Diethyl phenylphosphonate (**70**) ^{13}C-NMR spectrum in $CDCl_3$*

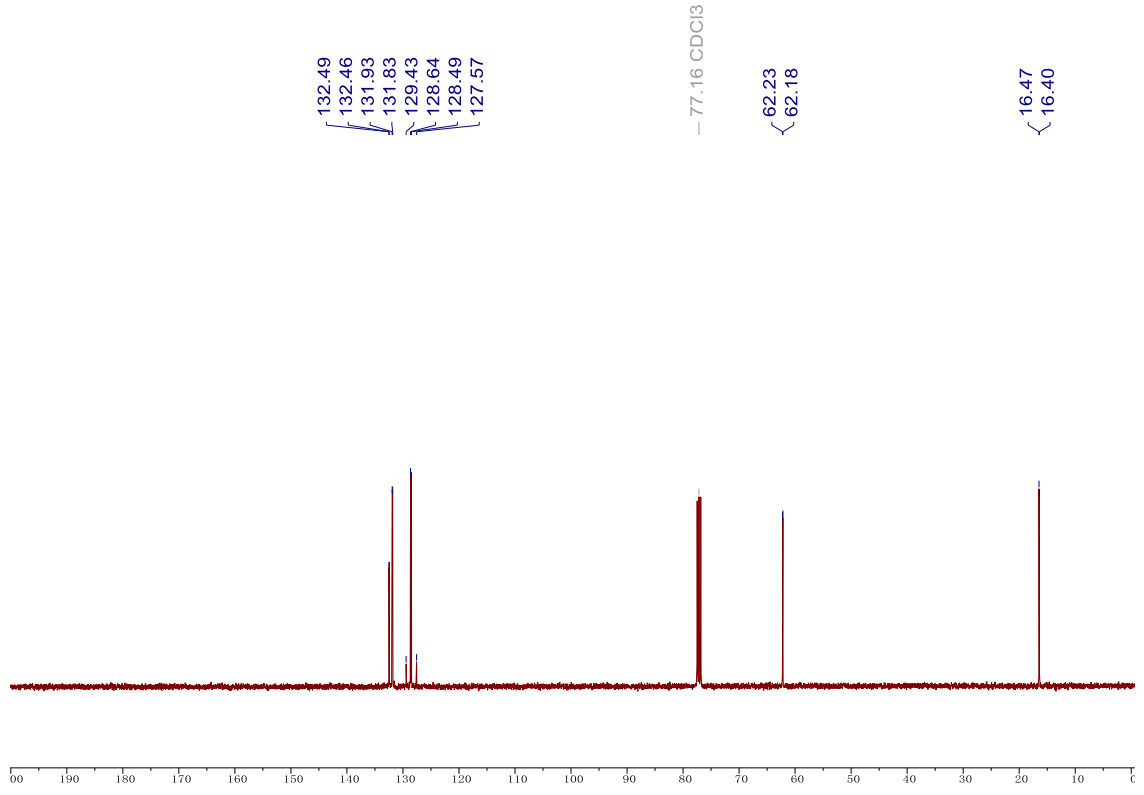

*Diethyl phenylphosphonate (**70**) ^{31}P-NMR spectrum in $CDCl_3$*

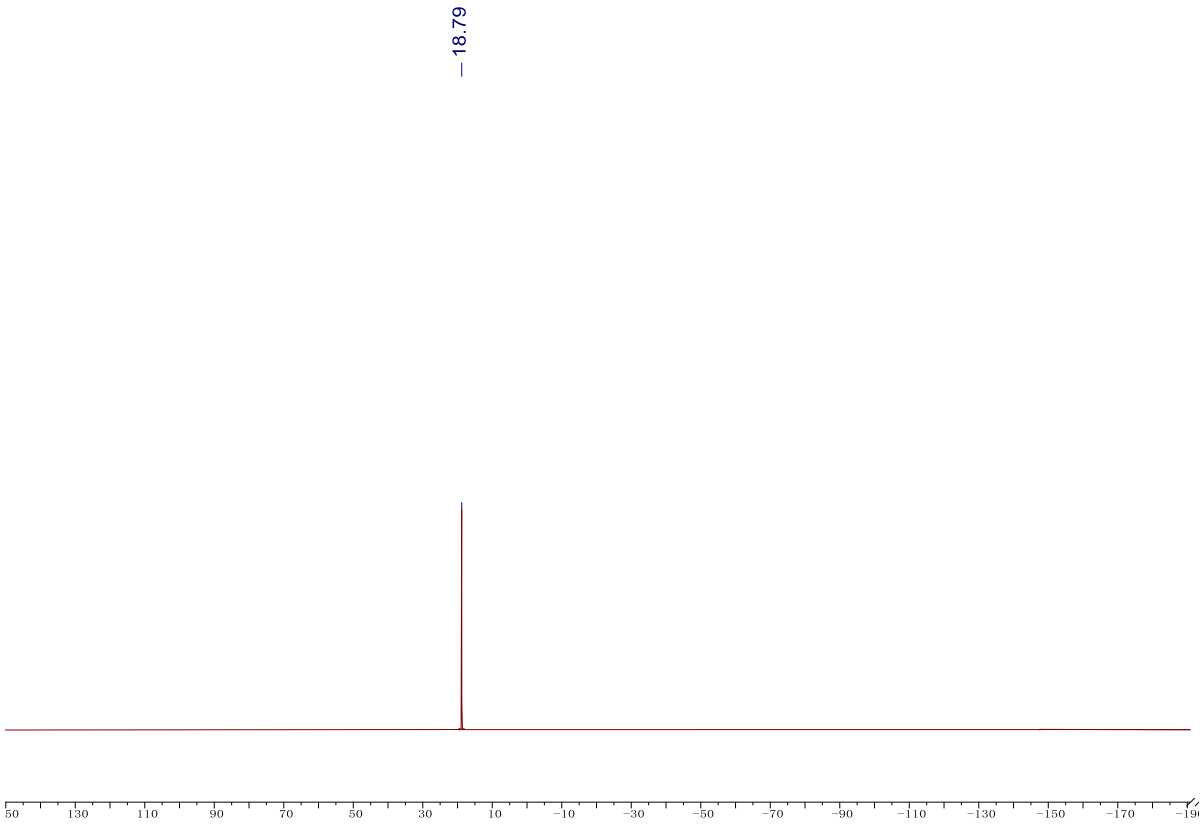

*Diethyl 4-methoxyphenylphosphonate (**71**) ^{1}H-NMR spectrum in $CDCl_3$*

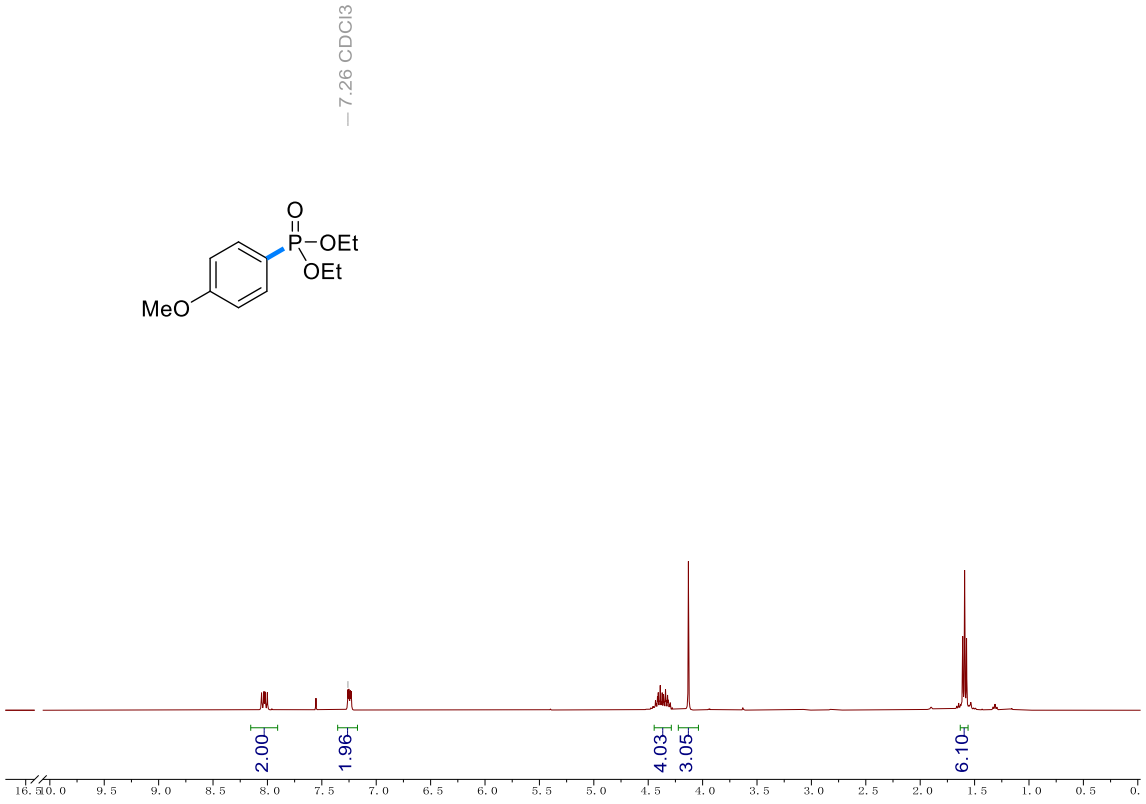

*Diethyl 4-methoxyphenylphosphonate (**71**) ^{13}C-NMR spectrum in $CDCl_3$*

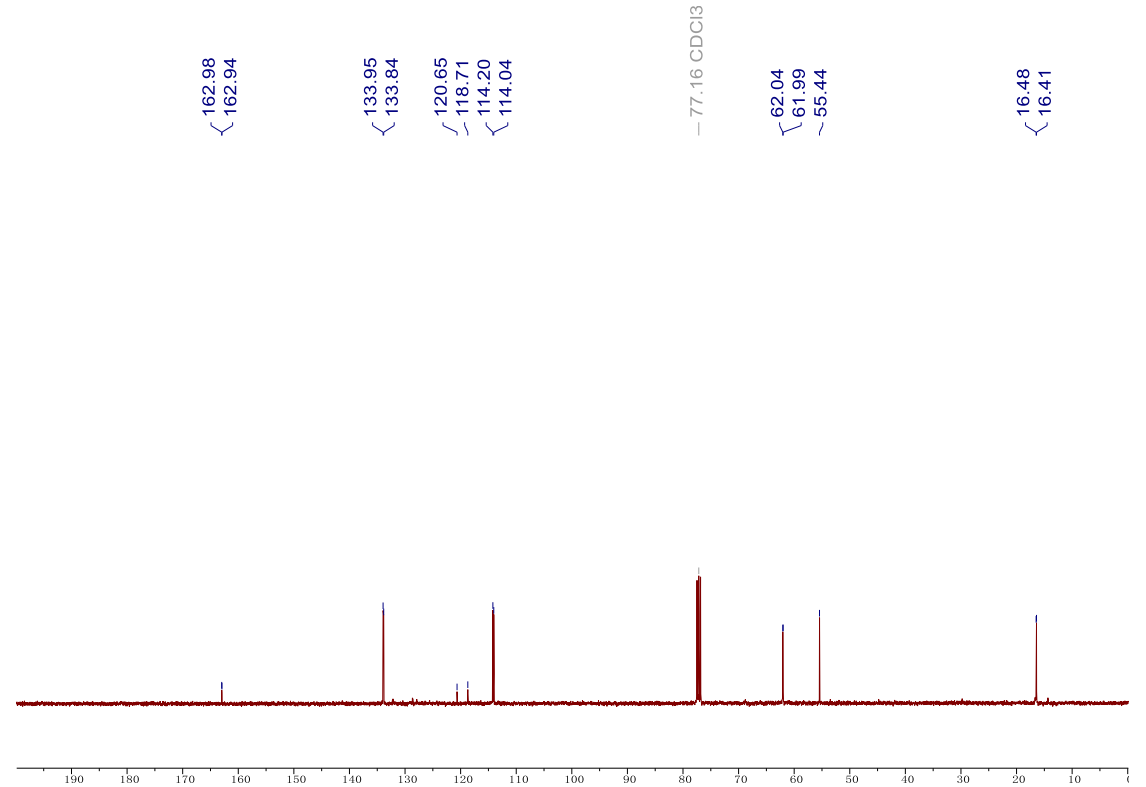

*Diethyl 4-methoxyphenylphosphonate (**71**) ^{31}P-NMR spectrum in $CDCl_3$*

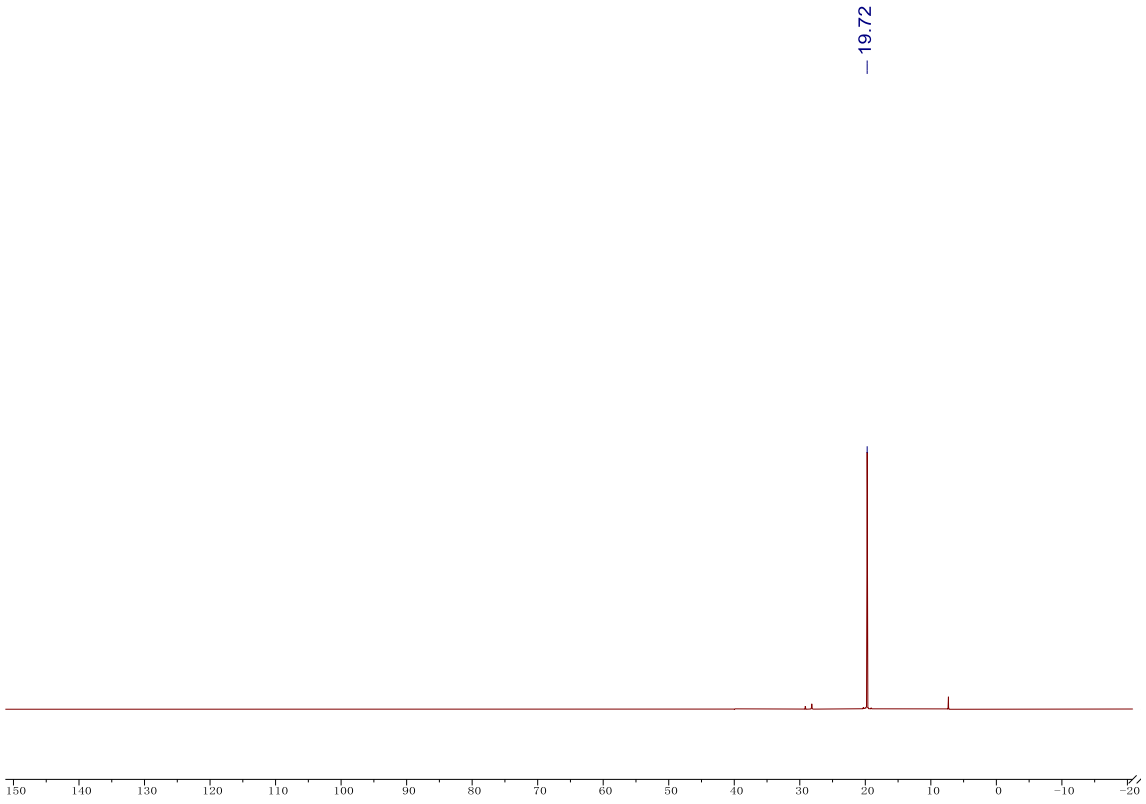

*Diethyl (m-tolyl)phosphonate (**72**) ^{1}H-NMR spectrum in $CDCl_3$*

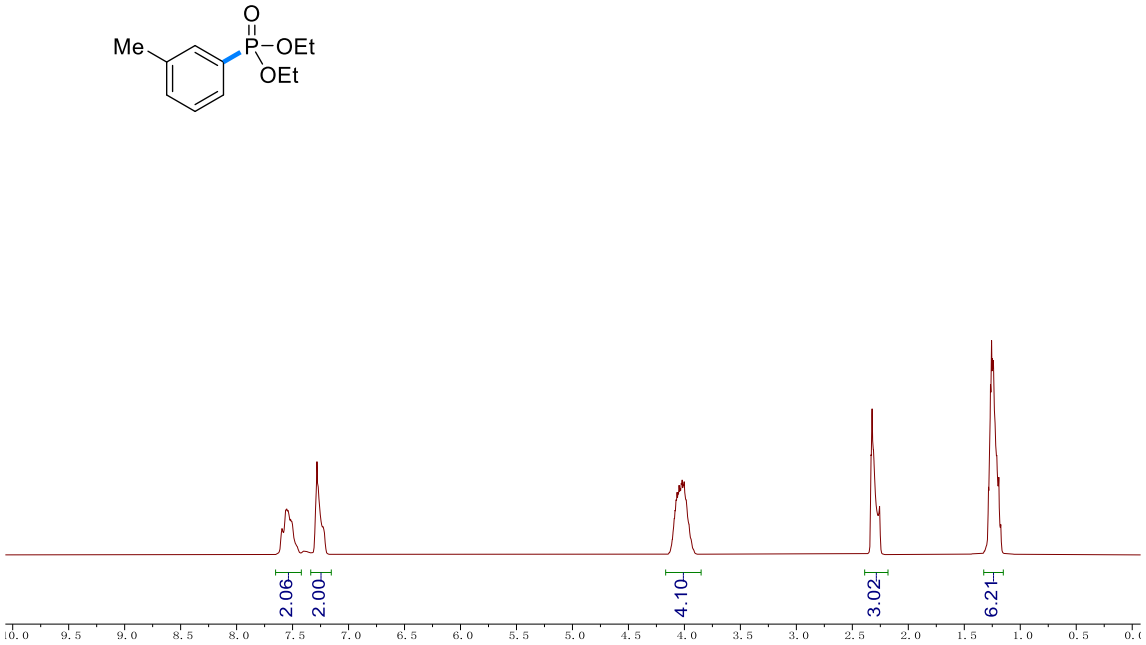

*Diethyl (m-tolyl)phosphonate (**72**) ^{13}C-NMR spectrum in $CDCl_3$*

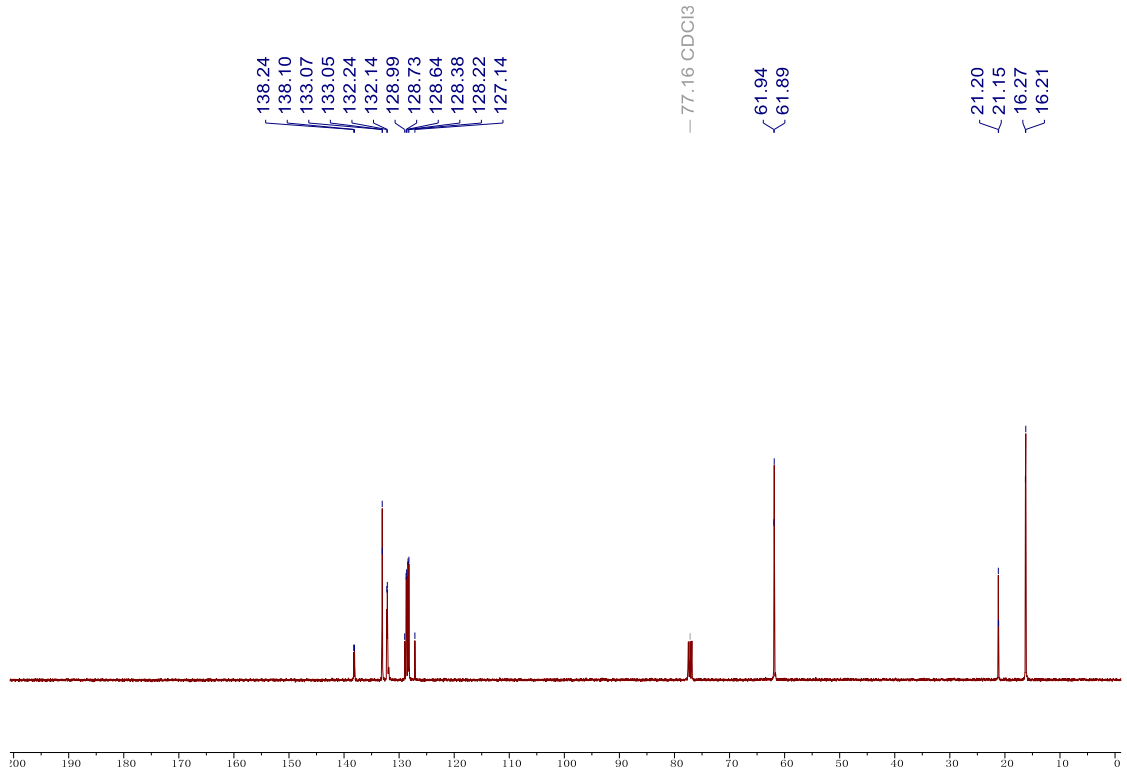

*Diethyl (m-tolyl)phosphonate (**72**) ^{31}P-NMR spectrum in $CDCl_3$*

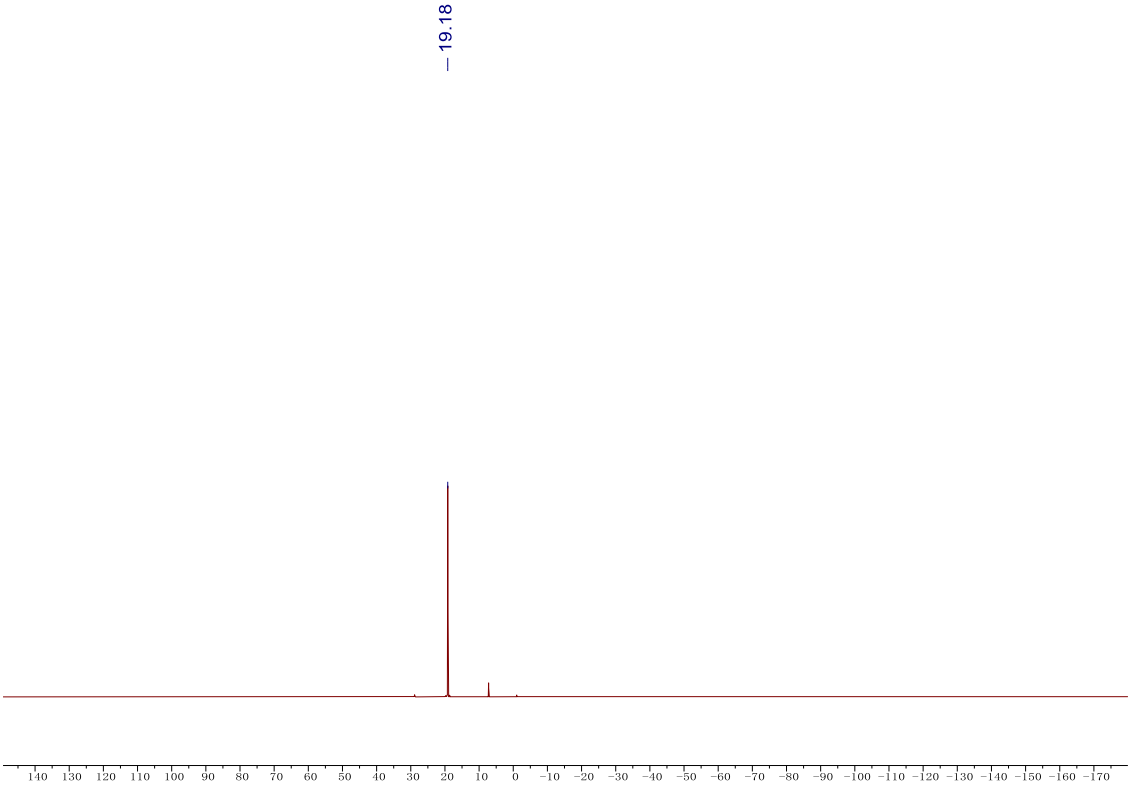

*1-Methyl-2-(4-cyanophenyl)pyrrole (**75**) ^{1}H-NMR spectrum in $CDCl_3$*

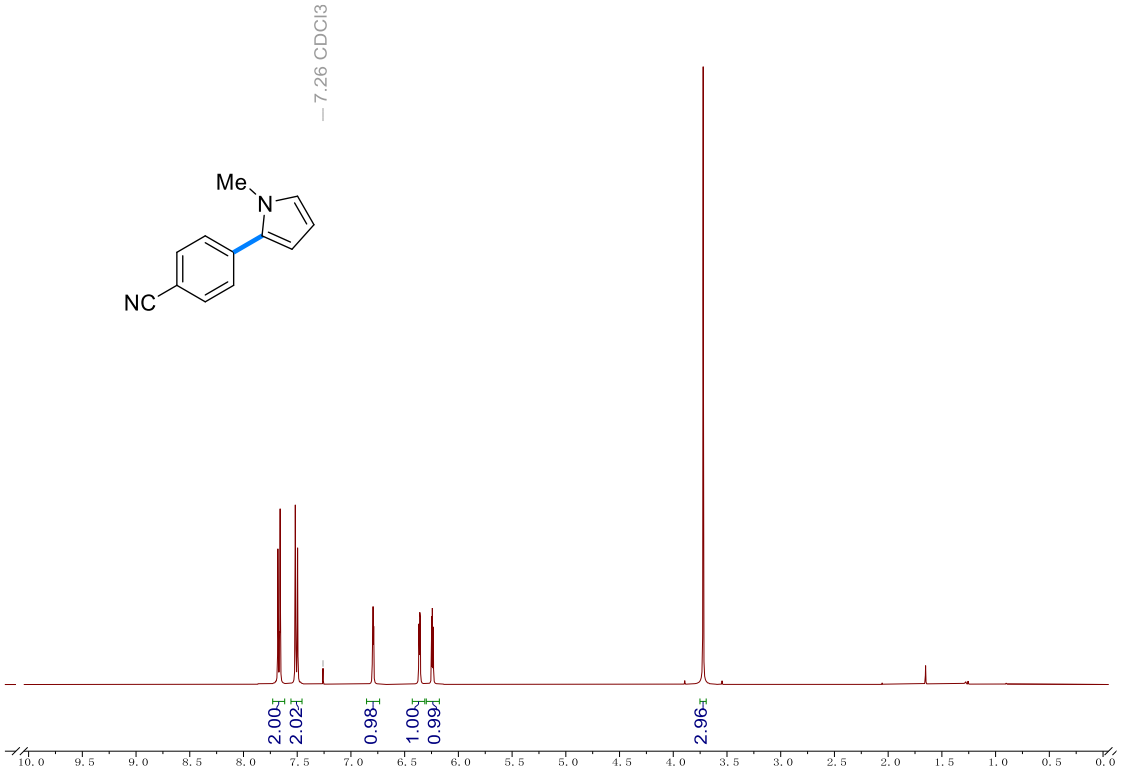

*1-Methyl-2-(4-cyanophenyl)pyrrole (**75**) ^{13}C-NMR spectrum in $CDCl_3$*

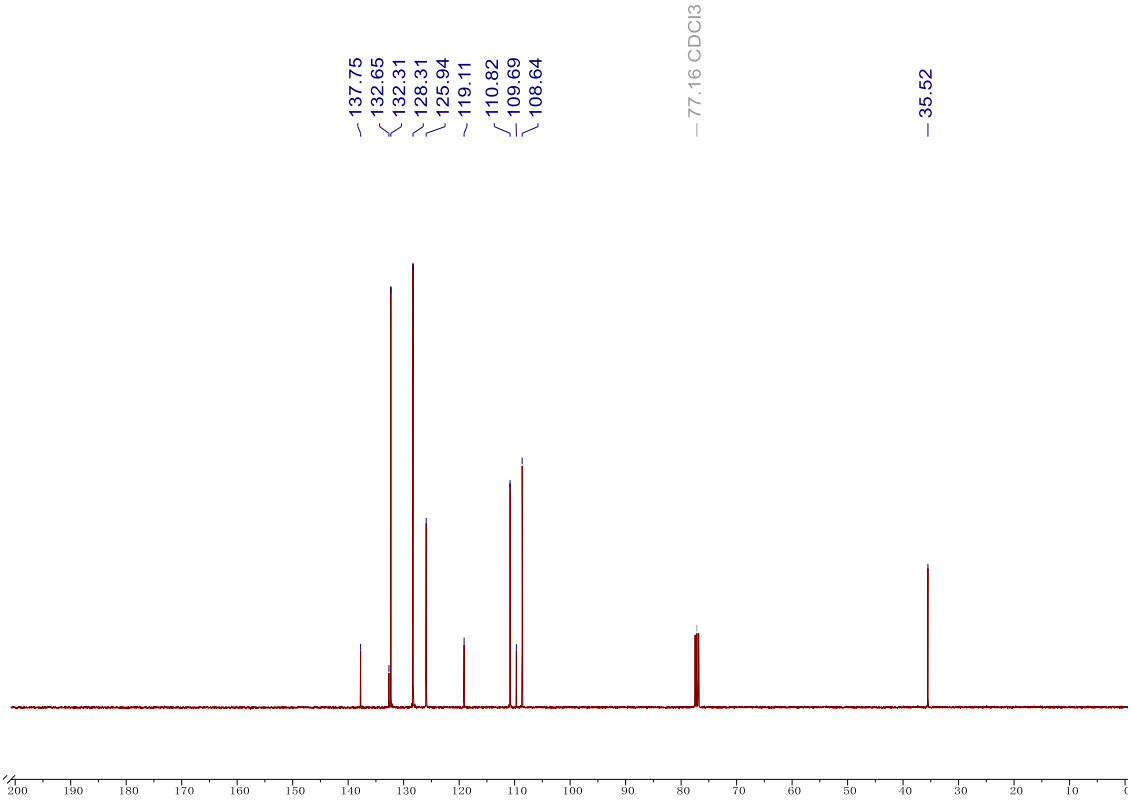

*2-(1-methyl-1H-pyrrol-2-yl)benzonitrile (**77**) ^{1}H-NMR spectrum in $CDCl_3$*

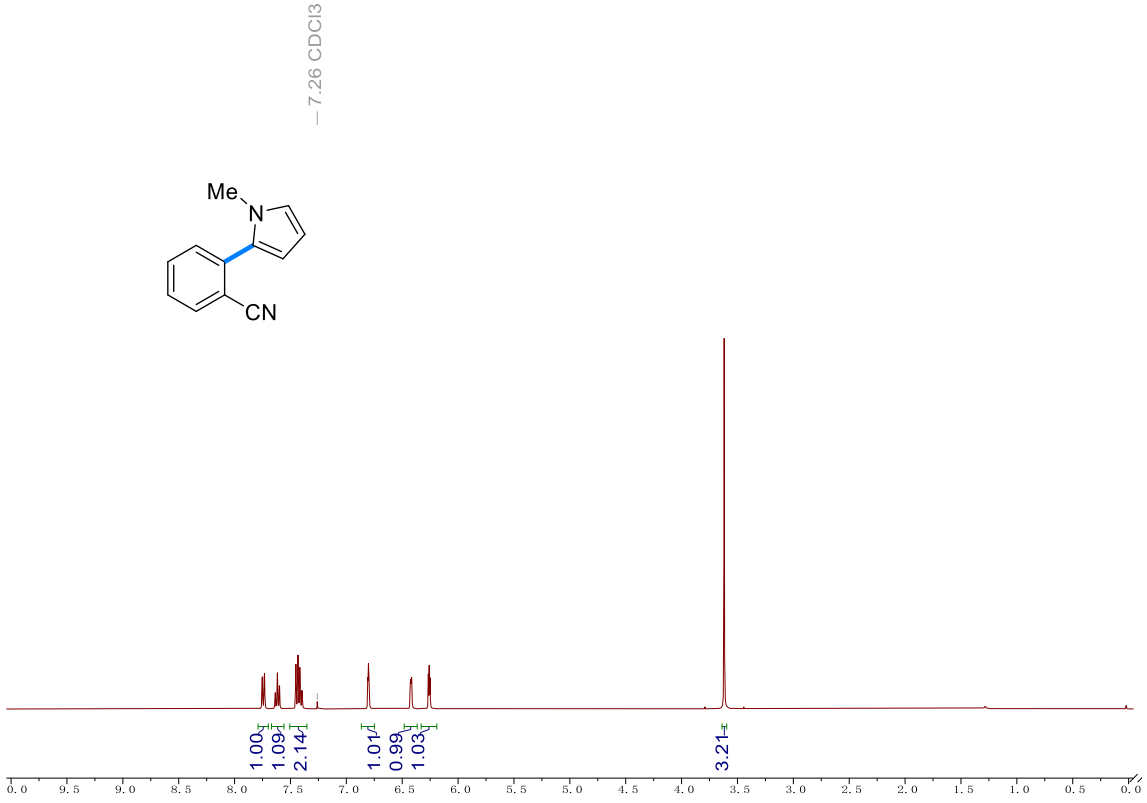

*2-(1-methyl-1H-pyrrol-2-yl)benzonitrile (**77**) ^{13}C-NMR spectrum in $CDCl_3$*

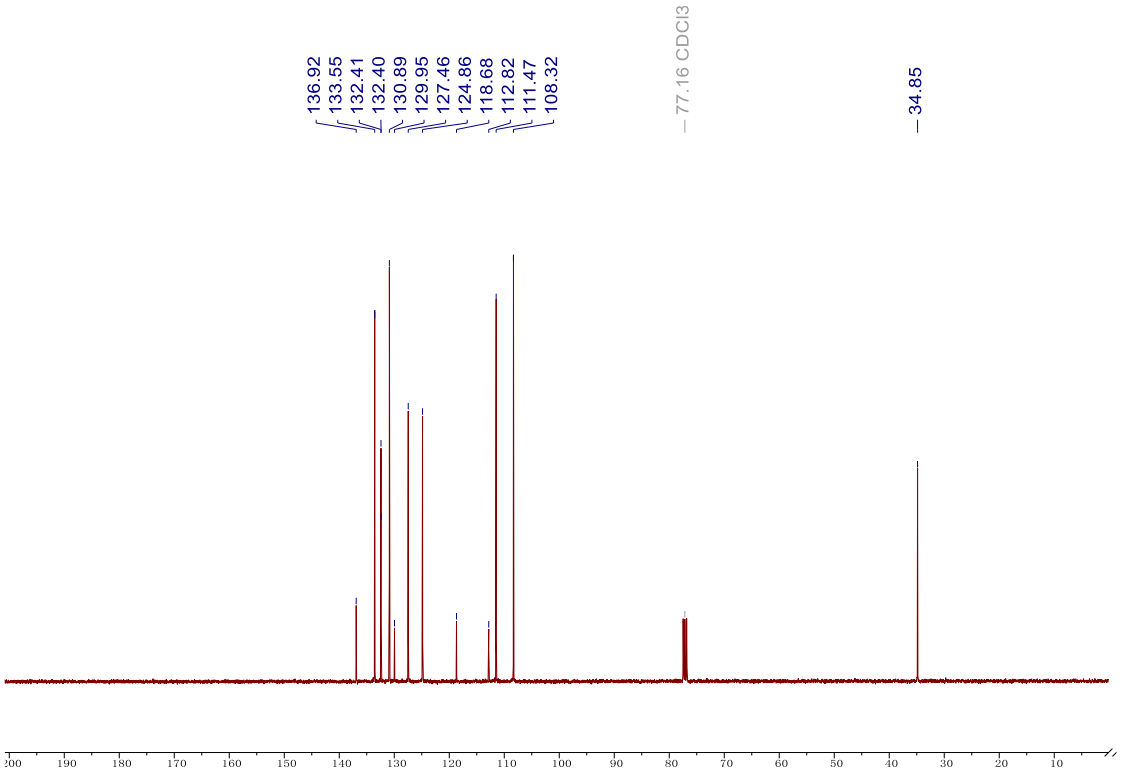

*1-(4-(1-methyl-1H-pyrrol-2-yl)phenyl)ethan-1-one (**78**) ^{1}H-NMR spectrum in $CDCl_3$*

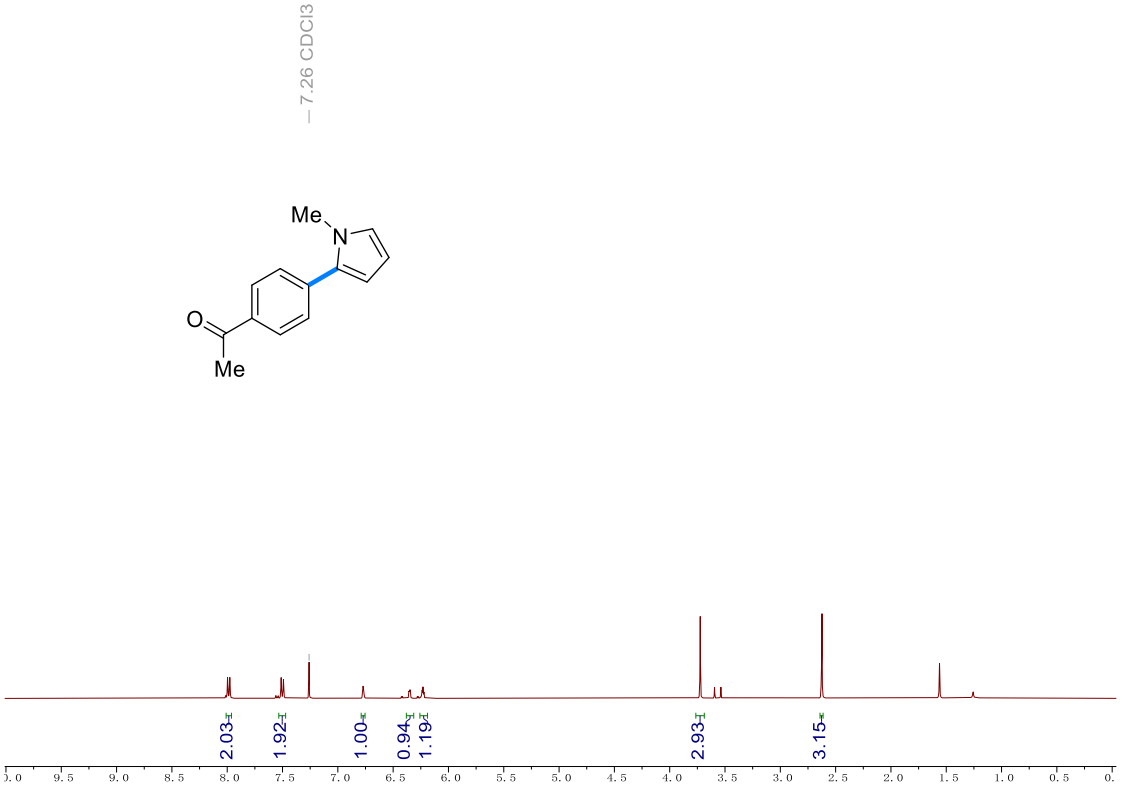

*1-(4-(1-methyl-1H-pyrrol-2-yl)phenyl)ethan-1-one (**78**) ^{13}C-NMR spectrum in $CDCl_3$*

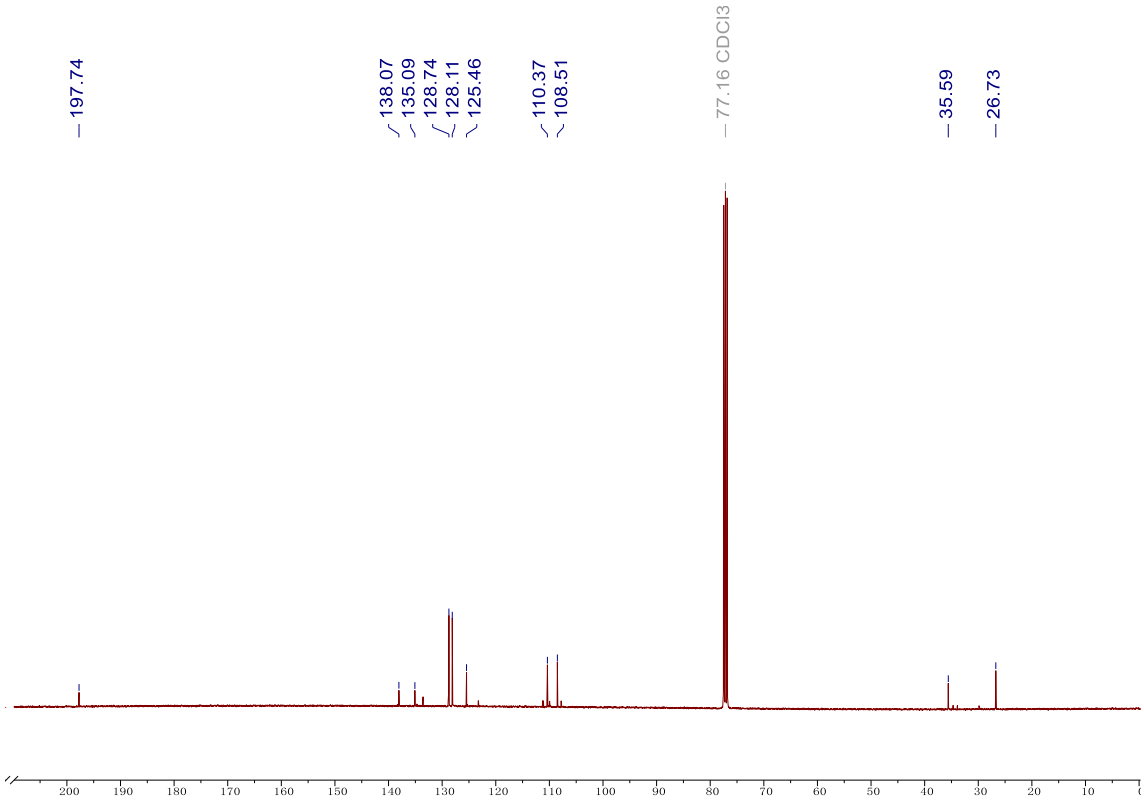

*1-benzyl-2-phenyl-1H-pyrrole (**80**) ^{1}H-NMR spectrum in $CDCl_3$*

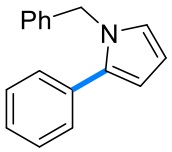

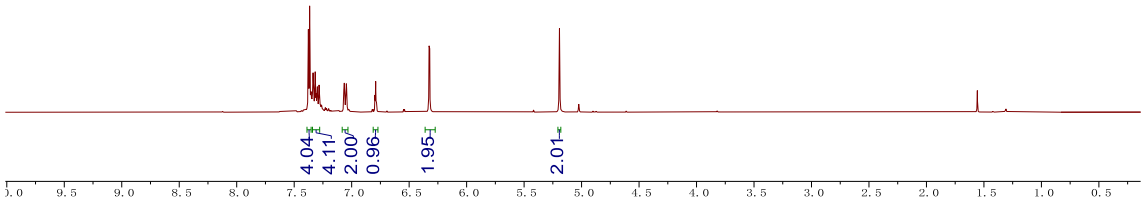

*1-benzyl-2-phenyl-1H-pyrrole (**80**) ^{13}C-NMR spectrum in $CDCl_3$*

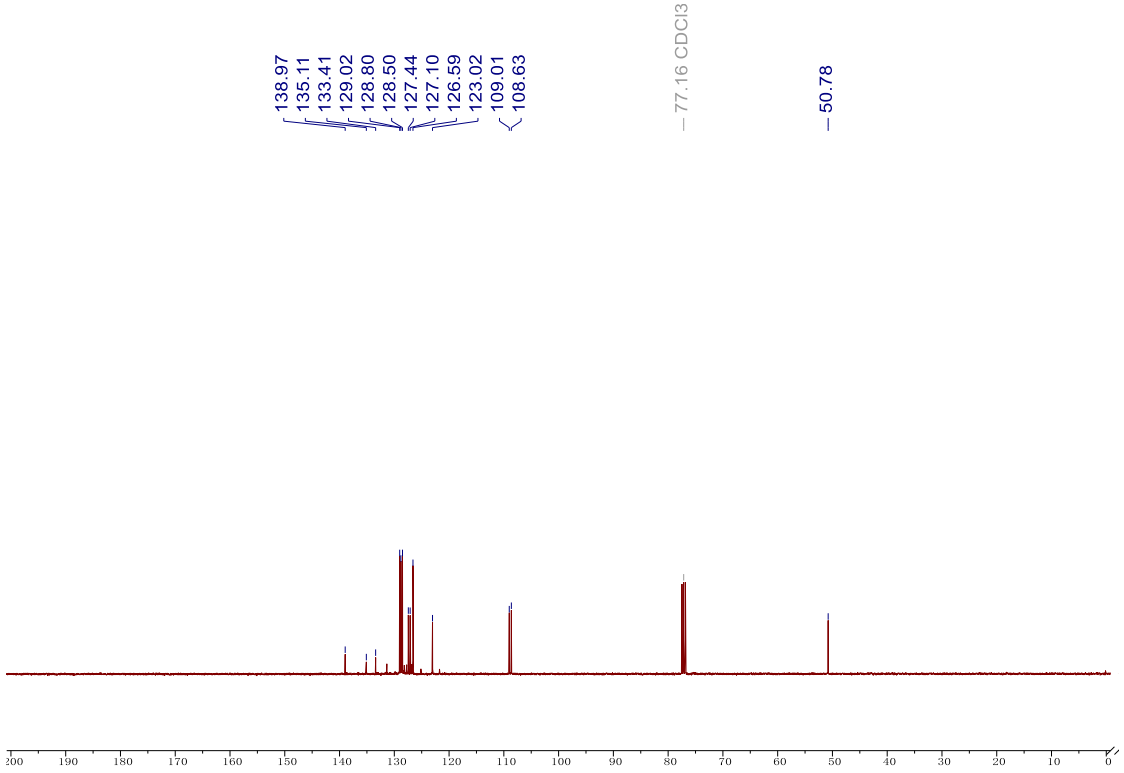

*4-Methylphenyl methylsulfide (**82**) ^{1}H-NMR spectrum in $CDCl_3$*

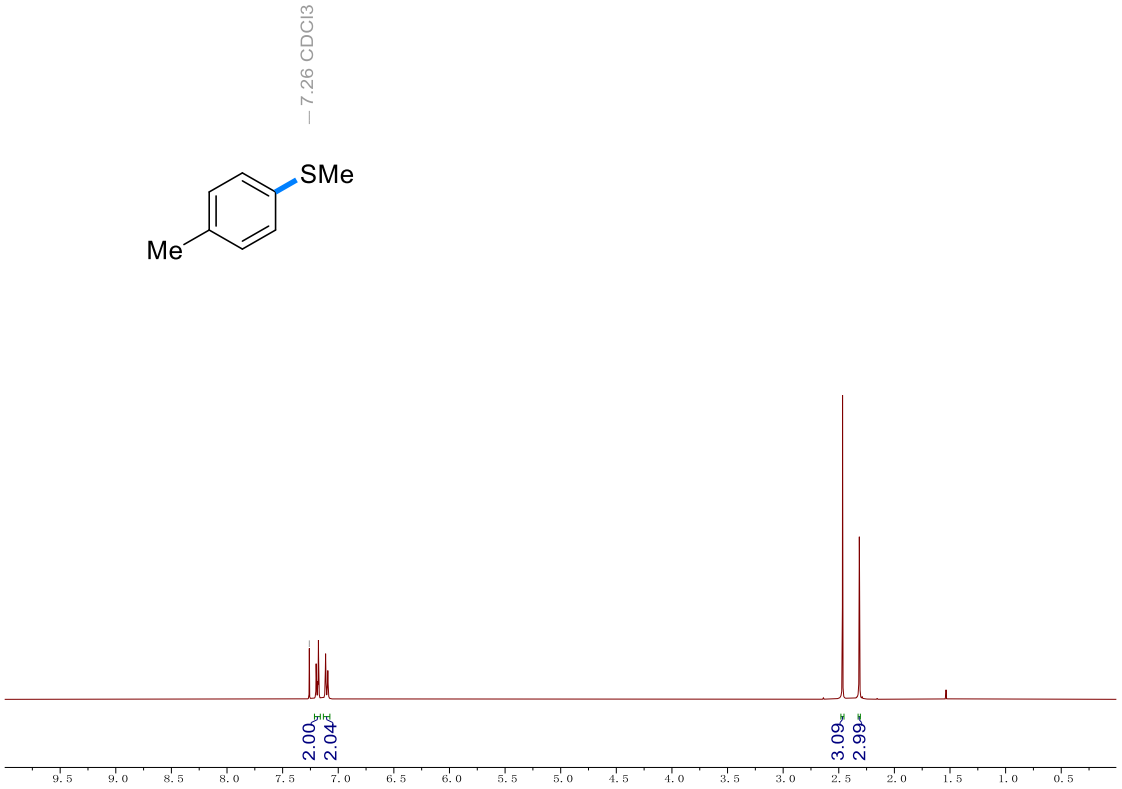

*4-Methylphenyl methylsulfide (**82**) ^{13}C-NMR spectrum in $CDCl_3$*

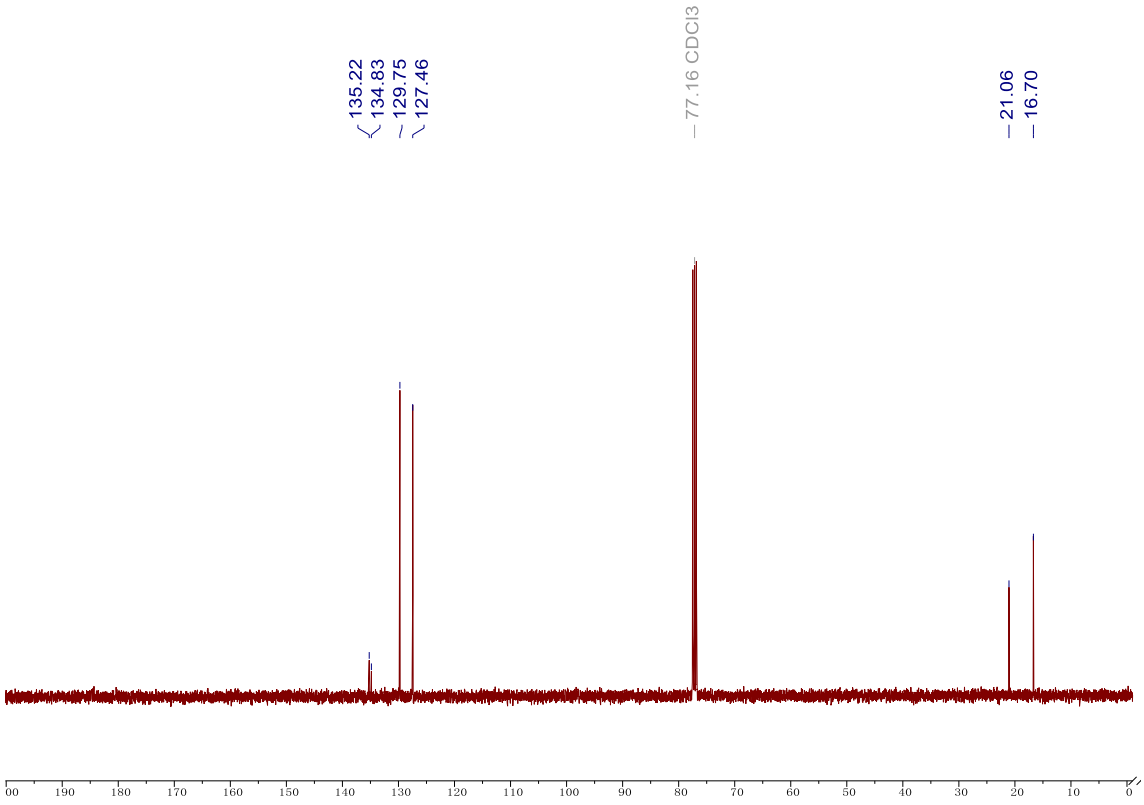

*4-Methoxythioanisole (**83**) ^{1}H-NMR spectrum in $CDCl_3$*

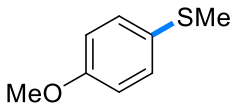

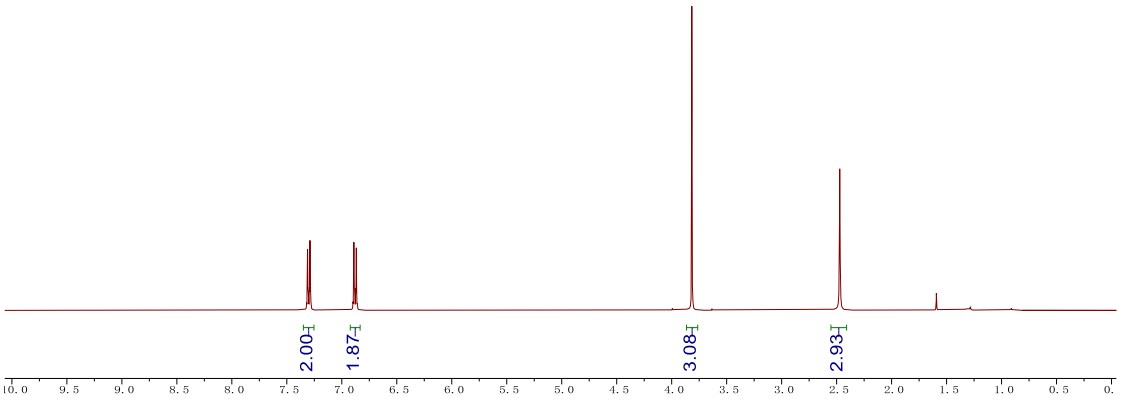

*4-Methoxythioanisole (**83**) ^{13}C-NMR spectrum in $CDCl_3$*

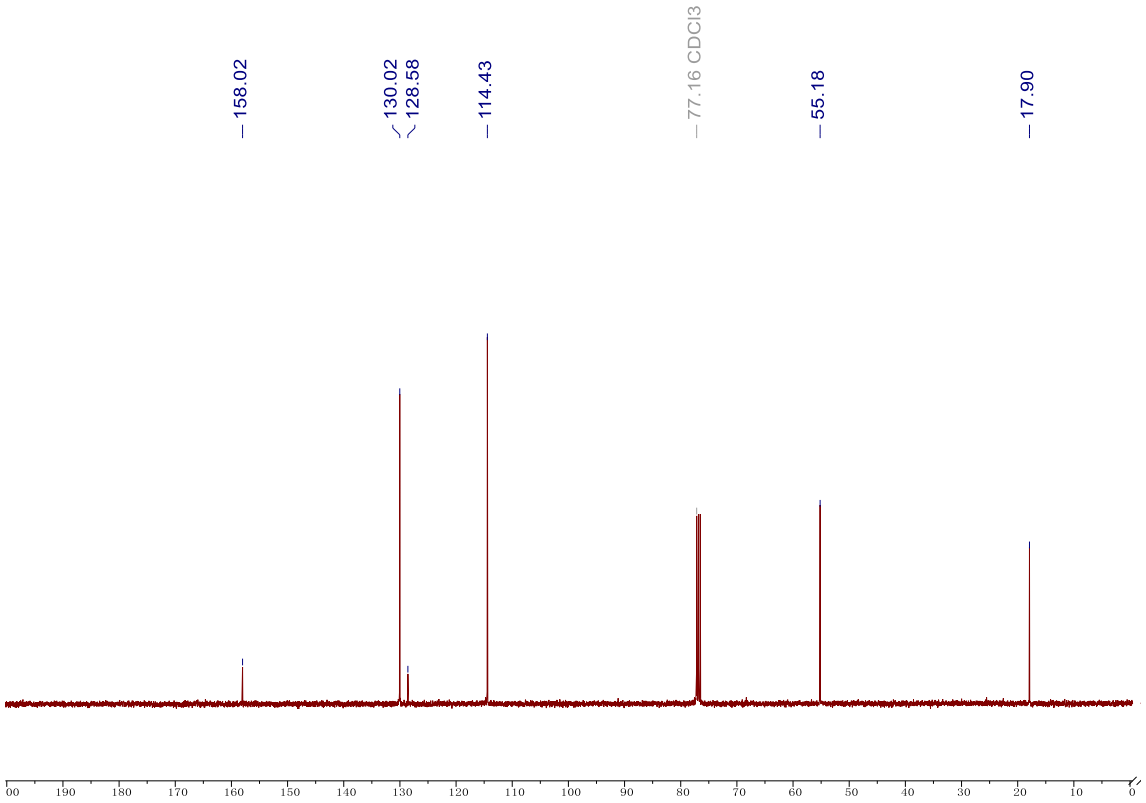

*3-Methoxythioanisole (**84**) ^{1}H-NMR spectrum in $CDCl_3$*

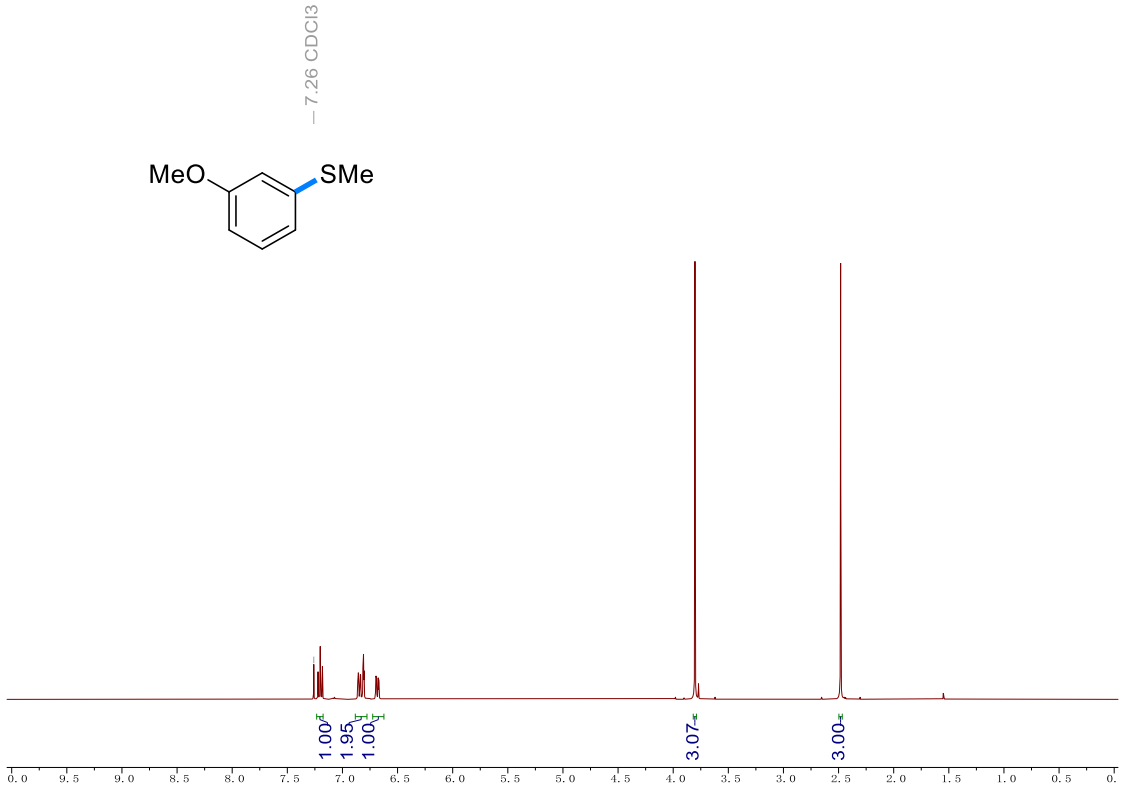

*3-Methoxythioanisole (**84**) ^{13}C-NMR spectrum in $CDCl_3$*

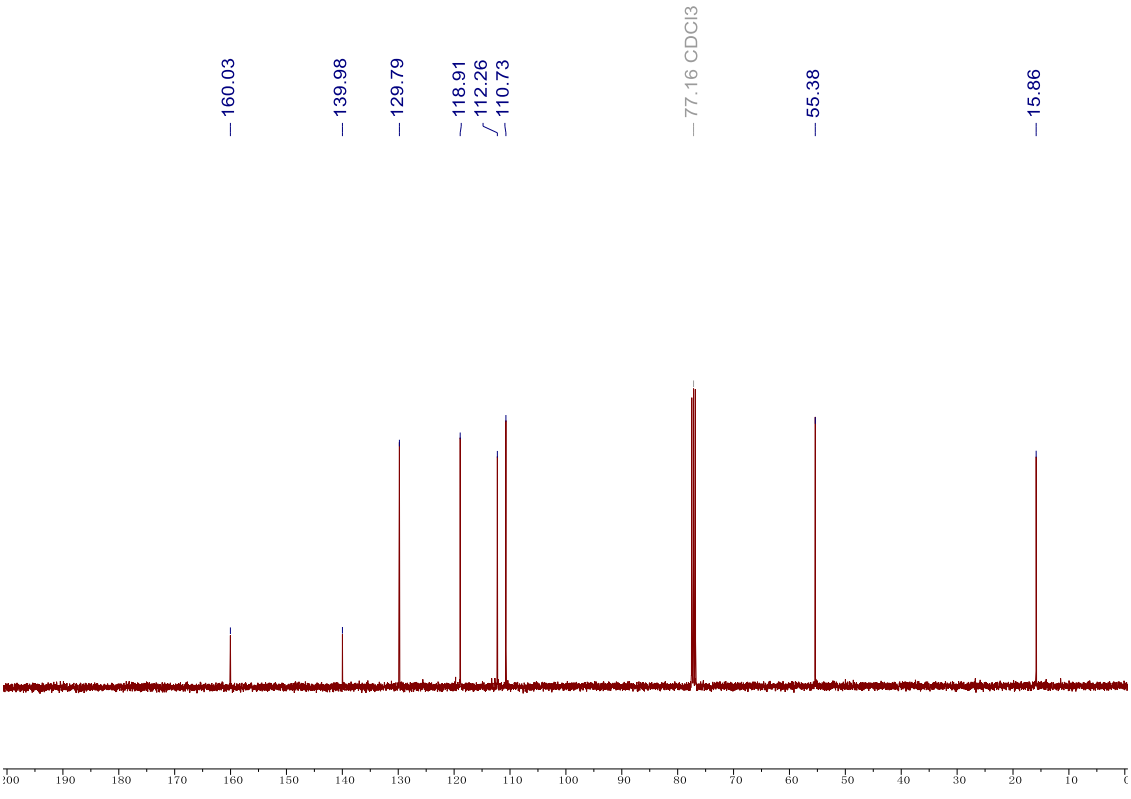

*2-Methoxythioanisole (**85**) ^{1}H-NMR spectrum in $CDCl_3$*

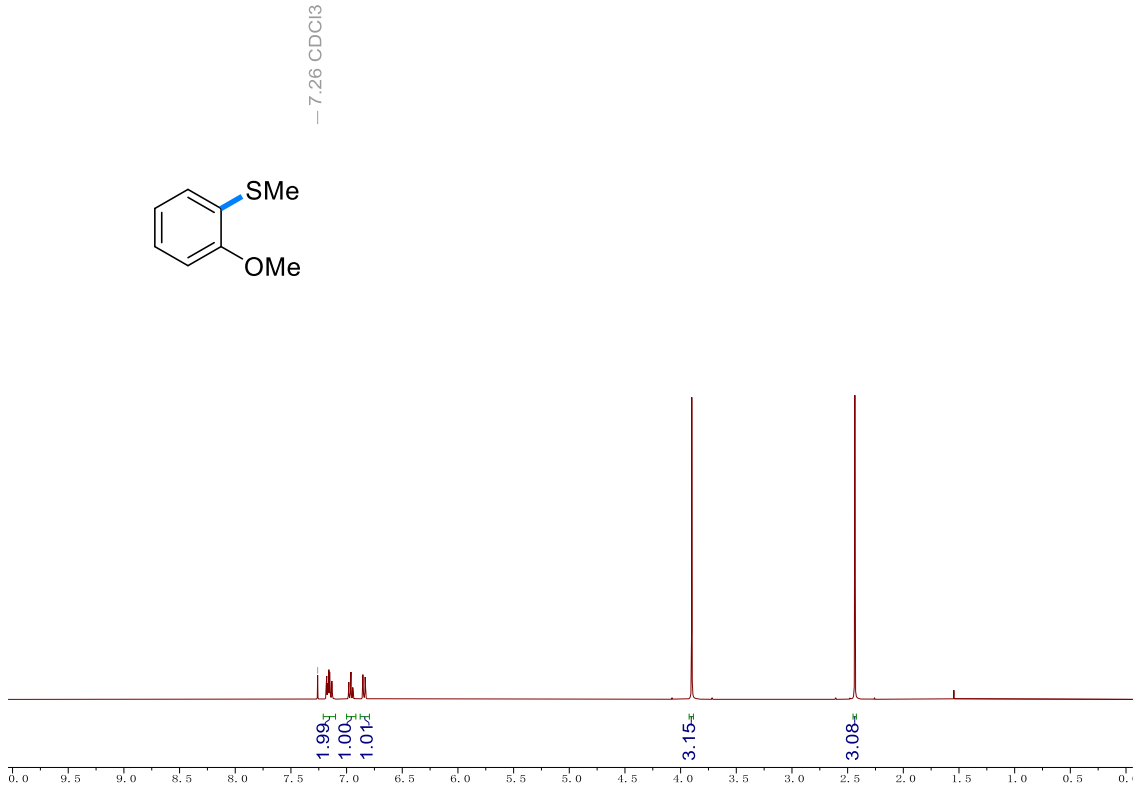

*2-Methoxythioanisole (**85**) ^{13}C-NMR spectrum in $CDCl_3$*

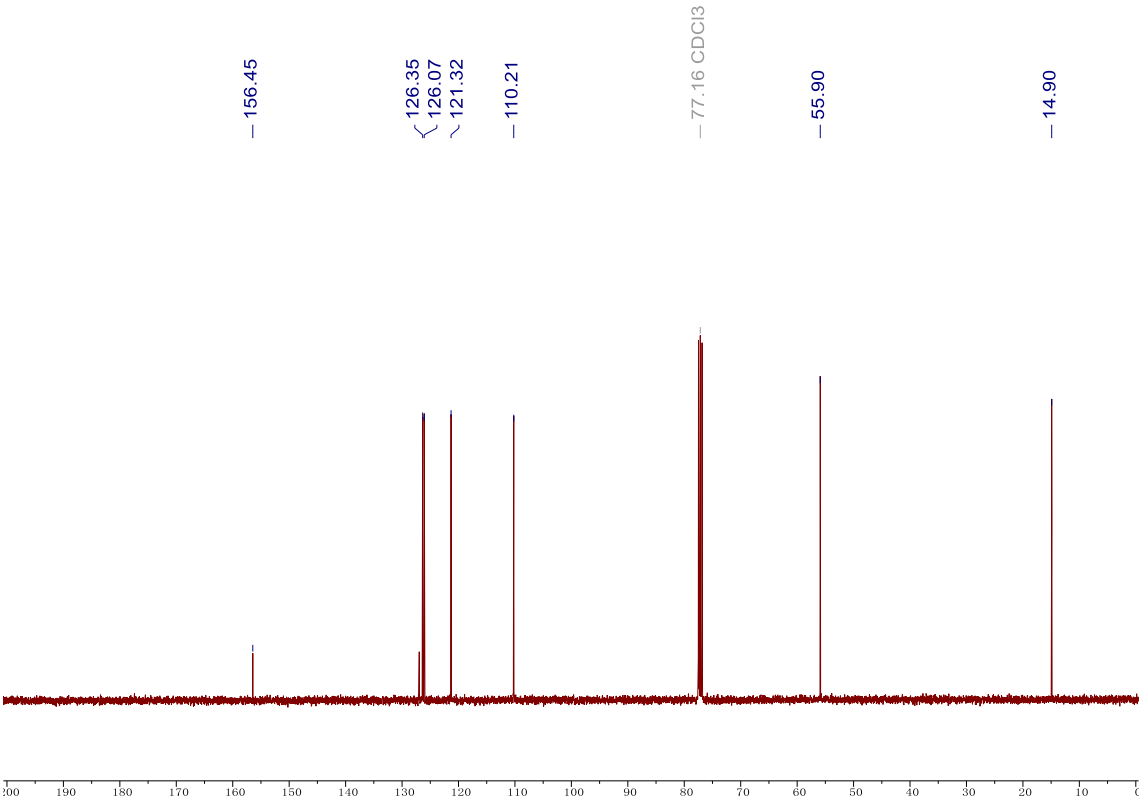

*Butyl(phenyl)selane (**86**) ^{1}H-NMR spectrum in $CDCl_3$*

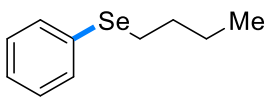

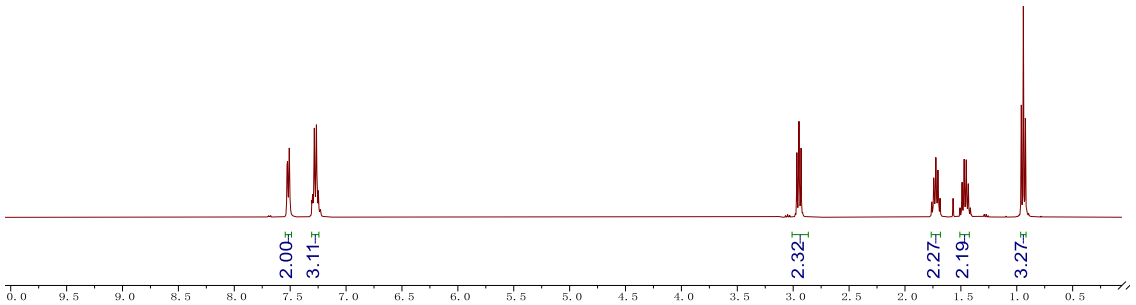

*Butyl(phenyl)selane (**86**) ^{13}C-NMR spectrum in $CDCl_3$*

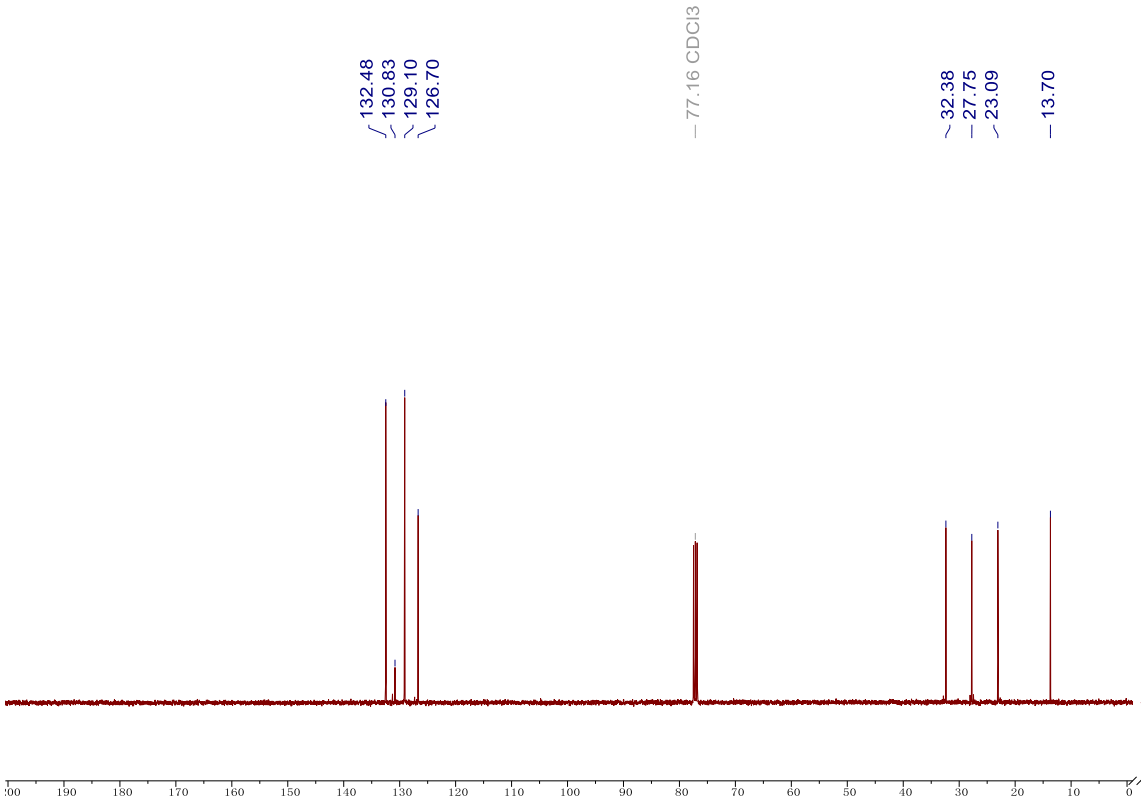

*4-fluorophenylboronic acid pinacol ester (**88**) ^{1}H-NMR spectrum in $CDCl_3$*

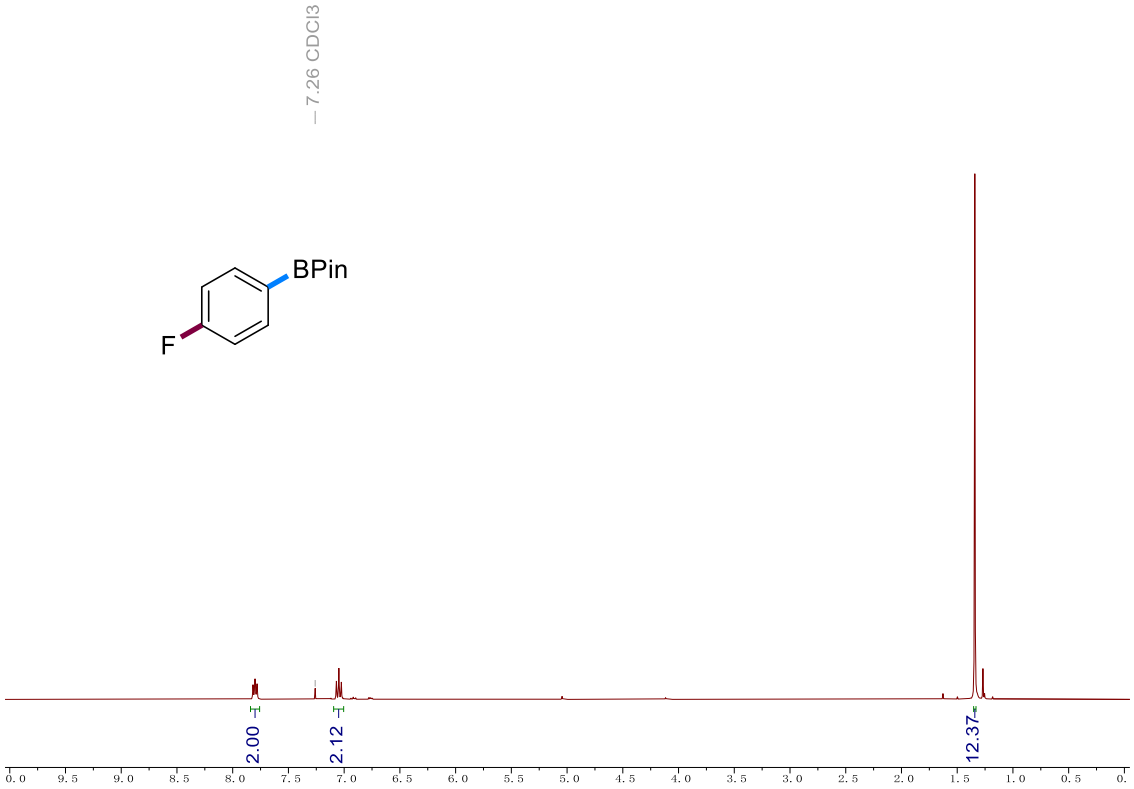

*4-fluorophenylboronic acid pinacol ester (**88**) ^{13}C-NMR spectrum in $CDCl_3$*

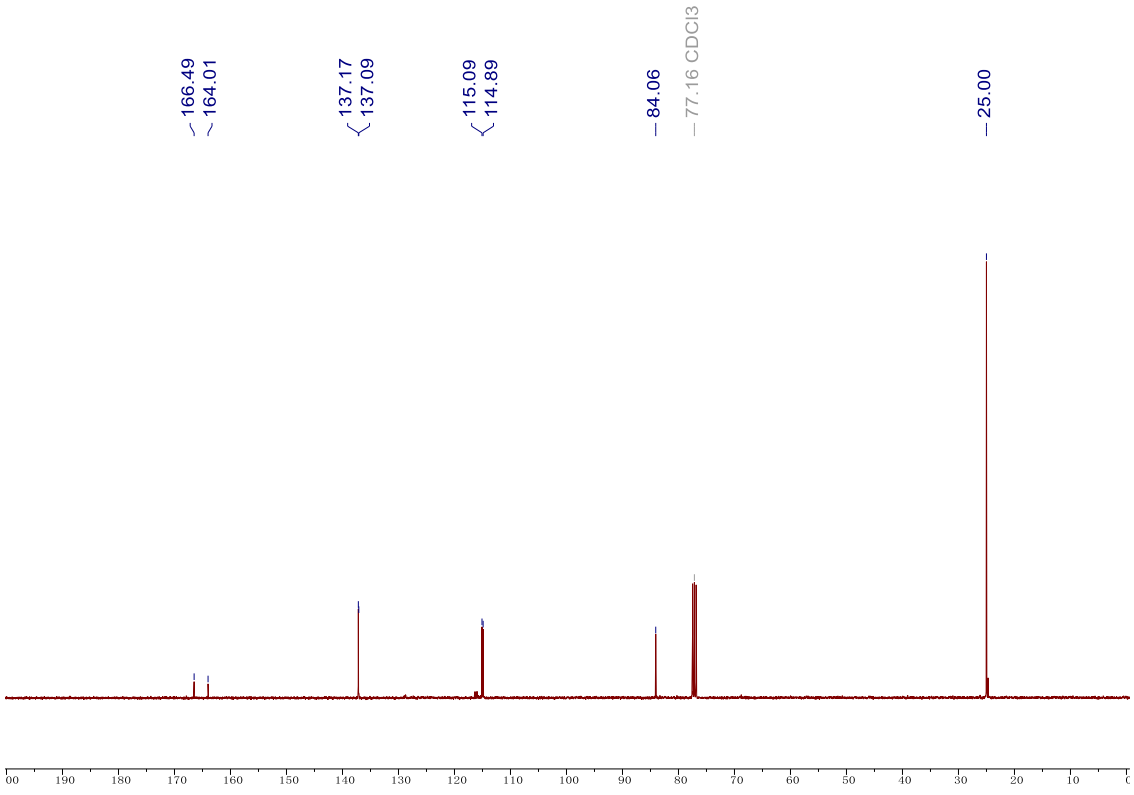

*4-fluorophenylboronic acid pinacol ester (**88**) ^{19}F-NMR spectrum in $CDCl_3$*

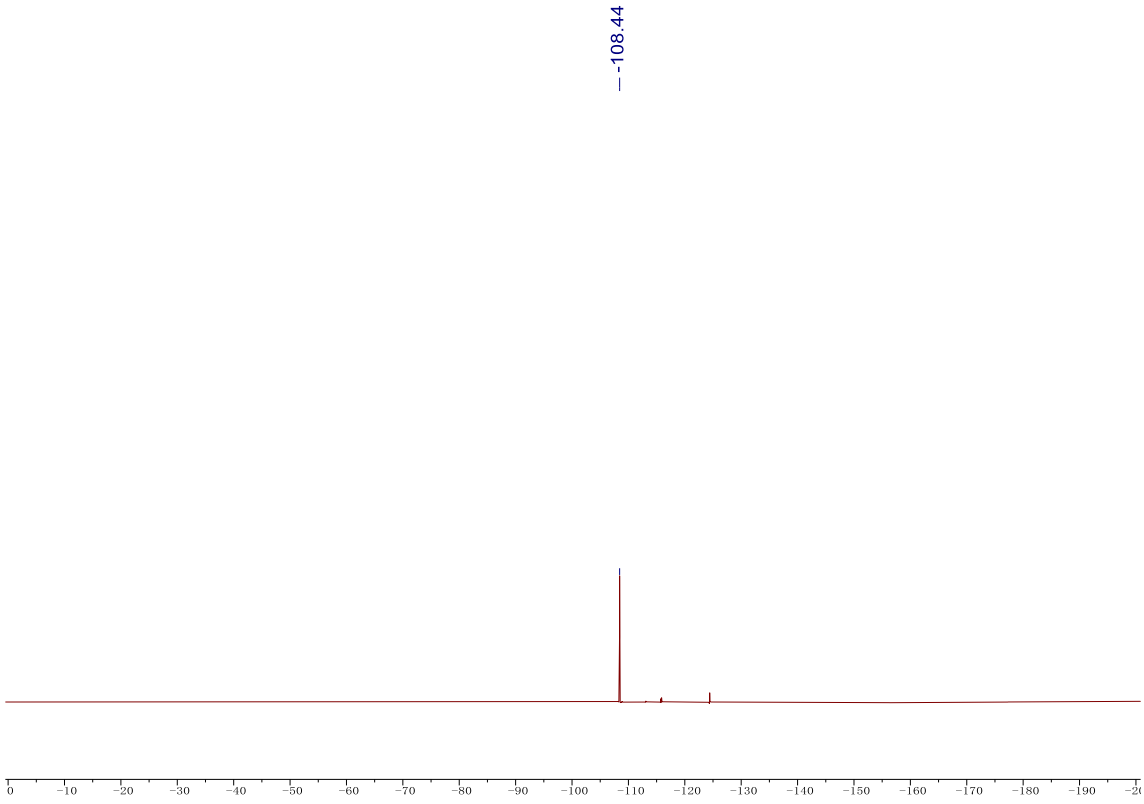
-108.44
0
−10
−20
−30
−40
−50
−60
−70
−80
−90
−100
−110
−120
−130
−140
−150
−160
−170
−180
−190

*4-(4-fluorophenyl)morpholine **(89)** ^{1}H-NMR spectrum in $CDCl_3$*

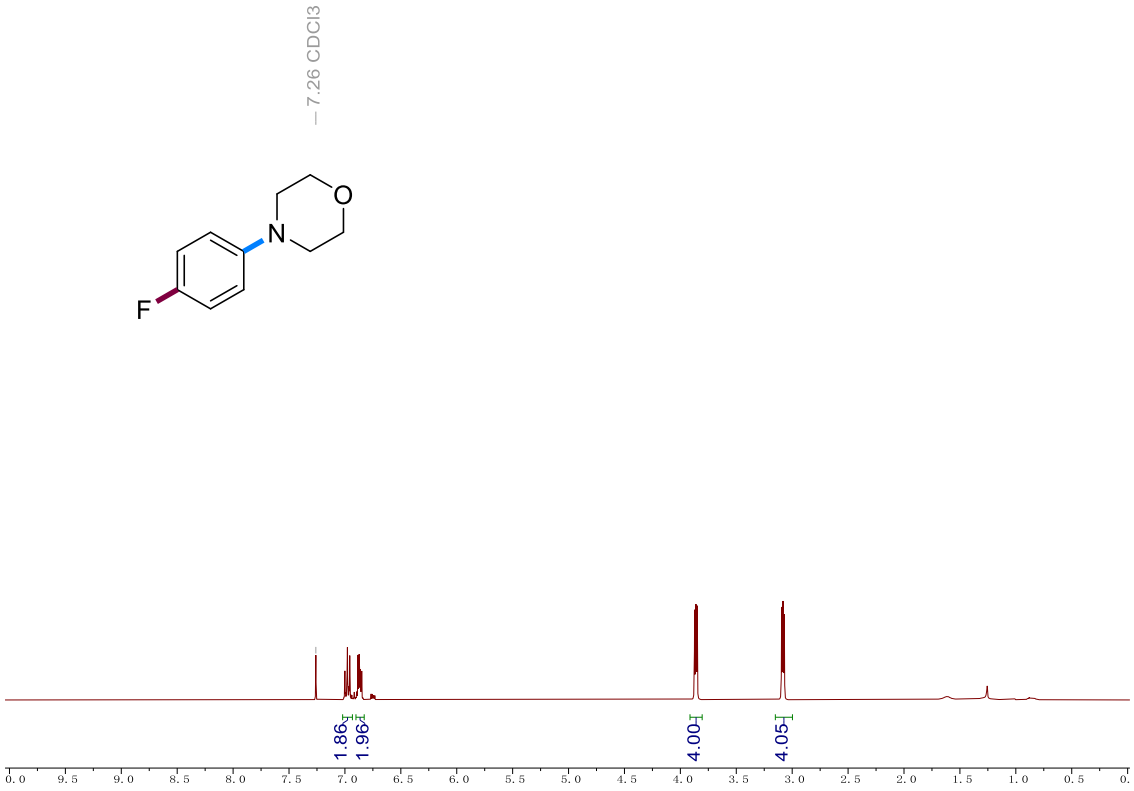

*4-(4-fluorophenyl)morpholine **(89)** ^{13}C-NMR spectrum in $CDCl_3$*

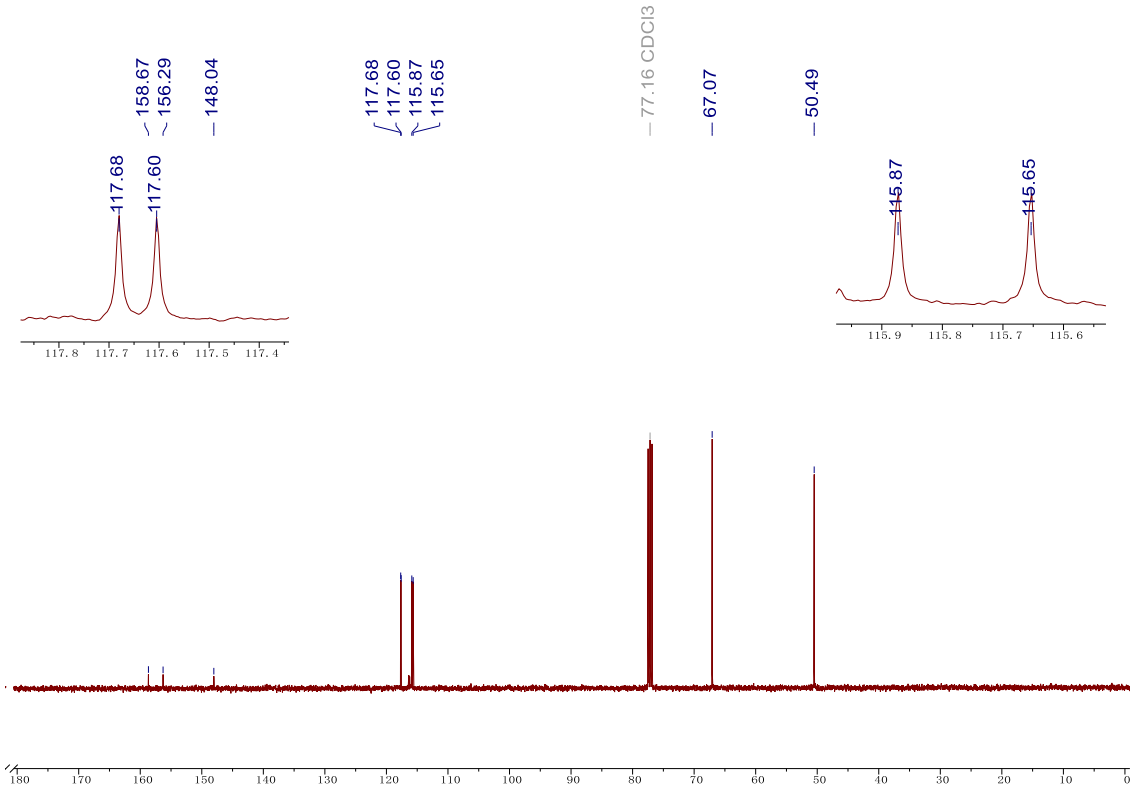

*4-[4-(4,4,5,5-tetramethyl-1,3,2-dioxaborolan-2-yl)phenyl]morpholine **(90)** ^{1}H-NMR spectrum in $CDCl_3$*

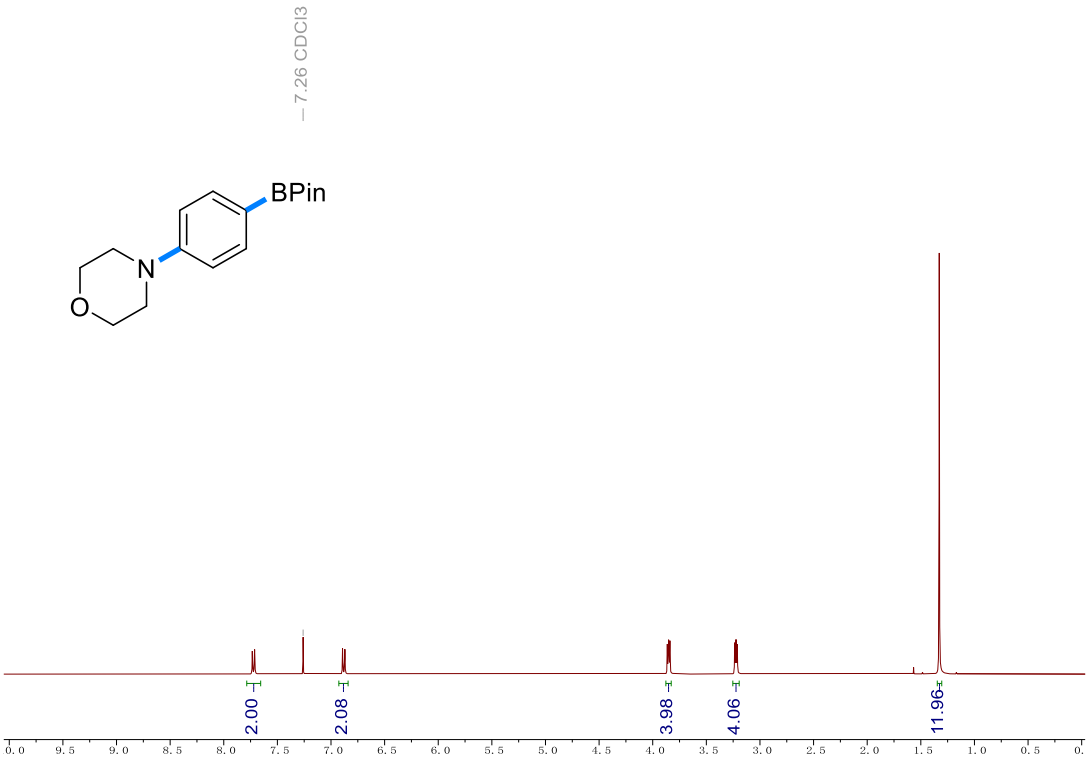

*4-[4-(4,4,5,5-tetramethyl-1,3,2-dioxaborolan-2-yl)phenyl]morpholine **(90)** ^{13}C-NMR spectrum in $CDCl_3$*

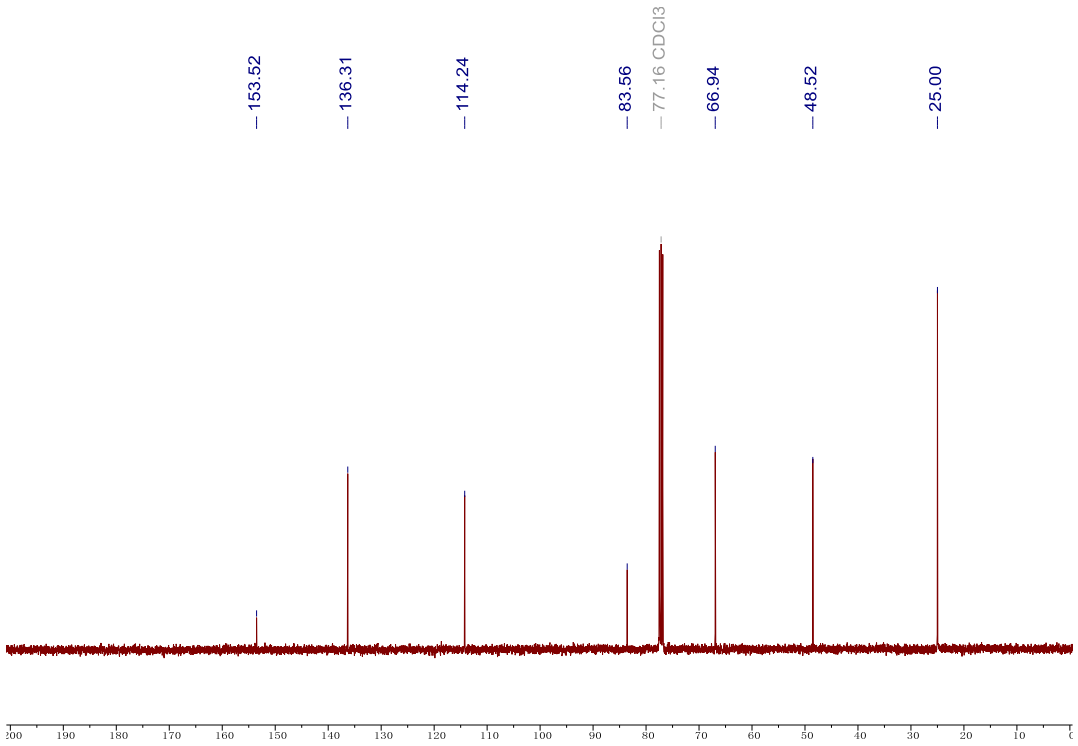

4,4,5,5-Tetramethyl-2-(4-((trifluoromethyl)thio)phenyl)-1,3,2-dioxaborolane (***92***) ^{1}*H-NMR spectrum in* $CDCl_3$

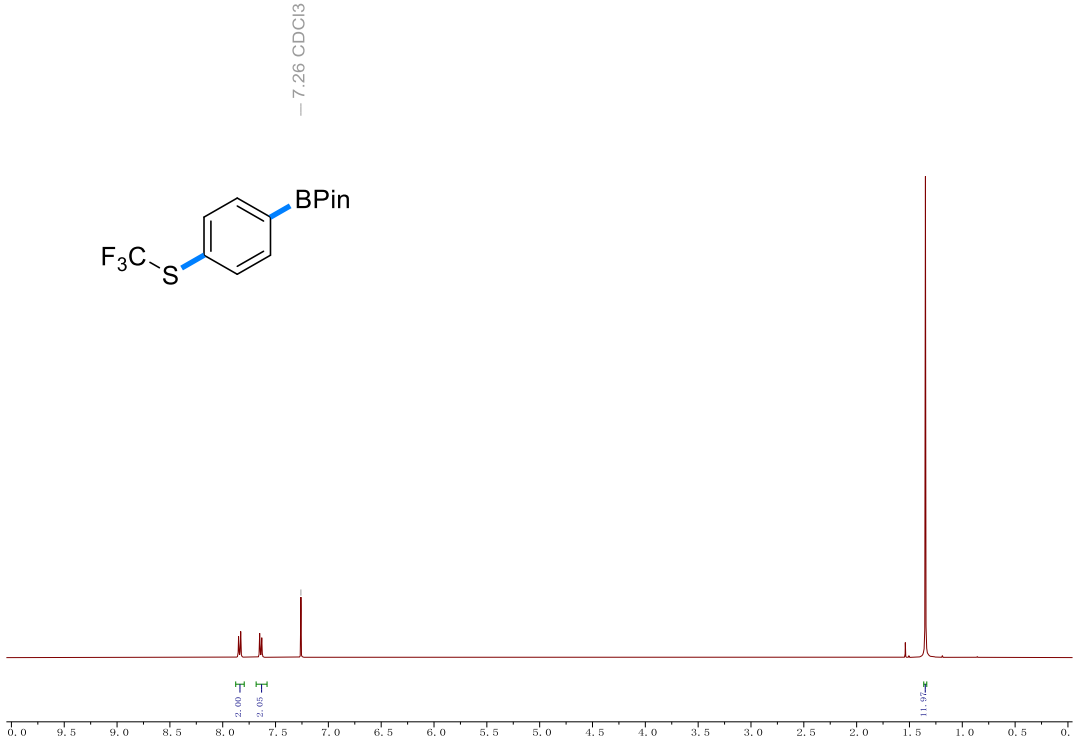

4,4,5,5-Tetramethyl-2-(4-((trifluoromethyl)thio)phenyl)-1,3,2-dioxaborolane (***92***) ^{13}*C-NMR spectrum in* $CDCl_3$

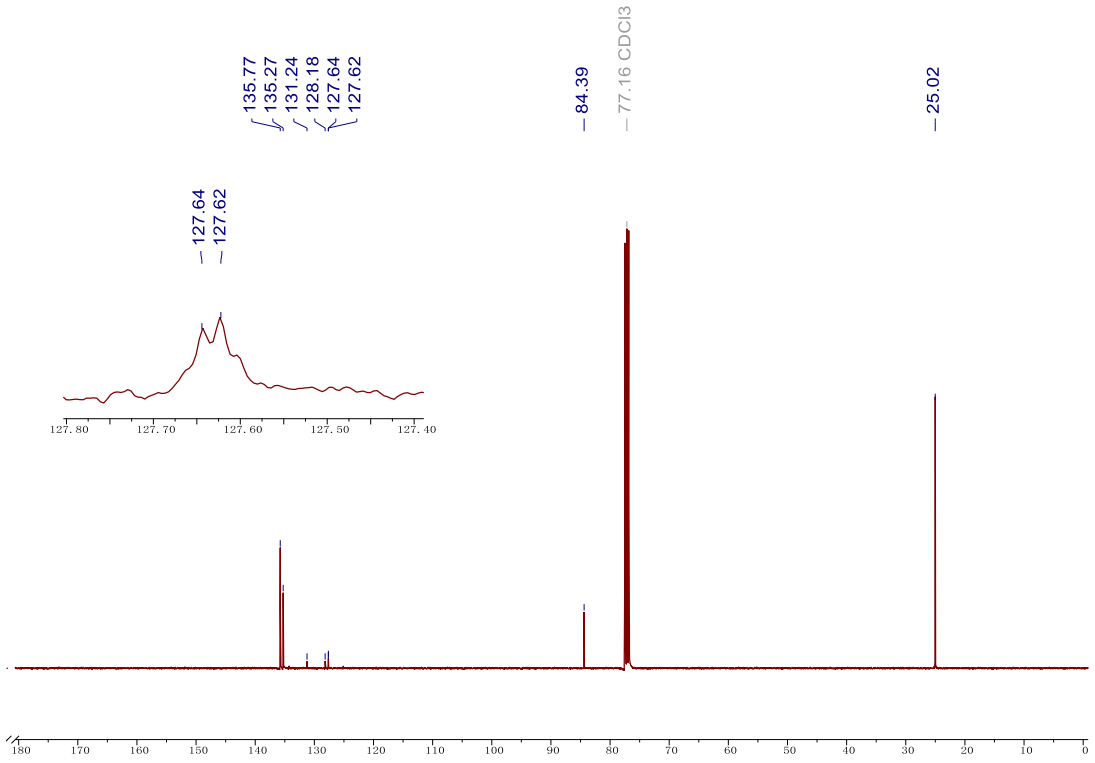

*4,4,5,5-Tetramethyl-2-(4-((trifluoromethyl)thio)phenyl)-1,3,2-dioxaborolane (**92**) ^{19}F-NMR spectrum in $CDCl_3$*

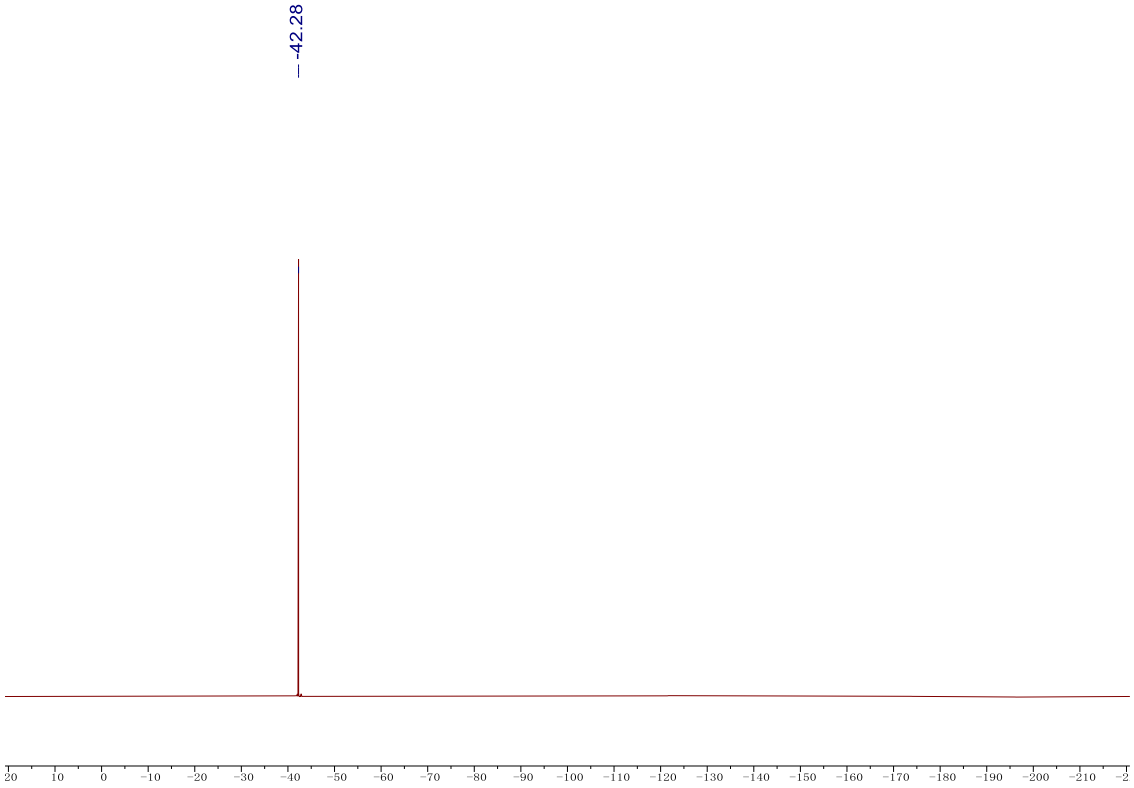

N,N-diethyl-4-((trifluoromethyl)thio)benzenesulfinamide ***(93)*** *^{1}H-NMR spectrum in $CDCl_3$*

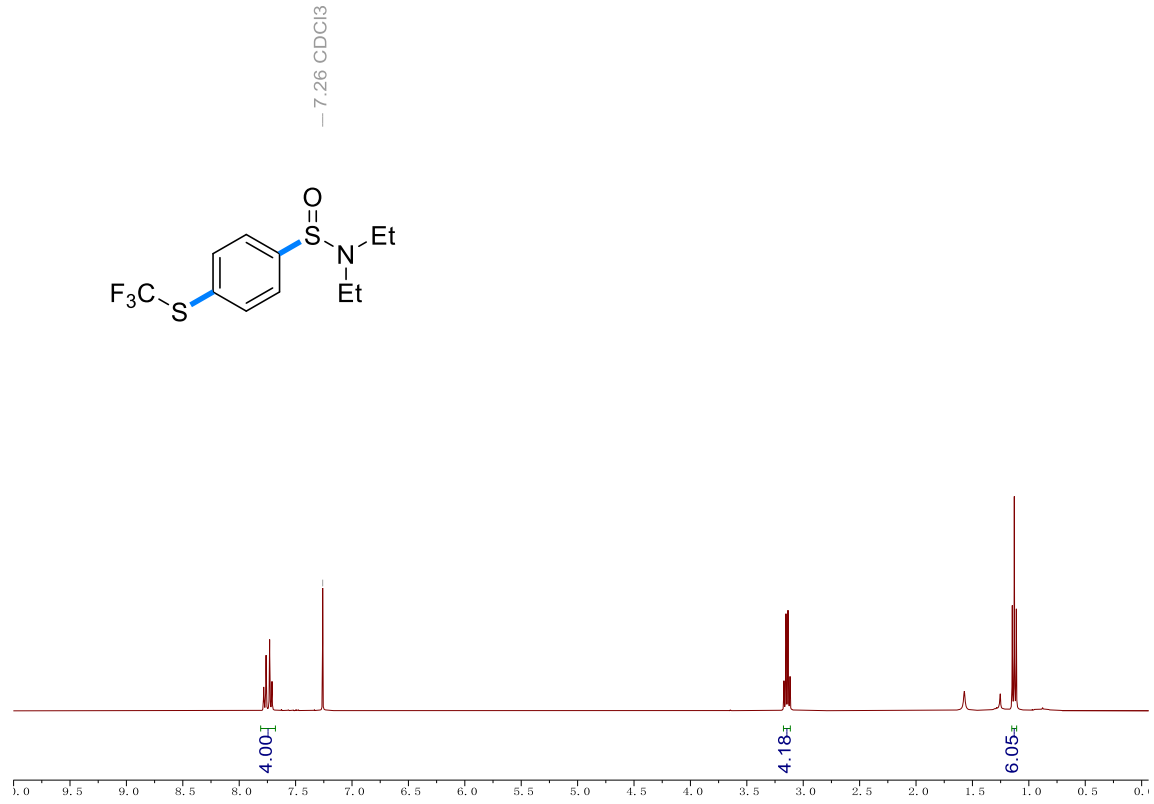

N,N-diethyl-4-((trifluoromethyl)thio)benzenesulfinamide ***(93)*** *^{13}C-NMR spectrum in $CDCl_3$*

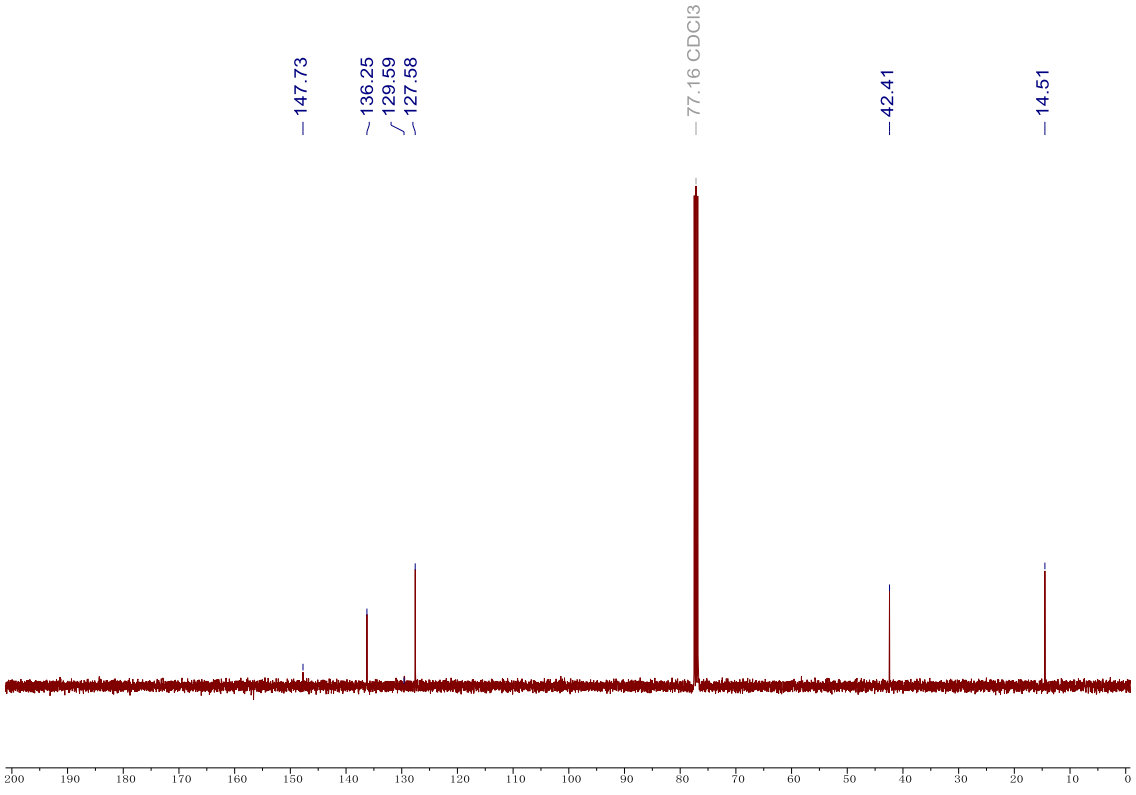

*N,N-diethyl-4-((trifluoromethyl)thio)benzenesulfinamide (**93**) ^{19}F-NMR spectrum in $CDCl_3$*

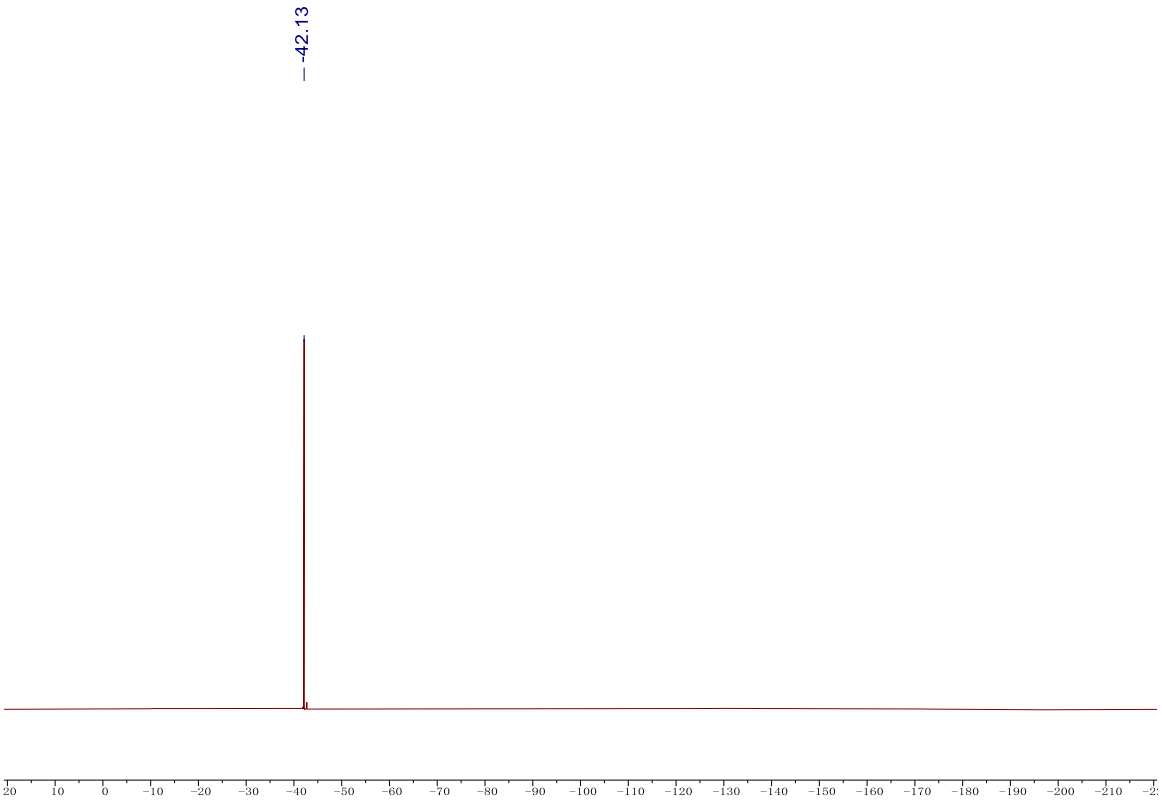

4'-((trifluoromethyl)thio)-[1,1'-biphenyl]-4-carbonitrile ***(94)*** *^{1}H-NMR spectrum in $CDCl_3$*

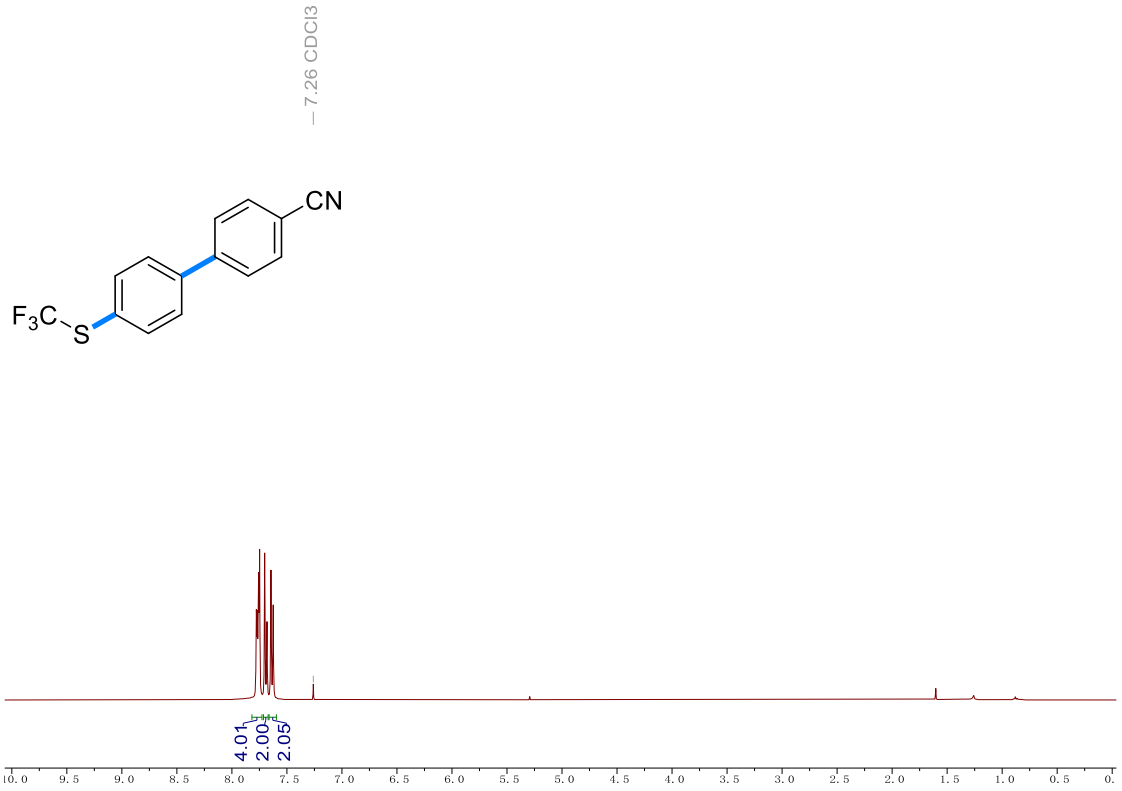

4'-((trifluoromethyl)thio)-[1,1'-biphenyl]-4-carbonitrile ***(94)*** *^{13}C-NMR spectrum in $CDCl_3$*

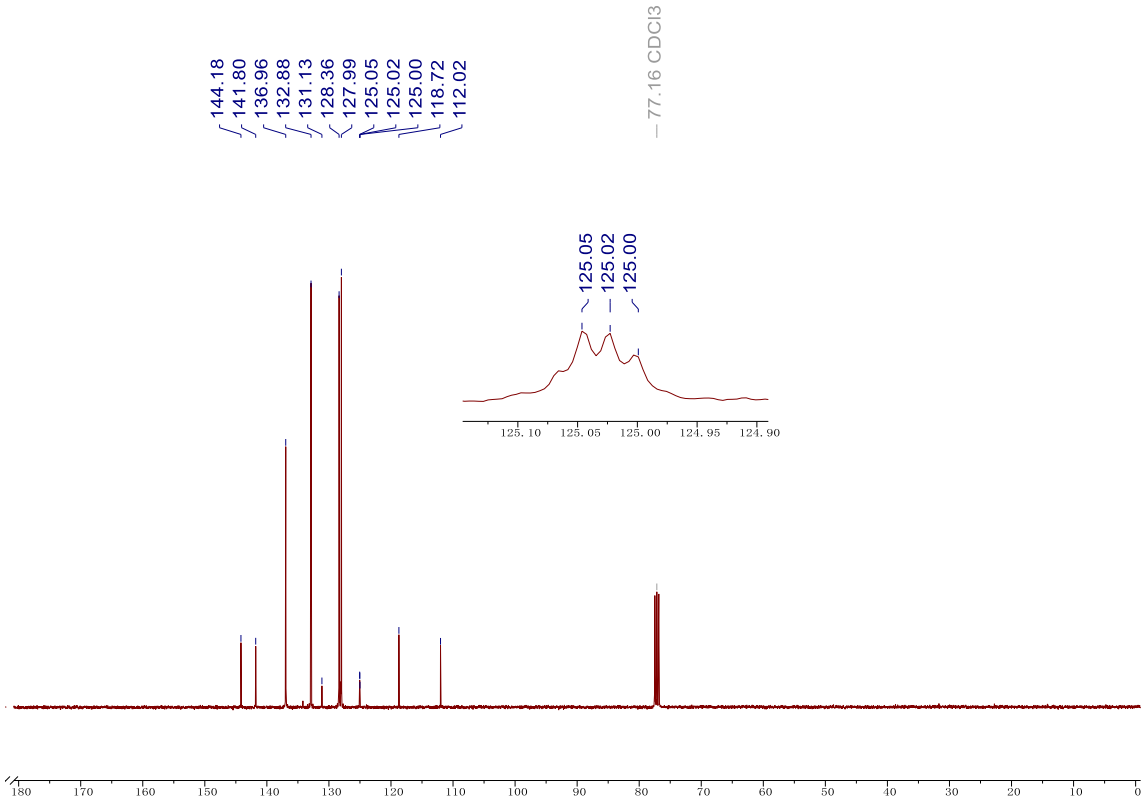

*4'-((trifluoromethyl)thio)-[1,1'-biphenyl]-4-carbonitrile **(94)** ^{19}F-NMR spectrum in $CDCl_3$*

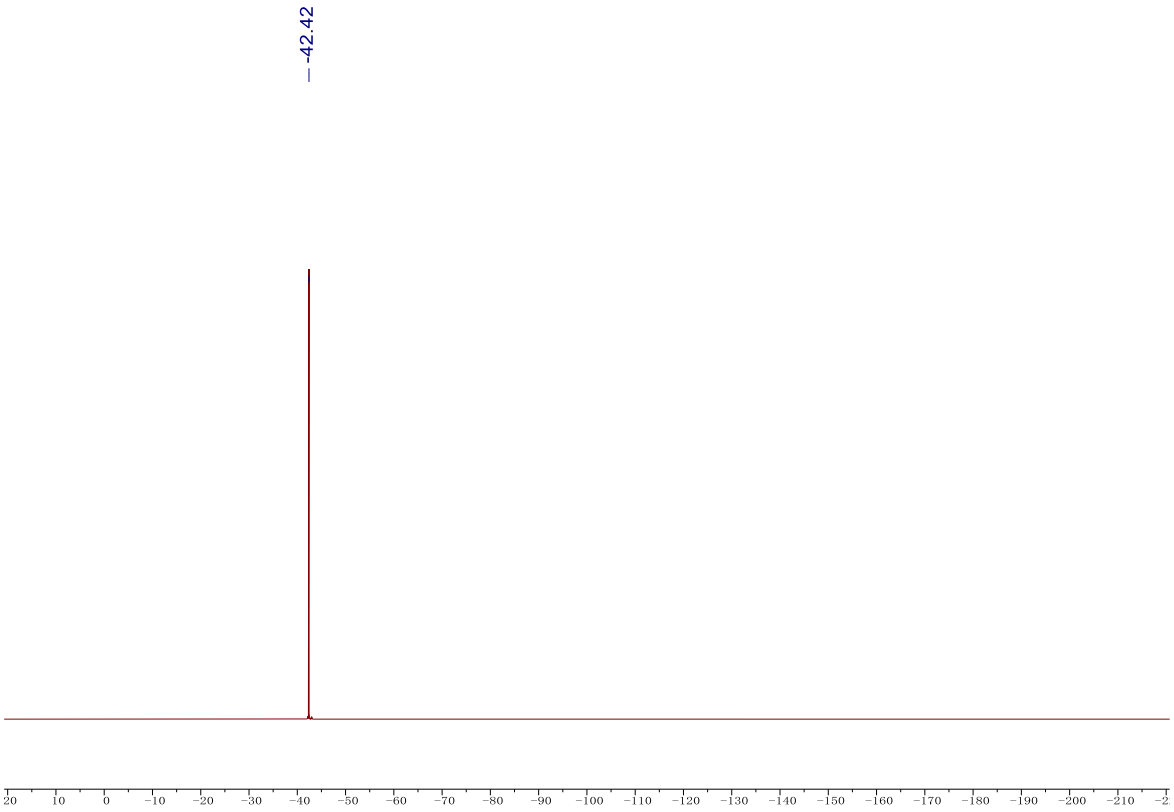

Poly(4-fluorostyrene) ^{1}H-NMR spectrum in $CDCl_3$

14.2 NMR spectra for polymer products

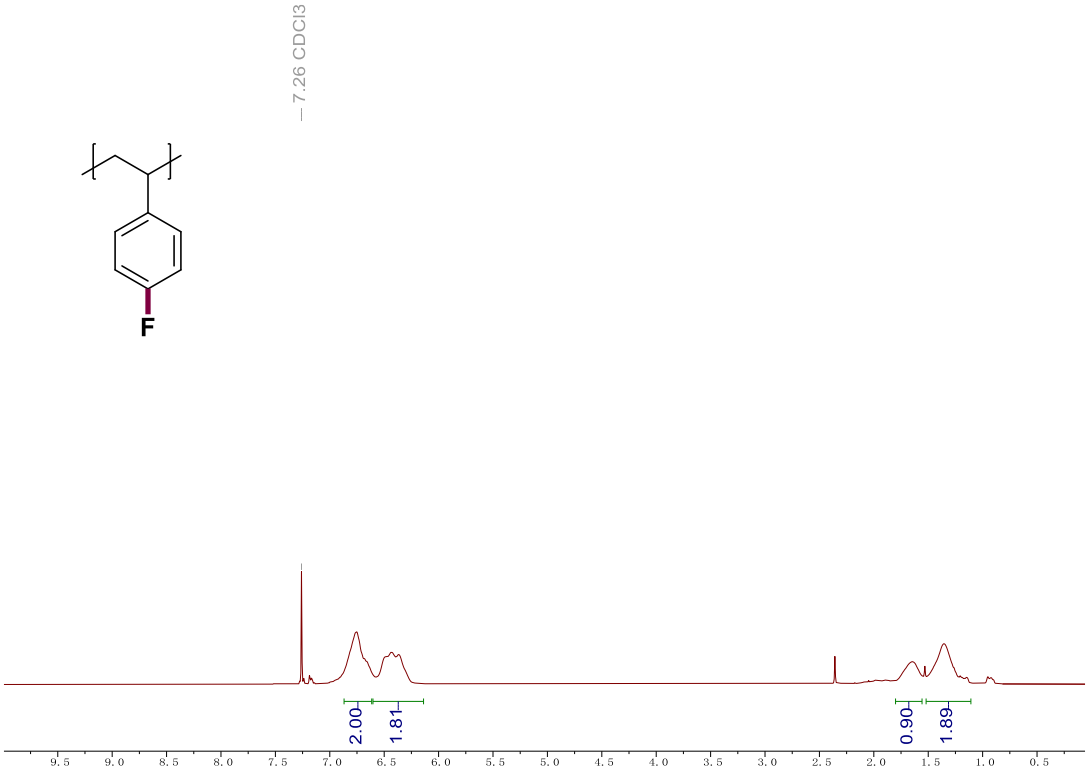

*(**46**) ^{1}H-NMR spectrum in $CDCl_3$*

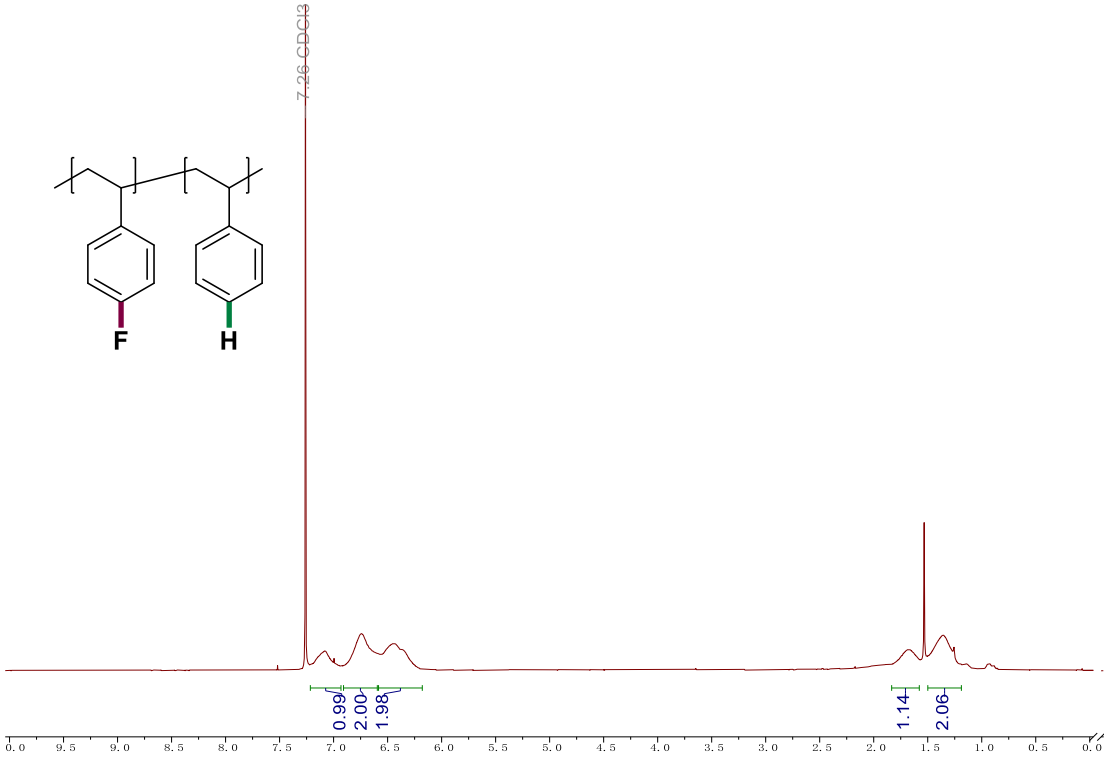

Poly(3-fluorostyrene) ^{1}H-NMR spectrum in $CDCl_3$

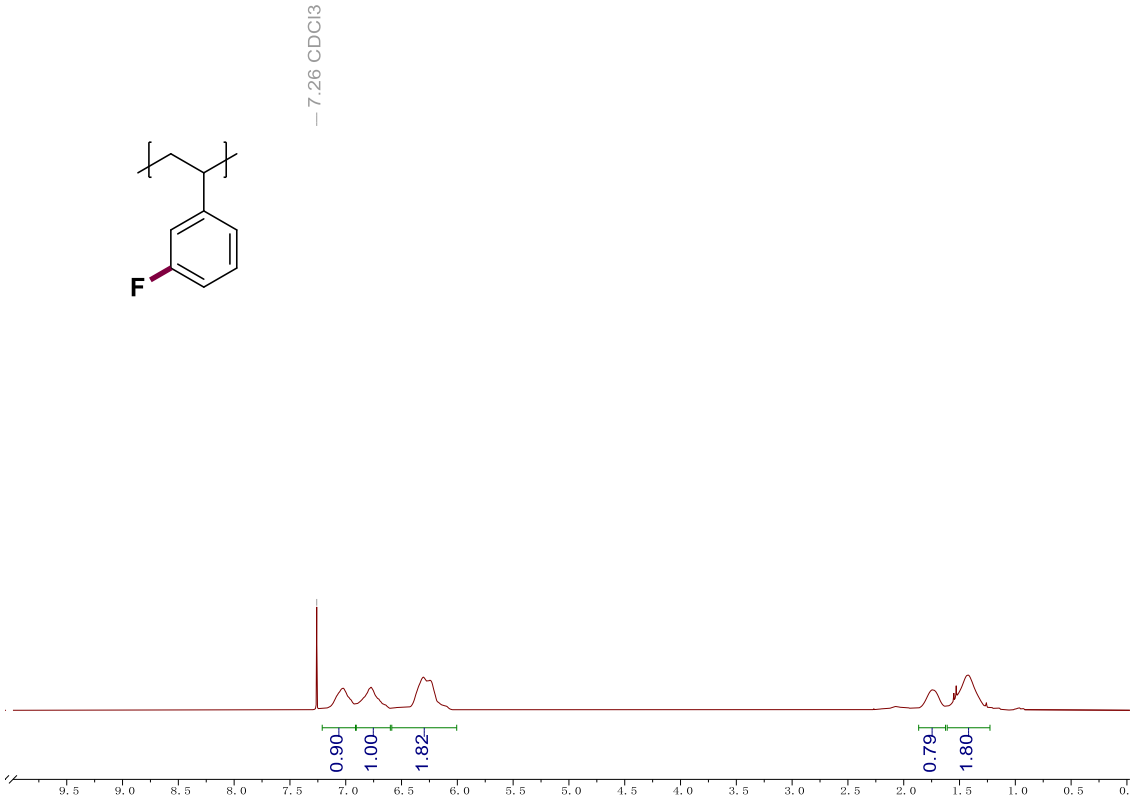

*(**47**) ^{1}H-NMR spectrum in $CDCl_3$*

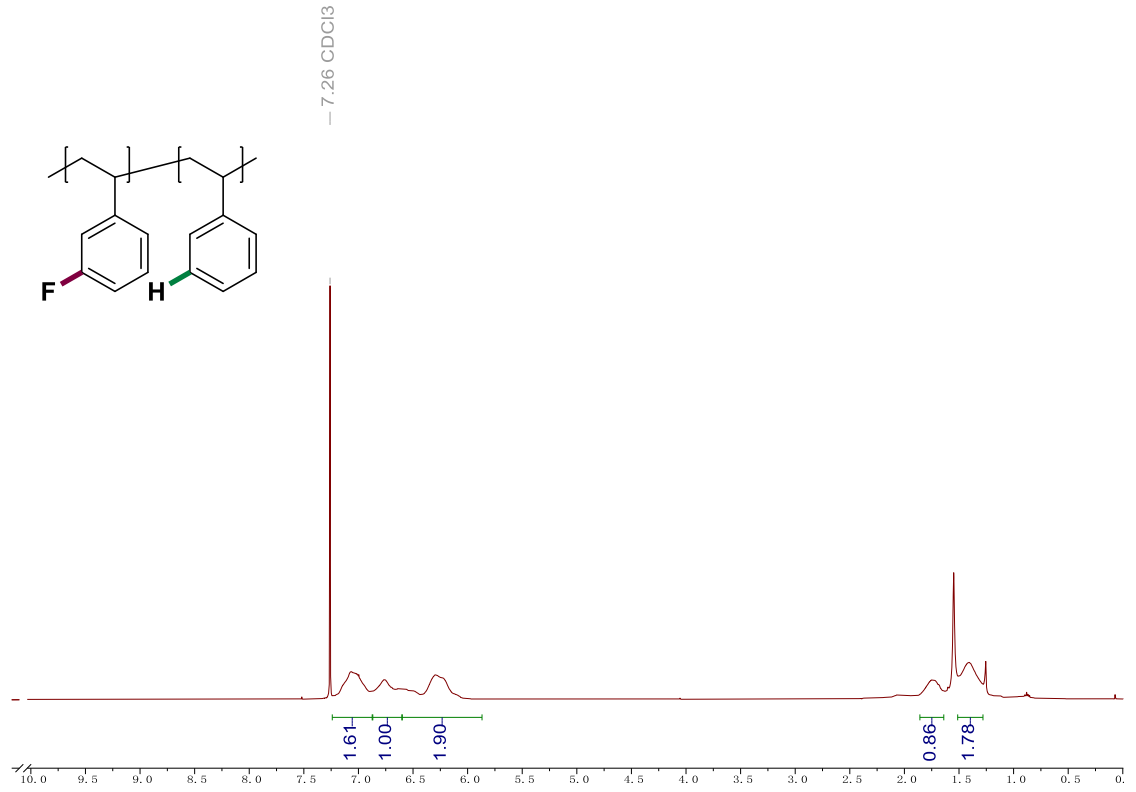

Poly(2-fluorostyrene) ^{1}H-NMR spectrum in $CDCl_3$

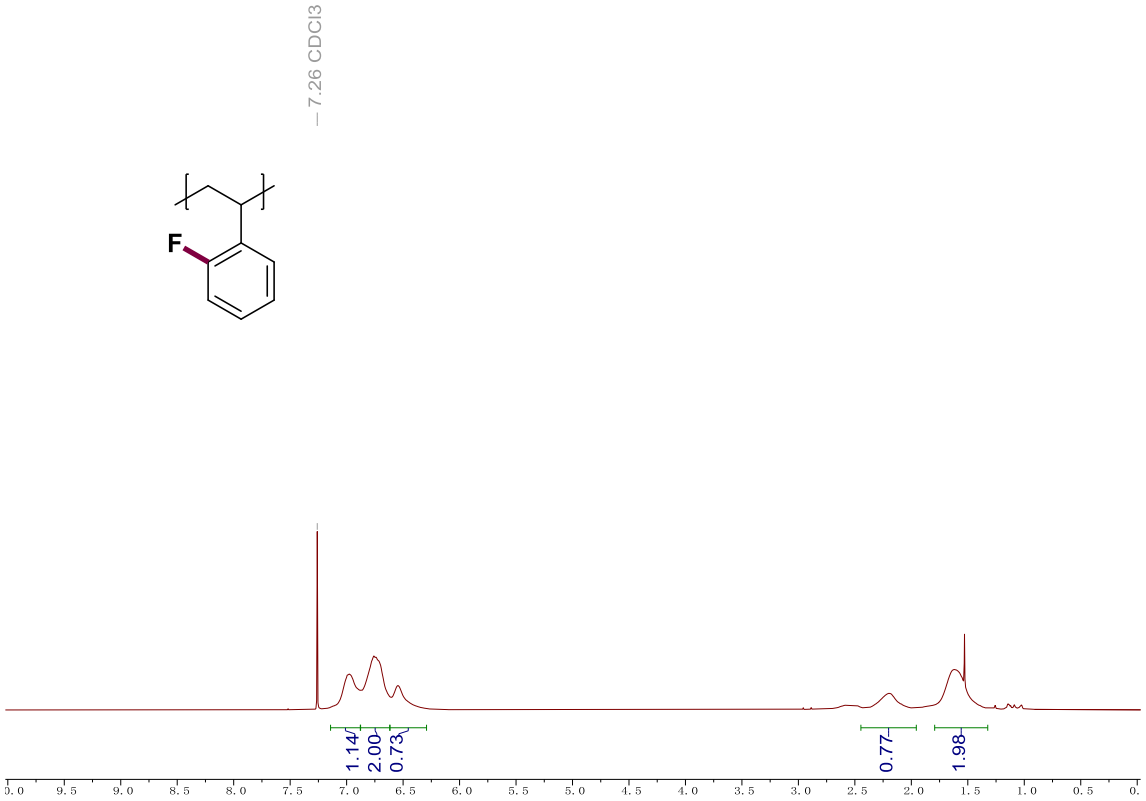

*(**48**) ^{1}H-NMR spectrum in $CDCl_3$*

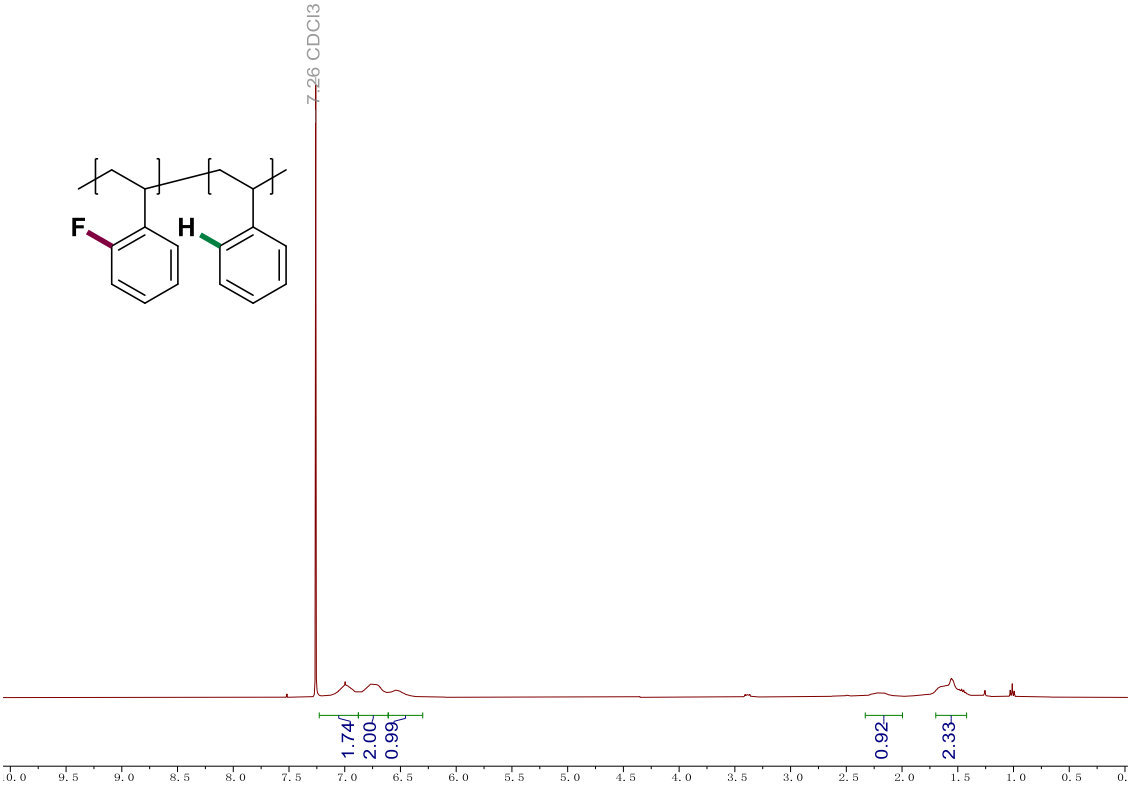

^{1}H-NMR spectrum in $CDCl_3$

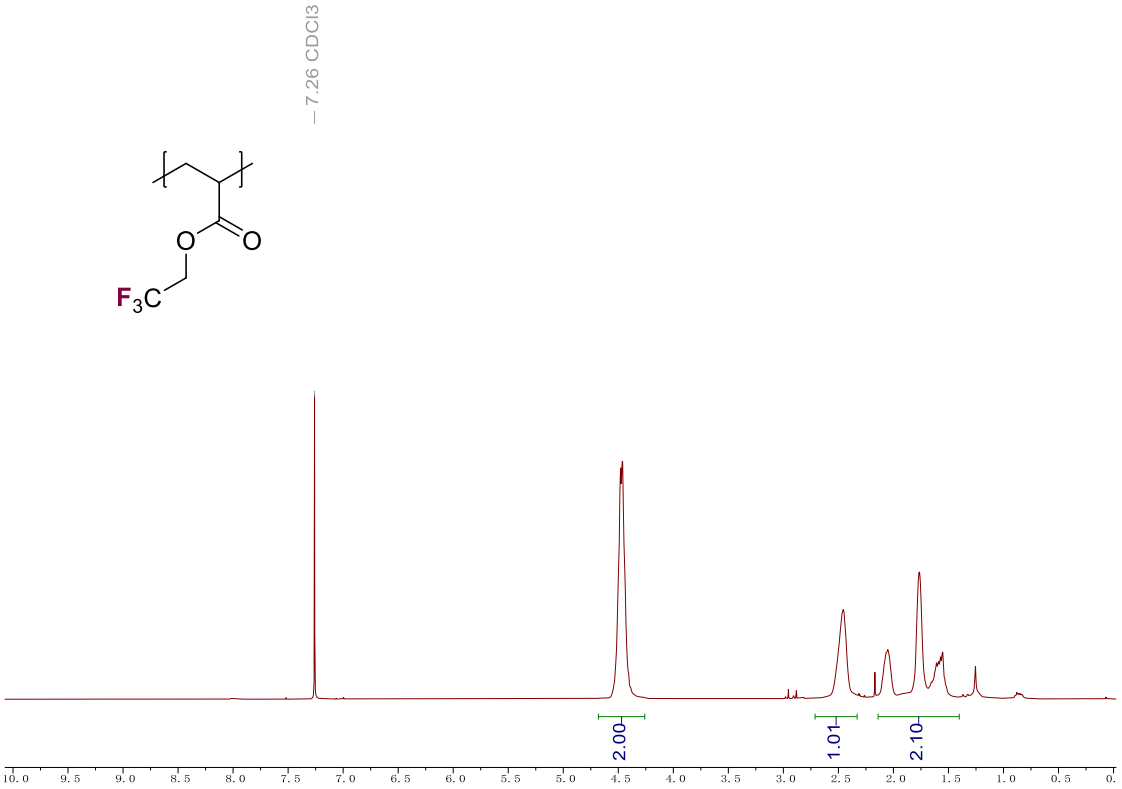

*(**49**) ^{1}H-NMR spectrum in $CDCl_3$*

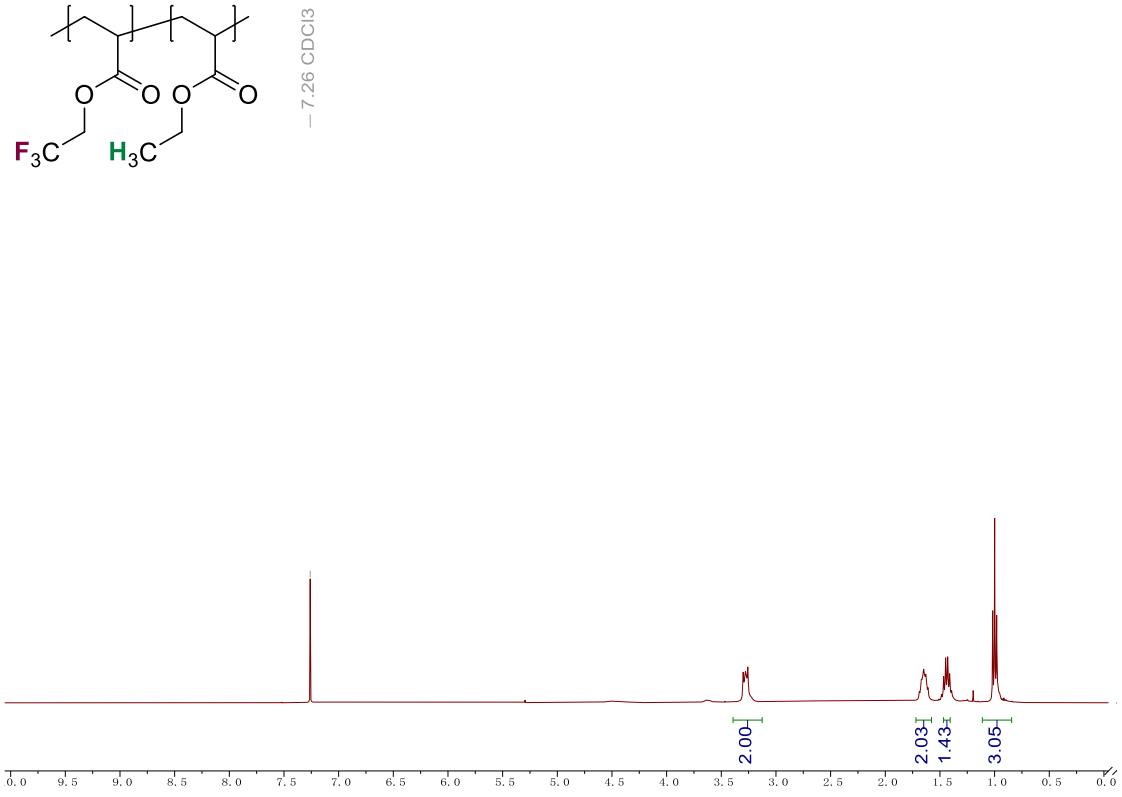

^{1}H-NMR spectrum in $CDCl_3$

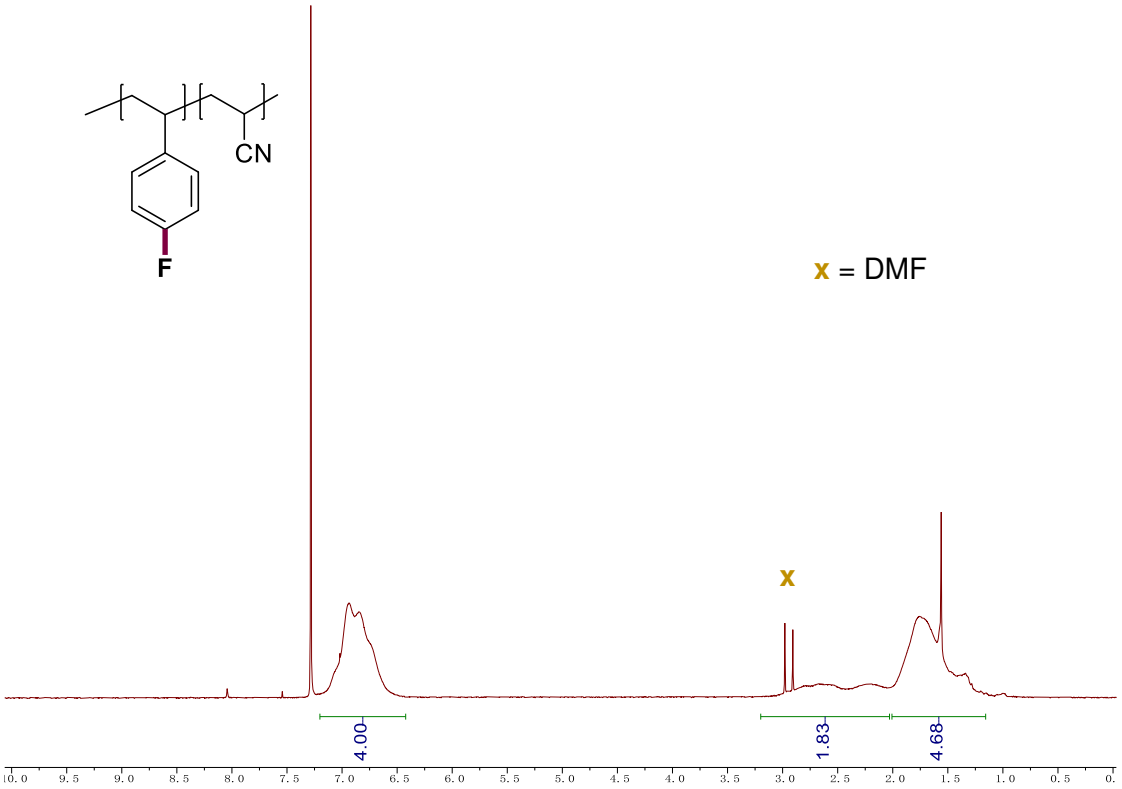

*(**50**) ^{1}H-NMR spectrum in $CDCl_3$*

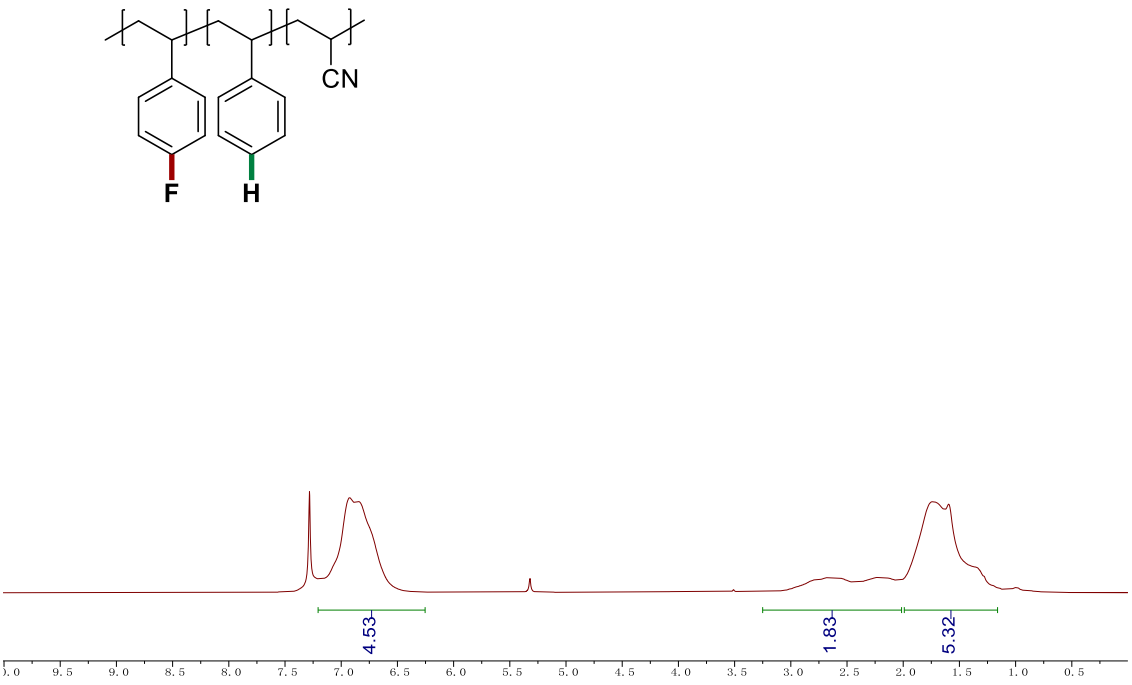

^{1}H-NMR spectrum in $CDCl_3$

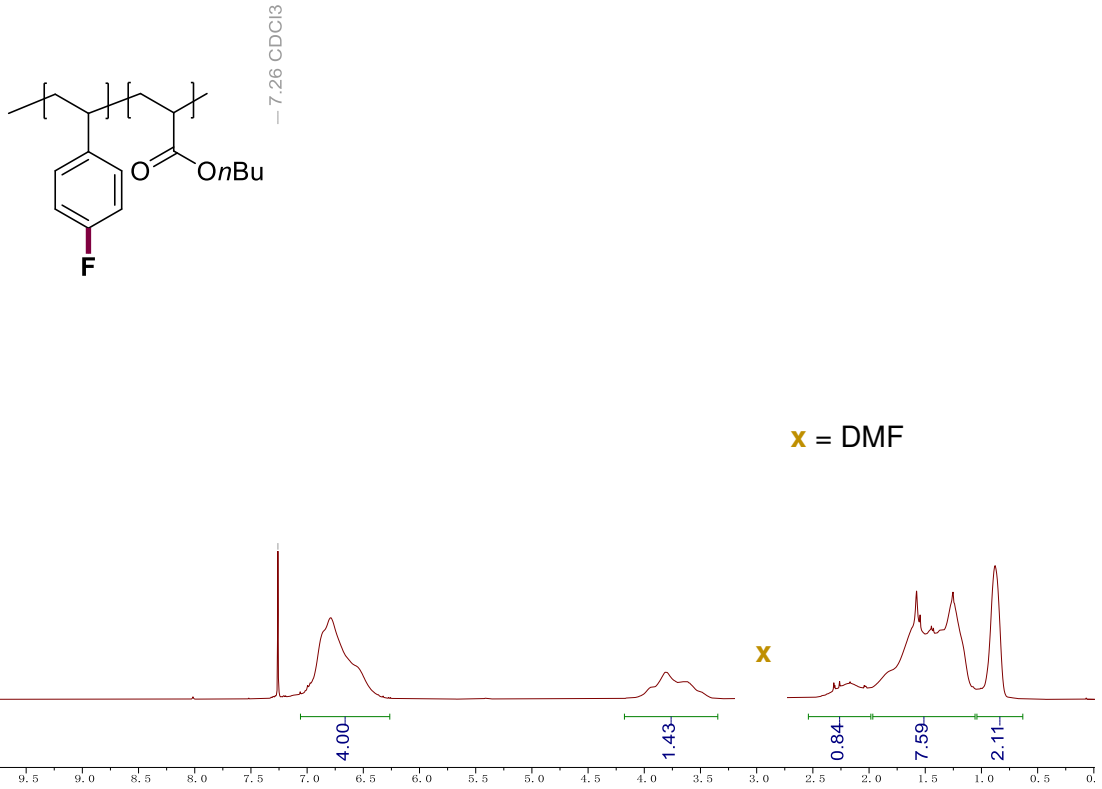

*(**51**) ^{1}H-NMR spectrum in $CDCl_3$*

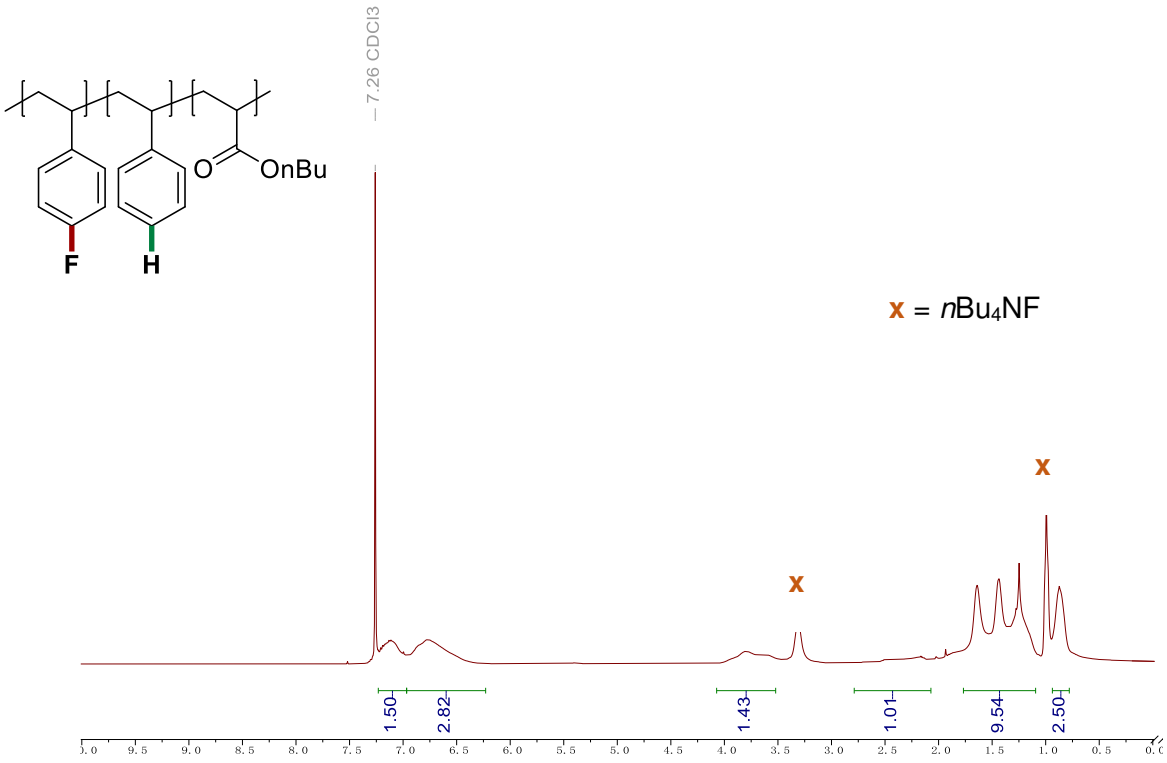

REFERENCES

1. Cole, J. P., Chen, D.-F., Kudisch, M., Pearson, R. M., Lim, C.-H. & Miyake, G. M. *J. Am. Chem. Soc.* 142, 13573–13581 (2020).

2. Ghosh, I., Ghosh, T., Bardagi, J. I. & König, B. *Science* 346, 725–728 (2014).

3. Cowper, N. G. W., Chernowsky, C. P., Williams, O. P. & Wickens, Z. K. *J. Am. Chem. Soc.* 142, 2093–2099 (2020).

4. H. Huang, C. Yu, Y. Zhang, Y. Zhang, P. S. Mariano, W. Wang. *J. Am. Chem. Soc.* 139, 9799–9802 (2017).

5. Siddiqi, Z. & Sarlah, D. *J. Am. Chem. Soc.* 143, 21264–21269 (2021).

6. Zhu, Y., Fan, Y., Li, S., Wei, P., Li, D., Liu, B., Cui, D., Zhang, Z., Li, G., Nie, Y. & Lu, G. *Mater. Horiz.,* 7, 1861-1871 (2020).

7. Wang, Z., Wang, M., Liu, J., Liu, D., & Cui, D. *Chem. Eur. J.* 23, 18151–18155 (2017).

8. Walsh, D. J., Schinski, D. A., Schneider, R. A. & Guironnet, D. *Nat. Commun.* 11, 3094 (2020).

9. Guo, Z., Pang, T., Yan, L., Wei, X., Chao, J. & Xi, C. *Green Chem.,* 23, 7534–7538 (2021).

10. Bai, X.-F., Ye, F., Zheng, L.-S., Lai, G.-Q., Xia, C.-G. & Xu, L.-W. *Chem Commun.,* 48, 8592–8594 (2012).

11. Thiyagarajan, S. & Gunanathan, C. *Org. Lett.* 21, 9774–9778 (2019).

12. Meng, Q.-Y., Wang, S., Huff, G. S. & König. B. *J. Am. Chem. Soc.* 140, 3198–3201 (2018).

13. Bhunia, S., Ghorpade, S., Huple, D. B. & Liu, R.-S. *Angew. Chem. Int. Ed.* 51, 2939–2942 (2012).

14. Zhang, K., Chang, L., An, Q., Wang, X. & Zuo, Z. *J. Am. Chem. Soc.* 141, 10556–10564 (2019).

15. Zhang, Y., Qian, J., Wang, M., Huang, Y. & Hu, P. *Org. Lett.* 24, 5972–5976 (2022).

16. Clerici, A., Ghilardi, A., Pastori, N., Punta, C. & Porta, O. *Org. Lett.* 10, 5063–5066 (2008).

17. O'Neill, P. M., Sabbani, S., Nixon, G. L., Schnaderbeck, M., Roberts, N. L., Shore, E. R., Riley, C., Murphy, B., McGillan, P., Ward, S. A., Davies, J. & Amewu, R. K. *Tetrahedron* 40, 6118–6126 (2016).

18. Zhang, G., Favela, D., Chow, W. L., Lyer, R. N., Pell, A. J. & Olson, D. E. *Org. Lett.* 24, 6208–6212 (2022).

19. Lovett, G. H., Chen, S., Xue, X.-S., Houk, K. N. & MacMillan, D. W. C. *J. Am. Chem. Soc*. 141, 20031–20036 (2019).

20. Modak, A., Naveen, T. & Maiti, D. *Chem. Commun.,* 49, 252–254 (2013).

21. Wang, J.-R., Song, Z.-Q., Li, C. & Wang, D.-H. *Org. Lett.* 23, 8450–8454 (2021).

22. Shen, T., Wang, T., Qin, C. & Jiao, N. *Angew. Chem. Int. Ed.* 52, 6677–6680 (2013).

23. Fukuyama, T., Fujita, Y., Miyoshi, H., Ryu, I., Kao, S.-C. & Wu, Y.-K. *Chem. Commun.,* 54, 5582–5585 (2018).

24. Li, Y., Zhang, J., Li, D. & Chen, Y. *Org. Lett.* 20, 3296–3299 (2018).

25. Nambo, M., Yar, M., Smith, J. D. & Crudden, C. M. *Org. Lett.* 17, 50–53 (2015).

26. Keith, D. J. & Townsend, S. D. *J. Am. Chem. Soc.* 141, 12939–12945 (2019).

27. Doboszewski, B. & Herdewijin, P. *Tetrahedron Lett.* 53, 2253–2256 (2012)

28. Rahim, N. H. C. A., Asari, A., Ismail, N., Abdullah, F., Osman, H. & Tahier, S. S. M. *Asian. J. Chem.* 30, 126–128 (2018).

29. Sisto, F., Carradori, S., Guglielmi, P., Traversi, C. B., Spano, M., Sobolev, A. P., Secci, D., Marcantonio, M. C. D., Haloci, E., Grande, R. & Mincione, G. *Pharmaceuticals*, 13, 405 (2020).

30. Germain, S., Schulz, E. & Hannedouche, J. *Chemcatchem*, 6, 2065–2073 (2014).

31. Qin, Y., Zhang, T., Ching, H. Y. V., Raman, G. S. & Das, S. *Chem* 8, 2472–2484 (2022).

32. Xing, B., Ni, C. & Bo, J. *Angew. Chem. Int. Ed.* 57, 9896–9900 (2018).

33. Funder, E. D., Trads, J. B. & Gothelf, K. V. *Org. Biomol. Chem.*, 13, 185–198 (2015).

34. Cui, X., Zhang, Y., Deng, Y. & Shi, F. *Chem. Commun.,* 50, 13521–13524 (2014).

35. Dale, H. J. A., Nottingham, C., Poree, C. & Lloyd-jones, G. C. *J. Am. Chem. Soc.* 143, 2097–2107 (2021).

36. Deng, J., Xue, T., Wu, H. & Wu, P. *New J. Chem.,* 46, 12169–12176 (2022).

37. Li, X., Feng, Y., Lin, L. & Zou, G. *J. Org. Chem.* 77, 10991–10995 (2012).

38. Ramachandran, P. V., Alawaed, A. A. & Hamann, H. J. *Org. Lett.* 24, 8481–8486 (2022).

39. Denis, J. D. S., Scully, C. C. G., Lee, F & Yudin, A. K. *Org. Lett.* 16, 1338–1341 (2014).

40. Hsieh, J. -C., Chu, Y. -H., Muralirajan, K & Cheng, C. -H. *Chem. Commun*., 53, 11584–11587 (2017).

41. Xu, J., Cao, J., Wu, X., Wang, H., Yang, X., Tang, X., Toh, R. W., Zhou, R., Yeow, E. K. L. & Wu, J. *J. Am. Chem. Soc.* 143, 13266–13273 (2021).

42. Zhang, W., Curran, D. P. & Chen, C. *Tetrahedron* 58, 3871–875 (2002).

43. Tang, L., Peng, T., Wang, G., Wen, X., Sun, Y., Zhang, S., Liu, S. & Wang, L. *Med. Chem. Commun.*, 9, 625–631 (2018).

44. Gatin-Fraudet, B., Pucher, M., Saux, Y. L., Doisneau, G., Bourdreux, Y., Jullien, L., Vauzeilles, B., Guianvarc'h, D. & Urban, D. *Chem. Eur. J.* 28, e202201543 (2022).

45. Levai, A. & Jekő, J. *J. Heterocycl. Chem.* 42, 739–742 (2005).

46. Miralles, N., Romero, R. M., Fernandez, E. & Muñiz, K. *Chem. Commun.,* 51, 14068–14071 (2015).

47. Srimontree, W., Guo, L. & Rueping, M. *Chem. Eur. J.* 26, 423–427 (2020).

48. Zhang, Q., Catti, L., Pleiss, J. & Tiefenbacher, K. *J. Am. Chem. Soc.* 139, 11482–11492 (2017).

49. Dai, P.-F., Ning, X.-S., Wang, H., Cui, X.-C., Liu, J., Qu, J.-P. & Kang, Y.-B. *Angew. Chem. Int. Ed.* 58, 5392–5395 (2019).

50. M. AI-Masum, A. Hira, S. Chrisman, N. T. Nguyen. *Tetrahedron Lett.* 60, 150936 (2019).

51. Jang, H.-G., Song, W., Lee, J. Y. & Hwang. S.-H. *RSC Adv.,* 5, 17030–17033 (2015).

52. V. Pathania, V. J. Roy, S. R. Roy. *J. Org. Chem.* 87, 16550–16566 (2022).

53. W. Chen, H.-J. L, Y.-F. Cheng, Y.-C. Wu. *Org. Biomol. Chem.*, 19, 1555–1564 (2021).

54. B. Zhang, Z. Fan, Z. Guo, C. Xi. *J. Org. Chem.* 84, 8661–8667 (2019).

55. W. Ren, S. Zhang, Z. Xu, X. Ma. *Dalton Trans.,* 48, 3109–3115 (2019).

56. Zhu, C. & Yamane, M. *Org. Lett.* 14, 4560–4563 (2012).

57. Li, J. & Wang, Z.-X. *Org. Lett.* 19, 3723–3726 (2017).

58. Q.-K. Kang, Y. Lin, Y. Li, H. Shi. *J. Am. Chem. Soc.* 142, 3706–3711 (2020).

59. Cheng, W.-M., Shang, R., Zhao, B., Xing, W.-L. & Fu, Y. *Org. Lett.* 19, 4291–4294 (2017).

60. Sun, H. & DiMagno, S. G. *J. Am. Chem. Soc.* 127, 2050–2051 (2005).

61. Cox. D. P., Terpinski, J., & Kawrynowicz, W. *J. Org. Chem.* 49, 3216–3219 (1984).

62. Shukla, J., & Mukhopadhyay, P. *Eur. J. Org. Chem.* 48, 7770–7786 (2019)

63. Saha, Sourav. Acc. Chem. Res, 51, 2225–2236 (2018)

64. Kobaisi, M. A., Bhosale, S. V., Latham, K., Raynor, A. M., & Bhosale, S. V. *Chem. Rev.* 116, 11685–11796 (2016).

65. Dawson, R. E., Hennig, A., Weimann, D. P., Emery, D., Ravikumar, V., Montenegro, J., Takeuchi, T., Gabutti, S., Mayor, M., Mareda, J., Schalley, C. A., & Matile S. *Nat. Chem.* 2, 533–538 (2010).

66. Guha, S., Goodson, F. S., Roy, S., Corson, L. J., Gravenmier, C. A., & Saha, S. *J. Am. Chem. Soc.* 133, 15256–15259 (2011).

67. Rieth, A. J., Gonzalez, M. I., Kudisch, B., Nava, M., & Nocera, D. G. *J. Am. Chem. Soc.* 2021, 143, 14352–14359 (2021).

68. Julino, M., & Stevens, M. F. G. *J. Chem. Soc., Perkin Trans. 2* 2, 291–296 (1998).

69. Hoffmann-Röder, A., Seiler, P., & Diederich, F. *Org. Biomol. Chem.,* 2, 2267-2269 (2004).

70. Meutermans, W. D. F., Alewood, P. F., Bourne, G. T., Hawkins, B., & Smythe, M. L. *Letters in Peptide Science*, 4, 79–84 (1997).

71. Li, H., Wenger, O. S. *Angew. Chem. Int. Ed*. 61, e202110491 (2022).

72. Parmenter, C. S. & Rau. J. D. *J. Chem Phys*. 51, 2242–2246 (1969).

73. Glaser, F., Kerzig, Christoph., Wenger, O. S. *Angew. Chem. Int. Ed.* 59, 10266–10284 (2020)

74. Chatterjee, A. & König, B. *Angew. Chem. Int. Ed.* 58, 14289–14294 (2019).

75. Sharma, R. K. & Fry, J. L. *J. Org. Chem.* 48, 2112–2114 (1983).

76. Gaussian 16, Revision C.01, et al. Gaussian, Inc., Wallingford CT, 2016.

77. Becke, A. D. *J. Chem. Phys*. 98, 5648–5652 (1993).

78. Lee, C., Yang, W. & Parr, R. G. *Phys. Rev. B*, 37, 785–789 (1988).

79. Vosko, S. H., Wilk, L. & Nusair, M. *Can. J. Phys.* 1980, 58, 1200–1211 (1980).

80. Stephens, P. J., Devlin, F. J., Chabalowski, C. F. & Frisch, M. J. *J. Phys.Chem*, 98, 11623–11627 (1994).

81. Chai, J. D. & Head-Gordon, M. *J. Chem. Phys*. 128, 084106 (2008).

82. Marenich, A. V., Cramer, C. J. & Truhlar, D. G. *J. Phys. Chem.* B, *113*, 6378–6396 (2009).

83. G. Luchini, J. V. Alegre-Requena, I. Funes-Ardoiz, R. S. Paton, *F1000Research* 9, 291 (2020).

84. Roth, H. G., Romero, N. A. & Nicewicz, D. A. *Synlett* 27, 714–723 (2016).

85. Guha, S. & Saha, S. *J. Am. Chem. Soc.* 132, 17674–17677 (2010).

86. A. Sau, N. F. Pompetti, A. R. Green, M. V. Popescu, R. S. Paton, G. M. Miyake, N. H. D. ACS Catal. 2024, 14, 4, 2252–2263.

APPENDIX B: SUPPLEMENTARY INFORMATION FOR CHAPTER 3

General Methods

All purchased reagents were used without further purification. NMR spectra were recorded on a Varian 300 MHz, 400 MHz, or 500MHz NMR Spectrometer as noted. All ^{1}H NMR are reported in δ units (parts per million – ppm) and were measured relative to the signals found in residual chloroform (7.26 ppm). All ^{13}C NMR were measured relative to $CDCl_3$ (77.16 ppm).

Photophysical Experiments. UV-Visible absorption spectra were collected with an HP 8452A diode array spectrophotometer using 1.0 cm pathlength quartz cuvettes. Emission spectra were collected using an Olis SLM 8000C fluorimeter with the appropriate wavelength-dependent correction (calculated as the multiplicative factor necessary to match the collected emission profiles of two solid emissive NIST standards - SRM
2940-B and SRM 2943 - to their true profiles) applied to the raw data. Most of the data collected herein utilized a configuration in which the slit-widths before and after each monochromator were set to 1 mm (which corresponds to an effective bandpass of 2 nm). TCSPC measurements were made using a DeltaFlex Modular Fluorescence Lifetime System from Horiba Scientific. A Horiba NanoLED-405L was used as the excitation source (402 nm center-wavelength [CWL], c. 220 ps full-width at half maximum [FWHM]). Temperatures were measured with a built-in digital temperature sensor in the Horiba device. Temperature was controlled by a Quantum Northwest TC-1 temperature control unit coupled with an aquarium pump submerged in a reservoir, and a jacketed sample holder.

Transient Absorption. Transient absorption data in Fig. 6 were collected using a home-built pump/probe spectrometer. Source laser pulses (796 nm, 150 fs, 1 kHz) were derived from a commercially available oscillator and regenerative amplifier (Spectra Physics Solstice Ace). The pulse was split using a 90:10 beam splitter to pump and probe paths, respectively. The probe arm was successively directed onto a linear stage (Newport; ILS250HA, 0.5 fs/step time resolution, 25 cm of travel) which enabled control of the relative delay of the pump and probe pulses. A supercontinuum was generated by attenuating the probe appropriately and then focusing it into the back of a 10 mm crystal of CaF_2 using a 100 mm focal length lens. Due to the low damage threshold of CaF_2, the crystal was continuously moved perpendicularly to the beam path using a linear actuator (Zaber T-series). The probe was directed into the sample with a 250 mm focal length concave mirror to a spot size of ~60 μm. To minimize chirp at the sample, only reflective optics were used between the point of supercontinuum generation and the sample. For the pump path, majority of the rest 796 nm amplifier output was transmitted through a 100 μm crystal of β-barium borate (Type I, 30°), which generated the 398-nm-centered second harmonic of the fundamental that served as the excitation pulse. The repetition rate of this pulse was reduced to 500 Hz using an optical chopper (Thorlabs; MC1000A) attenuated to approximately 400 nJ/pulse and then focused into the sample to a spot size of ~110 μm using a 300 mm focal length lens. In order to ensure that the two pulses maintained spatial overlap for the duration of their travel through the sample, they were focused at a very narrow (< 5°) angle. The relative polarization of the pump and probe beams was set to the magic angle (54.7°) by rotating the polarization of the 398 nm pump pulse prior to being focused into the sample. Detection was performed using a spectrograph (Chromex; 250IS) and charge coupled detector (CCD) (Andor; DU920P-OE). By focusing the beam onto a small vertical region (8 pixels) of the detector, acquisition of spectra on a shot-to-shot

basis was possible, eliminating noise due to any laser fluctuations on a timescale longer than 10s of milliseconds. Data processing was performed using home-built software programmed in Labview and Matlab. Outlying spectra (with photon counts outside of a region of 6 sigma from the median, due to small burns in the white-light generation medium) were removed and the remaining pump-on and pump-off spectra were averaged in 20 shot blocks and used to calculate ΔA. These 20 shots ΔA measurements were averaged over one period of the actuation of the CaF_2 between changing the time delay to ensure that, at each pump probe delay timepoint, the average white light quality was identical. Samples were prepared using UV-grade THF inside an Ar-filled glovebox before being sealed in a quartz cuvette using a KONTES valve. Samples were kept at a low optical density (~0.2) to avoid complete probe attenuation in near-UV regions of interest.

Photoreactors

The photoreactors used were custom designed and built in-house. The specifications have been published previously.[1] All LEDs were purchased from LED Engin and full emission spectra, as well as peak wavelength shift vs. temperature data, are available online in the respective manufacturer datasheets (see below). In the photoreactor, both the 385 nm and 405 nm LEDs were run at 700mA and a forward voltage of 13.5 V.

Table S3.1. LED Information

LED Peak Wavelength	Luminous Flux	Model #	URL
405 nm	4.1 W @ 700 mA	LZ4-40UB0000U8	https://media.osram.info/media/img/osram-dam-5412925//LED_Engin_Datasheet_LuxiGen_LZ4-00UB00_rev1.pdf

385 nm	1.1 W @ 700 mA	LZ1-10UBN0-00U4	https://www.mouser.com/datasheet/2/588/Ams_Osram_7_6_2022_LZ1_10UBN0_EN-2998940.pdf

Single LED Photoreactor Setup

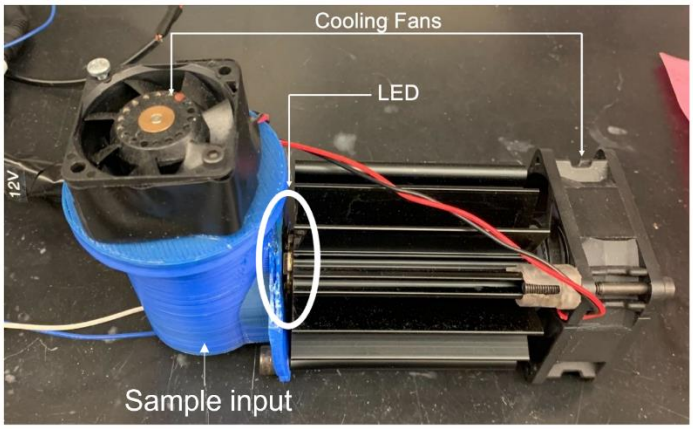

Double LED Photoreactor Setup

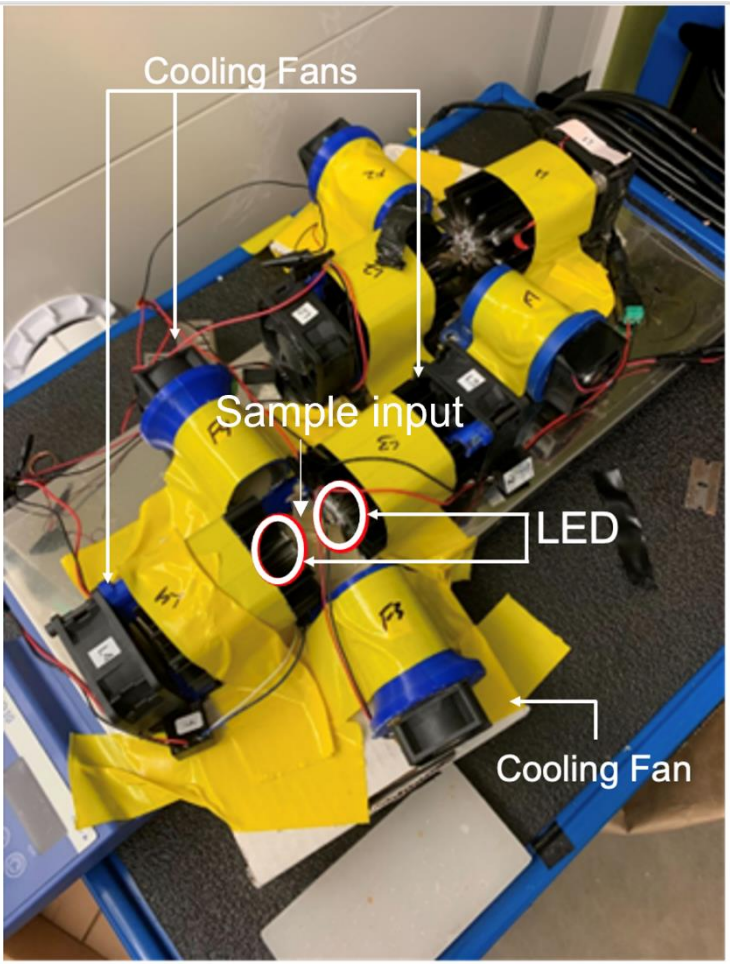

List of Abbreviations

PC Abbreviation	Structure

BPI-N	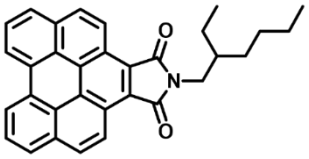
BPI-Br	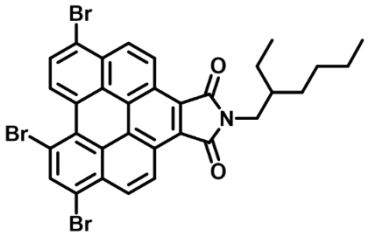
BPI-P	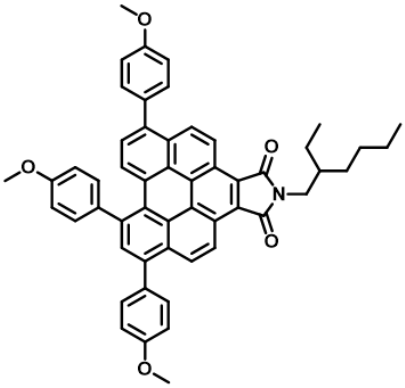
BPI-RO	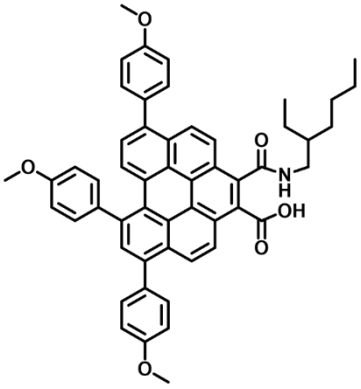

BPI-M	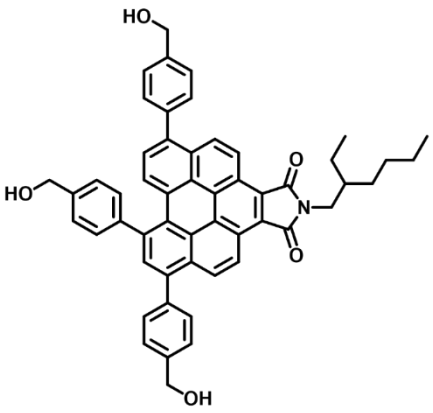
BPA-M	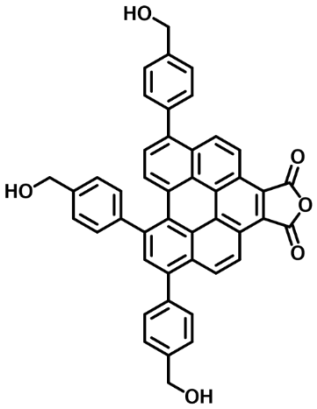
BPA-P	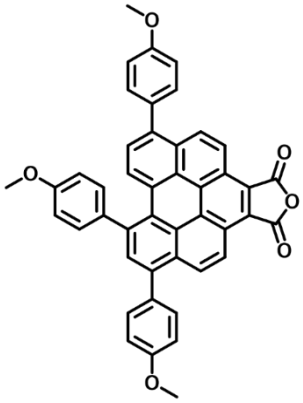
BPDE	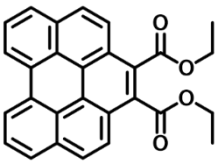

Catalyst Synthesis

2-(2-ethylhexyl)-1H-peryleno[1,12-efg]isoindole-1,3(2H)-dione ***(BPI-N)***

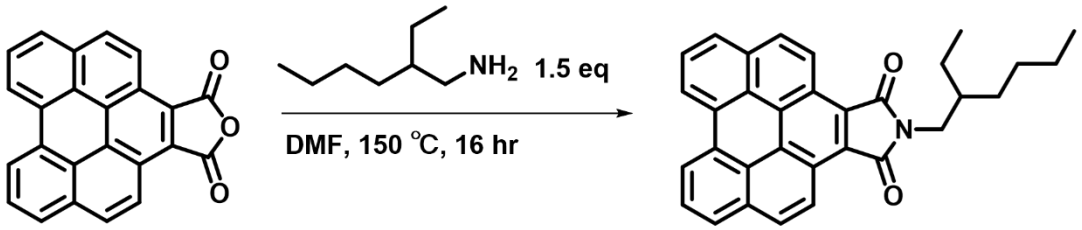

2-(2-ethylhexyl)-1H-peryleno[1,12-efg]isoindole-1,3(2H)-dione ***(BPI-N)*** was synthesized according to literature procedure.[2]

6,8,11-tribromo-2-(2-ethylhexyl)-1H-peryleno[1,12-efg]isoindole -1,3(2H)-dione ***(BPI-Br)***

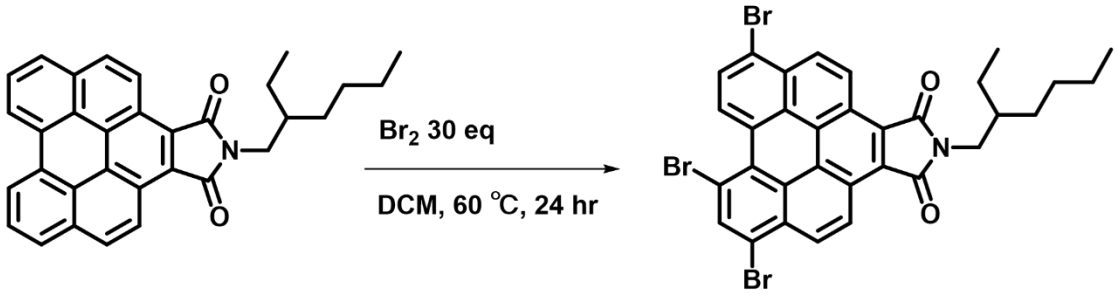

6,8,11-tribromo-2-(2-ethylhexyl)-1H-peryleno[1,12-efg]isoindole -1,3(2H)-dione ***(BPI-Br)*** was synthesized according to literature procedure.[2]

^{1}H NMR (400 MHz, CDCl3) δ 9.24 (d, J = 8.7 Hz, 0H), 8.69 (dd, J = 14.1, 9.1 Hz, 1H), 8.25 (s, 0H), 8.11 (d, J = 9.1 Hz, 0H), 7.99 (d, J = 9.1 Hz, 0H), 7.85 (d, J = 8.7 Hz, 0H), 3.75 (d, J = 7.2 Hz, 1H), 1.95 (t, J = 6.3 Hz, 1H), 1.54 – 1.35 (m, 1H), 1.05 (t, J = 7.4 Hz, 1H), 0.97 (t, J = 7.0 Hz, 1H) ppm. ^{13}C NMR (101 MHz, $CDCl_3$) ^{13}C NMR (101 MHz, $CDCl_3$) δ 168.6, 168.5, 138.3, 129.5, 128.0, 127.8, 127.8, 127.1, 125.6, 125.2, 125.2, 124.8, 123.8, 123.3, 123.3, 123.2, 123.1 123.1, 122.5, 122.3, 122.2, 121.3, 116.8, 77.3, 77.0, 76.7, 42.1, 38.8, 30.8, 28.7, 24.1, 23.2, 14.2, 10.6 ppm.

2-(2-ethylhexyl)-6,8,11-tris(4-(hydroxymethyl)phenyl)-1H-peryleno[1,12-efg]isoindole-1,3(2H)-dione ***(BPI-M)***

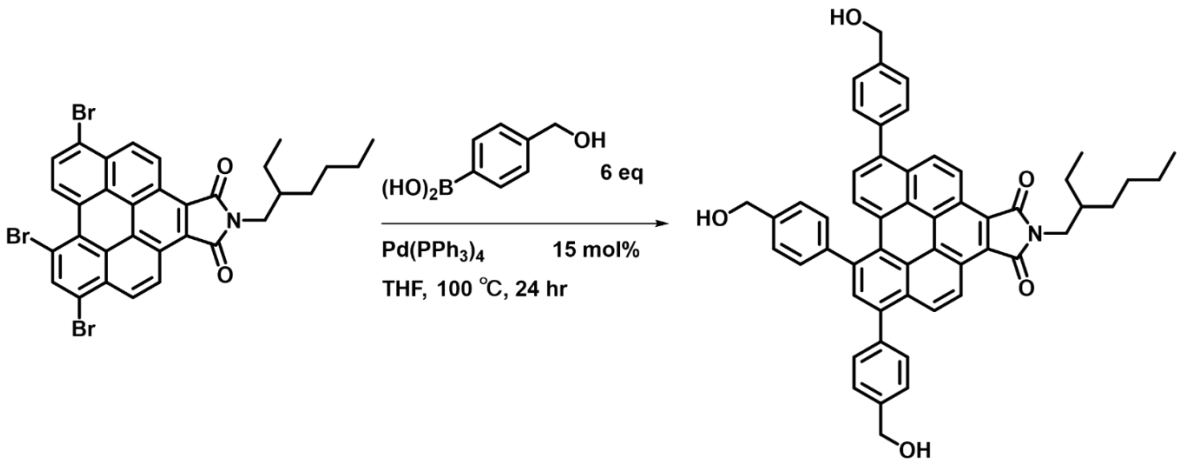

To a 100 mL storage tube **BPI-Br** (0.20 g, 0.29 mmol, 1.0 eq.) and 4-(Hydroxymethyl)phenylboronic acid (0.263 g, 1.74 mmol, 6.00 eq.) were added. The storage tube was then moved to a N_2 filled glovebox where $Pd(PPh_3)_4$ (0.050 g, 0.043 mmol, 0.15 eq) was added. 25.0 mL of THF was added and the storage tube was sealed with a Teflon screw cap and removed from the glovebox. Under a nitrogen atmosphere on a Schlenk line, 6.50 mL of 2.0 M aqueous K_2CO_3 was then added and sealed under N_2. The reaction was then heated to 100 °C for 24 hours. After completion, the THF was removed in vacuo, and the crude mixture was washed three times with DCM (3 x 50 mL) and water (3 x 50 mL), followed by brine and dried with anhydrous Na_2SO_4. TLC was performed on the crude reaction mixture with 95:5 DCM:MeOH where the product appears as an orange spot with rf 0.4. Purification via silica column chromatography using a DCM:MeOH (0-10%) gradient afforded a dark red solid (**BPI-M**) (140 mg, 63%). ^{1}H NMR (400 MHz, MeOD) δ 7.61 (d, J = 9.0 Hz, 1H), 7.43 (dd, J = 16.3, 8.2 Hz, 3H), 7.33 (d, J = 7.5 Hz, 5H), 7.23 (dd, J = 16.5, 7.4 Hz, 4H), 7.04 (d, J = 7.4 Hz, 3H), 6.80 (d, J = 7.8 Hz, 3H), 4.80 (s, 2H), 4.70 (s, 2H), 4.64 (s, 2H), 3.37 (s, 1H), 2.87 (s, 2H), 1.57 (s, 1H), 1.30 (s, 1H), 1.27 (s, 4H), 1.22 (s, 5H), 0.92 – 0.79 (m, 6H) ppm . ^{13}C NMR (101 MHz, MeOD) δ 91.3, 70.2, 54.5, 54.5, 54.4, 47.6, 47.4, 47.2, 47.0, 35.7, 27.3, 7.6. HRMS (ESI): Calculated for $[M+H]^+$ $C_{53}H_{46}NO_5$ 776.3371, measured 776.3361.

6,8,11-tris(4-(hydroxymethyl)phenyl)naphtho[2',1',8':3,4,5]pyreno[1,2-c]furan-1,3-dione ***(BPA-M)***

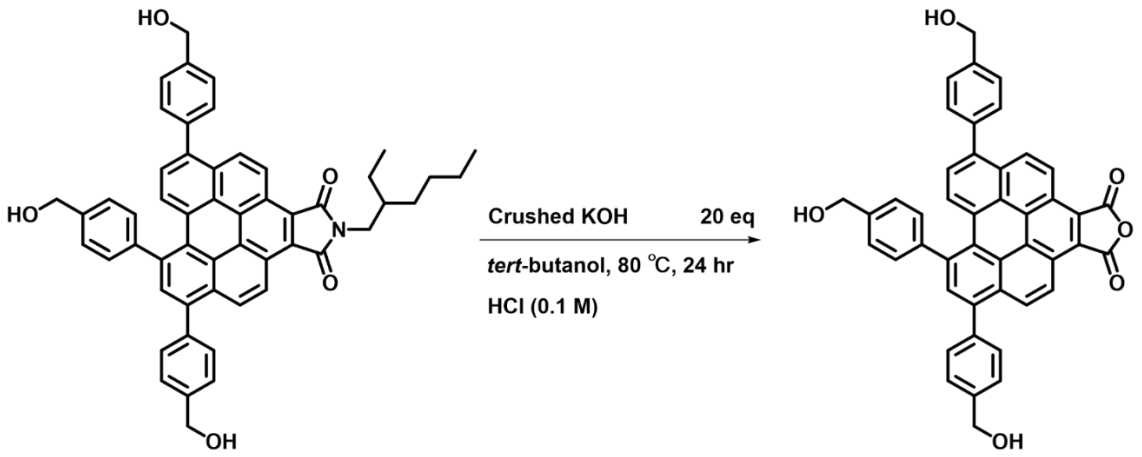

To a 100 mL round bottom flask, BPIPhCH$_2$OH (**BPI-M**) (0.100 g, 0.130 mmol, 1 eq), crushed potassium hydroxide (0.235 g, 2.60 mmol, 20 eq), and 18.0 mL tert-butanol were added, and the mixture was refluxed under a reflux condenser cooled by water at 80 °C for 24 hours open to air. The resulting solution turned a yellow color with cyan fluorescence. After the reaction was complete via monitoring with TLC (cyan intermediate rf of 0.3 in 8:2 hexanes : ethyl acetate), 0.10 M aq HCl was added dropwise, until the pH changed from 14 to 1, and the solution was stirred for an additional one hour until a red precipitate crashed out. The resulting suspension was cooled to 0 °C for 15 minutes and then filtered. The red precipitate was then rinsed with water followed by ether to give the target product in 49 % isolated yield (30 mg). ^{1}H NMR (400 MHz, THF) δ 9.07 – 8.91 (m, 1H), 8.58 – 8.41 (m, 1H), 8.11 (d, J = 1.6 Hz, 0H), 7.70 – 7.49 (m, 4H), 4.74 (dd, J = 12.3, 7.2 Hz, 2H), 4.46 – 4.24 (m, 1H) ppm. ^{13}C NMR (101 MHz, $CDCl_3$) δ 164.0, 159.6, 159.5, 159.4, 139.5, 139.4, 137.1, 134.7, 132.2, 132.0, 131.7, 131.6, 130.2, 129.6, 129.3, 129.1, 128.8, 128.4, 127.5, 126.6, 124.1, 123.1, 122.0, 121.7, 115.5, 114.2, 114.1, 77.3, 77.2, 77.0, 76.7, 55.5, 55.5, 55.4 ppm. HRMS (ESI): Calculated for $[M + H]^+$ $C_{45}H_{28}O_6$ 665.1964, measured 665.1955.

2-(2-ethylhexyl)-6,8,11-tris(4-methoxyphenyl)-1H-peryleno[1,12-efg]isoindole-1,3(2H)-dione ***(BPI-P)***

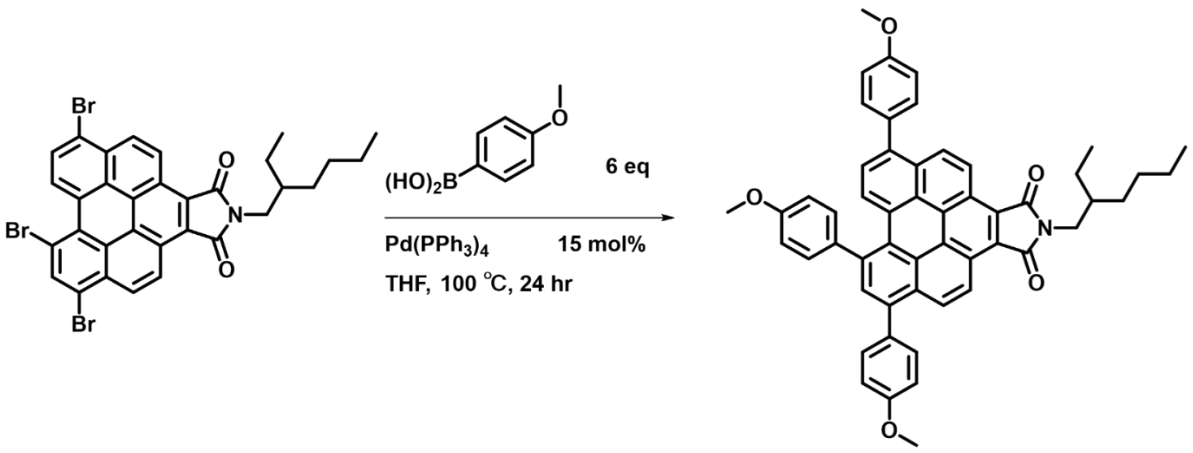

2-(2-ethylhexyl)-6,8,11-tris(4-methoxyphenyl)-1H-peryleno[1,12-efg]isoindole-1,3(2H)-dione (**BPI-P**) was synthesized according to literature procedure.[2] ^{1}H NMR (400 MHz, $CDCl_3$) δ 9.31 – 9.16 (m, 1H), 8.47 – 8.34 (m, 1H), 8.01 (s, 0H), 7.68 – 7.48 (m, 2H), 7.17 – 7.02 (m, 2H), 4.01 – 3.84 (m, 2H), 3.74 (d, *J* = 7.3 Hz, 1H), 3.49 (d, *J* = 5.5 Hz, 0H), 1.99 (d, *J* = 6.4 Hz, 0H), 1.52 – 1.27 (m, 3H), 0.99 (t, *J* = 7.4 Hz, 1H), 0.94 – 0.84 (m, 1H) ppm. ^{13}C NMR (101 MHz, $CDCl_3$) δ 170.2, 170.2, 159.4, 159.2, 159.2, 138.8, 138.7, 137.6, 133.8, 132.6, 132.4, 131.6, 131.6, 130.3, 129.2, 129.1, 128.9, 128.4, 128.2, 128.1, 127.9, 127.6, 127.4, 126.9, 126.4, 124.4, 123.7, 122.6, 122.3, 115.3, 114.1, 114.0, 77.3, 77.2, 77.0, 76.7, 55.5, 55.4, 41.9, 38.6, 30.7, 28.7, 24.1, 23.2, 14.1, 10.5 ppm.

6,8,11-tris(4-methoxyphenyl)naphtho[2',1',8':3,4,5]pyreno[1,2-c]furan-1,3-dione ***(BPA-P)***

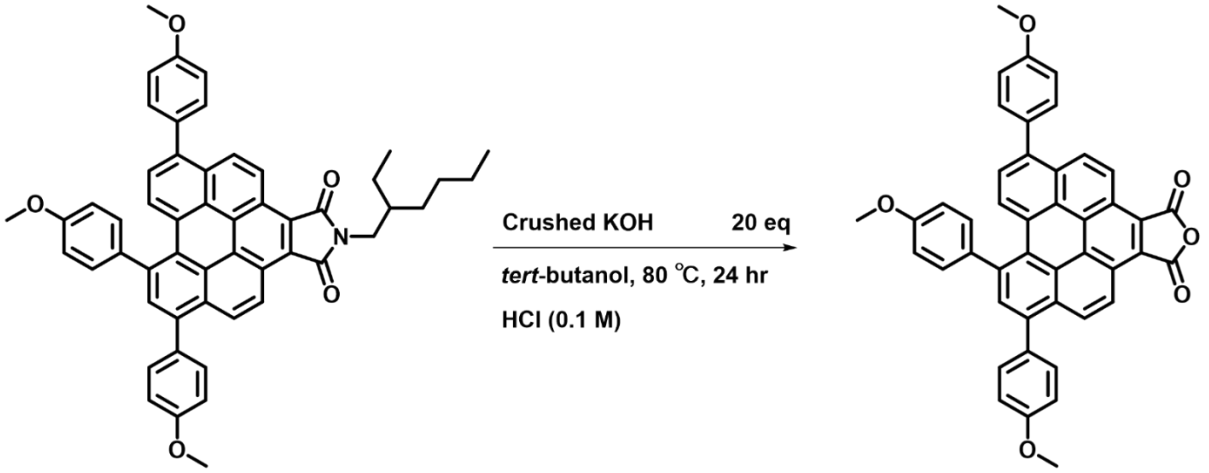

To a 100 mL round bottom flask, **BPI-P** (0.100 g, 0.130 mmol, 1 eq), crushed potassium hydroxide (0.235 mg, 2.60 mmol, 20 eq), and 18.0 mL tert-butanol were added, and the mixture refluxed using a reflux condenser, cooled with water, at 80 °C for 24 hours open to air. The resulting solution turned into a yellow color with cyan fluorescence. After the reaction was complete via monitoring with TLC (cyan intermediate rf of 0.3 in 8:2 hexanes: ethyl acetate), 0.10 M aq HCl was added dropwise, until the pH changed from 14 to 1, and the solution was stirred for an additional one hour until a red precipitate crashed out. The resulting red precipitate was cooled to 0 °C for 15 minutes and then filtered. The ~~solid~~ red precipitate was then rinsed with water followed by ether to give the target product in 49 % isolated yield (30 mg). ^{1}H NMR (400 MHz, THF) δ 9.07 – 8.91 (m, 1H), 8.58 – 8.41 (m, 1H), 8.11 (d, J = 1.6 Hz, 0H), 7.70 – 7.49 (m, 4H), 4.74 (dd, J = 12.3, 7.2 Hz, 2H), 4.46 – 4.24 (m, 1H) ppm. ^{13}C NMR (101 MHz, $CDCl_3$) δ 164.0, 159.6, 159.5, 159.4, 139.5, 139.4, 137.1, 134.7, 132.2, 132.1, 131.7, 131.6, 130.2, 129.6, 129.3, 129.1, 128.8, 128.4, 127.5, 126.6, 124.1, 123.1, 122.0, 121.7, 115.5, 114.2, 114.1, 77.3, 77.2, 77.0, 76.7, 55.5, 55.5, 55.4 ppm. HRMS (ESI): Calculated for $[M+H]^+$ $C_{45}H_{28}O_6$ 665.1964 measured 665.1955.

2-((2-ethylhexyl)carbamoyl)-5,8,10-tris(4-methoxyphenyl)benzo[ghi]perylene-1-carboxylic acid ***(BPI-RO)***

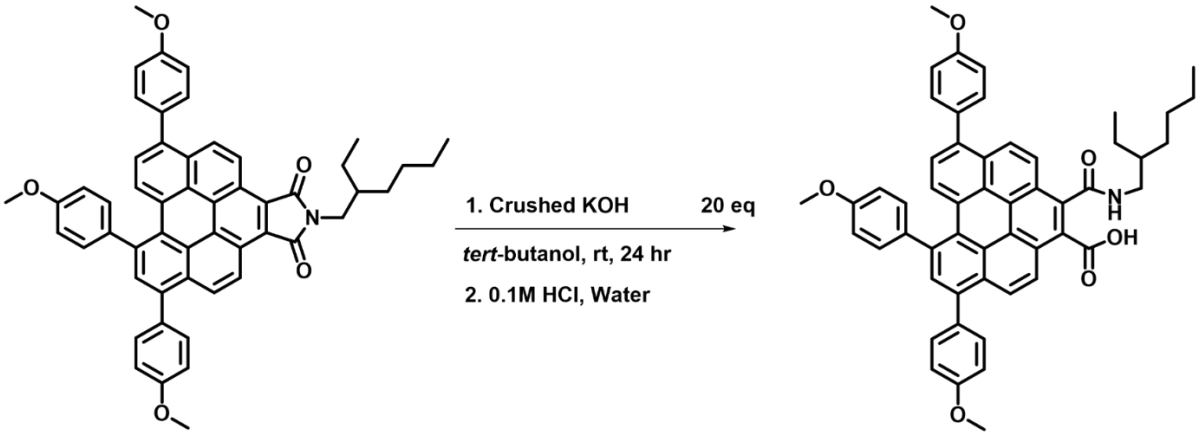

To a 100 mL round bottom flask, **BPI-P** (0.100 g, 0.130 mmol, 1 eq) crushed potassium hydroxide (0.235 mg, 2.60 mmol, 20 eq) and 18.0 mL tert-butanol were added and the mixture was stirred and refluxed with a reflux condenser cooled by water at 80 °C for 24 hours open to air. The resulting solution turned yellow with a cyan fluorescence as the reaction proceeded. An aliquot of the yellow solution was taken from the crude reaction mixture and 0.1 M HCl was added until the pH changed from 14 to 7, and water (50.0 mL) was added until precipitation occurred as a yellow solid. The filtered yellow solid gave 15 mg. HRMS (ESI): Calculated for $[M+H]^+$ $C_{53}H_{47}NO_6$ 794.3481, measured 794.3465.However, this species was found to be prone to anhydride formation in solution which precluded NMR characterization.

diethyl benzo[ghi]perylene-1,2-dicarboxylate **(BPDE)**

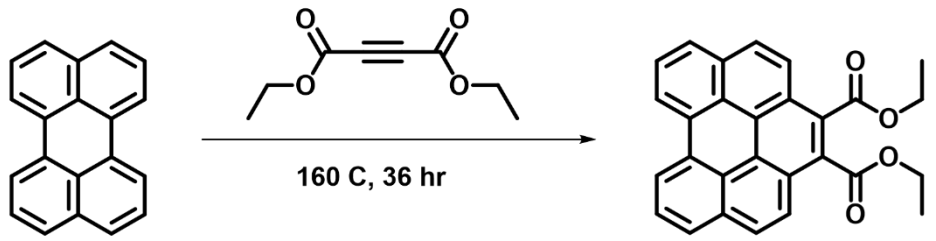

A modified literature procedure was used to synthesize this compound.[3] To a 50 mL round bottom flask, perylene (1.00 g, 4.00 mmol, 1.00 eq) was added with diethyl acetylenedicarboxylate (13.7 mL, 100.0 mmol 25.0 eq), and the mixture was stirred and refluxed with a reflux condensor, cooled with water at 150 °C in open air for 48 hours. The crude yellow solution was purified via silica column chromatography with a hexanes:ethyl acetate gradient (0-100 %). The resulting column fractions were recrystallized by layering DCM:MeOH (1:1 by volume) at 0 °C to form yellow needles, which were then filtered and collected for a 10 % yield (100 mg). ^{1}H NMR (400 MHz, $CDCl_3$) δ 9.06 (d, *J* = 7.8 Hz, 2H), 8.42 (d, *J* = 9.1 Hz, 2H), 8.23 (d, *J* = 7.7 Hz, 2H), 8.09 (t, *J* = 7.8 Hz, 2H), 4.63 (q, *J* = 7.2 Hz, 4H), 1.54 (dd, *J* = 7.9, 6.4 Hz, 6H) ppm. ^{13}C NMR (101 MHz, $CDCl_3$) δ 168.7, 132.3, 130.7, 129.2, 128.3, 127.4, 127.2, 125.6, 125.4, 125.1, 124.6, 121.5, 77.5, 77.4, 77.2, 76.8, 62.3, 14.4 ppm. HRMS (ESI): $[M+NH_4]^+$ Calculated for $C_{28}H_{24}NO_4$ 438.1706; measured 438.1683.

Synthetic methods and degradation study

Table S3.2. Optimization of photo-Birch reduction of benzene using tetramethylammonium hydroxide as a sacrificial electron donor with different PCs as discussed in the manuscript.[a]

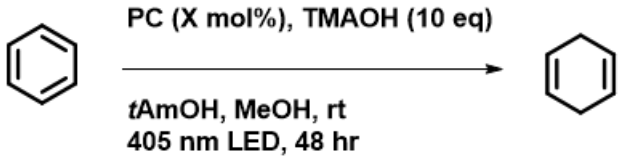

Entry	PC	X	Time	Conversion %[b]
1	BPI-P	0.25	48	30
2	BPI-M	0.25	48	9
3	BPI-M	0.25	120	9
4	BPI-M	1.0	48	23
5	BPI-M	1.2	48	26
6	BPI-M	1.4	48	25
7	BPI-M	1.6	48	25
8	BPI-M	1.8	48	17
9	BPI-M	2.0	48	16
10	BPI-M	2.5	48	13
11	BPA-P	0.25	48	20
12	BPA-M	1.2	48	0

[a]*Conditions:* *A mixture of specified photocatalyst (PC) (x mole% relative to benzene), benzene (0.50 mmol, 39.0 μL, 1.00 eq), tetramethylammonium hydroxide (TMAOH; 25 wt% solution in methanol) (5.0 mmol, 1.82 mL, 10.0 eq), tert-amyl alcohol (4.0 mmol, 0.45 mL, 8.0 eq), irradiated with 405 nm LEDs at room temperature.* [b]*Conversion determined by* ^{1}*H NMR. Note: Reactions with no PC, light, or reductant failed to show conversion.*

Table S3.3. Degradation of BPI-P as a function of heat and light and control experiments.[a]

Entry	Conditions (all ran for 48 hours)	% BPI Recovered
1	50 °C + TMAOH + PC	61
2	25 °C + TMAOH + PC	76
3	0 °C + TMAOH + PC	90
4	single 405 nm LED + PC	94
5	0 °C + single 405 nm LED + TMAOH + PC	92
6	25 °C + single 405 nm LED + TMAOH + PC[b]	76

[a]*Conditions: A mixture of BPI-P (0.01 g, 0.013 mmol, 1.00 eq), TMAOH (25 wt% solution in methanol) (93.3 µL, 0.260 mmol, 20.0 eq) and solvent system of 8:2 volume ratio MeOH:tert-amyl alcohol (1.9 mL) in a 2.0 mL dram vial was subjected to conditions shown. The crude reaction was then filtered, and the resulting residue was collected. Note: Full conversion to any ring opened species was not achieved in this experiment due to the poor solubility of* ***BPI-P*** *in methanol which is in contrast to the smaller scale experiment performed on* ***BPI-M*** *as seen in Figure 2C within the main text.*

[b]*Standard photo-Birch conditions with BPI-P excluding substrate.*

Table S3.4. Hydrodehalogenations with **BPDE** compared to **BPI-N.**

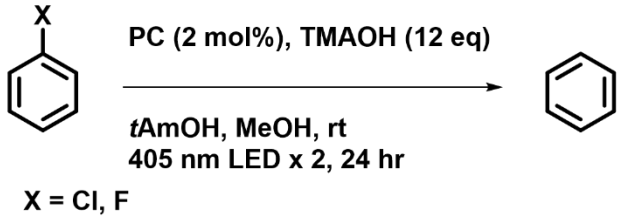

Entry	PC	Substrate	NMR Yield (%)
1	BPDE	Fluorobenzene	19
2	BPDE	Chlorobenzene	25
3	BPI-N	Fluorobenzene	0

4	BPI-N	Chlorobenzene	49

Conditions: A mixture of photocatalyst (PC)(0.005 mmol, 2.0 mol%), TMAOH (25 wt% solution in methanol) (1.09 mL, 3.00 mmol, 12.0 eq) and tert-amyl alcohol (0.48 mL, 4.50 mmol, 18 eq), THF (0.50 mL, 6.15 mmol, 24.6 eq), and substrate (0.25 mmol, 1.0 eq) in a 2.0 mL dram vial under N_2 were subjected to a dual photoreactor (fitted with 2 x 405 nm LEDs) for 24 hours. Mesitylene (42 uL, 0.25 mmol, 1 eq), used as an internal ^1H NMR standard, was then added via volumetric syringe to the crude reaction. ^1H NMR analysis, with integrations relative to the known concentration of mesitylene, was used to determine yields of conversion with respect to benzene formed.

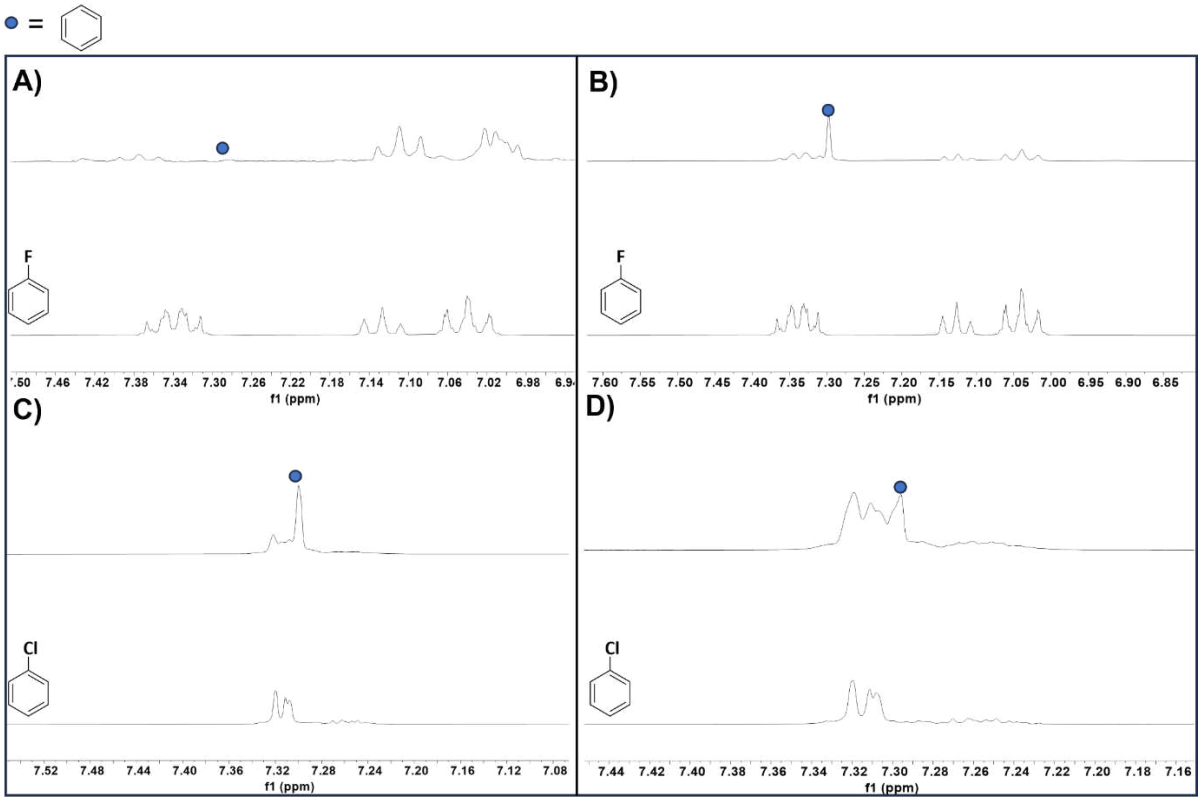

Figure S1. ^1H NMR of a 100 uL aliquot taken from crude reaction mixture (in 400 uL CD_3OD, 400 MHz) after running the dehalogenation reactions after 24 hours in conditions stated above in Table S4. ^1H NMR spectra of the starting materials, i.e. fluorobenzene or chlorobenzene are shown at the bottom of each for reference. A/B) Hydrodefluorination of fluorobenzene to benzene using BPI-N (A) and BPDE (B). As can be seen in (A), BPI-N fails to generate any detectable amount of benzene whereas a clear rise of the singlet resonance corresponding to benzene can be observed at 7.3 ppm after 24hr reaction with BPDE in (B). C/D) Hydrodechlorination of chlorobenzene to benzene using BPI-N and BPDE. In both cases formation of benzene is detected as a singlet resonance at 7.3ppm.

Electrochemistry

Cyclic voltammetry (CV), spectroelectrochemistry, and bulk electrolysis experiments were performed in a glovebox under an inert atmosphere of argon. For cyclic voltammetry, either anhydrous tetrahydrofuran (THF) or anhydrous dimethylacetamide (DMAc)was used to perform the experiment and is defined for each experiment within the text. Cyclic voltammetry was performed with an electrochemical analyzer (CH Instruments 601C) using a 3-electrode setup consisting of: a freshly polished platinum disk working electrode (3mm diameter), a 0.5mm platinum wire counter-electrode, and a freshly prepared 0.01M $Ag/AgNO_3$ reference electrode dissolved in either anhydrous DMAc or anhydrous acetonitrile(for those experiments run in THF) with a 0.1M tetrabutylammonium hexafluorophosphate ($TBAPF_6$) supporting electrolyte separated from solution with a porous frit. Cyclic voltammograms were scanned in the negative direction for all cyclic voltammetry experiments. After all cyclic voltammetry measurements were performed, ferrocene was spiked into solution to be used as an internal standard. A final cyclic voltammogram was collected containing the ferrocenium/ferrocene couple at the scan rate defined within the text. During post data collection analysis, the ferrocenium/ferrocene half-wave potential was used as the electrochemical reference, which is to say the ferrocenium/ferrocene half-wave was corrected so as to occur at 0V, and all electrochemical experiments are reported relative to this reference unless specified otherwise. For the scan rate experiments, data were collected from the slowest scan rate to the fastest scan rate. Before starting a new CV experiment, the solution was mixed via pipette to ensure homogeneity and allowed to rest for 1 minute before the next experiment was run.

Spectroelectrochemical measurements were performed in anhydrous THF using an electrochemical analyzer (CH Instruments 601C) in a 3-electrode setup with a constant applied

potential at values indicated in the text. Experiments were performed within a 2mm pathlength cuvette (1 cm wide and ~ 2 cm tall) which was equipped with a platinum mesh (0.6 cm x 2 cm) working electrode, 0.5mm platinum wire counter electrode, and a 0.01M Ag/AgNO3 reference electrode within a 0.1M $TBAPF_6$ MeCN solution separated from solution with a porous frit. Optical data collection was performed using an Avantes Avalight DHc white light source coupled with an Ocean Insight P600-2-VIS-NIR fiber optic cable which was passed into the glove box through an Avantes vacuum feedthrough (FC-VFT UVIR600) integrated into a custom milled KF flange. White light passed through the sample and coupled to a separate fiber optic cable back out through the glovebox in the same manner where it was collected with an Avantes Starlight Avaspec 3648 spectrometer then processed using Avasoft software. Absorption spectra, after applying a baseline correction and appropriate solvent (including electrolyte) blank to the software, were collected as a function of time at a constant applied potential.

Bulk electrolysis was performed using an electrochemical analyzer (CH Instruments 601C) with a 3-electrode setup and a constant applied potential at values indicated in the text. The experiment used a custom-built H-Cell where the working and counter electrode compartments were separated by a glass fritted disk. The electrode setup consisted of a 1 x 5 cm glassy carbon working electrode (IKA) placed within the working compartment, a 0.5mm diameter platinum wire contained within the counter electrode compartment, and a 0.01M $Ag/AgNO_3$ reference electrode within a 0.1M $TBAPF_6$ MeCN solution that is separated from the experimental solution with a porous frit and placed within the working compartment. To perform bulk electrolysis, **BPDE** was dissolved in a 0.1M $TBAPF_6$ THF electrolyte solution and added to the working compartment along with a Teflon stir bar and glassy carbon working electrode. To the counter electrode compartment was added an equal volume of 0.1M $TBAPF_6$ THF followed by 7 molar

equivalents (relative to **BPDE**) of triethyl amine as a sacrificial reductant added via 10 uL volumetric syringe. Bulk electrolysis of concentrated solutions of BPDE without the addition of triethyl amine resulted in polymerization of the THF solvent strictly within the counter electrode compartment. The solution was then electrolyzed at a constant potential as defined in the text. To generate **BPDE**$^{2-}$ the applied potential was –2.85V vs Fc^{+}/Fc, until the change in measured current approached zero. **[BP-H]**$^{-}$could be generated by adding either tert-amyl alcohol or methanol directly to the solution after 4 hours of electrolysis at this potential (see text for discussion). The amount of **[BP-H]**$^{-}$ could be greatly improved by adding a 1:1 tert-amyl alcohol:methanol solvent mixture to the working compartment (2:0.5:0.5 THF:tAmOH:MeOH by volume) after 4 hours of electrolysis and continuing electrolysis at –2.85V vs Fc^{+}/Fc for an additional hour. The optical absorption spectra of electrochemical products were characterized within the glovebox using the Avantes spectroscopy setup described above.

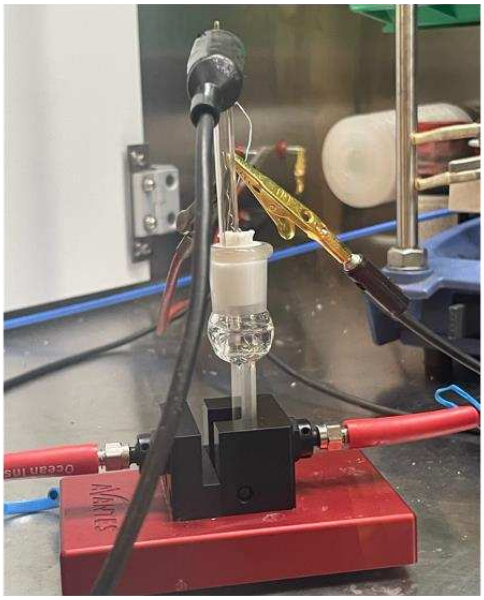

Figure S3.2. The three electrode spectroelecrochemical setup using a 2mm cuvette equipped with a platinum mesh (0.6 cm x 2 cm) working electrode, 0.5 mm platinum wire counter electrode, and a 0.01M Ag/AgNO$_3$ reference electrode in MeCN with 0.1M TBAPF$_6$ supporting electrolyte separated from experimental solution via a porous frit.

Figure S3.3. Example of a bulk electrolysis experiment performed on BPDE in 0.1M TBAPF$_6$ THF solution. The working compartment is on the left and contains BPDE dissolved in THF with supporting electrolyte, a stir bar, the glassy carbon working electrode and Ag/AgNO$_3$ reference electrode which is held in the small glass neck. The counter electrode compartment on the right contains a platinum wire counter electrode, 0.1M TBAPF$_6$ THF solution and 7 molar equivalents of triethylamine relative to BPDE.

Table S5. Electrochemical properties of catalysts studied in this work.

PC	$E_{1/2}$ **(PC/PC$^{\bullet-}$)**[a]	$E_{1/2}$ **(PC$^{\bullet-}$ /PC^{2-})**[a]
BPI-P	-1.62	-2.39
BPI-M	-1.62	-2.35
BPDE[b]	-2.22	-2.61

[a]*Values are reported versus the ferrocenium/ferrocene couple incorporated as an internal standard.*

[b]*Performed in a 0.1M $TBAPF_6$ THF electrolyte solution.*

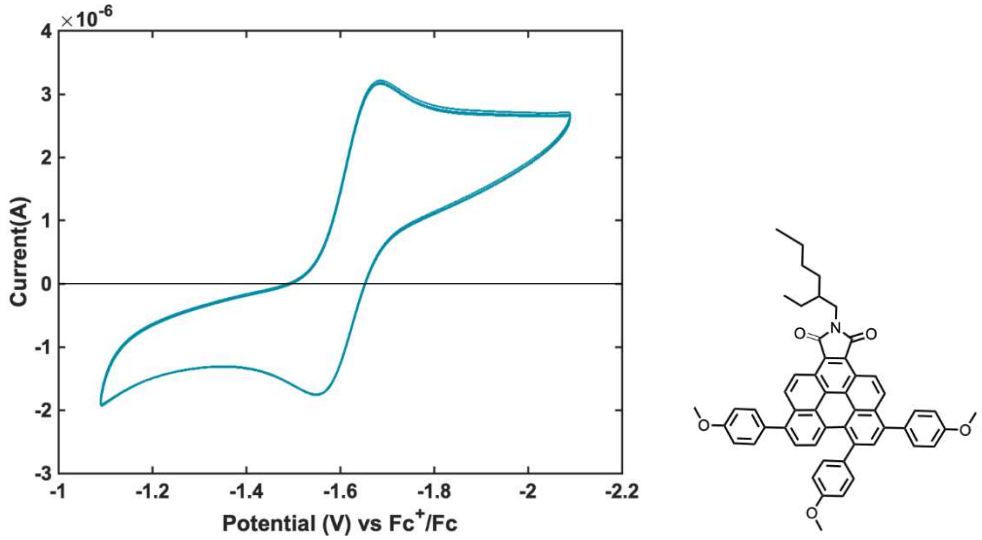

Figure S3.4. Cyclic voltammogram recorded at 100 mV/s for BPI-P in a 0.1M $TBAPF_6$ DMAc solution scanning from –1.1 to –2.1 V and back vs Fc^+/Fc.

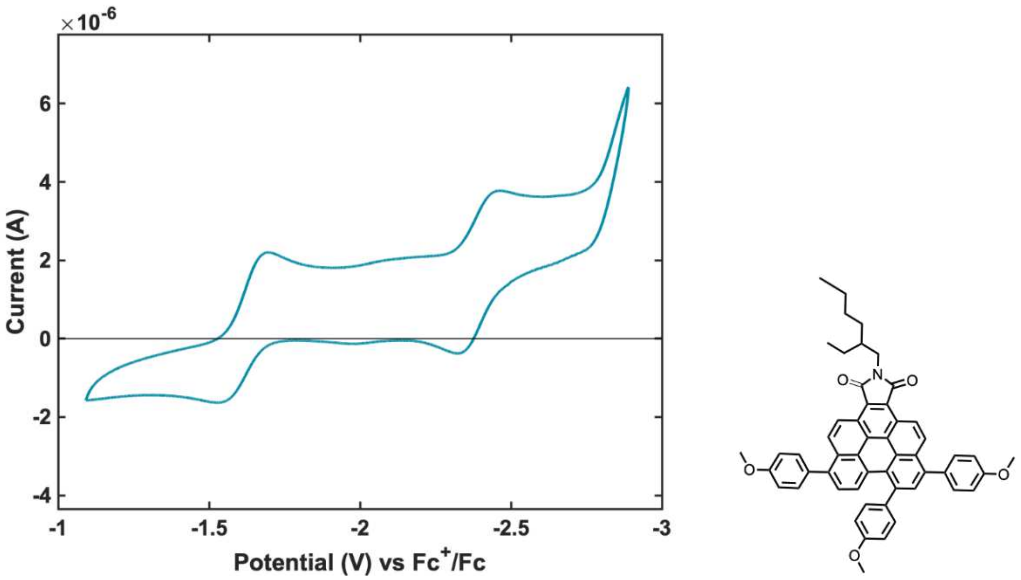

Figure S3.5. Cyclic voltammogram recorded at 100 mV/s for BPI-P in a 0.1M $TBAPF_6$ DMAc solution scanning from –1.1 to –2.8 V and back vs Fc^+/Fc.

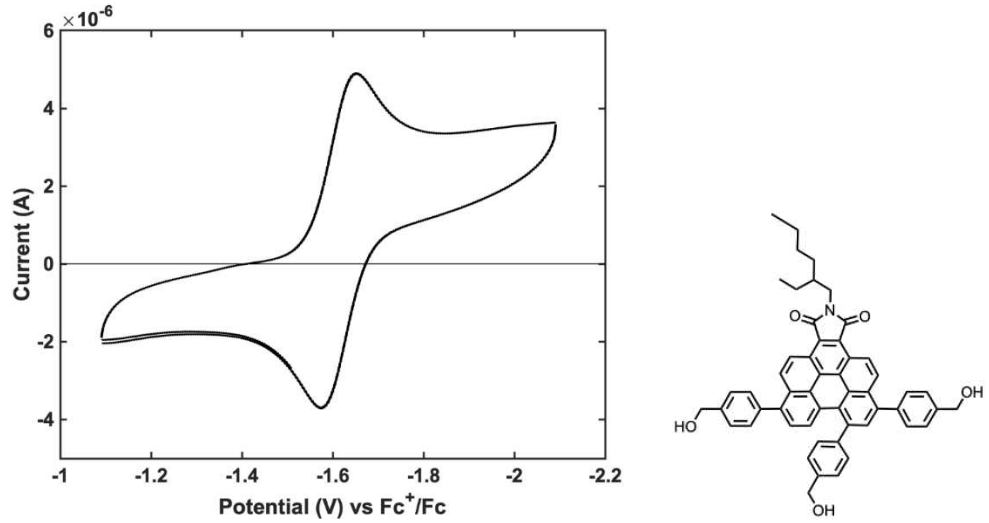

Figure S3.6. Cyclic voltammogram recorded at 100 mV/s for BPI-M in a 0.1M $TBAPF_6$ DMAc solution scanning from –1.1 to –2.1 V and back vs Fc^+/Fc.

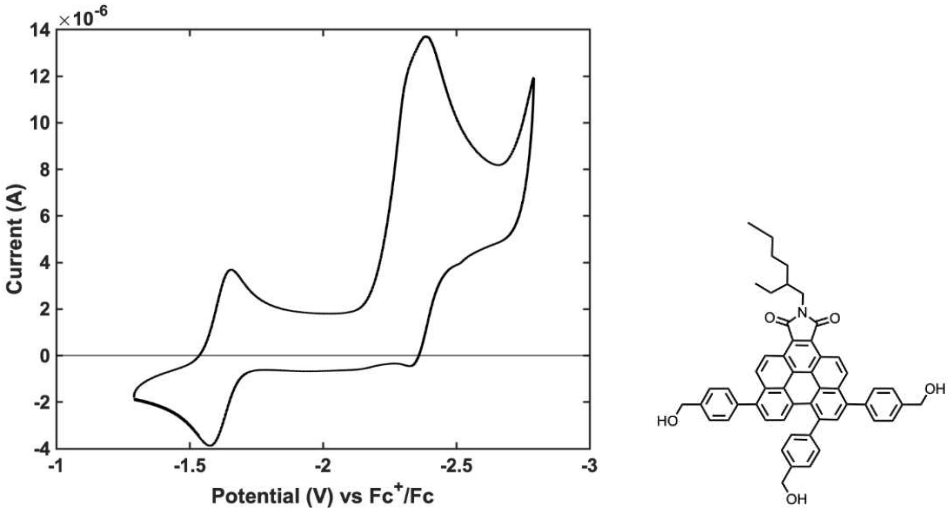

Figure S7. Cyclic voltammogram recorded at 100 mV/s for **BPI-M** in a 0.1M $TBAPF_6$ DMAc solution scanning from –1.3 to –2.8 V and back vs Fc^+/Fc.

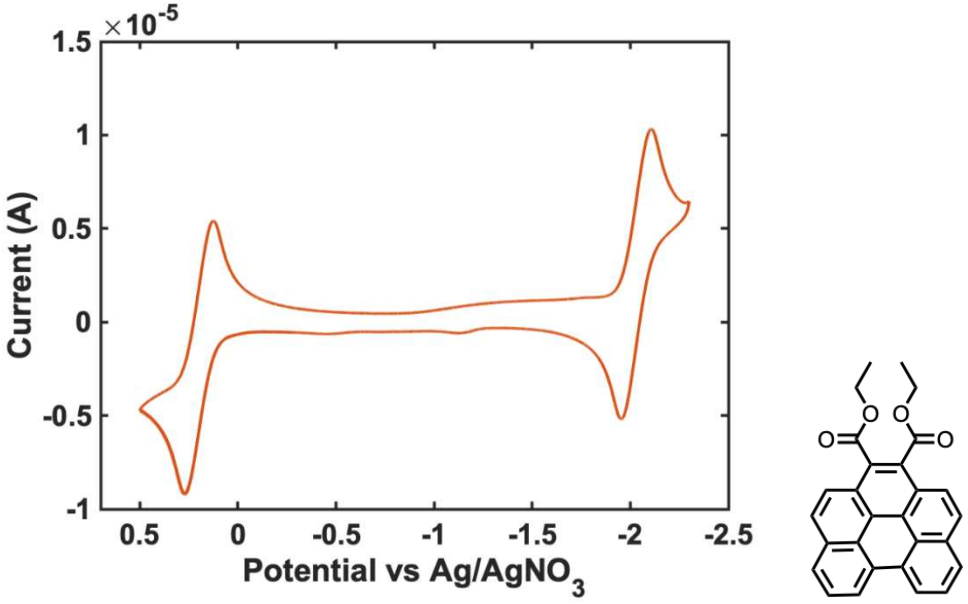

Figure S3.8. Cyclic voltammogram recorded at 100 mV/s for BPDE (1mM) and ferrocene in a 0.1M $TBAPF_6$ THF solution scanning from +0.5V to –2.4V and back vs $Ag/AgNO_3$. The cyclic voltammogram captures the ferrocenium/ferrocene couple with $E_{1/2}$ = +0.20V vs $Ag/AgNO_3$ and the first reduction couple of BPDE/$BPDE^{\bullet-}$ with $E_{1/2}$ = -2.0V vs $Ag/AgNO_3$.

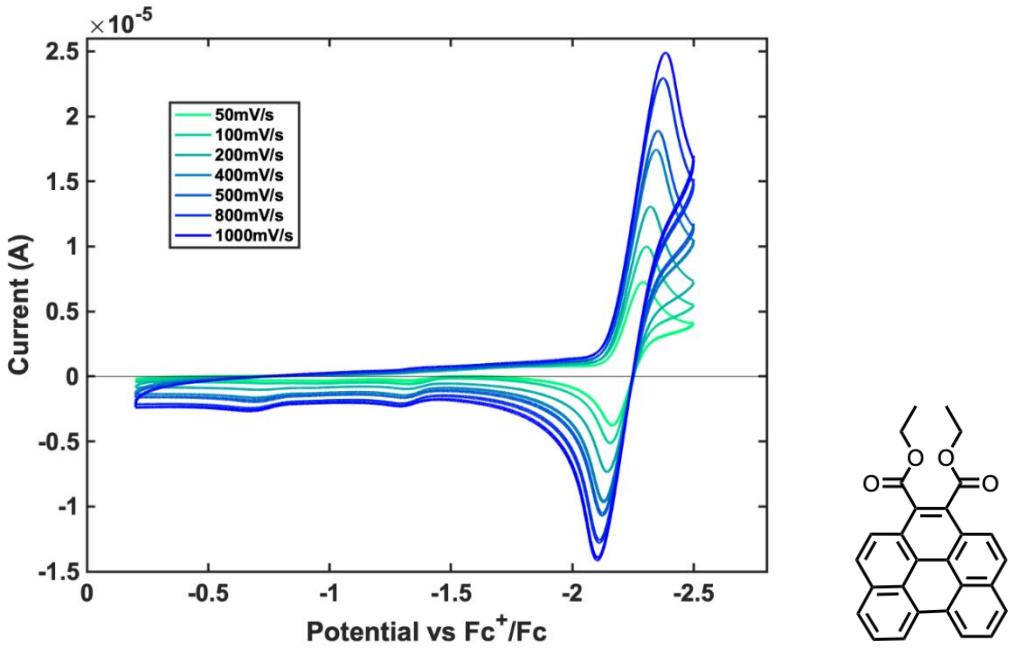

Figure S3.9. Cyclic voltammograms recorded at scan rates of 50 to 1000 mV/s of BPDE (1mM) in a 0.1M TBAPF$_6$ THF solution scanning from –0.2 to –2.5V and back vs Fc$^+$/Fc.

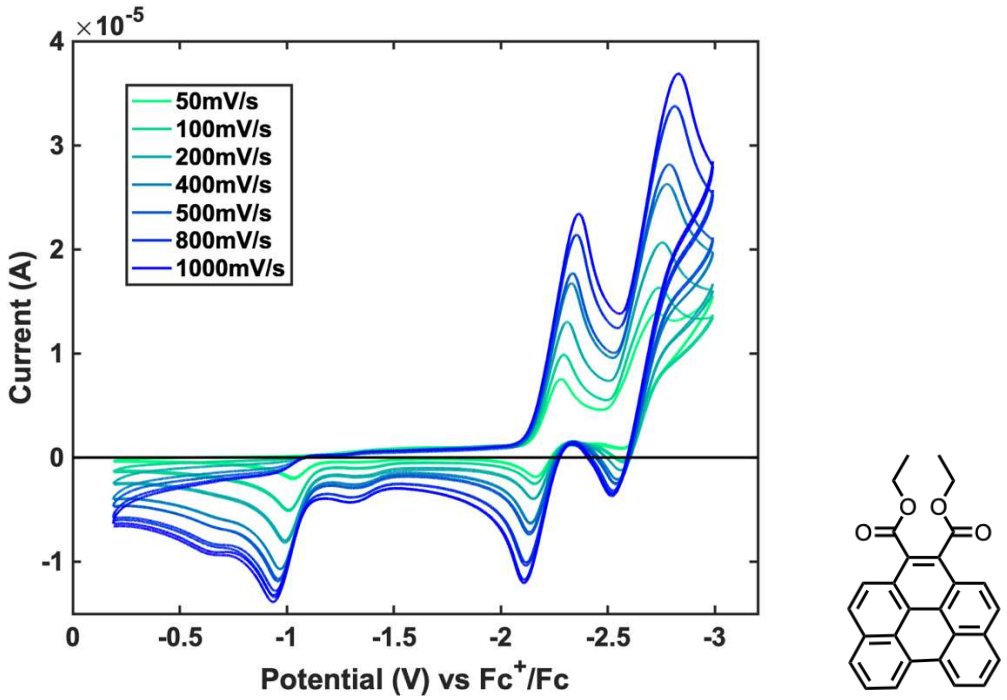

Figure S3.10. Cyclic voltammogram recorded at scan rates of 50 to 1000 mV/s of BPDE (1mM) at scan rates of 50 to 1000 mV/s in 0.1M TBAPF$_6$ THF solution going from –0.2 to –3V and back vs Fc$^+$/Fc.

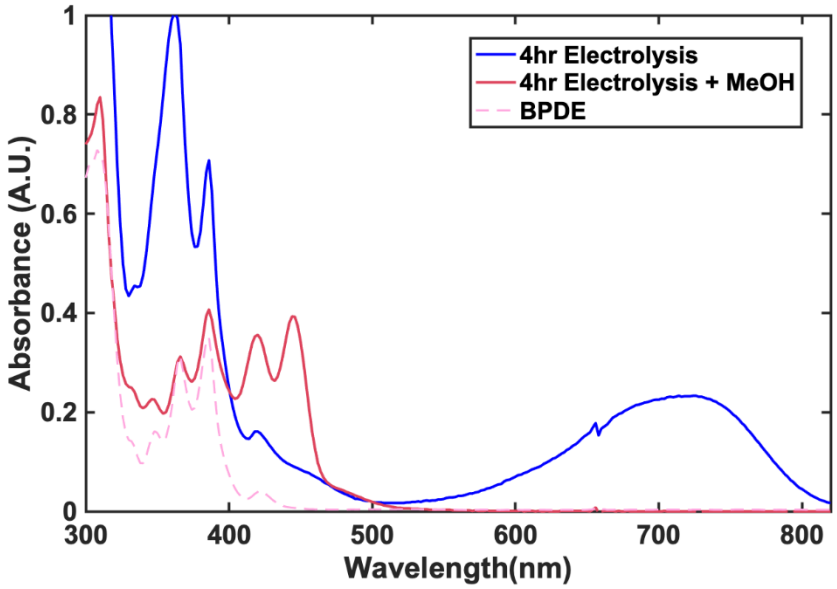

Figure S3.11. The steady state absorption profile of BPDE after 4 hours of bulk electrolysis at –2.85 V vs. Fc^{+}/Fc in a 0.1M $TBAPF_6$ THF solution (blue) under an argon atmosphere. After the first absorption spectrum was taken, methanol was added to the cuvette (resulting solvent mixture 3:1 THF:MeOH by volume). The cuvette was sufficiently mixed via a pipette and an absorption spectrum was immediately taken (red). After addition of methanol, the absorption features associated with $BPDE^{2-}$ are quenched and the vibronic progression of BPDE is reformed in addition to two new features centered at 420 and 446nm (corresponding to $[BP\text{-}H]^{-}$; refer to main text for further discussion). An absorption spectrum of ground state BPDE (dashed pink) in 0.1M $TBAPF_6$ THF solution is provided for comparison.

Determination of excited state reduction potential

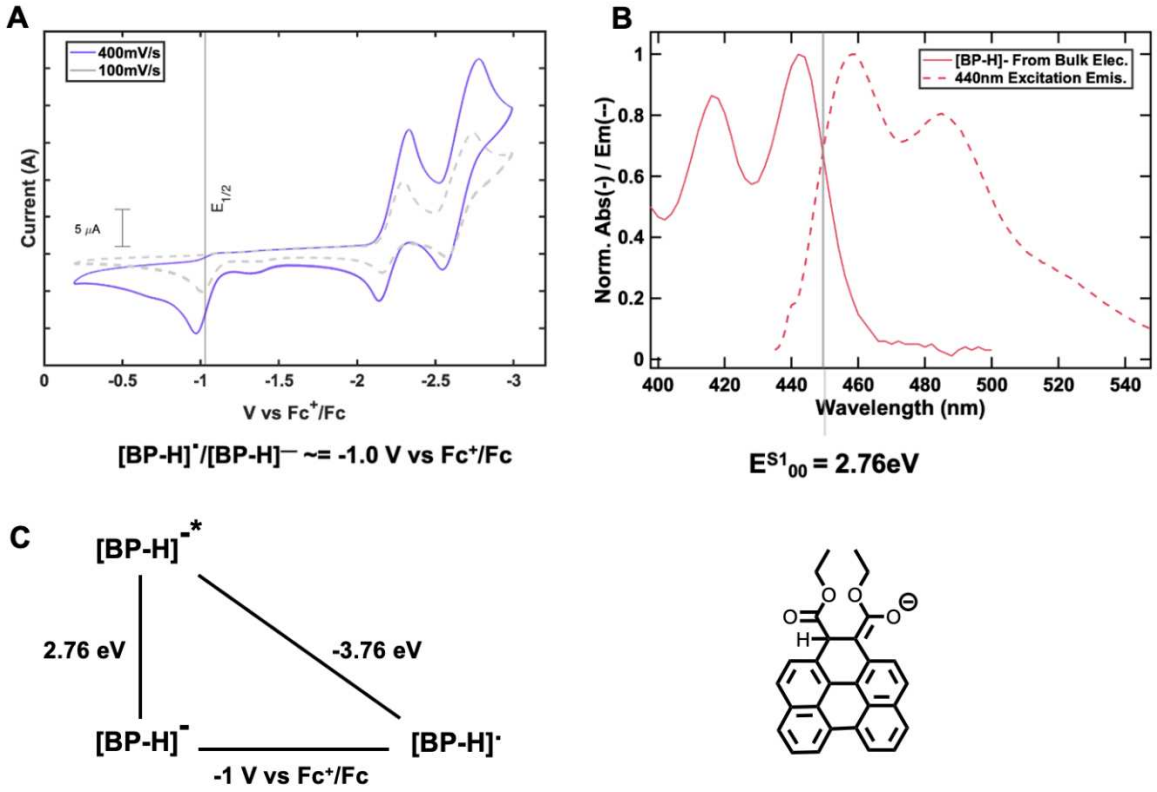

Figure S3.12. Latimer diagram describing the excited state redox potential of ***[BP-H]-*** *in THF.* ***A)*** *The oxidation potential of* ***[BP-H]-*** *to* ***[BP-H]•*** *garnered through cyclic voltammetry recorded at 400 mV/s (blue) of 1mM* ***BPDE*** *after passing the second reduction event of* ***BPDE*** *(****BPDE$^{\bullet-}$/BPDE^{2-}****) in a 0.1M TBAPF$_6$ THF solution . The oxidation of this species, which is coupled to a further loss of an electron and a proton, appears more reversible at a scan rate of 400mV/s in THF. The same experiment recorded at 100mV/s. (dashed gray line) is shown for comparison.* ***B)*** *The energy stored by the electrochemically generated* ***[BP-H]-*** *after absorption of a photon, represented as E^{S1}_{00}, estimated from the intersection of the normalized steady state absorbance and normalized emission profile (after proper Jacobian correction was applied) in THF under an inert argon atmosphere.* ***C)*** *Latimer diagram of* ***[BP-H]-*** *to calculate the excited state reduction potential using the following equation* $\boldsymbol{E^{*}_{red} = E_{red}\{[BP\text{-}H]^{\bullet} / [BP\text{-}H]^{-}\} - E^{S1}_{00}}$ *with the assumption of 1eV/V.*

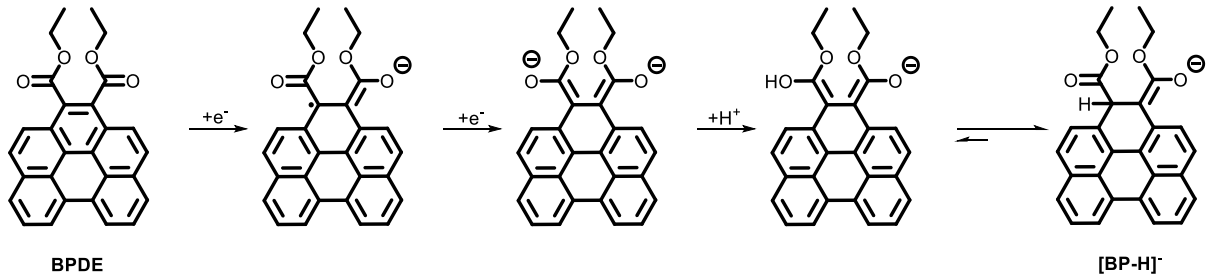

Figure S3.13. Anticipated mechanism with key resonance structures as BPDE undergoes two successive reductions followed by a protonation, to generate an enol which can then tautomerize leading to the perylene-like [BP-H]-.

Photophysical Studies

Absorption spectra comparison between BPI-P and BPI-M

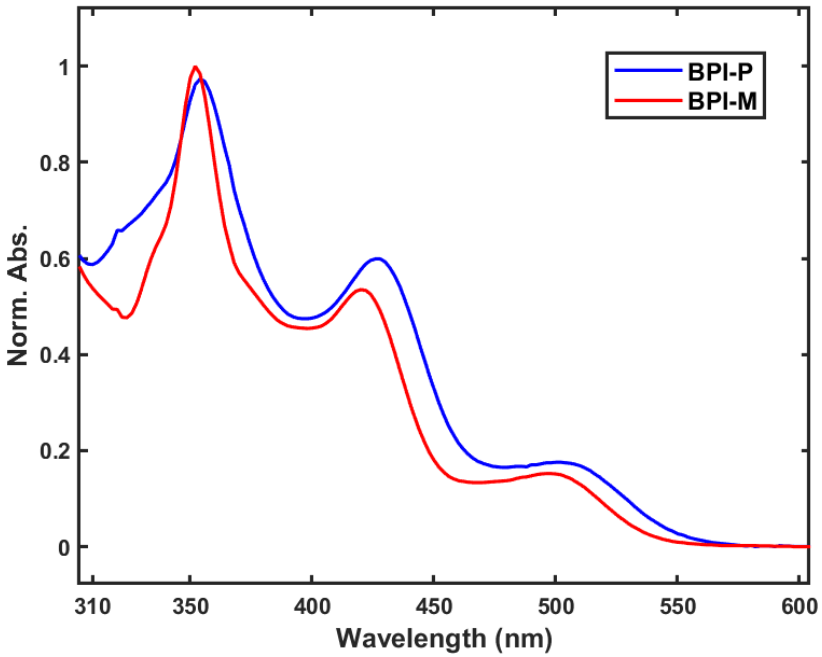

Figure S3.14. Comparing the absorption spectra of two BPI derivatives: BPI-P and BPI-M in DMAc. None of the 3 absorbance bands are significantly shifted as the core extension is changed from PhOMe (BPI-P) to $PhCH_2OH$ (BPI-M)

Tracking thermally induced changes to BPI-N upon reacting with TMAOH

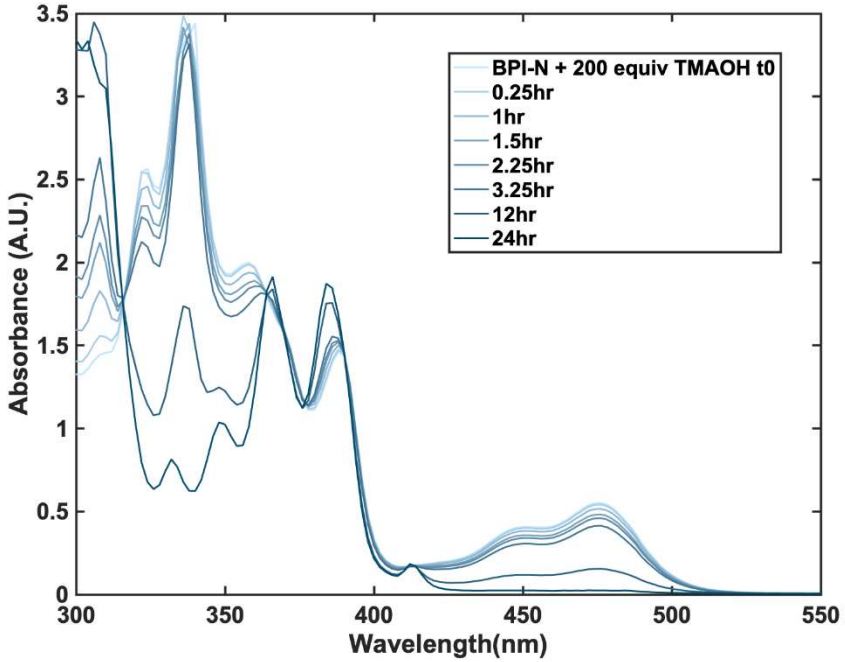

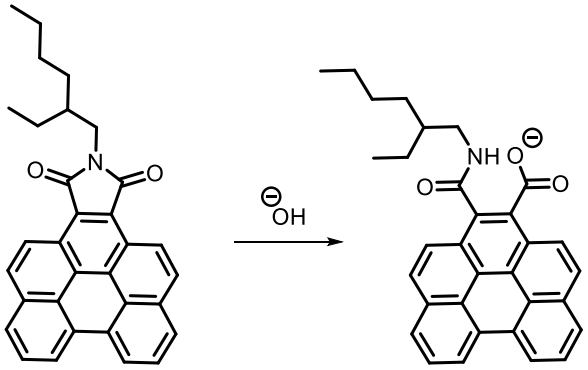

Figure S3.15. Steady state absorption spectra of 250uM BPI-N pre- and post-addition of 200 equivalents of TMAOH in 2:1 THF:MeOH mixture (by volume) excluding light in a 2mm cuvette sealed with a Kontese valve. The spectral changes were monitored as a function of time denoted in the legend. The intense absorbance feature at 338nm and the vibronic progression with lowest transition at 476nm are lost concomitant with a new feature rising at 384nm. The resulting vibronic progression after 24 hours (distorted due to the high optical density of the sample) is assigned to a ring-opened monoimide catalyst (right panel) which occurs thermally via hydroxide in solution. 200 equivalences of hydroxide were used in this experiment (which is 20x less than in the standard photo-Birch conditions) so that the spectral changes could be monitored slowly.

BPI-P radical anion characterization

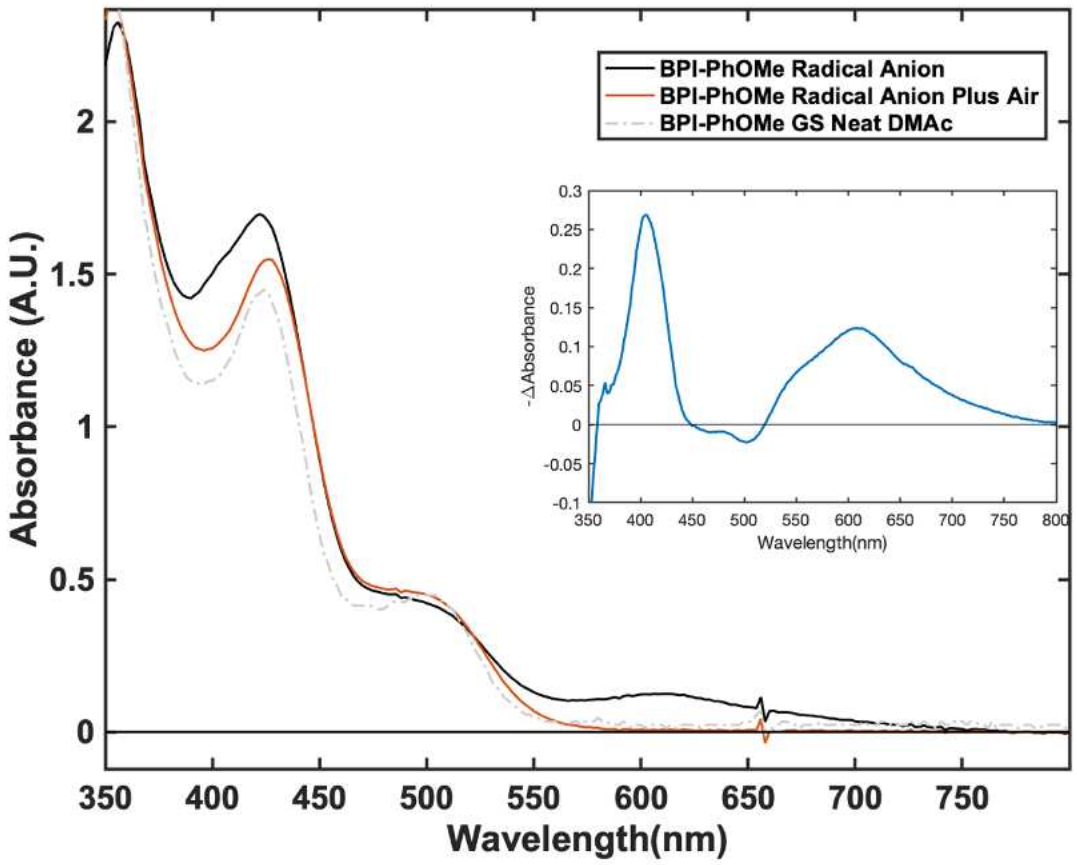

*Figure S3.16. Absorption spectra of **BPI-P** radical anion in DMAc which was generated via bulk electrolysis at –2V vs Fc^+/Fc before (black) and after air exposure (red). The ground state absorption spectrum of **BPI-P** (dashed gray) before electrolysis is also presented to demonstrate that the radical anion is quenched by oxygen to reproduce ground state **BPI-P**. Inset shows the negative delta absorption spectrum after exposure to air to highlight the absorbance profile of BPI-P radical anion as well as its sensitivity in the presence of air.*

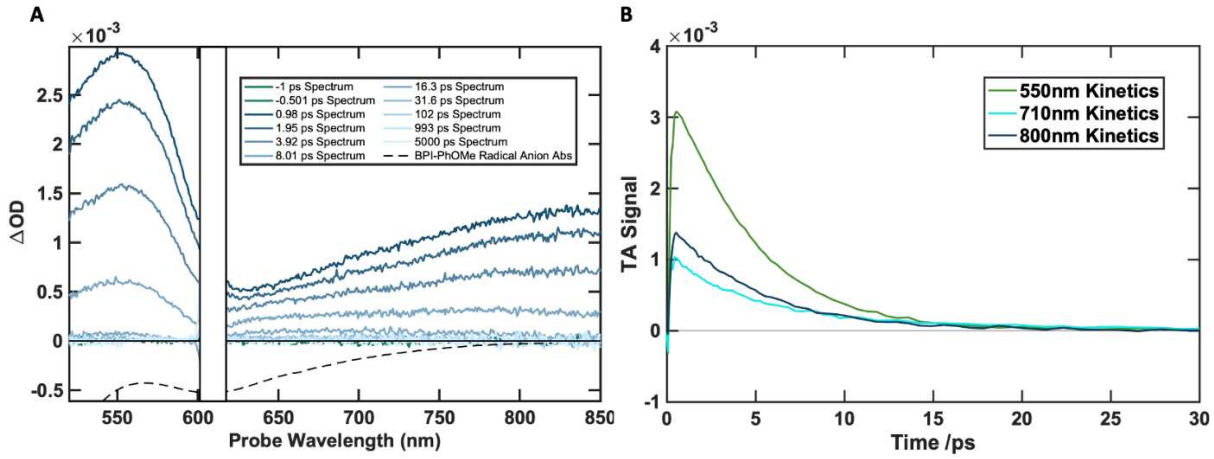

*Figure S3.17. A) Visible transient absorption spectral slices of **BPI-P** radical anion in DMAc generated via bulk electrolysis at –2V vs Fc^+/Fc in DMAc. The radical anion was excited at 630nm with an average pulse energy of 30 μJ at room temperature. The negative of the ground state absorption spectrum is shown in the figure as a dashed black line to aid in the identification of a superimposed ground state bleach overlaid on the broad excited state absorption feature. **B)** Selected single wavelength kinetics from the transient absorption experiment shown in panel A.*

Photophysics of BPDE and photochemically generated [BP-H]$^-$

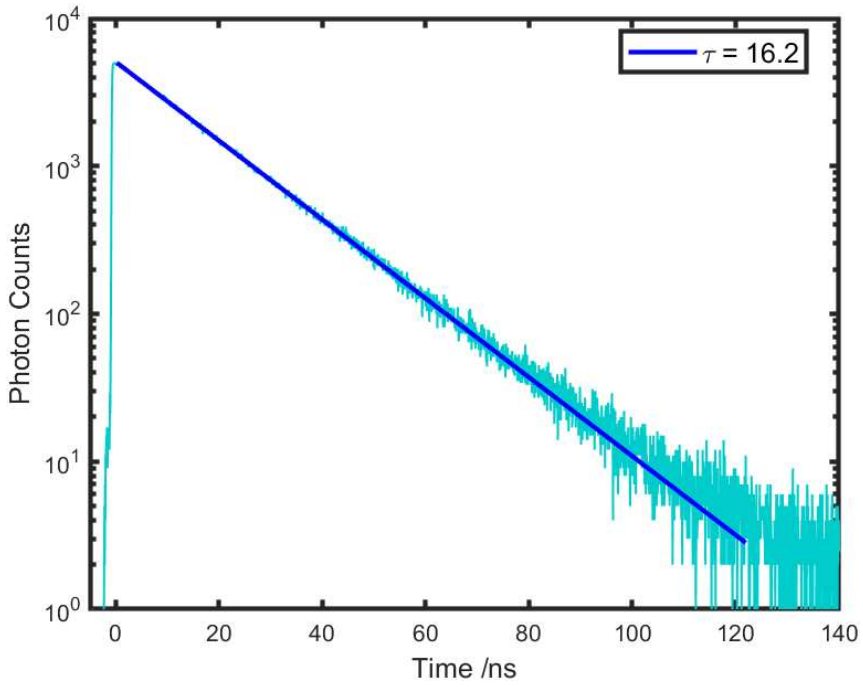

*Figure S3.18. Plot of fluorescence decay for **BPDE** in THF as measured by TCSPC following excitation at 405 nm. Monoexponential fit leads to a lifetime of 16.2 ns.*

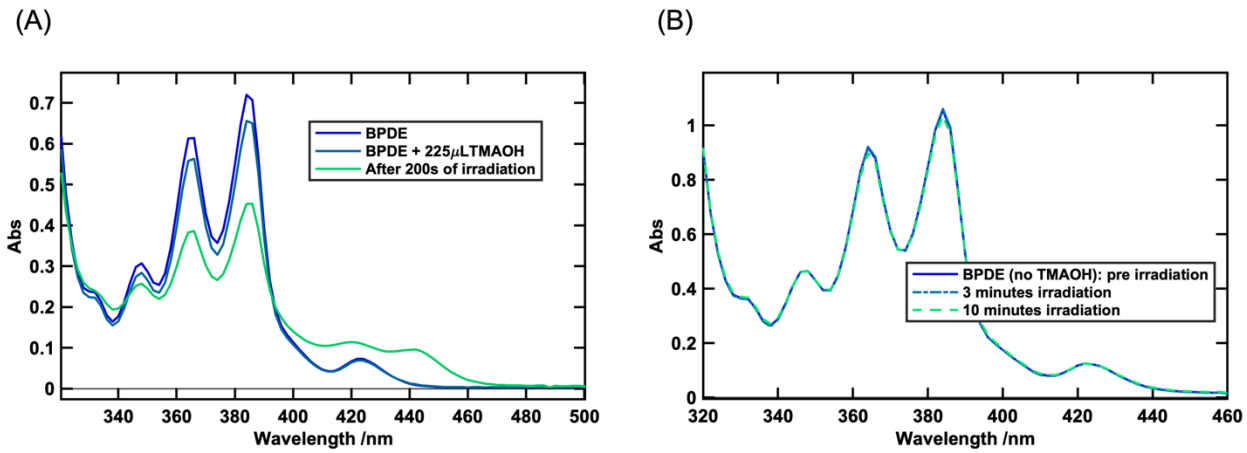

Figure S3.19. (A) Comparing the UV-Vis spectra of BPDE before and after addition of TMAOH and after irradiation with 385nm LEDs. No detectable changes, other than the effect of dilution, can be detected upon addition of 225 μL TMAOH in the 2:1 THF:MeOH solvent system suggesting no dark reactivity between BPDE and TMAOH. However, after 200s of irradiation, a clear decrease in the absorption of BPDE can be seen in the absorption spectrum along with growth of two new peaks. As described in the text, this is indication that [BP-H]$^-$ is being generated from BPDE with TMAOH and light. (B) A control experiment where BPDE was irradiated without TMAOH for up to 10 minutes. No changes were detected which proves that TMAOH is necessary for the generation of [BP-H]$^-$

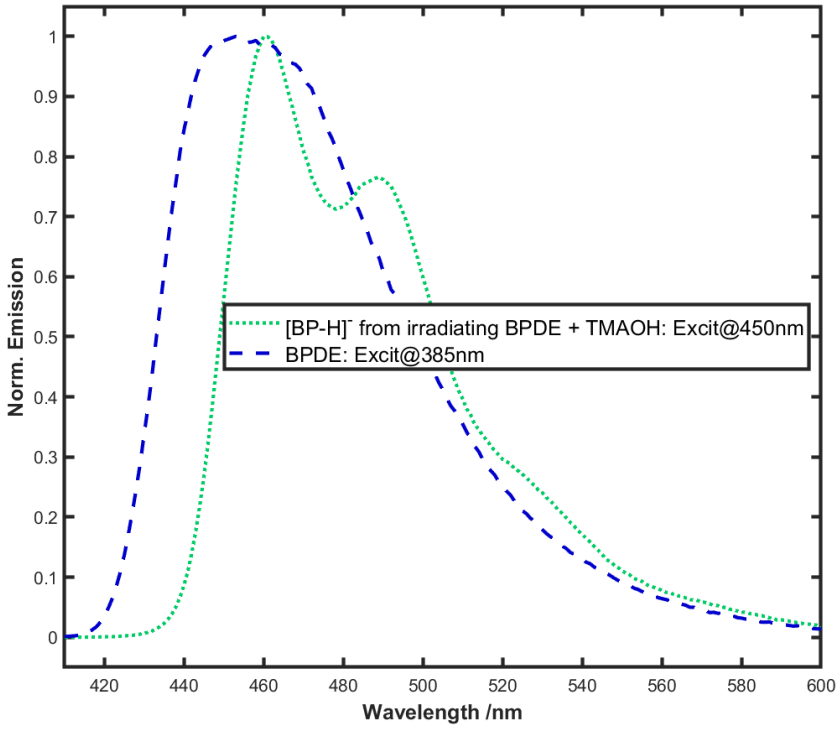

Figure S3.20. Comparing the normalized emission spectrum of BPDE to that of photochemically generated [BP-H]$^-$ (200s of irradiation in presence of 180 mM TMAOH) in 2:1 THF:MeOH solvent system. The [BP-H]$^-$ emission spectrum was obtained by selectively exciting the reaction mixture at 450 nm where BPDE absorbance is negligible (Figure S19).

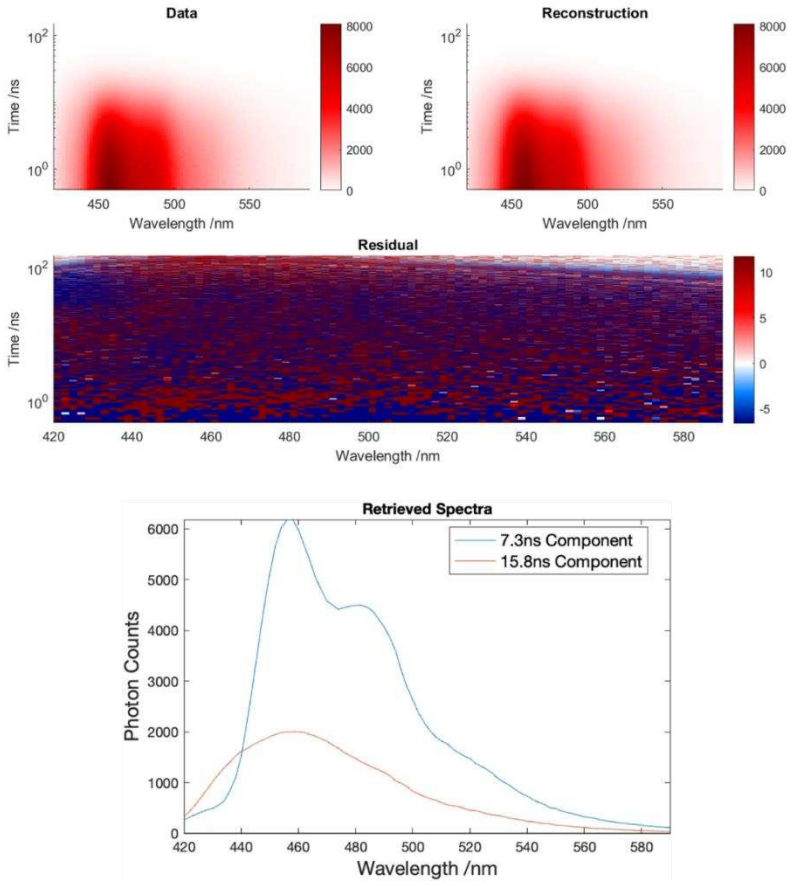

Figure S3.21. Time-resolved emission spectroscopy (TRES) on the irradiated BPDE + TMAOH solution (after 200s of irradiation). Excitation wavelength = 405 nm. The data are well-modeled using a bi-exponential function. The 15.8 ns fitted spectrum strongly resembles the steady state emission profile of BPDE while 7.3 ns matches the fluorescence spectrum of the new [BP-H]$^-$ species (Fig S20).

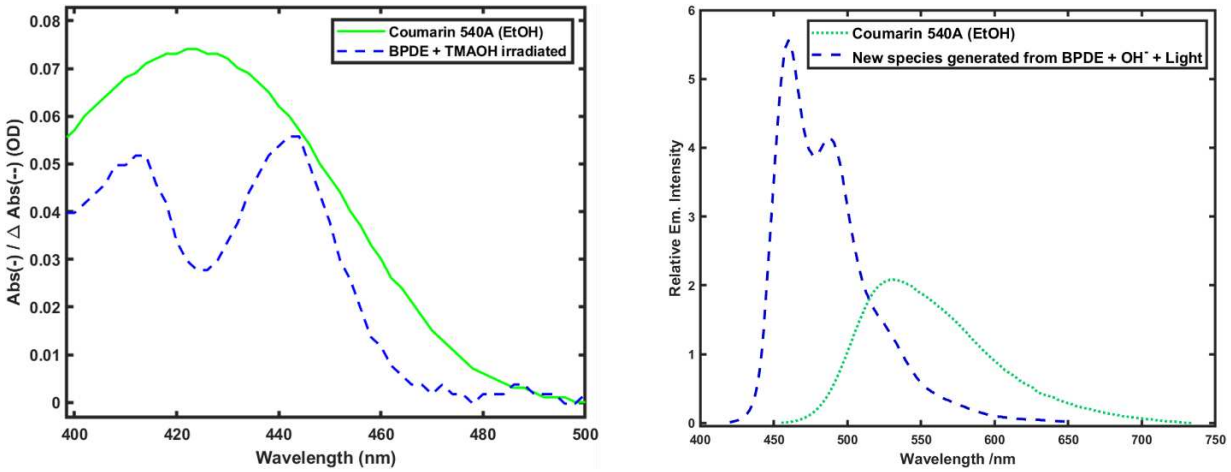

Figure S3.22. Data collected for emission quantum yield determination of the new [BP-H]⁻ species (which was generated by irradiating BPDE + TMAOH in a 2:1 THF: MeOH solvent system). Reference dye = Coumarin 540A (in ethanol) ($\Phi_{em}^{ref} = 0.544$). Excitation wavelength for both samples = 450 nm. The refractive index of the mixed THF:MeOH solvent system is calculated as the weighted average of refractive indices of THF and MeOH. Calculated $\Phi_{em} = 0.94$.

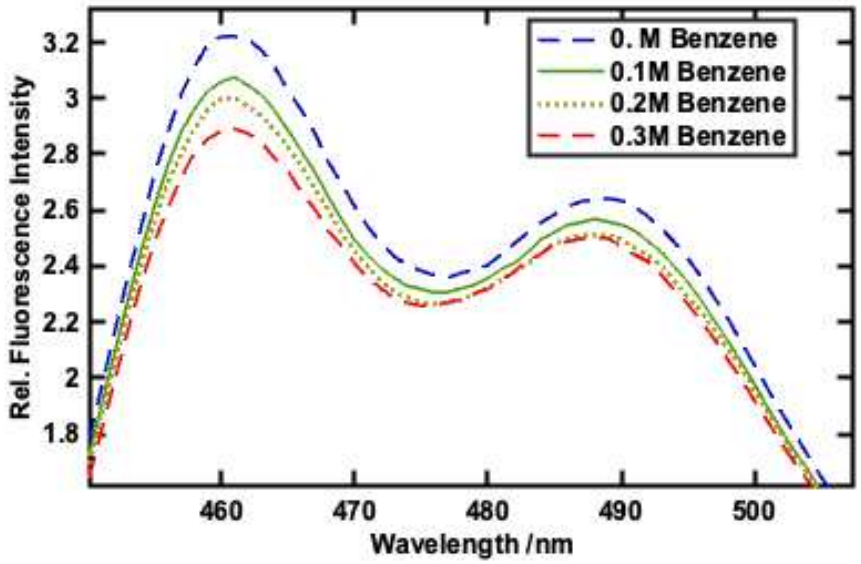

Figure S3.23. Steady-state fluorescence quenching of [BP-H]$^-$ in the presence of benzene as the quencher. 35 µM BPDE was irradiated for 200s with two 385nm LEDs in the presence of 180 mM TMAOH in a 2:1 THF:MeOH solvent mixture to generate the [BP-H]$^-$ species. The reference [BP-H]$^-$ fluorescence spectrum was obtained by selectively exciting the sample at 450 nm. 22 µL of benzene was then added to the cuvette (containing 2.5 mL solution) to achieve a concentration of 0.1M for benzene and another emission spectrum was collected. This was repeated two more times.

Photophysics of electrochemically generated [BP-H]$^-$

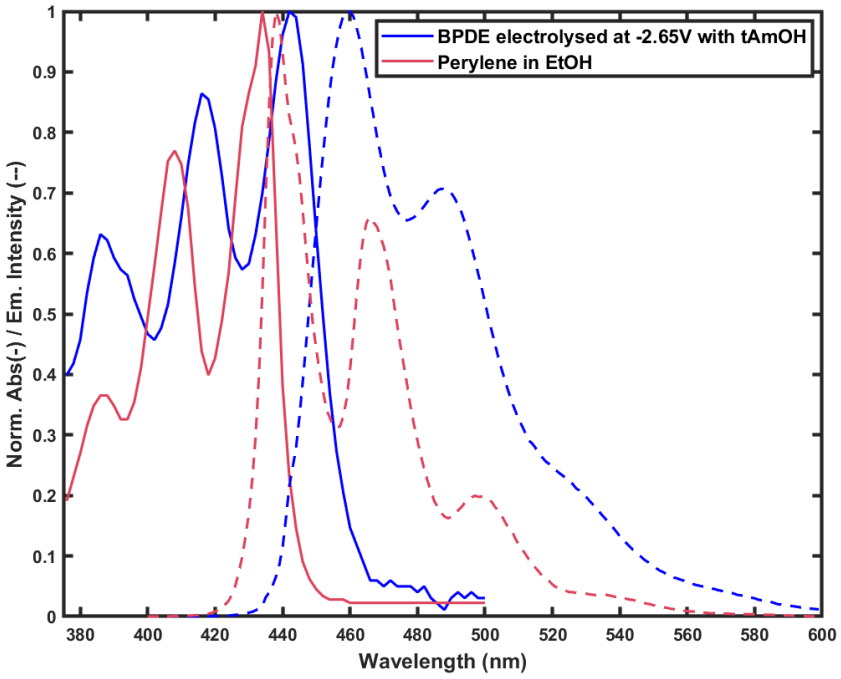

Figure S3.24. Comparing the absorption and emission spectra of electrochemically generated [BP-H]$^-$ (bulk electrolysis at -2.65 V vs Ag/AgNO$_3$ in the presence of tAmOH) with that of pure perylene (in ethanol). The sample does contain a small amount of BPDE as is evident by the shape of the peak at 385nm where BPDE absorbs most strongly.

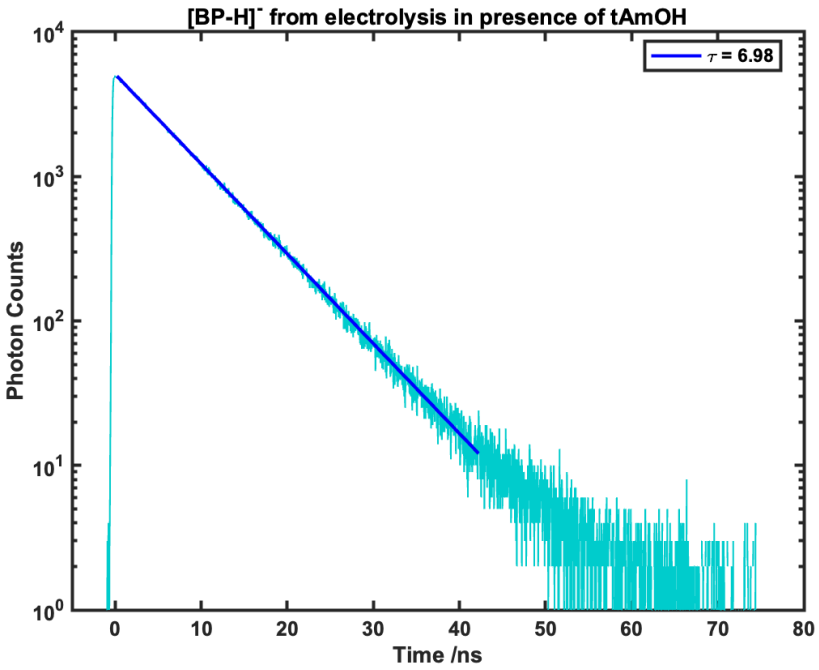

Figure S3.25. Plot of fluorescence decay of electrochemically generated [BP-H]⁻ in THF photoexcited at 405 nm. The detected emission wavelength = 460 nm. A monoexponential fit indicates in a lifetime of 6.98 ns.

Transient Absorption Studies

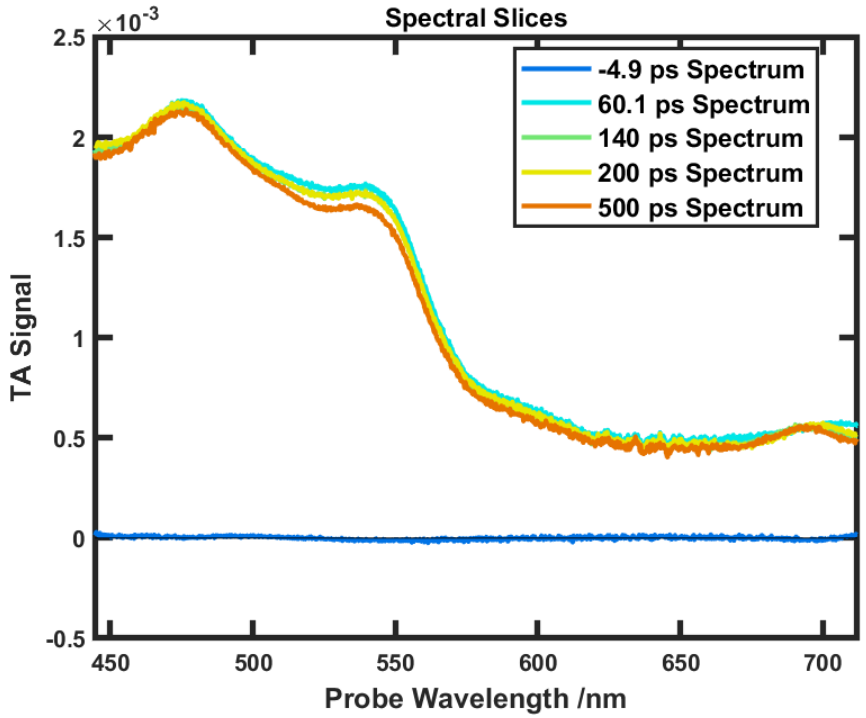

Figure S3.26. Picosecond transient absorption spectra for BPDE in THF. The S_1 lifetime of BPDE as determined from TCSPC is 16.2 ns which is why the signal has not decayed noticeably in 500 ps.

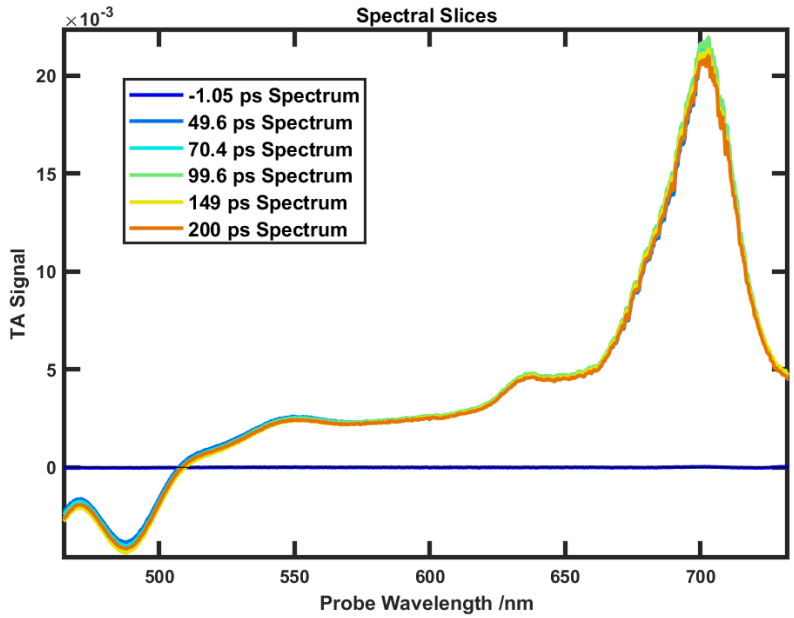

Figure S3.27. Picosecond transient absorption spectra for electrochemically generated [BP-H]$^-$ in THF (the sample does contain trace amount of MeOH which was used to quench BPDE^{2-}; however, its effect is presumably negligible). The S_1 lifetime as determined from TCSPC is ~7 ns which is why the signal has not decayed noticeably in 200 ps.

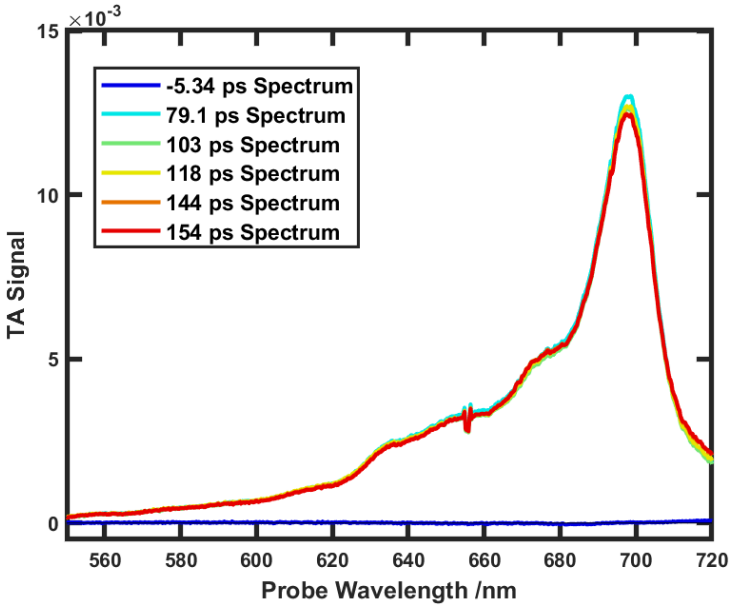

Figure S3.28. Picosecond transient absorption spectra for perylene in ethanol. Since only the excited state absorption ($S_1 \rightarrow S_n$) profile was needed for comparison with that of [BP-H]$^-$, just the early time spectral slices were collected.

Testing the sensitivity of $[BP\text{-}H]^-$ towards oxygen

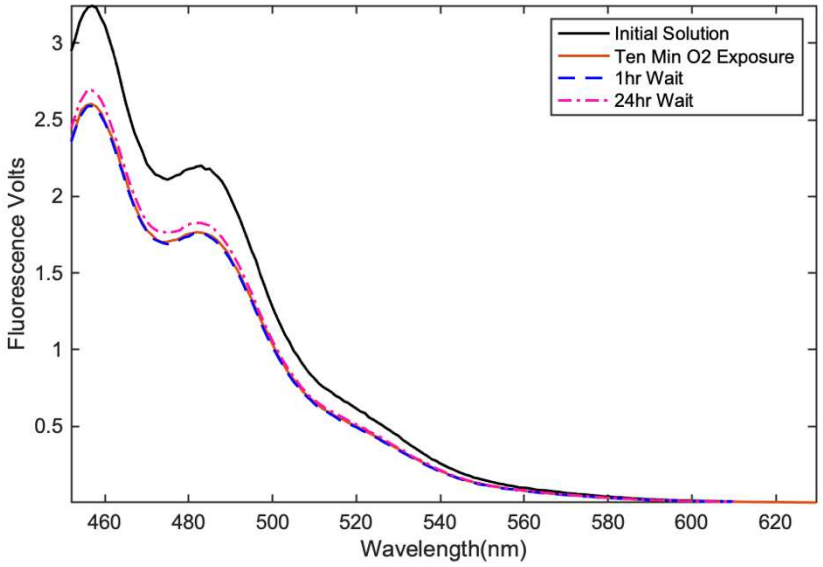

Figure S3.29. Fluorescence spectrum of the electrochemically generated $[BP\text{-}H]^-$, in THF before and after O_2 Exposure. The initial solution was prepared within an Argon filled glovebox with O_2 <1ppm, transferred to a 1cm cuvette sealed with a Kontes valve. The sample was then pumped out and the fluorescence spectrum was collected by exciting with 450nm light to target $[BP\text{-}H]^-$ fluorescence exclusively. After the initial fluorescence spectrum was collected, the solution was poured out from the 1cm cuvette into a scintillation vial wrapped in aluminum foil and stirred vigorously open to the atmosphere for 10 minutes. The solution was then transferred back to the 1cm cuvette, sealed with a Kontes valve and a fluorescence spectrum was immediately collected. Further spectra were collected at 1 and 24hr time intervals after the ten-minute air exposure.

Fluorescence Quenching Using Electrochemically Generated $[BP\text{-}H]^-$

Sample preparation: **BPDE** was electrolyzed at -2.85 V (vs Fc^+/Fc) in THF with $TBAPF_6$ as the supporting electrolyte (0.1M) in presence of tAmOH/MeOH to generate **[BP-H]**$^-$; typically, 15-30 µL of this electrolyzed solution was then diluted with 2.5 mL of 2:1 THF/MeOH solvent mixture inside an Ar-filled glovebox to prepare a sample which was then transferred into a cuvette sealed with a Kontes valve to keep it air-free for the duration of the experiment. The purpose of only using a small amount of **[BP-H]**$^-$ was to keep the absorbance <0.1 to avoid the effect of self-absorption. A steady-state fluorescence spectrum was collected by exciting the sample at 445 nm with an integration time of 0.2 seconds. This served as the reference spectrum (F_0) for the calculation of Stern-Volmer quenching rates. The cuvette was then again pumped into the glovebox where an appropriate amount of quencher was added to the sample to achieve the first quencher concentration mentioned in the figure legends. A second fluorescence spectrum was then collected by exciting the sample at the same wavelength (i.e. 445 nm). This process was repeated two more times at which point the fluorescence spectra for three different concentrations of the quencher had been collected in total. The Stern-Volmer (K_{SV}) rate constant was calculated using the following equation:

$$\frac{F_0}{F} = 1 + K_{SV}[Q]$$

Equation S3.1

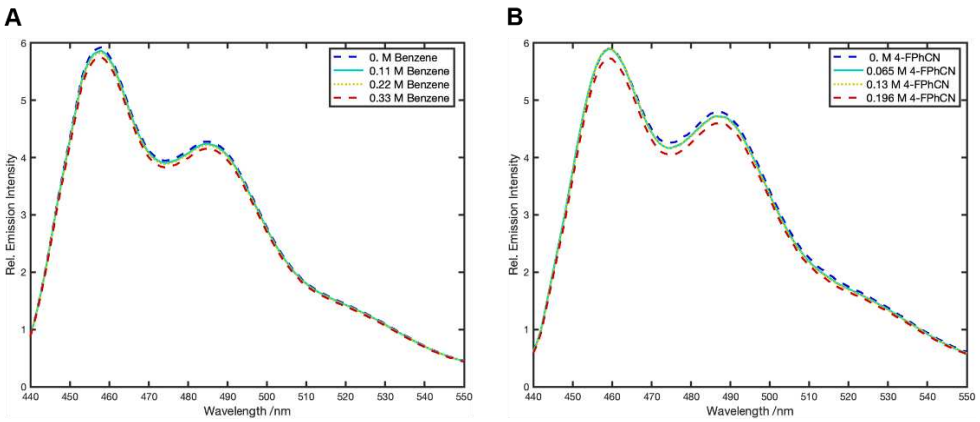

Figure S3.30. Attempted fluorescence quenching with electrochemically generated [BP-H]⁻ without presence of TMAOH. As evident from the unchanged fluorescence intensity, there is very little quenching due to either (A) benzene or (B) 4-fluorobenzonitrile.

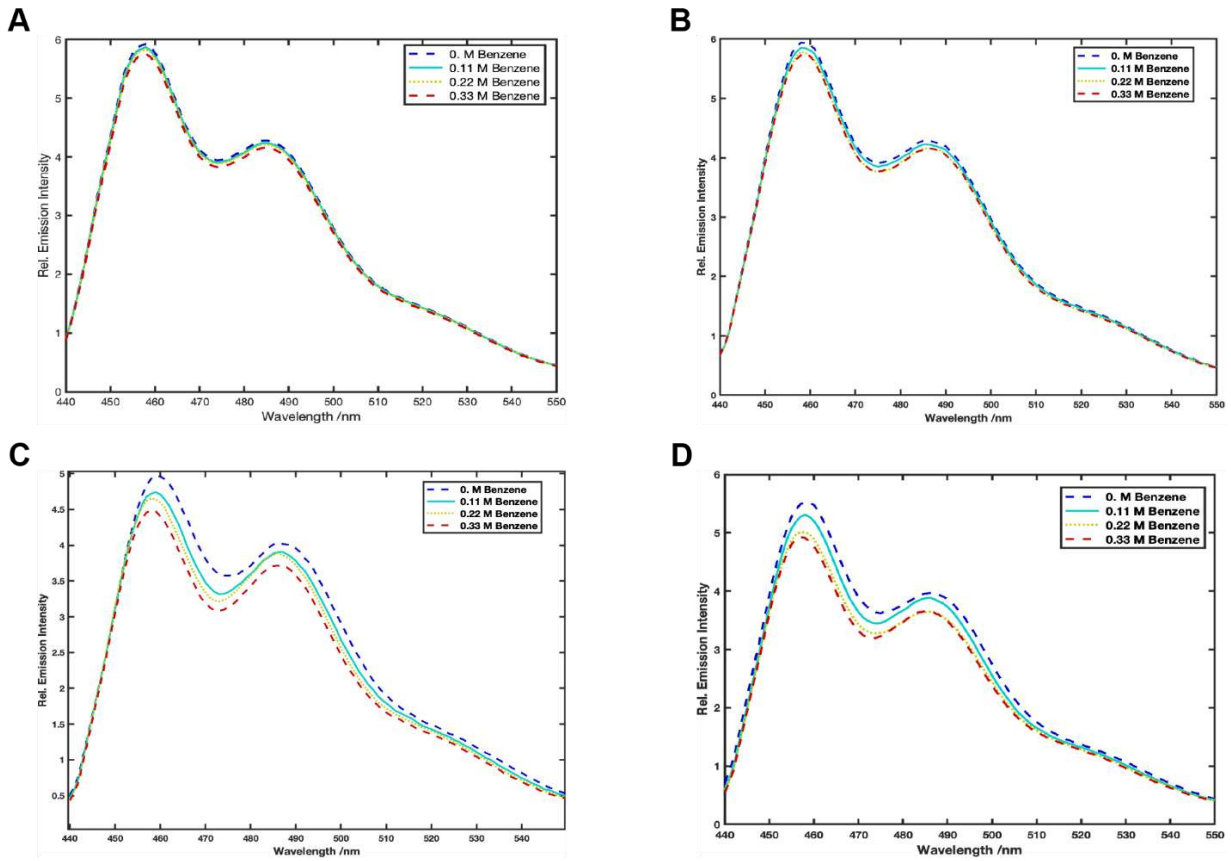

Figure S3.31a. Steady-state emission spectra: Effect of hydroxide concentration on fluorescence quenching with benzene as the quencher. The following amounts of TMAOH (25 wt% in MeOH) were added to the electrolyzed [BP-H]⁻ while preparing the sample. (A) no TMAOH. (B) 50 µL; [TMAOH] = 45 mM. (C) 200 µL; [TMAOH] = 185 mM. (D) 350 µL; [TMAOH] = 320 mM. The amount of THF was kept constant for all the samples while the volume of MeOH was adjusted so that together with the MeOH added with TMAOH, the THF to MeOH ratio remains 2:1.

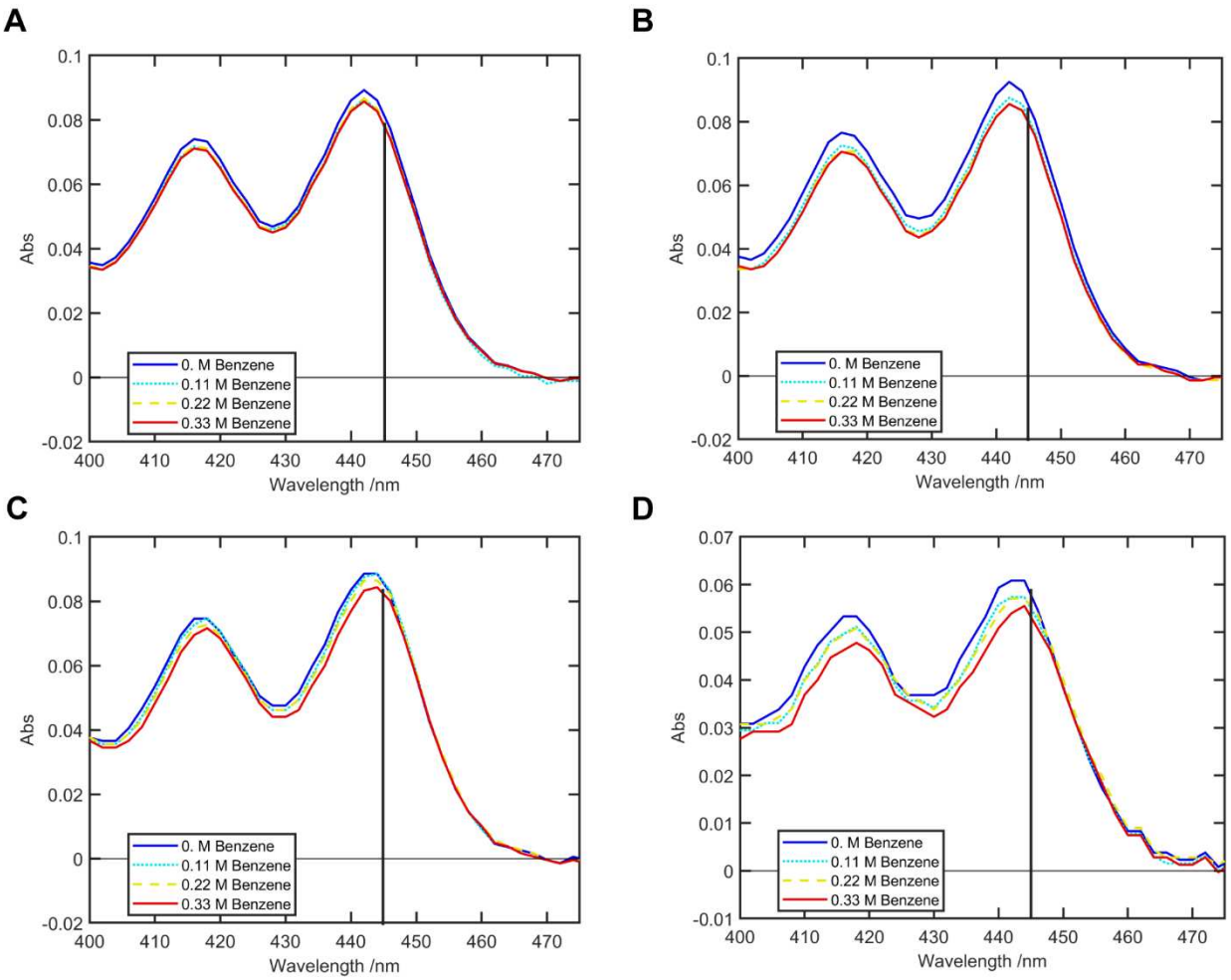

Figure S3.31b. Absorption spectra: UV-Visible spectra of the samples used for the fluorescence quenching experiments shown above in Fig. S31a. Only the 400-475 nm region is shown to highlight the [BP-H]$^-$ absorbance. The black vertical line indicates the excitation wavelength of 445 nm (the bandwidth of excitation monochromator was set to 1 nm). As can be seen in all four panels, the OD at 445 nm is only perturbed by a quite small amount even after introduction of varying amounts of benzene. (A) no TMAOH. (B) 50 µL; [TMAOH] = 45 mM. (C) 200 µL; [TMAOH] = 185 mM. (D) 350 µL; [TMAOH] = 320 mM.

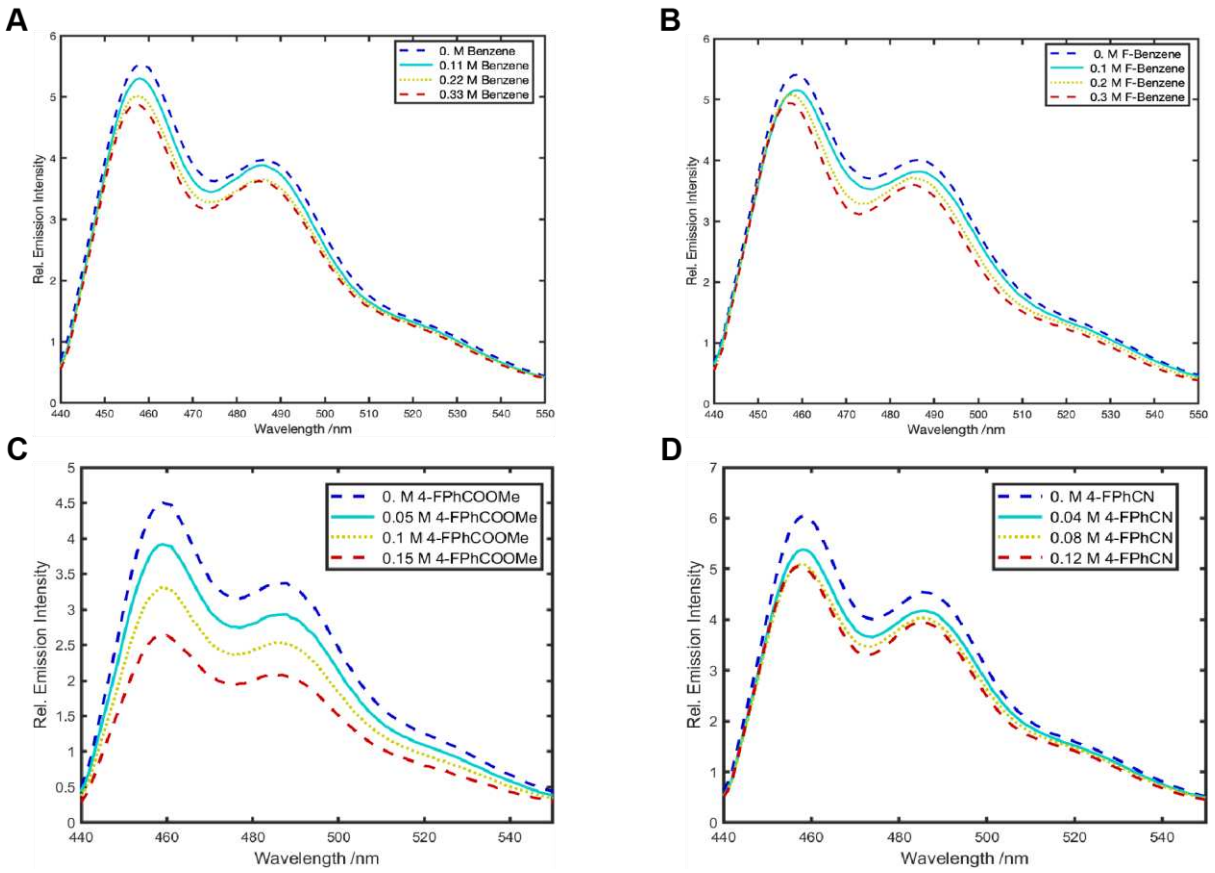

Figure S3.32a. Steady-state emission spectra: Fluorescence quenching with 4 different substrates (A) benzene, (B) fluorobenzene, (C) methyl 4-fluorobenzoate, (D) 4-fluorobenzonitrile. 300 µL of TMAOH (25 wt% in MeOH) were added to the electrolyzed [BP-H]⁻ (diluted with 2.5 mL 2:1 THF:MeOH) while preparing the samples for each of the quenchers. Since benzene, fluorobenzene and methyl-4-fluorobenzoate are all liquid, they were added directly in increments of 25, 25 and 17 µL respectively whereas a stock solution (400 mg/mL) in THF was prepared for 4-fluorobenzonitrile and was added to the cuvette in increments of 30 µL.

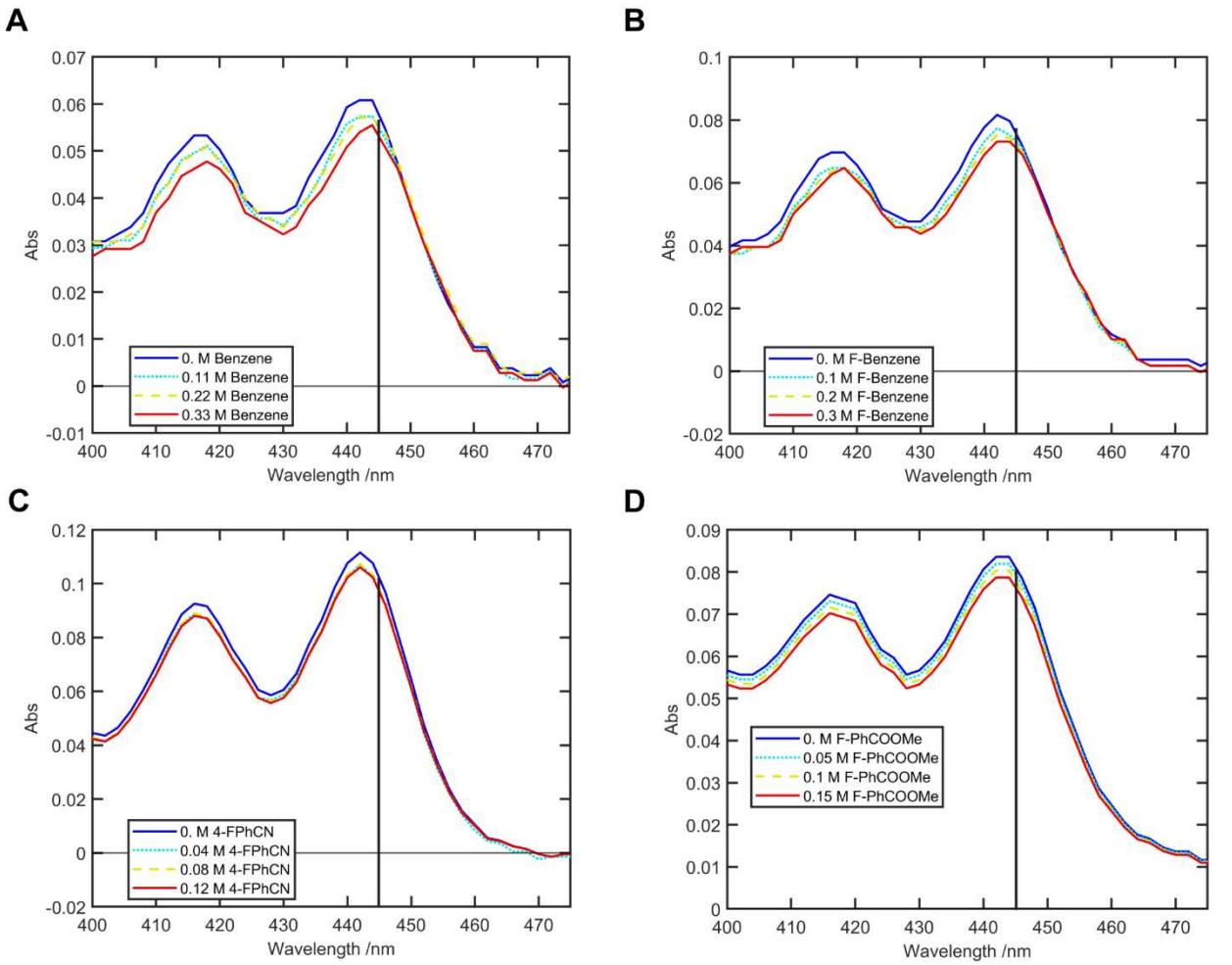

Figure S3.32b. Absorption spectra: UV-Visible spectra of the samples used for the fluorescence quenching experiments shown above in Fig. S32a. Only the 400-475 nm region is shown to highlight the [BP-H]$^-$ absorbance. The black vertical line indicates the excitation wavelength of 445 nm (the bandwidth of excitation monochromator was set to 1 nm). As can be seen in all four panels, the OD at 445 nm is only perturbed by a quite small amount even after introduction of varying amounts of substrates. (A) benzene, (B) fluorobenzene, (C) methyl 4-fluorobenzoate, (D) 4-fluorobenzonitrile.

Attempted quenching with TMACl

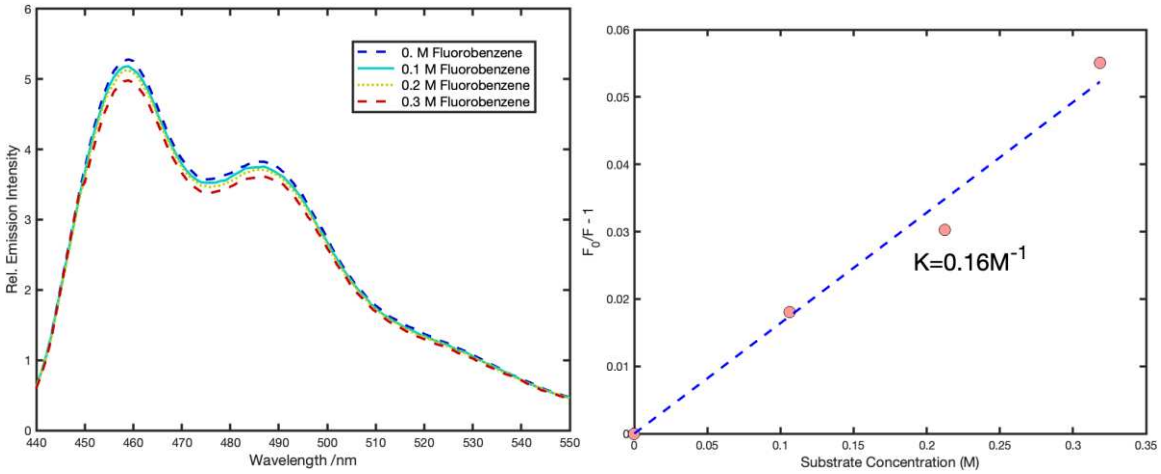

Figure S3.33. In order to investigate whether the tetramethylammonium (TMA^+) cation was playing a role in the quenching process, the static photoluminescence quenching experiment was repeated in the presence of 280 mM TMACl (no OH^- in this case) with fluorobenzene as the quencher. Notably, K_{sv} is significantly lower in this case than what was previously obtained (K_{sv} = 0.52 M^{-1}) from our experiment in the presence of 300 mM TMAOH.

Investigating the nature of fluorescence quenching

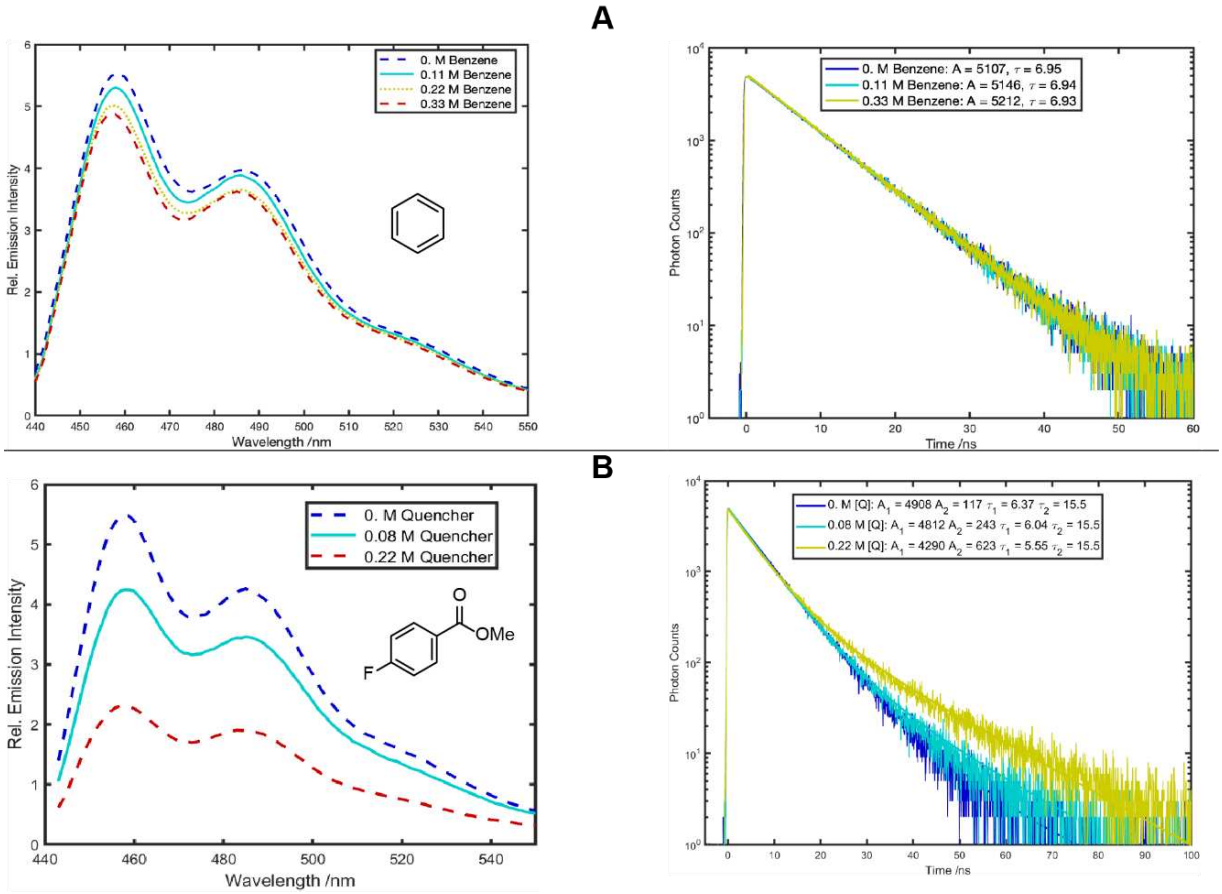

Figure S3.34. Tracking fluorescence lifetime (by TCSPC) of [BP-H]$^-$ along with its steady-state photoluminescence quenching with addition of (A) benzene and (B) methyl 4-fluorobenzoate. Both the experiments were done in the presence of 300 µL of TMAOH (25 wt% in MeOH) using electrochemically generated [BP-H]$^-$ (diluted with 2.5 mL 2:1 THF:MeOH). For the TCSPC experiment, the excitation wavelength is 405 nm. (A) With benzene the fluorescence decay traces are practically co-incident indicating no change in the lifetime. (B) Even with dramatically diminished fluorescence intensity with methyl 4-fluorobenzoate as the quencher, the photoluminescence lifetime of [BP-H]$^-$ species (τ_1) is only slightly decreased. τ_2 refers to the fluorescence lifetime of leftover BPDE species and this component gains more intensity as [BP-H]$^-$ fluorescence is quenched.

Attempted isolation of photochemically generated [BP-H]$^-$

To a scintillation vial, diethyl benzo[ghi]perylene-1,2-dicarboxylate (**BPDE)** (200 mg, 0.4 mmol, 1 eq), and tetramethylammonium hydroxide (TMAOH) (25 % by weight in MeOH, 350 uL, 3.2 mmol, 8 eq) were added and the mixture was irradiated for 30 minutes using a dual photoreactor (405 nm) under N_2. Progress was monitored by TLC. After the 30 minutes, volatiles were removed using a rotary evaporator and the resulting residue was run through a silica column using hexanes: ethyl acetate gradient. However, the **[BP-H]$^-$** fractions, when concentrated, were found to partially revert to **BPDE** as can be seen below in Fig. S35.

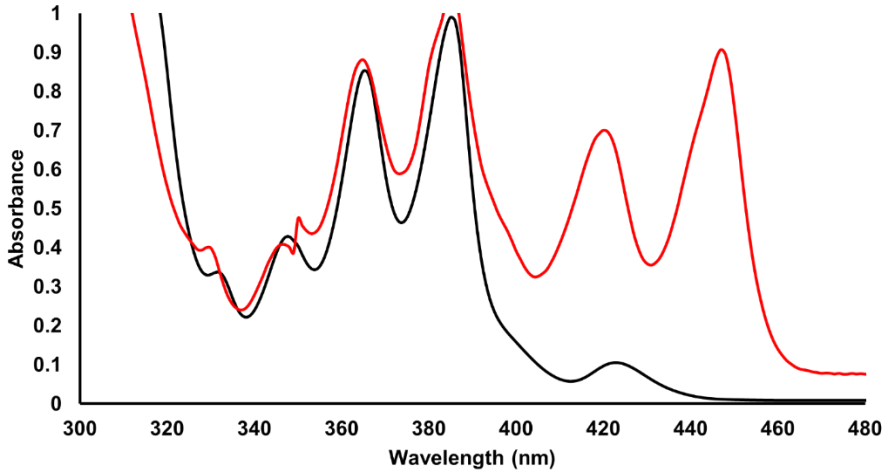

Figure S3.35. Comparing absorption spectra of BPDE (black trace) with the absorption of the isolated photochemically generated [BP-H]$^-$ (red trace). While the perylene-like vibronic progression with characteristic peaks at 420 and 445 nm confirms the presence of [BP-H]$^-$, the evident BPDE vibronic peaks in 340-390 nm region indicate that this is a mixture of BPDE and [BP-H]$^-$. This is indication that [BP-H]$^-$ tends to revert to BPDE when kept in high concentration, making NMR characterization of [BP-H]$^-$ unsuccessful.

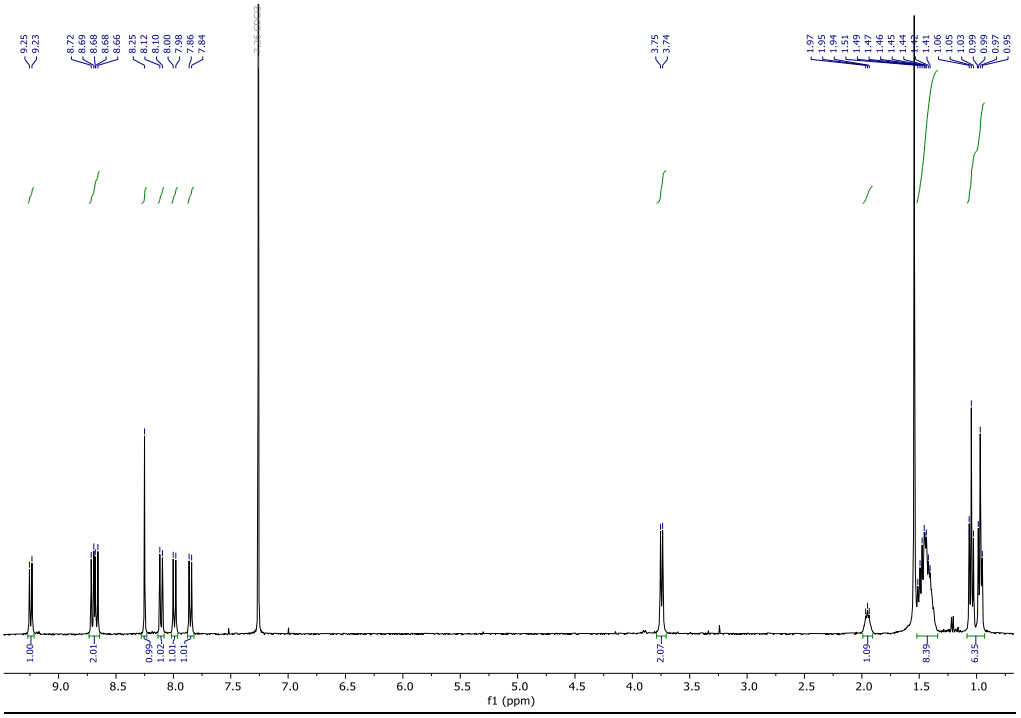

Figure S3.36. ^{1}H NMR of BPI-Br ($CDCl_3$, 400 MHz).

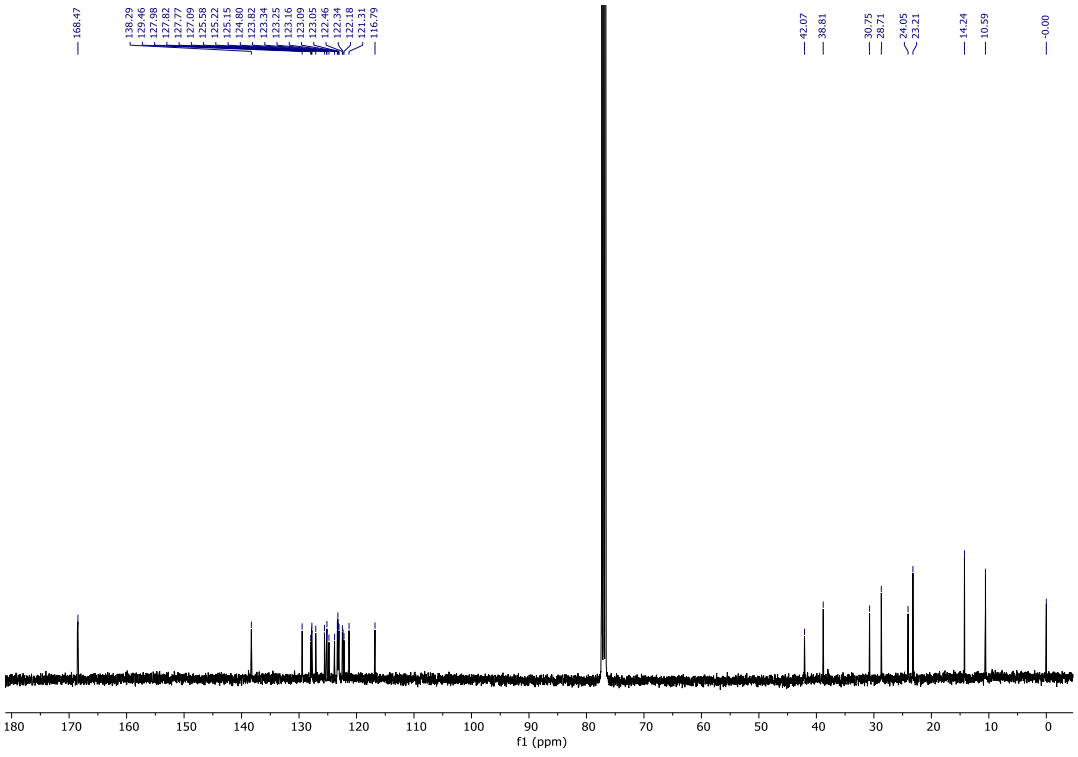

Figure S3.37. ^{13}C NMR of BPI-Br (CDCl3, 100 MHz).

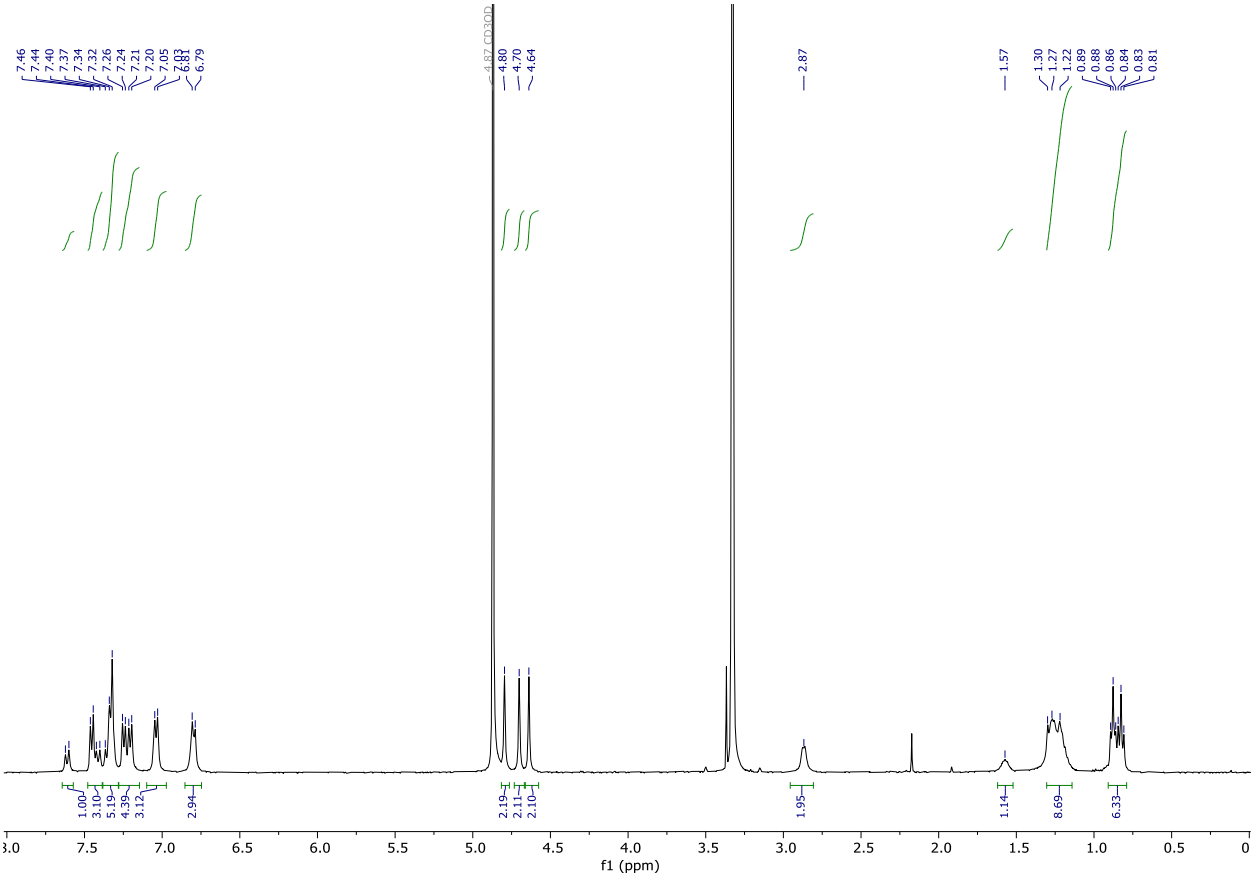

Figure S3.38. ^{1}H NMR of BPI-M (MeOD, 400 MHz).

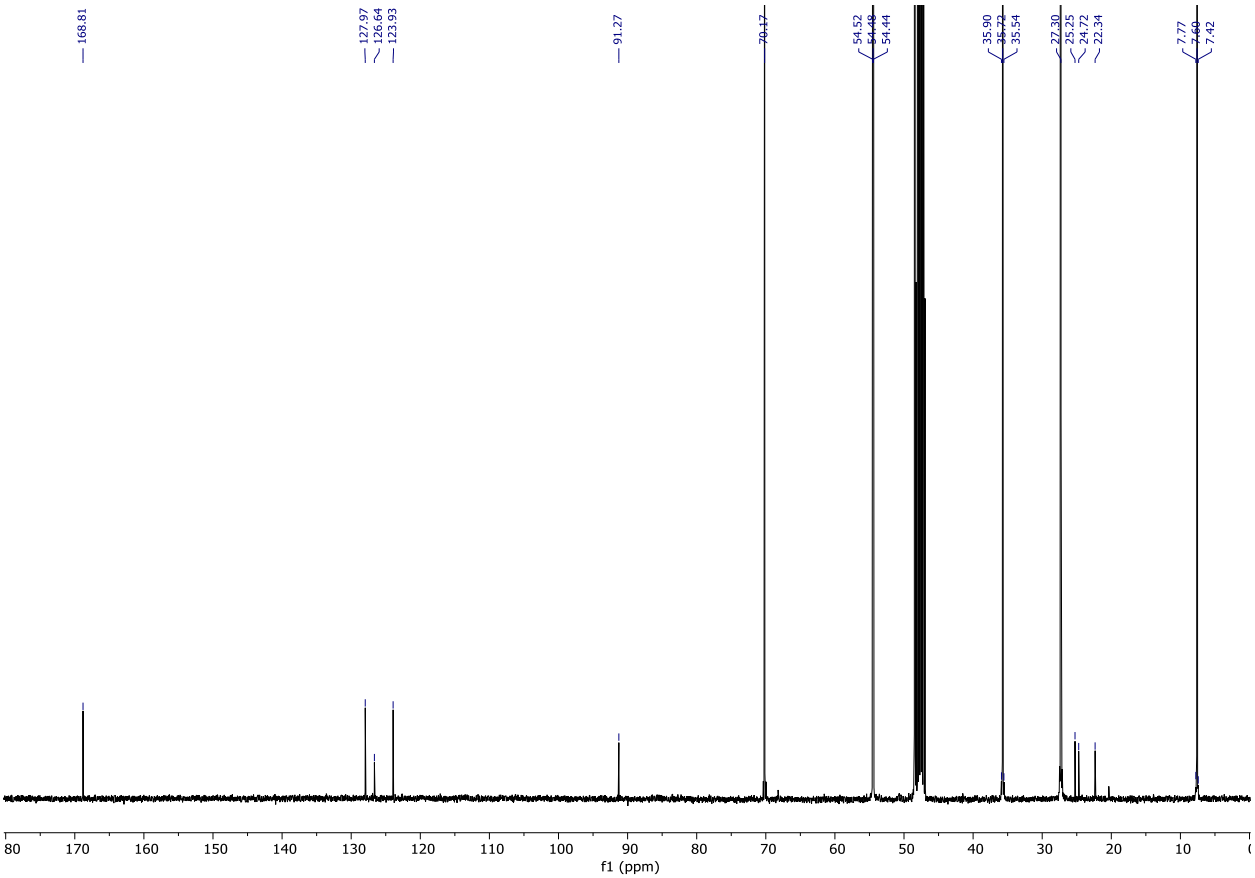

Figure S3.39. ^{13}C NMR of BPI-M (MeOD, 100 MHz).

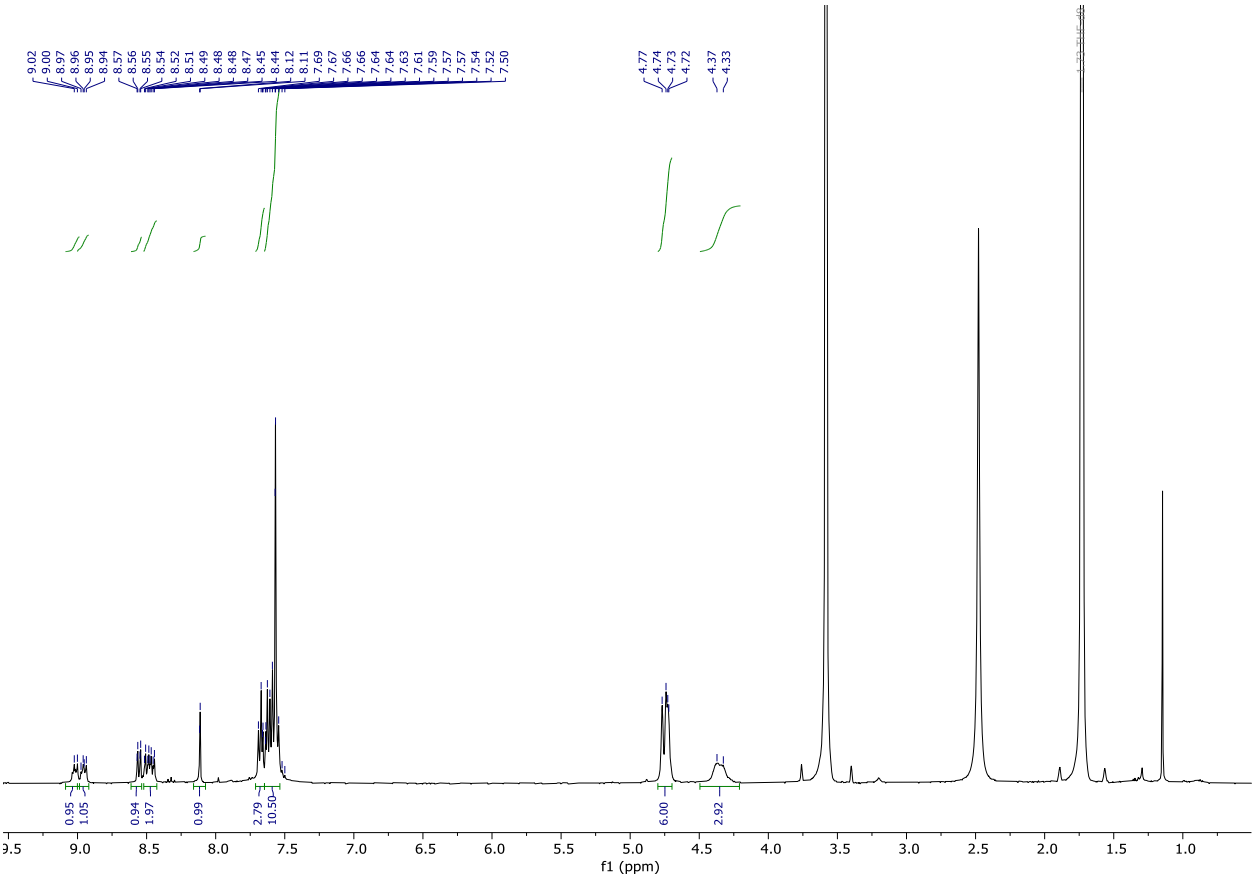

Figure S3.40. ^{1}H NMR of BPA-M (THF-d8, 400 MHz).

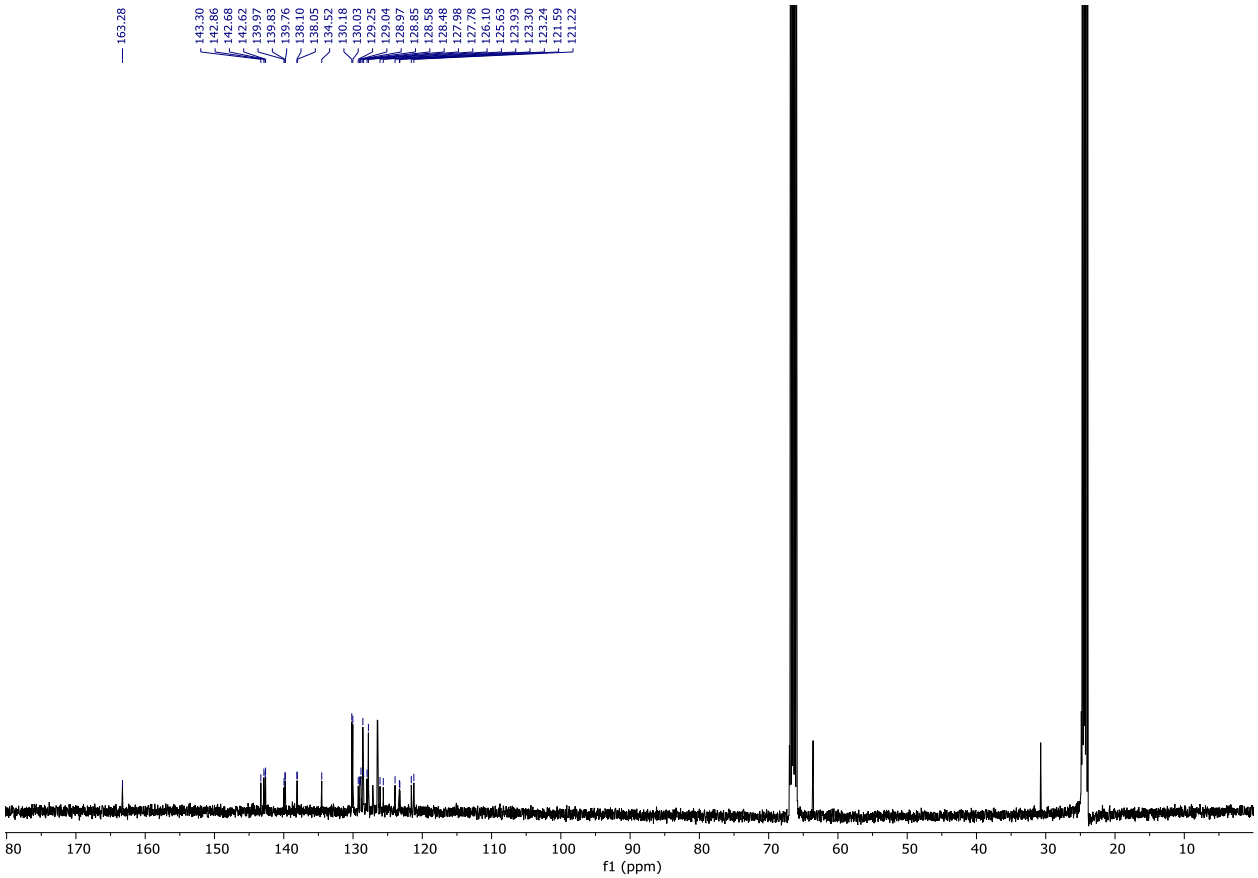

Figure S3.41. ^{13}C NMR of BPA-M (THF-d8, 100 MHz).

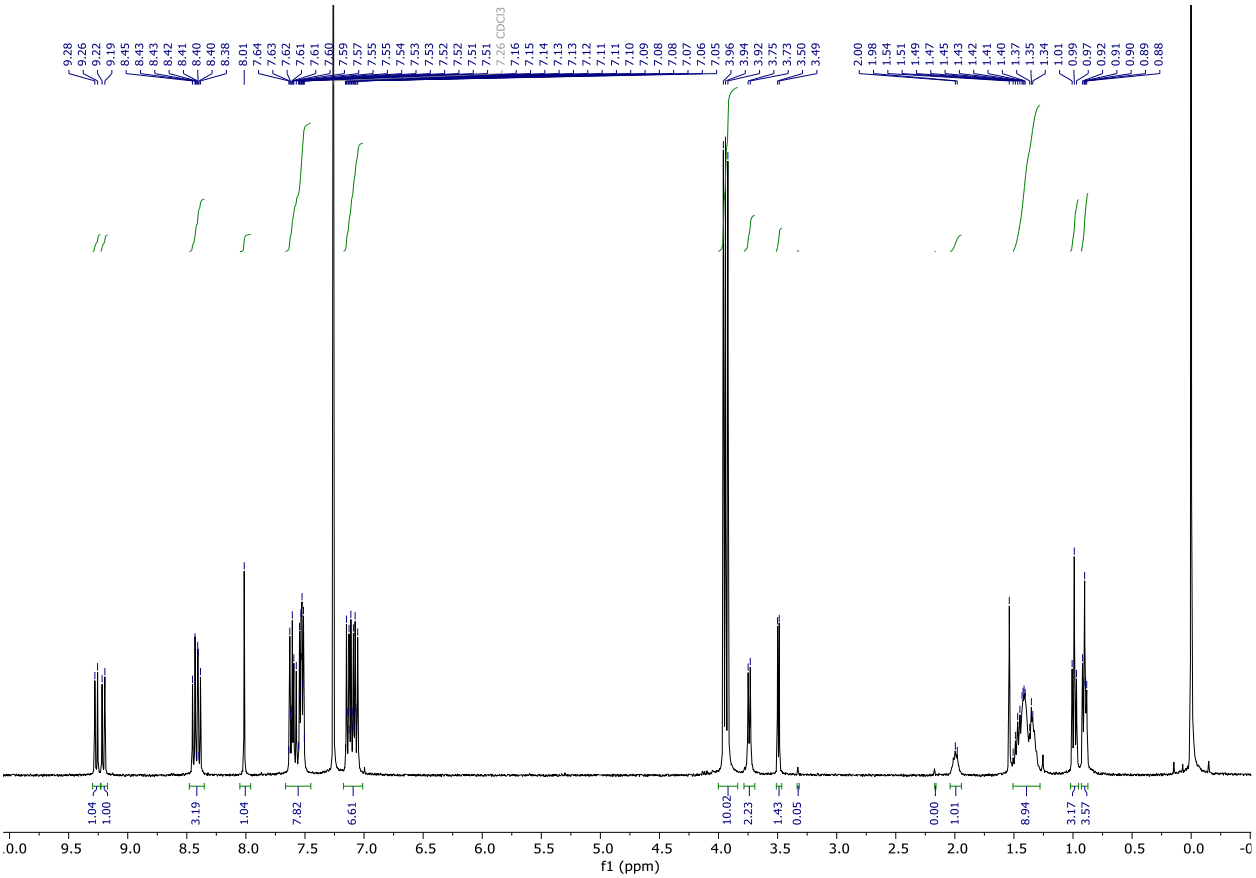

Figure S3.42. ^{1}H NMR of BPI-P ($CDCl_3$, 400 MHz).

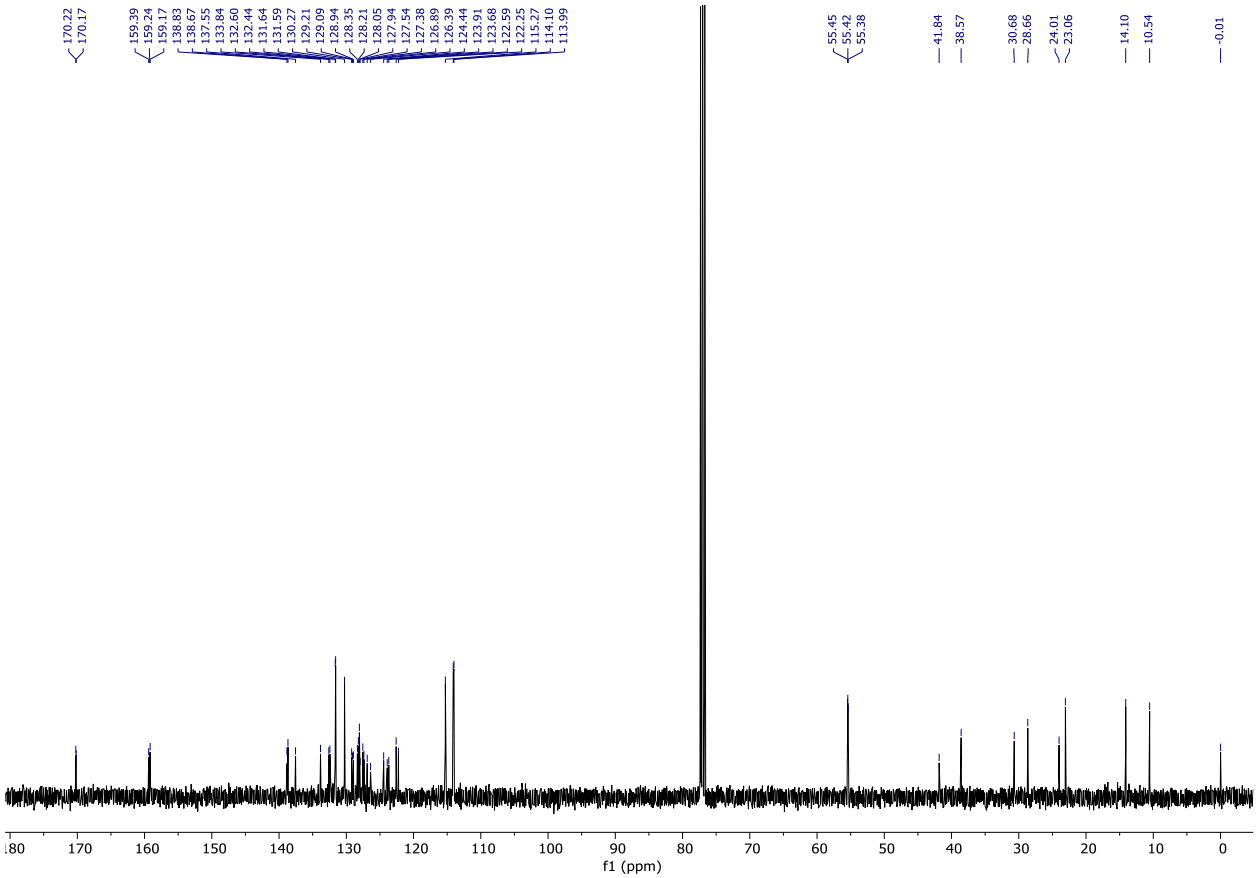

Figure S3.43. ^{13}C NMR of BPI-P ($CDCl_3$, 100 MHz).

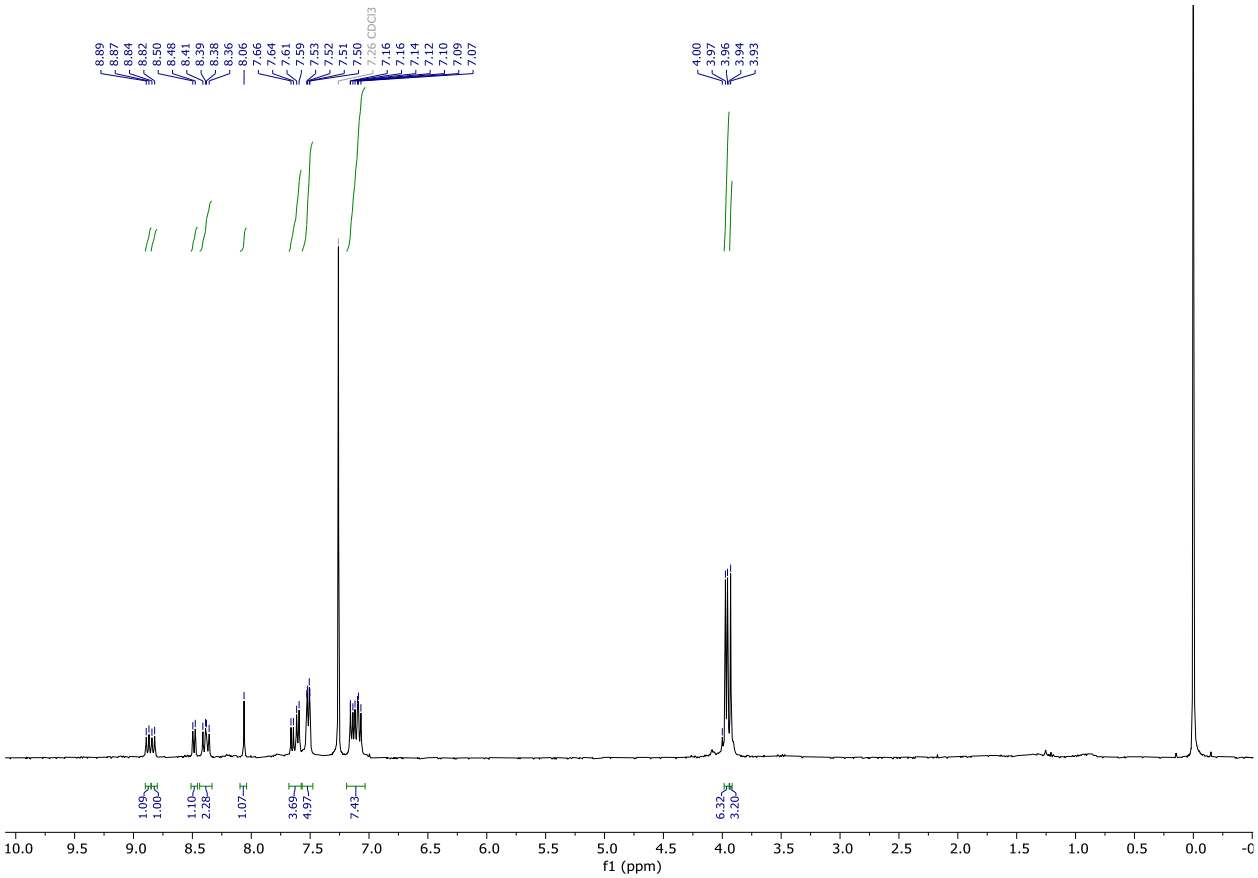

Figure S3.44. ^{1}H NMR of BPA-P ($CDCl_3$, 400 MHz).

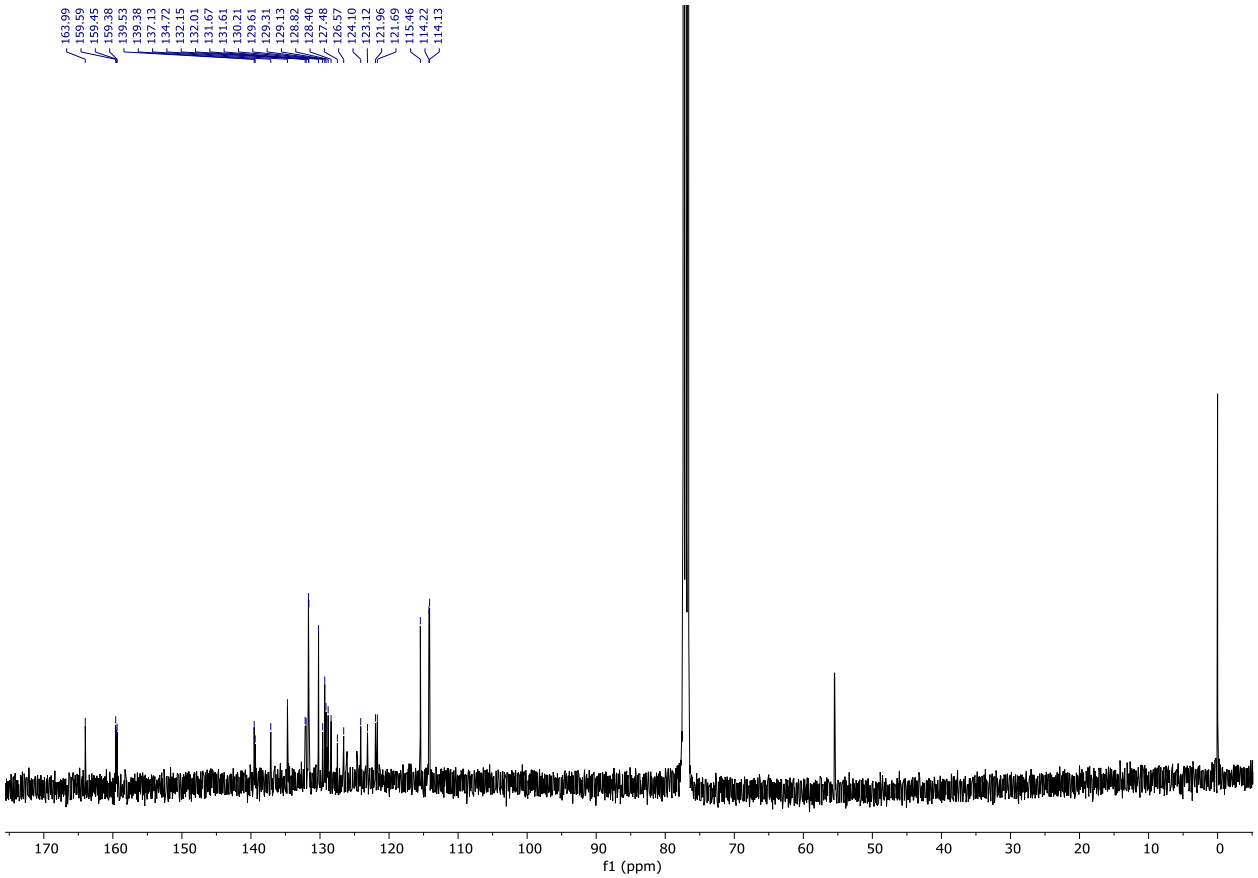

Figure S3.45. ^{13}C NMR of BPA-P ($CDCl_3$, 100 MHz).

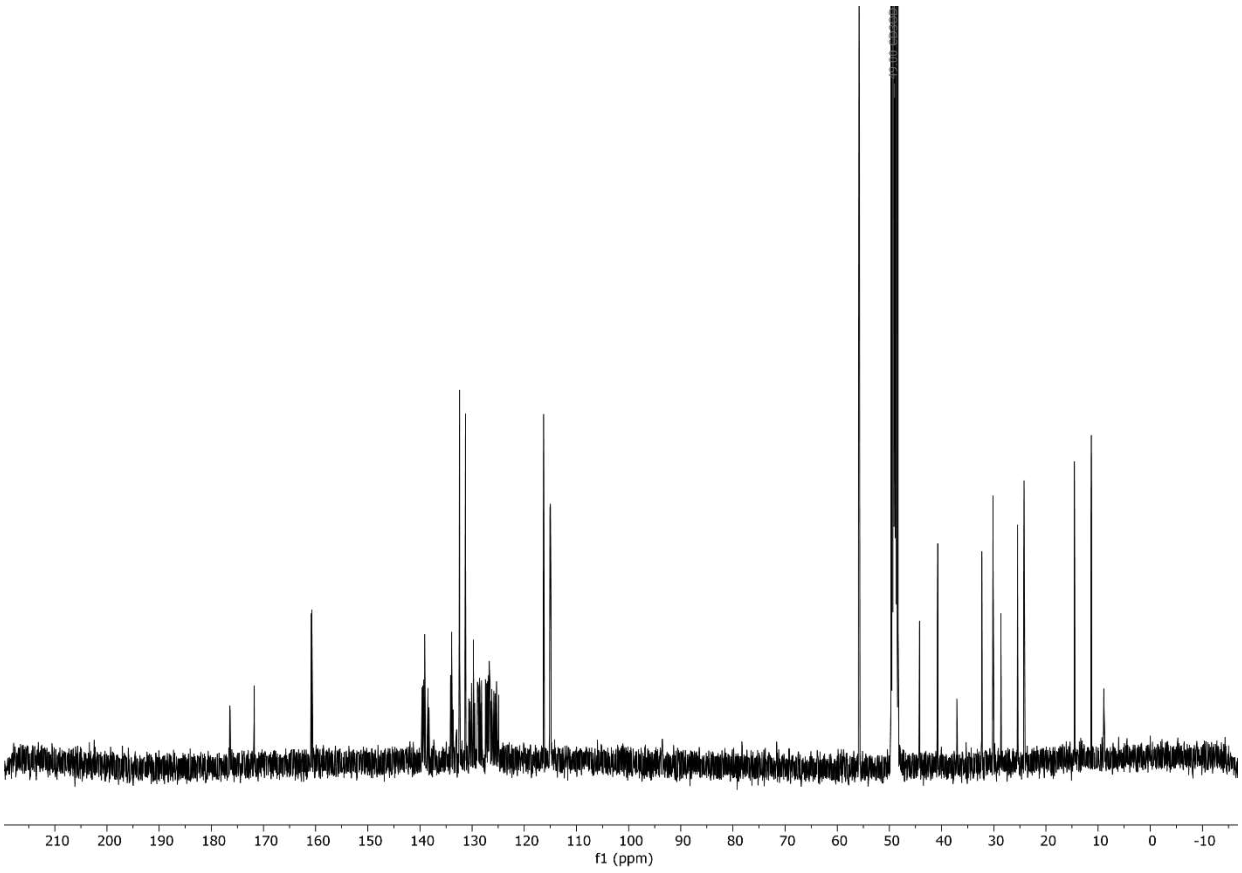

Figure S3.46. ^{13}C NMR of BPI-RO ($CDCl_3$, 100 MHz).

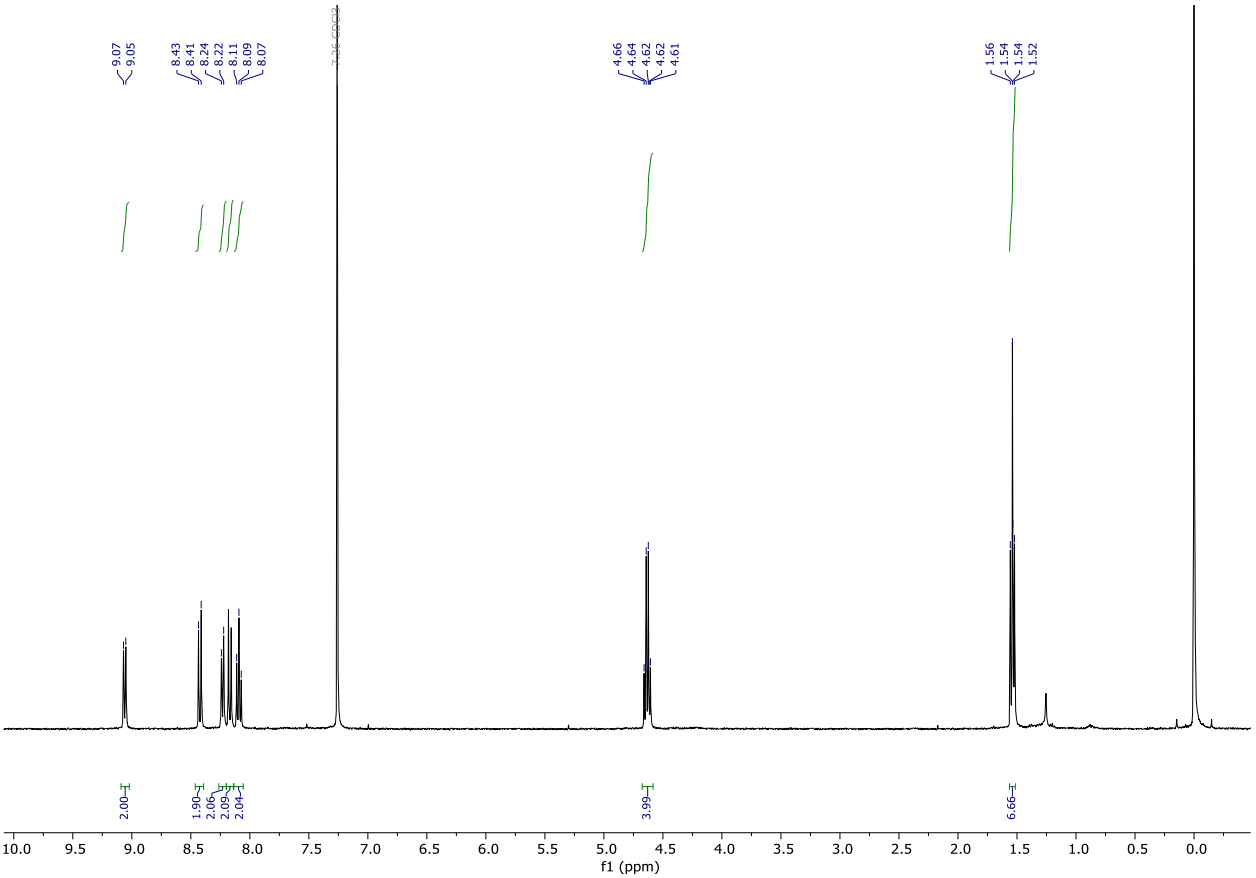

Figure S3.47. ^{1}H NMR of BPDE ($CDCl_3$, 400 MHz).

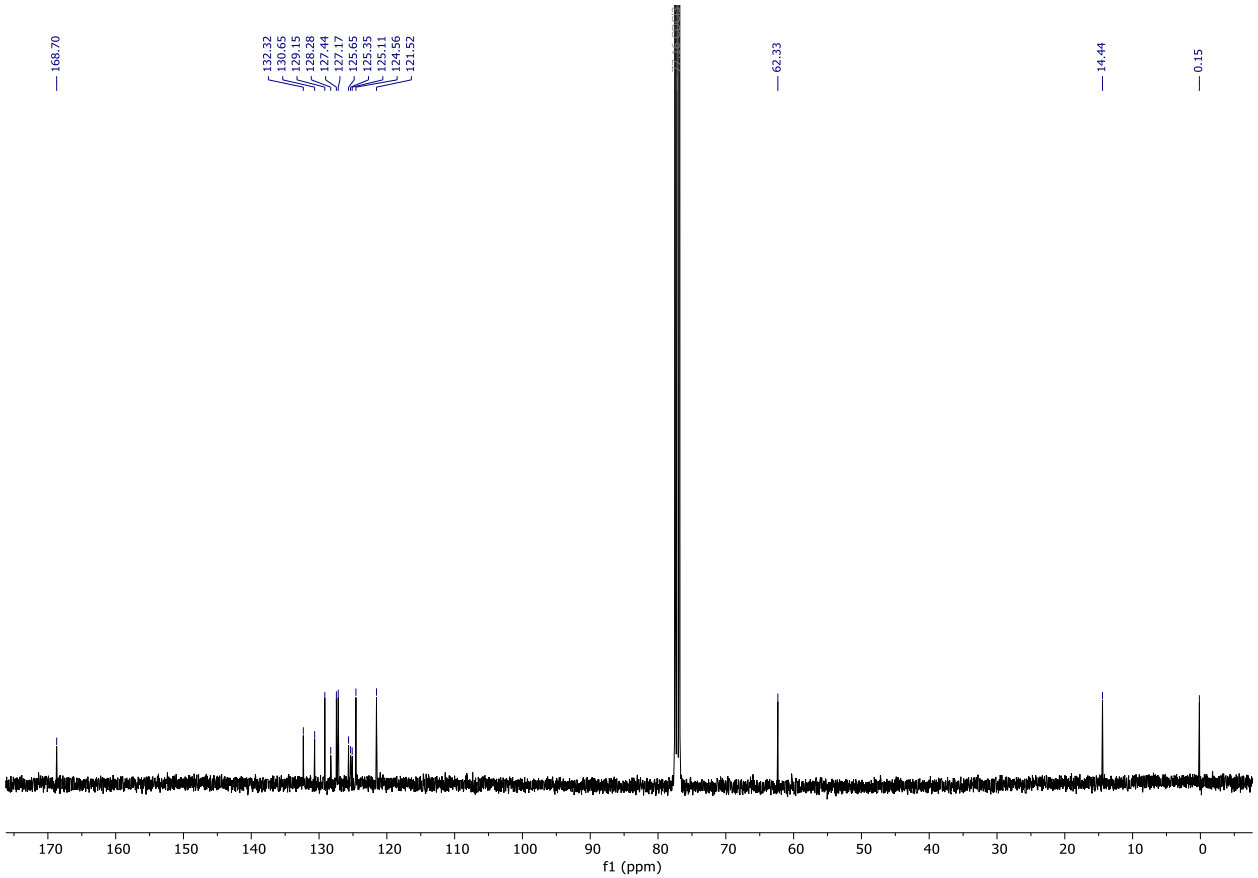

Figure S3.48. ^{13}C NMR of BPDE ($CDCl_3$, 100 MHz).

Computational Data and Methods

C.1 General Information

The hybrid meta-GGA M06-2X[4] density functional in conjunction with Pople's double-z 6-31+G(d,p)[5-9] basis set for the remaining atoms, were used together with Grimme's zero-damped D3 correction[10] to optimize all stationary point structures. To these optimized structures, single-point energy corrections were applied at the M06-2X-D3/6-311+G(d,p). For both optimization and single point calculations the integral equation formalism variant of the polarizable continuum model (IEF-PCM), with the SMD solvation model was applied to account for solvent effects (solvent=tetrahydrofuran).[11] Conformational sampling was performed manually. *Gaussian 16*[12] version C.01 was employed for all density functional theory (DFT) calculations, using an "ultrafine" pruned (99,590) grid for numerical integration of the exchange-correlation functional and its derivatives. Conformational analyses of all stationary points were performed manually. Input files for single-point energy corrections were generated automatically using the qprep function in AQME.[13] Molecular graphics were generated using *PyMol.*[14] Vibrational frequency calculations were performed to verify that stationary points were either minima or first-order saddle points on the potential energy surface (PES), and to calculate thermal corrections to Gibbs free energies (G). The computed thermochemistry data were corrected following Grimme's quasi-harmonic (QHA) model for entropy[15] with a frequency cut-off value of 100.0 cm^{-1} using the *GoodVibes*[16] program at 285.15 K, unless otherwise stated. Also, *GoodVibes* applied (i) 1 M standard concentration corrections to all individual calculations to account for reactions in solution (i.e. change in standard concentration from 1 atm to 1 M)[17] and (ii) multi-conformational

corrections (G_{conf}) to all final Boltzmann weighted G to include the entropic stabilization created by multiple accessible low-lying conformers.[18]

C.2. Calculation of electrochemical redox potentials

The M06-2X functional has been shown to give accurate half-wave one-electron reduction potential predictions in benchmarking studies when used with a double-z basis set; with predictions within a standard deviation of ±0.29 V versus experiment.[19] Here, we calculate redox potentials at the M06-2X-D3/6-311+G(d,p)//M06-2X-D3/6-31+G(d) in conjunction with the SMD implicit solvation for THF, in accordance with the following equation:

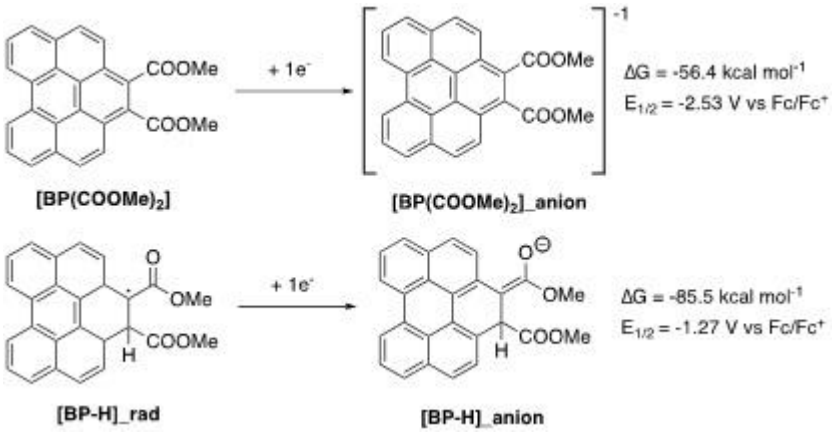

Figure S3.49: Computed half-wave potentials.

C.3. Computed Molecular Orbital Energies

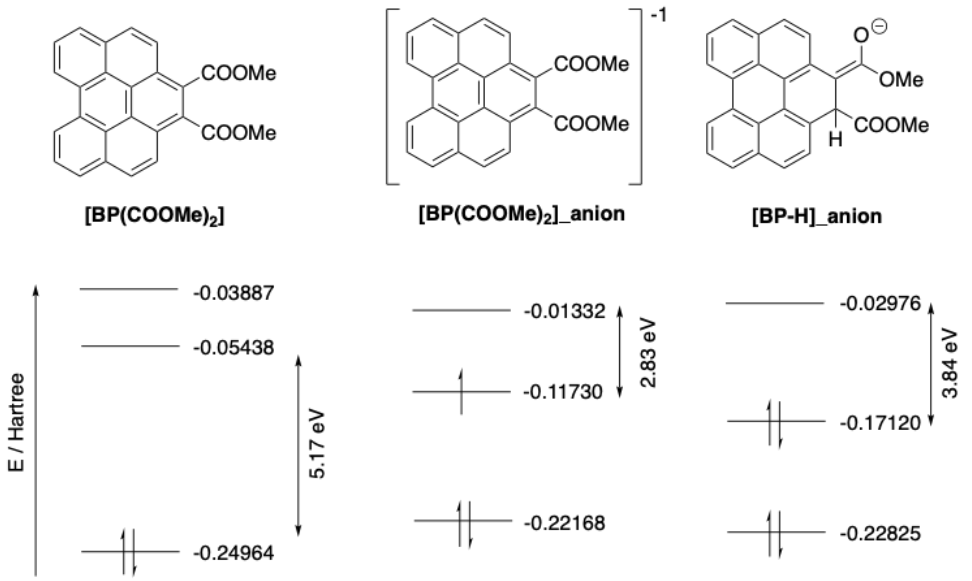

Figure S3.50: Diagram describing the computed frontier molecular orbitals.

C.4. Thermochemistry of the proposed photoactive species [BP-H]$^-$ anion

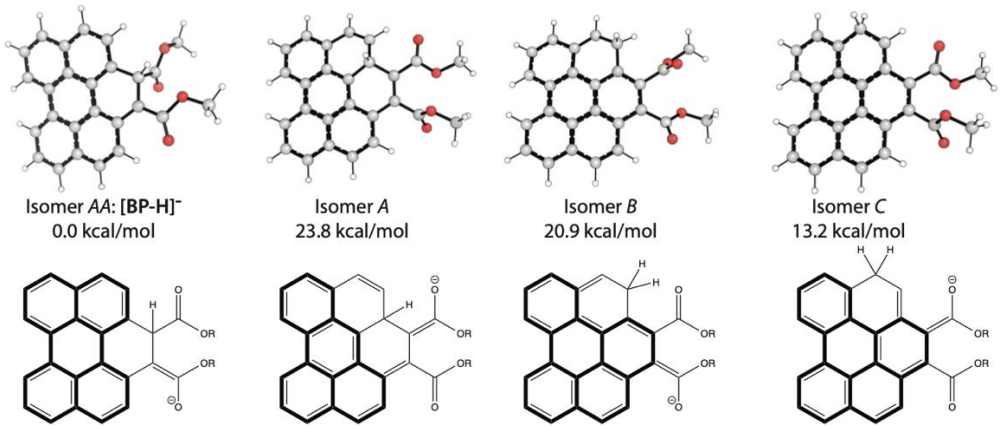

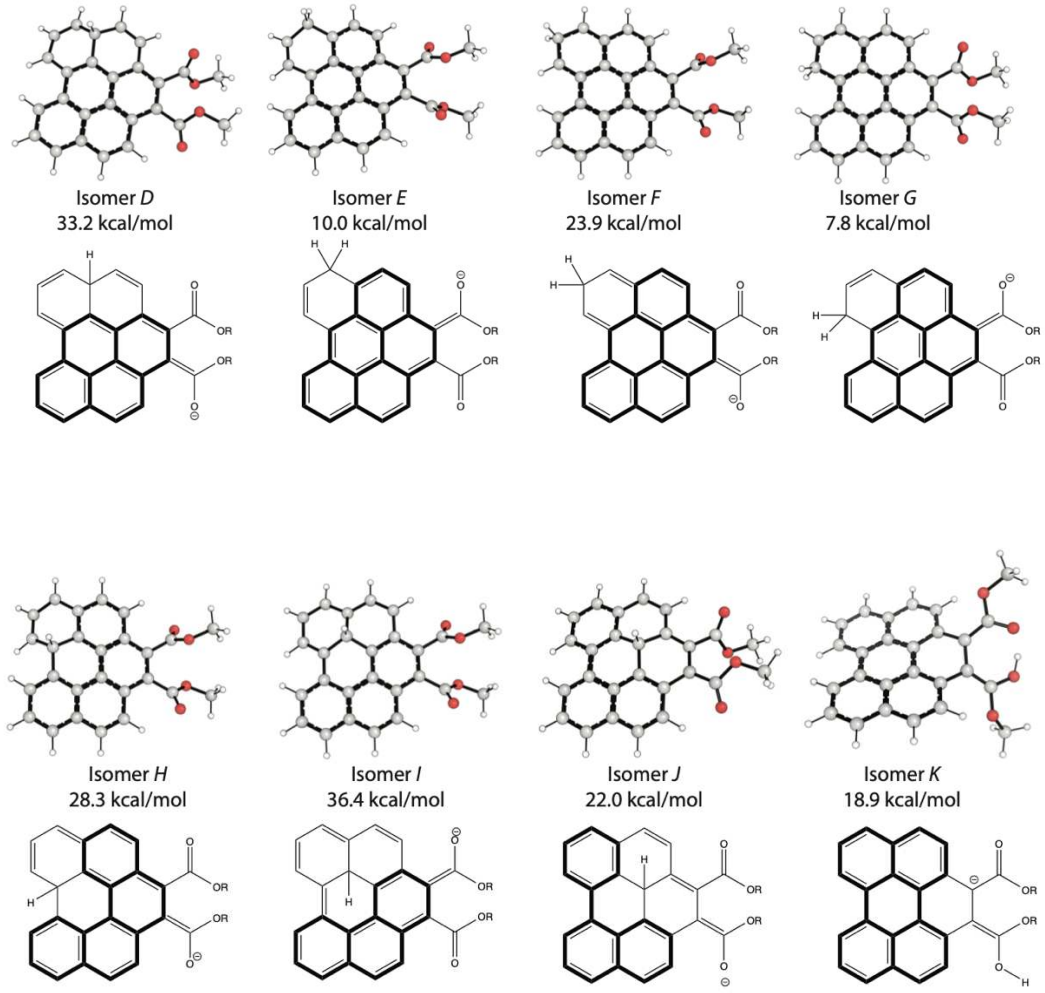

Figure S3.51: Computed thermochemistry for constitutional isomers of the [BP-H]⁻ anion.

C.5. Thermochemical Data

Legend:

E_{SPC} = energy obtained in the single-point energy corrections

E = energy obtained in the geometry optimizations

ZPE = zero-point energy

H_{SPC} = enthalpy corrected with E_{SPC}

T·S = temperature times entropy with no correction

T·qh-S = temperature times entropy with quasi-harmonic S correction

G(T) = Gibbs free energy corrected only with E_{SPC}

qh-G(T) = Gibbs free energy with ESPC and quasi-harmonic S correction

Name	E_{SPC}	E	ZPE	H_{SPC}	T·S	T·gh-S	G(T)	qh-G(T)
[BP-H]-rad_conf_1	-1301.806748	-1301.503882	0.366520	-1301.416276	0.073961	0.070438	-1301.490237	-1301.486714
[BP-H]-rad_conf_2	-1301.806440	-1301.503609	0.366352	-1301.416013	0.074543	0.070808	-1301.490556	-1301.486821
[BP-H]-rad_conf_3	-1301.807954	-1301.505078	0.366402	-1301.417550	0.074168	0.070553	-1301.491718	-1301.488103
[BP-H]-rad_conf_4	-1301.808387	-1301.505442	0.366351	-1301.418032	0.074269	0.070559	-1301.492301	-1301.488591
[BP-H]_anion_isomer_aa conf_1	-1301.942142	-1301.637565	0.365571	-1301.552537	0.073833	0.070078	-1301.626370	-1301.622615
[BP-H]_anion_isomer_aa conf_2	-1301.942433	-1301.637780	0.365579	-1301.552829	0.073630	0.070005	-1301.626458	-1301.622834

[BP-H]_anion_isomer_aa conf_3	-1301.944397	-1301.639704	0.365592	-1301.554890	0.073096	0.069710	-1301.627987	-1301.624600
[BP-H]_anion_isomer_aa conf_4	-1301.944540	-1301.639857	0.365811	-1301.554844	0.073261	0.069697	-1301.628105	-1301.624541
[BP-H]_anion_isomer_a_conf_1	-1301.909606	-1301.600722	0.364626	-1301.521056	0.072677	0.069619	-1301.593734	-1301.590675
[BP-H]_anion_isomer_a_conf_2	-1301.909309	-1301.600361	0.364538	-1301.520726	0.073284	0.069969	-1301.594010	-1301.590695
[BP-H]_anion_isomer_b_conf_1	-1301.913072	-1301.604572	0.364094	-1301.524838	0.072691	0.069837	-1301.597529	-1301.594675
[BP-H]_anion_isomer_b_conf_2	-1301.913004	-1301.604568	0.363939	-1301.524779	0.073171	0.070165	-1301.597950	-1301.594945
[BP-H]_anion_isomer_c_conf_1	-1301.925012	-1301.617025	0.364292	-1301.536521	0.073807	0.070322	-1301.610327	-1301.606842
[BP-H]_anion_isomer_c_conf_2	-1301.924474	-1301.616384	0.364176	-1301.535992	0.073612	0.070339	-1301.609603	-1301.606331
[BP-H]_anion_isomer_d_conf_1	-1301.894452	-1301.585258	0.363759	-1301.506638	0.072625	0.069701	-1301.579262	-1301.576339
[BP-H]_anion_isomer_d_conf_2	-1301.893523	-1301.584254	0.363536	-1301.505745	0.073113	0.070092	-1301.578859	-1301.575838
[BP-H]_anion_isomer_d_conf_4	-1301.892712	-1301.583480	0.363641	-1301.504839	0.073242	0.070136	-1301.578080	-1301.574974
[BP-H]_anion_isomer_e_conf_1	-1301.930464	-1301.622299	0.364268	-1301.542071	0.072646	0.069837	-1301.614718	-1301.611908
[BP-H]_anion_isomer_e_conf_2	-1301.929416	-1301.621251	0.364133	-1301.541038	0.073057	0.070107	-1301.614095	-1301.611145
[BP-H]_anion_isomer_e_conf_3	-1301.930337	-1301.622185	0.364000	-1301.542142	0.072801	0.069951	-1301.614943	-1301.612093
[BP-H]_anion_isomer_f_conf_1	-1301.907310	-1301.599239	0.363838	-1301.519089	0.073943	0.070611	-1301.593032	-1301.589700

[BP-H]_anion_isomer_f_conf_2	-1301.906535	-1301.598362	0.363545	-1301.518398	0.074898	0.071218	-1301.593296	-1301.589617
[BP-H]_anion_isomer_g_conf_1	-1301.934105	-1301.626027	0.364097	-1301.545931	0.072283	0.069632	-1301.618214	-1301.615563
[BP-H]_anion_isomer_g_conf_2	-1301.932972	-1301.624886	0.363982	-1301.544778	0.072804	0.069957	-1301.617581	-1301.614735
[BP-H]_anion_isomer_h_conf_1	-1301.902197	-1301.592910	0.364058	-1301.514041	0.073077	0.069872	-1301.587119	-1301.583913
[BP-H]_anion_isomer_h_conf_2	-1301.903094	-1301.593845	0.364443	-1301.514841	0.071740	0.069109	-1301.586581	-1301.583950
[BP-H]_anion_isomer_h_conf_3	-1301.901822	-1301.592536	0.364037	-1301.513650	0.073389	0.070053	-1301.587039	-1301.583703
[BP-H]_anion_isomer_h_conf_6	-1301.902797	-1301.593549	0.364438	-1301.514538	0.071902	0.069180	-1301.586440	-1301.583718
[BP-H]_anion_isomer_i_conf_1	-1301.889507	-1301.580088	0.363815	-1301.501713	0.072638	0.069612	-1301.574351	-1301.571325
[BP-H]_anion_isomer_i_conf_2	-1301.887765	-1301.578312	0.363553	-1301.500031	0.073522	0.070084	-1301.573553	-1301.570115
[BP-H]_anion_isomer_j_conf_1	-1301.913669	-1301.604711	0.365324	-1301.524599	0.072130	0.069150	-1301.596728	-1301.593749
[BP-H]_anion_isomer_j_conf_2	-1301.912720	-1301.603693	0.365092	-1301.523667	0.073070	0.069720	-1301.596737	-1301.593387
[BP-H]_anion_isomer_k_conf_1	-1301.917485	-1301.608955	0.364538	-1301.529282	0.072292	0.069140	-1301.601575	-1301.598423
[BP(COOMe2)]_anion_conf_1	-1301.333951	-1301.030795	0.351191	-1300.958576	0.073965	0.070681	-1301.032541	-1301.029257
[BP(COOMe2)]_anion_conf_2	-1301.335433	-1301.032271	0.351346	-1300.960092	0.072893	0.070137	-1301.032985	-1301.030229
[BP(COOMe2)]_conf_1	-1301.249105	-1300.948469	0.355271	-1300.869827	0.073124	0.069786	-1300.942951	-1300.939613

[BP(COOMe2)]_conf_2	-1301.250362	-1300.949757	0.355506	-1300.870993	0.072545	0.069418	-1300.943539	-1300.940411

Table S3.6: Compiled thermochemical data in atomic units for structures computed at the M06-2X-D3/6-311+G(d,p)(SMD=THF)//M06-2X-D3/6-31+G(d,p)(SMD=THF) level of theory

C.6. XYZ coordinates

47
[BP-H]-rad_conf_1 Eopt -1301.503882
C -0.040650 -2.987961 -0.790601
C 0.274827 -1.629433 -0.560163
C -0.731089 -0.690029 -0.345308
C -2.099080 -1.121421 -0.328766
C -2.401960 -2.494471 -0.554174
C -1.342844 -3.413047 -0.792480
C -0.407417 0.708934 -0.154596
C -3.158060 -0.200217 -0.081264
C -2.829523 1.212891 0.158861
C -1.465002 1.635395 0.103197
C -3.815402 2.161725 0.429764
C -4.467052 -0.673582 -0.074832
C -4.761719 -2.027149 -0.303932
C -3.747756 -2.928571 -0.540228
H -3.962983 -3.979346 -0.716815
H -5.796736 -2.355745 -0.291769
H 0.768504 -3.691928 -0.965904
H -1.585349 -4.456944 -0.974344
C 1.727961 -1.233959 -0.524823
C 1.974835 0.244797 -0.522056
C 0.950598 1.164013 -0.258987
C 1.207104 2.571565 -0.040067
C 0.205360 3.438993 0.237904
C -1.161491 3.013003 0.308924
H 2.225141 2.930291 -0.078946
H 0.425934 4.488459 0.417619
C -3.501518 3.507400 0.641279
H -4.297471 4.215827 0.850844
C -2.185183 3.932307 0.578772
H -1.928962 4.977053 0.735837
H -5.294990 0.001768 0.108215
H -4.857787 1.868262 0.480854
C 3.407384 0.540545 -0.709529
C 2.370256 -1.922870 0.694108
O 4.260865 -0.322780 -0.575743
O 2.802262 -3.051285 0.676009
O 3.712802 1.790417 -1.085740

O 2.325118 -1.156580 1.783536
C 2.874565 -1.734911 2.974767
H 2.329628 -2.643431 3.240965
H 2.755103 -0.978640 3.749476
C 5.107126 2.057778 -1.278558
H 5.165412 3.108657 -1.560051
H 5.661431 1.878745 -0.354495
H 2.239617 -1.693399 -1.379679
H 3.931981 -1.965763 2.826346
H 5.507532 1.427620 -2.075918
47
[BP-H]-rad_conf_2 Eopt -1301.503609
C 0.257823 -2.873705 -0.787283
C 0.426266 -1.496357 -0.518886
C -0.676758 -0.671191 -0.308547
C -1.992020 -1.242308 -0.329160
C -2.146279 -2.633578 -0.590676
C -0.993351 -3.430998 -0.827654
C -0.504564 0.750231 -0.091481
C -3.145382 -0.442064 -0.083169
C -2.969533 0.990803 0.195050
C -1.656956 1.555775 0.164147
C -4.052496 1.823751 0.476966
C -4.398168 -1.048015 -0.116549
C -4.546168 -2.419053 -0.381253
C -3.439677 -3.204974 -0.614926
H -3.540854 -4.267839 -0.819557
H -5.541691 -2.852743 -0.399330
H 1.138008 -3.485863 -0.964941
H -1.122957 -4.489077 -1.040446
C 1.826555 -0.949932 -0.428831
C 1.916853 0.546045 -0.432810
C 0.799393 1.348776 -0.174390
C 0.901511 2.773965 0.058862
C -0.189137 3.525038 0.339829
C -1.503272 2.954202 0.394208
H 1.875732 3.239635 0.034062
H -0.083150 4.589279 0.536086
C -3.884736 3.190374 0.716775
H -4.752442 3.805937 0.934908
C -2.620542 3.754115 0.670915
H -2.477789 4.817162 0.847896
H -5.295537 -0.466173 0.061480
H -5.057477 1.419394 0.515077
C 3.312514 0.989093 -0.606610
C 2.462230 -1.495931 0.863679

O 4.249250 0.214738 -0.485340
O 2.381087 -0.962341 1.944549
O 3.490084 2.270851 -0.956788
O 3.063039 -2.667445 0.651041
C 3.642525 -3.287342 1.807474
H 4.417343 -2.643334 2.229443
H 4.076117 -4.221483 1.452934
C 4.850682 2.685001 -1.128711
H 4.801988 3.740699 -1.393550
H 5.410378 2.549793 -0.200464
H 2.424008 -1.361901 -1.250709
H 2.873261 -3.483331 2.557855
H 5.323497 2.113089 -1.930240
47
[BP-H]-rad_conf_3 Eopt -1301.505078
C 0.558952 -2.738975 -0.739090
C 0.555420 -1.343959 -0.510827
C -0.640139 -0.660060 -0.302121
C -1.872221 -1.393903 -0.280445
C -1.851990 -2.801620 -0.493704
C -0.610947 -3.452219 -0.734847
C -0.647247 0.777673 -0.133067
C -3.114005 -0.738121 -0.037848
C -3.119946 0.716437 0.175570
C -1.890160 1.441332 0.103971
C -4.298432 1.417358 0.431906
C -4.278601 -1.500320 -0.016666
C -4.254529 -2.887937 -0.229994
C -3.061585 -3.533923 -0.467370
H -3.030098 -4.607533 -0.635186
H -5.185888 -3.446015 -0.206856
H 1.506070 -3.240324 -0.919591
H -0.607462 -4.524331 -0.914123
C 1.879694 -0.626283 -0.459239
C 1.784816 0.871099 -0.471172
C 0.570436 1.530812 -0.244538
C 0.493816 2.967791 -0.087054
C -0.682843 3.586991 0.169120
C -1.913054 2.857010 0.270256
H 1.403736 3.545503 -0.160438
H -0.713695 4.665412 0.305446
C -4.303697 2.803634 0.609606
H -5.241214 3.314205 0.809115
C -3.121543 3.520328 0.524643
H -3.114709 4.599850 0.652476
H -5.238992 -1.031311 0.165214

H -5.244084 0.891407 0.496171
C 3.067370 1.575633 -0.648535
C 2.603694 -1.089228 0.818829
O 3.243230 2.763434 -0.857990
O 2.467118 -0.578805 1.905233
O 4.103339 0.712736 -0.572036
O 3.362279 -2.161494 0.586409
C 4.033820 -2.707701 1.730445
H 4.710555 -1.964952 2.158813
H 4.594830 -3.564485 1.359643
C 5.405237 1.282605 -0.727475
H 6.102160 0.450254 -0.633407
H 5.502268 1.750310 -1.710060
H 2.497076 -0.972901 -1.296338
H 3.306241 -3.023392 2.481529
H 5.591558 2.024610 0.052527
47
[BP-H]-rad_conf_4 Eopt -1301.505442
C 0.315359 -2.886342 -0.729843
C 0.447160 -1.491086 -0.543943
C -0.673748 -0.691145 -0.335945
C -1.969839 -1.303182 -0.278391
C -2.086650 -2.711134 -0.455187
C -0.916597 -3.483911 -0.691595
C -0.541220 0.744568 -0.202351
C -3.139972 -0.526169 -0.037388
C -3.004049 0.926879 0.142036
C -1.711651 1.528724 0.037684
C -4.105798 1.742700 0.399109
C -4.371598 -1.172617 0.014998
C -4.482772 -2.560841 -0.164040
C -3.359954 -3.323528 -0.397274
H -3.432742 -4.398966 -0.538331
H -5.462809 -3.026402 -0.117361
H 1.209270 -3.479288 -0.903925
H -1.017985 -4.556103 -0.839084
C 1.835690 -0.903640 -0.548249
C 1.884513 0.596496 -0.572450
C 0.740529 1.374453 -0.344674
C 0.803834 2.814666 -0.216107
C -0.304638 3.549185 0.041109
C -1.596776 2.942967 0.174261
H 1.762900 3.301694 -0.315656
H -0.230375 4.628346 0.152581
C -3.975783 3.126776 0.546882
H -4.857187 3.728492 0.748066

C -2.732275 3.724604 0.430752
H -2.619407 4.800817 0.534812
H -5.280320 -0.609682 0.195629
H -5.096548 1.311666 0.487994
C 3.226821 1.173183 -0.769638
C 2.582016 -1.484895 0.667679
O 3.515928 2.337810 -0.984390
O 3.164320 -2.543894 0.655352
O 4.174320 0.213840 -0.701670
O 2.456471 -0.713386 1.746742
C 3.089604 -1.199536 2.938220
H 2.661211 -2.161504 3.228564
H 2.892256 -0.448512 3.701805
C 5.523790 0.650099 -0.881924
H 6.135122 -0.247419 -0.793232
H 5.649996 1.100556 -1.869235
H 2.381264 -1.310967 -1.408162
H 4.164618 -1.305686 2.775528
H 5.796435 1.374354 -0.110651
47
[BP-H]_anion_isomer_aa conf_1 Eopt -1301.637565
C -0.085296 -2.996329 -0.832849
C 0.271285 -1.656591 -0.555927
C -0.712430 -0.691720 -0.352935
C -2.093318 -1.091476 -0.363742
C -2.433255 -2.453443 -0.625742
C -1.397098 -3.394132 -0.875133
C -0.358088 0.705681 -0.164360
C -3.134514 -0.145973 -0.100643
C -2.769447 1.255327 0.178650
C -1.393204 1.647534 0.098870
C -3.729666 2.213781 0.492969
C -4.455789 -0.581580 -0.125039
C -4.783857 -1.922605 -0.391532
C -3.794697 -2.846950 -0.636715
H -4.038388 -3.887006 -0.841015
H -5.828681 -2.221890 -0.402206
H 0.710138 -3.718713 -1.003280
H -1.662656 -4.426407 -1.090182
C 1.741819 -1.313795 -0.424133
C 2.019262 0.161362 -0.585498
C 1.001712 1.112859 -0.324131
C 1.267844 2.526448 -0.165341
C 0.289725 3.421914 0.137834
C -1.074893 3.027296 0.282711
H 2.285830 2.875163 -0.264408

H 0.541389 4.471865 0.278037
C -3.397326 3.559269 0.708292
H -4.176591 4.275009 0.953930
C -2.079648 3.961422 0.590291
H -1.800790 5.003767 0.732529
H -5.267373 0.113910 0.057706
H -4.773766 1.929936 0.574769
C 3.411140 0.400900 -0.819804
C 2.247167 -1.908388 0.896066
O 4.269262 -0.491288 -0.806412
O 2.590311 -3.065397 1.034030
O 3.789526 1.686501 -1.101304
O 2.209338 -1.041799 1.915196
C 2.614393 -1.555934 3.184471
H 1.966427 -2.382386 3.487992
H 2.520395 -0.725789 3.884424
C 5.180460 1.884526 -1.317124
H 5.302171 2.954101 -1.497986
H 5.762840 1.585498 -0.441029
H 2.298648 -1.885636 -1.175693
H 3.650679 -1.901115 3.143519
H 5.528545 1.319138 -2.186230
47
[BP-H]_anion_isomer_aa conf_2 Eopt -1301.637780
C 0.161573 -2.861781 -0.941656
C 0.411405 -1.524898 -0.557637
C -0.646884 -0.644781 -0.339038
C -1.993873 -1.137321 -0.421952
C -2.226222 -2.499079 -0.783737
C -1.117232 -3.344195 -1.062504
C -0.398458 0.760837 -0.070896
C -3.106053 -0.286382 -0.128658
C -2.848776 1.116977 0.244942
C -1.504032 1.611547 0.215603
C -3.881105 1.985696 0.591308
C -4.391426 -0.812121 -0.218303
C -4.614029 -2.151907 -0.582236
C -3.554990 -2.985352 -0.861137
H -3.718761 -4.023402 -1.141398
H -5.633827 -2.523150 -0.642299
H 1.011119 -3.514480 -1.130500
H -1.301335 -4.374340 -1.358052
C 1.837955 -1.074912 -0.317288
C 2.011132 0.410531 -0.495109
C 0.926848 1.276156 -0.203456
C 1.086608 2.697232 0.014801

C 0.043226 3.502017 0.352893
C -1.289703 3.000171 0.467152
H 2.077613 3.122855 -0.058891
H 0.214820 4.559605 0.546263
C -3.650063 3.337738 0.882904
H -4.482503 3.981478 1.152257
C -2.364273 3.841288 0.805068
H -2.165422 4.892994 1.002140
H -5.256026 -0.190470 -0.013401
H -4.903237 1.624513 0.637008
C 3.370079 0.761773 -0.776733
C 2.261606 -1.537356 1.082436
O 4.301475 -0.052529 -0.812476
O 2.287552 -0.855859 2.082623
O 3.624216 2.078651 -1.054384
O 2.571330 -2.847229 1.092216
C 2.901840 -3.401192 2.367090
H 3.782279 -2.905070 2.783289
H 3.113076 -4.455507 2.188082
C 4.983647 2.399133 -1.317432
H 5.006863 3.477898 -1.482474
H 5.622466 2.137518 -0.469055
H 2.495311 -1.616712 -1.005697
H 2.062664 -3.296255 3.059597
H 5.345500 1.879362 -2.209256
47
[BP-H]_anion_isomer_aa conf_3 Eopt -1301.639704
C 0.531046 -2.731017 -0.851622
C 0.571278 -1.352767 -0.539836
C -0.609538 -0.646023 -0.322532
C -1.860896 -1.352815 -0.341655
C -1.877611 -2.752128 -0.625546
C -0.653756 -3.420677 -0.900827
C -0.589215 0.792496 -0.120127
C -3.091282 -0.676362 -0.063830
C -3.061406 0.771920 0.215183
C -1.813105 1.471469 0.136866
C -4.217967 1.485446 0.518951
C -4.274351 -1.408638 -0.080250
C -4.283894 -2.786147 -0.362664
C -3.110309 -3.451399 -0.632953
H -3.108518 -4.516431 -0.853293
H -5.230335 -3.320551 -0.367290
H 1.469561 -3.246665 -1.043419
H -0.674687 -4.481263 -1.139769
C 1.923458 -0.681163 -0.383295

C 1.853211 0.819553 -0.530750
C 0.637896 1.501893 -0.274613
C 0.576438 2.940310 -0.139020
C -0.583225 3.588154 0.156926
C -1.819519 2.888858 0.310283
H 1.493918 3.500985 -0.258159
H -0.583954 4.669882 0.281059
C -4.204306 2.872788 0.726372
H -5.128553 3.391654 0.964026
C -3.014595 3.567521 0.608288
H -2.985053 4.647150 0.742561
H -5.223740 -0.924619 0.120668
H -5.170121 0.970976 0.595909
C 3.099413 1.490005 -0.740330
C 2.500311 -1.094846 0.975870
O 3.333541 2.690383 -0.915860
O 2.399639 -0.474151 2.010225
O 4.155412 0.600978 -0.737011
O 3.111672 -2.291865 0.907848
C 3.604175 -2.810603 2.144967
H 4.357380 -2.141002 2.567895
H 4.049858 -3.776391 1.906741
C 5.438120 1.170305 -0.946704
H 6.142516 0.336778 -0.918839
H 5.494948 1.672169 -1.917223
H 2.602541 -1.115223 -1.124498
H 2.786613 -2.937199 2.859371
H 5.683301 1.890193 -0.160273
47
[BP-H]_anion_isomer_aa conf_4 Eopt -1301.639857
C 0.286772 -2.905400 -0.761884
C 0.458646 -1.520836 -0.533711
C -0.647251 -0.696585 -0.342090
C -1.959509 -1.282251 -0.316553
C -2.110810 -2.686332 -0.526982
C -0.957672 -3.482167 -0.766127
C -0.489454 0.741703 -0.205681
C -3.118216 -0.479355 -0.068701
C -2.948406 0.969721 0.149758
C -1.640125 1.543396 0.034649
C -4.028155 1.800429 0.436882
C -4.366161 -1.094219 -0.053142
C -4.508481 -2.476891 -0.266814
C -3.404615 -3.264251 -0.499470
H -3.505023 -4.334503 -0.664719
H -5.501858 -2.917627 -0.247832

H 1.171295 -3.517146 -0.926803
H -1.080035 -4.547982 -0.943352
C 1.873819 -0.978244 -0.442023
C 1.941774 0.520225 -0.631149
C 0.798019 1.323578 -0.394705
C 0.874843 2.765352 -0.310446
C -0.214642 3.531609 -0.030030
C -1.510100 2.960231 0.156719
H 1.839792 3.231756 -0.457303
H -0.110653 4.612209 0.054156
C -3.880608 3.187068 0.592470
H -4.748619 3.799741 0.818513
C -2.631878 3.760255 0.439373
H -2.497968 4.836192 0.533908
H -5.264207 -0.511570 0.120104
H -5.023206 1.381192 0.543696
C 3.245040 1.065780 -0.854664
C 2.473294 -1.471408 0.880421
O 3.592134 2.233147 -1.065798
O 3.018294 -2.547602 1.023271
O 4.212525 0.082735 -0.813425
O 2.282564 -0.618583 1.893593
C 2.766892 -1.044472 3.168057
H 2.273169 -1.969762 3.476293
H 2.525648 -0.238562 3.860910
C 5.543617 0.518678 -1.040440
H 6.165209 -0.376349 -0.977049
H 5.647448 0.973909 -2.029971
H 2.480658 -1.493899 -1.194245
H 3.848006 -1.201782 3.132719
H 5.856427 1.242926 -0.282442
47
[BP-H]_anion_isomer_a_conf_1 Eopt -1301.600722
O -3.273687 1.837546 1.375608
C -2.993532 1.289782 0.333805
O -3.772133 1.338121 -0.756846
C -5.044365 1.964383 -0.574405
C -1.710293 0.548686 0.066892
C -1.702738 -0.820845 -0.085075
C -2.953288 -1.573860 -0.130389
O -3.927062 -1.064354 0.662262
C -5.236630 -1.585872 0.453016
O -3.151617 -2.563280 -0.822325
C -0.539388 1.347320 -0.044963
C -0.569489 2.769162 -0.011924
C 0.571135 3.519319 -0.021003

C 1.863977 2.886864 -0.027831
C 3.045699 3.641544 -0.025806
C 4.287347 3.010293 -0.035693
C 4.380342 1.625096 -0.038356
C 3.219996 0.821368 -0.031952
C 1.947001 1.457098 -0.038201
C 0.733247 0.670265 -0.093900
C 0.800138 -0.717356 -0.175410
C -0.439806 -1.524242 -0.557680
H -0.473973 -1.597148 -1.668944
C -0.335414 -2.943292 -0.040327
C 0.849739 -3.526489 0.183408
C 2.057781 -1.372513 -0.057624
C 2.110058 -2.799978 0.058396
C 3.329389 -3.449612 0.166023
C 4.529663 -2.721754 0.167743
C 4.494252 -1.339657 0.100375
C 3.275717 -0.634622 0.002358
H -4.920652 3.021045 -0.323499
H -5.601207 1.463734 0.222365
H -5.565275 1.860832 -1.525968
H -5.259797 -2.662622 0.638317
H -5.570398 -1.386820 -0.570349
H -5.879958 -1.071106 1.167330
H -1.531413 3.277232 0.020970
H 0.524387 4.605218 -0.010270
H 2.979226 4.727232 -0.018975
H 5.196225 3.607274 -0.040549
H 5.363988 1.169017 -0.047488
H -1.252421 -3.510006 0.082458
H 0.902289 -4.566630 0.501768
H 3.346758 -4.532905 0.269750
H 5.482039 -3.238535 0.246504
H 5.432949 -0.796611 0.138133
47
[BP-H]_anion_isomer_a_conf_2 Eopt -1301.600361
O 3.769569 1.465079 -1.030691
C 3.054236 1.219658 -0.083465
O 3.295816 1.655677 1.155658
C 4.518079 2.377604 1.327145
C 1.746234 0.480657 -0.182456
C 1.708943 -0.894553 -0.247057
C 2.946278 -1.665986 -0.310985
O 3.970515 -1.103697 0.376371
C 5.266657 -1.629707 0.103740
O 3.097201 -2.707757 -0.934605

C 0.584540 1.293956 -0.277097
C 0.643246 2.714634 -0.313813
C -0.481529 3.487917 -0.287594
C -1.783696 2.882443 -0.185920
C -2.949270 3.660845 -0.148624
C -4.200391 3.055758 -0.053095
C -4.318122 1.674289 0.016623
C -3.174258 0.847561 -0.008125
C -1.893025 1.455710 -0.122119
C -0.699584 0.641676 -0.211426
C -0.794317 -0.746763 -0.212996
C 0.410330 -1.596760 -0.615695
H 0.385935 -1.725989 -1.721848
C 0.308118 -2.985399 -0.021790
C -0.873456 -3.532289 0.294062
C -2.054488 -1.368750 0.009806
C -2.125692 -2.787232 0.201462
C -3.348486 -3.405623 0.407526
C -4.533851 -2.654103 0.436644
C -4.477445 -1.277937 0.299158
C -3.253681 -0.603649 0.100445
H 4.564789 2.633130 2.385272
H 5.369992 1.751671 1.048732
H 4.516347 3.285086 0.717596
H 5.958571 -1.050798 0.716141
H 5.512996 -1.510971 -0.955597
H 5.321857 -2.686894 0.374942
H 1.614780 3.203645 -0.371875
H -0.414972 4.571823 -0.333640
H -2.863240 4.744028 -0.198397
H -5.097037 3.670601 -0.031585
H -5.308398 1.238815 0.089630
H 1.220065 -3.564448 0.078451
H -0.926881 -4.554518 0.665837
H -3.379378 -4.481950 0.566060
H -5.489613 -3.146932 0.591281
H -5.402835 -0.714463 0.359033
47
[BP-H]_anion_isomer_b_conf_1 Eopt -1301.604572
O -3.235981 -2.570028 -0.382340
C -2.957434 -1.535507 0.192765
O -3.827821 -0.921582 1.016144
C -5.151283 -1.459963 1.036406
C -1.674502 -0.796613 0.093830
C -0.438755 -1.487088 0.039868
C 0.765429 -0.738859 -0.024915

C 2.033242 -1.413067 -0.074685
C 3.249610 -0.673795 -0.121834
C 4.449224 -1.377667 -0.261685
C 4.480501 -2.773787 -0.309640
C 3.305281 -3.501038 -0.207951
C 2.075121 -2.834571 -0.093121
C 0.842495 -3.563326 0.014115
C -0.352819 -2.927196 0.090700
C 3.218686 0.792394 0.018846
C 1.954729 1.445266 -0.054745
C 0.742501 0.689922 -0.093922
C 4.378977 1.524944 0.268246
C 4.283561 2.922495 0.491438
C 3.088014 3.585998 0.442826
C 1.855008 2.898865 0.122010
C 0.651214 3.539954 0.004863
C -0.539736 2.810954 -0.550916
H -0.546644 2.842580 -1.661625
H -1.472457 3.284628 -0.234982
C -0.516417 1.352264 -0.143691
C -1.684278 0.608689 0.013938
C -3.002317 1.330939 -0.017624
O -3.740293 0.960264 -1.075085
C -5.052857 1.526541 -1.139106
O -3.363861 2.161069 0.784804
H -5.580232 -1.455817 0.030299
H -5.142826 -2.481794 1.423600
H -5.723736 -0.811281 1.699207
H 5.385802 -0.836073 -0.342738
H 5.432534 -3.285564 -0.421278
H 3.319259 -4.588424 -0.226585
H 0.887226 -4.650075 0.035147
H -1.265469 -3.504593 0.169612
H 5.344953 1.041827 0.355620
H 5.192178 3.478539 0.717627
H 3.045007 4.658722 0.623850
H 0.584503 4.613581 0.166738
H -4.995030 2.609970 -1.269926
H -5.531556 1.066467 -2.003104
H -5.609024 1.299018 -0.225748
47
[BP-H]_anion_isomer_b_conf_2 Eopt -1301.604568
O 3.064047 -2.876096 0.502562
C 2.883059 -1.787888 -0.009470
O 3.846326 -1.162375 -0.712717
C 5.147395 -1.749318 -0.654521

C 1.640829 -0.981930 0.049619
C 0.360470 -1.590934 0.025247
C -0.794466 -0.766533 0.057406
C -2.104590 -1.354295 0.017013
C -3.270947 -0.536372 0.025393
C -4.519791 -1.162519 0.067357
C -4.645236 -2.554378 0.059340
C -3.516225 -3.355360 0.000304
C -2.240362 -2.769636 -0.019100
C -1.054075 -3.575719 -0.082464
C 0.183284 -3.019562 -0.074760
C -3.137472 0.929161 -0.051628
C -1.838782 1.491795 0.107975
C -0.683574 0.655440 0.177745
C -4.233691 1.748827 -0.319039
C -4.035622 3.144774 -0.473512
C -2.802798 3.723239 -0.340383
C -1.633463 2.940796 0.000518
C -0.396742 3.495786 0.195160
C 0.724205 2.670173 0.761296
H 1.697690 3.086972 0.480137
H 0.711203 2.675861 1.871728
C 0.610914 1.228355 0.311227
C 1.732700 0.414886 0.181621
C 3.082555 1.050169 0.371257
O 3.450903 1.786422 -0.679529
C 4.716614 2.442272 -0.559171
O 3.747470 0.940905 1.379320
H 5.129744 -2.764477 -1.057721
H 5.785979 -1.113016 -1.266867
H 5.507724 -1.769405 0.377712
H -5.422682 -0.562991 0.113619
H -5.633834 -3.003961 0.094937
H -3.602235 -4.439368 -0.022003
H -1.168449 -4.655970 -0.140700
H 1.059350 -3.653901 -0.123433
H -5.224776 1.337643 -0.469443
H -4.894016 3.770654 -0.712991
H -2.681608 4.797584 -0.468962
H -0.258633 4.569673 0.089244
H 4.704902 3.144359 0.278726
H 4.863205 2.975345 -1.497902
H 5.511348 1.706778 -0.409739
47
[BP-H]_anion_isomer_c_conf_1 Eopt -1301.617025
O 3.388974 2.089021 0.970569

C	3.038520	1.319203	0.104196
O	3.774019	1.065736	-0.989403
C	5.072605	1.663544	-1.006550
C	1.725167	0.586432	0.072218
C	0.550535	1.374937	0.026906
C	0.577771	2.799609	-0.009040
C	-0.563473	3.544238	-0.033998
C	-1.851311	2.906576	-0.007962
C	-3.031880	3.663923	0.004736
C	-4.272253	3.036478	0.029511
C	-4.361295	1.649719	0.047534
C	-3.202702	0.848414	0.039612
C	-1.930652	1.478238	0.005693
C	-0.715627	0.686293	-0.016893
C	-0.780522	-0.706940	-0.081084
C	-2.067770	-1.365802	-0.061151
C	-3.268077	-0.611762	0.054689
C	-4.500340	-1.288041	0.172586
C	-4.563518	-2.667711	0.161946
C	-3.384781	-3.410238	0.007293
C	-2.155628	-2.785827	-0.119656
C	-0.930806	-3.632675	-0.377143
H	-0.958856	-4.511055	0.284137
H	-1.007850	-4.050067	-1.397262
C	0.362624	-2.890628	-0.216332
C	0.437996	-1.535662	-0.113536
C	1.703690	-0.797337	0.020789
C	2.981002	-1.534085	0.086357
O	3.871791	-0.948116	0.922267
C	5.196106	-1.475209	0.885180
O	3.261168	-2.560814	-0.505581
H	5.553015	1.302256	-1.915514
H	5.642752	1.358579	-0.124753
H	4.992856	2.753436	-1.028077
H	1.537769	3.307727	-0.007073
H	-0.520983	4.630112	-0.058142
H	-2.961650	4.749307	-0.007889
H	-5.181840	3.632019	0.032144
H	-5.345128	1.195327	0.055309
H	-5.421695	-0.727552	0.285238
H	-5.520323	-3.172284	0.265739
H	-3.429803	-4.497653	-0.026001
H	1.269160	-3.480357	-0.255208
H	5.778964	-0.861710	1.572856
H	5.607962	-1.410981	-0.126683
H	5.205759	-2.517846	1.212947

47

[BP-H]_anion_isomer_c_conf_2 Eopt -1301.616384

O	-3.776229	1.128541	1.280605
C	-3.111729	1.098812	0.267132
O	-3.453381	1.740725	-0.854473
C	-4.709401	2.422192	-0.813928
C	-1.771644	0.421426	0.155258
C	-0.641578	1.265725	0.193753
C	-0.747652	2.683973	0.300952
C	0.348102	3.492923	0.294362
C	1.666582	2.932378	0.157318
C	2.799102	3.756850	0.103831
C	4.068552	3.204468	-0.032817
C	4.233382	1.827935	-0.121525
C	3.124011	0.960412	-0.074263
C	1.825034	1.513260	0.071656
C	0.660784	0.651183	0.132828
C	0.802481	-0.736269	0.128933
C	2.120953	-1.317356	0.004493
C	3.267304	-0.491471	-0.158414
C	4.523285	-1.091692	-0.387378
C	4.661317	-2.464971	-0.439706
C	3.539070	-3.279532	-0.232891
C	2.290610	-2.730637	0.004943
C	1.134660	-3.646713	0.329630
H	1.295097	-4.056775	1.343151
H	1.174108	-4.522703	-0.333615
C	-0.207913	-2.982289	0.246660
C	-0.368837	-1.632341	0.188705
C	-1.680837	-0.962392	0.128875
C	-2.918585	-1.755325	0.073373
O	-3.913545	-1.113204	-0.589408
C	-5.211951	-1.688955	-0.474991
O	-3.098083	-2.869008	0.536179
H	-4.695029	3.209732	-0.055597
H	-5.516043	1.718203	-0.593193
H	-4.843492	2.854662	-1.804996
H	-1.733495	3.136173	0.387651
H	0.247693	4.572088	0.375872
H	2.670608	4.834762	0.172386
H	4.941157	3.852055	-0.067142
H	5.238094	1.432537	-0.215386
H	5.402709	-0.475443	-0.537648
H	5.634331	-2.909748	-0.630202
H	3.646076	-4.363029	-0.244311
H	-1.074131	-3.627328	0.304350

H -5.223347 -2.704066 -0.879190
H -5.874238 -1.047930 -1.057590
H -5.530790 -1.709188 0.571485
47
[BP-H]_anion_isomer_d_conf_1 Eopt -1301.585258
O 3.216647 -2.555397 0.648028
C 2.974277 -1.547646 0.007004
O 3.907668 -0.981599 -0.789930
C 5.227791 -1.510965 -0.673833
C 1.698317 -0.808823 -0.019416
C 0.450535 -1.495562 0.034967
C -0.756948 -0.758348 -0.014856
C -2.021960 -1.430667 0.004054
C -3.245436 -0.694357 -0.018459
C -4.448848 -1.404275 -0.031976
C -4.481546 -2.801517 -0.004031
C -3.300051 -3.523734 0.039142
C -2.065761 -2.853709 0.040303
C -0.828496 -3.576712 0.071370
C 0.368392 -2.935012 0.071519
C -3.212032 0.777389 -0.028195
C -4.346506 1.557511 0.172161
C -4.191971 2.960696 0.451056
C -3.031030 3.610637 0.203889
C -1.935776 2.886438 -0.548012
H -2.149925 2.972505 -1.640068
C -1.938680 1.408594 -0.182381
C -0.748168 0.681238 -0.127829
C 0.528471 1.346970 -0.166225
C 0.528923 2.805461 -0.125621
C -0.598317 3.518052 -0.273180
C 1.701276 0.597186 -0.120116
C 3.005985 1.340188 -0.088035
O 3.685545 1.092983 1.042290
C 4.986174 1.682107 1.118742
O 3.398108 2.103503 -0.942060
H 5.250483 -2.559531 -0.980889
H 5.585305 -1.427408 0.356826
H 5.846920 -0.911632 -1.341702
H -5.390257 -0.866095 -0.074376
H -5.438293 -3.316547 -0.017731
H -3.312166 -4.611073 0.066607
H -0.866439 -4.663870 0.093575
H 1.285192 -3.510226 0.099765
H -5.314915 1.101496 0.345106
H -5.022163 3.485373 0.923053

H -2.883665 4.654439 0.474694
H 1.469316 3.321171 0.048080
H -0.562868 4.605653 -0.220987
H 5.418587 1.324900 2.052983
H 5.596324 1.365553 0.268366
H 4.913123 2.772553 1.127805
47
[BP-H]_anion_isomer_d_conf_2 Eopt -1301.584254
O 3.048698 -2.829395 0.786000
C 2.897356 -1.771085 0.200329
O 3.911903 -1.193078 -0.481413
C 5.204912 -1.761203 -0.279552
C 1.663369 -0.970165 0.129622
C 0.377184 -1.586041 0.090929
C -0.783184 -0.779456 0.011495
C -2.083051 -1.376721 -0.061851
C -3.260499 -0.569636 -0.115418
C -4.498988 -1.207575 -0.218599
C -4.611177 -2.600994 -0.250386
C -3.476263 -3.391848 -0.177609
C -2.207883 -2.795039 -0.087197
C -1.016277 -3.588799 -0.024438
C 0.213429 -3.018109 0.062471
C -3.144127 0.897301 -0.060686
C -4.241023 1.734278 0.117322
C -4.020623 3.111820 0.471750
C -2.812772 3.701630 0.314873
C -1.724630 2.948458 -0.418819
H -1.881149 3.094808 -1.514256
C -1.831034 1.458525 -0.123203
C -0.689141 0.660944 -0.038800
C 0.621939 1.250942 0.018690
C 0.706299 2.703771 0.118374
C -0.367782 3.488977 -0.055301
C 1.746322 0.435179 0.093141
C 3.079308 1.102001 0.290293
O 3.485991 1.763048 -0.796991
C 4.737922 2.443642 -0.671822
O 3.697440 1.088868 1.333231
H 5.486036 -1.701837 0.775797
H 5.888215 -1.166752 -0.886219
H 5.224104 -2.803898 -0.605397
H -5.405597 -0.614756 -0.284777
H -5.593288 -3.058766 -0.332363
H -3.550795 -4.476920 -0.195299
H -1.115841 -4.671978 -0.049589

H 1.094453 -3.645459 0.112632
H -5.241598 1.329639 0.220974
H -4.842633 3.662609 0.927993
H -2.619343 4.720443 0.645221
H 1.664276 3.156259 0.366544
H -0.272752 4.569719 0.042987
H 5.532954 1.733487 -0.430162
H 4.681455 3.208382 0.107384
H 4.921729 2.904700 -1.641714
47
[BP-H]_anion_isomer_d_conf_4 Eopt -1301.583480
O -3.048424 -2.859757 0.639799
C -2.901486 -1.770107 0.113361
O -3.922029 -1.155811 -0.525139
C -5.212497 -1.738575 -0.349080
C -1.667132 -0.966492 0.083460
C -0.381528 -1.584077 0.035392
C 0.783042 -0.779613 0.033280
C 2.083669 -1.377744 -0.020710
C 3.264130 -0.573025 -0.016303
C 4.505371 -1.213904 -0.036245
C 4.615967 -2.606966 -0.082777
C 3.476602 -3.394351 -0.113499
C 2.206574 -2.795050 -0.081012
C 1.011323 -3.585017 -0.115381
C -0.219878 -3.013192 -0.065163
C 3.147446 0.894020 0.014549
C 4.229934 1.743885 -0.196931
C 3.982446 3.132102 -0.487024
C 2.787599 3.710531 -0.221757
C 1.769977 2.920374 0.571845
H 2.042419 3.002846 1.651373
C 1.843099 1.449973 0.187236
C 0.694905 0.658133 0.132145
C -0.614579 1.250523 0.172792
C -0.700865 2.705655 0.230810
C 0.385743 3.477643 0.387553
C -1.744270 0.439596 0.126375
C -3.082338 1.111039 0.274434
O -3.467332 1.734039 -0.842976
C -4.727656 2.406784 -0.769625
O -3.718890 1.134399 1.305571
H -5.230598 -2.760628 -0.734756
H -5.900881 -1.112128 -0.916462
H -5.487609 -1.741153 0.709480
H 5.415630 -0.623626 -0.006784

H 5.600297 -3.067199 -0.095729
H 3.549232 -4.478737 -0.158661
H 1.109397 -4.666266 -0.186678
H -1.102953 -3.638852 -0.089316
H 5.221592 1.347496 -0.385082
H 4.767463 3.700345 -0.985255
H 2.562504 4.736950 -0.504871
H -1.675899 3.175260 0.121463
H 0.280058 4.561742 0.413346
H -4.895045 2.829354 -1.759783
H -4.694824 3.200636 -0.018669
H -5.520954 1.698143 -0.518018
47
[BP-H]_anion_isomer_e_conf_1 Eopt -1301.622299
O 3.402570 2.140500 -0.929164
C 3.058304 1.343682 -0.085248
O 3.819593 1.014084 0.967594
C 5.140840 1.564300 0.968174
C 1.738038 0.629112 -0.062196
C 0.548531 1.405986 -0.049198
C 0.566078 2.835617 -0.023987
C -0.588757 3.555197 0.005132
C -1.874247 2.915884 0.003633
C -3.060651 3.665954 0.001624
C -4.290717 3.005650 0.002019
C -4.368759 1.622073 -0.000190
C -3.197850 0.811978 -0.008041
C -1.925277 1.486538 0.001376
C -0.708245 0.732658 -0.008434
C -0.755801 -0.696505 0.023662
C -2.028234 -1.358486 0.061292
C -3.236573 -0.606500 -0.023996
C -4.459989 -1.349550 -0.284069
C -4.538269 -2.690453 -0.181579
C -3.383448 -3.485214 0.369472
H -3.527858 -3.638923 1.455200
H -3.353652 -4.491356 -0.066783
C -2.064774 -2.777804 0.131792
C -0.874782 -3.490828 0.078263
C 0.370749 -2.868288 0.025680
C 0.454486 -1.463802 0.027402
C 1.708299 -0.750429 -0.014793
C 2.988372 -1.510600 -0.005894
O 3.859549 -1.042247 -0.918529
C 5.172179 -1.606359 -0.867745
O 3.250846 -2.447429 0.719171

H 5.668410 1.283560 0.052521
H 5.100437 2.653503 1.046201
H 5.636542 1.140555 1.841025
H 1.518639 3.355592 -0.033428
H -0.555409 4.642364 0.023581
H -3.007294 4.751649 0.004512
H -5.210494 3.587115 0.013270
H -5.346019 1.151419 0.030335
H -5.326299 -0.801390 -0.648709
H -5.451445 -3.212830 -0.458406
H -0.915954 -4.579422 0.108238
H 1.272388 -3.467982 0.013202
H 5.612197 -1.459597 0.122793
H 5.138108 -2.674561 -1.095456
H 5.750231 -1.077828 -1.625566
47
[BP-H]_anion_isomer_e_conf_2 Eopt -1301.621251
O -3.819981 1.044283 1.268419
C -3.142194 1.087772 0.264736
O -3.497661 1.749315 -0.838806
C -4.775423 2.392808 -0.787113
C -1.788493 0.446863 0.132391
C -0.649449 1.291373 0.130479
C -0.756065 2.714228 0.219722
C 0.350698 3.506009 0.225954
C 1.672054 2.949246 0.135841
C 2.808444 3.771756 0.111722
C 4.076032 3.190679 0.027937
C 4.239052 1.816675 -0.037306
C 3.120810 0.934397 -0.027965
C 1.811632 1.526664 0.068717
C 0.645816 0.697857 0.081685
C 0.779042 -0.725372 0.047960
C 2.089479 -1.306900 -0.003864
C 3.244406 -0.476588 -0.107879
C 4.500195 -1.129529 -0.445502
C 4.664884 -2.465726 -0.410950
C 3.583026 -3.360655 0.133845
H 3.785150 -3.574012 1.199860
H 3.592664 -4.337634 -0.365418
C 2.215020 -2.723065 -0.002385
C 1.068383 -3.504728 -0.029296
C -0.213993 -2.958859 0.007572
C -0.382763 -1.564784 0.074820
C -1.679672 -0.928829 0.120356
C -2.916406 -1.750047 0.184589

O -3.895831 -1.241162 -0.586768
C -5.185934 -1.835441 -0.429700
O -3.071021 -2.756557 0.845696
H -4.791902 3.146571 0.004308
H -5.562111 1.655503 -0.607826
H -4.908595 2.862364 -1.760988
H -1.739167 3.173897 0.285574
H 0.251768 4.586983 0.295644
H 2.689764 4.850943 0.164720
H 4.957721 3.828485 0.022888
H 5.243746 1.408330 -0.071113
H 5.318402 -0.512285 -0.810582
H 5.599346 -2.914525 -0.740757
H 1.175477 -4.589057 -0.051748
H -1.077620 -3.611907 0.011728
H -5.843254 -1.301184 -1.115309
H -5.153742 -2.896439 -0.688059
H -5.533187 -1.717886 0.600534
47
[BP-H]_anion_isomer_e_conf_3 Eopt -1301.622185
O 3.418982 2.131836 0.917993
C 3.059535 1.343512 0.072399
O 3.802538 1.024053 -0.996626
C 5.123282 1.575028 -1.015763
C 1.738763 0.629372 0.063051
C 0.548849 1.405749 0.078838
C 0.565377 2.835500 0.090453
C -0.590137 3.554560 0.090847
C -1.875137 2.914814 0.072390
C -3.061441 3.665000 0.068207
C -4.291266 3.004808 0.043639
C -4.368794 1.621620 0.013448
C -3.197792 0.811504 0.003036
C -1.925594 1.485556 0.047502
C -0.708171 0.732085 0.047801
C -0.755328 -0.697161 0.012139
C -2.027732 -1.360114 0.021797
C -3.236215 -0.606319 -0.043329
C -4.459516 -1.343216 -0.321180
C -4.537811 -2.686245 -0.253636
C -3.382133 -3.496118 0.272533
H -3.525733 -3.682683 1.353202
H -3.352192 -4.488589 -0.193931
C -2.063876 -2.781010 0.055239
C -0.873523 -3.491609 -0.014569
C 0.371659 -2.867818 -0.063047

C 0.454964 -1.463567 -0.030339
C 1.708785 -0.749314 -0.004761
C 2.989156 -1.508429 -0.037176
O 3.870945 -1.049917 0.870137
C 5.183153 -1.612771 0.797197
O 3.243102 -2.437492 -0.775184
H 5.080903 2.664771 -1.084775
H 5.603955 1.158328 -1.900340
H 5.666803 1.287749 -0.111568
H 1.517517 3.355698 0.107951
H -0.557552 4.641832 0.104254
H -3.008160 4.750485 0.089419
H -5.211309 3.585850 0.054911
H -5.346463 1.151092 0.022227
H -5.326754 -0.786769 -0.670338
H -5.451641 -3.200790 -0.542722
H -0.914021 -4.580648 -0.009813
H 1.272377 -3.466089 -0.119549
H 5.152404 -2.683050 1.015418
H 5.610292 -1.456609 -0.197531
H 5.770685 -1.090931 1.552341
47
[BP-H]_anion_isomer_f_conf_1 Eopt -1301.599239
O -3.251202 -2.565788 -0.570207
C -3.008832 -1.529842 0.028730
O -3.959181 -0.923406 0.780007
C -5.282209 -1.436986 0.643993
C -1.734052 -0.800141 0.047570
C -0.479001 -1.494550 -0.012625
C 0.731409 -0.769996 0.006584
C 1.994007 -1.456181 -0.023815
C 3.231724 -0.740245 -0.022148
C 4.417498 -1.469540 -0.027017
C 4.432512 -2.871605 -0.047048
C 3.244147 -3.572839 -0.057912
C 2.018285 -2.879559 -0.043222
C 0.776568 -3.588794 -0.037926
C -0.413316 -2.932609 -0.023405
C 3.224871 0.746989 -0.018258
C 4.368644 1.477646 -0.060762
C 4.436746 2.983499 -0.038933
H 4.988453 3.345867 -0.925377
C 3.064086 3.594205 0.022956
C 1.919794 2.860419 0.057439
C 1.920801 1.400974 0.040466
C 0.733578 0.680188 0.058661

C -0.545236 1.350222 0.126885
C -0.538682 2.797186 0.134368
C 0.613809 3.502293 0.103024
C -1.724451 0.604110 0.130602
C -3.021907 1.362223 0.120567
O -3.694924 1.168797 -1.023857
C -4.984705 1.782101 -1.088262
O -3.410471 2.099711 0.998786
H -5.328802 -2.477681 0.974324
H -5.615112 -1.372325 -0.396508
H -5.909116 -0.814124 1.282806
H 5.371641 -0.953946 -0.014116
H 5.383467 -3.397303 -0.051746
H 3.235199 -4.660473 -0.073216
H 0.802392 -4.676549 -0.041486
H -1.336521 -3.497637 -0.022749
H 5.329962 0.974250 -0.113183
H 5.056470 3.317554 0.813237
H 2.989333 4.681230 0.034883
H -1.484763 3.328608 0.172221
H 0.583949 4.590771 0.109715
H -4.894297 2.870818 -1.054308
H -5.414720 1.468554 -2.039180
H -5.607831 1.442868 -0.256219
47
[BP-H]_anion_isomer_f_conf_2 Eopt -1301.598362
O -3.101932 -2.812207 0.703167
C -2.948493 -1.725584 0.167464
O -3.981572 -1.102258 -0.449299
C -5.274595 -1.655338 -0.216171
C -1.710360 -0.941615 0.099181
C -0.421222 -1.575898 0.060346
C 0.751583 -0.793118 0.018730
C 2.045163 -1.415903 -0.044035
C 3.246142 -0.639717 -0.068061
C 4.463970 -1.309600 -0.143906
C 4.545874 -2.709015 -0.189853
C 3.393928 -3.467836 -0.163329
C 2.137115 -2.835711 -0.092992
C 0.931422 -3.603887 -0.077359
C -0.287771 -3.007387 -0.004688
C 3.168466 0.844892 -0.010031
C 4.276025 1.630145 0.000569
C 4.269361 3.137335 0.037709
H 4.815997 3.534835 -0.837114
C 2.867873 3.680337 0.087820

C 1.759974 2.892082 0.083299
C 1.833683 1.434786 0.029702
C 0.684195 0.656351 0.039297
C -0.625580 1.262418 0.076044
C -0.691871 2.705719 0.141754
C 0.423599 3.468787 0.143282
C -1.766957 0.462720 0.092243
C -3.088133 1.162329 0.259506
O -3.485232 1.777086 -0.858890
C -4.728156 2.478478 -0.767302
O -3.699766 1.218661 1.304521
H -5.971407 -1.026803 -0.771269
H -5.327385 -2.684355 -0.579813
H -5.513499 -1.632114 0.851119
H 5.391494 -0.747947 -0.170914
H 5.519998 -3.186988 -0.247884
H 3.437021 -4.554159 -0.198969
H 1.008622 -4.687988 -0.128582
H -1.182448 -3.616300 0.009282
H 5.262049 1.174491 -0.021684
H 4.859300 3.492365 0.901962
H 2.741550 4.761649 0.133671
H -1.664229 3.190648 0.190980
H 0.340985 4.553250 0.194250
H -4.661145 3.282573 -0.029573
H -5.531158 1.791832 -0.487035
H -4.909145 2.890135 -1.759735
47
[BP-H]_anion_isomer_g_conf_1 Eopt -1301.626027
O -3.419211 2.144490 -0.911431
C -3.065497 1.345386 -0.073445
O -3.814255 1.017018 0.989207
C -5.132758 1.572853 1.009092
C -1.746336 0.628719 -0.065167
C -0.559279 1.401925 -0.067310
C -0.565297 2.830214 -0.061750
C 0.595522 3.543689 -0.048333
C 1.875245 2.895105 -0.038397
C 3.072087 3.630976 -0.036780
C 4.296605 2.962238 -0.022303
C 4.363748 1.576554 -0.006271
C 3.179343 0.783526 -0.005438
C 1.915016 1.466212 -0.025923
C 0.697260 0.717351 -0.030310
C 0.745286 -0.705470 0.003730
C 2.025060 -1.370141 0.020552

C 3.220071 -0.630497 0.012114
C 4.575343 -1.310563 0.025679
H 5.164856 -0.965656 0.894437
H 5.172588 -0.985806 -0.845478
C 4.495494 -2.811207 0.043179
C 3.331112 -3.479818 0.049924
C 2.042986 -2.805885 0.040077
C 0.847814 -3.511327 0.047652
C -0.394897 -2.880276 0.044999
C -0.468650 -1.473879 0.027572
C -1.717246 -0.753890 -0.007194
C -3.001112 -1.506619 0.009336
O -3.874266 -1.033728 -0.900381
C -5.190519 -1.587635 -0.841110
O -3.268116 -2.441464 0.735494
H -5.619127 1.147445 1.886418
H -5.673531 1.298737 0.099173
H -5.086623 2.661549 1.091517
H -1.514160 3.356741 -0.076628
H 0.569035 4.631174 -0.047540
H 3.029770 4.717283 -0.047107
H 5.219923 3.538160 -0.022090
H 5.335222 1.094498 0.006116
H 5.436295 -3.358771 0.050815
H 3.326290 -4.569547 0.063347
H 0.887639 -4.600262 0.061190
H -1.300514 -3.472664 0.069613
H -5.166451 -2.656004 -1.069484
H -5.623110 -1.438279 0.152357
H -5.769721 -1.054372 -1.594814
47
[BP-H]_anion_isomer_g_conf_2 Eopt -1301.624886
O -3.816049 1.057069 1.280523
C -3.145340 1.096830 0.271779
O -3.507919 1.758002 -0.829943
C -4.783082 2.405511 -0.768419
C -1.794455 0.452091 0.131215
C -0.655954 1.290597 0.113879
C -0.747874 2.713826 0.185071
C 0.366791 3.497289 0.177671
C 1.681942 2.926719 0.099312
C 2.832191 3.732349 0.080629
C 4.093665 3.138502 0.010454
C 4.242898 1.760521 -0.040330
C 3.108154 0.897468 -0.023667
C 1.807021 1.503140 0.044144

C 0.637674 0.682474 0.061502
C 0.767169 -0.734713 0.029709
C 2.082140 -1.320989 -0.044035
C 3.230882 -0.510816 -0.074820
C 4.621760 -1.109499 -0.157278
H 5.155420 -0.711433 -1.039234
H 5.233156 -0.770192 0.698304
C 4.628992 -2.611536 -0.207913
C 3.507248 -3.348416 -0.176650
C 2.183643 -2.752511 -0.091718
C 1.033045 -3.527111 -0.056988
C -0.242999 -2.971291 0.030723
C -0.399198 -1.573474 0.078397
C -1.689055 -0.927274 0.131704
C -2.931074 -1.739023 0.207544
O -3.909189 -1.231062 -0.567275
C -5.202693 -1.814785 -0.401270
O -3.092963 -2.737949 0.878474
H -4.790383 3.160932 0.021583
H -5.570622 1.671205 -0.580711
H -4.923353 2.873590 -1.742032
H -1.726557 3.183570 0.245726
H 0.276942 4.579916 0.231712
H 2.726891 4.813584 0.122624
H 4.980541 3.768935 -0.003330
H 5.240563 1.338125 -0.092182
H 5.598903 -3.101636 -0.272231
H 3.565709 -4.435960 -0.215191
H 1.135306 -4.611363 -0.095210
H -1.110919 -3.616533 0.073199
H -5.858952 -1.280533 -1.087972
H -5.179284 -2.877737 -0.652596
H -5.545340 -1.688233 0.629442
47
[BP-H]_anion_isomer_h_conf_1 Eopt -1301.592910
O 3.046388 -2.823002 -0.696773
C 2.903320 -1.762234 -0.118048
O 3.905599 -1.192287 0.580370
C 5.195509 -1.784295 0.420262
C 1.673004 -0.940762 -0.091491
C 0.371473 -1.556131 -0.048000
C -0.780353 -0.750195 -0.086080
C -2.089794 -1.351500 -0.025272
C -3.271358 -0.563643 -0.120058
C -4.504782 -1.192352 -0.074575
C -4.619740 -2.587466 0.075534

C -3.484795 -3.362560 0.173253
C -2.208250 -2.760374 0.119451
C -1.016803 -3.547919 0.194019
C 0.214602 -2.977156 0.105243
C -3.197695 0.931362 -0.350747
H -3.479965 1.108796 -1.415136
C -4.159405 1.726368 0.513289
C -4.007674 3.076461 0.542389
C -2.849400 3.714826 -0.014264
C -1.704360 2.928072 -0.200606
C -1.807172 1.501255 -0.177069
C -0.672613 0.693884 -0.143849
C 0.637576 1.279195 -0.185102
C 0.731199 2.701848 -0.316779
C -0.384027 3.486202 -0.324465
C 1.773031 0.443307 -0.145870
C 3.120172 1.095852 -0.292216
O 3.478429 1.767699 0.804140
C 4.745654 2.429117 0.735291
O 3.785759 1.059449 -1.304368
H 5.870018 -1.197033 1.043095
H 5.506803 -1.736080 -0.626996
H 5.185618 -2.824670 0.753329
H -5.408703 -0.596062 -0.173993
H -5.604259 -3.046513 0.107045
H -3.552400 -4.442585 0.283616
H -1.113698 -4.624437 0.317461
H 1.098699 -3.600884 0.153638
H -4.971096 1.223571 1.031411
H -4.740040 3.691772 1.065835
H -2.756502 4.797784 0.009759
H 1.710001 3.169045 -0.397728
H -0.284659 4.567763 -0.400113
H 4.742005 3.180623 -0.058494
H 4.883693 2.903956 1.705976
H 5.541166 1.703097 0.548899
47
[BP-H]_anion_isomer_h_conf_2 Eopt -1301.593845
O 3.215597 -2.537474 -0.559394
C 2.972737 -1.530872 0.078796
O 3.879509 -0.980163 0.909821
C 5.195163 -1.533373 0.847498
C 1.701348 -0.770451 0.053115
C 0.440007 -1.460578 0.006488
C -0.754397 -0.720756 -0.058687
C -2.026484 -1.400493 -0.092275

C -3.247188 -0.680212 -0.217959
C -4.441128 -1.381458 -0.262751
C -4.478782 -2.785762 -0.174826
C -3.305086 -3.496465 -0.048288
C -2.066516 -2.818936 -0.010897
C -0.835070 -3.538911 0.094682
C 0.362112 -2.894228 0.093530
C -3.251290 0.824855 -0.384637
H -3.479839 1.031115 -1.456810
C -4.311192 1.521480 0.449235
C -4.244281 2.875143 0.549886
C -3.094894 3.605875 0.100266
C -1.895627 2.896308 -0.053377
C -1.909833 1.467175 -0.103012
C -0.729547 0.728069 -0.045195
C 0.544280 1.391686 0.010357
C 0.553322 2.822685 -0.048598
C -0.608017 3.536308 -0.076939
C 1.725540 0.619107 0.063231
C 3.041498 1.343744 0.059636
O 3.773881 1.028492 -1.018460
C 5.085445 1.598812 -1.059017
O 3.400737 2.141847 0.895598
H 5.797196 -0.942573 1.537797
H 5.185600 -2.581077 1.157660
H 5.592835 -1.458883 -0.168840
H -5.373427 -0.835746 -0.386199
H -5.433984 -3.302510 -0.213462
H -3.312578 -4.582319 0.015352
H -0.873208 -4.623546 0.169625
H 1.278479 -3.467461 0.163261
H -5.122171 0.948739 0.889878
H -5.044087 3.419973 1.052300
H -3.068419 4.689675 0.180972
H 1.502507 3.349584 -0.047698
H -0.572249 4.624454 -0.093820
H 5.647169 1.320910 -0.163032
H 5.558918 1.187752 -1.950141
H 5.026733 2.687781 -1.128927
47
[BP-H]_anion_isomer_h_conf_3 Eopt -1301.592536
O 3.019902 -2.740028 0.966744
C 2.898882 -1.738448 0.286867
O 3.927519 -1.231813 -0.421940
C 5.209677 -1.804267 -0.160335
C 1.670585 -0.926855 0.133519

C 0.371364 -1.546458 0.077249
C -0.776431 -0.742612 -0.043528
C -2.082148 -1.348595 -0.130547
C -3.257748 -0.558695 -0.272898
C -4.486097 -1.191333 -0.369313
C -4.602991 -2.593499 -0.321300
C -3.474232 -3.371080 -0.181324
C -2.201999 -2.764257 -0.089363
C -1.014418 -3.553376 0.020720
C 0.214980 -2.975628 0.091407
C -3.179698 0.949111 -0.391408
H -3.391261 1.201654 -1.457051
C -4.203809 1.677347 0.459427
C -4.060543 3.021281 0.601799
C -2.872330 3.701538 0.172832
C -1.712256 2.932940 0.000890
C -1.806741 1.508676 -0.088439
C -0.671510 0.702790 -0.037832
C 0.636108 1.292166 0.012958
C 0.727820 2.720912 0.017469
C -0.390583 3.500993 0.012750
C 1.770963 0.456840 0.077322
C 3.113038 1.119616 0.225164
O 3.520756 1.694034 -0.908885
C 4.788030 2.356071 -0.843705
O 3.734499 1.170028 1.264199
H 5.908619 -1.271940 -0.805213
H 5.479820 -1.664759 0.890085
H 5.211638 -2.869656 -0.401968
H -5.383173 -0.590819 -0.500735
H -5.583397 -3.055566 -0.400300
H -3.542829 -4.456169 -0.148039
H -1.111741 -4.636789 0.037521
H 1.096455 -3.599687 0.171797
H -5.044527 1.135767 0.883797
H -4.829520 3.594697 1.120288
H -2.786811 4.779043 0.289583
H 1.706261 3.194979 0.039790
H -0.293913 4.585051 0.042985
H 4.753714 3.177097 -0.122867
H 4.971938 2.739957 -1.846491
H 5.569848 1.648307 -0.556404
47
[BP-H]_anion_isomer_h_conf_6 Eopt -1301.593549
O 3.169541 -2.482083 0.830532
C 2.964452 -1.541165 0.087658

O	3.916279	-1.069377	-0.741286
C	5.225340	-1.610641	-0.555538
C	1.696168	-0.782807	-0.028196
C	0.429982	-1.465610	0.008421
C	-0.760915	-0.723098	-0.082929
C	-2.037389	-1.395211	-0.066159
C	-3.257680	-0.670563	-0.168768
C	-4.456485	-1.364720	-0.164938
C	-4.499332	-2.767116	-0.053526
C	-3.326062	-3.482473	0.049683
C	-2.083110	-2.811860	0.040387
C	-0.852939	-3.538112	0.112425
C	0.347194	-2.899191	0.089638
C	-3.264186	0.832014	-0.349561
H	-3.565309	1.031580	-1.404942
C	-4.258491	1.545660	0.547829
C	-4.180536	2.901417	0.611969
C	-3.066395	3.616265	0.059188
C	-1.880262	2.898625	-0.156744
C	-1.904027	1.469706	-0.170116
C	-0.726665	0.723723	-0.151728
C	0.550793	1.378543	-0.209380
C	0.564895	2.808635	-0.285350
C	-0.592576	3.529599	-0.260501
C	1.728964	0.600208	-0.157197
C	3.047002	1.321366	-0.156642
O	3.721517	1.114443	0.983123
C	5.029861	1.691499	1.036682
O	3.451370	2.033692	-1.047728
H	5.865610	-1.085643	-1.264339
H	5.566974	-1.439855	0.469503
H	5.230157	-2.682856	-0.766031
H	-5.388414	-0.813069	-0.265317
H	-5.457953	-3.278960	-0.054686
H	-3.337601	-4.567097	0.131184
H	-0.894622	-4.623203	0.178358
H	1.261658	-3.476912	0.144295
H	-5.032476	0.982298	1.061597
H	-4.938334	3.462044	1.160121
H	-3.030488	4.701383	0.116213
H	1.515274	3.328608	-0.355339
H	-0.550867	4.617170	-0.294306
H	4.968486	2.781679	0.993070
H	5.638831	1.326933	0.204920
H	5.453809	1.374341	1.988929

47

[BP-H]_anion_isomer_i_conf_1 Eopt -1301.580088

O	-3.315783	2.354586	-0.676222
C	-2.991354	1.449786	0.061405
O	-3.778081	0.992014	1.045567
C	-5.097764	1.544517	1.091275
C	-1.689660	0.711759	0.000803
C	-0.470690	1.435188	-0.021033
C	-0.433916	2.873308	0.026749
C	0.743111	3.546145	-0.020514
C	1.997596	2.846199	-0.084067
C	3.211561	3.561888	-0.088045
C	4.412072	2.874069	-0.097218
C	4.426460	1.474942	-0.082682
C	3.245120	0.723472	-0.063176
C	2.004743	1.430663	-0.103604
C	0.746922	0.701516	-0.089770
C	0.730673	-0.703802	-0.185999
C	2.008186	-1.458691	-0.523385
H	2.060411	-1.502730	-1.643999
C	3.242783	-0.734315	-0.007889
C	4.343756	-1.463219	0.364135
C	4.347362	-2.884345	0.441501
C	3.135250	-3.553227	0.325103
C	1.949215	-2.887818	-0.000269
C	0.702536	-3.537264	-0.036233
C	-0.483571	-2.859667	-0.222487
C	-0.487796	-1.419741	-0.153133
C	-1.694123	-0.675122	-0.030490
C	-3.006554	-1.399036	0.014052
O	-3.834150	-0.979657	-0.956344
C	-5.157929	-1.521845	-0.914723
O	-3.306786	-2.257863	0.811847
H	-5.606510	1.390563	0.135799
H	-5.612592	1.012196	1.890419
H	-5.055103	2.613442	1.313775
H	-1.366509	3.422984	0.087786
H	0.758712	4.633234	0.008083
H	3.187577	4.649009	-0.083345
H	5.353472	3.417250	-0.117435
H	5.385307	0.966006	-0.104348
H	5.246340	-0.940050	0.675750
H	5.248463	-3.408565	0.744846
H	3.080808	-4.621003	0.542668
H	0.678704	-4.617411	0.115440
H	-1.423969	-3.397274	-0.219821
H	-5.706090	-1.024211	-1.714204

H -5.133182 -2.600669 -1.086421
H -5.621369 -1.317578 0.054395
47
[BP-H]_anion_isomer_i_conf_2 Eopt -1301.578312
O 3.788170 0.928057 1.369448
C 3.095749 1.119736 0.392813
O 3.456114 1.909882 -0.621580
C 4.750636 2.511764 -0.505679
C 1.745979 0.498074 0.184735
C 0.586789 1.307338 0.148096
C 0.656441 2.740083 0.260815
C -0.461962 3.503726 0.184944
C -1.759712 2.902155 0.028681
C -2.915549 3.707468 -0.003983
C -4.161703 3.113625 -0.099747
C -4.281219 1.720123 -0.143326
C -3.161392 0.880495 -0.097398
C -1.872187 1.492816 -0.050506
C -0.675065 0.669221 -0.007938
C -0.754777 -0.728451 -0.157422
C -2.066139 -1.373483 -0.581605
H -2.066700 -1.377789 -1.704282
C -3.268799 -0.574847 -0.100058
C -4.437859 -1.231398 0.188679
C -4.549445 -2.650503 0.208825
C -3.385361 -3.404684 0.130652
C -2.137671 -2.819430 -0.108751
C -0.941375 -3.557725 -0.104298
C 0.300198 -2.965807 -0.208715
C 0.406177 -1.533687 -0.093978
C 1.657132 -0.881851 0.101358
C 2.923290 -1.677014 0.188026
O 3.847866 -1.214222 -0.668988
C 5.152953 -1.786974 -0.545366
O 3.123685 -2.609807 0.932749
H 4.883498 3.100264 -1.412642
H 5.519511 1.737893 -0.436182
H 4.795585 3.155106 0.376558
H 1.623378 3.214558 0.401161
H -0.399893 4.586608 0.262857
H -2.811858 4.788619 0.048042
H -5.057804 3.727512 -0.142457
H -5.273008 1.287064 -0.230885
H -5.315159 -0.653796 0.475301
H -5.501545 -3.115634 0.445509
H -3.421961 -4.480298 0.309845

H -1.004527 -4.640571 0.013220
H 1.197768 -3.571179 -0.175703
H 5.549877 -1.605120 0.456941
H 5.119005 -2.861645 -0.738767
H 5.766379 -1.287515 -1.294669
47
[BP-H]_anion_isomer_j_conf_1 Eopt -1301.604711
O -3.169918 -2.748769 -0.109001
C -2.948015 -1.560421 -0.343765
O -3.959959 -0.782286 -0.847230
C -5.264701 -1.336833 -0.774176
C -1.716341 -0.827005 -0.199616
C -0.437586 -1.492850 -0.008070
C 0.755199 -0.765847 -0.130088
C 2.017146 -1.401870 0.023614
C 3.247244 -0.667030 -0.077188
C 4.448675 -1.354693 -0.069023
C 4.502424 -2.754166 0.105653
C 3.339479 -3.464248 0.293497
C 2.085577 -2.808708 0.253395
C 0.867687 -3.521613 0.408693
C -0.340536 -2.891470 0.302802
C 3.185580 0.812215 -0.082208
C 1.952601 1.454933 -0.264357
C 0.714656 0.660767 -0.654249
H 0.729110 0.595086 -1.766433
C -0.582682 1.362471 -0.277303
C -0.570313 2.801120 -0.207438
C 0.578204 3.519163 -0.241429
C -1.725424 0.606356 -0.176621
C -3.015567 1.327172 0.107317
O -3.542256 0.948159 1.283794
C -4.818372 1.508338 1.591319
O -3.516989 2.187670 -0.584189
C 1.874871 2.861392 -0.174141
C 3.036037 3.609583 0.056129
C 4.262345 2.972991 0.219288
C 4.333104 1.585999 0.169257
H -5.538533 -1.557698 0.263301
H -5.934535 -0.578916 -1.184474
H -5.337192 -2.253673 -1.365286
H 5.385156 -0.818225 -0.184401
H 5.465565 -3.256802 0.109860
H 3.362097 -4.539401 0.459525
H 0.910106 -4.590173 0.611699
H -1.255167 -3.454539 0.429468

H -1.518138 3.326090 -0.140239
H 0.554171 4.605684 -0.206620
H -4.747250 2.592682 1.711544
H -5.535530 1.277883 0.798376
H -5.127949 1.045839 2.528582
H 2.963431 4.692936 0.124778
H 5.160447 3.554750 0.409057
H 5.289440 1.105818 0.346529
47
[BP-H]_anion_isomer_j_conf_2 Eopt -1301.603693
O 2.979818 -3.023525 0.144613
C 2.857446 -1.817846 -0.072612
O 3.958102 -1.096393 -0.456972
C 5.212388 -1.742787 -0.299296
C 1.666920 -1.006771 -0.015283
C 0.334467 -1.589241 0.068601
C -0.798975 -0.780276 -0.098331
C -2.107444 -1.333523 -0.044010
C -3.277653 -0.510362 -0.176401
C -4.520708 -1.112330 -0.267943
C -4.677661 -2.511303 -0.164920
C -3.578271 -3.308155 0.055200
C -2.283099 -2.740087 0.117535
C -1.126477 -3.539546 0.313665
C 0.124642 -2.988784 0.312396
C -3.118014 0.959838 -0.101990
C -1.837152 1.522069 -0.192963
C -0.640548 0.658391 -0.561570
H -0.610715 0.636397 -1.675244
C 0.678897 1.252188 -0.096702
C 0.765325 2.683099 0.026111
C -0.327087 3.484164 -0.022491
C 1.763626 0.420295 0.034652
C 3.072930 1.063129 0.410021
O 3.618839 1.751908 -0.602196
C 4.860138 2.392672 -0.306377
O 3.557703 1.031671 1.520735
C -1.667036 2.914668 -0.035190
C -2.785466 3.730088 0.179182
C -4.058677 3.173909 0.255476
C -4.222027 1.799102 0.132947
H 5.963353 -1.022002 -0.627192
H 5.385301 -2.009819 0.748157
H 5.271026 -2.644341 -0.914833
H -5.410792 -0.506984 -0.407700
H -5.670691 -2.945713 -0.238957

H -3.682924 -4.385206 0.169514
H -1.250549 -4.610362 0.464628
H 0.989527 -3.617940 0.472084
H 1.743402 3.139677 0.162261
H -0.230189 4.563649 0.062949
H 5.599675 1.657426 0.021854
H 4.728245 3.147343 0.474135
H 5.180427 2.863771 -1.235530
H -2.644158 4.801732 0.302942
H -4.923109 3.808229 0.432896
H -5.216439 1.379244 0.240350
47
[BP-H]_anion_isomer_k_conf_1 Eopt -1301.608955
C -0.711981 2.803237 0.352779
C -0.699395 1.395891 0.067866
C 0.547269 0.737139 0.109187
C 1.757124 1.462887 0.332590
C 1.702827 2.855560 0.630333
C 0.429025 3.493747 0.640819
C 0.616516 -0.694570 -0.162234
C 3.037225 0.827890 0.241663
C 3.107952 -0.585220 -0.182537
C 1.890607 -1.315737 -0.365534
C 4.316514 -1.231033 -0.410420
C 4.177446 1.570058 0.526808
C 4.109899 2.932293 0.867468
C 2.888457 3.570984 0.903725
H 2.819209 4.630361 1.141866
H 5.024624 3.475837 1.086769
H -1.663667 3.318183 0.372924
H 0.379559 4.552233 0.888993
C -1.907881 0.639566 -0.194904
C -1.837253 -0.811822 0.117148
C -0.554911 -1.457495 -0.222256
C -0.467259 -2.820789 -0.623110
C 0.738786 -3.417086 -0.878804
C 1.952532 -2.692218 -0.731836
H -1.382455 -3.390972 -0.731260
H 0.785296 -4.457900 -1.191767
C 4.369759 -2.584132 -0.794717
H 5.335887 -3.051541 -0.964940
C 3.209485 -3.307538 -0.947997
H 3.238172 -4.356292 -1.235106
H 5.156364 1.103731 0.487719
H 5.253623 -0.696389 -0.298431
C -2.857519 -1.485464 0.710185

C -3.074879 1.179943 -0.760375
O -4.032712 -0.931850 1.053608
O -4.155080 0.547430 -0.958811
O -2.778422 -2.822817 0.984041
O -3.030035 2.489585 -1.157436
C -4.229018 3.018411 -1.705035
H -4.514332 2.490705 -2.619655
H -4.010121 4.062958 -1.935031
C -3.312872 -3.196273 2.248990
H -3.075398 -4.253914 2.377764
H -2.843407 -2.615372 3.052801
H -5.053613 2.960409 -0.988555
H -4.396298 -3.054283 2.281417
H -4.274178 -0.305892 0.284460
46
[BP(COOMe2)]_anion_conf_1 Eopt -1301.030795
C 0.491007 2.852758 0.231641
C 0.538840 1.449939 0.081058
C -0.691325 0.713099 0.048311
C -1.947904 1.410422 0.111162
C -1.952181 2.838288 0.240540
C -0.709925 3.524884 0.309420
C -0.681420 -0.704648 -0.039957
C -3.182976 0.697887 0.056143
C -3.167237 -0.741957 -0.068385
C -1.918061 -1.428806 -0.104589
C -4.361746 -1.507559 -0.150323
C -4.394686 1.435691 0.127646
C -4.382209 2.820336 0.248273
C -3.186450 3.527406 0.304699
H -3.182493 4.610354 0.402035
H -5.327237 3.356860 0.301687
H 1.415860 3.416472 0.286659
H -0.721172 4.606360 0.425100
C 1.774913 0.707328 0.019584
C 1.772671 -0.665982 -0.012950
C 0.561462 -1.418292 -0.061956
C 0.551545 -2.830128 -0.171735
C -0.627783 -3.527910 -0.245675
C -1.890612 -2.858940 -0.212736
H 1.493559 -3.372936 -0.199449
H -0.619388 -4.611927 -0.331458
C -4.319107 -2.888901 -0.257158
H -5.250531 -3.447375 -0.319266
C -3.102516 -3.571839 -0.286440
H -3.075423 -4.655656 -0.369243

H -5.349972 0.925278 0.093268
H -5.327996 -1.016978 -0.132972
C 3.073352 -1.413213 -0.104448
C 3.108180 1.376715 0.018552
O 3.769336 -1.452451 -1.095472
O 4.051826 1.014836 0.693198
O 3.351648 -2.074038 1.021479
O 3.184397 2.402967 -0.837548
C 4.444917 3.079684 -0.886589
H 4.694695 3.492858 0.093787
H 4.319273 3.879990 -1.615114
C 4.571837 -2.822499 1.013101
H 4.642788 -3.280320 1.999055
H 4.541790 -3.592234 0.237515
H 5.232127 2.393317 -1.207230
H 5.420954 -2.157145 0.839252
46
[BP(COOMe2)]_anion_conf_2 Eopt -1301.032271
C 0.682247 2.714618 0.177103
C 0.604239 1.301037 0.108890
C -0.683190 0.670402 0.057962
C -1.870063 1.475568 0.043553
C -1.751997 2.904053 0.099764
C -0.448980 3.489561 0.172198
C -0.785782 -0.745798 0.025117
C -3.160309 0.871635 -0.019885
C -3.269207 -0.568562 -0.077646
C -2.083526 -1.362016 -0.050746
C -4.524250 -1.228285 -0.158537
C -4.302575 1.717346 -0.027176
C -4.171874 3.095694 0.024323
C -2.913472 3.697385 0.086718
H -2.816704 4.779579 0.128731
H -5.064929 3.716621 0.017361
H 1.655199 3.196554 0.232673
H -0.371883 4.573055 0.223501
C 1.763162 0.470905 0.127370
C 1.674179 -0.902190 0.129533
C 0.391796 -1.562515 0.068720
C 0.255996 -2.965674 0.004131
C -0.984615 -3.560861 -0.082436
C -2.178621 -2.791580 -0.105879
H 1.143871 -3.587391 0.029978
H -1.065401 -4.644541 -0.130321
C -4.600077 -2.615618 -0.210102
H -5.576504 -3.091638 -0.271983

C -3.453753 -3.401032 -0.184684
H -3.519169 -4.485622 -0.225424
H -5.297855 1.290572 -0.070841
H -5.444121 -0.656153 -0.184196
C 2.926202 -1.702107 0.231908
C 3.105641 1.132250 0.263185
O 3.090128 -2.673736 0.940460
O 3.780192 1.104126 1.269935
O 3.897784 -1.214389 -0.559654
O 3.459378 1.789766 -0.843435
C 4.728161 2.450279 -0.789380
H 4.730760 3.208966 -0.002562
H 4.860107 2.915435 -1.765539
C 5.194706 -1.788641 -0.380415
H 5.846563 -1.272205 -1.084522
H 5.538999 -1.630402 0.645179
H 5.523535 1.724409 -0.601688
H 5.173452 -2.858493 -0.600333
46
[BP(COOMe2)]_conf_1 Eopt -1300.948469
C -0.521866 -2.851812 0.198657
C -0.538019 -1.419703 0.074831
C 0.684580 -0.711190 0.046349
C 1.929156 -1.426300 0.107641
C 1.911850 -2.843276 0.221505
C 0.651616 -3.528953 0.269386
C 0.685053 0.712272 -0.047816
C 3.172707 -0.735032 0.063348
C 3.174003 0.730049 -0.061171
C 1.931849 1.423913 -0.109820
C 4.354191 1.472108 -0.130970
C 4.351062 -1.479784 0.135746
C 4.327515 -2.873007 0.248547
C 3.122716 -3.552593 0.290371
H 3.097582 -4.635855 0.378174
H 5.264580 -3.419367 0.303311
H -1.461210 -3.394228 0.240141
H 0.657721 -4.611599 0.367170
C -1.753024 -0.687025 0.023767
C -1.753953 0.691108 -0.020420
C -0.537031 1.422955 -0.077049
C -0.515553 2.854185 -0.212077
C 0.660021 3.527695 -0.284659
C 1.918601 2.840329 -0.228406
H -1.452576 3.398777 -0.260957
H 0.668429 4.609567 -0.390876

C 4.334359 2.865147 -0.246970
H 5.272838 3.409274 -0.299618
C 3.131183 3.546996 -0.295347
H 3.108512 4.630019 -0.386762
H 5.315751 -0.985855 0.106855
H 5.317620 0.975973 -0.097819
C -3.082677 1.389073 -0.073703
C -3.073488 -1.401225 0.093868
O -3.921175 1.167770 -0.918990
O -3.861878 -1.265290 1.002520
O -3.238394 2.261056 0.921021
O -3.270942 -2.195201 -0.956590
C -4.515482 -2.910545 -0.969927
H -4.581782 -3.569398 -0.100916
H -4.507793 -3.492197 -1.890395
C -4.489864 2.964584 0.941100
H -4.440128 3.623372 1.806693
H -4.611282 3.545159 0.023661
H -5.350933 -2.207129 -0.967593
H -5.315249 2.256979 1.044573
46
[BP(COOMe2)]_conf_2 Eopt -1300.949757
C 0.642630 2.751094 0.199587
C 0.574898 1.316544 0.131324
C -0.686485 0.681718 0.072750
C -1.885392 1.472822 0.043958
C -1.784651 2.889903 0.101324
C -0.488118 3.500300 0.185068
C -0.770872 -0.742122 0.039763
C -3.166447 0.857131 -0.032427
C -3.253664 -0.609362 -0.093388
C -2.056513 -1.378448 -0.047233
C -4.473525 -1.281124 -0.190415
C -4.297826 1.674738 -0.048275
C -4.192078 3.067509 0.007714
C -2.950265 3.673691 0.081265
H -2.860803 4.756087 0.126421
H -5.094592 3.671606 -0.005526
H 1.610932 3.237009 0.267684
H -0.432254 4.584529 0.239831
C 1.743338 0.511579 0.160875
C 1.662598 -0.866414 0.167467
C 0.404611 -1.526277 0.099904
C 0.298163 -2.959031 0.043707
C -0.913938 -3.561381 -0.051500
C -2.127354 -2.797128 -0.095691

H	1.199791	-3.559520	0.079016
H	-0.986859	-4.645123	-0.097098
C	-4.536047	-2.676952	-0.238371
H	-5.503245	-3.165171	-0.314104
C	-3.377376	-3.431694	-0.190121
H	-3.417912	-4.517447	-0.225905
H	-5.289316	1.239568	-0.101639
H	-5.404243	-0.726470	-0.232029
C	2.929722	-1.663621	0.261722
C	3.097038	1.156189	0.272465
O	3.126782	-2.555525	1.055265
O	3.821231	1.032564	1.234919
O	3.829939	-1.255478	-0.637467
O	3.402747	1.874118	-0.806346
C	4.695408	2.497205	-0.788680
H	4.766956	3.198568	0.045858
H	4.779810	3.023082	-1.738445
C	5.135393	-1.837917	-0.524436
H	5.730051	-1.378887	-1.312966
H	5.560050	-1.614152	0.457246
H	5.474830	1.736317	-0.700881
H	5.081726	-2.919140	-0.668553

REFERENCES

1. Lim, C.-H.; Kudisch, M.; Liu, B.; Miyake, G. M., C–N cross-coupling via photoexcitation of nickel–amine complexes. *J. Am. Chem. Soc.* **2018,** *140* (24), 7667-7673.
2. Cole, J. P.; Chen, D. F.; Kudisch, M.; Pearson, R. M.; Lim, C. H.; Miyake, G. M., Organocatalyzed Birch Reduction Driven by Visible Light. *J. Am. Chem. Soc.* **2020,** *142* (31), 13573-13581.
3. Fort, E. H.; Donovan, P. M.; Scott, L. T., Diels− Alder Reactivity of Polycyclic Aromatic Hydrocarbon Bay Regions: Implications for Metal-Free Growth of Single-Chirality Carbon Nanotubes. *J. Am. Chem. Soc.* **2009,** *131* (44), 16006-16007.
4. Zhao, Y.; Truhlar, D. G., The M06 suite of density functionals for main group thermochemistry, thermochemical kinetics, noncovalent interactions, excited states, and transition elements: two new functionals and systematic testing of four M06-class functionals and 12 other functionals. *Theor. Chem. Acc.* **2008,** *120*, 215-241.
5. Francl, M. M.; Pietro, W. J.; Hehre, W. J.; Binkley, J. S.; Gordon, M. S.; DeFrees, D. J.; Pople, J. A., Self-consistent molecular orbital methods. XXIII. A polarization-type basis set for second-row elements. *J. Chem. Phys.* **1982,** *77* (7), 3654-3665.
6. McLean, A.; Chandler, G., Contracted Gaussian basis sets for molecular calculations. I. Second row atoms, Z= 11–18. *J. Chem. Phys.* **1980,** *72* (10), 5639-5648.
7. Krishnan, R.; Binkley, J. S.; Seeger, R.; Pople, J. A., Self-consistent molecular orbital methods. A basis set for correlated wave functions. *J. Chem. Phys.* **1980,** *72* (1), 650-654.
8. Hariharan, P. C.; Pople, J. A., The influence of polarization functions on molecular orbital hydrogenation energies. *Theor. Chim. Acta* **1973,** *28*, 213-222.
9. Hehre, W. J.; Ditchfield, R.; Pople, J. A., Self—consistent molecular orbital methods. XII. Further extensions of Gaussian—type basis sets for use in molecular orbital studies of organic molecules. *J. Chem. Phys.* **1972,** *56* (5), 2257-2261.
10. Grimme, S.; Antony, J.; Ehrlich, S.; Krieg, H., A consistent and accurate ab initio parametrization of density functional dispersion correction (DFT-D) for the 94 elements H-Pu. *J. Chem. Phys.* **2010,** *132* (15).
11. Marenich, A. V.; Cramer, C. J.; Truhlar, D. G., Universal solvation model based on solute electron density and on a continuum model of the solvent defined by the bulk dielectric constant and atomic surface tensions. *J. Phys. Chem. B* **2009,** *113* (18), 6378-6396.
12. Frisch, M. J.; Trucks, G. W.; Schlegel, H. B.; Scuseria, G. E.; Robb, M. A.; Cheeseman, J. R.; Scalmani, G.; Barone, V.; Petersson, G. A.; Nakatsuji, H.; Li, X.; Caricato, M.; Marenich, A. V.; Bloino, J.; Janesko, B. G.; Gomperts, R.; Mennucci, B.; Hratchian, H. P.; Ortiz, J. V.; Izmaylov, A. F.; Sonnenberg, J. L.; Williams; Ding, F.; Lipparini, F.; Egidi, F.; Goings, J.; Peng, B.; Petrone, A.; Henderson, T.; Ranasinghe, D.; Zakrzewski, V. G.; Gao, J.; Rega, N.; Zheng, G.; Liang, W.; Hada, M.; Ehara, M.; Toyota, K.; Fukuda, R.; Hasegawa, J.; Ishida, M.; Nakajima, T.; Honda, Y.; Kitao, O.; Nakai, H.; Vreven, T.; Throssell, K.; Montgomery Jr., J. A.; Peralta, J. E.; Ogliaro, F.; Bearpark, M. J.; Heyd, J. J.; Brothers, E. N.; Kudin, K. N.; Staroverov, V. N.; Keith, T. A.; Kobayashi, R.; Normand, J.; Raghavachari, K.; Rendell, A. P.; Burant, J. C.; Iyengar, S. S.; Tomasi, J.; Cossi, M.; Millam, J. M.; Klene, M.; Adamo, C.; Cammi, R.; Ochterski, J. W.; Martin, R. L.; Morokuma, K.; Farkas, O.; Foresman, J. B.; Fox, D. J. *Gaussian 16 Rev. C.01*, Wallingford, CT, 2016.

13. Alegre-Requena, J. V.; Sowndarya SV, S.; Pérez-Soto, R.; Alturaifi, T. M.; Paton, R. S., AQME: Automated quantum mechanical environments for researchers and educators. *Wiley Interdiscip. Rev. Comput. Mol. Sci.* **2023**, e1663.
14. Schrodinger, LLC, The PyMOL Molecular Graphics System, Version 1.8. 2015.
15. Grimme, S., Supramolecular binding thermodynamics by dispersion-corrected density functional theory. *Chem. Eur. J.* **2012,** *18* (32), 9955-9964.
16. Luchini, G.; Alegre-Requena, J. V.; Funes-Ardoiz, I.; Paton, R. S., GoodVibes: automated thermochemistry for heterogeneous computational chemistry data. *F1000Research* **2020,** *9* (291), 291.
17. Bryantsev, V. S.; Diallo, M. S.; Goddard Iii, W. A., Calculation of solvation free energies of charged solutes using mixed cluster/continuum models. *J. Phys. Chem. B* **2008,** *112* (32), 9709-9719.
18. Plata, R. E.; Singleton, D. A., A case study of the mechanism of alcohol-mediated Morita Baylis–Hillman reactions. The importance of experimental observations. *J. Am. Chem. Soc.* **2015,** *137* (11), 3811-3826.
19. Roth, H. G.; Romero, N. A.; Nicewicz, D. A., Experimental and calculated electrochemical potentials of common organic molecules for applications to single-electron redox chemistry. *Synlett* **2016,** *27* (05), 714-723.

APPENDIX C: SUPPLEMENTARY INFORMATION FOR CHAPTER 4

1. General information

Unless noted below, all the substrates and reagents were used as received from commercial suppliers. All purchased reagents were used without further purification. All experiments were performed under nitrogen atmosphere by using standard Schlenk technique or in a glove box, if not stated otherwise. All liquid substrates were sparged with nitrogen and used in a nitrogen filled glovebox.

Solvents such as Tetrahydrofuran (THF), dimethylformamide (DMF), dichloromethane (DCM), and toluene were dried using a solvent purification system from MBRAUN Inert Gas-System GmbH. Anhydrous dimethylacetamide (DMAc), acetonitrile (MeCN), methanol (MeOH), isopropyl alcohol (*i*PrOH), *tert*-Amyl alcohol (*tert*-AmylOH), were purchased from Sigma Aldrich. All solvents were stored in the glovebox. Reductants such as *Tetra*-methylammonium hydroxide (Me_4NOH), *tetra*-nbutylammonium fluoride (nBu_4NF), *tetra*-nbutylammonium chloride (nBu_4NCl), *tetra*-nbutylammonium bromide (nBu_4NBr) were purchased from Sigma Aldrich and directly stored in the glovebox upon receiving.

For thin layer chromatography (TLC), pre–coated Merck glass backed silica gel plates (Silica gel 60 F254) were used. Visualization was achieved using ultraviolet light (254 nm) or staining with iodine (absorbed on silica gel). Flash column chromatography was undertaken on Fluka or Material Harvest silica gel (230–400 mesh) under a positive pressure of air. Flash chromatography purification system (Combiflash® Rf 150) was also used to purify the products

using a gradient of ethyl acetate and hexane as mobile phase. NMR spectra were recorded at ambient temperature on either a Bruker Ultrashield-400 (400 MHz) spectrometer, a Varian 400 MR (400 MHz) spectrometer or an Agilent Inova 400 (400 MHz) spectrometer in the Colorado State University Analytical Resources Core (ARC). Chemical shifts (δ) are quoted to the nearest 0.01 ppm relative to the residual protons in $CDCl_3$ (δ 7.26 ppm), CD_3OD (δ 3.31 ppm). Carbon chemical shifts are internally referenced to the deuterated solvent signals in $CDCl_3$ (δ 77.1 ppm) and CD_3OD (δ 49.00 ppm). NMR shifts are reported as delta (δ) units in parts per million (ppm) and coupling constants (J) are reported in Hertz (Hz). High Resolution Mass spectroscopy (HRMS) analysis was performed on a 6224 Time-of-Flight LC/MS (Agilent) at Colorado State University Central Instrument Facility.

Photophysical Experiments. UV-Visible absorption spectra were collected with an HP 8452A diode array spectrophotometer using 1.0 cm pathlength quartz cuvettes. Emission spectra were collected using an Olis SLM 8000C fluorimeter with the appropriate wavelength-dependent correction (calculated as the multiplicative factor necessary to match the collected emission profiles of two solid emissive NIST standards – SRM 2940-B and SRM 2943 - to their true profiles) applied to the raw data. Most of the data collected herein utilized a configuration in which the slit-widths before and after each monochromator were set to 1 mm (which corresponds to an effective bandpass of 2 nm). TCSPC measurements were made using a DeltaFlex Modular Fluorescence Lifetime System from Horiba Scientific. A Horiba NanoLED-405L was used as the excitation source (402 nm center-wavelength [CWL], c. 220 ps full-width at half maximum [FWHM]). Temperatures were measured with a built-in digital temperature sensor in the Horiba

device. Temperature was controlled by a Quantum Northwest TC-1 temperature control unit coupled with an aquarium pump submerged in a reservoir, and a jacketed sample holder.

Transient Absorption. Transient absorption data in Fig. 6 were collected using a home-built pump/probe spectrometer. Source laser pulses (796 nm, 150 fs, 1 kHz) were derived from a commercially available oscillator and regenerative amplifier (Spectra Physics Solstice Ace). The pulse was split using a 90:10 beam splitter to pump and probe paths, respectively. The probe arm was successively directed onto a linear stage (Newport; ILS250HA, 0.5 fs/step time resolution, 25 cm of travel) which enabled control of the relative delay of the pump and probe pulses. A supercontinuum was generated by attenuating the probe appropriately and then focusing it into the back of a 10 mm crystal of CaF_2 using a 100 mm focal length lens. Due to the low damage threshold of CaF_2, the crystal was continuously moved perpendicularly to the beam path using a linear actuator (Zaber T-series). The probe was directed into the sample with a 250 mm focal length concave mirror to a spot size of ~60 μm. To minimize chirp at the sample, only reflective optics were used between the point of supercontinuum generation and the sample. For the pump path, majority of the rest 796 nm amplifier output was transmitted through a 100 μm crystal of β-barium borate (Type I, 30°), which generated the 398-nm-centered second harmonic of the fundamental that served as the excitation pulse. The repetition rate of this pulse was reduced to 500 Hz using an optical chopper (Thorlabs; MC1000A) attenuated to approximately 400 nJ/pulse and then focused into the sample to a spot size of ~110 μm using a 300 mm focal length lens. In order to ensure that the two pulses maintained spatial overlap for the duration of their travel through the sample, they were focused at a very narrow (< 5°) angle. The relative polarization of the pump and probe beams was set to the magic angle (54.7°) by rotating the polarization of the 398 nm pump

pulse prior to being focused into the sample. Detection was performed using a spectrograph (Chromex; 250IS) and charge coupled detector (CCD) (Andor; DU920P-OE). By focusing the beam onto a small vertical region (8 pixels) of the detector, acquisition of spectra on a shot-to-shot basis was possible, eliminating noise due to any laser fluctuations on a timescale longer than 10s of milliseconds. Data processing was performed using home-built software programmed in Labview and Matlab. Outlying spectra (with photon counts outside of a region of 6 sigma from the median, due to small burns in the white-light generation medium) were removed and the remaining pump-on and pump-off spectra were averaged in 20 shot blocks and used to calculate ΔA. These 20 shots ΔA measurements were averaged over one period of the actuation of the CaF_2 between changing the time delay to ensure that, at each pump probe delay timepoint, the average white light quality was identical. Samples were prepared using UV-grade THF inside an Ar-filled glovebox before being sealed in a quartz cuvette using a KONTES valve. Samples were kept at a low optical density (~0.2) to avoid complete probe attenuation in near-UV regions of interest.

Photoreactors. The photoreactors used were custom designed and built in-house and the specifications have been published previously.[1] All LEDs were purchased from LED Engin and full emission spectra, as well as peak wavelength shift vs. temperature data, are available online in the respective manufacturer datasheets (see below). In the photoreactor, both the 385 nm and 405 nm LEDs were run at 700mA and a forward voltage of 13.5 V.

Table S4.1. LED Information

LED Peak Wavelength	**Luminous Flux**	**Model #**	**URL**

405 nm	4.1 W @ 700 mA	LZ4-40UB0000U8	https://media.osram.info/media/img/osram-dam-5412925//LED_Engin_Datasheet_LuxiGen_LZ4-00UB00_rev1.pdf
385 nm	1.1 W @ 700 mA	LZ1-10UBN0-00U4	https://www.mouser.com/datasheet/2/588/Ams_Osram_7_6_2022_LZ1_10UBN0_EN-2998940.pdf

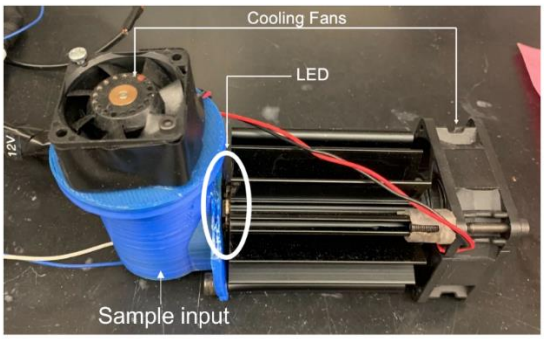

Figure S4.1. Single LED Photoreactor Setup

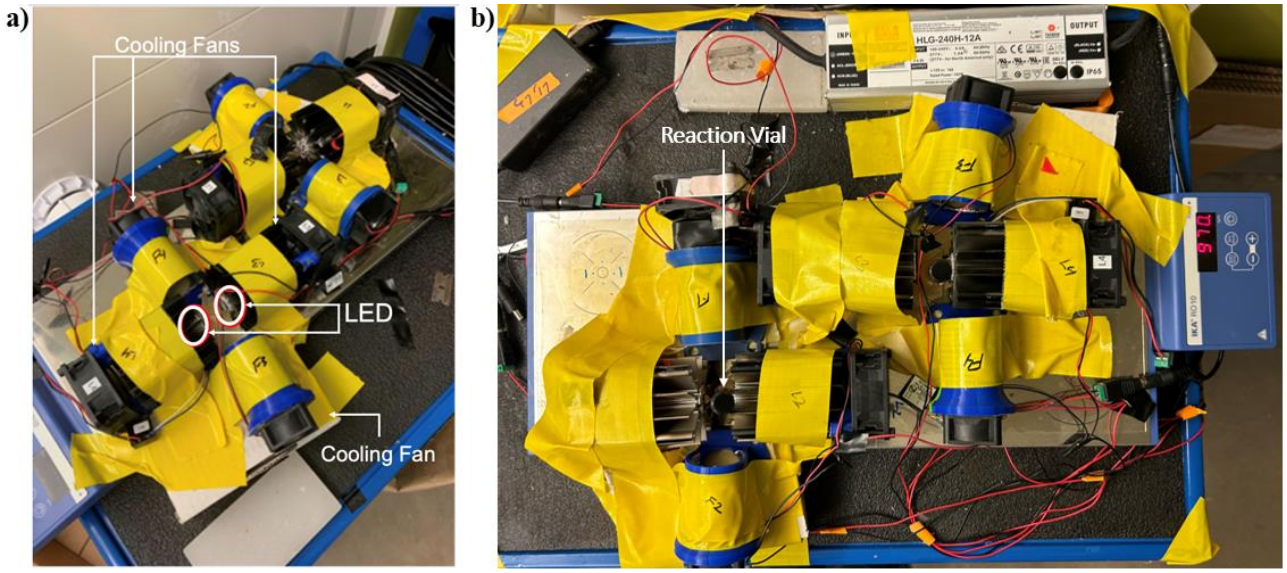

Figure S4.2. a) Double LED Photoreactor Setup with 405 nm LED; b) reactor with a 1.5-dram vial (reaction vial)

List of Abbreviations

PC Abbreviation	Structure
1	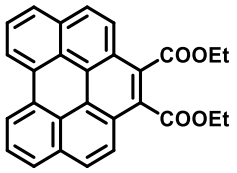
2	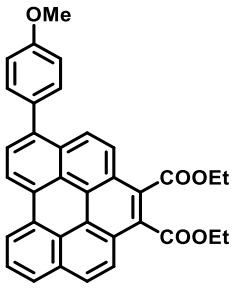
3	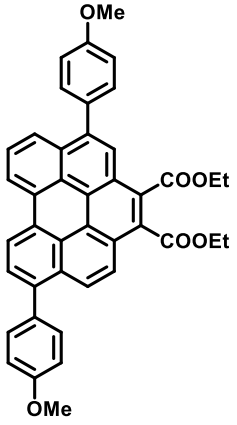
4-H	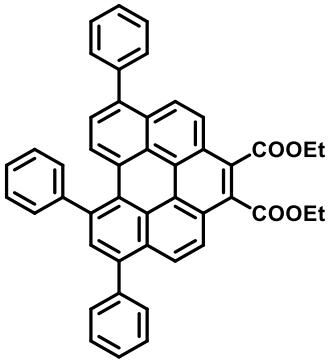

4-OMe	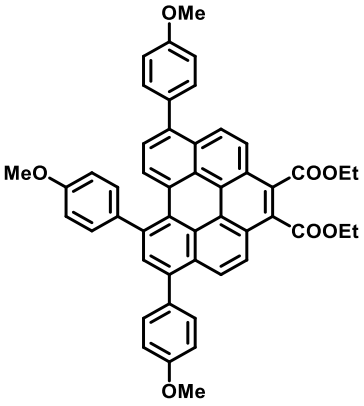 OMe MeO COOEt COOEt OMe
4-CF_3	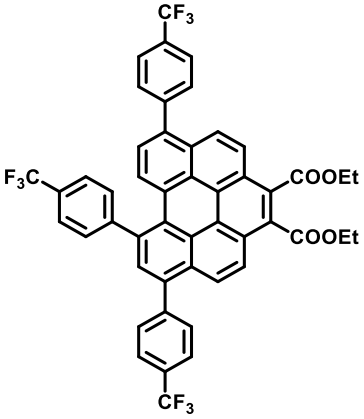 CF3 F3C COOEt COOEt CF3
5	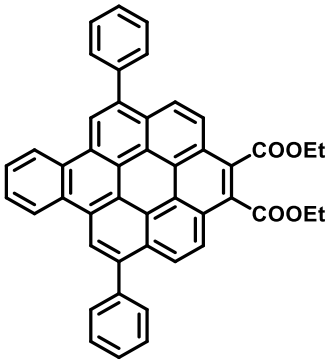 COOEt COOEt
6	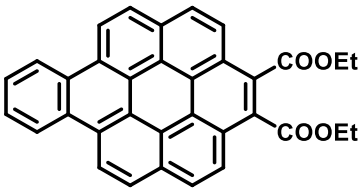 COOEt COOEt

7	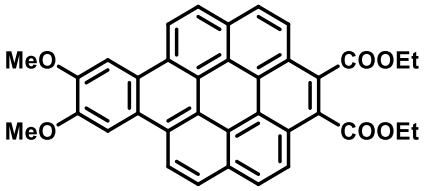
8	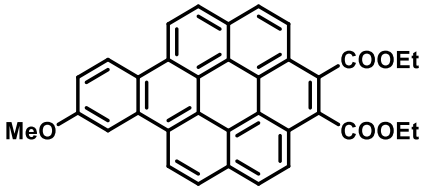
7a	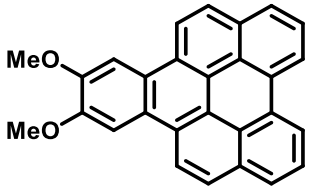
[6-H]$^-$	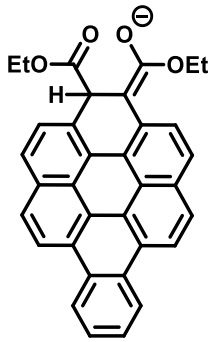
[7-H]$^-$	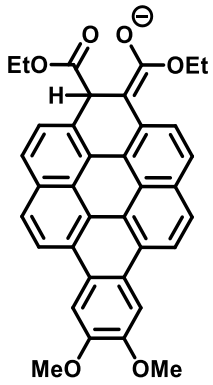

entry	PC	Substrate scope	Benzene reduction (% yield)	Reaction time (h)
1	$Ir[dF(CF_3)ppy]_2(dtbpy)PF_6$	• Limited to aromatic compounds with low triplet energy • Cannot reduce benzene or related compounds	Cannot reduce benzene	-
2	BPI-OMe	• Multiple catalyst loading • Long reaction time • Unable to reduce electron-rich substrate • Not tested on electron-deficient substrates such as benzoic acid	80	96
3	Thiolate anion	• Limited substrate scope • Not tested on electron-deficient substrates such as benzoic acid	32	20
4	Boron carbonitride semiconductor	• Not tested on electron-deficient substrates such as benzoic acid • Not tested on electron-rich substrates	27	24
5	Present work (7)	✓ Can reduce electron-rich such as toluene, anisole, *p*-cymene, 4-*tert*-butyl anisole, 1,3-, and 1,4-dimethoxybenzene ✓ Can reduce deficient substrate such as benzoic acid, 2,6-dimethyl benzoic acid, and 3,5-dimethyl benzoic acid ✓ Approx 70 substrate scope (upto % yield) ✓ Less reaction time	**78**	**4**

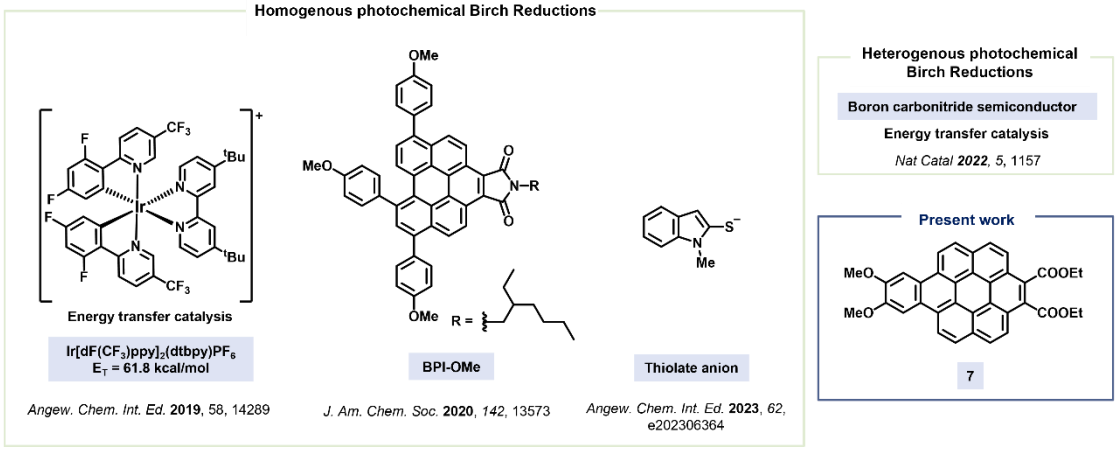

Figure S4.3: A survey of other photo-Birch reductions[2].

2. Catalyst Synthesis

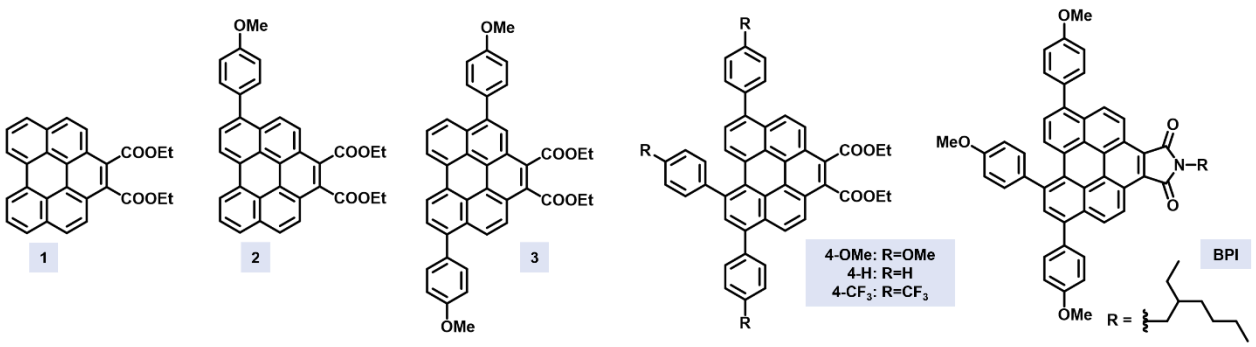

General procedure A (for Buchwald-Hartwig coupling): A 100 mL flask was charged with reactant (1.00 mmol, 1.00 eq) and boronic acid (6.00 mmol, 6.00 eq) and was transferred into an N_2 filled glovebox. Thereafter, $Pd(PPh_3)_4$ (173 mg, 0.15 mmol, 15 mol%) and 25.0 mL of THF was added and the flask was removed from the glovebox. After that, 25.0 mL of 2 M aqueous K_2CO_3 was added under positive nitrogen flow. The reaction was then heated to 100 °C for 24 hours. The reaction mixture was extracted with water-dichloromethane mixture. The organic layer was washed with water (3×100 mL) and dried over sodium sulphate. The crude product was purified by silica-gel column chromatography to yield the target product with eluent combination: hexane/DCM (10:1).

General procedure B (for anhydride synthesis by Diels-Alder reaction): A 100 mL reaction flask was charged with reactant (1.00 mmol, 1.00 eq), *p*-chloranil (565 mg, 2.30 mmol, 2.30 eq), and maleic anhydride (39.0 g, 40.0 mmol, 40.0 eq). The reaction mixture was then refluxed at 220 °C for 24 hours. After the completion of the reaction, the flask was cooled to 100 °C, and EtOH (100 mL) was added to it and stirred at that temperature for an additional 30 minutes. The solids were filtered while hot and repeatedly rinsed with EtOH (3 x 25 mL). The resulting solid was

dried. The product was used without further purification (products were not characterized via NMR because of their insolubility).

General procedure C (for anhydride synthesis by ring-opening of imide): A 100 mL round bottom flask was charged with reactant (1.00 mmol, 1.00 eq), potassium hydroxide (11.2 g, 20.0 mmol, 20.0 eq), and 30.0 mL tert-butanol was added to it. The reaction mixture was refluxed at 80 °C for 24 hours. After the reaction was complete, the flask was cooled to 0 °C, and to it 0.1 M aq. HCl was added dropwise until the pH changed from 14 to 1, and the solution was stirred for an additional one hour at 0 °C until the red precipitate crashed out. The residue was then washed with water (3 x 25 mL) and ether (25 mL) to give the target product.

General procedure D (for ring opening of anhydride): Under a nitrogen atmosphere, *anhydride* (1.00 mmol, 1.00 eq) was suspended in ethanol (50.0 mL) and acetonitrile (100 mL). Subsequently, ethyl iodide (400 µL, 5.0 mmol, 5.0 eq) was added, and the reaction mixture was cooled to 0 °C, and 1,8-diazabicyclo[5.4.0]undec-7-ene (DBU) (608 µL, 4.0 mmol, 4 eq) was added dropwise. The reaction mixture was allowed to warm up to room temperature and then heated at 65 °C for 12 hours. The mixture was cooled to room temperature, and 10% NH_3(aq)-solution (25.0 mL) was carefully added (to quench excess methyl iodide). The resulting mixture was extracted with dichloromethane. The organic phases were washed with water (3 x 50 mL), dried over $MgSO_4$, and concentrated under reduced pressure. The crude product was purified by silica-gel column chromatography to yield the target product with eluent combination: hexane/DCM (10:1).

2a. Schematic outline for synthesis of 1:

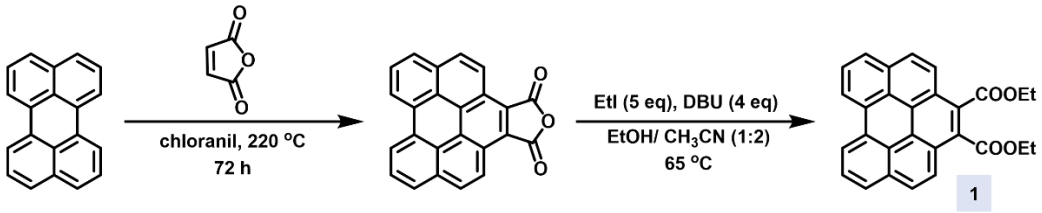

Diethyl benzo[ghi]perylene-1,2-dicarboxylate (1):

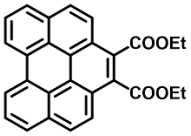

Benzo[ghi]perylene-1,2-dicarboxylic Anhydride **(1)** was synthesized according to literature procedure[3].

2b. Schematic outline for synthesis of 2:

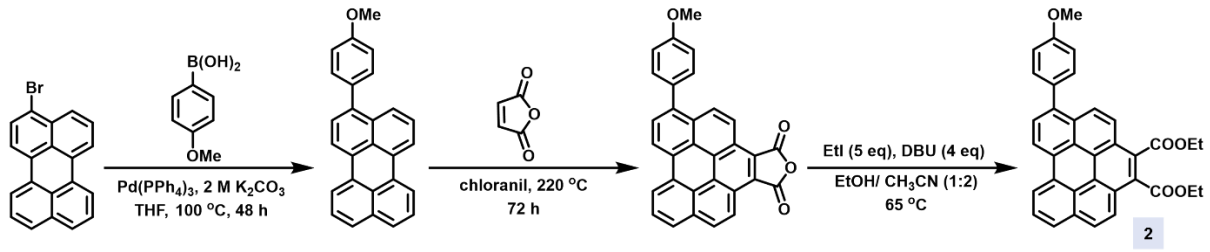

Diethyl 5-(4-methoxyphenyl)benzo[ghi]perylene-1,2-dicarboxylate (2):

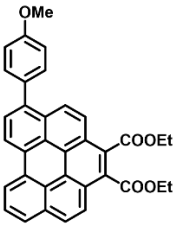

2 was prepared starting from 1-bromoperylene (331 mg, 1.00 mmol, 1.00 eq). The reactions were performed using general procedure A, B, and D on 1.00 mmol scale each. The crude product was purified by silica-gel column chromatography, eluent combination: hexane/DCM (10:1). The yellow-colored solid product (**2**) was obtained in (373 mg) 71% yield when starting with 1.00 mmol of 1-bromoperylene. The desired product is fully characterized by ^{1}H, and ^{13}C NMR spectroscopies, along with mass spectrometry.

^{1}H NMR (400 MHz, $CDCl_3$) δ 8.71 – 8.66 (m, 1H), 8.59 – 8.55 (m, 1H), 8.24 – 8.11 (m, 3H), 7.90 – 7.81 (m, 3H), 7.76 (t, *J* = 7.7 Hz, 1H), 7.61 – 7.52 (m, 2H), 7.16 – 7.10 (m, 2H), 4.64 (dq, *J* = 16.5, 7.2 Hz, 4H), 3.96 (d, *J* = 3.4 Hz, 3H), 1.61 – 1.51 (m, 6H); $^{13}C\{^{1}H\}$ NMR (101 MHz, $CDCl_3$) δ 168.7, 168.6, 159.4, 159.3, 140.3, 138.8, 133.1, 133.0, 131.6, 131.6, 131.6, 131.4, 131.3, 130.2, 129.9, 129.9, 129.5, 129.1, 128.6, 128.6, 128.5, 128.1, 128.0, 127.9, 127.8, 127.0, 126.9, 126.7, 126.5, 126.4, 125.4, 125.2, 125.1, 125.0, 125.0, 125.0, 124.8, 124.6, 124.2, 124.1, 124.1, 124.0, 121.3, 120.9, 120.9, 120.7, 114.0, 62.2, 62.1, 55.5, 14.4, 14.4 ppm.

HRMS: (ESI) Calc. for $C_{35}H_{27}O_5$ 527.1860 (calculated) $[M+H]^+$, found 527.1856 (experimental).

2c. Schematic outline for synthesis of 3:

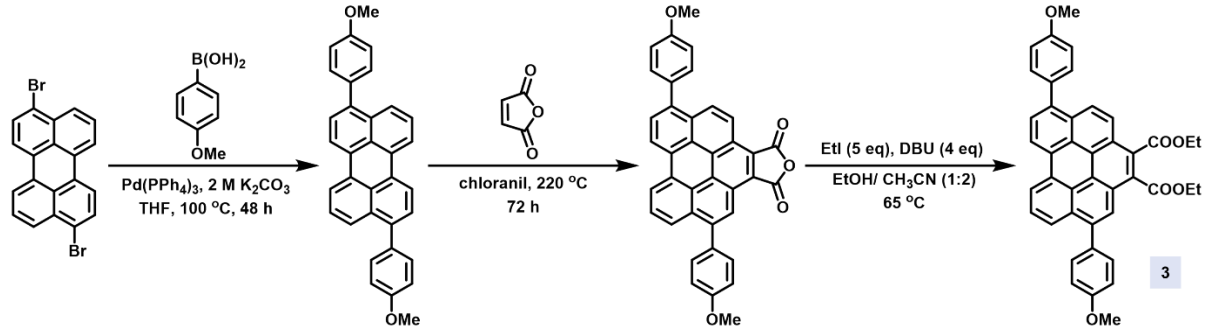

Diethyl 4,10-bis(4-methoxyphenyl)benzo[ghi]perylene-1,2-dicarboxylate (3):

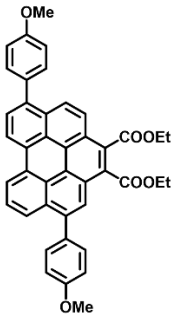

3 was prepared starting from 3,9-dibromoperylene (410 mg, 1.00 mmol, 1.00 eq). The reactions were performed using general procedure A, B, and D on 1.00 mmol scale each. The crude product was purified by silica-gel column chromatography, eluent combination: hexane/DCM (10:1). The yellow-colored solid product (**2**) was obtained in (510 mg) 81% yield when starting with 1.00 mmol of 3,9-bromoperylene. The desired product is fully characterized by ^{1}H, and ^{13}C NMR spectroscopies, along with mass spectrometry.

^{1}H NMR (400 MHz, $CDCl_3$) δ 8.98 (dd, J = 8.1, 2.8 Hz, 2H), 8.31 (q, J = 3.0 Hz, 2H), 8.26 – 8.21 (m, 2H), 8.00 – 7.94 (m, 2H), 7.61 – 7.53 (m, 4H), 7.15 – 7.08 (m, 4H), 4.66 – 4.57 (m, 4H), 3.95 (d, J = 3.1 Hz, 6H), 1.52 (dt, J = 10.1, 7.1 Hz, 6H); $^{13}C\{^{1}H\}$ NMR (101 MHz, $CDCl_3$) δ 168.7, 168.6, 159.4, 159.3, 140.5, 140.4, 139.1, 133.0, 132.9, 131.7, 131.6, 131.6, 131.4, 130.8, 130.7, 129.7, 129.6, 128.9, 128.4, 128.3, 128.2, 127.1, 126.8, 125.7, 125.6, 125.3, 125.3, 125.2, 125.2, 125.0, 125.0, 124.8, 124.4, 124.3, 121.5, 121.3, 121.1, 114.0, 62.2, 55.5, 14.4, 14.4 ppm.

HRMS: (ESI) Calc. for $C_{42}H_{36}NO_6$ 650.2543 (calculated) $[M+NH_4]^+$, found 650.2540 (experimental).

2d. Schematic outline for synthesis of 4-OMe, 4-H, 4-CF_3:

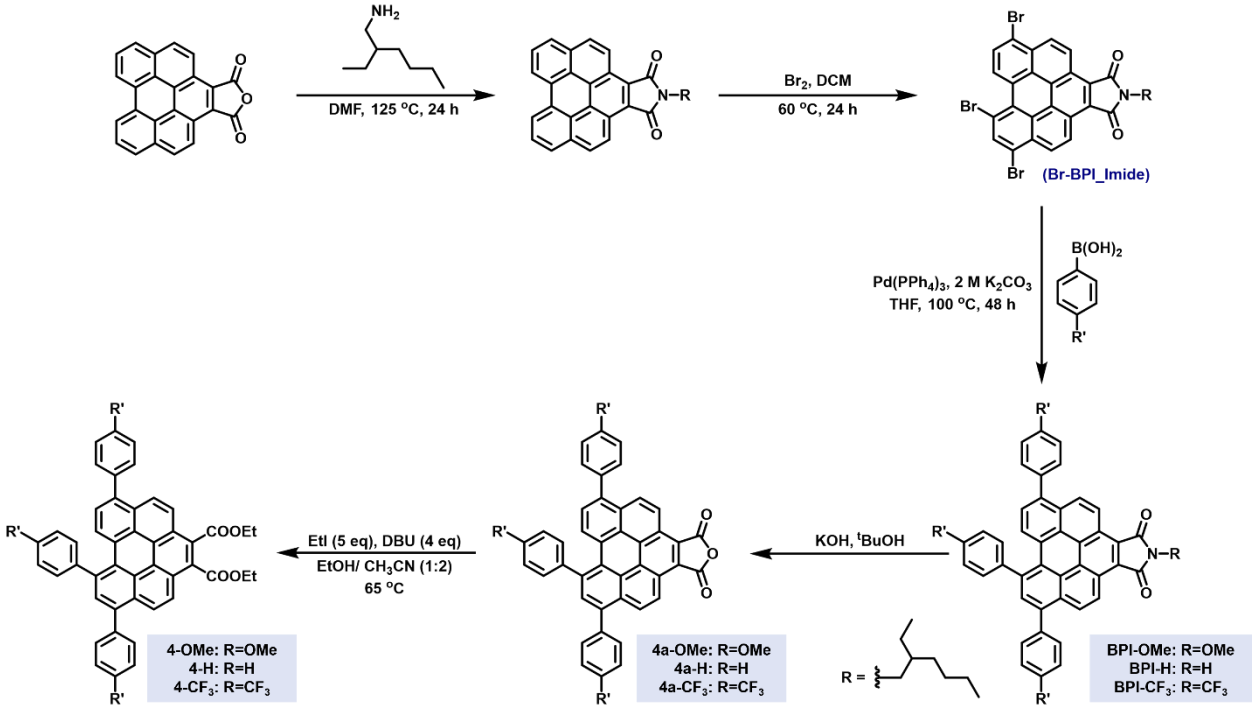

6,8,11-tris(4-methoxyphenyl)naphtho[2',1',8':3,4,5]pyreno[1,2-c]furan-1,3-dione (4a-OMe):

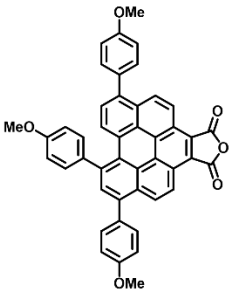

6,8,11-tris(4-methoxyphenyl)naphtho[2',1',8':3,4,5]pyreno[1,2-c]furan-1,3-dione **(4a-OMe)** was synthesized according to literature procedure[3]. The red colored solid was obtained in 80% yield. The desired product is fully characterized by ^{1}H, and ^{13}C NMR spectroscopies.

^{1}H NMR (400 MHz, $CDCl_3$) δ 9.16 – 8.95 (m, 2H), 8.40 – 8.22 (m, 3H), 7.97 (dd, *J* = 4.4, 2.2 Hz, 1H), 7.64 – 7.57 (m, 2H), 7.57 – 7.44 (m, 5H), 7.18 – 7.01 (m, 6H), 4.00 – 3.89 (m, 9H), 3.66 (q, *J* = 7.2 Hz, 2H), 2.00 – 1.87 (m, 1H), 1.49 – 1.27 (m, 8H), 0.97 (t, *J* = 7.4 Hz, 3H), 0.90 (t, *J* = 6.8 Hz, 3H); ^{13}C{^{1}H} NMR (101 MHz, $CDCl_3$) δ 170.3, 159.5, 159.3, 159.3, 138.8, 137.7, 133.9, 132.7, 132.5, 131.8, 131.7, 130.4, 129.3, 128.4, 128.3, 128.1, 127.6, 123.7, 122.7, 122.3, 115.4, 114.2, 114.1, 55.6, 55.5, 55.5, 41.9, 38.7, 30.8, 28.8, 24.16, 23.2, 14.2, 10.6 ppm.

6,8,11-Triphenylnaphtho[2',1',8':3,4,5]pyreno[1,2-c]furan-1,3-dione (4a-H):

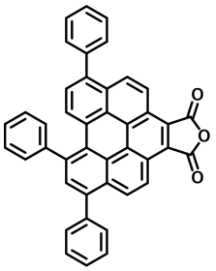

BPI-H[2b] was synthesized according to literature procedure[3] using phenylboronic acid (732 mg, 6.00 mmol, 6.00 eq) and **Br-BPI_Imide** (694 mg, 1.00 mmol, 1.00 eq). Further, **4a-H** was obtained using general procedure C on **BPI-H** (685 mg, 1.00 mmol, 1.00 eq). The red colored solid was obtained in (487 mg) 85% yield. The desired product is fully characterized by ^{1}H, and ^{13}C NMR spectroscopies, along with mass spectrometry.

^{1}H NMR (400 MHz, $CDCl_3$) δ 8.83 – 8.67 (m, 2H), 8.41 (dt, *J* = 8.4, 1.9 Hz, 1H), 8.38 – 8.25 (m, 2H), 8.09 (d, *J* = 1.1 Hz, 1H), 7.70 – 7.49 (m, 16H); ^{13}C{^{1}H} NMR (101 MHz, $CDCl_3$) δ 163.8, 144.9, 140.1, 140.0, 139.9, 139.8, 139.7, 134.7, 130.6, 130.5, 130.1, 129.5, 129.4, 129.3, 129.2,

129.1, 129.0, 128.8, 128.7, 128.7, 128.5, 128.1, 128.0, 127.8, 127.6, 126.4, 125.9, 124.5, 124.0, 123.1, 123.1, 122.2, 121.8 ppm.

HRMS: (ESI) Calc. for $C_{42}H_{23}O_3$ 575.1647 (calculated) $[M+H]^+$, found 575.1660 (experimental).

6,8,11-Tris(4-(trifluoromethyl)phenyl)naphtho[2',1',8':3,4,5]pyreno[1,2-c]furan-1,3-dione (4a-CF_3):

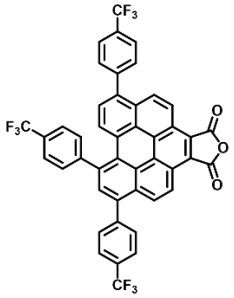

BPI-CF_3[2b] was synthesized according to literature procedure[3] using (4-(trifluoromethyl)phenyl)boronic acid (1.14 g, 6.00 mmol, 6.00 eq) and **Br-BPI_Imide** (694 mg, 1.00 mmol, 1.00 eq). Further, **4a-CF_3** was obtained using general procedure C on **BPI-CF_3** (889 mg, 1.00 mmol, 1.00 eq). The red colored solid was obtained in (614 mg) 79% yield. The desired product is fully characterized by ^{1}H, and ^{13}C NMR spectroscopies, along with mass spectrometry.

^{1}H NMR (400 MHz, $CDCl_3$) δ 8.82 (d, *J* = 9.1 Hz, 1H), 8.74 (s, 1H), 8.42 (d, *J* = 8.3 Hz, 1H), 8.25 (ddd, *J* = 22.9, 9.6, 2.0 Hz, 2H), 8.07 (s, 1H), 7.95 – 7.79 (m, 11H), 7.72 (dd, *J* = 8.3, 2.4 Hz, 3H); ^{13}C{^{1}H} NMR (101 MHz, $CDCl_3$) δ 163.4, 148.2, 143.2, 143.0, 139.1, 138.8, 138.6, 134.3, 130.9, 130.8, 129.6, 129.5, 129.3, 128.7, 128.5, 128.4, 127.2, 125.9, 125.6, 124.0, 123.5, 123.1, 122.9, 122.4, 66.0, 15.4 ppm.

^{19}F NMR (376 MHz, $CDCl_3$) δ -62.50 ppm.

HRMS: (ESI) Calc. for $C_{45}H_{20}F_9O_3$ 779.1269 (calculated) $[M+H]^+$, found 779.1316 (experimental).

Diethyl 5,7,10-tris(4-methoxyphenyl)benzo[ghi]perylene-1,2-dicarboxylate (4-OMe):

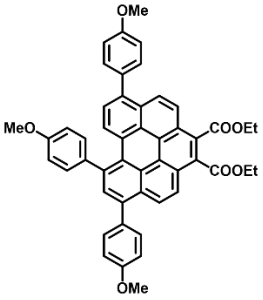

4-OMe was prepared starting from **4a-OMe** (664 mg, 1.00 mmol, 1.00 eq) using general procedure D. The crude product was purified by silica-gel column chromatography, eluent combination: hexane/DCM (10:1). The yellow-colored solid product (**4-OMe**) was obtained in (594 mg) 83% yield. The desired product is fully characterized by ^{1}H, and ^{13}C NMR spectroscopies, along with mass spectrometry.

^{1}H NMR (400 MHz, $CDCl_3$) δ 8.43 – 8.30 (m, 5H), 7.97 (s, 1H), 7.64 – 7.59 (m, 2H), 7.54 (dd, *J* = 8.4, 4.8 Hz, 5H), 7.14 – 7.04 (m, 6H), 4.61 (q, *J* = 7.2 Hz, 4H), 3.96 – 3.89 (m, 9H), 1.52 (t, *J* = 7.2 Hz, 6H); $^{13}C\{^{1}H\}$ NMR (101 MHz, $CDCl_3$) δ 168.8, 168.7, 159.4, 159.3, 159.2, 138.5, 138.4, 138.3, 137.8, 133.5, 132.9, 132.7, 131.7, 131.6, 130.4, 129.4, 129.3, 129.09, 128.45, 128.2, 128.1, 127.6, 127.3, 127.2, 127.1, 126.9, 126.7, 126.1, 126.0, 125.6, 125.2, 124.2, 123.9, 115.4, 114.1, 114.0, 62.2, 55.6, 55.5, 55.5, 14.4 ppm.

HRMS: (ESI) Calc. for $C_{49}H_{28}O_7$ 739.2698 (calculated) $[M+Na]^+$, found 739.2688 (experimental).

Diethyl 5,7,10-triphenylbenzo[ghi]perylene-1,2-dicarboxylate (4-H):

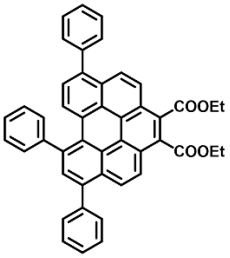

4-H was prepared starting from **4a-H** (574 mg, 1.00 mmol, 1.00 eq) using general procedure D. The crude product was purified by silica-gel column chromatography, eluent combination: hexane/DCM (10:1). The yellow-colored solid product (**4-H**) was obtained in (479 mg) 74% yield. The desired product is fully characterized by ^{1}H, and ^{13}C NMR spectroscopies, along with mass spectrometry.

^{1}H NMR (400 MHz, $CDCl_3$) δ 8.42 – 8.28 (m, 5H), 8.01 (s, 1H), 7.70 (d, J = 7.5 Hz, 2H), 7.66 – 7.43 (m, 15H), 4.61 (q, J = 7.2 Hz, 4H), 1.51 (t, J = 7.1 Hz, 6H); $^{13}C\{^{1}H\}$ NMR (101 MHz, $CDCl_3$) δ 168.4, 168.3, 148.8, 143.9, 143.7, 137.9, 137.6, 137.2, 132.8, 130.9, 130.8, 130.1, 129.8, 129.8, 129.3, 129.2, 129.2, 129.0, 128.8, 128.8, 128.3, 127.1, 127.1, 127.0, 127.0, 126.9, 126.6, 126.5, 126.2, 125.8, 125.8, 125.7, 125.7, 125.6, 125.6, 125.6, 125.5, 125.5, 124.8, 123.0, 62.5, 14.4 ppm.

HRMS: (ESI) Calc. for $C_{46}H_{33}O_4$ 649.2376 (calculated) $[M+H]^+$, found 649.2348 (experimental).

Diethyl 5,7,10-tris(4-(trifluoromethyl)phenyl)benzo[ghi]perylene-1,2-dicarboxylate (4-CF_3):

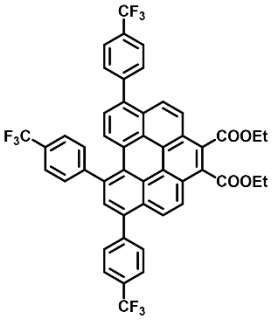

4-CF_3 was prepared starting from **4a-CF_3** (778 mg, 1.00 mmol, 1.00 eq) using general procedure D. The crude product was purified by silica-gel column chromatography, hexane/DCM (10:1). The yellow-colored solid product (**4-CF_3**) was obtained in (639 mg) 75% yield. The desired product is fully characterized by ^{1}H, and ^{13}C NMR spectroscopies, along with mass spectrometry.

Yield: 0.26 g, 89%. ^{1}H NMR (400 MHz, $CDCl_3$) δ 8.46 (dd, *J* = 16.7, 9.4 Hz, 2H), 8.30 – 8.22 (m, 3H), 7.95 (s, 1H), 7.80 (ddt, *J* = 31.6, 14.9, 8.1 Hz, 12H), 7.57 (d, *J* = 8.3 Hz, 1H), 4.62 (q, *J* = 7.1 Hz, 4H), 1.52 (t, *J* = 7.1 Hz, 7H); ^{13}C{^{1}H} NMR (101 MHz, $CDCl_3$) δ 168.7, 168.6, 145.4, 140.5, 140.3, 139.0, 138.8, 138.7, 133.3, 130.6, 130.5, 129.9, 129.4, 129.3, 129.2, 129.1, 128.7, 128.6, 128.5, 128.3, 127.8, 127.8, 127.6, 127.5, 127.2, 127.1, 126.8, 126.6, 126.0, 125.9, 125.6, 125.3, 124.5, 124.1, 62.3, 14.4 ppm.

^{19}F NMR (377 MHz, $CDCl_3$) δ -62.41 ppm.

HRMS: (ESI) Calc. for $C_{49}H_{29}F_9NaO_4$ 875.1820 (calculated) $[M+Na]^+$, found 875.1814 (experimental)

3. Photoannulation of 4-H

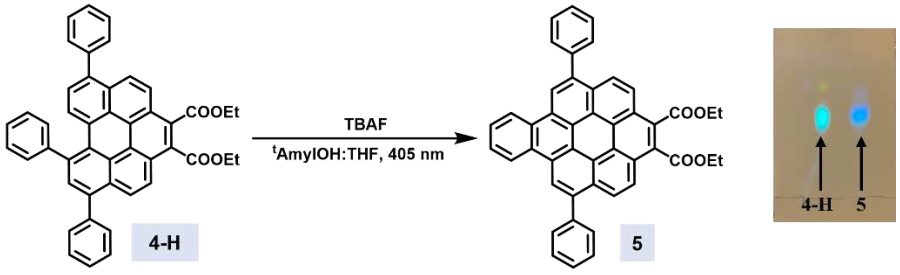

A 2.00 mL scintillation vial was charged with a Teflon-coated stir bar and **4-H** (9.00 mg, 0.01 mmol, 1.00 eq). Subsequently, the vial was transferred to an N_2-filled glovebox where *t*-amyl alcohol (0.40 mL), THF (8.00 mL), and TBAF (11 µL, 0.04 mmol, 4.00 eq (1 M solution in THF)) were added sequentially. The sealed vial was removed from the glovebox and placed into the light reactor. The reaction mixture was stirred for 9 hours under constant 405 nm irradiation inside the light reactor at room temperature. The reaction mixture was stopped and concentrated *in vacuo*. The crude mixture was purified by column chromatography using eluent combination: hexane/DCM (10:1). The desired products were well-characterized by ^{1}H, and ^{13}C NMR spectroscopies, along with mass spectrometry.

Diethyl 7,14-diphenylbenzo[a]coronene-3,4-dicarboxylate (5): Yellow solid (5.74 mg, 89%), eluent combination: hexane/DCM (10:1).

^{1}H NMR (400 MHz, $CDCl_3$) δ 9.52 (s, 2H), 9.21 (dd, *J* = 6.4, 3.4 Hz, 2H), 8.96 (d, *J* = 9.2 Hz, 2H), 8.87 (d, *J* = 9.2 Hz, 2H), 7.91 (dd, *J* = 6.4, 3.2 Hz, 2H), 7.89 – 7.85 (m, 4H), 7.74 – 7.68 (m,

4H), 7.67 – 7.61 (m, 2H), 4.71 (q, *J* = 7.2 Hz, 4H), 1.59 (d, *J* = 7.2 Hz, 7H); ^{13}C NMR (75 MHz, $CDCl_3$) δ 168.9, 141.3, 139.1, 131.0, 129.1, 128.8, 128.7, 128.1, 127.9, 127.4, 126.3, 126.2, 124.9, 124.7, 124.3, 123.9, 123.6, 123.4, 121.7, 77.3, 76.8, 62.4, 29.8, 14.5 ppm.

HRMS: (ESI) Calc. for $C_{46}H_{31}O_4$ 647.2224 (calculated) $[M+H]^+$, found 647.2230 (experimental).

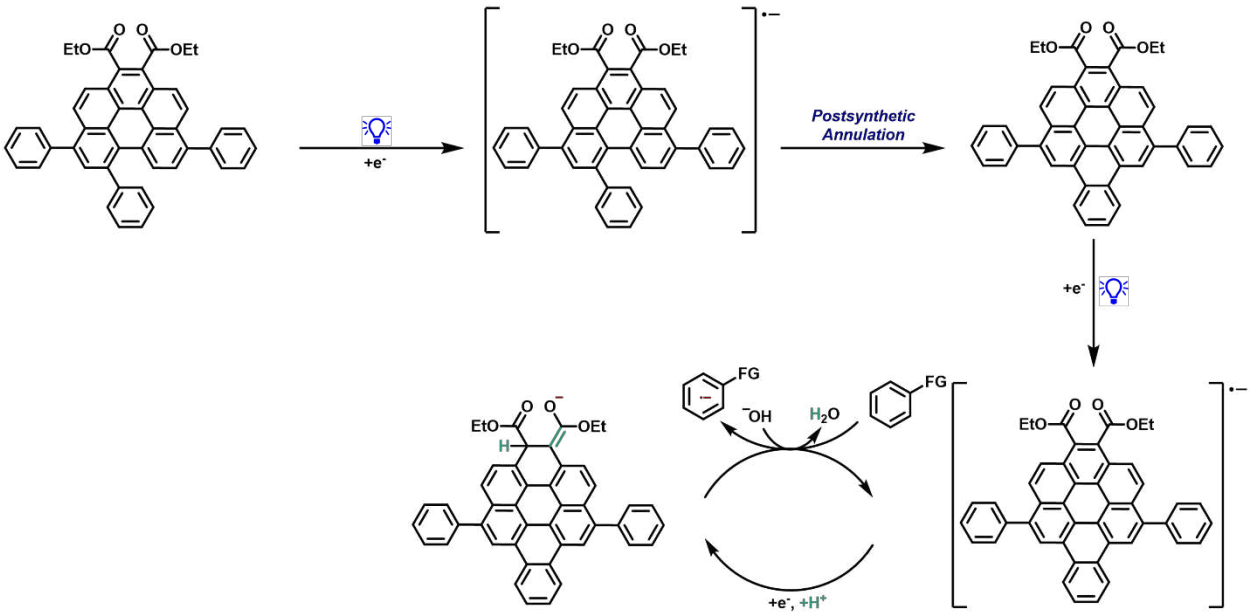

Scheme S4.1: Plausible mechanism for post-synthetic annulation of 4-H

4. Synthesis of Beno(a)coronene diester (6, 7, 8):

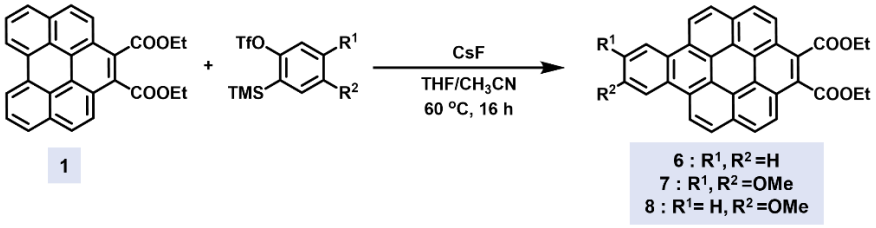

1

6 : R^1, R^2 =H
7 : R^1, R^2 =OMe
8 : R^1= H, R^2 =OMe

A 100 mL Schlenk tube was charged with **1** (83 mg, 0.19 mmol, 1.00 eq), 2-(trimethylsilyl) phenyl trifluoromethanesulfonate (114 mg, 0.594 mmol, 3.10 eq) or 4-methoxy-2-(trimethylsilyl)phenyl trifluoromethanesulfonate (195 mg, 0.594 mmol, 3.10 eq) or 4,5-dimethoxy-2-(trimethylsilyl)phenyl trifluoromethanesulfonate (212 mg, 0.594 mmol, 3.10 eq) and CsF (270 mg, 1.78 mmol, 9.00 eq). To it, THF/CH_3CN (1:1, 9.6 mL) was added and the rection mixture was stirred at 60 °C for 16 hours. After completion of the reaction, the reaction mixture was cooled to room temperature and concentrated *in vacuo*. The resulting mixture was extracted with dichloromethane. The crude product was purified by silica-gel column chromatography using eluent combination: hexane/DCM (10:1) to afford respective compound **(6, 7, 8**) as a yellow solid.

Diethyl benzo[a]coronene-3,4-dicarboxylate (6): Yellow solid (61 mg, 65%), eluent combination: hexane/DCM (10:1).

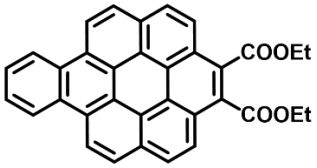

^{1}H NMR (400 MHz, $CDCl_3$) δ 9.26 (d, *J* = 8.8 Hz, 2H), 9.13 (dd, *J* = 6.4, 3.4 Hz, 2H), 8.85 (d, *J* = 8.8 Hz, 2H), 8.56 (dd, *J* = 8.8, 6.0 Hz, 4H), 8.00 (dd, *J* = 6.3, 3.2 Hz, 2H), 4.78 (q, *J* = 7.2 Hz, 4H), 1.66 (t, *J* = 7.2 Hz, 7H); ^{13}C NMR (101 MHz, $CDCl_3$) δ 128.6, 127.7, 127.1, 126.3, 123.9, 123., 121.7, 62.3, 14.6 ppm.

HRMS: (ESI) Calc. for $C_{34}H_{22}O_4$ 494.1518 (calculated) $[M]^+$, found 494.1525 (experimental).

Diethyl 10,11-dimethoxybenzo[a]coronene-3,4-dicarboxylate (7): Yellow solid (79 mg, 72%), eluent combination: hexane/DCM (10:1).

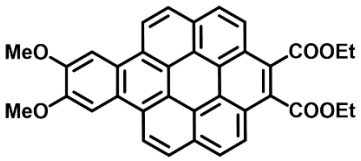

^{1}H NMR (400 MHz, $CDCl_3$) δ 8.31 (dd, *J* = 8.6, 1.5 Hz, 2H), 7.71 (d, *J* = 8.7 Hz, 2H), 7.52 (d, *J* = 8.5 Hz, 2H), 7.29 (d, *J* = 8.4 Hz, 2H), 7.08 (s, 2H), 4.84 – 4.74 (m, 4H), 4.04 (d, *J* = 1.4 Hz, 6H), 1.70 (td, *J* = 7.2, 1.4 Hz, 6H); ^{13}C NMR (101 MHz, $CDCl_3$) δ 169.1, 148.4, 127.5, 127.2, 126.5, 124.2, 123.5, 123.4, 122.3, 122.0, 121.9, 120.3, 119.6, 118.2, 102.7, 62.1, 55.8, 14.6 ppm.

HRMS: (ESI) Calc. for $C_{36}H_{37}O_6$ 555.1809 (calculated) $[M+H]^+$, found 555.1795 (experimental).

Diethyl 10-methoxybenzo[a]coronene-3,4-dicarboxylate (8): Yellow solid (67 mg, 68%), eluent combination: hexane/DCM (10:1).

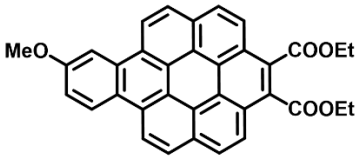

^{1}H NMR (400 MHz, $CDCl_3$) δ 8.43 (dd, *J* = 11.1, 8.7 Hz, 2H), 8.22 (d, *J* = 9.0 Hz, 1H), 8.15 (d, *J* = 8.6 Hz, 1H), 8.07 (d, *J* = 8.6 Hz, 1H), 7.95 (dd, *J* = 8.8, 2.1 Hz, 2H), 7.70 (dd, *J* = 17.9, 8.5 Hz, 2H), 7.58 (d, *J* = 2.6 Hz, 1H), 7.22 (dd, *J* = 8.9, 2.5 Hz, 1H), 4.80 (q, *J* = 7.2 Hz, 4H), 4.10 (s, 3H), 1.71 (dd, *J* = 7.6, 6.8 Hz, 6H); ^{13}C NMR (101 MHz, $CDCl_3$) δ 169.0, 158.0, 129.0, 128.3, 127.7, 127.5, 127.0, 126.8, 125.2, 124.9, 124.8, 124.6, 124.2, 123.8, 123.6, 123.1, 122.6, 122.4, 122.3, 122.0, 120.7, 120.7, 120.4, 120.2, 120.1, 118.5, 116.4, 103.8, 62.2, 55.5, 14.6 ppm.

HRMS: (ESI) Calc. for $C_{35}H_{25}O_5$ 525.1704 (calculated) $[M+H]^+$, found 525.1700 (experimental).

5. Synthesis of 10,11-dimethoxynaphtho[1,2,3,4-ghi]perylene (7a):

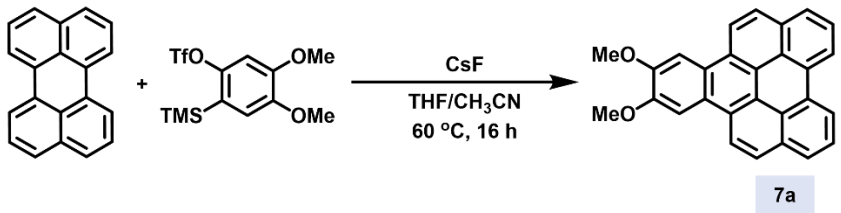

A 100 mL Schlenk tube was charged with perylene (50 mg, 0.198 mmol, 1.00 eq), 4,5-dimethoxy-2-(trimethylsilyl)phenyl trifluoromethanesulfonate (212 mg, 0.594 mmol, 3.10 eq) and CsF (270 mg, 1.78 mmol, 9.00 eq). To it, THF/CH_3CN (1:1, 9.6 mL) was added and the rection mixture was stirred at 60 ^oC for 16 hours. After completion of the reaction, the reaction mixture was cooled to room temperature and concentrated *in vacuo*. The resulting mixture was extracted with dichloromethane. The crude product was purified by silica-gel column chromatography using eluent combination: hexane/DCM (10:1) to afford respective compound **(7a**) as a yellow solid.

10,11-dimethoxynaphtho[1,2,3,4-ghi]perylene (7a): Yellow solid (65 mg, 85%), eluent combination: hexane/DCM (10:1).

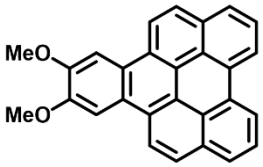

^1H NMR (400 MHz, $CDCl_3$) δ 8.83 (dd, *J* = 7.8, 1.1 Hz, 2H), 8.60 (d, *J* = 9.1 Hz, 2H), 8.12 (s, 2H), 8.10 – 8.02 (m, 4H), 7.89 (t, *J* = 7.7 Hz, 2H), 4.19 (s, 6H); ^{13}C NMR (101 MHz, $CDCl_3$) δ 149.5, 132.1, 130.6, 127.4, 126.8, 126.6, 126.0, 125.4, 123.6, 122.4, 121.9, 120.5, 103.4, 77.3, 56.1 ppm. The NMR spectroscopic data is in agreement with the literature[4] .

6. General procedures

General Procedure for Photoredox Organocatalyzed Birch Reduction: A 1.5-dram scintillation vial was charged with a Teflon-coated stir bar and 7 (2.5 mg, 0.005 mmol, 2.0 mol%). If the substrate is solid it was weighed into the 1.5-dram scintillation vial outside the glove box. Subsequently, the vial was transferred to an N_2-filled glovebox where liquid substrate (0.25 mmol, 1.00 eq) which was sparged with nitrogen and transferred to the glovebox was added. Then *t*-amyl alcohol (0.50 mL), THF (0.50 mL), and TMAOH (1.0 mL, 2.75 mmol, 11 eq (25% solution in MeOH)) were added sequentially. The sealed vial was removed from the glovebox and placed into the light reactor. The reaction mixture was stirred for 4 hours under constant irradiation inside the light reactor with fans placed in line of the vials for cooling (temperatures measured via IR ranged between 25-30 °C). The reaction mixture was stopped and concentrated *in vacuo*. The crude mixture was purified by column chromatography using hexane/ethyl acetate (10:1) as eluent. The desired products were well-characterized by ^{1}H, and ^{13}C NMR spectroscopies, along with mass spectrometry.

General Procedure for reductions of plethora of carbocycle, heterocycle, alkenes/alkynes: A 1.5-dram scintillation vial was charged with a Teflon-coated stir bar and 7 (1.3 mg, 0.0025 mmol, 1 mol%). If the substrate is solid it was weighed into the 1.5-dram scintillation vial outside the glove box. Subsequently, the vial was transferred to an N_2-filled glovebox where liquid substrate (0.25 mmol, 1.00 eq) which was sparged with nitrogen and transferred to the glovebox was added. Then *t*-amyl alcohol (0.50 mL), THF (0.50 mL), and TMAOH (1.0 mL, 2.75 mmol, 11 eq (25% solution in MeOH)) were added sequentially. The sealed vial was removed from the glovebox and placed into the light reactor. The reaction mixture was stirred for 3 hours under constant irradiation inside the light reactor with fans placed in line of the vials for cooling

(temperatures measured via IR ranged between 25-30 °C). The reaction mixture was stopped and concentrated *in vacuo*. The crude mixture was purified by column chromatography using hexane/ethyl acetate (10:1) as eluent. The desired products were well-characterized by ^{1}H, and ^{13}C NMR spectroscopies, along with mass spectrometry.

7. Synthesis of starting materials

Synthesis of (1R,2R,4R)-1,7,7-Trimethylbicyclo[2.2.1]heptan-2-yl 3,5-dimethylbenzoate (59a):

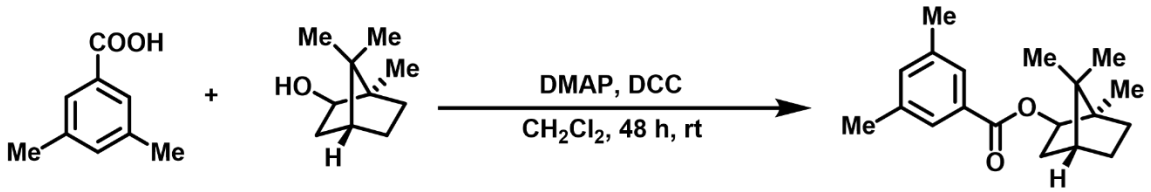

(59a, 75%)

To a 50 mL round bottom flask containing a magnetic stirring bar, 4-dimethylaminopyridine (12 mg, 0.1 mmol, 0.10 eq), *N,N'*-dicyclohexylcarbodiimide (206 mg, 1.00 mmol, 1.00 eq), 3,5-dimethyl benzoic acid (166 mg, 1.0 mmol, 1.00 eq) and isobernol (308 mg, 2.00 mmol, 2.00 eq) were added. To it, 5.0 mL dichloromethane was added. The reaction mixture was stirred at room temperature for 48 hours. After completion, the reaction mixture was filtered, the organic phase was washed with water (3 x 50 mL), and then dried over anhydrous sodium sulfate. The reaction mixture was stopped and concentrated *in vacuo*. The crude mixture was purified by column chromatography using hexane/ethyl acetate (10:1) as eluent. The desired products were well-characterized by ^{1}H, and ^{13}C NMR spectroscopies, along with mass spectrometry.

(1R,2R,4R)-1,7,7-Trimethylbicyclo[2.2.1]heptan-2-yl 3,5-dimethylbenzoate (59a): White solid (214 mg, 75%), eluent combination: hexane/ethyl acetate (10:1).

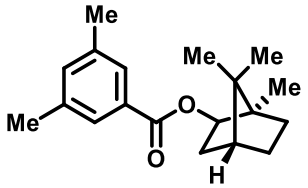

^{1}H NMR (400 MHz, $CDCl_3$) δ 7.63 (s, 2H), 7.17 (s, 1H), 4.92 (t, *J* = 5.6 Hz, 1H), 2.36 (s, 6H), 1.91 (d, *J* = 6.7 Hz, 2H), 1.83 – 1.68 (m, 2H), 1.61 (td, *J* = 12.1, 4.0 Hz, 1H), 1.29 – 1.17 (m, 2H), 1.14 (d, *J* = 1.9 Hz, 4H), 0.94 (d, *J* = 1.7 Hz, 3H), 0.90 (s, 4H); ^{13}C{^{1}H} NMR (101 MHz, $CDCl_3$) δ 166.4, 138.0, 134.4, 130.9, 127.2, 81.4, 49.1, 47.1, 45.2, 38.9, 33.8, 27.1, 21.3, 20.2, 20.1, 11.7 ppm. The NMR spectroscopic data is in agreement with the literature[5].

Synthesis of (3S,8S,9S,10R,13R,14S,17R)-10,13-Dimethyl-17-((R)-6-methylheptan-2-yl)-2,3,4,7,8,9,10,11,12,13,14,15,16,17-tetradecahydro-1H-cyclopenta[a]phenanthren-3-yl benzo[b]thiophene-2-carboxylate (60a):

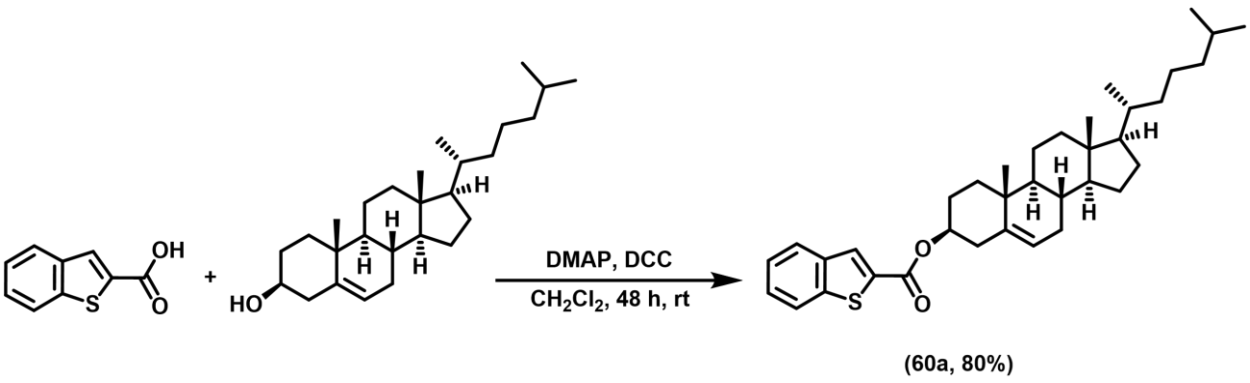

(60a, 80%)

To a 50 mL round bottom flask containing a magnetic stirring bar, 4-dimethylaminopyridine (12 mg, 0.1 mmol, 0.1 eq), *N,N'*-dicyclohexylcarbodiimide (206 mg, 1.00 mmol, 1.00 eq),

benzo[b]thiophene-2-carboxylic acid (178 mg, 1.0 mmol, 1.00 eq) and cholesterol (772 mg, 2.00 mmol, 2.00 eq) were added. To it, 5.0 mL dichloromethane was added. The reaction mixture was stirred at room temperature for 48 hours. After completion, the reaction mixture was filtered, the organic phase was washed with water (3 x 50 mL), and then dried over anhydrous sodium sulfate. The reaction mixture was stopped and concentrated *in vacuo*. The crude mixture was purified by column chromatography using hexane/ethyl acetate (10:1) as eluent. The desired products were well-characterized by ^{1}H, and ^{13}C NMR spectroscopies, along with mass spectrometry.

(3S,8S,9S,10R,13R,14S,17R)-10,13-Dimethyl-17-((R)-6-methylheptan-2-yl) 2,3,4,7,8,9,10,11,12,13,14,15,16,17-tetradecahydro-1H-cyclopenta[a]phenanthren-3-yl benzo[b]thiophene-2-carboxylate (60a): White solid (436 mg, 80%), eluent combination: hexane/ethyl acetate (10:1).

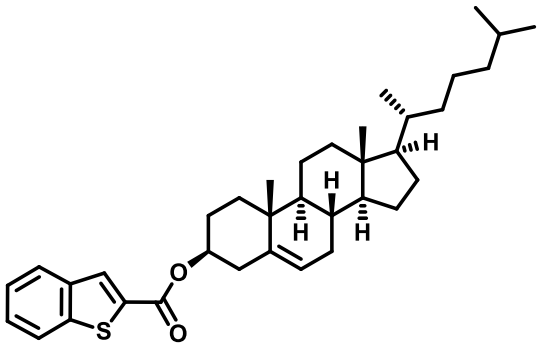

^{1}H NMR (400 MHz, $CDCl_3$) δ 7.11 – 7.03 (m, 2H), 6.69 – 6.58 (m, 2H), 4.68 – 4.59 (m, 1H), 4.08 (dtd, *J* = 11.4, 8.4, 4.5 Hz, 1H), 1.74 – 1.67 (m, 2H), 1.28 – 0.95 (m, 6H), 0.86 – 0.33 (m, 16H), 0.29 (s, 4H), 0.27 – 0.18 (m, 4H), 0.14 (d, *J* = 6.6 Hz, 3H), 0.09 (dd, *J* = 6.6, 1.8 Hz, 6H), -0.09 (s, 3H); $^{13}C\{^{1}H\}$ NMR (101 MHz, $CDCl_3$) δ 162.3, 142.3, 139.6, 138.9, 134.5, 130.3, 126.9, 125.6,

124.9, 123.1, 122.8, 75.5, 56.8, 56.2, 50.1, 42.4, 39.8, 39.6, 38.3, 37.1, 36.7, 36.3, 35.9, 32.0, 32.0, 28.3, 28.1, 28.0, 24.4, 23.9, 22.9, 22.7, 21.2, 19.5, 18.8, 12.0 ppm.

HRMS: (ESI) Calc. for $C_{36}H_{51}SO_2$ 547.3612 (calculated) $[M+H]^+$, found 547.3602 (experimental).

8. Optimization Table: *Benchmark benzene reduction*

8a. Screening different catalyst

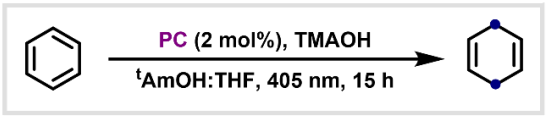

entry	PC	% conversion via NMR (15 h)
1	**1**	5
2	**2**	7
3	**3**	11
4	**4-OMe**	88
5	**4-H**	73
6	**4-CF_3**	78
7	**BPI**	38

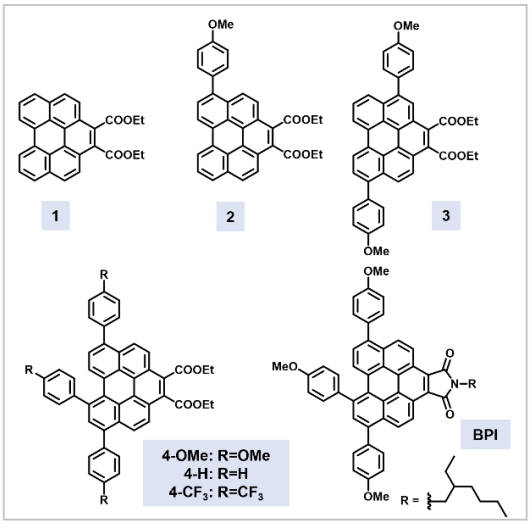

Reaction Conditions: PC (0.005 mmol, 2.0 mol%), benzene (20 µL, 0.25 mmol, 1.00 eq), TMAOH (1.0 mL, 2.75 mmol, 11 eq (25% solution in MeOH)), t-amyl alcohol (0.50 mL), THF (0.50 mL), 405 nm LEDs (2 lights).

8b. Solvent screening:

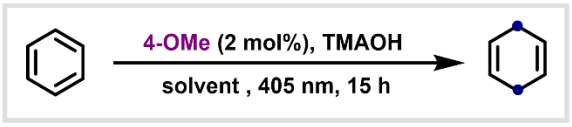

entry	solvent	% conversion via NMR (15 h)
1	Only THF	72
2	Only ^{t}AmOH	78
3	THF:^{t}AmOH (1:1)	88
4	DCM	n.r.
5	DMF	n.r.
6	DMAc	n.r.
7	CH_3CN	n.r.

Reaction Conditions: 7 (2.5 mg, 0.005 mmol, 2.0 mol%), benzene (20 µL, 0.25 mmol, 1.00 eq), TMAOH (1.0 mL, 2.75 mmol, 11 eq (25% solution in MeOH)), t*-amyl alcohol (0.50 mL), THF (0.50 mL), 405 nm LEDs (2 lights), n.r- no reaction.*

8c. Screening light sources:

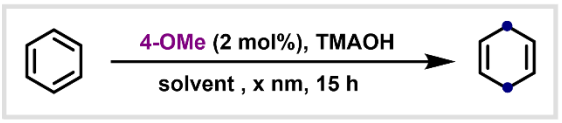

entry	Light source	% conversion via NMR (15 h)
1	365 nm (two light)	35
2	390 nm (two light)	59
3	405 nm (one light)	32
4	405 nm (two light)	88
5	455 nm (two Kessil lamp)	46

Reaction Conditions: 7 (2.5 mg, 0.005 mmol, 2.0 mol%), benzene (20 µL, 0.25 mmol, 1.00 eq), TMAOH (1.0 mL, 2.75 mmol, 11 eq (25% solution in MeOH)), *t*-amyl alcohol (0.50 mL), THF (0.50 mL), 365 to 455 nm LEDs.

8d. Varying catalyst loading:

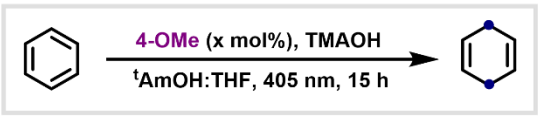

entry	Catalyst loading	% conversion via NMR
1	0.5	37
2	1	59
3	2	88
4	3	86
5	5	89

Reaction Conditions: 7 (x mol%), benzene (20 µL, 0.25 mmol, 1.00 eq), TMAOH (1.0 mL, 2.75 mmol, 11 eq (25% solution in MeOH)), t*-amyl alcohol (0.50 mL), THF (0.50 mL), 405 nm LEDs (2 lights).*

8e. Varying sacrificial reductants and its amount:

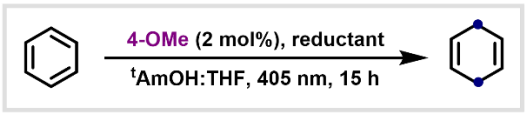

entry	sacrificial reductant	equiv	% conversion via NMR (15 h)
1	Me_3N	11	n.r.
2	DIPEA	11	n.r.
3	TBAF	11	2
4	TMAOH	5	60
5	TMAOH	11	88
6	TMAOH	25	83

Reaction Conditions: 7 (2.5 mg, 0.005 mmol, 2.0 mol%), benzene (20 µL, 0.25 mmol, 1.00 eq), reductant (x eq), t*-amyl alcohol (0.50 mL), THF (0.50 mL), 405 nm LEDs (2 lights), n.r- no reaction.*

8f. Optimizing reaction condition with the modified benzo[a]coronene diester:

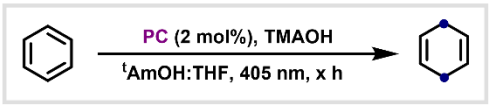

entry	PC	% yield (4 h)	% yield (6 h)	% yield (15 h)
1	4-OMe	-	28	88
2	5	65	75	90
3	6	45	70	79
4	8	55	72	-
5	7	72	76	-

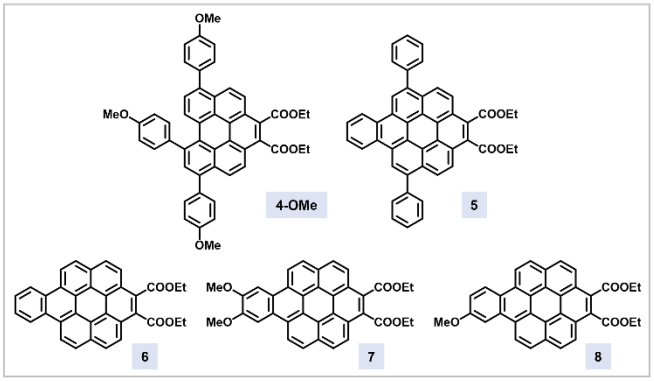

Reaction Conditions: 7 (0.005 mmol, 2.0 mol%), benzene (20 µL, 0.25 mmol, 1.00 eq), TMAOH (1.0 mL, 2.75 mmol, 11 eq (25% solution in MeOH)), t*-amyl alcohol (0.50 mL), THF (0.50 mL), 405 nm LEDs (2 lights).*

8g. Control reactions:

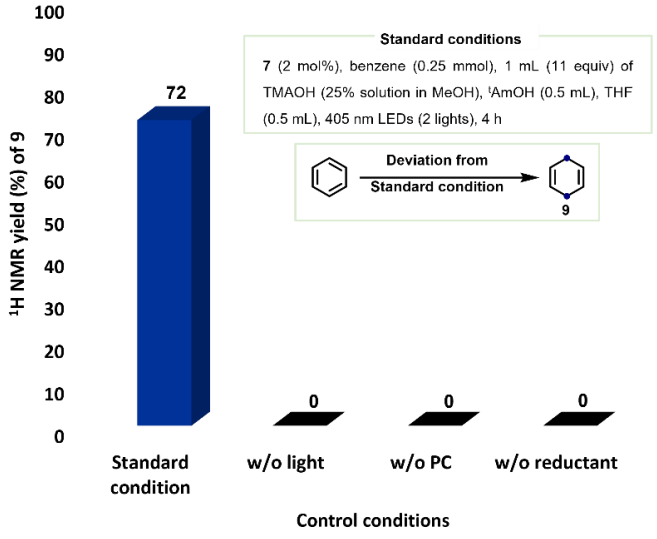

8h. Optimization for simple reduction (hydrogenation) reactions:

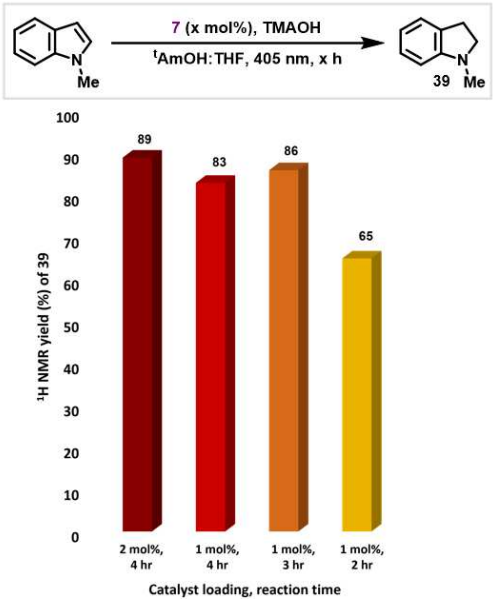

Reaction Conditions: 7 (x mol%), benzene (20 µL, 0.25 mmol, 1.00 eq), TMAOH (1.0 mL, 2.75 mmol, 11 eq (25% solution in MeOH)), t*-amyl alcohol (0.50 mL), THF (0.50 mL), 405 nm LEDs (2 lights).*

9. Other reactivity:

9a. Reactivity of 4-OMe towards various classes of arenes

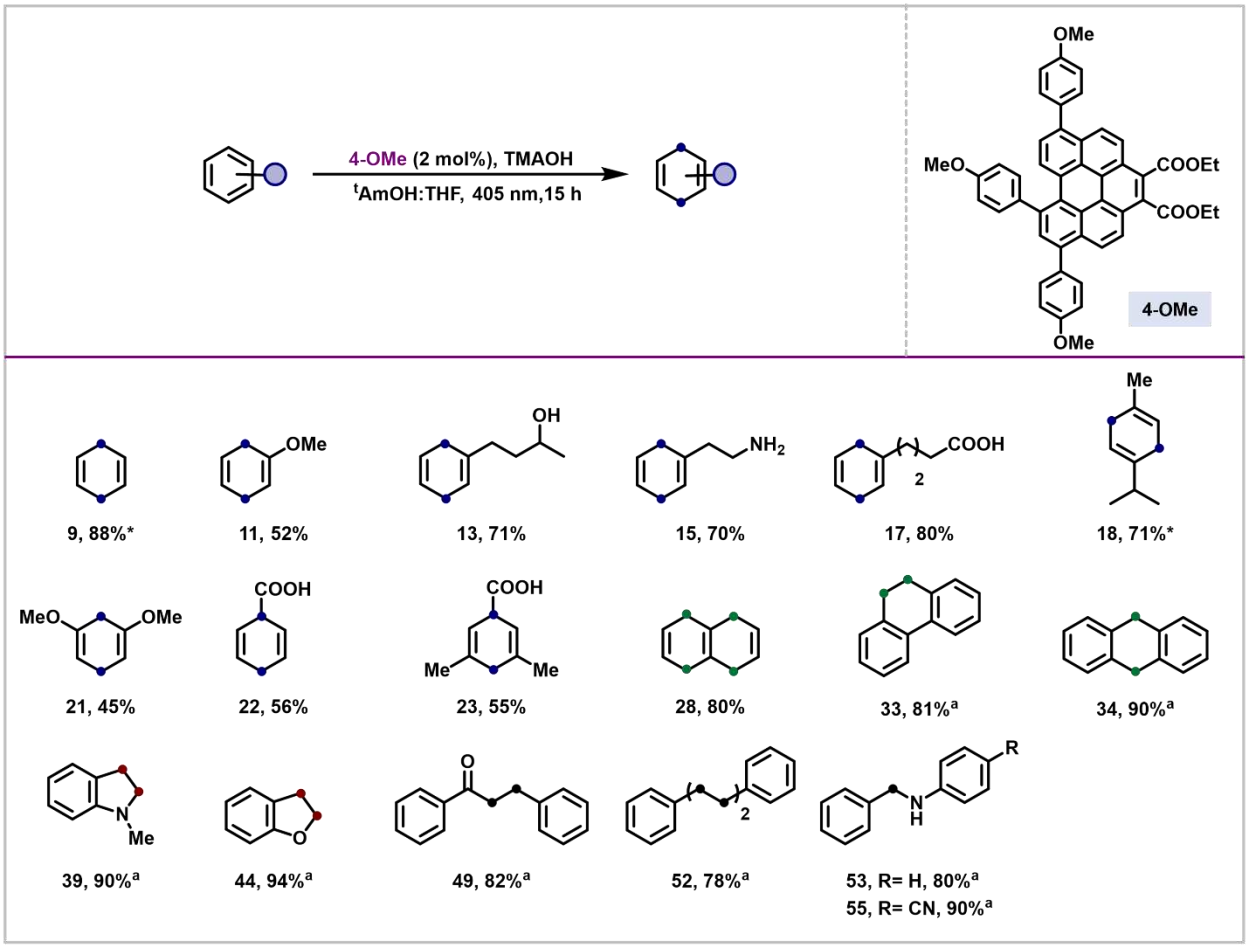

Reaction Conditions: 4-OMe (2.5 mg, 0.005 mmol, 2.0 mol%), benzene (20 µL, 0.25 mmol, 1.00 eq), TMAOH (1.0 mL, 2.75 mmol, 11 eq (25% solution in MeOH)), t*-amyl alcohol (0.50 mL), THF (0.50 mL), 405 nm LEDs (2 lights), isolated yield, *: NMR yield with mesitylene as internal standard, a: reaction time- 7 hours*

9b. Other reductive transformations:

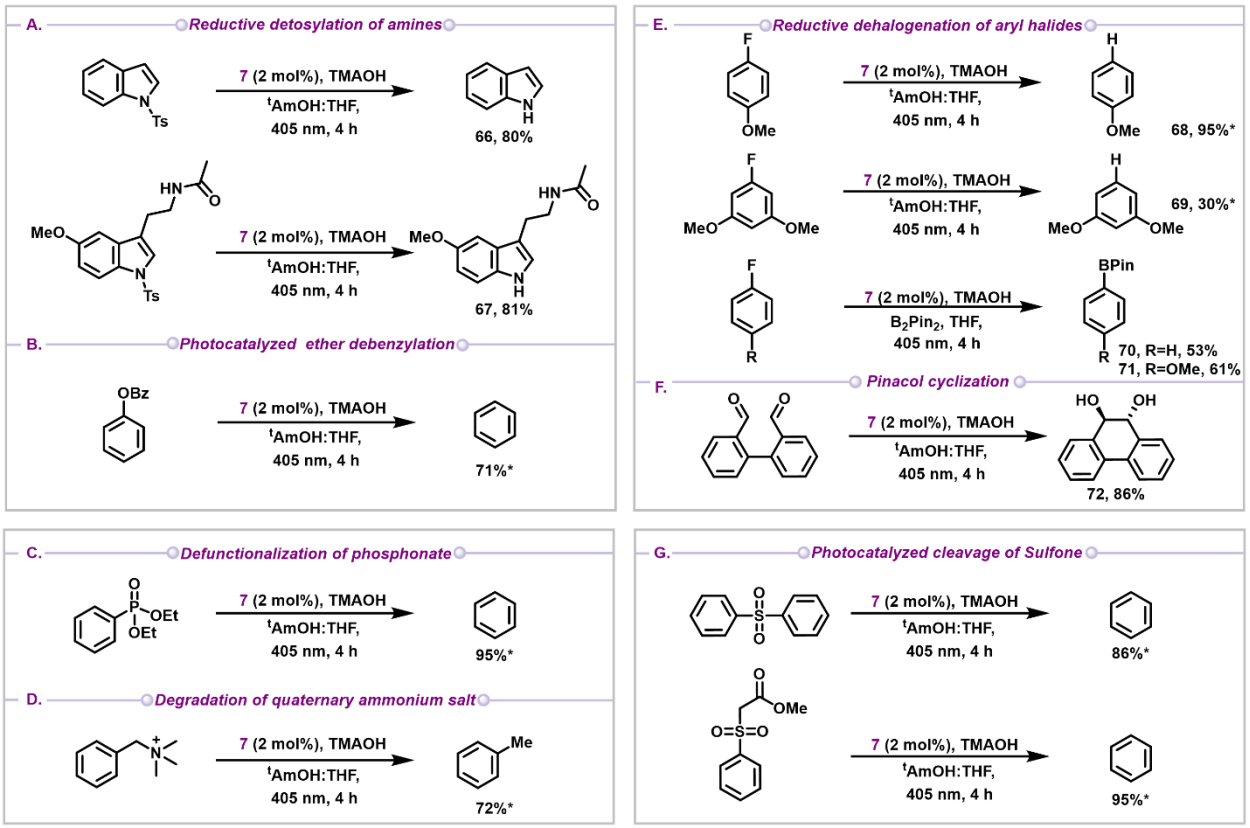

9c. Reductive alkylation of benzoic acid:

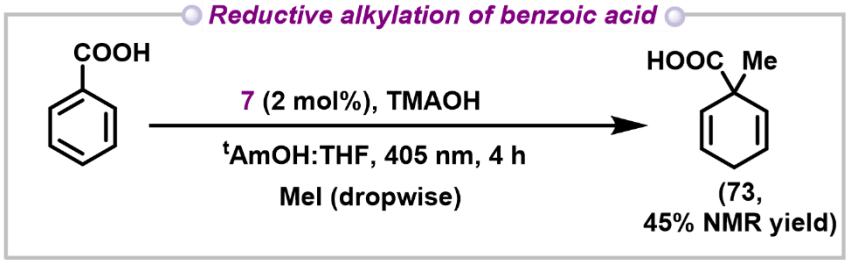

Procedure: A 1.5-dram scintillation vial was charged with a Teflon-coated stir bar, 7 (2.5 mg, 0.005 mmol, 2 mol%), and benzoic acid (30.0 mg, 0.25 mmol, 1.00 eq). Subsequently, the vial was transferred to an N_2-filled glovebox where *t*-amyl alcohol (0.50 mL), THF (0.50 mL), and TMAOH (1.0 mL, 2.75 mmol, 11 eq (25% solution in MeOH)) were added sequentially. The sealed vial was removed from the glovebox and placed into the light reactor. Methyl Iodide was added dropwise into the reaction mixture via syringe inserted into rubber septa cap over the interval of 2 hours. The reaction mixture was stirred for 4 hours under constant irradiation inside the light reactor with fans placed in line of the vials for cooling (temperatures measured via IR ranged between 25-30 °C). The reaction mixture was stopped and 0.25 mmol of mesitylene (internal standard) was added. Next, 100 µL of the crude mixture was added to 400 µL of CD_3OD and was subjected to ^1H spectroscopy to obtain ^1H NMR yield.

9e. Photochemical Lignin Fragmentation

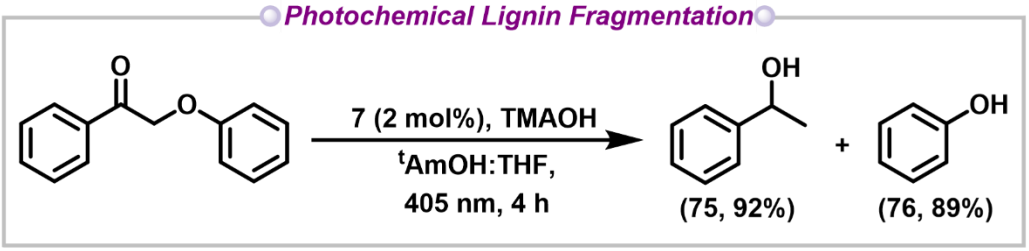

Procedure: A 1.5-dram scintillation vial was charged with a Teflon-coated stir bar, 7 (2.5 mg, 0.005 mmol, 2 mol%), and 2-phenoxy-1-phenylethanol (38 mg, 0.25 mmol, 1.00 eq). Subsequently, the vial was transferred to an N_2-filled glovebox where *t*-amyl alcohol (0.50 mL), THF (0.50 mL), and TMAOH (1.0 mL, 2.75 mmol, 11 eq (25% solution in MeOH)) were added sequentially. The sealed vial was removed from the glovebox and placed into the light reactor. The reaction mixture was stirred for 4 hours under constant 405 nm irradiation inside the light reactor with fans placed in line of the vials for cooling (temperatures measured via IR ranged between 25-30 °C). The reaction mixture was stopped and concentrated *in vacuo*. The crude mixture was purified by column chromatography using hexane/ethyl acetate (10:1) as eluent. The desired products were well-characterized by ^{1}H, and ^{13}C NMR spectroscopies, along with mass spectrometry.

10. Mechanistic investigation

10a. Test for over-reduction of 1, 4-cyclohexadiene

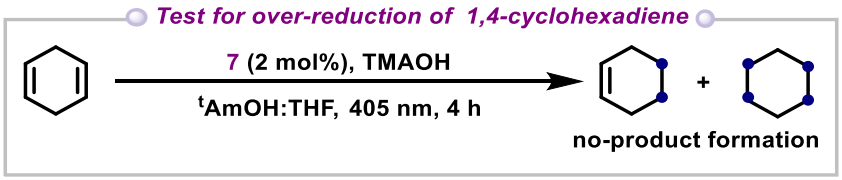

Procedure: A 1.5-dram scintillation vial was charged with a Teflon-coated stir bar and 7 (2.5 mg, 0.005 mmol, 2 mol%). Subsequently, the vial was transferred to an N_2-filled glovebox where liquid substrate 1,4-cyclohexadiene (23.0 µL, 0.25 mmol, 1.00 eq) which was sparged with nitrogen was added. Next, *t*-amyl alcohol (0.50 mL), THF (0.50 mL), and TMAOH (1.0 mL, 2.75 mmol, 11 eq (25% solution in MeOH)) were added sequentially. The sealed vial was removed from the glovebox and placed into the light reactor. The reaction mixture was stirred for 4 hours under constant 405 nm irradiation inside the light reactor with fans placed in line of the vials for cooling (temperatures measured via IR ranged between 25-30 °C). The reaction mixture was stopped and 0.25 mmol of mesitylene (internal standard) was added. Next, 100 µL of the crude mixture was added to 400 µL of CD_3OD and was subjected to ^1H spectroscopy. No over-reduced product was identified via ^1H spectroscopy.

10b. Competition experiments on the chemoselectivity in Birch reductions of aromatic hydrocarbons:

a) Procedure for intermolecular competition reaction: A 1.5-dram scintillation vial was charged with a Teflon-coated stir bar and 7 (2.5 mg, 0.005 mmol, 2 mol %). Solid substrates were weighed into the 1.5-dram scintillation vial. Subsequently, the vial was transferred to an N_2-filled glovebox where liquid substrate, which was sparged with nitrogen and transferred to the glovebox was added. The two-substrate subjected to competition reaction was added in 0.125 mmol each. Next, *t*-amyl alcohol (0.50 mL), THF (0.50 mL), and TMAOH (1.0 mL, 2.75 mmol, 11 eq (25% solution in MeOH)) were added sequentially. The sealed vial was removed from the glovebox and placed into the light reactor. The reaction mixture was stirred for 1.5 hours under constant irradiation inside the light reactor with fans placed in line of the vials for cooling (temperatures measured via IR ranged between 25-30 °C). The reaction mixture was stopped and 100 µL of the crude mixture was added to 400 µL of CD_3OD and was subjected to ^1H spectroscopy to obtain % conversion and product distribution.

Table S4.2. Intermolecular competition reactions in the chemoselectivity in Birch reductions

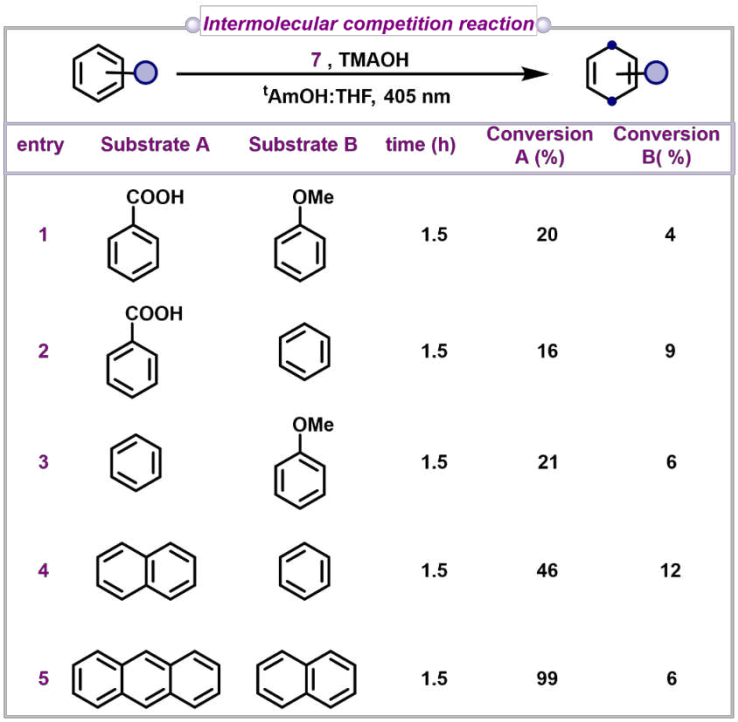

Reaction Conditions: 7 (2.5 mg, 0.005 mmol, 2.0 mol%), substrate A/substrate B (0.125 mmol), TMAOH (1.0 mL, 2.75 mmol, 11 eq (25% solution in MeOH)), t*-amyl alcohol (0.50 mL), THF (0.50 mL), 405 nm LEDs (2 lights).*

b) Procedure for intramolecular competition reaction: A 1.5-dram scintillation vial was charged with a Teflon-coated stir bar, 7 (2.5 mg, 0.005 mmol, 2 mol %) and 4-benzylbenzoic acid (53 mg, 0.25 mmol, 1.00 eq). Subsequently, the vial was transferred to an N_2-filled glovebox where *t*-amyl alcohol (0.5 mL), THF (0.50 mL), and TMAOH (1.0 mL, 2.75 mmol, 11 eq (25% solution in MeOH)) were added sequentially. The sealed vial was removed from the glovebox and placed into the light reactor. The reaction mixture was stirred for 4 hours under constant irradiation inside the light reactor with fans placed in line of the vials for cooling (temperatures measured via IR ranged between 25-30 °C). The reaction mixture was stopped and 100 µL of the crude mixture was added to 400 µL of CD_3OD and was subjected to ^1H spectroscopy to obtain % conversion.

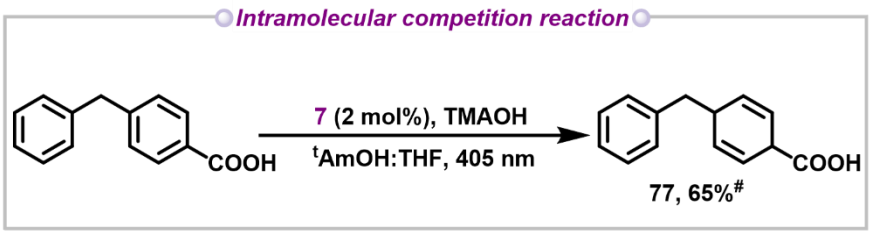

*Reaction Conditions: **7** (2.5 mg, 0.005 mmol, 2.0 mol%), benzene (20 µL, 0.25 mmol, 1.00 eq), TMAOH (1.0 mL, 2.75 mmol, 11 eq (25% solution in MeOH)),* t*-amyl alcohol (0.50 mL), THF (0.50 mL), 405 nm LEDs (2 lights), 65 % conversion with respect to the reactant*

11. Comparing TON/TOF for 4, OMe, 6, and 7:

Calculating TON/TOF for 4-OMe:

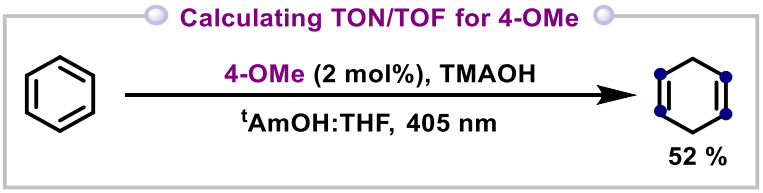

$$\text{Turn over number} = \frac{\text{Moles of desired product}}{\text{Moles of catalyst}} = \frac{0.13}{0.002} = 65$$

$$\text{Turn over frequency} = \frac{\text{Turn over number}}{\text{Time of reaction}} = \frac{65}{27{,}000} = 2.4 \text{ x } 10^{-3}\ s^{-1}$$

Reaction was stopped after 7.5 h.

Calculating TON/TOF for 6:

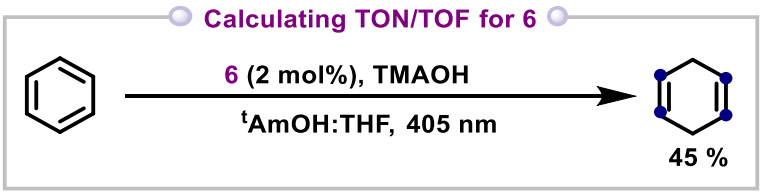

$$\text{Turn over number} = \frac{\text{Moles of desired product}}{\text{Moles of catalyst}} = \frac{0.11}{0.002} = 55$$

$$\text{Turn over frequency} = \frac{\text{Turn over number}}{\text{Time of reaction}} = \frac{55}{10{,}800} = 5.1 \text{ x } 10^{-3}\ s^{-1}$$

Reaction was stopped after 4 h.

Calculating TON/TOF for 7:

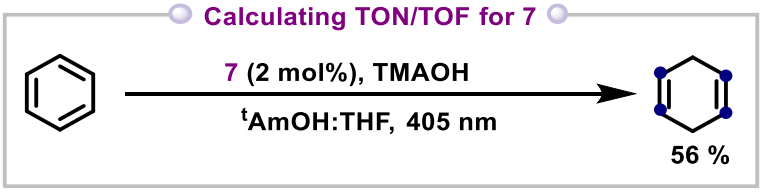

$$\text{Turn over number} = \frac{\text{Moles of desired product}}{\text{Moles of catalyst}} = \frac{0.14}{0.002} = 70$$

$$\text{Turn over frequency} = \frac{\text{Turn over number}}{\text{Time of reaction}} = \frac{70}{7{,}200} = 9.7 \text{ x } 10^{-3}\ s^{-1}$$

Reaction was stopped after 2 h.

Table S4.3: Comparing TOF for 4-OMe, 6, and 7

entry	catalyst	Time (hours)	% yield of 9	TON	TOF (x 10^{-3} s^{-1})
1.	**4-OMe**	7.5	52	65	2.4
2.	**6**	4	45	55	5.1
3.	**7**	2	56	70	9.7

12. Kinetic experiments

12a. General procedure for monitoring the kinetics of the reaction: A 1.5-dram scintillation vial was charged with a Teflon-coated stir bar and 7 (2.5 mg, 0.005 mmol2 mol %). Subsequently, the vial was transferred to an N_2-filled glovebox where benzene (20 µL, 0.25 mmol, 1.00 eq), *t*-amyl alcohol (0.50 mL), THF (0.50 mL), and TMAOH (1.0 mL, 2.75 mmol, 11 eq (25% solution in MeOH)) were added sequentially. The sealed vial was removed from the glovebox and placed into the 405 nm light reactor with fans placed in line of the vials for cooling (temperatures measured via IR ranged between 25-30 °C). At each timepoint, the lights were turned off and using a Hamilton syringe 25 µL each were taken from the reaction mixture into a NMR tube containing 450 µL d-MeOH. Conversion was analyzed by ^{1}H NMR.

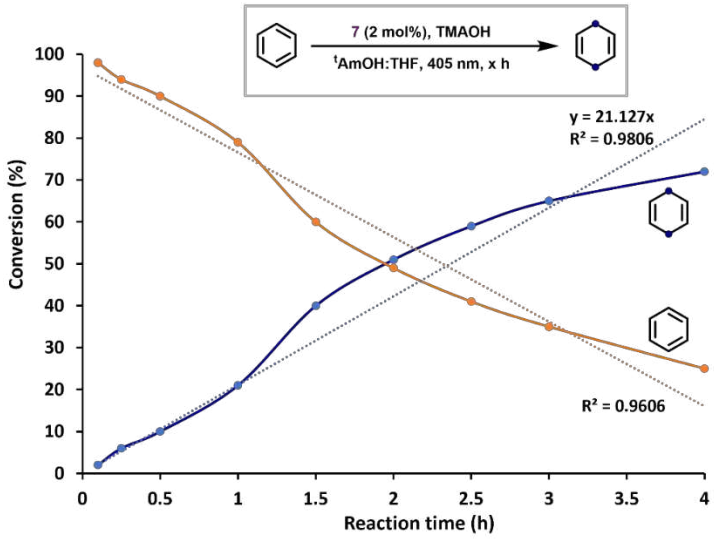

Figure S4.4. Product growth profile for 1,4-cyclohexadiene synthesis. The orange line represents the decay of benzene over time. The blue curve exhibits the growth of product i.e, 1,4-cyclohexadiene over time.

13. Light on/off reaction

A 1.5-dram scintillation vial was charged with a Teflon-coated stir bar and 7 (2.5 mg, 0.005 mmol, 2 mol %). Subsequently, the vial was transferred to an N_2-filled glovebox where benzene (20 µL, 0.25 mmol, 1.00 eq), *t*-amyl alcohol (0.50 mL), THF (0.50 mL), and TMAOH (1.0 mL, 2.75 mmol, 11 eq (25% solution in MeOH)) were added sequentially. The sealed vial was removed from the glovebox and placed into the light reactor with fans placed in line of the vials for cooling (temperatures measured via IR ranged between 25-30 °C). For the first thirty minutes the reaction was performed when the lights were turned on and then the lights were turned off for next 30 minutes. This was repeated for 3 cycles. At each timepoint, using a Hamilton syringe 25 µL each were taken from the reaction mixture into a NMR tube containing 450 µL d-MeOH. Conversion was analyzed by ^{1}H NMR.

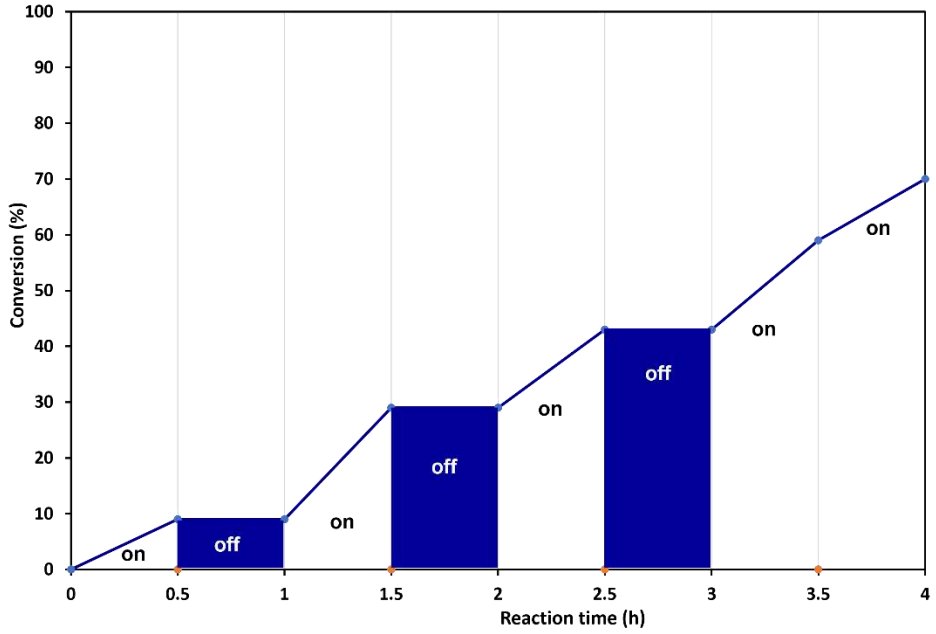

Figure S4.5. Light on/off reaction profile plot.

14. Photophysical Characterization of Photocatalysts

Table S4.4. Photophysical properties of the photocatalysts studied in this work.

PC	λ_{Max} /Abs (nm)	ϵ_{Max} ($M^{-1}cm^{-1}$)	$\lambda_{Local,Max}$ /Abs (nm)	ϵ_{Max} ($M^{-1}cm^{-1}$)	$\lambda_{Local,Max}$ /Abs (nm)	ϵ_{Max} ($M^{-1}cm^{-1}$)	λ_{Max} /Emission (nm)[a]	τ_{em} (ns)
2	314	52835	394	23948	--	--	460	15.0
3	316	58499	406	33216	--	--	469	11.9
4-OMe	324	47870	414	24175	--	--	496	6.7
4-H	323	50514	407	24420	--	--	475	TBD
4-CF_3	322	67843	408	32634	--	--	469	TBD
5	328	TBD	374	TBD	450	TBD	462	TBD
6	320	98342	362	23000	442	2090	452	24.8
7	348	81488	370	44938	422	2060	460	TBD
8	324	TBD	366	TBD	445	TBD	457	TBD

All the characterization was done in THF. [a]Emission data was obtained by exciting the sample at 380 nm.

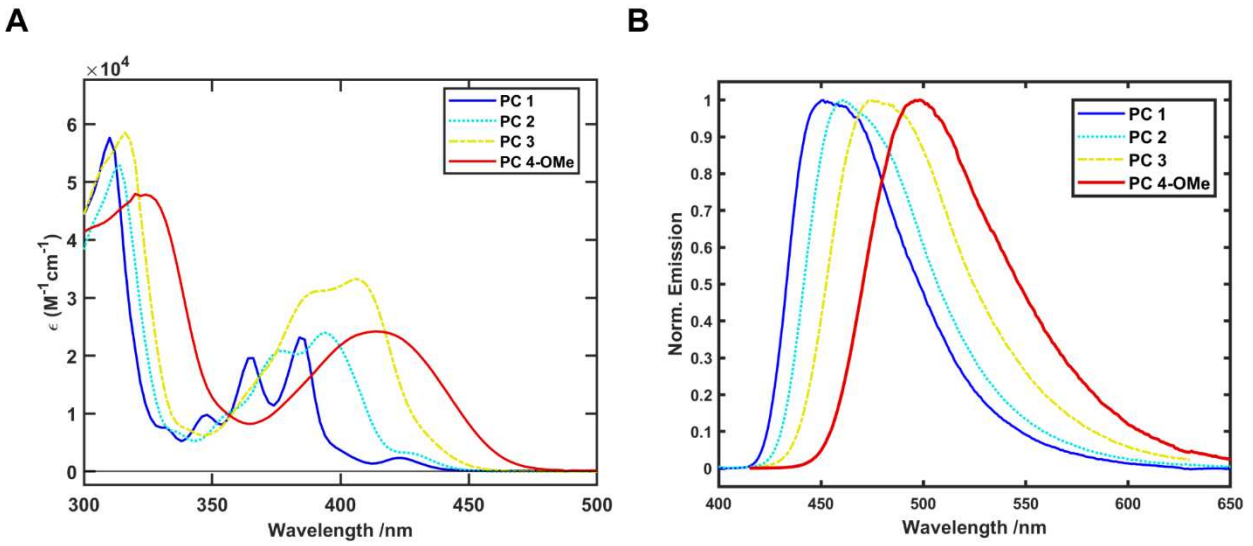

Figure S4.6. (A) Molar extinction coefficients and (B) normalized fluorescence spectra for 1, 2, 3 and 4-OMe. As the number of PhOMe groups increases from 0 (in 1) to 3 (in 4-OMe) a consistent red shift (~8-9 nm with each added PhOMe) can be seen in the absorption spectra along with a broadening of the absorbance band (centered around 380-410 nm). A similar red shift is observed in the fluorescence spectra as well.

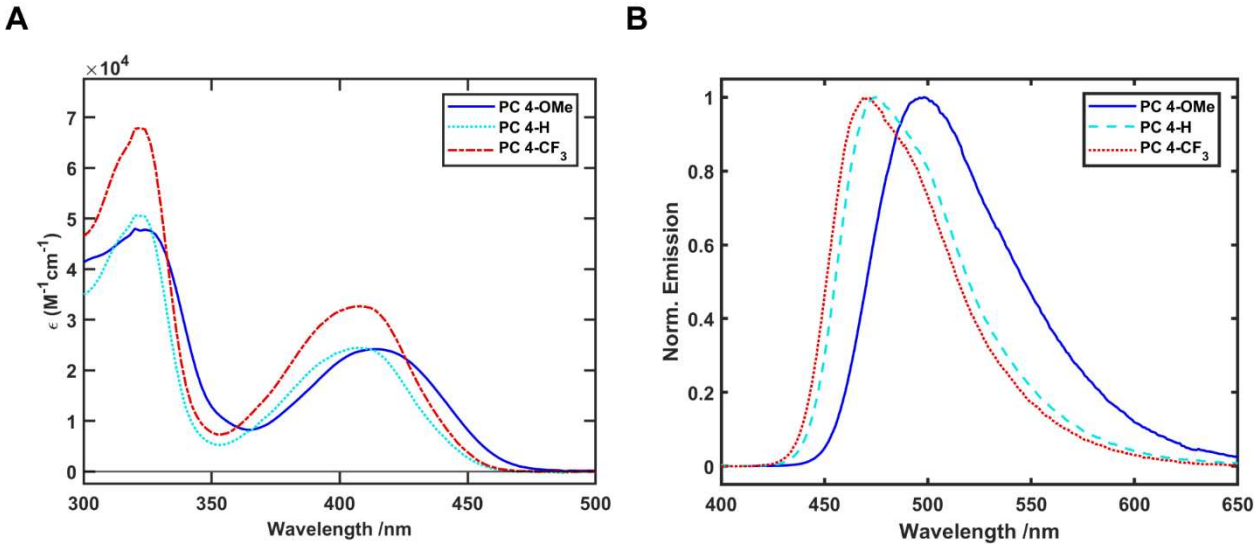

Figure S4.7. (A) Molar extinction coefficients and (B) normalized fluorescence spectra for 4-OMe, 4-H and 4-CF_3 exploring the effect of electron withdrawing vs donating effect of the substituent on the phenyl group. Both PC 4-H and 4-CF_3 have very similar absorption and emission profiles while for 4-OMe a red shift can be observed. We attribute this to the +M effect of the OMe group.

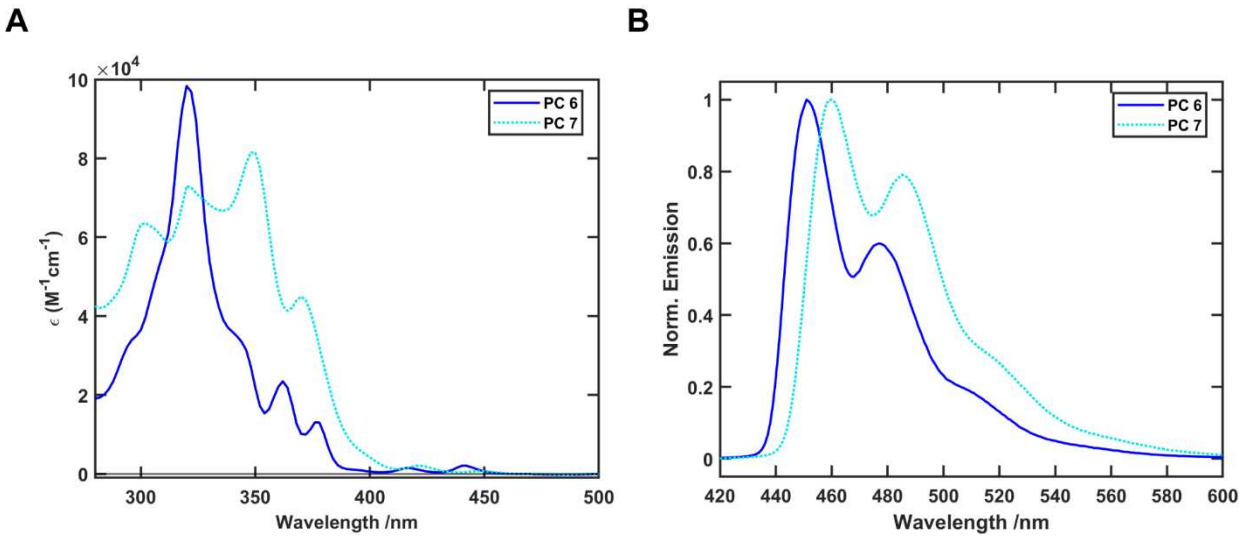

Figure S4.8. (A) Molar extinction coefficients and (B) normalized fluorescence spectra for 6 and 7 exploring the effect of dimethoxy substitution. As can be seen in (A), the relative intensities of the different vibronic peaks are significantly altered due to the OMe groups. Especially the absorption at 405 nm (peak output of the LEDs used in our the photoreactor) is enhanced in 7 compared to 6.

15. Supplemental Beer-Lambert Law Studies

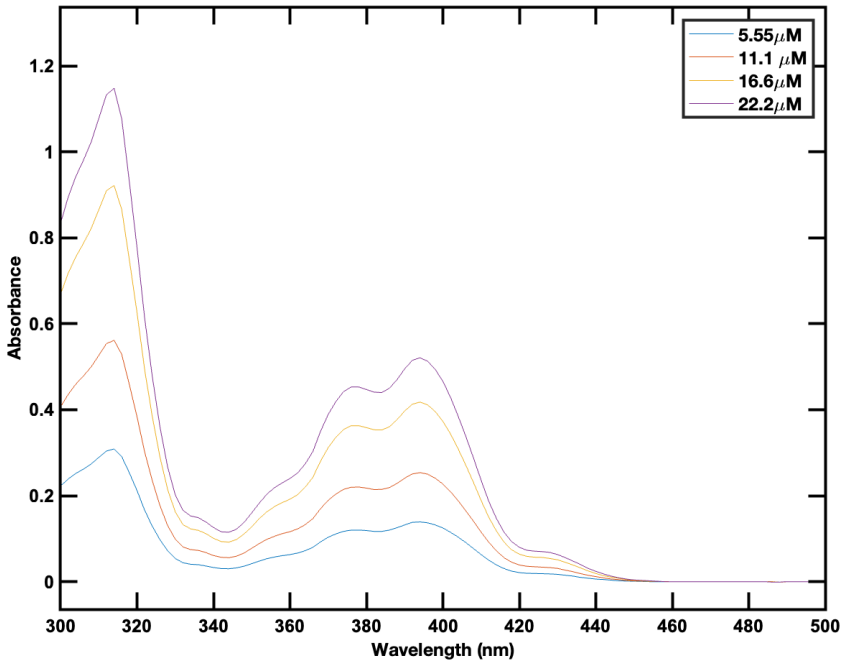

Figure S4.9. UV-Vis absorption spectra of 2 taken at different concentrations (mentioned in the legend) in THF. Path length is 1 cm.

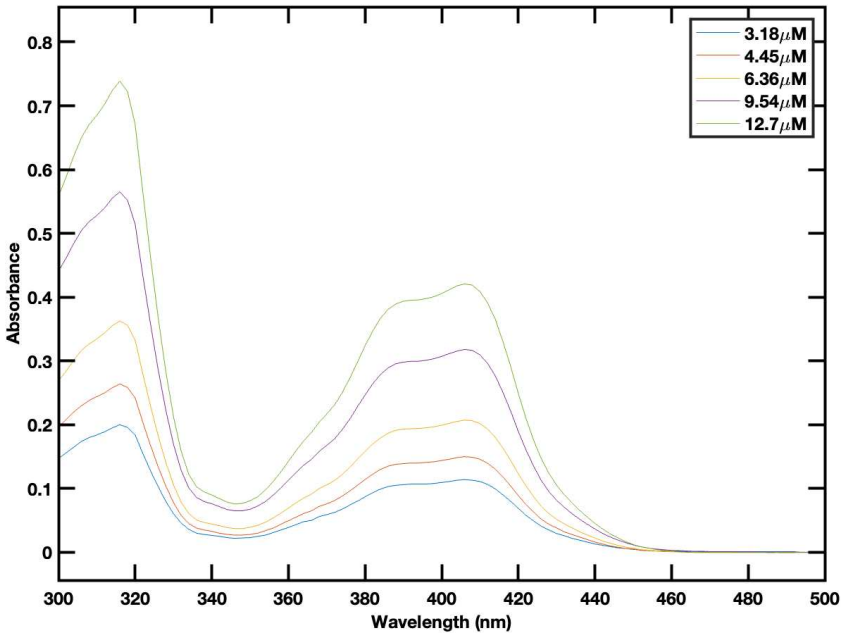

Figure S4.10. UV-Vis absorption spectra of 3 taken at different concentrations (mentioned in the legend) in THF. Path length is 1 cm.

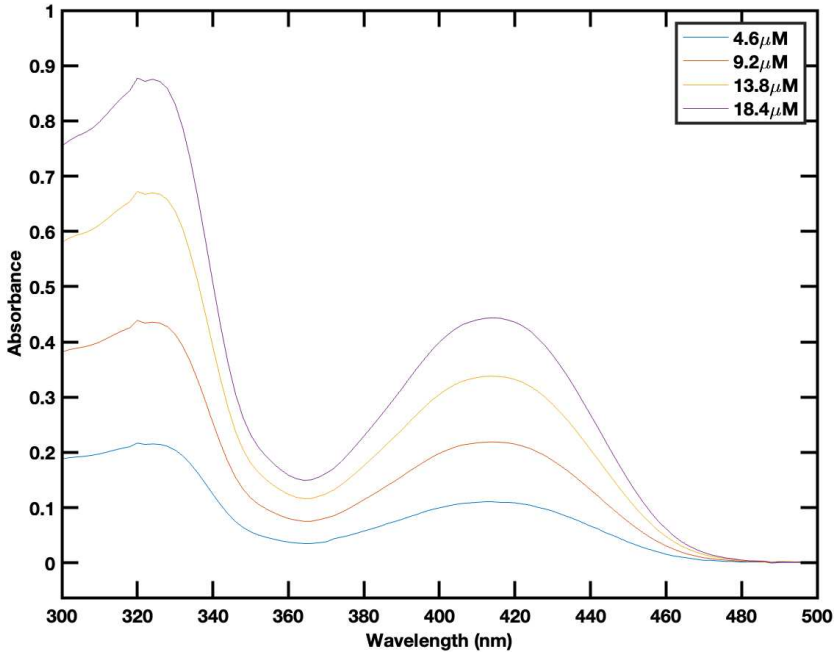

Figure S4.11. UV-Vis absorption spectra of 4-OMe taken at different concentrations (mentioned in the legend) in THF. Path length is 1 cm.

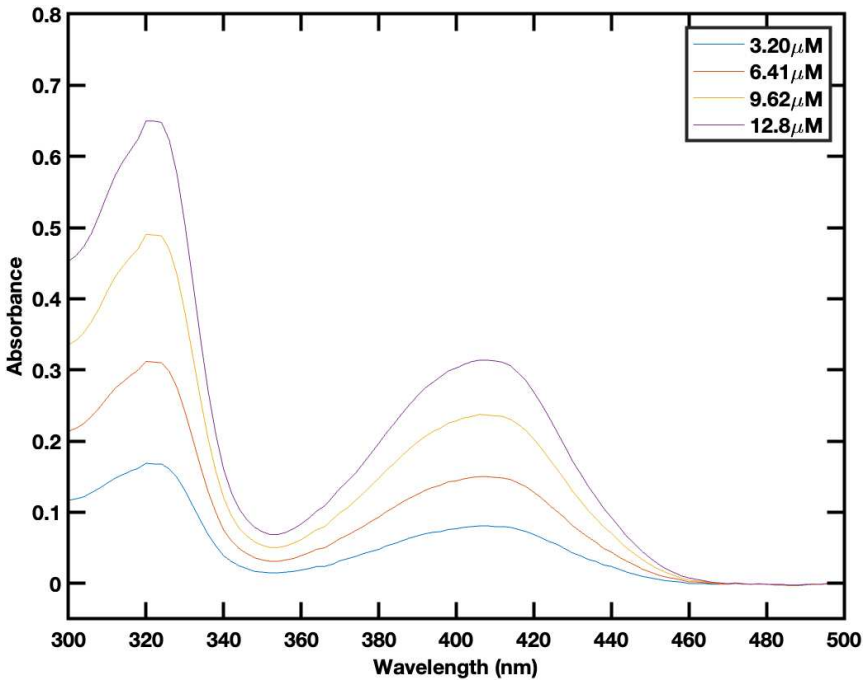

Figure S4.12. UV-Vis absorption spectra of 4-H taken at different concentrations (mentioned in the legend) in THF. Path length is 1 cm.

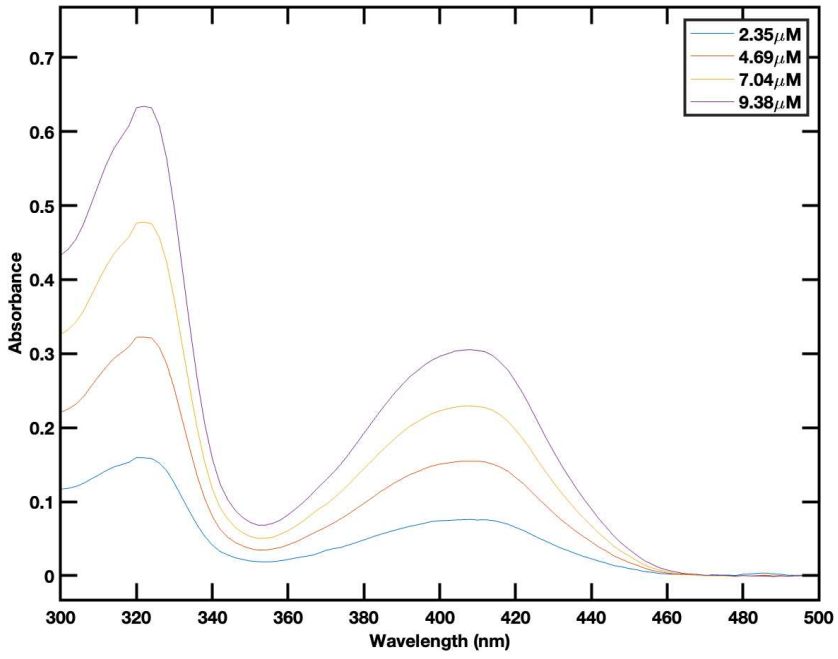

Figure S4.13. UV-Vis absorption spectra of 4-CF_3 taken at different concentrations (mentioned in the legend) in THF. Path length is 1 cm

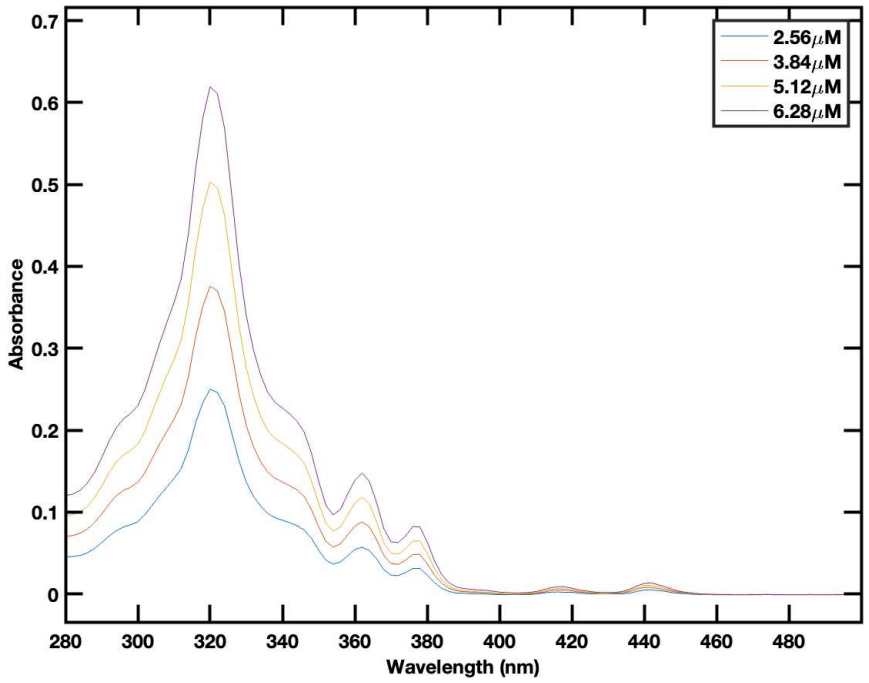

Figure S4.14. UV-Vis absorption spectra of 6 taken at different concentrations (mentioned in the legend) in THF. Path length is 1 cm.

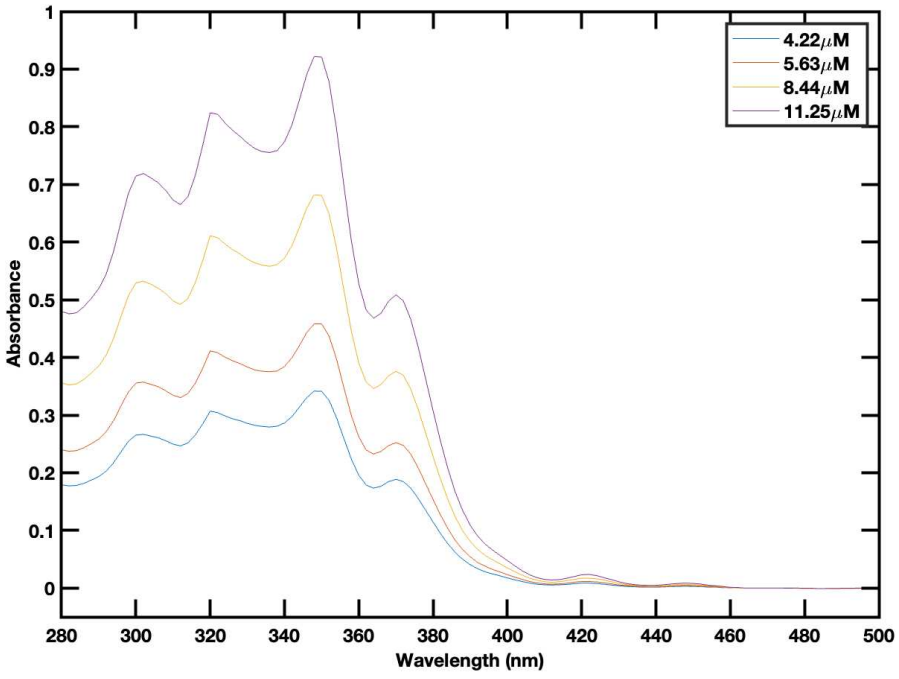

Figure S4.15. UV-Vis absorption spectra of 7 taken at different concentrations (mentioned in the legend) in THF. Path length is 1 cm.

16. Supplemental Fluorescence Lifetime Data

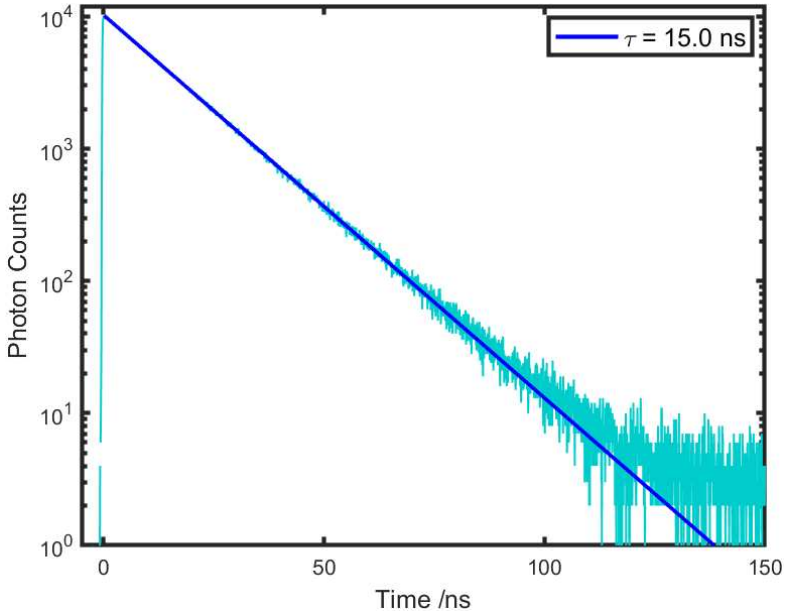

Figure S4.16. Plot of fluorescence decay for 2 in THF as measured by TCSPC following excitation at 405 nm. Monoexponential fit leads to a lifetime of 15.0 ns.

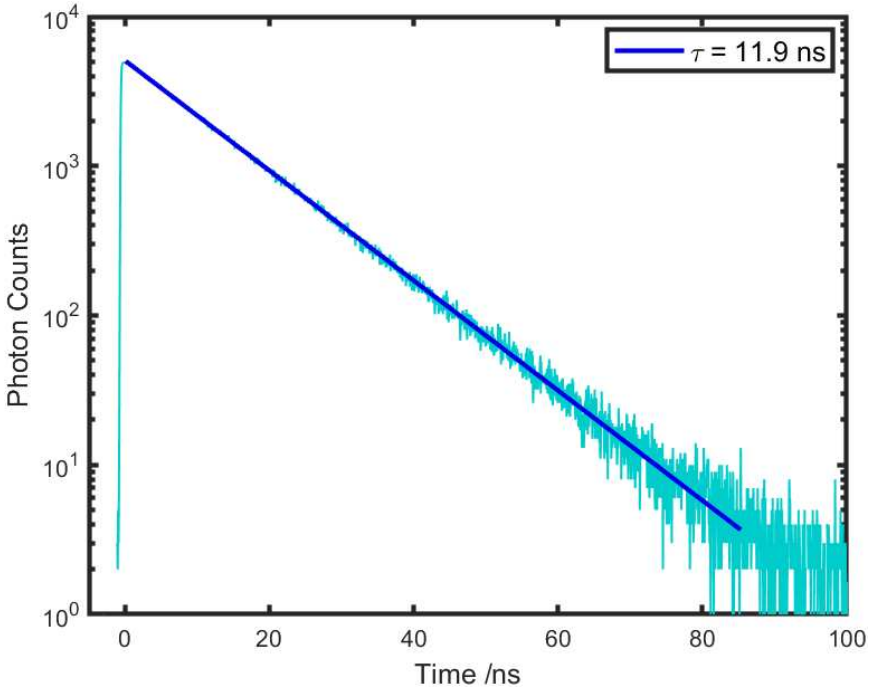

Figure S4.17. Plot of fluorescence decay for 3 in THF as measured by TCSPC following excitation at 405 nm. Monoexponential fit leads to a lifetime of 11.9 ns.

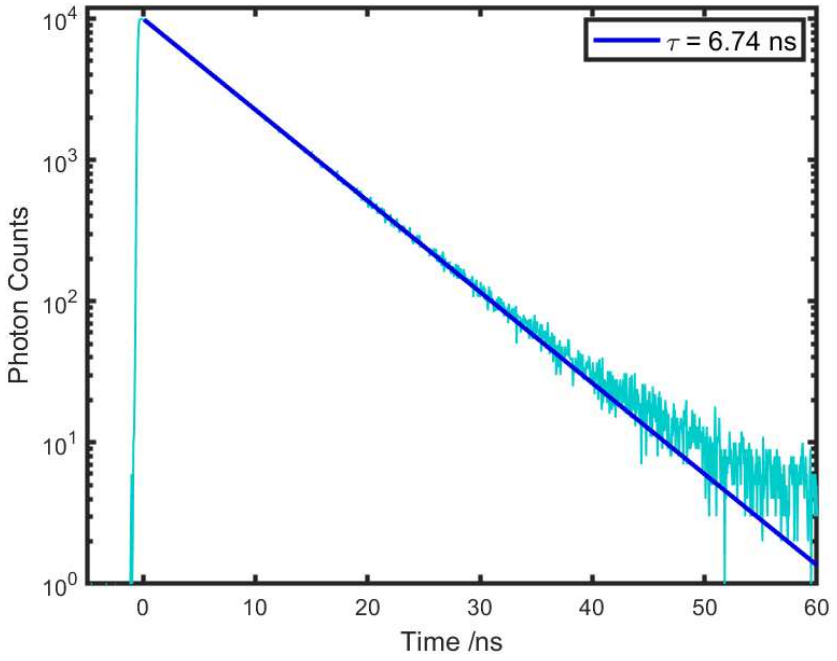

Figure S4.18. Plot of fluorescence decay for 4-OMe in THF as measured by TCSPC following excitation at 405 nm. Monoexponential fit leads to a lifetime of 6.74 ns.

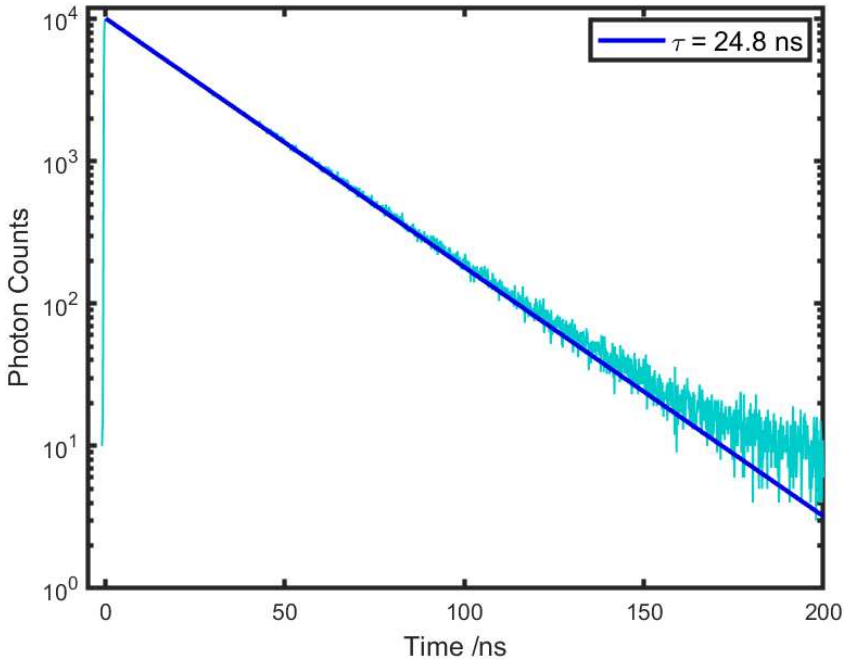

Figure S4.19. Plot of fluorescence decay for 6 in THF as measured by TCSPC following excitation at 405 nm. Monoexponential fit leads to a lifetime of 24.8 ns.

17. Electrochemical Characterization of Catalysts

Cyclic voltammetry (CV), spectroelectrochemistry, and bulk electrolysis experiments were performed in a glovebox under an inert atmosphere of argon. For cyclic voltammetry, anhydrous tetrahydrofuran (THF) was used to perform the experiment. Cyclic voltammetry was performed with an electrochemical analyzer (CH Instruments 601C) using a 3-electrode setup consisting of: a freshly polished platinum disk working electrode (3 mm diameter), a 0.5 mm platinum wire counter-electrode, and a freshly prepared 0.01 M $Ag/AgNO_3$ reference electrode dissolved in anhydrous acetonitrile (given $AgNO_3$ is insoluble in THF) with a 0.1 M tetrabutylammonium hexafluorophosphate ($TBAPF_6$) supporting electrolyte separated from solution with a porous frit. Cyclic voltammograms were scanned in the negative direction for all cyclic voltammetry experiments. After all cyclic voltammetry measurements were performed, ferrocene was spiked into the solution to be used as an internal standard. A final cyclic voltammogram was collected containing the ferrocenium/ferrocene couple at the scan rate defined within the text. During post data collection analysis, the ferrocenium/ferrocene half-wave potential was used as the electrochemical reference, which is to say the ferrocenium/ferrocene half-wave was corrected so as to occur at 0 V, and all electrochemical experiments are reported relative to this reference unless specified otherwise. For the scan rate experiments, data were collected from the slowest scan rate to the fastest scan rate. Before starting a new CV experiment, the solution was mixed via pipette to ensure homogeneity and allowed to rest for 1 minute before the next experiment was run.

Spectroelectrochemical measurements were performed in anhydrous THF using an electrochemical analyzer (CH Instruments 601C) in a 3-electrode setup with a constant applied

potential at values indicated in the text. Details of this setup can be found in our previous publication.

Bulk electrolysis was performed using a previously described custom-made H-cell. To perform bulk electrolysis, **PC** (photocatalyst) was dissolved in a 0.1 M $TBAPF_6$ THF electrolyte solution and added to the working compartment along with a Teflon stir bar and glassy carbon working electrode. To generate $\mathbf{PC}^{2-}$ the applied potential was raised 100 mV above the second reduction potential and the electrolysis was continued till the change in measured current approached zero. $\mathbf{[PC\text{-}H]}^{-}$ could be generated by adding either tert-amyl alcohol or methanol directly to this electrolyzed solution after (see text for discussion).

Table S4.5. Electrochemical properties of relevant photocatalysts studied in this work.

PC	$E_{1/2}$ ($PC/PC^{\bullet-}$)[a]	$E_{1/2}$ ($PC^{\bullet-}/PC^{2-}$)[a]	$E_{1/2}$ (PC^{2-}/PC^{3-})[a]	$E_{1/2}$ ([PC-H]$^{\bullet}$ /[PC-H]$^{-}$)[a,b]
1[x]	-2.22	-2.61	N/A	-1
4-OMe	-2.20	-2.58	N/A	-1.02
6	-2.22	-2.51	-2.75	-1
7	-2.25	-2.53	-2.80	-1.01
$\mathbf{Fc^{+}/Fc}$	0.22[b]			

[a]*Values are reported versus the ferrocenium/ferrocene couple incorporated as an internal standard.* [b]*$E_{1/2}$ (Fc^{+}/Fc) was determined to be 0.22 V vs $Ag/AgNO_3$ (see Fig. S20 below)*

[b]*This redox couple is irreversible. We believe the resulting* $\mathbf{[PC\text{-}H]^{\bullet}}$ *is further oxidized at this potential leading to regeneration of* ***PC****.*

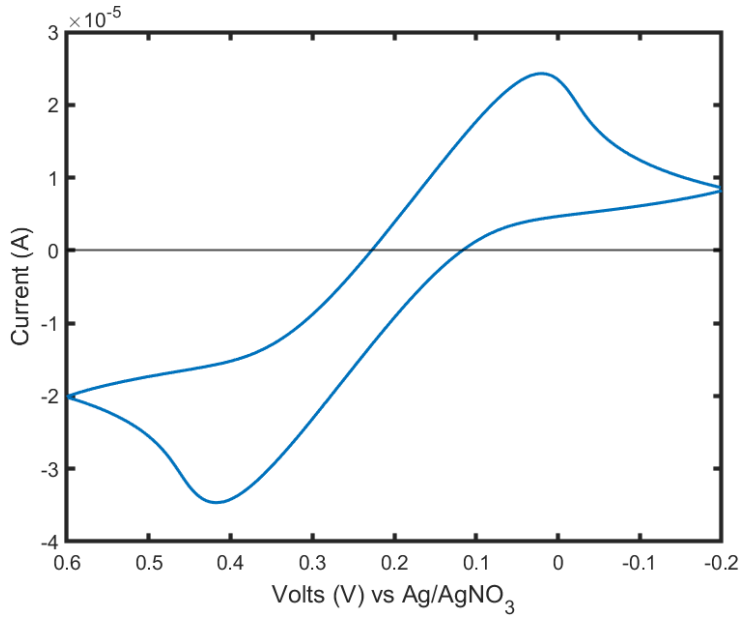

Figure S4.20. Cyclic voltammogram recorded at 100 mV/s for ferrocene in a 0.1 M $TBAPF_6$ THF solution scanning from +0.6 V to –0.2 V and back vs $Ag/AgNO_3$.

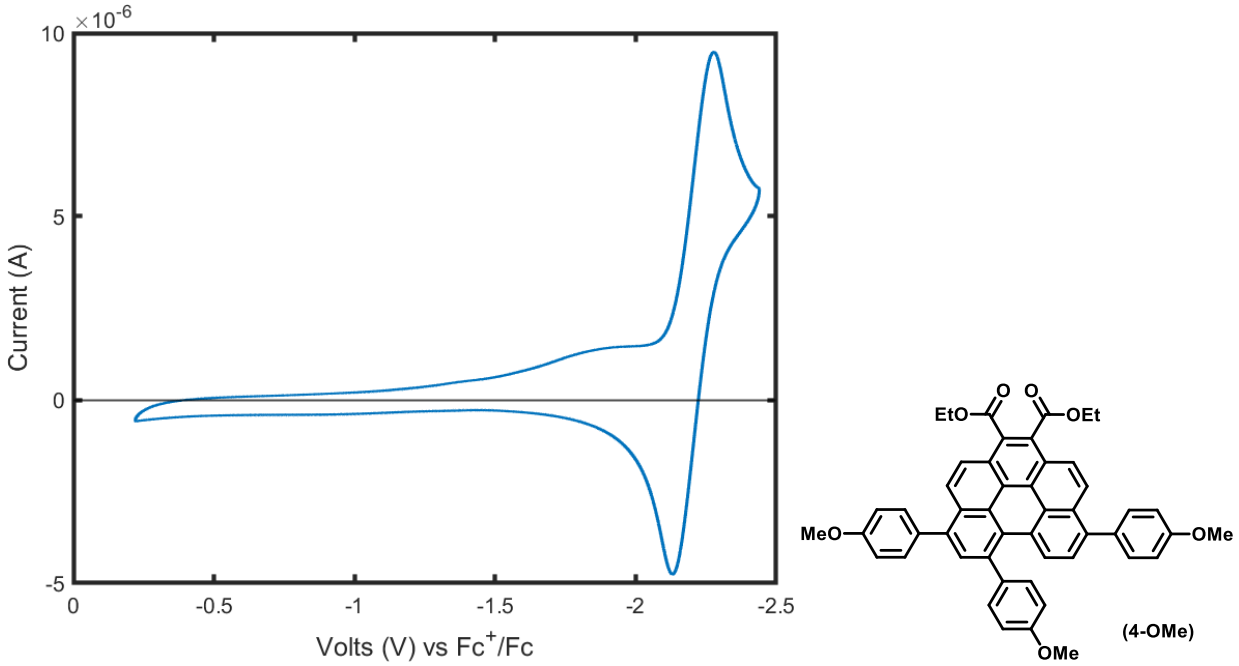

Figure S4.21. Cyclic voltammogram recorded at 100 mV/s for 4-OMe in a 0.1 M $TBAPF_6$ THF solution scanning from –0.2 to –2.45 V and back vs Fc^+/Fc.

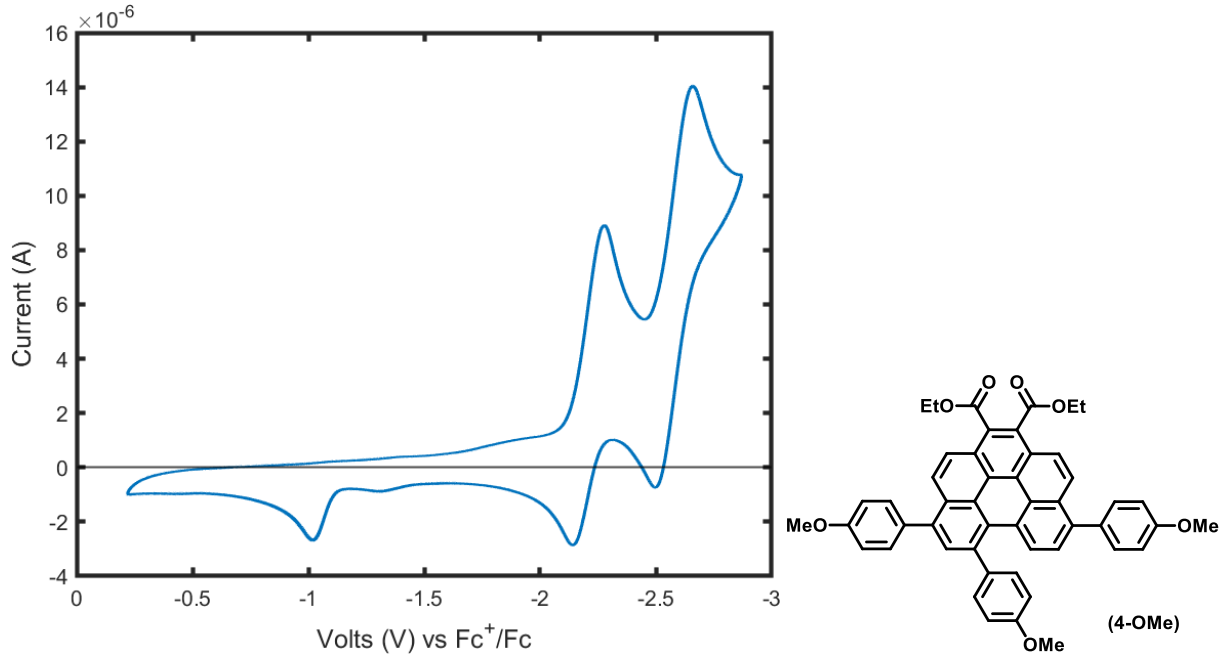

Figure S4.22. Cyclic voltammogram recorded at 100 mV/s for 4-OMe in a 0.1 M $TBAPF_6$ THF solution scanning from –0.2 to –2.86 V and back vs Fc^+/Fc.

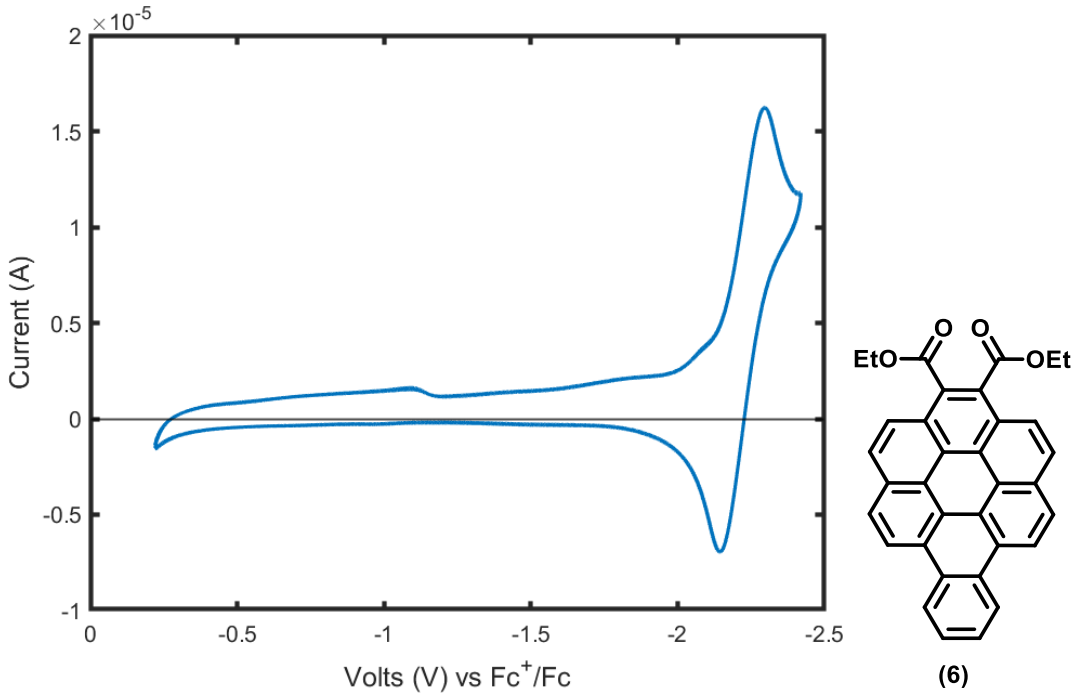

Figure S4.23. Cyclic voltammogram recorded at 100 mV/s for 6 in a 0.1 M $TBAPF_6$ THF solution scanning from –0.2 to –2.42 V and back vs Fc^+/Fc.

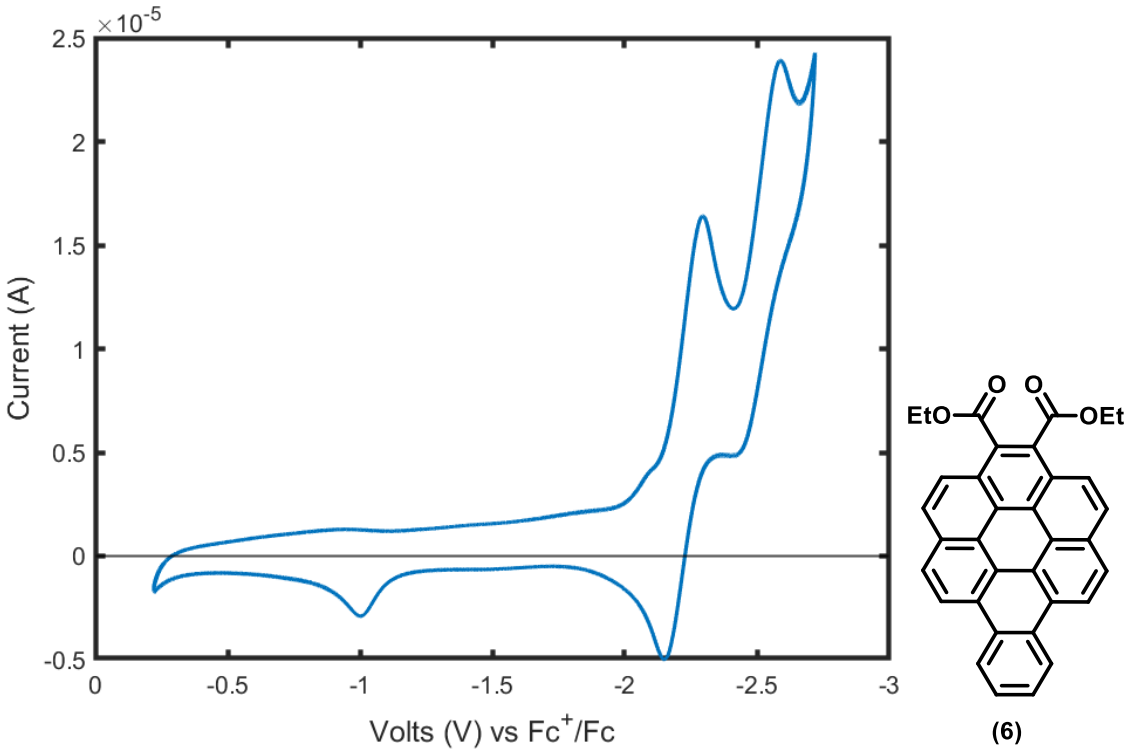

Figure S4.24. Cyclic voltammogram recorded at 100 mV/s for 6 in a 0.1 M $TBAPF_6$ THF solution scanning from –0.2 to –2.72 V and back vs Fc^+/Fc.

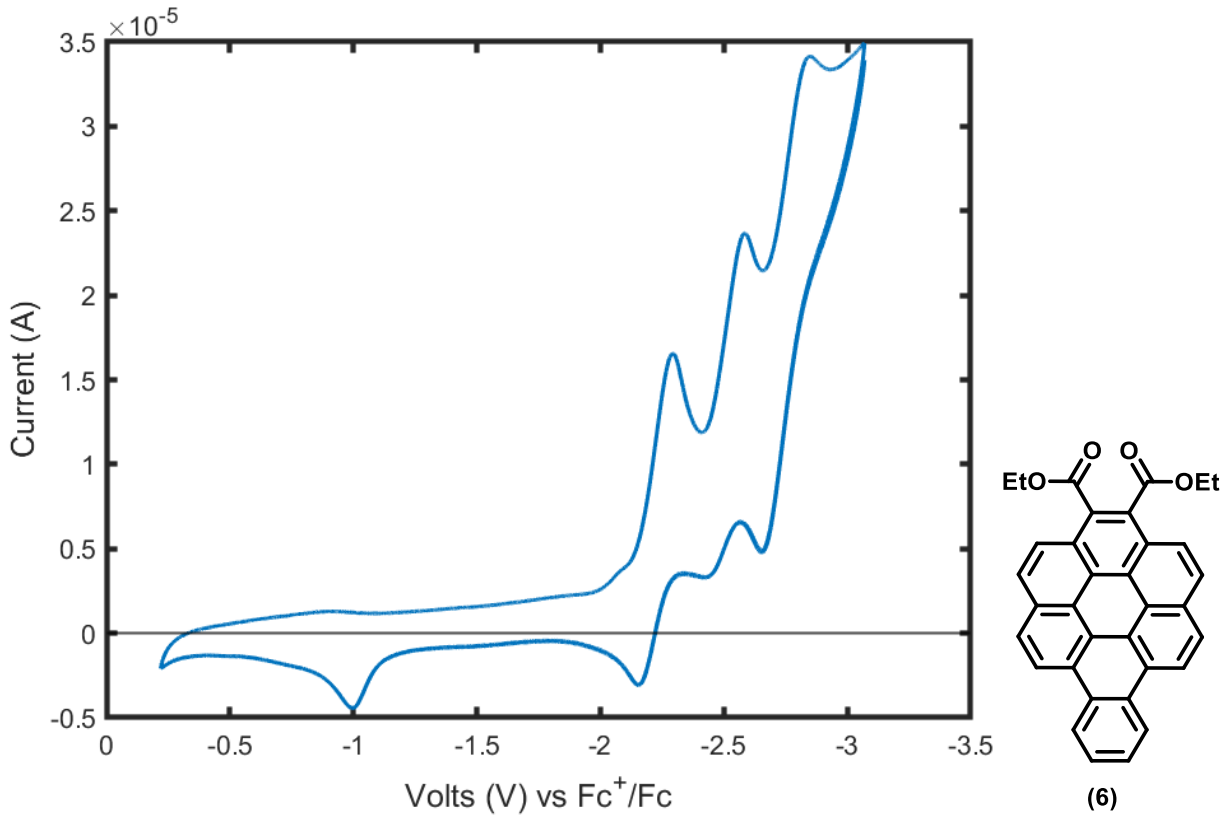

Figure S4.25. Cyclic voltammogram recorded at 100 mV/s for 6 in a 0.1 M TBAPF$_6$ THF solution scanning from –0.2 to –3.07 V and back vs Fc$^+$/Fc.

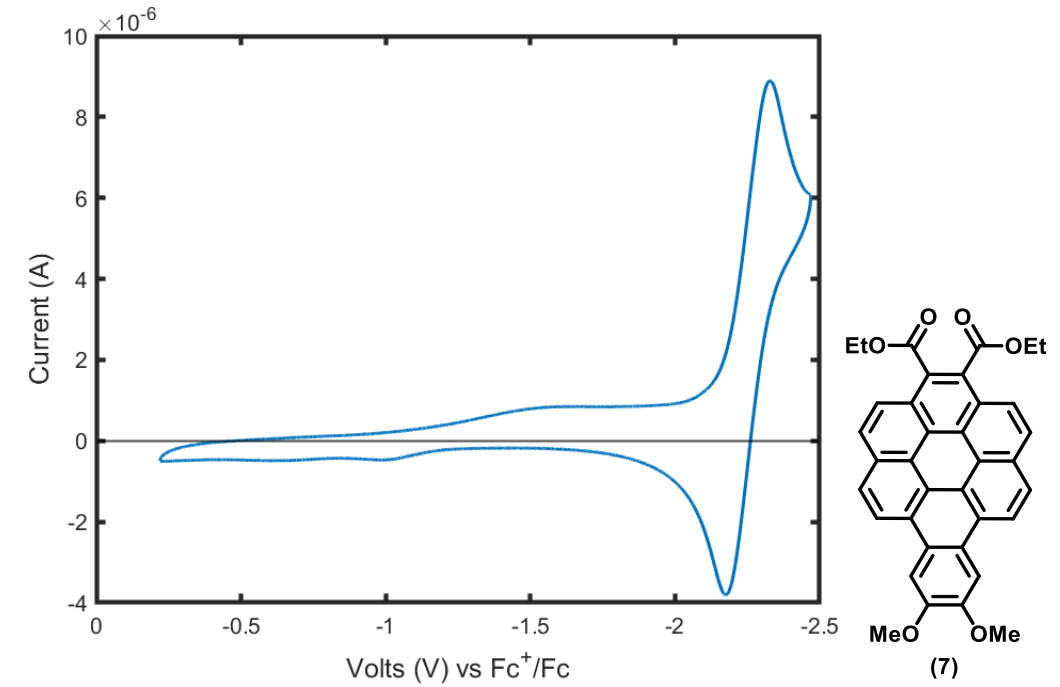

Figure S4.26. Cyclic voltammogram recorded at 100 mV/s for 7 in a 0.1 M $TBAPF_6$ THF solution scanning from –0.2 to –2.5 V and back vs Fc^+/Fc.

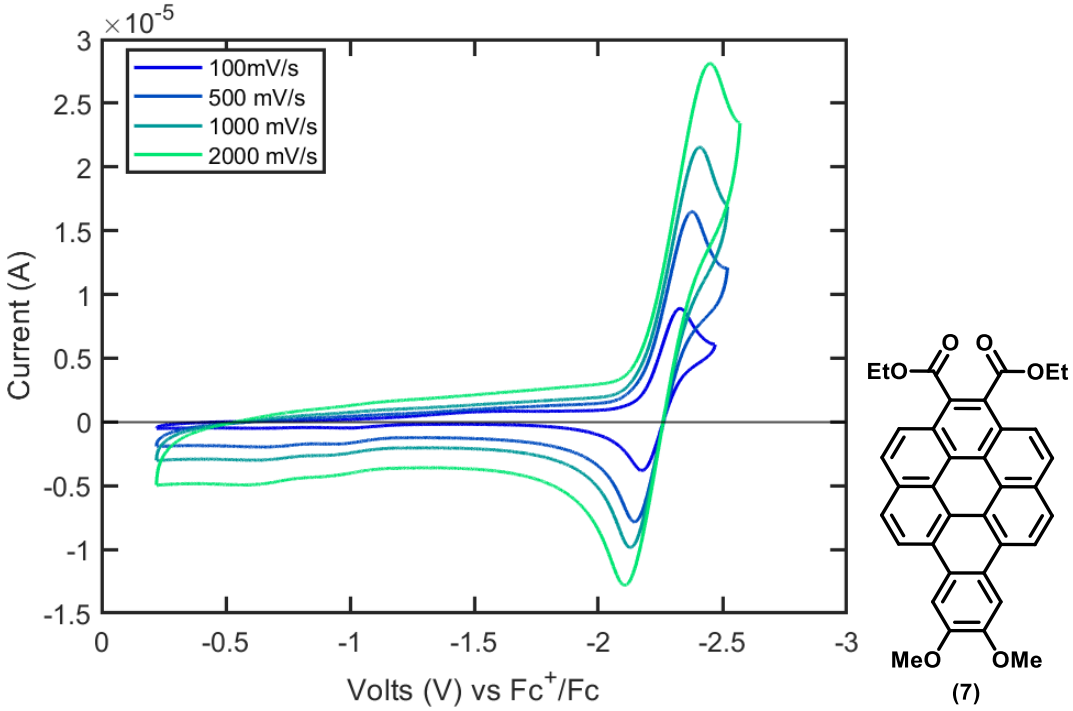

Figure S4.27. Cyclic voltammograms recorded at scan rates of 100 to 2000 mV/s of 7 in a 0.1 M $TBAPF_6$ THF solution just capturing the first reduction event.

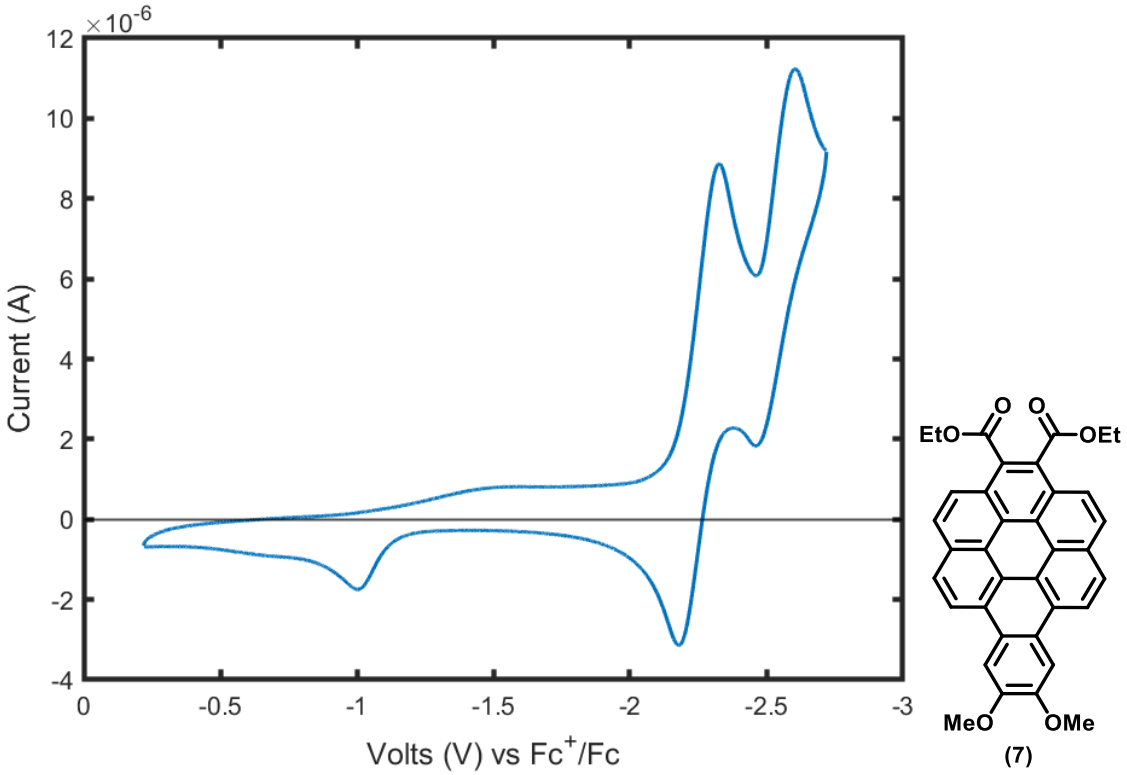

Figure S4.28. Cyclic voltammogram recorded at 100 mV/s for 7 in a 0.1 M $TBAPF_6$ THF solution scanning from –0.2 to –2.72 V and back vs Fc^+/Fc.

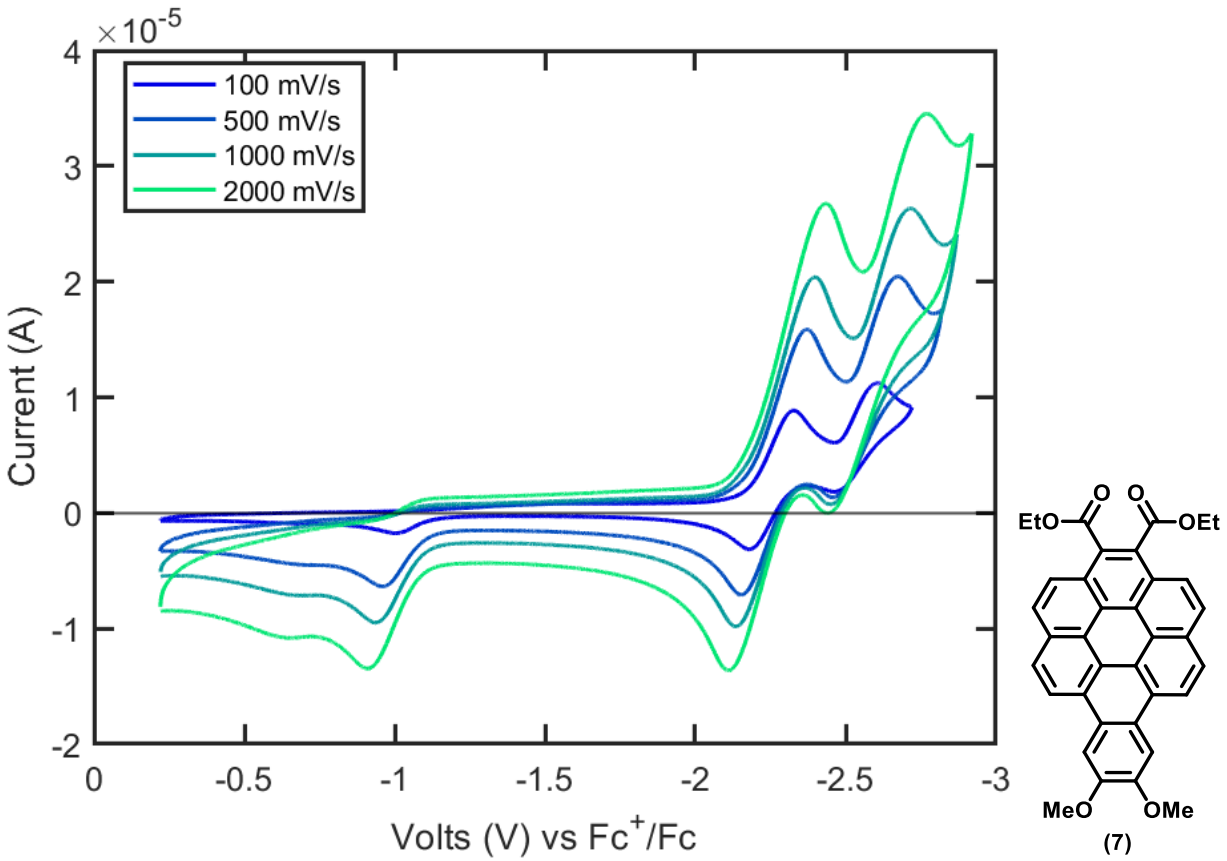

Figure S4.29. Cyclic voltammogram recorded at scan rates of 50 to 1000 mV/s of 7 at scan rates of 100 to 2000 mV/s in 0.1 M $TBAPF_6$ THF solution capturing till the second reduction event.

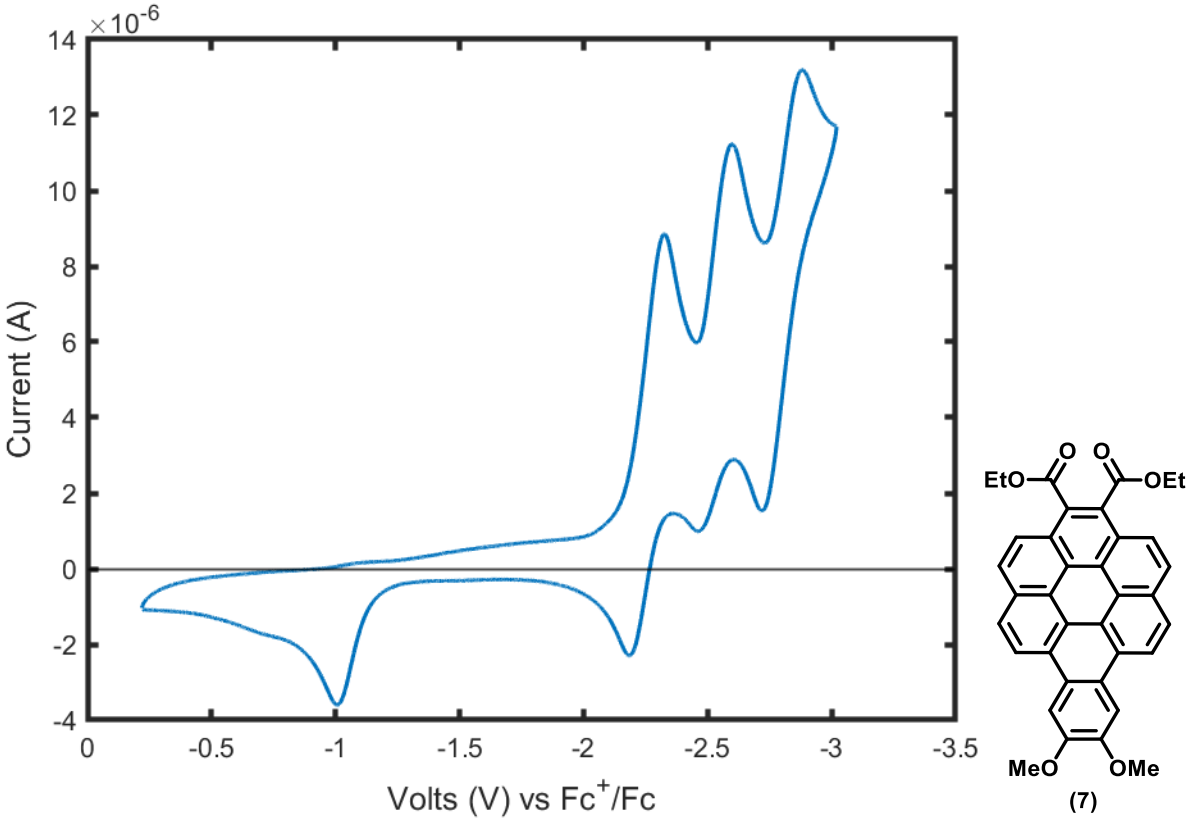

Figure S4.30. Cyclic voltammogram recorded at 100 mV/s for 7 in a 0.1 M $TBAPF_6$ THF solution scanning from –0.2 to –3.1 V and back vs Fc^+/Fc.

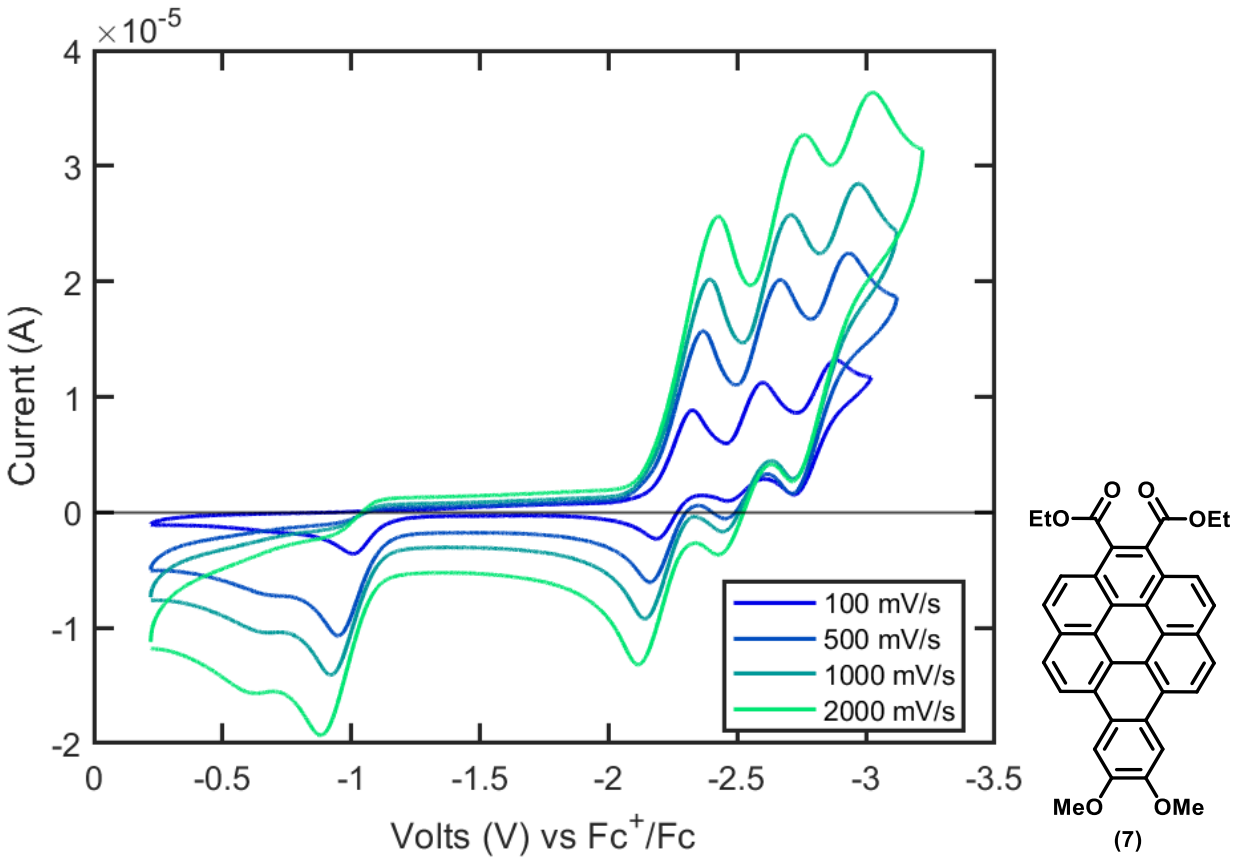

Figure S4.31. Cyclic voltammogram recorded at scan rates of 50 to 1000 mV/s of 7 (1 mM) at scan rates of 50 to 1000 mV/s in 0.1 M $TBAPF_6$ THF solution capturing the third reduction event.

18. Spectroelectrochemistry

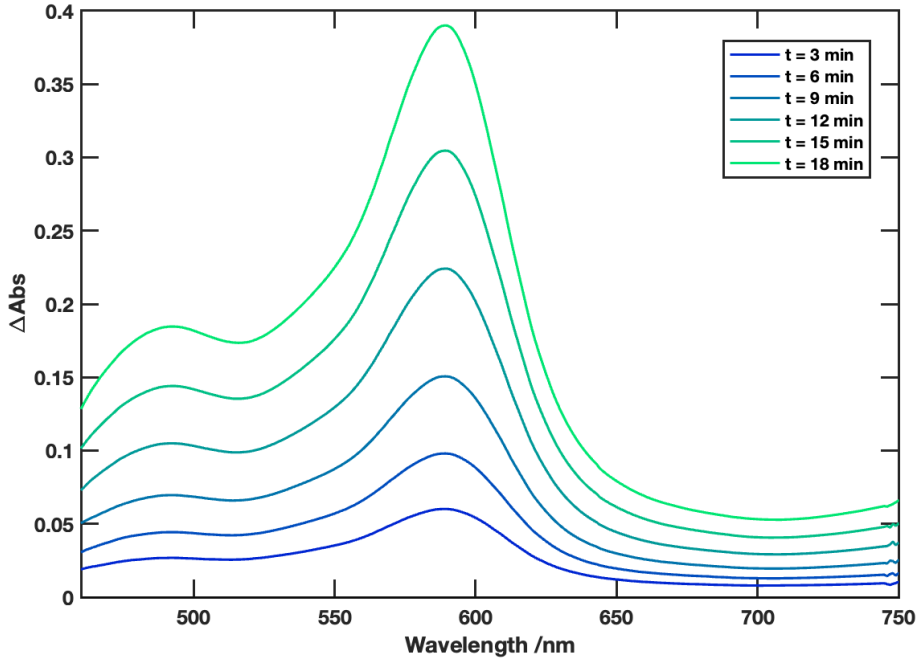

Figure S4.32. Spectroelectrochemical study of 4-OMe in 0.1 M $TBAPF_6$ THF solution with the Pt mesh working electrode held just past the $1e^-$ reducing potential at –2.3 V vs Fc^+/Fc. Legend indicates the times at which the spectral slices were taken after turning on the reductive potential.

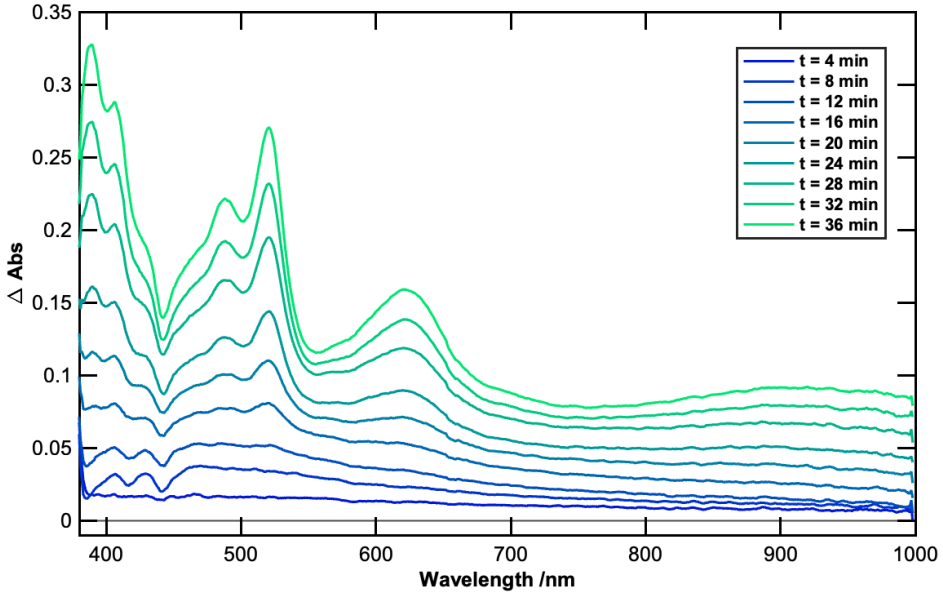

Figure S4.33. *Spectroelectrochemical study of **6** in 0.1 M $TBAPF_6$ THF solution with the Pt mesh working electrode held just past the $1e^-$ reducing potential at –2.35 V vs Fc^+/Fc. Legend indicates the times at which the spectral slices were taken after turning on the reductive potential.*

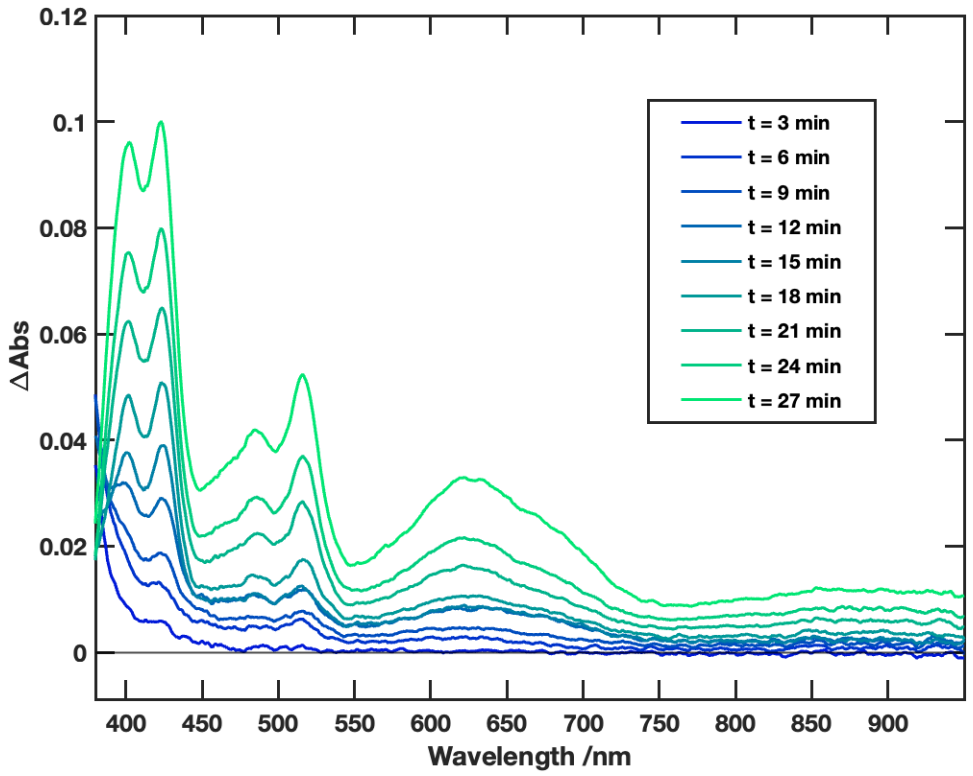

Figure S4.34. Spectroelectrochemical study of 7 in 0.1 M $TBAPF_6$ THF solution with the Pt mesh working electrode held just past the $1e^-$ reducing potential at –2.35 V vs Fc^+/Fc. Legend indicates the times at which the spectral slices were taken after turning on the reductive potential.

19. Bulk Electrolysis

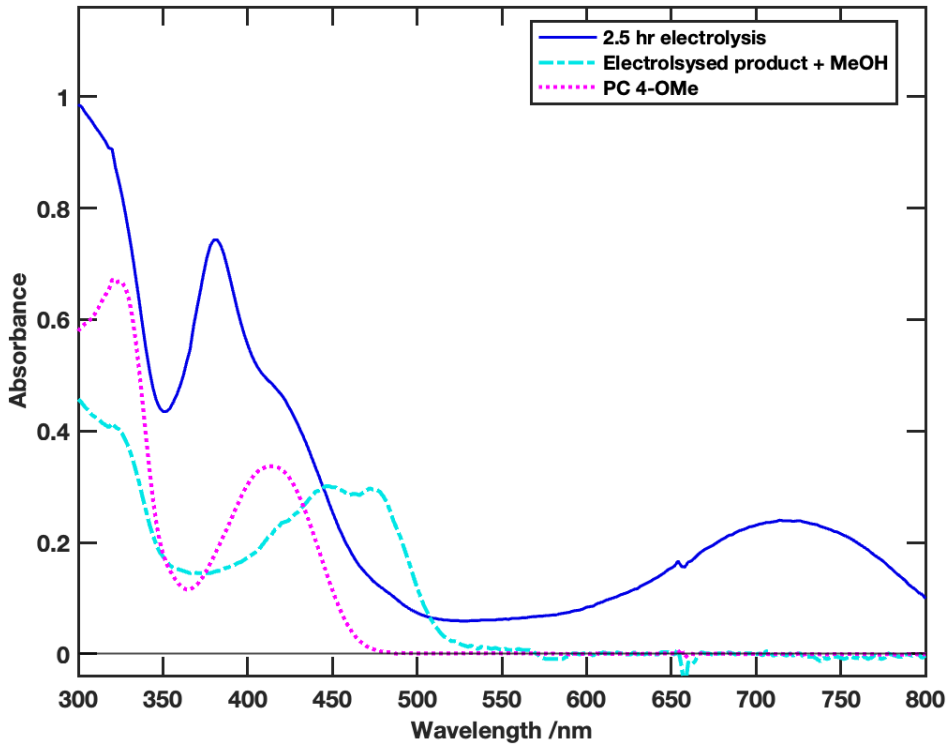

Figure S4.35. The steady state absorption profile of 4-OMe after 2.5 hours of bulk electrolysis at –2.65 V vs. Fc^{+}/Fc in a 0.1 M $TBAPF_6$ THF solution (blue) under an argon atmosphere. After the first absorption spectrum was taken, 15 μL methanol was added to the cuvette and an absorption spectrum was immediately taken (cyan). After addition of methanol, the absorption features associated with $4\text{-}OMe^{2-}$ are quenched in addition to new features centered at 446 and 474 nm (corresponding to $[PC\text{-}H]^{-}$; refer to main text for further discussion). An absorption spectrum of ground state 4-OMe (dotted pink) in THF solution is provided for comparison.

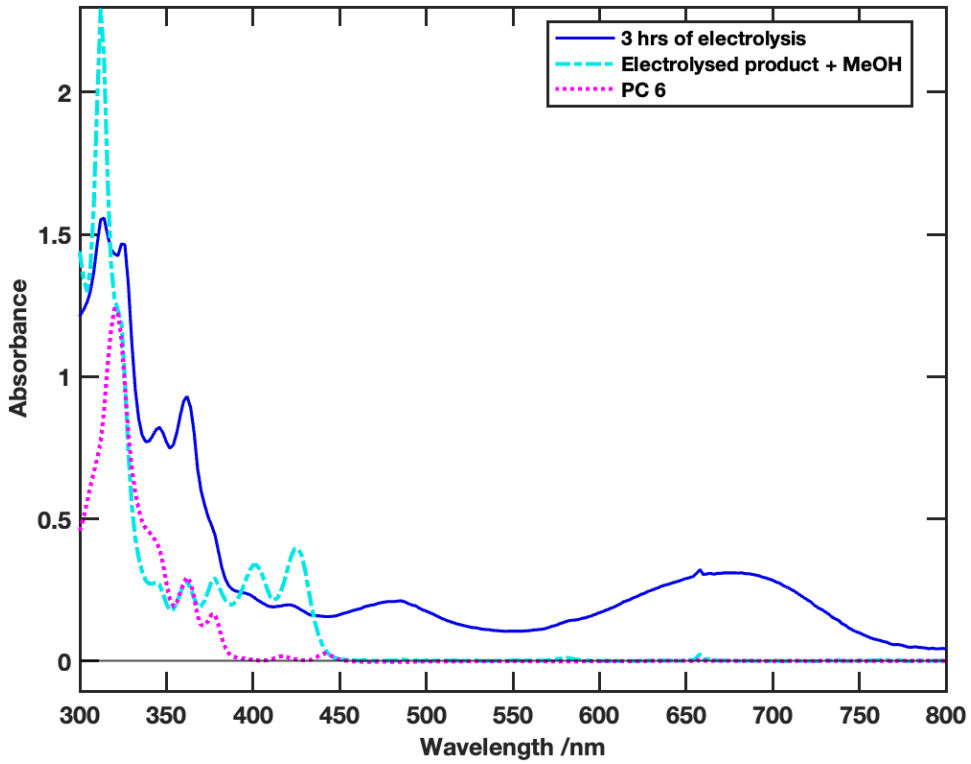

Figure S4.36. The steady state absorption profile of 6 after 3 hours of bulk electrolysis at –2.65 V vs. Fc^+/Fc in a 0.1 M $TBAPF_6$ THF solution (blue) under an argon atmosphere. After the first absorption spectrum was taken, 15 μL methanol was added to the cuvette and an absorption spectrum was immediately taken (cyan). After addition of methanol, the absorption features associated with 6^{2-} are quenched and a new vibronic progression appears with peaks centered at 378, 400 and 425 nm (corresponding to $[PC\text{-}H]^-$; refer to main text for further discussion). The peak at 362 nm coincides with 6 absorption, and we reason, indicates presence of leftover starting material. An absorption spectrum of ground state 6 (dotted pink) in THF solution is provided for comparison.

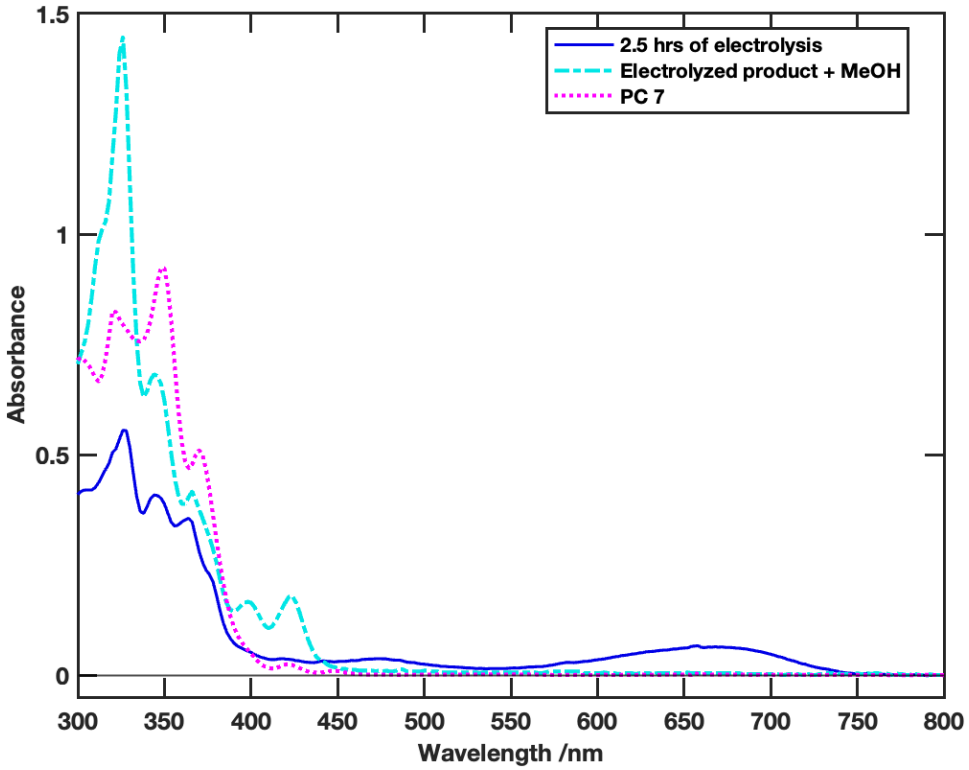

Figure S4.37. The steady state absorption profile of 7 after 2.5 hours of bulk electrolysis at –2.65 V vs. Fc^{+}/Fc in a 0.1 M $TBAPF_6$ THF solution (blue) under an argon atmosphere. After the first absorption spectrum was taken, 15 μL methanol was added to the cuvette and an absorption spectrum was immediately taken (cyan). After addition of methanol, the absorption features associated with 7^{2-} are quenched and a new vibronic progression appears with peaks centered at 400 and 425 nm (corresponding to $[PC\text{-}H]^{-}$; refer to main text for further discussion). The peaks at 345 and 366 nm coincides with 7 absorption, and we reason, indicate presence of leftover starting material. An absorption spectrum of ground state 7 (dotted pink) in THF solution is provided for comparison.

20. Reductant and light induced transformations to the PCs

20a. With TMAOH as reductant

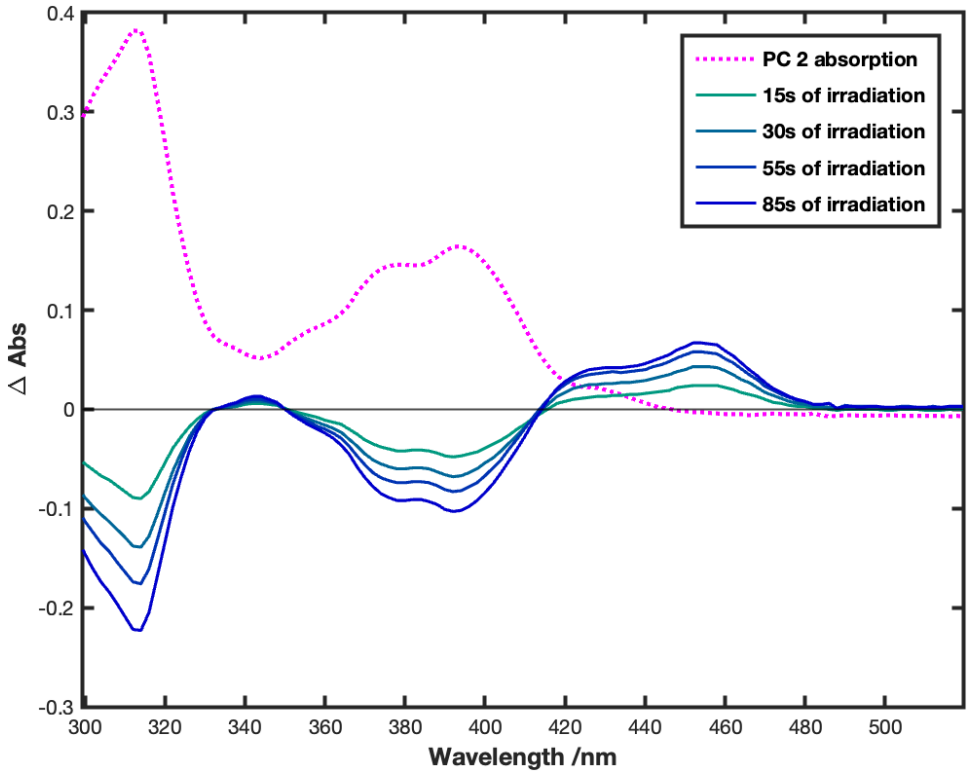

Figure S4.38. Comparing the UV-Vis spectra of 2 before and after irradiation with a 405 nm LED in presence of 225 µL TMAOH in the 2:1 THF:MeOH solvent system. The change in the absorption spectrum is monitored as a difference spectrum. Starting material absorbance is shown as a reference.

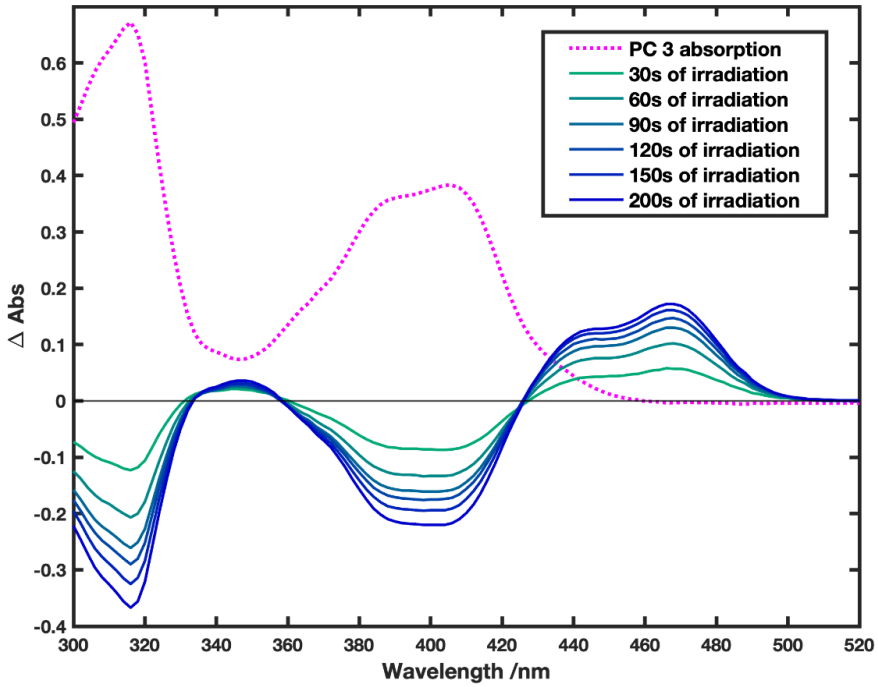

Figure S4.39. Comparing the UV-Vis spectra of 3 before and after irradiation with a 405 nm LED in presence of 225 µL TMAOH in the 2:1 THF:MeOH solvent system. The change in the absorption spectrum is monitored as a difference spectrum. Starting material absorbance is shown as a reference.

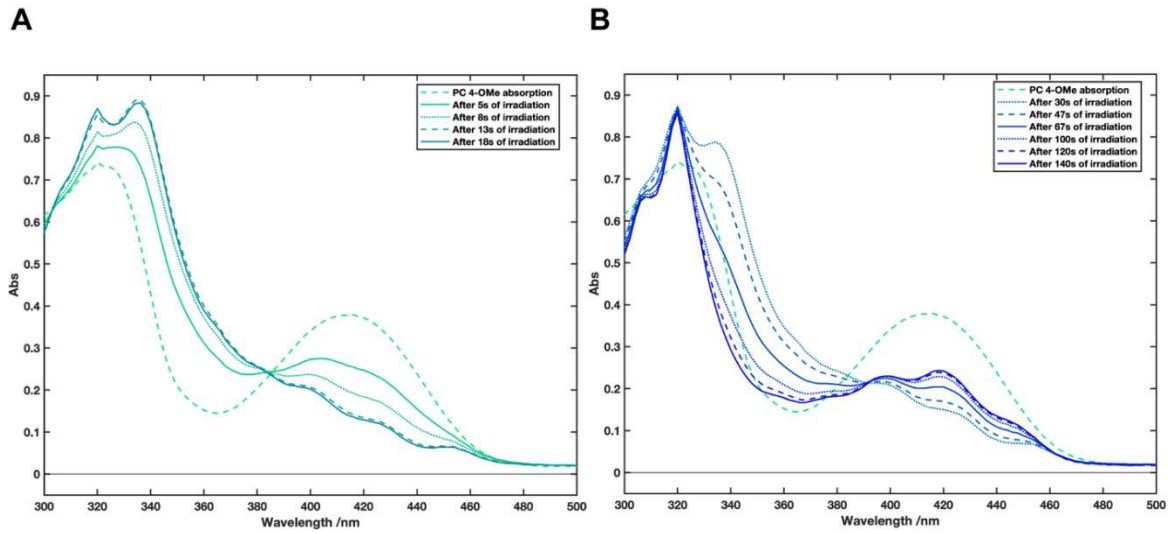

Figure S4.40. Comparing the UV-Vis spectra of 4-OMe before and after irradiation with a 405nm LED in presence of 225 µL TMAOH in the 2:1 THF:MeOH solvent system. The change in the absorption spectrum is monitored as a difference spectrum. Starting material absorbance is shown as a reference.

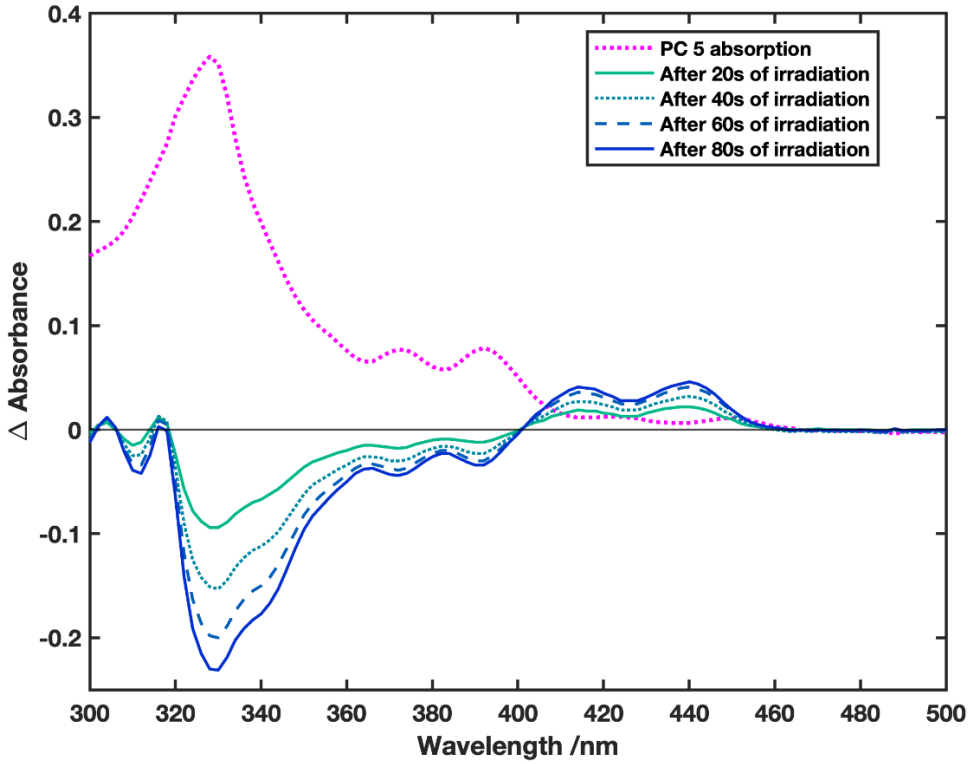

Figure S4.41. Comparing the UV-Vis spectra of 5 before and after irradiation with a 405 nm LED in presence of 225 µL TMAOH in the 2:1 THF:MeOH solvent system. The change in the absorption spectrum is monitored as a difference spectrum. Starting material absorbance is shown as a reference.

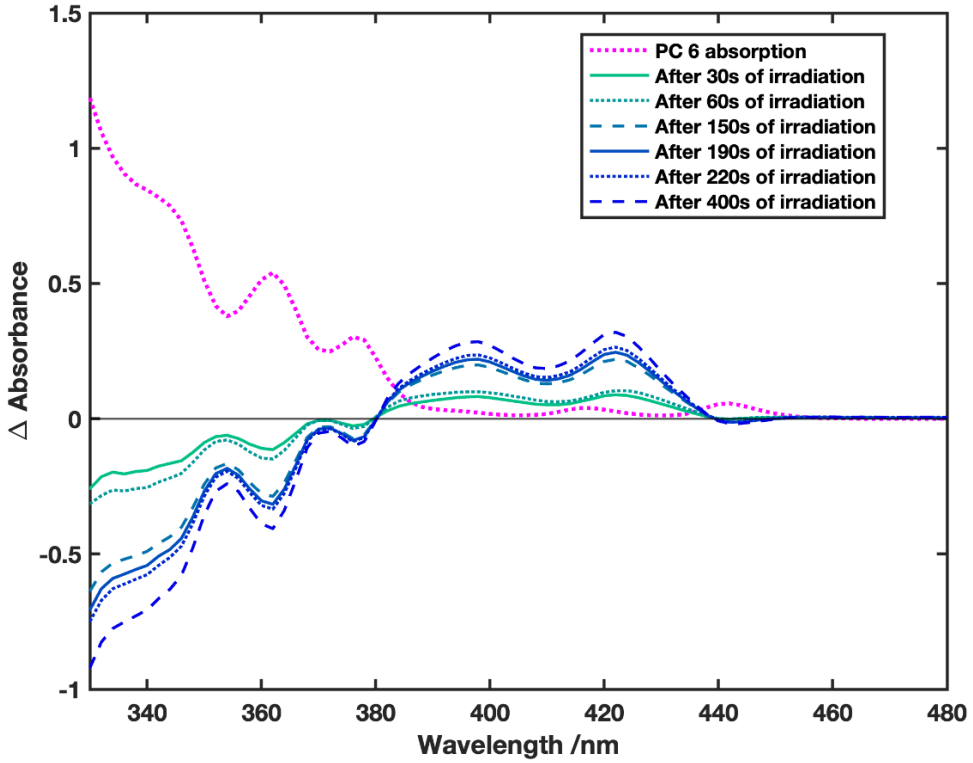

Figure S4.42. Comparing the UV-Vis spectra of 6 before and after irradiation with a 405nm LED in presence of 225 µL TMAOH in the 2:1 THF:MeOH solvent system. The change in the absorption spectrum is monitored as a difference spectrum. Starting material absorbance is shown as a reference.

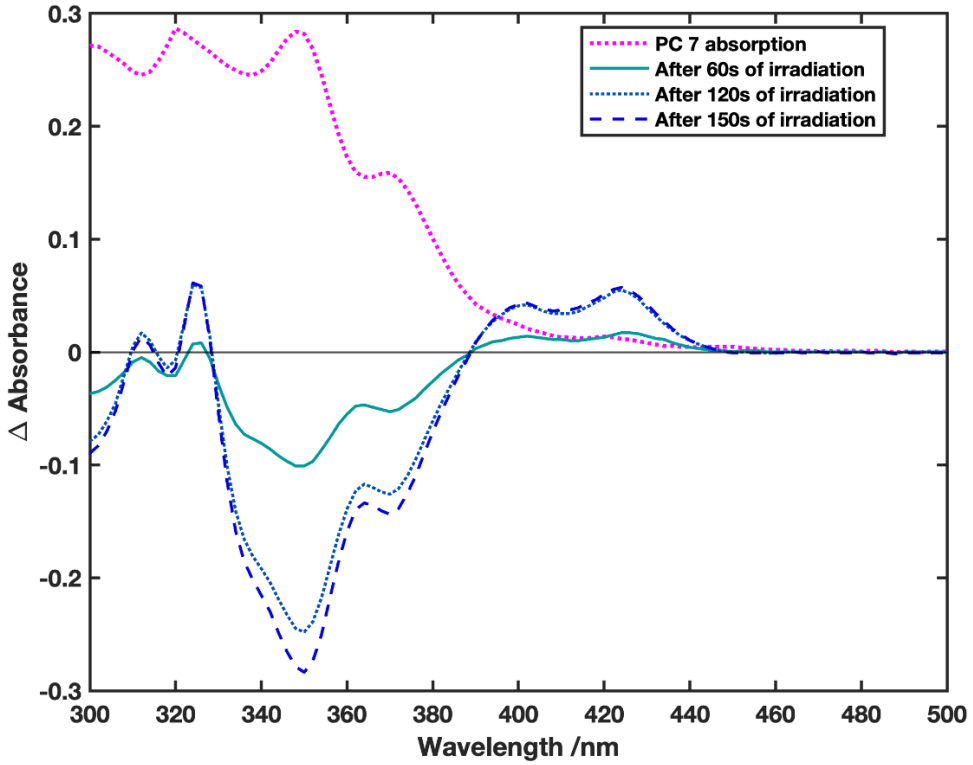

Figure S4.43. Comparing the UV-Vis spectra of 7 before and after irradiation with a 405nm LED in presence of 225 µL TMAOH in the 2:1 THF:MeOH solvent system. The change in the absorption spectrum is monitored as a difference spectrum. Starting material absorbance is shown as a reference.

20b. With *n*Bu$_4$F as reductant

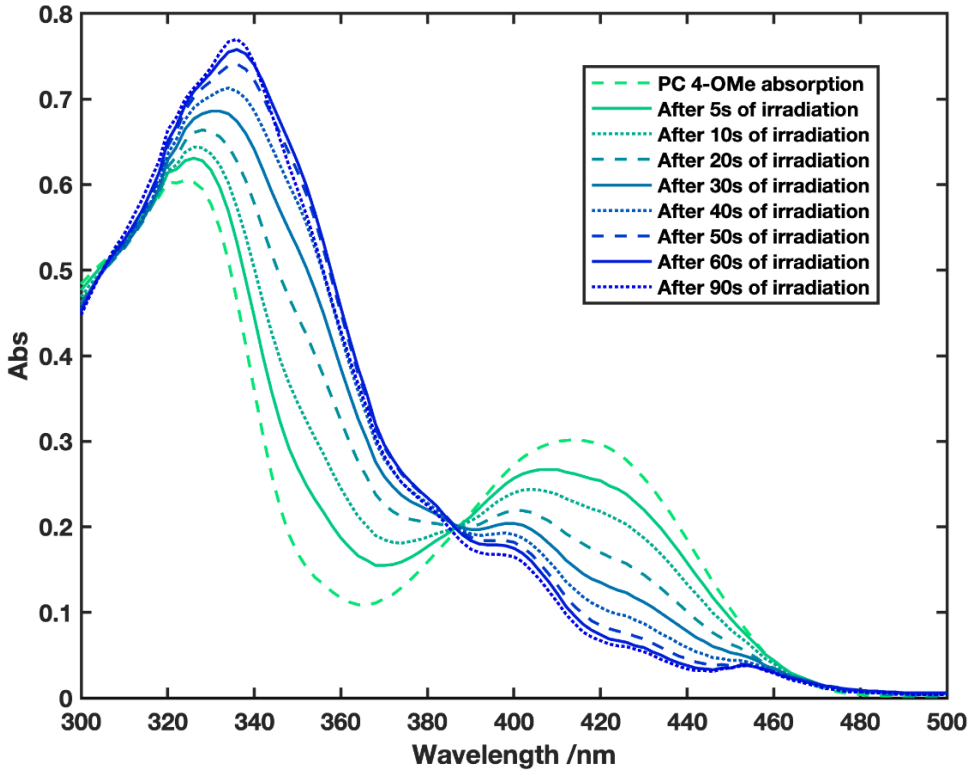

Figure S4.44. Comparing the UV-Vis spectra of 4-OMe before and after irradiation with a 405 nm LED in presence of 25 µL TBAF in the 95:5 THF:tAmOH solvent system. The change in the absorption spectrum is monitored as a function of irradiation time.

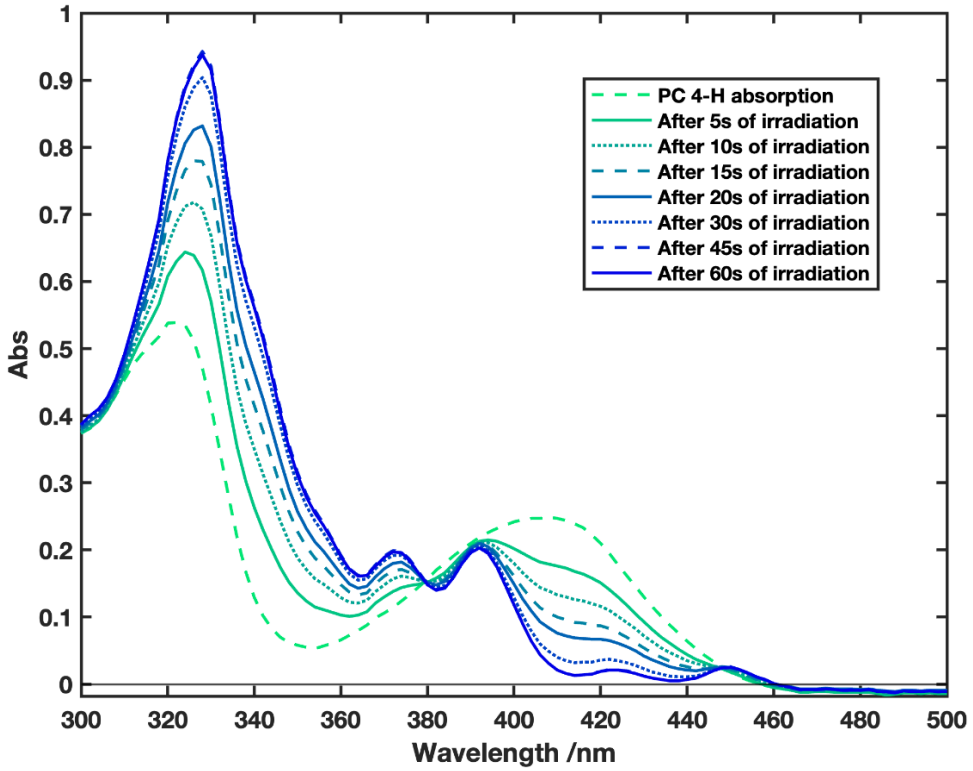

Figure S4.45. Comparing the UV-Vis spectra of 4-H before and after irradiation with a 405 nm LED in presence of 25 µL TBAF in the 95:5 THF:tAmOH solvent system. The change in the absorption spectrum is monitored as a function of irradiation time.

21. Photophysics of electrochemically generated [PC-H]$^-$

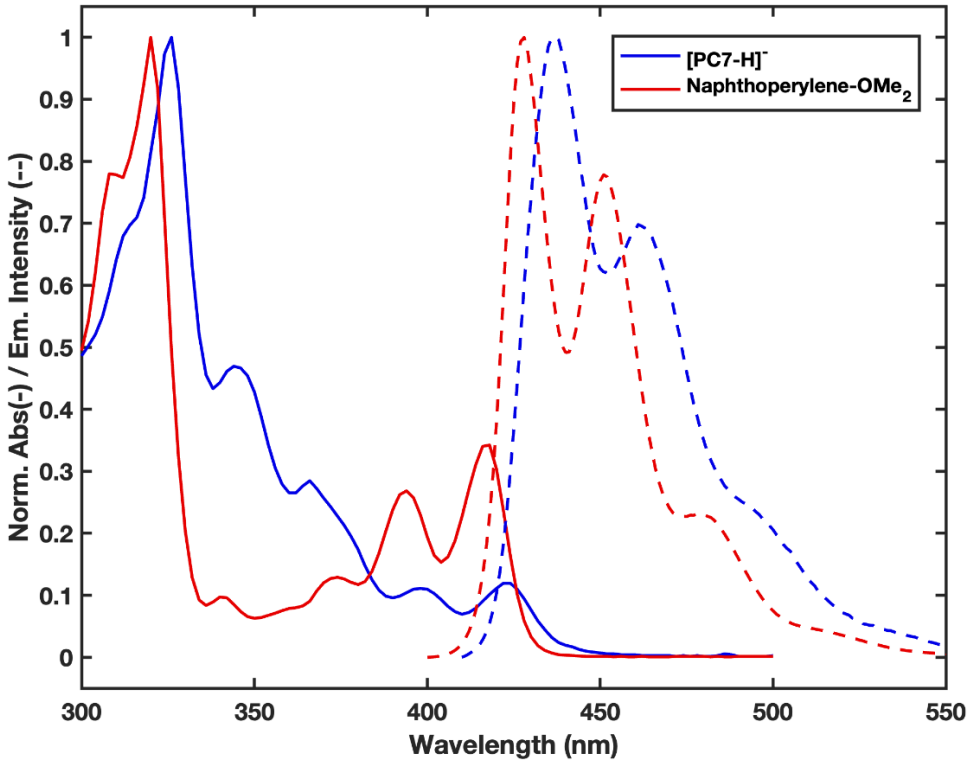

Figure S4.46. Comparing the absorption and emission spectra of electrochemically generated [7-H]$^-$ (electrolyzed at -2.45 V vs Ag/AgNO$_3$ and quenched with MeOH) with that of dimethoxy naphthoperylene (7a) (in THF). The sample does contain a small amount of 7 as is evident by the shape of the peaks at 346 and 366 nm where 7 absorbs strongly.

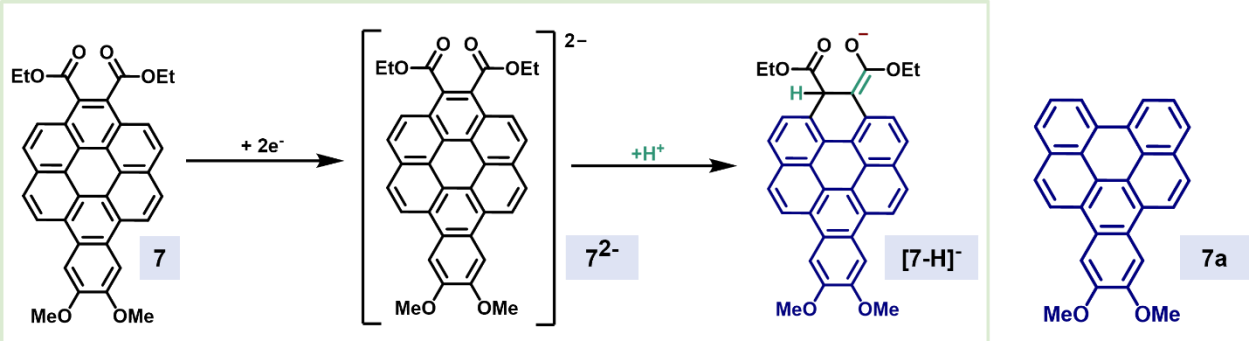

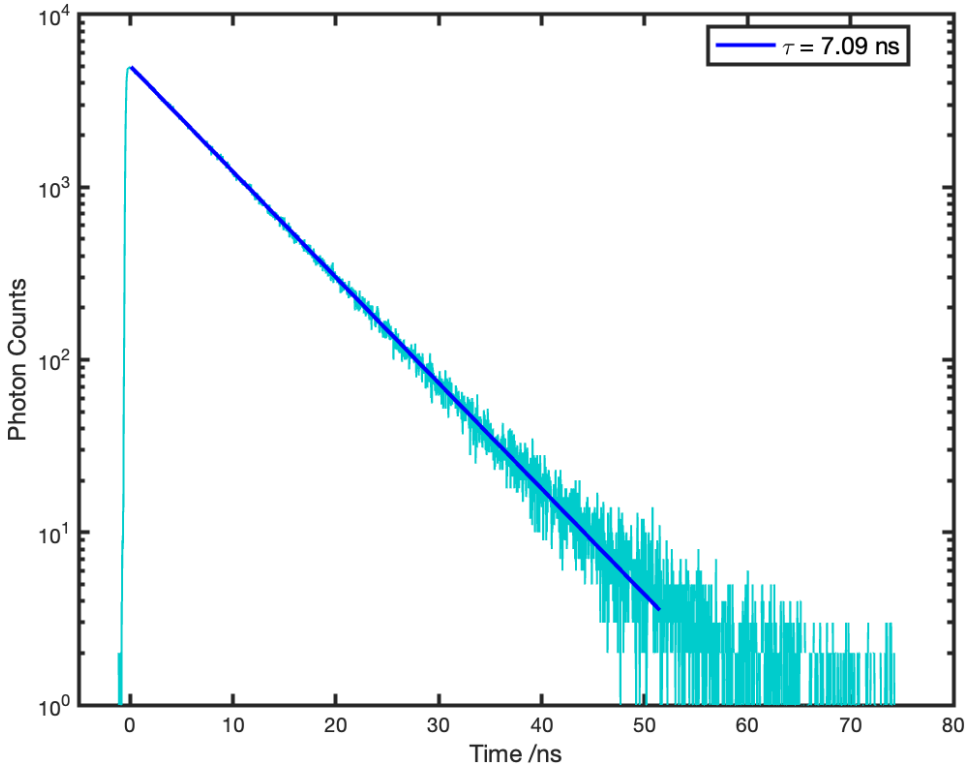

Figure S4.47. Plot of fluorescence decay of electrochemically generated [7-H]⁻ in THF photoexcited at 405 nm. The detected emission wavelength = 435 nm. A monoexponential fit indicates a lifetime of 7.09 ns.

22. Transient Absorption Studies

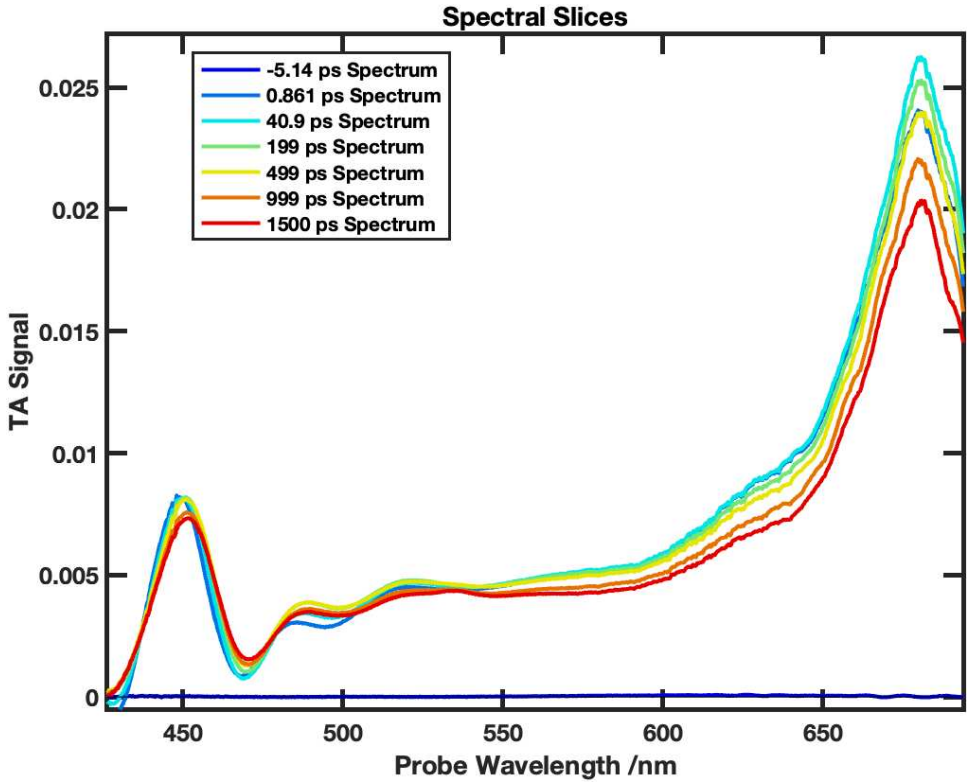

Figure S4.48. Picosecond transient absorption spectra for electrochemically generated [6-H]$^-$ in THF (the sample does contain trace amount of MeOH which was used to quench PC^{2-}; however, its effect is presumably negligible).

23. Fluorescence Quenching Using Electrochemically Generated [PC-H]$^-$

Sample preparation: **7** was electrolyzed at -2.85 V (vs Fc^+/Fc) in THF with $TBAPF_6$ as the supporting electrolyte (0.1M) in presence of tAmOH/MeOH to generate **[7-H]**$^-$; typically, 15-30 µL of this electrolyzed solution was then diluted with 2.5 mL of 2:1 THF/MeOH solvent mixture inside an Ar-filled glovebox to prepare a sample which was then transferred into a cuvette sealed with a Kontes valve to keep it air-free for the duration of the experiment. The purpose of only using a small amount of **[7-H]**$^-$ was to keep the absorbance <0.1 to avoid the effect of self-

absorption. A steady-state fluorescence spectrum was collected by exciting the sample at 445 nm with an integration time of 0.2 seconds. This served as the reference spectrum (F_0) for the calculation of Stern-Volmer quenching rates. The cuvette was then again pumped into the glovebox where an appropriate amount of quencher was added to the sample to achieve the first quencher concentration mentioned in the figure legends. A second fluorescence spectrum was then collected by exciting the sample at the same wavelength (i.e. 445 nm). This process was repeated two more times at which point the fluorescence spectra for three different concentrations of the quencher had been collected in total. The Stern-Volmer (K_{SV}) rate constant was calculated using the following equation:

$$\frac{F_0}{F} = 1 + K_{SV}[Q] \qquad \text{- Equation S4.1}$$

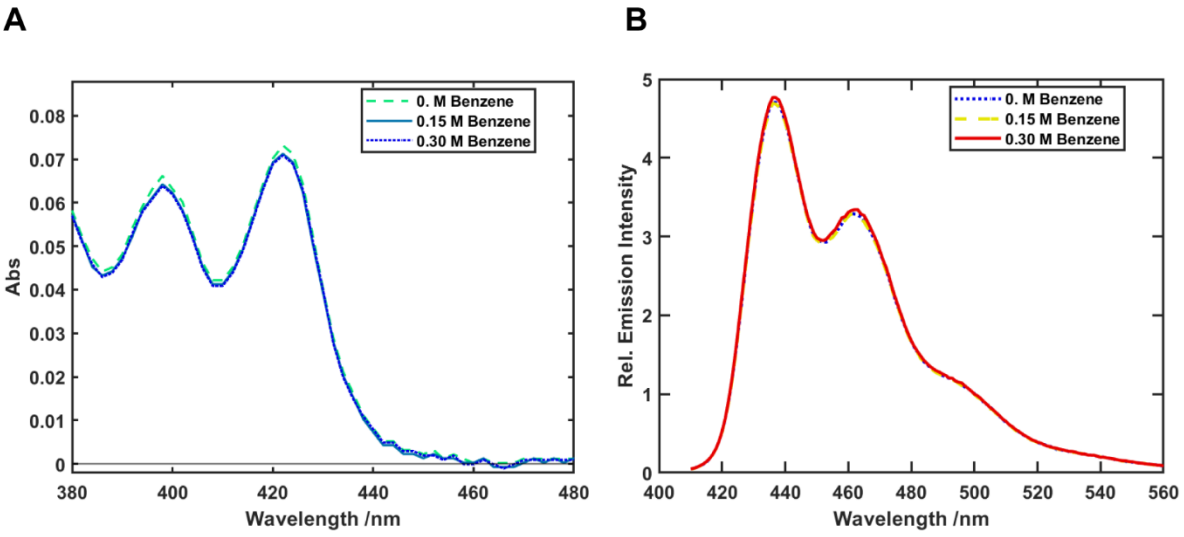

Figure S4.49. Attempted fluorescence quenching with electrochemically generated [7-H]⁻ without presence of TMAOH. (A) UV-Visible spectra of the samples used for the fluorescence quenching experiments shown in panel B. (B) Steady-state emission spectra of [7-H]⁻ collected in presence of 3 different concentration of benzene. As evident from the unchanged fluorescence intensity, there is very little quenching when there is no base.

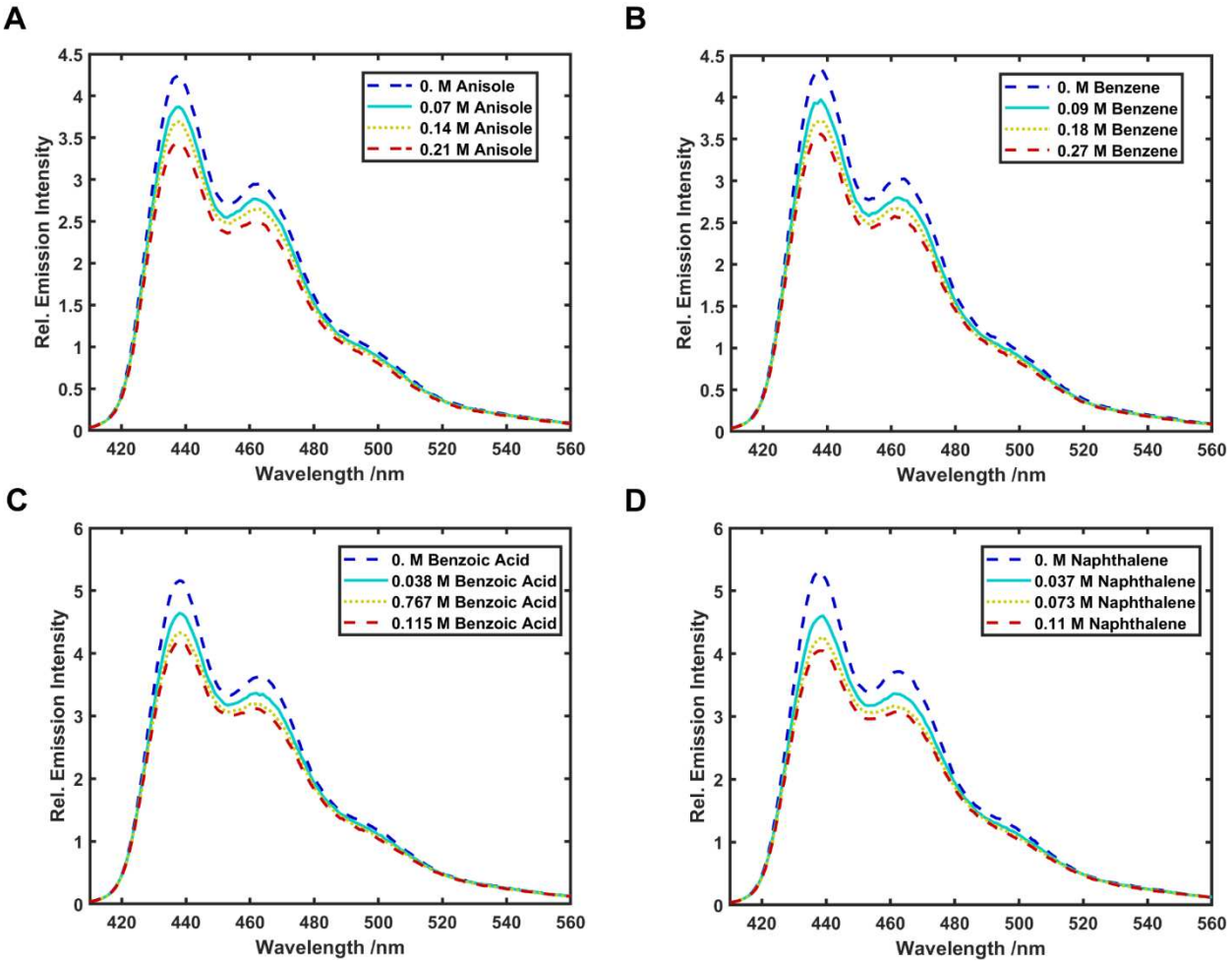

Figure S4.50a. Steady-state emission spectra: Fluorescence quenching with 4 different substrates (A) anisole, (B) benzene, (C) benzoic acid, (D) naphthalene. 300 µL of TMAOH (25 wt% in MeOH) were added to the electrolyzed [7-H]$^-$ (diluted with 2.5 mL 2:1 THF:MeOH) while preparing the samples for each of the quenchers. Since anisole and benzene are all liquids, they were added directly in increments of 20 µL respectively whereas stock solutions (394 mg/mL) in THF was prepared for both benzoic acid and naphthalene and were added to the cuvettes in increments of 30 µL.

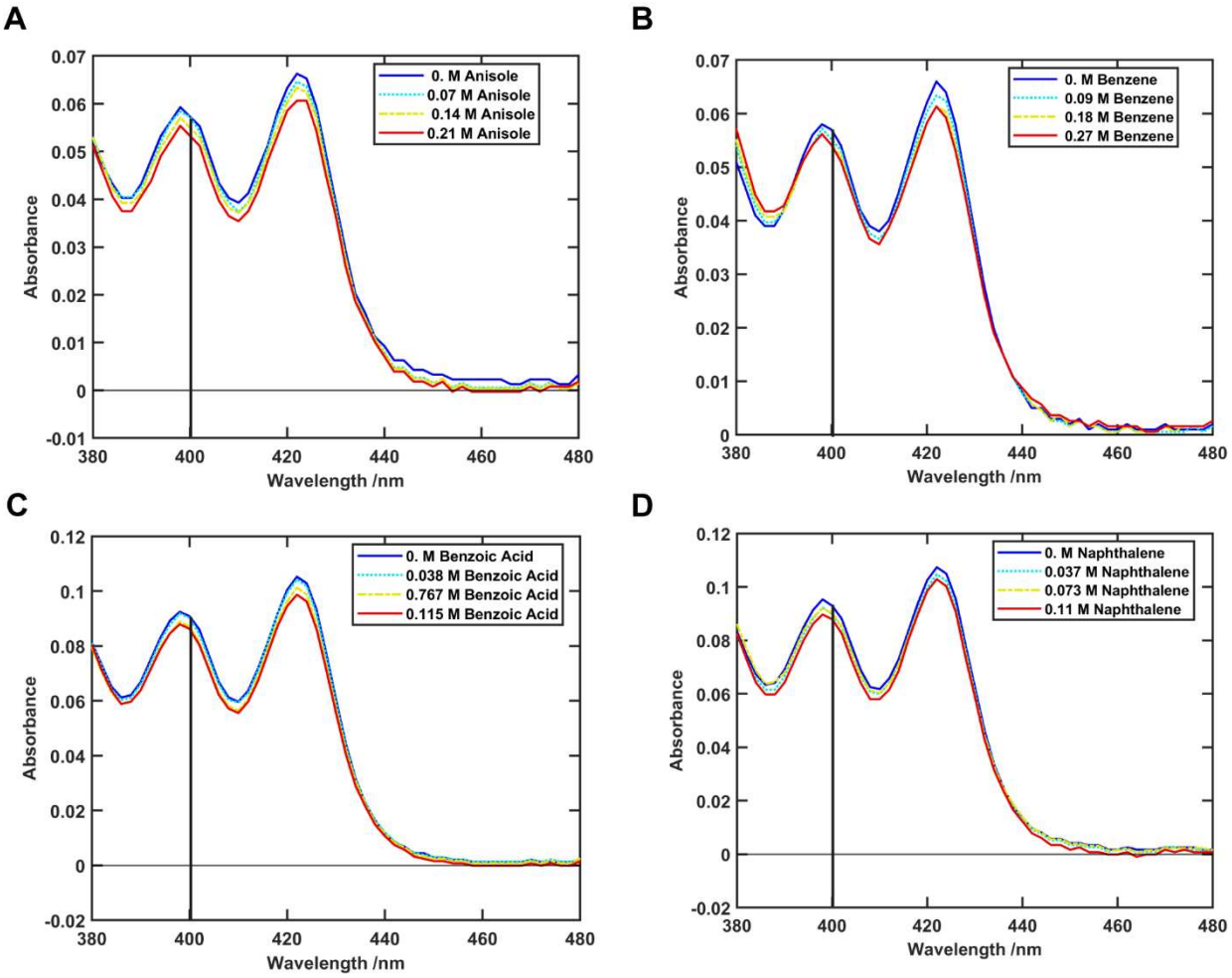

Figure S4.50b. Absorption spectra: UV-Visible spectra of the samples used for the fluorescence quenching experiments shown above in Fig. S50a. Only the 380-480 nm region is shown to highlight the [7-H]$^-$ absorbance. As can be seen in all four panels, the OD at the excitation wavelength 400 nm is only perturbed by a small amount even after introduction of varying amounts of substrates (A) anisole, (B) benzene, (C) benzoic acid, (D) naphthalene.

24. Estimating $E_{0,0}$ values for benzo[a]coronene based PCs

$$E_{0,0}^{S_1} = \frac{1240}{\lambda_{0,0}} = 2.79\ eV$$

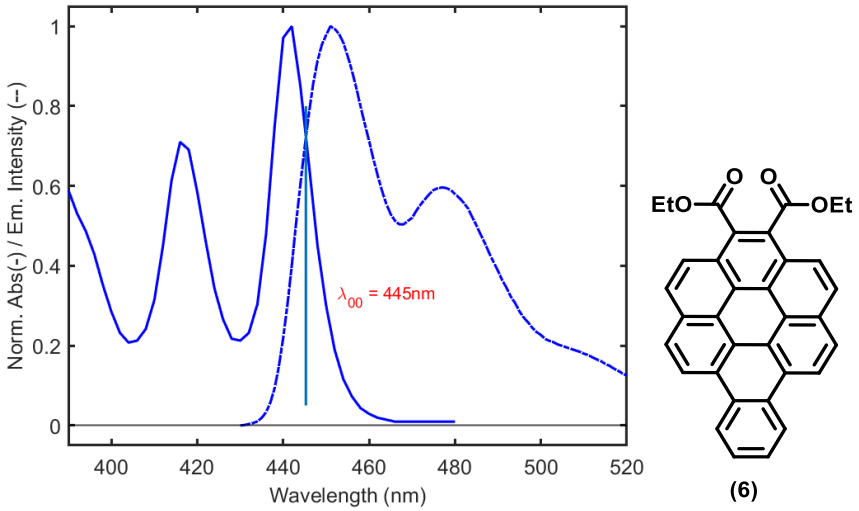

Figure S4.51. Energy stored by the lowest, vibrationally cooled singlet excited state of 6 after absorption of a photon, represented as $E_{0,0}^{S_1}$, estimated from the intersection of the normalized steady state absorbance and normalized emission profiles.

$$E_{0,0}^{S_1} = \frac{1240}{\lambda_{0,0}} = 2.74\ eV$$

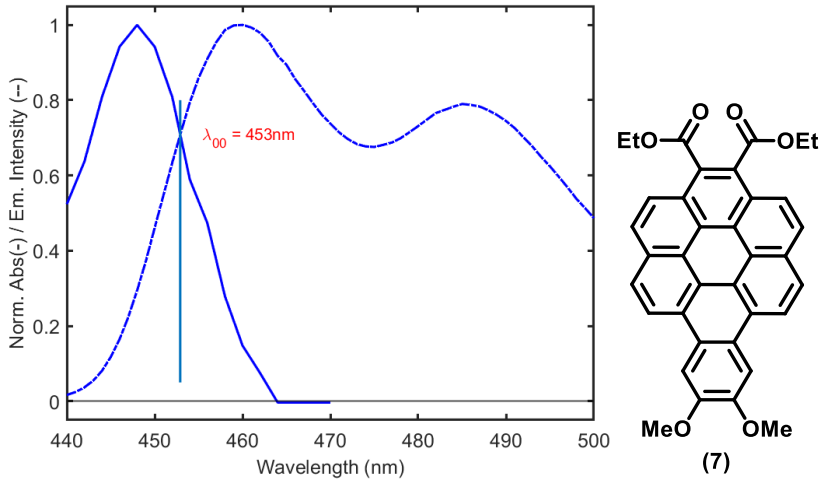

Figure S4.52. Energy stored by the lowest, vibrationally cooled singlet excited state of 7 after absorption of a photon, represented as $E_{0,0}^{S_1}$, estimated from the intersection of the normalized steady state absorbance and normalized emission profiles

$$E_{0,0}^{S_1} = \frac{1240}{\lambda_{0,0}} = 2.88\ eV$$

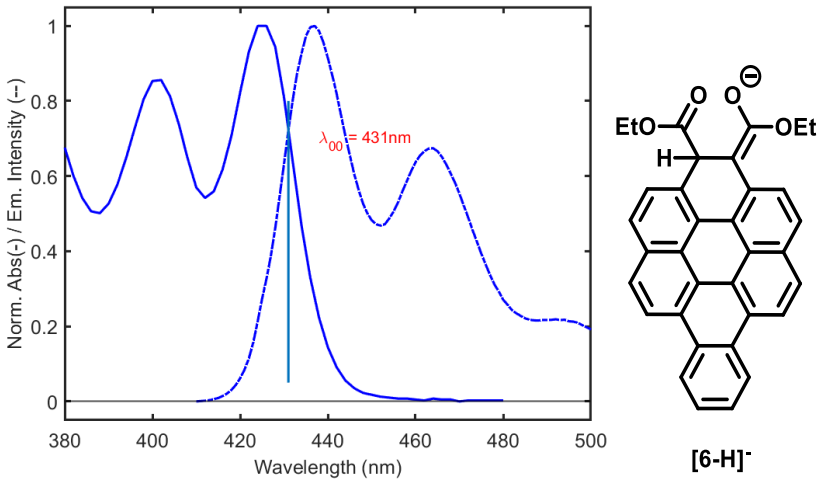

Figure S4.53. Energy stored by the lowest, vibrationally cooled singlet excited state of electrochemically generated [6-H]⁻ after absorption of a photon, represented as $E_{0,0}^{S_1}$, estimated from the intersection of the normalized steady state absorbance and normalized emission profiles.

$$E_{0,0}^{S_1} = \frac{1240}{\lambda_{0,0}} = 2.89\ eV$$

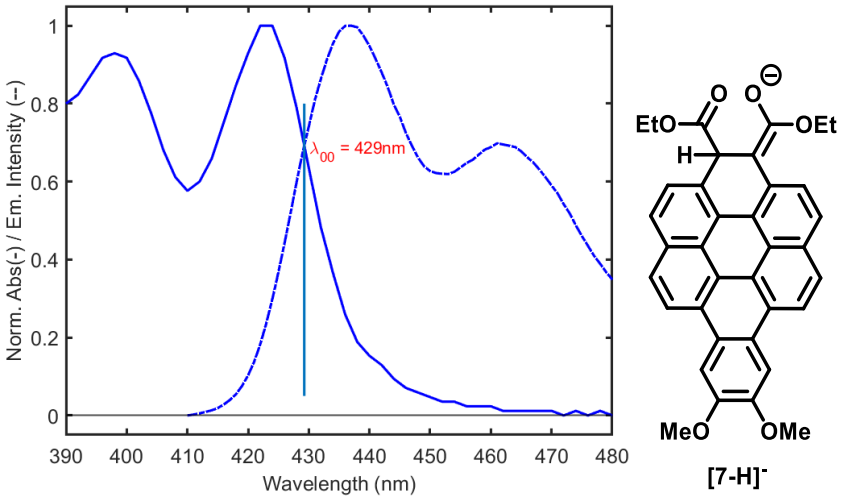

Figure S4.54. Energy stored by the lowest, vibrationally cooled singlet excited state of electrochemically generated [7-H]⁻ after absorption of a photon, represented as $E_{0,0}^{S_1}$, estimated from the intersection of the normalized steady state absorbance and normalized emission profiles.

25. Determination of excited state reduction potential

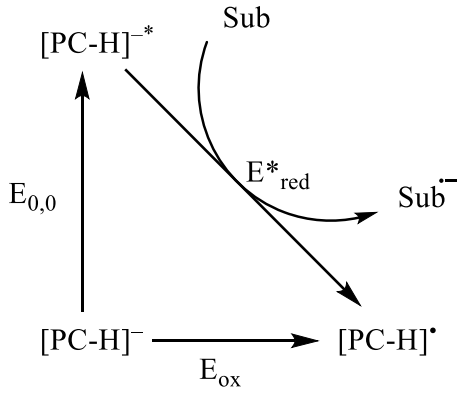

$$E^*_{red} = E_{ox} - E_{0,0}$$

Entry	$E_{0,0}$ (eV)	E_{ox} (vs Fc^+/Fc)	E^*_{red} (vs Fc^+/Fc)
[**6-H**]$^-$	2.88	-1	-3.88
[**7-H**]$^-$	2.89	-1.01	-3.9

Entry	$E_{0,0}$ (eV)	E_{ox} (vs Fc^+/Fc)	E^*_{red} (vs Fc^+/Fc)	E^*_{red} (vs SCE)	E^*_{red} (vs SCE)
[**6-H**]$^-$	2.88	-1	-3.88	-0.62	-3.5
[**7-H**]$^-$	2.89	-1.01	-3.9	-0.63	-3.52

Figure S4.55. Latimer diagram describing the excited state redox potential of [PC-H]$^-$. The oxidation potential of [PC-H]$^-$ to [PC-H]$^•$ was garnered through cyclic voltammetry (see the Electrochemistry section). The oxidation of this species is coupled to a further loss of an electron and a proton. However, for the purposes of determining the driving force for one electron reduction of the substrates, [PC-H]$^•$ is used as the oxidized intermediate.

26. Computational details and coordinates for computed structures

In progress

27. ^{1}H and ^{13}C NMR spectra for synthesized compounds

28. Analytical data:

1-Methoxycyclohexa-1,4-diene (11): Colorless oil (16 mg, 59%), eluent combination: hexane/ethyl acetate (10:1).

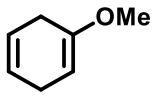

^{1}H NMR (400 MHz, MeOD) δ 5.45 (tt, *J* = 3.1, 1.4 Hz, 2H), 4.43 (t, *J* = 3.8 Hz, 1H), 3.31 (s, 3H), 2.57 (dddd, *J* = 11.5, 6.5, 3.4, 1.4 Hz, 2H), 2.45 (dddd, *J* = 9.0, 7.5, 2.8, 1.3 Hz, 2H); ^{13}C{^{1}H} NMR (101 MHz, MeOD) δ 153.9, 125.5, 124.0, 91.4, 53.9, 29.33, 27.2 ppm.

HRMS: (ESI) Calc. for $C_7H_{10}O$ 111.0812 (calculated) $[M+H]^+$, found 111.0802 (experimental).

4-(Cyclohexa-1,4-dien-1-yl)butan-2-ol (13): Colorless oil (30 mg, 81%), eluent combination: hexane/ethyl acetate (10:1).

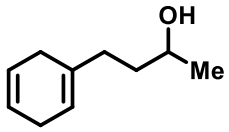

^{1}H NMR (400 MHz, $CDCl_3$) δ 5.70 (dq, *J* = 2.8, 1.5 Hz, 2H), 5.46 (dq, *J* = 3.3, 1.7 Hz, 1H), 3.81 (h, *J* = 6.2 Hz, 1H), 2.73 – 2.57 (m, 4H), 2.14 – 1.97 (m, 2H), 1.57 (dtd, *J* = 8.8, 6.9, 3.0 Hz, 3H), 1.49 (d, *J* = 3.4 Hz, 1H), 1.20 (d, *J* = 6.2 Hz, 3H); ^{13}C{^{1}H} NMR (101 MHz, $CDCl_3$) δ 134.9, 124.4, 124.3, 118.8, 68.1, 36.8, 33.9, 29.0, 26.8, 23.6 ppm. The NMR spectroscopic data is in agreement with the literature[6] .

3-(Cyclohexa-1,4-dien-1-yl)propan-1-ol (14): Colorless oil (26 mg, 76%), eluent combination: hexane/ethyl acetate (10:1).

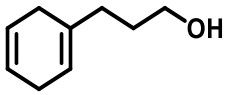

^{1}H NMR (400 MHz, $CDCl_3$) δ 5.70 (hept, *J* = 1.3 Hz, 2H), 5.45 (tt, *J* = 3.2, 1.3 Hz, 1H), 3.64 (t, *J* = 6.5 Hz, 2H), 2.74 – 2.56 (m, 4H), 2.09 – 2.00 (m, 2H), 1.75 – 1.63 (m, 2H); ^{13}C{^{1}H} NMR (101 MHz, $CDCl_3$) δ 134.6, 124.3, 124.3, 118.8, 62.8, 33.8, 30.3, 29.0, 26.8 ppm. The NMR spectroscopic data is in agreement with the literature[2b] .

2-(Cyclohexa-1,4-dien-1-yl)ethan-1-amine (15): Colorless oil (20 mg, 66%), eluent combination: hexane/ethyl acetate (10:1).

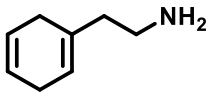

^{1}H NMR (400 MHz, $CDCl_3$) δ 5.71 – 5.56 (m, 2H), 5.48 – 5.38 (m, 1H), 2.78 – 2.59 (m, 4H), 2.59 – 2.47 (m, 2H), 2.11 – 1.99 (m, 2H), 1.06 (d, *J* = 3.0 Hz, 2H); ^{13}C NMR (101 MHz, $CDCl_3$) δ 132.3, 124.2, 124.1, 120.3, 41.6, 39.6, 28.7, 26.7 ppm. The NMR spectroscopic data is in agreement with the literature[7] .

4-(cyclohexa-1,4-dien-1-yl)butanoic acid (17): Colorless oil (30 mg, 75%), eluent combination: hexane/ethyl acetate (10:1).

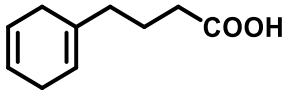

^{1}H NMR (400 MHz, $CDCl_3$) δ 5.70 (dq, *J* = 2.7, 1.8 Hz, 2H), 5.44 (dq, *J* = 3.3, 1.4 Hz, 1H), 2.75 – 2.63 (m, 2H), 2.63 – 2.54 (m, 2H), 2.35 (t, *J* = 7.5 Hz, 2H), 2.07 – 1.97 (m, 2H), 1.81 – 1.72 (m, 2H); ^{13}C{^{1}H} NMR (101 MHz, $CDCl_3$) δ 179.9, 133.8, 124.3, 124.3, 119.5, 36.7, 33.5, 28.8, 26.8, 22.3 ppm. The NMR spectroscopic data is in agreement with the literature[2b].

1,5-Dimethoxycyclohexa-1,4-diene (21): Colorless oil (15 mg, 44%), eluent combination: hexane/ethyl acetate (10:1).

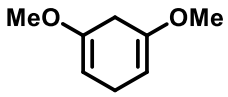

^{1}H NMR (400 MHz, $CDCl_3$) δ 4.43 – 4.37 (m, 1H), 3.31 (d, *J* = 2.3 Hz, 3H), 2.59 (ddd, *J* = 6.6, 3.4, 1.1 Hz, 1H), 2.56 – 2.49 (m, 1H); ^{13}C{^{1}H} NMR (101 MHz, $CDCl_3$) δ 152.0, 90.8, 90.7, 77.5, 77.1, 76.8, 54.2, 54.2, 31.1, 25.0 ppm. The NMR spectroscopic data is in agreement with the literature[8].

Cyclohexa-2,5-diene-1-carboxylic acid (22): White solid (19 mg, 61%), eluent combination: hexane/ethyl acetate (10:1).

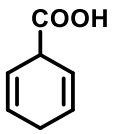

^{1}H NMR (400 MHz, $CDCl_3$) δ 12.14 (s, 1H), 5.90 (dtd, *J* = 10.4, 3.2, 1.8 Hz, 2H), 5.82 (ddt, *J* = 10.4, 3.7, 2.0 Hz, 2H), 3.83 – 3.71 (m, 1H), 2.69 (ddq, *J* = 9.1, 3.5, 2.0 Hz, 2H); ^{13}C{^{1}H} NMR (101 MHz, $CDCl_3$) δ 179.4, 126.9, 121.5, 41.5, 25.8 ppm. The NMR spectroscopic data is in agreement with the literature[7].

2,6-Dimethylcyclohexa-2,5-diene-1-carboxylic acid (23): White solid (21 mg, 55%), eluent combination: hexane/ethyl acetate (10:1).

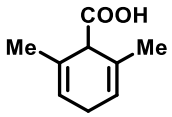

^{1}H NMR (400 MHz, $CDCl_3$) δ 11.41 (s, 1H), 5.72 – 5.64 (m, 2H), 3.47 (t, *J* = 6.3 Hz, 1H), 2.86 – 2.58 (m, 2H), 1.77 (t, *J* = 1.7 Hz, 6H); ^{13}C{^{1}H} NMR (101 MHz, $CDCl_3$) δ 178.7, 128.5, 122.5, 52.2, 27.6, 21.9 ppm. The NMR spectroscopic data is in agreement with the literature[6].

3,5-Dimethylcyclohexa-2,5-diene-1-carboxylic acid (24): White solid (20 mg, 52%), eluent combination: hexane/ethyl acetate (10:1).

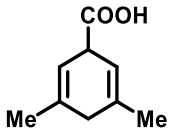

^{1}H NMR (400 MHz, $CDCl_3$) δ 11.41 (s, 1H), 5.52 (dt, *J* = 3.5, 1.7 Hz, 2H), 3.75 (dddq, *J* = 8.9, 5.3, 3.5, 1.7 Hz, 1H), 2.50 (t, *J* = 8.5 Hz, 2H), 1.75 (s, 6H); ^{13}C{^{1}H} NMR (101 MHz, $CDCl_3$) δ 179.7, 134.5, 115.7, 44.0, 35.7, 23.1 ppm. The NMR spectroscopic data is in agreement with the literature[6].

2,3,4,7-tetrahydro-1H-indene **(25):** Colorless oil (20 mg, 66%), eluent combination: hexane/ethyl acetate (10:1).

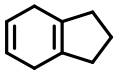

^{1}H NMR (400 MHz, $CDCl_3$) δ 5.77 (d, *J* = 1.2 Hz, 2H), 2.66 (d, *J* = 1.3 Hz, 4H), 2.28 (t, *J* = 7.4 Hz, 4H), 1.86 (t, *J* = 7.4 Hz, 2H); ^{13}C{^{1}H} NMR (101 MHz, $CDCl_3$) δ 131.9, 124.8, 35.6, 27.7, 21.5 ppm. The NMR spectroscopic data is in agreement with the literature[9].

1,4,5,8-Tetrahydronaphthalene (28): Colorless oil (25 mg, 75%), eluent combination: hexane/ethyl acetate (10:1).

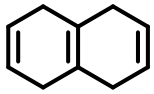

^{1}H NMR (400 MHz, $CDCl_3$) δ 5.72 (d, *J* = 3.8 Hz, 4H), 2.54 (d, *J* = 5.1 Hz, 8H); ^{13}C{^{1}H} NMR (101 MHz, $CDCl_3$) δ 181.6, 175.8, 175.8, 173.3, 173.2, 173.2, 172.1, 124.7, 124.4, 124.1, 77.1, 77.15 ppm. The NMR spectroscopic data is in agreement with the literature[6].

1,2,3,4-Tetrahydronaphthalene-2-carboxylic acid (29): White solid (31 mg, 71%), eluent combination: hexane/ethyl acetate (10:1).

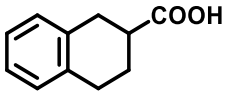

^{1}H NMR (400 MHz, $CDCl_3$) δ 11.96 (s, 1H), 7.14 (d, *J* = 6.2 Hz, 4H), 3.14 – 3.02 (m, 2H), 2.94 (ddt, *J* = 16.8, 11.4, 5.6 Hz, 2H), 2.88 – 2.78 (m, 1H), 2.29 (dq, *J* = 13.1, 4.5 Hz, 1H), 1.99 – 1.86 (m, 1H); ^{13}C{^{1}H} NMR (101 MHz, $CDCl_3$) δ 182.3, 135.6, 134.6, 129.2, 129.0, 126.1, 126.0, 39.9, 31.4, 28.4, 25.7 ppm. The NMR spectroscopic data is in agreement with the literature[7].

6-Methoxy-1,2,3,4,5,8-hexahydronaphthalene (30): Colorless oil (33 mg, 80%), eluent combination: hexane/ethyl acetate (10:1).

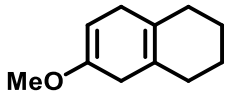

^{1}H NMR (400 MHz, $CDCl_3$) δ 4.62 (t, *J* = 3.4 Hz, 1H), 3.54 (s, 3H), 2.68 – 2.62 (m, 2H), 2.61 – 2.53 (m, 2H), 1.90 (dd, *J* = 6.1, 3.0 Hz, 4H), 1.63 (ddd, *J* = 6.4, 3.8, 2.6 Hz, 4H) ppm. The NMR spectroscopic data is in agreement with the literature[7].

4,9-Dihydro-1H-fluorene (31): White solid (30 mg, 71%), eluent combination: hexane/ethyl acetate (10:1).

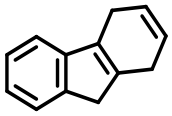

^{1}H NMR (400 MHz, $CDCl_3$) δ 7.39 (d, *J* = 7.3 Hz, 1H), 7.25 – 7.21 (m, 1H), 7.18 (d, *J* = 7.3 Hz, 1H), 7.12 (td, *J* = 7.3, 1.3 Hz, 1H), 5.89 (dtd, *J* = 13.3, 9.8, 1.6 Hz, 2H), 3.25 (s, 2H), 3.09 (s, 4H); ^{13}C{^{1}H} NMR (101 MHz, $CDCl_3$) δ 145.5, 142.7, 138.0, 133.4, 126.2, 124.5, 124.2, 124.1, 123.4, 117.8, 40.4, 27.4, 24.1 ppm. The NMR spectroscopic data is in agreement with the literature[10].

1,2-Dihydroacenaphthylene (32): White solid (35 mg, 92%), eluent combination: hexane/ethyl acetate (10:1).

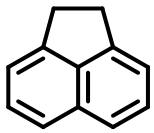

^{1}H NMR (400 MHz, $CDCl_3$) δ 7.61 (d, *J* = 8.2 Hz, 2H), 7.46 (dd, *J* = 8.2, 6.8 Hz, 2H), 7.30 (d, *J* = 6.9 Hz, 2H), 3.42 (s, 4H); ^{13}C{^{1}H} NMR (101 MHz, $CDCl_3$) δ 146.1, 139.4, 131.7, 127.9, 122.3, 119.2, 30.4 ppm. The NMR spectroscopic data is in agreement with the literature[2d].

9,10-Dihydrophenanthrene (33): White solid (38 mg, 85%), eluent combination: hexane/ethyl acetate (10:1).

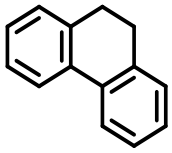

^{1}H NMR (400 MHz, $CDCl_3$) δ 7.78 (dt, *J* = 7.8, 1.0 Hz, 2H), 7.37 – 7.30 (m, 2H), 7.26 (dd, *J* = 4.0, 1.2 Hz, 4H), 2.90 (s, 4H); ^{13}C{^{1}H} NMR (101 MHz, $CDCl_3$) δ 137.5, 134.6, 128.2, 127.5, 127.0, 123.8, 29.1 ppm. The NMR spectroscopic data is in agreement with the literature[2c].

9,10-Dihydroanthracene (34): White solid (441 mg, 92%), eluent combination: hexane/ethyl acetate (10:1).

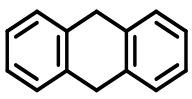

^{1}H NMR (400 MHz, $CDCl_3$) δ 7.27 (dt, *J* = 4.5, 2.2 Hz, 2H), 7.17 (dd, *J* = 5.6, 3.4 Hz, 2H), 3.92 (s, 2H); $^{13}C\{^1H\}$ NMR (101 MHz, $CDCl_3$) δ 136.8, 127.5, 126.2, 36.2 ppm. The NMR spectroscopic data is in agreement with the literature[2d].

2,3,6,7-Tetramethoxy-9,10-dihydroanthracene (35): White solid (64 mg, 86%), eluent combination: hexane/ethyl acetate (10:1).

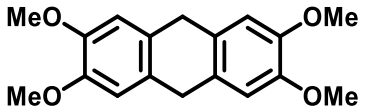

^{1}H NMR (400 MHz, $CDCl_3$) δ 6.83 (s, 4H), 4.76 (d, *J* = 13.8 Hz, 2H), 3.84 (s, 13H), 3.55 (d, *J* = 13.8 Hz, 2H); $^{13}C\{^1H\}$ NMR (101 MHz, $CDCl_3$) δ 147.8, 131.9, 113.2, 56.1, 36.6 ppm.

HRMS: (ESI) Calc. for $C_{18}H_{21}O_4$ -301.1442 (calculated) $[M+H]^+$, found -301.1438 (experimental).

(9,10-Dihydroanthracen-9-yl)(phenyl)methanol (36): White solid (48 mg, 86%), eluent combination: hexane/ethyl acetate (10:1).

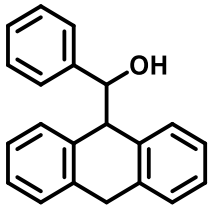

^{1}H NMR (400 MHz, $CDCl_3$) δ 7.29 (ddd, *J* = 11.3, 8.5, 4.8 Hz, 4H), 7.21 (td, *J* = 5.5, 3.3 Hz, 4H), 4.12 (d, *J* = 18.5 Hz, 1H), 3.88 – 3.78 (m, 3H), 1.61 (s, 1H), 1.11 (d, *J* = 5.7 Hz, 3H); $^{13}C\{^1H\}$

NMR (101 MHz, $CDCl_3$) δ 137.1, 136.9, 136.8, 136.7, 129.3, 129.2, 128.2, 127.9, 126.9, 126.7, 126.2, 126.2, 70.8, 55.5, 35.9, 20.5 ppm.

HRMS: (ESI) Calc. for $C_{21}H_{19}O$ 287.1438 (calculated) $[M+H]^+$, found 287.1428 (experimental).

9,10-Dimethyl-9,10-dihydroanthracene (37): White solid (48 mg, 93%), eluent combination: hexane/ethyl acetate (10:1).

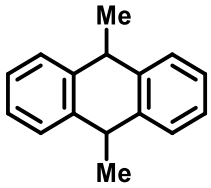

^1H NMR (400 MHz, $CDCl_3$) δ 7.43 (dd, *J* = 5.6, 3.4 Hz, 2H), 7.34 (dd, *J* = 5.4, 3.4 Hz, 2H), 7.31 – 7.23 (m, 4H), 4.14 (qd, *J* = 7.2, 2.6 Hz, 2H), 1.68 (dd, *J* = 7.1, 1.1 Hz, 3H), 1.62 (dd, *J* = 7.3, 1.2 Hz, 3H); $^{13}C\{^1H\}$ NMR (101 MHz, $CDCl_3$) δ 141.3, 140.5, 127.9, 126.3, 126.2, 125.8, 40.1, 38.5, 28.6, 18.9 ppm. The NMR spectroscopic data is in agreement with the literature[11].

2-(2,3-Dihydro-1H-inden-1-yl) acetic acid (38): White solid (33 mg, 76%), eluent combination: hexane/ethyl acetate (10:1).

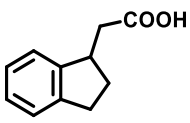

^1H NMR (400 MHz, $CDCl_3$) δ 11.89 (s, 1H), 7.41 – 7.23 (m, 4H), 3.69 (dt, *J* = 13.5, 6.7 Hz, 1H), 3.11 – 2.90 (m, 3H), 2.56 (dddd, *J* = 30.6, 16.6, 8.7, 3.1 Hz, 2H), 1.88 (dq, *J* = 12.4, 7.8 Hz, 1H); $^{13}C\{^1H\}$ NMR (101 MHz, $CDCl_3$) δ 179.5, 145.4, 144.0, 127.0, 126.5, 124.7, 123.5, 77.5, 77.1,

76.8, 41.1, 39.8, 39.8, 32.5, 31.3 ppm. The NMR spectroscopic data is in agreement with the literature[12].

1-Methylindoline (39): Yellow oil (28 mg, 84%), eluent combination: hexane/ethyl acetate (10:1).

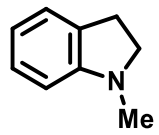

^{1}H NMR (400 MHz, $CDCl_3$) δ 7.21 – 7.09 (m, 2H), 6.82 – 6.69 (m, 1H), 6.59 – 6.53 (m, 1H), 3.35 (tdd, *J* = 8.0, 5.9, 1.6 Hz, 2H), 3.00 (t, *J* = 8.1 Hz, 2H), 2.82 (dd, *J* = 6.4, 1.6 Hz, 3H); ^{13}C{^{1}H} NMR (101 MHz, $CDCl_3$) δ 153.4, 130.3, 127.4, 124.3, 117.8, 107.3, 56.2, 36.3, 28.8 ppm. The NMR spectroscopic data is in agreement with the literature[2d].

1-Methylindoline-5-carboxylic acid (40): White solid (33 mg, 76%), eluent combination: hexane/ethyl acetate (10:1).

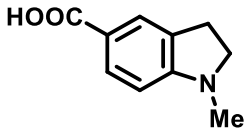

^{1}H NMR (400 MHz, $CDCl_3$) δ 7.89 (dd, *J* = 8.3, 1.8 Hz, 1H), 7.74 (q, *J* = 1.4 Hz, 1H), 6.37 (d, *J* = 8.3 Hz, 1H), 3.50 (t, *J* = 8.5 Hz, 2H), 3.01 (t, *J* = 8.5 Hz, 2H), 2.85 (s, 3H); ^{13}C{^{1}H} NMR (101 MHz, $CDCl_3$) δ 171.8, 132.2, 126.2, 117.1, 104.8, 77.3, 55.2, 34.5, 27.8 ppm.

HRMS: (ESI) Calc. for $C_{10}H_{10}NO$ 176.071 (calculated) $[M-H]^+$, found 176.0711 (experimental).

***N*-Methyl-1-(1-methylindolin-5-yl)methanamine (41):** Yellow oil (29 mg, 66%), eluent combination: hexane/ethyl acetate (10:1).

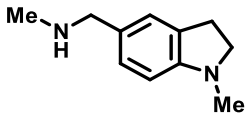

^{1}H NMR (400 MHz, $CDCl_3$) δ 7.06 (d, *J* = 1.7 Hz, 1H), 7.01 (dd, *J* = 7.9, 1.8 Hz, 1H), 6.44 (d, *J* = 7.9 Hz, 1H), 3.63 (s, 2H), 3.28 (t, *J* = 8.1 Hz, 2H), 2.92 (t, *J* = 8.1 Hz, 2H), 2.74 (s, 3H), 2.44 (s, 3H); ^{13}C{^{1}H} NMR (101 MHz, $CDCl_3$) δ 152.7, 130.7, 129.8, 127.4, 124.7, 106.9, 56.5, 56.1, 36.5, 36.0, 28.7 ppm.

HRMS: (ESI) Calc. for $C_{11}H_{16}N_2$ 176.1313 (calculated) $[M]^+$, found 176.1320 (experimental).

2,3-Dihydrobenzo[b]thiophene-2-carboxylic acid (42): White solid (39 mg, 86%), eluent combination: hexane/ethyl acetate (10:1).

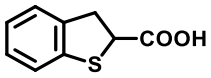

^{1}H NMR (400 MHz, $CDCl_3$) δ 11.87 (s, 1H), 7.23 – 7.12 (m, 3H), 7.06 (td, *J* = 7.1, 1.8 Hz, 1H), 4.43 (dd, *J* = 8.8, 4.8 Hz, 1H), 3.66 (dd, *J* = 16.0, 4.8 Hz, 1H), 3.49 (ddd, *J* = 15.9, 8.7, 1.1 Hz, 1H); ^{13}C{^{1}H} NMR (101 MHz, $CDCl_3$) δ 178.3, 178.3, 138.8, 138.1, 127.8, 125.0, 124.7, 121.8, 48.4, 38.0 ppm.

HRMS: (ESI) Calc. for $C_9H_7O_2S$ 179.0165 (calculated) $[M-H]^+$, found 179.0159 (experimental).

6-Methyl-2,3-dihydrobenzo[b]thiophene-2-carboxylic acid (43): White solid (38 mg, 79%), eluent combination: hexane/ethyl acetate (10:1).

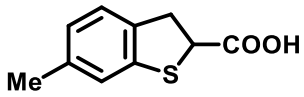

^{1}H NMR (400 MHz, $CDCl_3$) δ 7.07 (d, *J* = 7.7 Hz, 1H), 6.99 (s, 1H), 6.86 (d, *J* = 7.6 Hz, 1H), 4.42 (dd, *J* = 8.7, 4.7 Hz, 1H), 3.61 (dd, *J* = 15.8, 4.8 Hz, 1H), 3.44 (dd, *J* = 15.8, 8.7 Hz, 1H), 2.28 (s, 3H); ^{13}C{^{1}H} NMR (101 MHz, $CDCl_3$) δ 176.8, 138.8, 137.8, 135.2, 125.9, 124.4, 122.4, 77.3, 48.6, 37.8, 21.2 ppm.

HRMS: (ESI) Calc. for $C_{10}H_9O_2S$ 193.0322 (calculated) $[M-H]^+$, found 193.0300(experimental).

2,3-Dihydrobenzofuran (44): Colorless oil (27 mg, 90%), eluent combination: hexane/ethyl acetate (10:1).

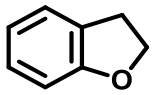

^{1}H NMR (400 MHz, $CDCl_3$) δ 7.20 (dd, *J* = 7.1, 1.4 Hz, 1H), 7.11 (td, *J* = 7.6, 1.1 Hz, 1H), 6.89 – 6.78 (m, 2H), 4.57 (t, *J* = 8.7 Hz, 2H), 3.22 (t, *J* = 8.7 Hz, 2H); ^{13}C{^{1}H} NMR (101 MHz, $CDCl_3$) δ 160.1, 128.0, 126.9, 125.0, 120.4, 109.4, 71.1, 29.8 ppm. The NMR spectroscopic data is in agreement with the literature[2d].

2-Methyl-2,3-dihydrobenzofuran (45): Colorless oil (25 mg, 75%), eluent combination: hexane/ethyl acetate (10:1).

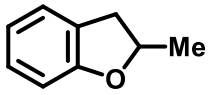

^{1}H NMR (400 MHz, $CDCl_3$) δ 7.22 – 7.07 (m, 2H), 6.91 – 6.83 (m, 1H), 6.80 (dd, *J* = 8.6, 2.8 Hz, 1H), 5.01 – 4.88 (m, 1H), 3.34 (dd, *J* = 15.4, 8.7 Hz, 1H), 2.90 – 2.79 (m, 1H), 1.56 – 1.45 (m, 3H); ^{13}C{^{1}H} NMR (101 MHz, $CDCl_3$) δ 159.6, 128.0, 127.1, 125.0, 120.2, 109.4, 79.5, 37.2, 21.8 ppm. The NMR spectroscopic data is in agreement with the literature[13].

(2,3-Dihydrobenzofuran-5-yl)methanol (46): Colorless oil (24 mg, 65%), eluent combination: hexane/ethyl acetate (10:1).

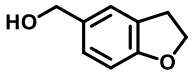

^{1}H NMR (400 MHz, $CDCl_3$) δ 7.21 (s, 1H), 7.08 (d, *J* = 8.1 Hz, 1H), 6.75 (d, *J* = 8.1 Hz, 1H), 4.60 – 4.53 (m, 4H), 3.19 (t, *J* = 8.6 Hz, 2H), 1.84 (s, 1H); ^{13}C{^{1}H} NMR (101 MHz, $CDCl_3$) δ 159.8, 133.2, 127.5, 127.4, 124.4, 109.2, 71.4, 65.4, 29.7 ppm.

HRMS: (ESI) Calc. for $C_9H_{11}O$ 151.0761 (calculated) $[M+H]^+$, found 151.0754 (experimental).

2,3-Dihydrobenzofuran-5-carboxylic acid (47): White solid (38 mg, 93%), eluent combination: hexane/ethyl acetate (10:1).

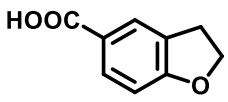

^{1}H NMR (400 MHz, $CDCl_3$) δ 12.03 (s, 1H), 7.99 – 7.91 (m, 2H), 6.82 (d, *J* = 8.8 Hz, 1H), 4.68 (t, *J* = 8.8 Hz, 2H), 3.26 (t, *J* = 8.8 Hz, 2H); ^{13}C{^{1}H} NMR (101 MHz, $CDCl_3$) δ 171.8, 165.1, 132.1, 127.6, 127.5, 121.7, 109.3, 77.3, 72.3, 29.1 ppm.

HRMS: (ESI) Calc. for $C_9H_8O_3$ 164.0473 (calculated) $[M]^+$, found 164.0463 (experimental).

2,3-Dihydrobenzofuran-5-sulfonic acid (48): White solid (23 mg, 47%), eluent combination: hexane/ethyl acetate (10:1).

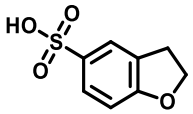

^{1}H NMR (400 MHz, $CDCl_3$) δ 5.87 – 5.84 (m, 1H), 5.81 – 5.76 (m, 1H), 4.93 (d, *J* = 8.3 Hz, 1H), 2.79 (t, *J* = 8.8 Hz, 2H), 1.42 (t, *J* = 8.8 Hz, 2H); ^{13}C{^{1}H} NMR (101 MHz, MeOD) δ 163.3, 137.9, 128.8, 127.6, 124.1, 109.3, 72.9, 30.1 ppm.

HRMS: (ESI) Calc. for $C_8H_9SO_4$ 201.0223 (calculated) $[M+H]^+$, found 201.0218 (experimental).

1,3-Diphenylpropan-1-one (49): Colorless oil (47 mg, 89%), eluent combination: hexane/ethyl acetate (10:1).

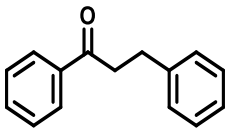

^{1}H NMR (400 MHz, $CDCl_3$) δ 7.92 – 7.87 (m, 2H), 7.52 – 7.46 (m, 1H), 7.42 – 7.35 (m, 2H), 7.27 – 7.18 (m, 4H), 7.18 – 7.12 (m, 1H), 3.27 – 3.21 (m, 2H), 3.01 (dd, *J* = 8.5, 6.9 Hz, 2H); ^{13}C{^{1}H}

NMR (101 MHz, $CDCl_3$) δ 199.3, 141.4, 136.9, 133.1, 128.7, 128.6, 128.5, 128.1, 126.2, 40.5, 30.2 ppm. The NMR spectroscopic data is in agreement with the literature[14].

3-Phenylpropanoic acid (50): Whie solid (28 mg, 75%), eluent combination: hexane/ethyl acetate (10:1).

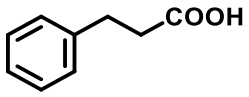

^{1}H NMR (400 MHz, $CDCl_3$) δ 11.35 (s, 1H), 7.34 – 7.27 (m, 2H), 7.22 (ddt, *J* = 8.1, 3.4, 2.1 Hz, 3H), 2.97 (t, *J* = 7.8 Hz, 2H), 2.70 (dd, *J* = 8.4, 7.2 Hz, 2H); ^{13}C{^{1}H} NMR (101 MHz, $CDCl_3$) δ 178.9, 140.2, 128.7, 128.4, 126.5, 35.6, 30.7 ppm. The NMR spectroscopic data is in agreement with the literature[15].

1,2-Diphenylethane (51): White solid (35 mg, 78%), eluent combination: hexane/ethyl acetate (10:1).

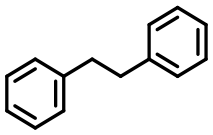

^{1}H NMR (400 MHz, $CDCl_3$) δ 7.40 – 7.33 (m, 4H), 7.28 (td, *J* = 6.3, 1.6 Hz, 6H), 3.01 (s, 4H); ^{13}C{^{1}H} NMR (101 MHz, $CDCl_3$) δ 141.9, 128.5, 128.4, 126.0, 38.0 ppm. The NMR spectroscopic data is in agreement with the literature[9].

1,4-Diphenylbutane (52): Colorless oil (35 mg, 71%), eluent combination: hexane/ethyl acetate (10:1).

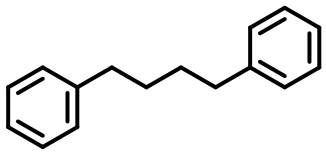

^{1}H NMR (400 MHz, $CDCl_3$) δ 7.36 – 7.28 (m, 4H), 7.23 (td, *J* = 5.5, 3.1 Hz, 6H), 2.75 – 2.65 (m, 4H), 1.78 – 1.69 (m, 4H); $^{13}C\{^1H\}$ NMR (101 MHz, $CDCl_3$) δ 142.6, 128.5, 128.3, 125.7, 35.9, 31.2 ppm. The NMR spectroscopic data is in agreement with the literature[16].

N-Benzylaniline (53): Colorless oil (38 mg, 84%), eluent combination: hexane/ethyl acetate (10:1).

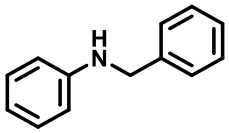

^{1}H NMR (400 MHz, $CDCl_3$) δ 7.43 – 7.35 (m, 4H), 7.33 – 7.26 (m, 1H), 7.23 – 7.17 (m, 2H), 6.75 (tt, *J* = 7.4, 1.1 Hz, 1H), 6.69 – 6.64 (m, 2H), 4.36 (s, 2H), 4.10 (s, 1H); $^{13}C\{^1H\}$ NMR (101 MHz, $CDCl_3$) δ 148.2, 139.5, 129.3, 128.7, 127.6, 127.3, 117.7, 113.0, 48.4 ppm. The NMR spectroscopic data is in agreement with the literature[14].

***N*-(4-Methoxybenzyl)aniline (54):** Colorless oil (40 mg, 76%), eluent combination: hexane/ethyl acetate (10:1).

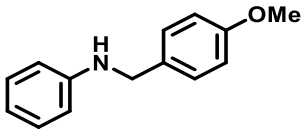

^{1}H NMR (400 MHz, $CDCl_3$) δ 7.34 – 7.27 (m, 2H), 7.19 (tt, *J* = 7.4, 0.8 Hz, 2H), 6.92 – 6.87 (m, 2H), 6.73 (tt, *J* = 7.4, 1.0 Hz, 1H), 6.68 – 6.63 (m, 2H), 4.27 (s, 2H), 3.99 (s, 1H), 3.82 (s, 3H); ^{13}C{^{1}H}NMR (101 MHz, $CDCl_3$) δ 159.0, 148.3, 131.5, 129.3, 128.9, 117.6, 114.1, 112.9, 55.4, 47.9 ppm. The NMR spectroscopic data is in agreement with the literature[14].

4-((Phenylamino)methyl)benzonitrile (55): Colorless oil (46 mg, 88%), eluent combination: hexane/ethyl acetate (10:1).

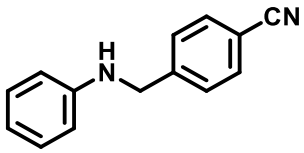

^{1}H NMR (400 MHz, $CDCl_3$) δ 7.66 – 7.60 (m, 2H), 7.50 – 7.46 (m, 2H), 7.20 – 7.14 (m, 2H), 6.74 (tt, *J* = 7.3, 1.1 Hz, 1H), 6.61 – 6.53 (m, 2H), 4.43 (s, 2H); ^{13}C{^{1}H} NMR (101 MHz, $CDCl_3$) δ 147.5, 145.5, 132.5, 129.5, 127.8, 119.1, 118.2, 113.0, 111.0, 47.9 ppm. The NMR spectroscopic data is in agreement with the literature[17].

***N*-(4-Nitrobenzyl)aniline (56):** Yellow solid (41 mg, 72%), eluent combination: hexane/ethyl acetate (10:1).

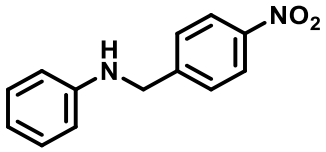

^{1}H NMR (400 MHz, $CDCl_3$) δ 8.12 – 8.04 (m, 2H), 7.42 – 7.29 (m, 5H), 6.62 – 6.53 (m, 2H), 4.89 (s, 1H), 4.43 (s, 2H); $^{13}C\{^{1}H\}$ NMR (101 MHz, $CDCl_3$) δ 153.1, 138.5, 137.4, 129.1, 128.0, 127.4, 126.5, 111.4, 77.3, 47.8 ppm. The NMR spectroscopic data is in agreement with the literature[18].

1,2-Diphenylhydrazine (57): Yellow solid (29 mg, 63%), eluent combination: hexane/ethyl acetate (10:1).

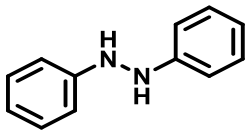

^{1}H NMR (400 MHz, $CDCl_3$) δ 7.18 – 7.11 (m, 5H), 6.78 (dt, *J* = 8.4, 1.5 Hz, 6H), 5.53 (s, 2H); $^{13}C\{^{1}H\}$ NMR (101 MHz, $CDCl_3$) δ 148.9, 129.4, 120.0, 112.4 ppm. The NMR spectroscopic data is in agreement with the literature[19].

(3S,8S,9S,10R,13R,14S,17R)-10,13-Dimethyl-17-((R)-6-methylheptan-2-yl)-2,3,4,7,8,9,10,11,12,13,14,15,16,17-tetradecahydro-1H-cyclopenta[a]phenanthren-3-yl 2,3-dihydrobenzo[b]thiophene-2-carboxylate (60): White solid (90 mg, 66%), eluent combination: hexane/ethyl acetate (10:1).

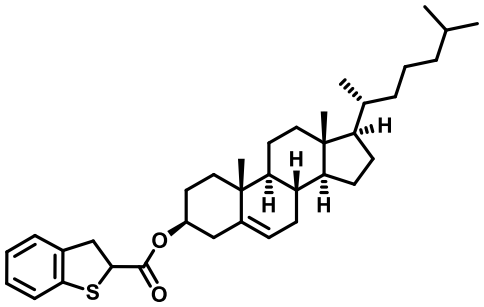

^{1}H NMR (400 MHz, $CDCl_3$) δ 7.20 – 7.10 (m, 3H), 7.03 (td, *J* = 7.1, 1.8 Hz, 1H), 5.37 (dt, *J* = 4.1, 1.9 Hz, 1H), 4.70 – 4.60 (m, 1H), 4.42 (dd, *J* = 8.8, 6.1 Hz, 1H), 3.68 (dd, *J* = 15.9, 6.0 Hz, 1H), 3.45 (dd, *J* = 15.9, 8.8 Hz, 1H), 2.39 – 2.27 (m, 2H), 2.06 – 1.79 (m, 6H), 1.66 – 1.28 (m, 12H), 1.13 (tdd, *J* = 14.0, 7.4, 4.4 Hz, 7H), 1.02 (s, 4H), 0.92 (d, *J* = 6.5 Hz, 3H), 0.87 (dd, *J* = 6.6, 1.8 Hz, 6H), 0.68 (s, 3H); $^{13}C\{^1H\}$ NMR (101 MHz, $CDCl_3$) δ 171.2, 139.6, 139.5, 139.3, 138.6, 127.6, 124.7, 124.6, 122.9, 121.7, 75.4, 56.8, 56.2, 50.1, 49.0, 48.9, 42.4, 39.8, 39.6, 38.1, 38.1, 38.0, 37.9, 37.0, 37.0, 36.7, 36.7, 36.3, 35.9, 32.0, 31.9, 28.3, 28.1, 27.7, 27.6, 24.4, 23.9, 22.9, 22.7, 21.1, 19.4, 18.8, 11.9 ppm.

HRMS: (ESI) Calc. for $C_{36}H_{52}O_2S$ 548.3688 (calculated) $[M]^+$, found 548.3676 (experimental).

9*H*-Fluorene (62): White solid (30 mg, 72%), eluent combination: hexane/ethyl acetate (10:1).

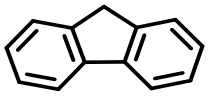

^{1}H NMR (400 MHz, $CDCl_3$) δ 7.83 (dt, *J* = 7.6, 1.0 Hz, 2H), 7.58 (dt, *J* = 7.5, 1.0 Hz, 2H), 7.41 (td, *J* = 7.4, 1.2 Hz, 2H), 7.34 (td, *J* = 7.4, 1.2 Hz, 2H), 3.93 (s, 2H); $^{13}C\{^1H\}$ NMR (101 MHz, $CDCl_3$) δ 143.3, 141.8, 126.8, 126.8, 125.1, 120.0, 37.0 ppm. The NMR spectroscopic data is in agreement with the literature[20].

4-Phenylbutanoic acid (63): White solid (28 mg, 69%), eluent combination: hexane/ethyl acetate (10:1).

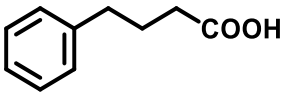

^{1}H NMR (400 MHz, $CDCl_3$) δ 7.30 (ddt, *J* = 8.7, 5.3, 1.6 Hz, 2H), 7.21 (tt, *J* = 8.0, 1.4 Hz, 3H), 2.69 (td, *J* = 7.6, 1.8 Hz, 2H), 2.39 (td, *J* = 7.5, 1.8 Hz, 2H), 2.03 – 1.93 (m, 2H); ^{13}C{^{1}H} NMR (101 MHz, $CDCl_3$) δ 180.2, 141.3, 128.6, 128.5, 126.1, 35.1, 33.4, 33.4, 26.3 ppm. The NMR spectroscopic data is in agreement with the literature[2b].

3-Phenylpropan-1-ol (64): Colorless oil (29 mg, 85%), eluent combination: hexane/ethyl acetate (10:1).

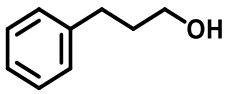

^{1}H NMR (400 MHz, $CDCl_3$) δ 7.34 – 7.28 (m, 2H), 7.23 (d, *J* = 7.3 Hz, 3H), 3.68 (t, *J* = 6.5 Hz, 2H), 2.73 (dd, *J* = 8.8, 6.8 Hz, 2H), 1.97 – 1.86 (m, 2H); ^{13}C{^{1}H} NMR (101 MHz, $CDCl_3$) δ 141.9, 128.5, 128.4, 125.9, 62.2, 34.2, 32.1 ppm. The NMR spectroscopic data is in agreement with the literature[2b].

4-Phenylbutan-2-ol (65): Colorless oil (22 mg, 59%), eluent combination: hexane/ethyl acetate (10:1).

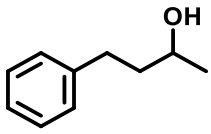

^{1}H NMR (400 MHz, $CDCl_3$) δ 7.41 – 7.34 (m, 2H), 7.29 (dt, *J* = 8.2, 2.0 Hz, 3H), 3.97 – 3.88 (m, 1H), 2.90 – 2.72 (m, 2H), 1.92 – 1.83 (m, 2H), 1.32 (d, *J* = 6.2 Hz, 3H); ^{13}C{^{1}H} NMR (101 MHz,

$CDCl_3$) δ 142.1, 128.5, 125.9, 67.6, 40.9, 32.2, 23.7 ppm. The NMR spectroscopic data is in agreement with the literature[21].

Indole (66): White solid (23 mg, 80%), eluent combination: hexane/ethyl acetate (10:1).

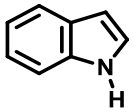

^{1}H NMR (400 MHz, $CDCl_3$) δ 8.17 (s, 1H), 7.71 (d, *J* = 7.9 Hz, 1H), 7.45 (d, *J* = 8.1 Hz, 1H), 7.32 – 7.23 (m, 2H), 7.21 – 7.15 (m, 1H), 6.62 (t, *J* = 2.8 Hz, 1H); ^{13}C{^{1}H} NMR (101 MHz, $CDCl_3$) δ 135.9, 124.2, 122.1, 120.8, 119.9, 111.1, 102.7, 77.3 ppm. The NMR spectroscopic data is in agreement with the literature[20].

Melatonin (67): White solid (47 mg, 81%), eluent combination: hexane/ethyl acetate (10:1).

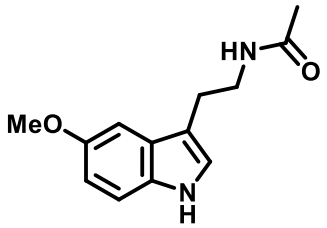

^{1}H NMR (400 MHz, $CDCl_3$) δ 8.03 (s, 1H), 7.26 (d, *J* = 1.4 Hz, 1H), 7.09 – 6.99 (m, 2H), 6.87 (dd, *J* = 8.8, 2.4 Hz, 1H), 5.66 (s, 1H), 3.86 (s, 3H), 3.59 (q, *J* = 6.4 Hz, 2H), 2.95 (t, *J* = 6.8 Hz, 2H), 1.94 (s, 3H); ^{13}C{^{1}H} NMR (101 MHz, $CDCl_3$) δ 170.3, 154.2, 131.6, 127.8, 122.9, 112.8, 112.6, 112.1, 100.6, 77.3, 56.0, 39.9, 25.4, 23.4 ppm. The NMR spectroscopic data is in agreement with the literatur[20].

(4,4,5,5- Tetramethyl-1,3,2-dioxaborolan-2-yl)benzene (70): White solid (27 mg, 53%), combination: hexane/ethyl acetate (10:1).

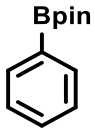

^{1}H NMR (400 MHz, $CDCl_3$) δ 7.85 – 7.79 (m, 2H), 7.50 – 7.44 (m, 1H), 7.42 – 7.35 (m, 2H), 1.36 (s, 13H); ^{13}C NMR (101 MHz, $CDCl_3$) δ 134.8, 131.3, 127.8, 83.8, 25.0 ppm. The NMR spectroscopic data is in agreement with the literature[20].

2-(4-Methoxyphenyl)-4,4,5,5,-tetramethyl-1,2,3-dioxaborolane (71): White solid (35 mg, 61%), eluent combination: hexane/ethyl acetate (10:1).

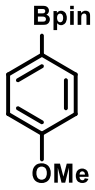

^{1}H NMR (400 MHz, $CDCl_3$) δ 7.82 – 7.71 (m, 2H), 6.96 – 6.85 (m, 2H), 3.82 (s, 3H), 1.34 (s, 13H); ^{13}C NMR (101 MHz, $CDCl_3$) δ 162.2, 136.6, 113.3, 83.6, 55.1, 24.9 ppm. The NMR spectroscopic data is in agreement with the literature[2c].

(9R,10R)-9,10-dihydrophenanthrene-9,10-diol (72): White solid (45 mg, 86%), eluent combination: hexane/ethyl acetate (10:1).

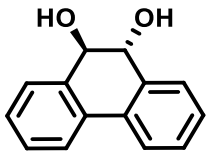

^{1}H NMR (400 MHz, $CDCl_3$) δ 7.76 (d, *J* = 7.4 Hz, 2H), 7.71 – 7.63 (m, 2H), 7.40 (t, *J* = 6.0 Hz, 4H), 4.76 (s, 2H), 2.54 (s, 2H); ^{13}C{^{1}H} NMR (101 MHz, $CDCl_3$) δ 136.1, 132.5, 128.5, 128.4, 125.2, 123.8, 74.1 ppm. The NMR spectroscopic data is in agreement with the literature[22].

3-Methylcyclohex-3-en-1-one (74): Yellow oil (18 mg, 65%), eluent combination: hexane/ethyl acetate (10:1).

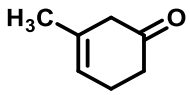

^{1}H NMR (400 MHz, $CDCl_3$) δ 5.57 – 5.52 (m, 1H), 2.74 (s, 2H), 2.39 (d, *J* = 3.4 Hz, 4H), 1.68 (s, 3H); ^{13}C{^{1}H} NMR (101 MHz, $CDCl_3$) δ 211.0, 132.1, 121.0, 44.5, 38.3, 25.0, 22.7 ppm. The NMR spectroscopic data is in agreement with the literature[23].

1-Phenylethan-1-ol (75): Colorless oil (28 mg, 92%), eluent combination: hexane/ethyl acetate (10:1).

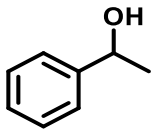

^{1}H NMR (400 MHz, $CDCl_3$) δ 7.32 – 7.25 (m, 4H), 7.24 – 7.17 (m, 1H), 4.81 (q, *J* = 6.5 Hz, 1H), 2.22 (d, *J* = 35.3 Hz, 1H), 1.42 (d, *J* = 6.4 Hz, 3H); ^{13}C{^{1}H} NMR (101 MHz, $CDCl_3$) δ 145.9,

128.6, 127.5, 125.5, 70.5, 25.2 ppm. The NMR spectroscopic data is in agreement with the literature[24].

Phenol (76): White solid (21 mg, 89%), eluent combination: hexane/ethyl acetate (10:1).

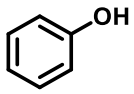

^{1}H NMR (400 MHz, $CDCl_3$) δ 7.29 – 7.19 (m, 2H), 6.99 – 6.89 (m, 1H), 6.88 – 6.79 (m, 2H), 5.00 (s, 1H); $^{13}C\{^{1}H\}$ NMR (101 MHz, $CDCl_3$) δ 155.4, 155.4, 129.8, 121.0, 120.9, 115.4, 115.4 ppm. The NMR spectroscopic data is in agreement with the literature[25].

REFERENCES

1. Lim, C.-H.; Kudisch, M.; Liu, B.; Miyake, G. M. C–N Cross-Coupling via Photoexcitation of Nickel–Amine Complexes. *J. Am. Chem. Soc.* **140**, 7667-7673 (2018)
2. a) Chatterjee, A.; König, B. *Angew. Chem., Int. Ed.,* **58**, 14289 (2019); b) Cole, J. P.; Chen, D.-F.; Kudisch, M.; Pearson, R. M.; Lim, C.-H.; Miyake, G. M. Organocatalyzed birch reduction driven by visible light. *J. Am. Chem. Soc.* **142**, 13573−13581 (2020); c) Wu, S.; Schiel, F.; Melchiorre, P. *Angew. Chem. Int. Ed.* **62**, e202306364 (2023); d) Yuan, T., Sun, L., Wu, Z. Mild and metal-free Birch-type hydrogenation of (hetero)arenes with boron carbonitride in water. *Nat Catal* **5**, 1157–1168 (2022)
3. Fort, E. H.; Donovan, P. M.; Scott, L. T. Diels−Alder Reactivity of Polycyclic Aromatic Hydrocarbon Bay Regions: Implications for Metal-Free Growth of Single-Chirality Carbon Nanotubes. *J. Am. Chem. Soc.* **131**, 16006−16007 (2009)
4. Pavlyuk, D. E.; Gundala, S.; Kovalev, I. S. Reactions of Perylene with Aryne Intermediates. *Russ J Org Chem* **55**, 409–411 (2019).
5. Furukawa, T.; Tobisu, M.; Chatani, N. C−H Borylation by Platinum Catalysis. *Bull. Chem. Soc. Jpn.* **90**, 332−342 (2017)
6. Peters, B. K.; Rodriguez, K. X.; Reisberg, S. H.; Beil, S. B.; Hickey, D. P.; Kawamata, Y.; Collins, M.; Starr, J.; Chen, L.; Udyavara, S.; Klunder, K.; Gorey, T. J.; Anderson, S. L.; Neurock, M.; Minteer, S. D.; Baran, P. S. Scalable and safe synthetic organic electroreduction inspired by Li-ion battery chemistry. *Science* **363**, 838-845 (**2019**)
7. Burrows, J.; Kamo, S.; Koide, K. Scalable Birch reduction with lithium and ethylenediamine in tetrahydrofuran. *Science* **374**, 741-746 (2021).
8. Wada, Y.; Murata, R.; Fujii, U.; Asano**,** K.; Matsubara, S. Org. Lett. **22**, 12, 4710–4715 (2020)
9. Lei, P.; Ding, Y.; Zhang, X.; Adijiang, A.; Li, H.; Ling, Y.; An**,** J. Org. Lett. **20**, 3439–3442 (2018)
10. Silver, S.; Leino, R. *Eur. J. Org. Chem.* 1965–1977 (2006)
11. Segawa, Y.; Stephan, D. W. ***Chem. Commun.*** **48**, 11963-11965 (2012)
12. Senboku, H.; Michinishi, J.; Hara, S. *Synlett* **11**, 1567-1572 (**2011**)
13. Zhou, B.; Chandrashekhar, V. G.; Ma, Z.; Kreyenschulte, C.; Bartling, S.; Lund, H.; Beller, M.; Jagadeesh, R. V. *Angew. Chem.Int. Ed.* **62**, e2022156 (2023)
14. Wang, D.; Zhao, K.; Xu, C.; Miao, H.; Ding, Y. ACS Catal. **4**, 3910–3918 (2014)
15. Ren, W.; Sheng, X.; Fan, C.; Shi, Y. Org. Lett. **25**, 7786–7790 (2023)
16. Maytum, H. C.; Francos, J.; Whatrup, D. J.; Williams, J. M. J. *Chem. Asian J*. **5**, 538 – 542 (2010)
17. Cho, B. T.; Kang, S. K. *Tetrahedron* **61**, 5725–5734 (2005)
18. Apodaca, R.; Xiao, W. Org. Lett. **3**, 1745–1748 (2001)
19. Dey, S.; Panja, D.; Sau, A.; Thakur, S. D.; Kundu, S. J. Org. Chem. **88**, 10048–10057 (2023)
20. Huang, B.; Guo, L.; Xia, W. ***Green Chem.*** **23**, 2095-2103 (2021)
21. Kreissl, H.; Jin, J.; Lin, S. H.; Schette, D.; Stçrtte, S.; Levin, N.; Chaudret, B.; Vorholt, A. J.; Bordet, A.; Leitner, W. *Angew. Chem. Int. Ed.* **60**, 26639–26646 (2021)
22. Yasui, M.; Hanaya, K.; Sugai, T.; Higashibayashi, S. *RSC Adv.,* **11**, 24652–24655 (2021)
23. Pero, J. E.; McAtee, J. J.; Behm, D. J.; Briand, J.; Millbrandt, G. G.; Erhard, K.; Roberts, A. D.; Rivero, R. A.; Holt, D. A.; Lawhorn, B. G. ACS Med. Chem. Lett. **12**, 1498–1502 (2021)
24. Liu, S.; Liu, H.; Zhou, H.; Liu, Q.; Lv, J. Org. Lett. **20**, 1110–1113 (2018)

25. Guo, T.; Lin, Y.; Pan, D.; Zhang, X.; Zhu, W.; Cai, X. W.; Huang, G.; Wang, H.; Xu, D.; Kühn, F. E.; Zhang. B.; Zhang, T. *Nat. Comm.* **14**, 6076 (2023)